UTILISATION OF FLY ASH IN THE MANUFACTURE OF ZEOLITES

by

ROBERTO PETER ZYGMUNT SOMMERVILLE

Thesis submitted to the University of Birmingham
for the Degree of
DOCTOR OF PHILOSOPHY

School of Chemical Engineering
College of Engineering & Physical Sciences
University of Birmingham
SEPTEMBER 2016

Abstract

Disposal of Coal Fly Ash (CFA) is a problem of increasing concern, due to its environmental impact. Beneficiation processes such as the RockTron process are capable of producing various value-added products with specialist applications, such as low density cenospheres, and the Alpha product: a pozzolanic replacement for cement and concrete. The Delta product from the RockTron process has few applications other than as an aggregate and is apt for use in the synthesis of zeolites due to its reduced iron and carbon content.

The current study explores the hydrothermal extraction process, the fusion assisted extraction process and a novel microwave fusion process with a performance comparable to the fusion process. The extraction process is optimised for the Delta ash, and compared to other ashes. The hydrothermal extraction of Si from rice husk ash is also assessed.

In the optimisation of the crystallisation process, the influence of sodium aluminate addition on the properties of zeolites which form was examined. The effects of alkalinity, sodium source and salt concentration were investigated using XRD, SEM, AAS, CEC and PSD. A concurrent decrease in the concentration of Si and Al in the crystallisation solution was observed as amorphous material is consumed during the crystal growth phase. This crystal growth phase occurs earlier with higher concentrations of sodium aluminate and NaCl. Limited addition of NaCl at concentrations similar to seawater improve crystallinity, yield and CEC of zeolites, whilst also decreasing particle size. The optimised results demonstrated good repeatability with the best measured yield being 233 g/kg FA with a CEC of 4.6 meq/g, and the best estimated yield being 264 g/kg FA, with a CEC of 4.8 meq/g.

Buoyant zeolites were synthesised through seeding of the crystallisation process with cenospheres. The resulting products consisted of 77% cenospheres and 23% zeolite. The crystallisation process was also applied successfully to rice husk ash, producing zeolite A at high yields.

It is therefore concluded that waste materials such as Delta ash and rice husk ash are well suited for utilisation in the manufacture of zeolites.

Acknowledgements

I would like to express my gratitude to a number of people who have supported me during this project. Firstly I would like to thank my supervisor Professor Neil Rowson for his patience, support, and guidance throughout my time at at the University of Birmingham. I would like to thank Dr. Rob Blissett for his advice, and collaboration in published papers. I would like to thank Dr. Sav Savva for his recommendations on analysis techniques, and Jo Fitzpatrick for proof reading the spelling and grammar of this thesis. I would also like to thank Prof. Stuart Blackburn, Dr. Jackie Deans, and Dr Phil Robbins.

I would like to thank the Engineering and Physical Sciences Research Council of the United Kingdom, RockTron Research Ltd, The Royal Commission for the Exhibition of 1851, and the University of Birmingham for funding and facilitating this project.

I'd like to thank Dave, Ridhi, Lisa and Helen for their support and good humour in the last decade. I thank my friends from Purple Mermaid who have encouraged me, and I thank my friends from the lunch and board games group, who have been an excellent sounding board during the more testing parts of this project. I owe special thanks to Mish for her unwavering support and optimism throughout this project.

And finally thanks to my Nonna, my parents, and family for their understanding and encouragement.

Contents

List of Figures

List of Tables

Nomenclature

AAS	Atomic Absorption Spectrometry
CEC	Cation Exchange Capacity
CFA	Coal fly ash
FA	Fly Ash
LOI	Loss On Ignition
PSD	Particle Size Distribution
RTP	Room Temperature and Pressure
SA	Sodium Aluminate
SEM	Scanning Electron Microscopy
XRD	X-Ray Diffraction
XRF	X-Ray Fluorescence

Chapter 1

Introduction

1.1 Objective of Thesis

The overall objective of this work is to make use of and derive value from waste products. The waste products utilised are processed coal fly ash and rice husk ash. These waste products were leached to produce a solution rich in silicon, to which aluminium was added to produce synthetic zeolites. The specific objectives were to study the extraction process, the crystallisation process, and the properties and yield of the zeolites produced from these processes.

1.2 Fly Ash

Pulverised coal fly ash is removed from the flue gasses of coal-fired power stations that burn pulverised coal. Coal fly ash (CFA) is a grey, abrasive, refractory powder that is heterogeneous in nature. European standard EN450 describes pulverised fly ash as "a fine-grained powder which is mainly composed of spherical glassy particles, produced during the combustion of pulverized coal". CFA is considered a pollutant if unutilised. Different coals and combustion conditions result in the formation of various minerals or mineral groups. To date approximately 188 minerals or mineral groups have been identified in various coal fly ashes [1–4]. The most abundant components of coal fly ash are silica and

alumina, but content varies depending on coal type and combustion conditions [1, 3].

1.3 Production of Fly Ash

Coal is 5-20 % mineral matter [5, 6]. Combustion of pulverised coal produces two main byproducts: fly ash and bottoms ash. The fly ash forms the majority of the combustion residue at 60-88 %, and is the main focus of this work [3, 4, 7, 8]. Fly ash is commonly separated from the flue gasses of thermoelectric power plants using electrostatic precipitators, however gravity chambers, cyclones, wet scrubbers and bag filters have also been used [3, 4, 9, 10]. Electrostatic precipitators are favoured due to energy efficiency, as well as reliable operation over different particle size ranges and gas flow rates, whilst having low operational and maintenance costs [11]. In 2013, 41.3 % of the world's electricity supply was derived from a combination of coal, peat and oil shale [12]. It is estimated that 750 million tonnes of CFA is generated globally per year [13]. Only 25 % of this CFA is utilised, meaning that the majority is disposed of, with common methods of disposal including landfill and lagoons. Such disposal methods are costly, and are under increasing scrutiny due to land availability and environmental concerns [2, 7, 13–15]. Toxic elements present in coal are concentrated in CFA, and their slow release renders land used as a CFA dump unsuitable for agriculture in future. Elements such as As, B and Mg have been noted to accumulate in plants, whilst the pH of the soil is increased due to the release of CaO and MgO present in CFA [7, 9, 16–18]. Such toxic contamination is attributed to water-soluble toxic components being dissolved by rainwater and contaminating soil and groundwater, however weathered fly ash is noted to have a significantly reduced toxicity [9].

1.4 Uses of Fly Ash

CFA can be utilised for a variety of applications. European CFA utilisation trends are shown in Figure 1.1 along with a breakdown of proportions of current applications of the

47 % which is utilised.

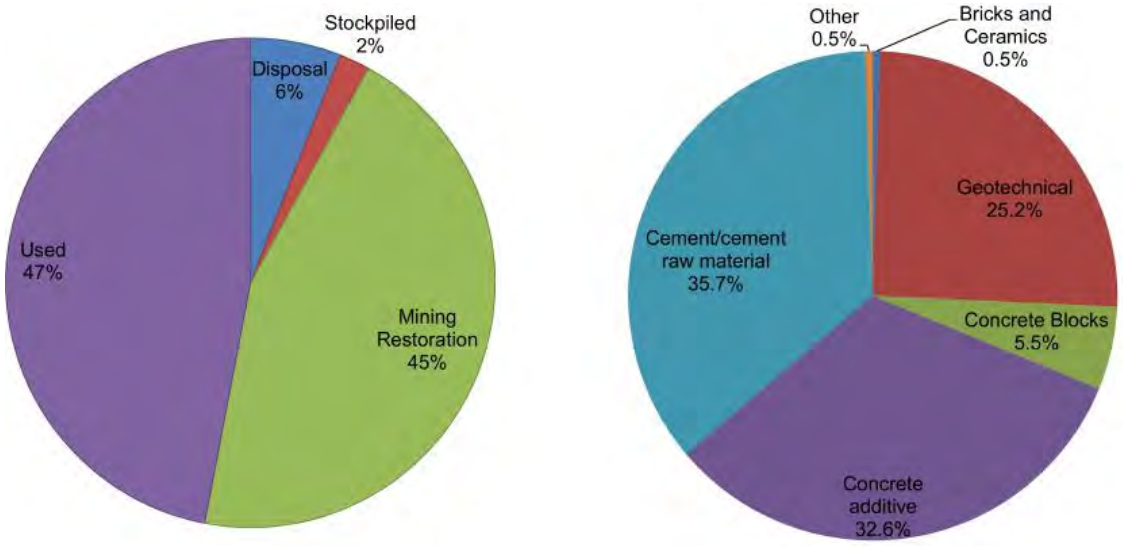

Figure 1.1: CFA utilisation trends in Europe. The right-hand pie chart shows a breakdown of the used component of the left-hand chart (from Blissett [1]).

The most common application of CFA exploits the pozzolanic properties of CFA for use in cement and as a concrete additive. A pozzolan is a material which is not itself cementitious, but which, when of a fine particle size, will react with calcium hydroxide to form a cementitious material [1, 19]. Such use is subject to strict standards, stipulated in ASTM C 618 by the American Society for Testing and Materials and EN 450-1 in Europe [1–3, 9, 13]. Utilisation of CFA in concrete or mortar can decrease costs, density and hydration heat, whilst increasing leaching resistance, workability and compressive strength [9, 10, 15]. Using 1 ton of CFA in lieu of 1 ton of cement saves the equivalent of 1 barrel of oil, thus use of CFA is ideal for reducing the carbon cost of cement [3]. Blocks and bricks that incorporate CFA are lighter and have reduced heat transfer whilst also being cheaper [9]. Construction applications such road bases, bitumen filler, embankments, grout mixes, and stabilising clay exploit the geotechnical properties of CFA, such as consolidation characteristics, specific gravity, internal angular friction and permeability [2, 3, 9, 14, 20]. Cement and construction demand is insufficient to consume all CFA produced [7, 14].

Uses outside of construction include ceramics and composite materials. Composites

such as metals and polymers show improvements in: hardness, elastic moduli, abrasive resistance, and tensile strength [9, 14, 21]. CFA can be used in land reclamation on the condition that the ash is non-polluting (i.e, has been weathered) and that the area is delimited by a reef [9]. CFA is a potential feedstock for metal extraction. Al extraction has been investigated, as well as Ti, Fe, Ge, Ga and other metals [3, 9, 14, 22–24]. The surface area, water retention, particle size and porosity of CFA allow for it to be used as an adsorbent [2, 9, 14], and a sorbent for flue gas desulphurisation [3].

Fly ash has been used as a settling aid, and chemical oxygen demand reducer in water purification, the alkalinity of the ash is of use in neutralising acidic water [9]. The alkalinity of fly ashes can also be exploited to neutralise acidic mining spoils [9].

CFA has been used to ameliorate clay soils, rendering improvements in crop yield, but also increasing the concentration of potentially toxic trace elements in plant tissues. Alkaline ashes have been used to treat acidic soils. Additionally, such neutralisation prevented the toxic effects of Al^{3+} and Mn^{2+} [9, 11, 14, 25]. CFA treatment of soil reduces the bulk density, improves aeration and water retention, however such soil amelioration applications must be undertaken with care. Insufficiently weathered ash used to treat soil raises the B content sufficiently to have a negative effect. Increasing Mo and Se content in plants could become a potential hazard through bio-accumulation further up the food chain [9, 14].

Transportation costs of fly ash are high compared to the relative (null) cost of the fly ash, so applications should be as close as possible to the source of the ash [9]. It has been noted that CFA bears a similar composition to volcanic ashes, which are precursors to natural zeolites [3, 26, 27]. CFA can be used as a feedstock for the production of synthetic zeolites [28], which is the application of CFA explored in this thesis.

Chapter 2

Zeolitisation

2.1 Zeolite Overview

Ideal aluminosilicate zeolites are defined by J. Weitkamp [29] as "Crystallised solids characterised by a structure which comprises: a three-dimensional and regular framework formed by linked TO_4 tetrahedra (T = Si, Al), each oxygen being shared between two T elements; channels and cavities with molecular sizes which can host the charge-compensating cations, water or other molecules and salts. The microporosity must be "open", and the framework must have enough stability to allow the transfer of matter between the interior of the crystals and the exterior".

The zeolite framework has a negative charge due to the presence of Al within the framework. Each Al is counterbalanced by a cation, thus the total number of cations is equal to the number of Al atoms within the zeolite [3, 30, 31]. The negative charge of the framework through substitution of $[SiO_4]$ for $[AlO_4]^-$ and counterbalancing with a metal cation is shown in Figure 2.1.

The porosity of the framework not only stores cations but can also store water, with 18-48 % porosity available for storage [27, 30]. The open frameworks allow for reversible exchange of guest ions and molecules, depending on the pore size of the structure. Due to the size of the framework allowing entry to only certain sizes of ions or molecules, zeolites

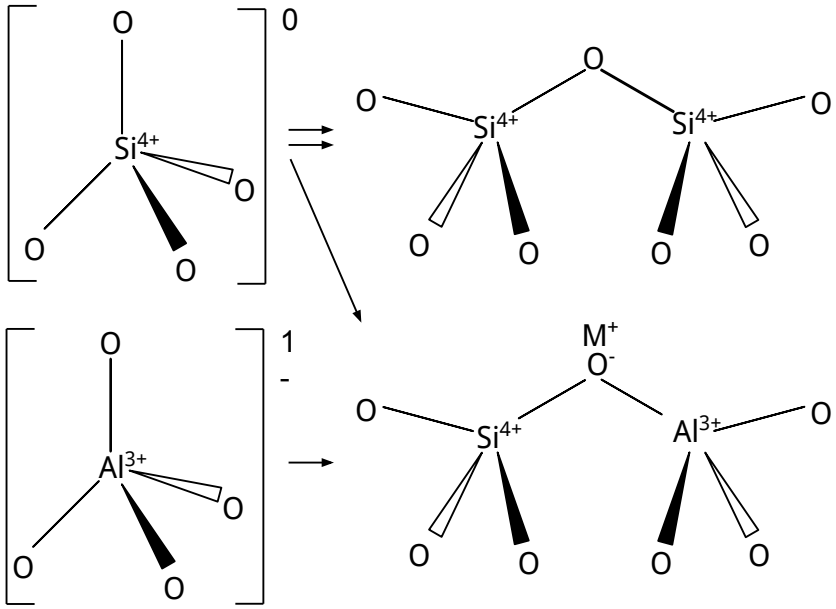

Figure 2.1: Diagram showing negative zeolite charge and counter-balancing metal cation M^+

are described as molecular sieves [30–32].

The maximum ratio of Si to Al in synthetic zeolites is 1:1 [30], thus synthetic zeolites can have a CEC up to 5 meq/g [3]. This gives synthetic zeolites superior sorption properties when compared to zeolites found in nature [29, 33]. Natural zeolites form under a variety of conditions, including the exposure of volcanic sediments to alkaline environments [34]. Over 150 synthetic zeolite types have been identified [33]. Some of the most common zeolites, their pore sizes, and a comparison between their pore sizes and the sizes of some gaseous molecules are shown in Figure 2.2.

At the top of Figure 2.2, the structure of 3 zeolites are shown. Zeolite A is a synthetic zeolite, also referred to as Linde Type A (LTA), zeolite 4A (due to the 4 Å pore size), or zeolite Na-A (due to the counterbalancing Na^+) [8, 30, 35]. Zeolite A is cubic in structure [36, 37], and SEM images of zeolite A look like cubes [8, 35, 38–43]. The framework is shown in more detail in Figure 2.3.

Zeolite X and zeolite Y are also synthetic zeolites, with a larger pore size than zeolite A. Sodalite is a contaminant or byproduct for many zeolite synthesis processes. The

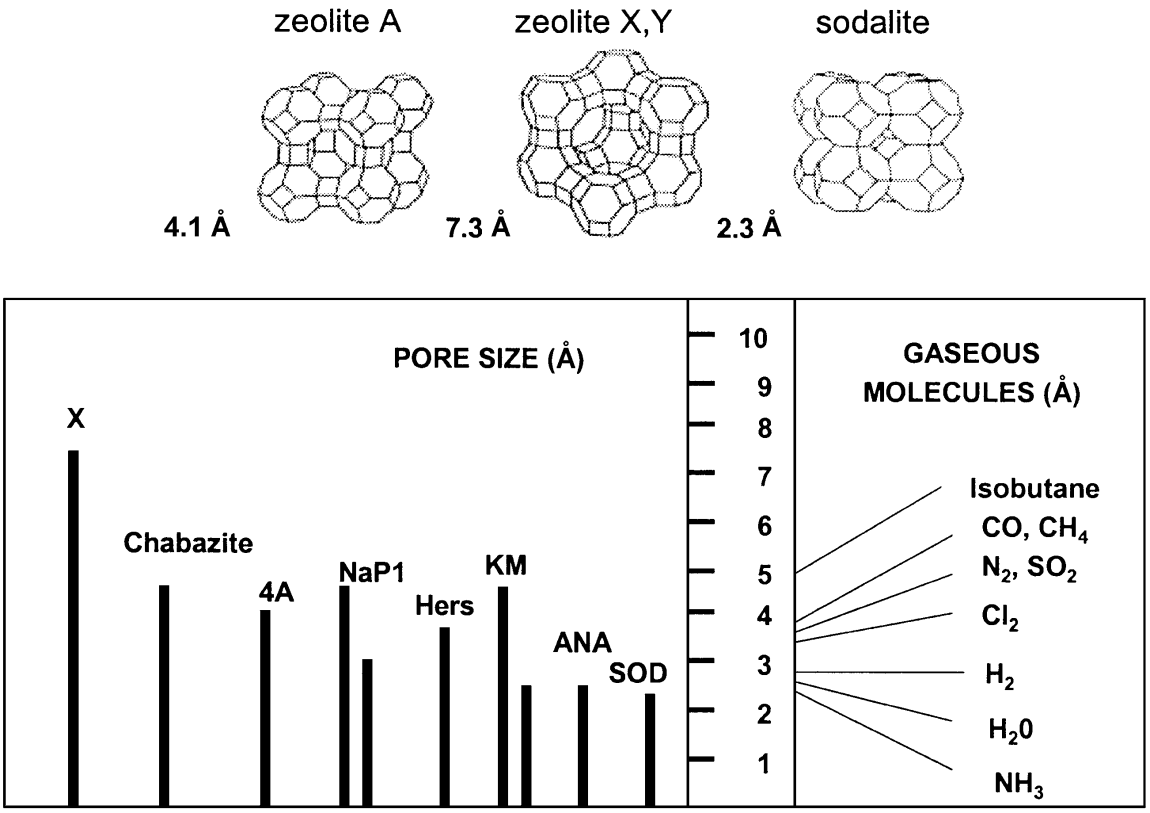

Figure 2.2: Comparison of pore sizes between different zeolites from Querol et al. [3]

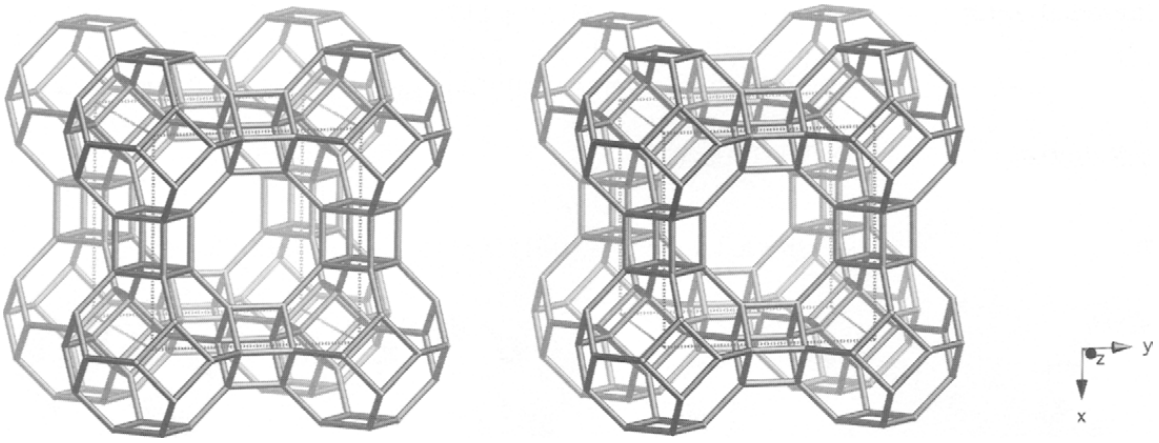

Figure 2.3: Framework of zeolite A from Baerlocher et al. [36]

smaller pore size limits its CEC, narrowing the potential applications it has. Sodalite is similar in structure to the basic building blocks of zeolite A, zeolite X and zeolite Y, as shown in Figure 2.2.

2.2 Motivation for Zeolitisation

Natural and synthetic zeolites have found applications in agriculture, water treatment, environmental protection, aquaculture, husbandry, paper manufacture, adsorbents and sequestration, and catalysts [6, 25, 31, 33, 35]. Demand for synthetic zeolites in the US was around 300,000 tonnes in 1993 [25].

Synthetic zeolites have been used to remove organic compounds from aqueous and gaseous systems. Zeolite Na-X and Na-P1 have been used to clean up simulated land-based petroleum spills with higher sorption capacities than commercial mineral sorption products [33].

2.2.1 Zeolite Use in Water Treatment

Due to the open framework of synthetic zeolites, and their ability to exchange the counter-balancing cations within their framework for cations outside of their framework, synthetic zeolites are highly suited to adsorb cations from water.

Synthetic zeolites are used for heavy metal [5, 26, 27, 33, 44–46] adsorption from industrial wastewater and acid mine drainage. Synthetic zeolites can also be utilised to isolate radionuclides [6, 33, 47].

2.2.1.1 Acid Mine Drainage

Acid mine drainage (AMD) is a term used to describe acidic water that originates from mines and spoil heaps. Acid mine drainage occurs due to the reaction of pyrite (FeS_2) with water, oxygen and Thiobacillus bacteria, which results in the production of sulphuric acid. The acidic environment dissolves metal in the mine or spoil heap. When this acidic, metal-laden water leaves the mine or spoil heap, it becomes diluted, less acidic, and these metals precipitate out. In the case of iron, this can result in red precipitates in waterways. If this metal content is too high, this causes the poisoning of waterways.

Figure 2.4 shows AMD during and after treatment at the Wheal Jane mine in Corn-

(a) AMD during processing, showing Fe-rich AMD (b) AMD at point of entry in to waterway

Figure 2.4: Photographs of AMD treatment at the Wheal Jane mine in Cornwall

wall. Whilst much of the metal content is removed at the processing facility, some remains in the effluent stream, iron being the most obvious, due to the red colouring of the water. Treatment of acidic wastewaters with chemicals (alkaline precipitation) is a process that must be closely monitored. Addition of too much alkaline material can harm the environment. Adsorbing the cations from the water stream by using synthetic zeolites is far preferable, as the synthetic zeolites can be applied in excess without the risk of adversely affecting the quality of the water. Synthetic zeolites are thus apt for passive remediation of waste streams without close monitoring. They are especially apt for polishing effluents from other remediation systems [27]. Zeolites can be regenerated by washing with NaCl solution [48].

2.2.2 Applications in High Performance Paints

An Innovate UK grant with Rolls-Royce has been researching alternatives to corrosion resistant paints with chromium. Corrosion resistant paints are used in gas turbines to protect turbine blades. Such corrosion resistant paints have thus far contained chromium, however due to the toxicity of chromium, alternatives are being sought. Synthetic zeolite A produced in the current study has been found suitable for such an application. The zeolite is first saturated with lanthanum nitrate before being added to a paint formula-

tion. The lanthanum is stable within the zeolite particles and does not precipitate out. Upon scratching of the paint surface, the lanthanum is released stabilising the paint and preventing further corrosion.

2.2.3 Zeolite Use in Detergents

Sodium tripolyphosphate has been used as a softener in detergents to remove calcium and magnesium from water. The reduced Ca and Mg content increases the efficiency of the detergent. Phosphates from cleaning processes contribute significantly toward eutrophiaction in bodies of water. Such eutrophication is harmful to marine life [49, 50].

Zeolites can remove calcium and magnesium from water and do not result in eutrophication [49]. Zeolites have thus found application in detergents, and can form 19.6-34.2 % of laundry powder or tablets [51]. An estimate by the Association of Detergent Zeolite Producers in 2000 put zeolite use in detergents at 1,000,000 tonnes per annum [52].

2.2.4 Zeolites A, X and P

Zeolite A is the most commonly manufactured zeolite [31, 49]. The ion exchange properties of zeolite A make it valued for use as a builder in commercial detergents [5, 25, 32, 43, 53]. Human risk assessments of zeolite use in detergents, as well as toxicological studies, have deemed zeolite A to not be harmful to consumers [49, 51]. The chamfered-edged cubes that zeolite A can form are especially suited for use as detergent builders, as the chamfered edges of the cubes inhibit excessive incrustation of fibres [32, 52]. Zeolite A synthesised from CFA has been shown to be as effective at removing calcium ions in water as commercial detergent grade zeolite A, with similar toxicological properties [49].

Zeolite A also has applications in drying gases and liquids, and separation of branched and straight paraffins [8, 32], whereas zeolites such as zeolite P have 2 channel sizes, making gasses difficult to trap (compared to A and X) [3]. Zeolite P and zeolite A have a higher affinity for heavy metals than they have for Ca and Mg. This is advantageous in the context of AMD remediation, as removing Ca and Mg is not the desired outcome in

this case; removal of heavy metals is the goal. This allows zeolite P and zeolite A to be used to remove wastewater metals up to 0.6 and 0.8 g/L [3].

Zeolite P has a smaller pore size (0.26 nm) than zeolite A (0.42 nm) [53], and the CEC of zeolite A has been shown to be higher than that of zeolite P [3]. Ammonium acetate CEC comparisons of Na-X with Na-A shows zeolite A to have a higher CEC (3.1 vs 3.9 meq/g), however zeolite A has been shown to have a lower BET surface area than zeolite X (10-15 vs 250-300 m^2/g). This is attributed to the smaller pore size of zeolite A compared to zeolite X (0.42 vs 0.74 nm) [54]. Zeolite P is a GIS-type zeolite (it has a structure related to that of gismondite). The structure is known to come in 3 main variants: cubic, referred to as Na-P1; tetragonal, referred to as Na-P2; and (rarely) orthorhombic, referred to as Na-P3 [55, 56]. Na-P1 is commonly synthesised from CFA and identified in literature. However, said literature is not always specific about the variant that has been synthesised, thus some literature will describe synthesis of zeolite Na-P1, whilst similar conditions in another paper will discuss the synthesis of Zeolite Na-P or a GIS-type zeolite, depending on how precise the literature is inclined to be. It has also been shown that zeolite Na-P2 can be converted to Na-P1 by heating at temperatures below 100°C in air [56]. Scant literature has been produced on the synthesis of zeolite Na-P2 or zeolite Na-P3 from CFA [43]. Henceforth, all references to zeolite Na-P1 will be described as zeolite P.

2.2.5 Use of CFA in the Synthesis of Zeolites

In the large scale manufacture of synthetic zeolites, feedstocks for the processes are commonly: silica gel, NaOH and Al salts, clay minerals, silicate group minerals and fly ash [25, 30, 33]. The amorphous nature of the aluminosilicate glass prevalent in CFA makes it suitable for use in zeolite synthesis because the glass is the most readily soluble phase [38, 39].

Using CFA as a feedstock for the synthesis of zeolites greatly improves the CEC of the CFA. CFA is partially dissolved to form a solution rich in aluminium and silicon, from

which zeolites can crystallise, forming zeolitised coal fly ash. Zeolitised coal fly ash has a variety of applications.

The improved CEC of zeolitised CFA makes it suited for use as a soil amendment agent [5, 25]. Zeolitised ash can also increase the rate of strength development in concrete [57].

Zeolitised CFA has been shown to immobilise ammonium and phosphates from water, and could be used to treat agricultural run off in order to prevent eutrophication [46, 58, 59]. The zeolite component of the zeolitised CFA retains cations such as ammonium and metals, whilst the calcium, iron and aluminium oxides present in the CFA can fixate anions such as phosphates [58, 59]. Ammonium rich zeolitised ash could then be used as a soil treatment agent to slowly release the ammonium into the soil [46].

Despite repeated washes with deionised water, zeolitised CFA is observed to increase the pH of acidic electroplating waste solutions [25]. When utilised to reduce the heavy metal content of acidic solutions, it was noted that the pH was increased due to the addition of zeolitised CFA. The reduction in concentration of heavy metals in such solutions can be attributed to precipitation due to the change in pH, rather than adsorption if the applied quantity of zeolitised CFA is too high [25].

2.3 Zeolite Synthesis Theory

2.3.1 Mechanism Overview

Eight mechanisms proposed from 1959-2004 for zeolite synthesis from pure reagents are described in Cundy and Cox [60]. Of these mechanisms, 3 were studied in the context of zeolite Na-A synthesis. Of the mechanisms discussed, of particular note are the "solution-mediation" model and the "gel-rearrangement" model, which were summarised by a "generalised mechanism for zeolite synthesis" [39, 60]. In the "solution-mediation" model, Si and Al from amorphous material is in equilibrium with Si and Al in solution, which in turn is in equilibrium with crystalline material. This is modelled by Lowe [61]

and described in Figure 2.5.

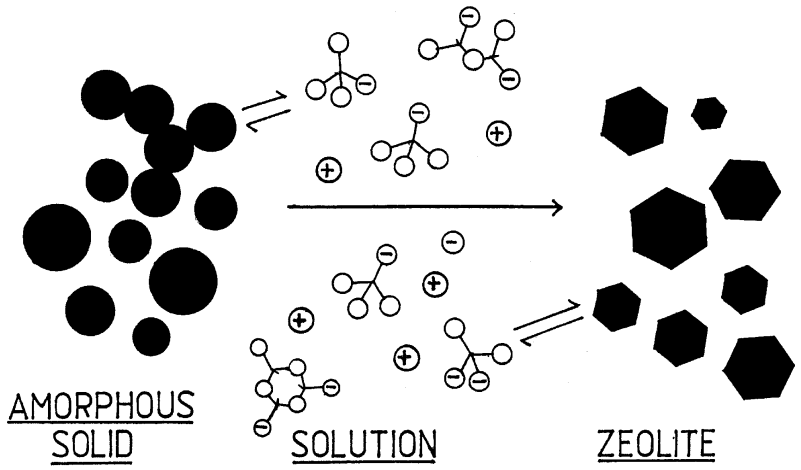

Figure 2.5: Original sketch by Lowe describing the basis for the equilibrium model [61] from [60]

.

This mechanism, along with others was summarised by Cundy's "generalised mechanism for zeolite synthesis" described and illustrated by Cundy and Cox [60]. This is shown in Figure 2.6.

2.3.2 Nucleation

The nucleation process will have a large influence on the final product, deciding particle size distribution, and which zeolites will form [29, 44, 53].

Cundy and Cox [60] describes nucleation as a discrete event defined as "a phase transition whereby a critical volume of a semi-ordered gel network is transformed into a structure which is sufficiently well ordered to form a viable growth centre from which the crystal lattice can propagate".

Upon the mixing of the necessary reagents for the synthesis of zeolties, nucleation does not occur immediately, but has a resting period described by equation 2.1, where τ is the nucleation induction period, t_r is the equilibration time for reagents to reach temperature and silicate and aluminate ion distribution, t_n is time taken for a stable nucleus to form,

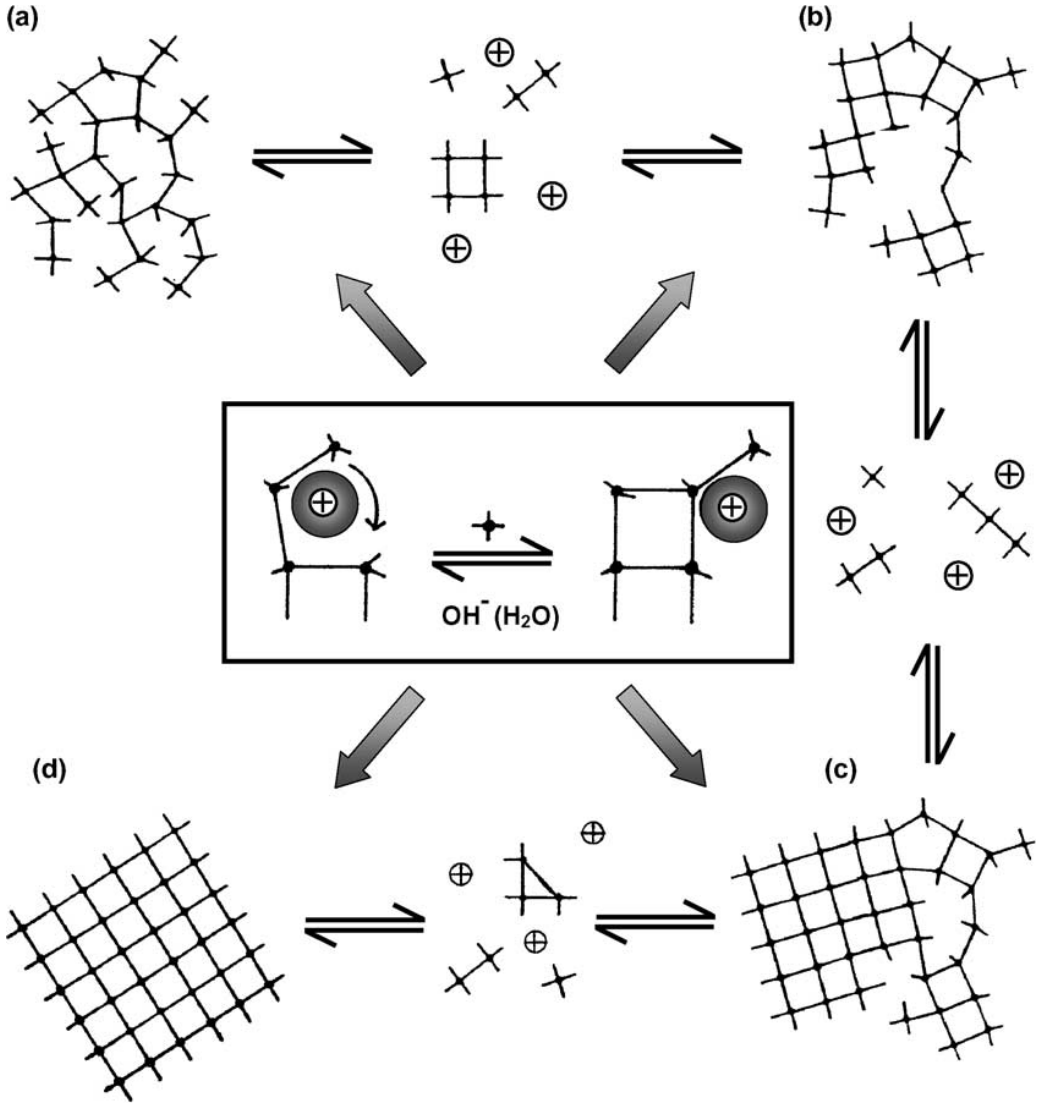

Figure 2.6: "A generalised mechanism for zeolite synthesis. A fragment or domain of amorphous material (a) equilibrates with solution species (anions and cations) to develop elements of local order (b). In due course, the equilibration process leads to an area of sufficient order for a periodic structure to become established—i.e. nucleation has occurred (c). The same equilibration reactions (Si,Al-O-Si,Al bond-making and bond-breaking) then allow the nascent crystal to grow and the amorphous areas to dissolve (d). The self-assembly process is mediated by the associated solvated cations, which act as coordination centres (templates) for the construction of the framework (central insert). These transformations most usually take place via a bulk solution phase, but may occur within a solvated layer at the surface of a "dry" solid (apparent solid-phase transformation)." [60]

.

and t_g is time taken for said nucleus to grow to a detectable size [60].

$$\tau = t_r + t_n + t_g \tag{2.1}$$

The rate of nucleation increases as solubility increases, thus an increase in the concentration of $[OH]^-$ will increase the rate of nucleation [29], in relation to equation 2.1 additional hydroxide would decrease t_r. Seeding can be used to eliminate t_n, however seeds may remain inert, dissolve, be used as the only seeds, or add to the seed count. Studying of nucleation is difficult, because nuclei are small, and are generally made up of the material that surrounds them, thus the point at which viable nuclei form comes before the point at which nuclei can be detected, thus t_g is included in equation. A review of literature on the nucleation process of zeolite A finds disagreement on the specific details of the nucleation process [60]. Ageing at a lower temperature encourages nucleation. A high quantity of nuclei present in solution prior to crystal growth will result in a finer particle size of the final product [32, 60].

2.3.2.1 Ostwald Ripening

Ostwald ripening is the coarsening of particle size "driven by the tendency of solid particles dispersed in saturated or supersaturated solution to achieve a minimum in total surface free energy. Thus the smaller particles dissolve, the larger grow, the size distribution narrows and the mean crystal size increases." [60]. Ostwald ripening would only be significant for particles ≤ 1 μm, and appears to have not been observed to operate in crystallisation processes [60].

2.3.3 Crystal Growth

Crystal growth is modelled as: [60]

- Nucleation on the surface of, or near an amorphous particle.
- Growth of the particle due to attachment of monomers from solution.

- Solution replenishing its stock of monomers by equilibrating with amorphous or less ordered material until the amorphous material has been completely dissolved.

The rate of crystallisation is directly proportional to temperature, with higher temperatures resulting in more rapid crystal growth [30, 62]. Zeolites grow slower than ionic or molecular crystals (such as salt or sugar). Nucleation of a new layer is slower than the lateral spread of a layer [60].

2.3.4 Ostwald's Rule of Successive Transformations

Ostwald's rule of successive transformations states: "If a system is far from equilibrium, intermediate metastable phases crystallise generally before the thermodynamically stable phase" [29]. Thus, the first phases that form are not necessarily stable, and can be successively replaced by more stable phases [34].

Amorphous gel is able to precipitate much faster than zeolite, and it can be considered the first phase to form in Ostwald's successive transformations [60]. In zeolite synthesis, the target zeolite is often meta-stable, and is not the final, most thermodynamically stable phase [32, 34, 60]. If zeolite synthesis experiments run for too long, the desired zeolite product can decompose to produce a more dense phase, such as sodalite forming from zeolite A [32, 60, 63, 64]. Zeolite A is metastable in comparison to zeolite P, which is in turn metastable in comparison to sodalite. Such metastability has been noted to affect zeolites A, X, Y and P [30]. The metastability of one zeolite form to another makes pure synthesis of each form harder to achieve. The concentration of NaOH in a solution will influence Ostwald's law of successive transformations. For crystallisation conditions with lower concentrations of NaOH, zeolite A can be converted to zeolite P if the zeolite A is not separated from the alkaline crystallisation solution. If the NaOH concentration is higher, zeolite A can be converted directly to sodalite [5, 6, 29, 53, 65].

Degradation of one zeolite to another is expedited by the presence of seeds of the next phase. Therefore crystallisation systems in which nuclei of sodalite form early will produce sodalite through dissolution of another phase faster than systems in which sodalite does

not nucleate [60].

2.3.5 Influence of Experimental Conditions on Zeolite Synthesis

Various experimental conditions will influence the synthesis of zeolites. For synthesis from pure reagents, variables that can influence the process, final product, and the properties of the final product are [30]:

- Temperature.
- Pressure.
- Chemical composition and ratio of reagents.
- OH- as mineralising catalyst.
- Structure directing effect of cations.
- Directing effects of anions other than $[OH]^-$.
- Role of added salts.
- Equilibration period (also called the resting, ageing, induction or ripening period).

2.3.5.1 Temperature

Rate of nucleation is inversely proportional to temperature [62], whilst crystal growth increases with increases in temperature [32]. If the temperature for the crystallisation process is too high, it can encourage more rapid conversion to thermodynamically stable forms, such as sodalite [42].

Microwave heating speeds crystallisation, but only due to better heat transfer. Selective heating of different phases can control which zeolites form (e.g: sodalite absorbing microwaves more effectively than phillipsite, effectively increasing the temperature of sodalite over phillipsite, increasing yield of sodalite [66]), but no athermal effects have been

observed [60]. Microwaves have been observed to aid in the dissolution of silica and alumina from coal fly ash [67–69], however nucleation of Na-P1 (with the ash still present) was hindered by microwave heating when compared to conventional heating [67].

High temperatures encourage better dissolution of CFA [3, 32, 42, 70], however higher CEC zeolites will not form under higher temperatures (125-200°C). Reducing crystallisation temperature gives a lower yield of zeolite and a slower reaction [3, 42].

2.3.5.2 Pressure

Commercial synthesis of zeolite A is conducted at atmospheric pressure [68]. High pressure experiments would increase costs, and thus zeolitisation conditions explored and discussed in this thesis will focus on crystallisation at atmospheric pressure, although the influence of pressure on zeolite synthesis will be discussed.

2.3.5.3 Chemical Composition and Ratio of Reagents

The Si/Al ratio has a significant influence on the final product [40, 54, 62], however literature on the synthesis of zeolites from CFA offers conflicting reports on which zeolites are formed under which conditions [40]. The presence of excess Al has been shown to increase the crystallisation rate of zeolite A, whilst for similar conditions an increased Si content has been shown to decrease the crystallisation rate [35, 71]. The Al content of a crystallisation solution can be the limiting factor during synthesis of zeolites from CFA, thus addition of Al can be beneficial to the crystallisation process [57]. A higher SiO_2/ H_2O ratio can encourage the formation of zeolite P rather than sodalite, however the crystallisation rate will decrease as the crystallisation solution becomes more dilute [72]. However, the description of the experimental method by Musyoka et al. [72] is ambiguous. Altering the SiO_2/H_2O ratio in this manner would appear to also dilute the NaOH content, as no mention of additional NaOH is made. The alkalinity of the crystallisation solution will have a significant influence on which nuclei form, and a higher NaOH content will expedite Ostwald's rule of successive transformations, encouraging

the formation of sodalite. Thus the parameter that is most influential on the form of the zeolite product in this set of experiments is more likely to be the alkalinity than the SiO_2/H_2O ratio.

2.3.5.4 Role of $[OH^-]$

$[OH]^-$ is considered a mineraliser, as it dissolves amphoteric oxides and hydroxides making them available for reaction within a solution, but does not stabilise such oxides and hydroxides to the point that they become inert [30, 60, 70, 71, 73].

As the hydroxide content increases, the nucleation rate also increases, with more nuclei forming sooner [60, 62]. The increased solubility of the zeolite leaves more Si and Al in solution, decreasing the yield of zeolite in a given crystallisation experiment with an increasing hydroxide content [60]. The yield of the desired zeolite product may also decrease with an increase in hydroxide content due to Ostwald's rule of successive transformations (see section 2.3.4), and the more rapid dissolution of one zeolite phase in favour of the formation of the next most thermodynamically stable form [30]. Such conditions narrow the opportunity for the zeolite to be isolated from the alkaline crystallisation solution which will render them stable and stop the transformation process.

An increased $[OH]^-$ content has been shown to produce zeolites with a higher Al content (and therefore a higher cation exchange capacity) under certain conditions [30], however if the hydroxide content is too high, literature has many examples of the formation of sodalite in lieu of useful zeolite phases [42, 58, 74, 75]. Various sources in literature have noted that a concentration of 2 M NaOH is optimal for the synthesis of zeolites [25, 32, 49, 58, 73, 74].

2.3.5.5 Structure Directing Role of Cations

The nucleation process is mediated by the presence of cations, and as such, the cations that are present will influence which zeolites form [30, 42, 60, 75]. Zeolite A forms in the presence of Na [30], whilst it has been recognised that the presence of some Ca and

Mg can result in the formation of zeolite X [38, 40]. The presence of Ca has been noted to interfere with the crystallisation process, such that if the concentration of Ca is too high ($\geq$ 0.01 M), zeolitisation is not possible, or only sodalite will form [5, 20, 72, 76, 77]. Organic bases and structure-directing molecules, such as EDTA can be used to alter the structure of zeolites to be formed [60].

2.3.5.6 Influence Of Salts In Zeolite Formation

Salts can occupy the voids and pores within a zeolite during formation, and can be incorporated into the structure, thus changing the structure itself. Addition of salt to zeolite synthesis can increase the yield and improve crystallinity [30].

2.3.5.7 Equilibration Period

The equilibration period is also referred to as the resting, ageing, induction or ripening period by literature. During this period, the amorphous material equilibrates with the solution, and nuclei form. The conditions during this period will govern the nucleation process, and thus the properties of the final product. Nucleation of zeolite A has been noted to occur more rapidly than the nucleation of zeolite X, for conditions in which nucleation of either is possible [43, 53, 68].

2.3.6 Synthesis Process

The process for hydrothermal zeolite synthesis from pure reagents (rather than fly ash) typically consists of: [60]

- Amorphous Si and Al are mixed in an alkaline solution.
- The solution is heated.
- Reagents remain amorphous for a time (referred to as the "induction period").
- Crystalline zeolites are detected.

- Amorphous material is gradually replaced with zeolite crystals.

Synthesis of zeolites from a heterogeneous material such as CFA is not as simple, however the yield, purity, and crystallinity of the product can be improved through processing (through beneficiation such as magnetic separation) of the CFA prior to zeolitisation [73, 73]. A large amount of literature exists on the formation of zeolites from coal fly ash and other aluminosilicates, however much of the information is contradictory with regard to which zeolites form under which conditions [40]. Sodium aluminate is used as a reagent in industrial zeolite synthesis in order to adjust the Si/Al ratio of the crystallisation solution [60]. Aluminate solution could be obtained from aluminium finishing industry [26].

2.4 Zeolitisation Methods

Most methods for the hydrothermal synthesis of zeolites from CFA can be summarised by Figure 2.7. Non-hydrothermal methods such as the molten salt method used by Park et al. [78] will not be discussed in detail, as the onerous experimental conditions outweigh the usefulness of the zeolites synthesised.

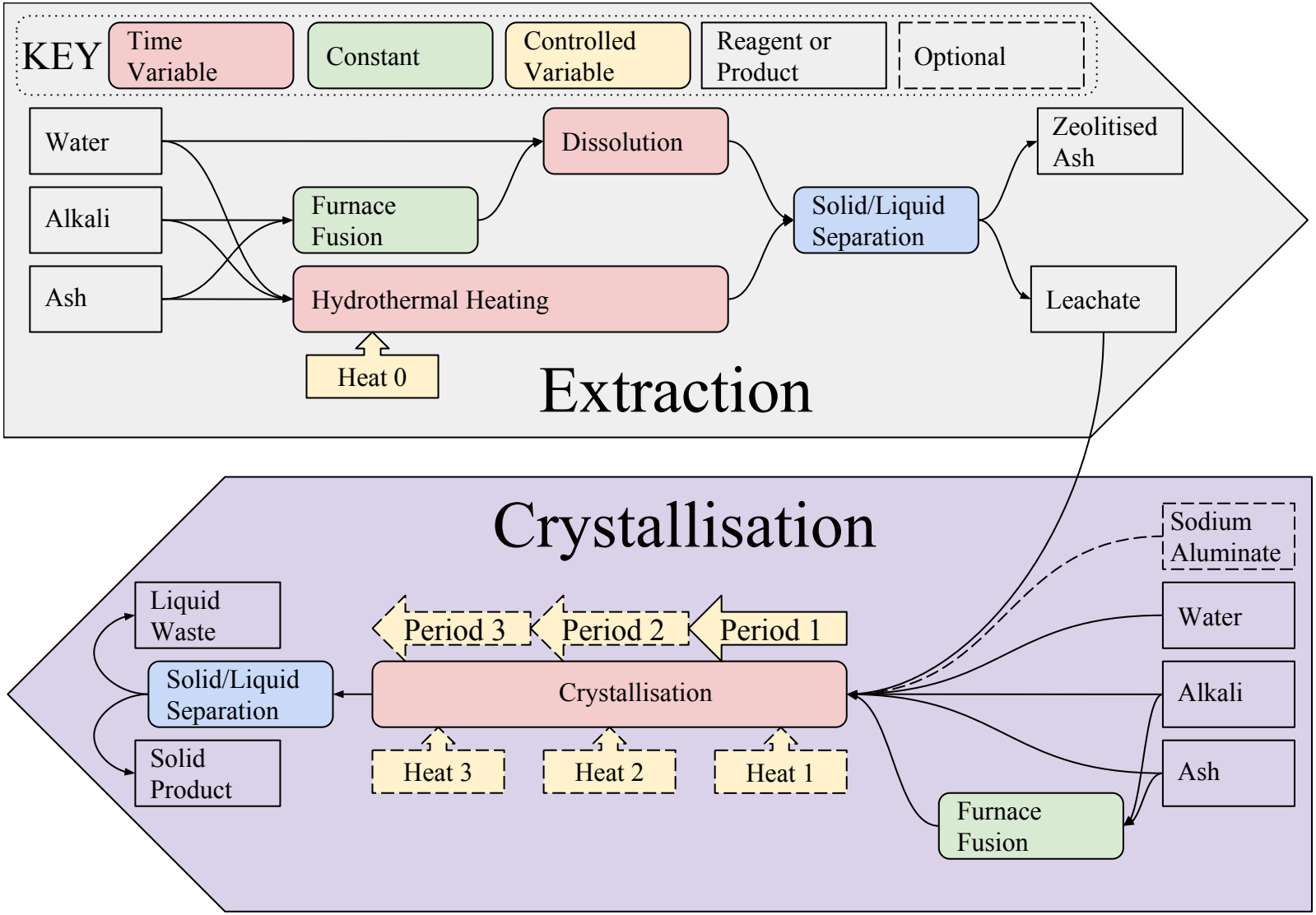

Figure 2.7: Block diagram of common extraction and crystallisation processes described in literature

The synthesis process can be divided into 2 main approaches: in-situ zeolitisation of ash with no solid byproduct, and the precipitation of zeolites from ash leachate with a byproduct of undissolved ash. Both approaches can incorporate a fusion step in order to improve the solubility of Si and Al in the CFA [6, 53, 54, 57].

Several experimental parameters are explored in literature. These parameters are listed below, with the relevant part of Figure 2.7 in parenthesis.

- Pressure (Crystallisation).
- Heat source (Heat 0-3).
- Temperature (Heat 0-3).
- Duration (Extraction: hydrothermal heating. Crystallisation: Period 1-3).
- Alkalinity (quantity of Alkali).
- Solids loading (ratio of Water to Ash).

2.4.1 In-Situ Zeolitisation of Ash Without Fusion

The simplest approach to zeolitisation is to mix CFA in a hot alkaline solution. The alkaline solution dissolves silica and alumina from the ash. The resulting hot alkaline solution rich in silica and alumina is similar in content and condition to the solutions from which zeolites are synthesised from laboratory reagents. This approach is shown in Figure 2.8.

The products of the in-situ zeolitisation of coal fly ash are often intermixed with or deposited on unreacted particles fly ash [57]. Such findings are based on the presence of quartz and mullite in XRD patterns and SEM images showing structures other than the zeolite crystals. Literature indicates that crystallisation begins on the surface of ash particles, with SEM-EDX (Scanning Electron Microscope Energy-Dispersive X-ray spectroscopy) indicating that zeolites preferentially crystallise on the amorphous glassy surfaces of ash particles, rather than iron microspheres, quartz crystals, or carbon residues

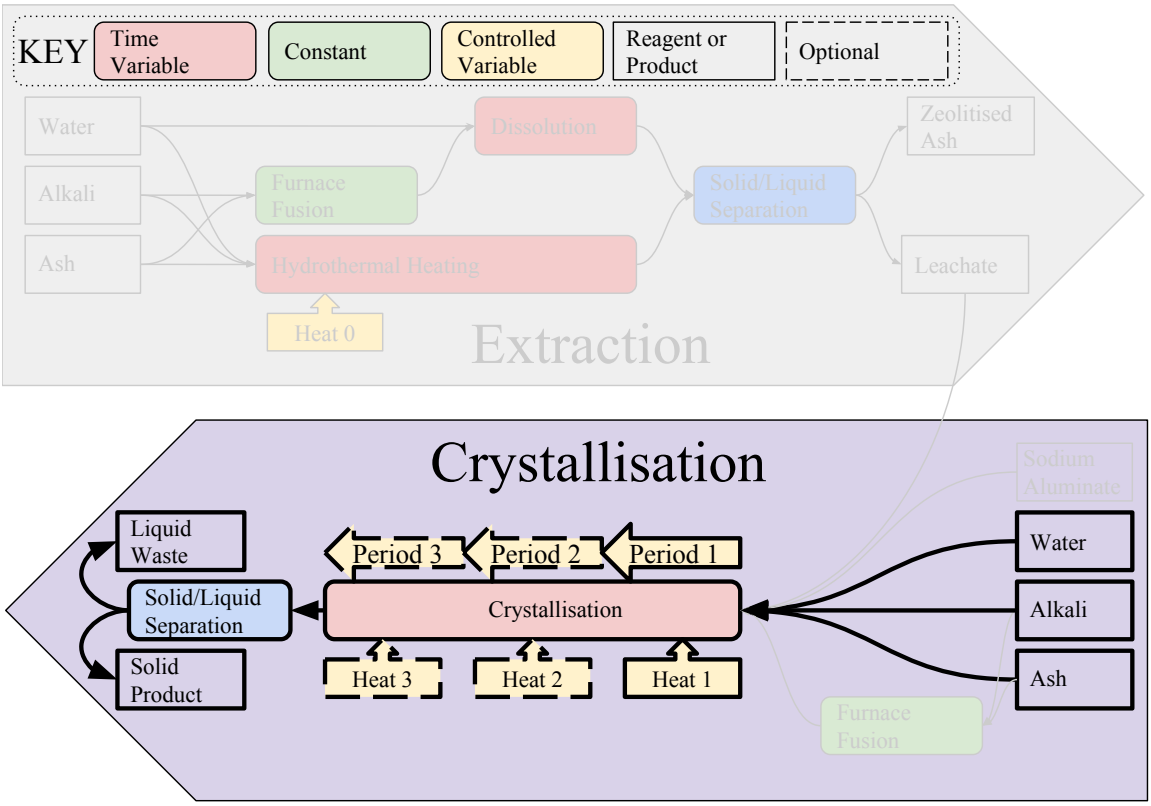

Figure 2.8: Block diagram of process for hydrothermal zeolitisation of ash described by literature

[42, 70]. Experiments carried out on CFA that has undergone beneficiation processes to reduce the magnetic content have shown that beneficiation improves results [6].

2.4.1.1 Pressure

Experiments at elevated pressures are conducted by heating sealed vessels. When comparing reflux conditions to hydrostatic pressure experiments, the CEC of zeolitised ash from higher pressure conditions was lower than the CEC of zeolitised ash from the ambient pressure experiments with similar conditions [73]. XRD analysis showed the presence of more quartz and mullite in experiments under hydrostatic conditions than those under reflux conditions. These inferior results were attributed to decreased dissolution of the CFA at higher pressures compared to dissolution of CFA under reflux conditions. The difference in dissolution of CFA was more pronounced at lower concentrations of NaOH. The CEC was similarly affected, with a larger gap in CEC between reflux and hydrostatic conditions

at low concentrations of NaOH than higher concentrations of NaOH. Both hydrostatic and reflux conditions produced zeolite P, with hydrostatic conditions also synthesising chabazite (general formula: $(Na,K,Ca_{0.5})x(H_2O)_{12}|$ $[Al_x\ Si_{12-x}\ O_{24}]$ x = 2.5 - 4.8). Other works also report synthesis of NaP1, sodalite and analcime ($Na(H_2O)[AlSi_2O_6]$) at hydrostatic pressures and temperatures of 100-160°C. [7, 41, 72, 79–81].

Moriyama et al. [76] conducted zeolitisation experiments at 0.3, 0.5 and 0.8 MPa on two CFA samples. The experiments had a solids loading an order of magnitude higher than solids loadings in many other experiments (813-1429 g CFA/L). The reaction vessel was equipped with kneaders rather than stirrers in order to accommodate the high solids loading. After crystallisation, one ash exhibited improved CEC as pressure increased, where XRD pattens showed the synthesis of a GIS-type zeolite (zeolite P being a GIS-type zeolite [55, 56]) with mullite and quartz still present. Another ash sample under the same conditions exhibited a decrease in CEC with increasing pressure, with XRD results showing synthesis of a GIS-type zeolite with undissolved quartz and mullite at 0.5 MPa, and analcime at 0.8 MPa with no other crystalline phases apparent. The authors noted that the high pressure allowed for a smaller quantity of NaOH to be used. Whilst this approach did demonstrate efficiencies in the use of NaOH, the sensitivity of the process to the properties of the fly ash used, and the incomplete dissolution of the mullite and quartz indicates that this high pressure, high solids loading approach is less attractive than the hydrothermal approach at atmospheric pressure described by other authors.

2.4.1.2 Temperature, Time and Heating Method

Zeolite synthesis experiments frequently "age" the solution at lower temperatures (47°C) prior to heating to induce more rapid crystallisation [7, 41, 72, 82]. This ageing process lasted 48 hours, and was followed by a higher tempreature crystallisation step at 100-160°C [7, 41, 72, 79, 82]. These authors made zeolites A, X and P.

Other authors reversed this approach and conducted the high temperature heat treatment first (120-130 °C) for 7 hours, followed by a 16 hour to 1 month ageing step at

25°C. These experiments produced mixtures of zeolites A, F, P and sodalite, as well as investigating concentration of NaOH and KOH [42].

Amrhein et al. [25] synthesised zeolite P in 100°C experiments for 72 hours. It was found that increasing the temperature above 100°C by using pressure bombs reduced the CEC and made zeolite X. A review by Ahmaruzzaman [2] found that it was not possible to synthesise zeolites A and X if the crystallisation temperature was raised to 125-200°C, however dissolution of the CFA was increased. Experiments by Wałek et al. [70] show a clear linear relationship between dissolution of CFA and temperature between 60°C and reflux (104°C) temperatures, with more CFA being dissolved at higher temperatures.

Using a microwave as a heat source for the crystallisation process was investigated by Inada et al. [67]. The authors aged their solution for 2 hours at room temperature prior to heating. Following the ageing step, the solution was heated for 2 hours. It was found that constant microwave heating raised the CEC of the product more rapidly than conventional heating, but the increase in CEC would plateau from 60 minutes and was overtaken by the CEC of the products of the conventional heating synthesis method by 2 hours. Another method investigated was 15 minutes of microwave heating, followed by 105 minutes of conventional heating. With reference to Figure 2.8, this later method could be described as "Periods 1, 2 and 3" being 120 minutes, 15 minutes and 105 minutes, and "Heat 1, 2 and 3" being ambient, microwave, and reflux. These improved results produced zeolite P, and the authors concluded that microwave irradiation aids dissolution of ash, but inhibits zeolite formation.

After ageing for 24 hours at room temperature and pressure (RTP) , Molina and Poole [6] heated their crystallisation solutions to 40, 60 or 90°C to produce different zeolites. At 60°C zeolite A was synthesised, which had a higher CEC than the mixture of zeolite A and zeolite X that was synthesised at 90°C.

2.4.1.3 Alkalinity of Solution

Various sources have established that NaOH is more effective than Na_2CO_3 or KOH in zeolitising fly ash [20, 21, 42, 74, 75], hence the use of NaOH in this study. This superior performance is attributed to better dissolution of CFA, and NaOH being a better mineraliser, increasing the solubility of silica and alumina in solution, which is attributed to increased nucleation [60].

More silica and alumina are leached from CFA as the NaOH content increases [21, 74, 83]. Many sources [25, 32, 49, 58, 73, 74] found 2 M NaOH to be the best concentration to yield zeolitised ash with the highest CEC, making zeolite P, whilst DuPlessis et al. [82] leached solutions in 5 M NaOH at a lower temperature, before diluting the solution and raising the temperature to encourage crystallisation. Berkgaut and Singer [44] synthesised zeolite P from CFA with a low CaO content after refluxing with 3.5 M NaOH for 6 hours, however the same conditions applied to an ash with a higher CaO content synthesised sodalite.

Sources showing examples of sodalite synthesised at high concentrations of NaOH are plentiful [3, 42, 46, 58, 70, 74, 75, 82], which is also in agreement with section 2.3.5.4, which states that increased concentrations of NaOH expedite Ostwald's rule of successive transformations and result in the formation of sodalite.

Experiments by Molina and Poole [6] aged solutions of CFA and NaOH at concentrations of 2.94-5.88 M NaOH for 24 hours, and then heated the solutions to 90°C for 6 hours. At the lowest concentration of NaOH, only mullite and quartz were detected, and the product had the lowest CEC. At 3.52 M NaOH, the highest CEC for the hydrothermal process was achieved, having synthesised a mixture of zeolite A and X at a NaOH:CFA ratio of 1.2:1. As the alkalinity increased, sodalite formed at the expense of formation of zeolites A and X and the CEC decreased. Prolonged crystallisation experiments at a NaOH:CFA ratio of 1.2:1, crystallising at 90°C rendered no zeolitic materials at 2 hours, a mixture of zeolites A and X at 8 hours, X at 24 hours, X and P at 72 hours and zeolite P at 96 hours. Mullite and quartz were detected in all samples. This is an example of

Ostwald's rule of successive transformations, where metastable zeolite A forms first, but is gradually displaced by more stable zeolite X, which is in turn displaced by the more stable zeolite P. Experiments were CFA underwent magnetic separation prior to zeolitisation exhibited higher CEC under all experimental conditions [6]. The improvement in CEC is attributed to the decrease in Fe, that results in the precipitation of less iron hydroxide, which would lessen the effective NaOH content though the synthesis of materials that may interfere with the crystallisation process, but which are not incorporated into the zeolite. These results are in agreement with work by Wang et al. [84], who also increased the CEC of their synthesised zeolite through reducing the iron content of the ash by washing with a 10 % HCl solution prior to zeolitisation.

2.4.1.4 Solids Loading

Experiments where low solid/liquid ratios (4 g CFA/L) were used were found to produce a higher yield of zeolite than experiments with a higher solid/liquid ratio (100 g CFA/L), however such conditions are acknowledged to not be cost-effective [70]. Experiments where the quantity of water added to the crystallisation solution was varied found that insufficient water resulted in the synthesis of sodalite, whilst the addition of more water resulted in a slower crystallisation process [72, 82].

Various authors have synthesised zeolite P from CFA using solids loadings of 100 g CFA/L [20, 25, 58, 70]. A review by Querol et al. [3] identified solids loadings of 50-100 g CFA/L to be optimal.

Experiments by Moutsatsou et al. [20] compared the hydrothermal zeolitisation of Ca rich ashes in solids loadings from 25-150 g CFA/L at 1 M NaOH. Ash that had a high content of CaO (35 %) formed no crystalline material at low solids loadings (25 g CFA/L), and formed zeolite P at solids loadings of 50-150 g CFA/L, with Herschelite at 150 g CFA/L along with zeolite P. For CFA with a lower (but still high compared to many other ashes discussed in literature) CaO content of 12 %, zeolite P was formed at all solids loadings with cancrinite formed at 25 and 100 g CFA/L solids loadings and

sodalite formed at 100-150 g CFA/L. The authors concluded that a solids loading of 50 g CFA/L was optimal for the highest CEC and SSA for high-Ca ashes, of which 30-45 % of the material had been converted to zeolite P.

2.4.1.5 Additional Reagents

Wu et al. [73] conducted experiments with additional halide salts, silica and alumina added to the zeolitisation process. Such experiments were conducted at 0.5-2 M NaOH. These experiments found that

- Addition of halide salts did not alter which zeolite formed (in comparison to control experiments without added salts).
- The CEC is increased by the addition of salts, and the improvement in CEC is more pronounced at lower concentrations of NaOH.
- NaF increases CEC more than NaCl. This improved performance is attributed to better dissolution of CFA and higher solubility of silica and alumina in solutions of $[F]^-$, as $[F]^-$ acts as a mineraliser. The function of $[F]^-$ as a mineraliser is discussed in more detail by Cundy and Cox [60].

Altering of the Si/Al ratio through addition of silica and alumina in solid form or as a solution can change which zeolite forms. It is noted that the addition of excess alumina has been shown to result in the synthesis of sodalite rather than zeolite P [73, 74].

Inclusion of unburned coal from CFA appeared to function as a seed material for the crystallisation of zeolite P in experiments by Berkgaut and Singer [44]. Experiments where the ash was heated to 700°C prior to synthesis produced sodalite. The inclusion of zeolite P zeolitised ash or inclusion of pulverised coal in the crystallisation step was noted to result in the synthesis of zeolite P, rather than sodalite in the same conditions.

2.4.1.6 Closed Loop System

In an attempt to reduce the disposal costs of alkaline metal-rich effluents from the zeolitisation process, experiments were conducted where the leachate was reused in the zeolitisation process. Wu et al. [73] found that the CEC decreased after repeated uses, which was improved slightly through the addition of more NaOH, but not entirely rectified. Amrhein et al. [25] found that four cycles of the same leachate did not result in a significant decrase in the CEC of the zeolitised ash. Attempts to reuse the same leachate 10 times resulted in the synthesis of analcime rather than zeolite P in experiments conducted by DuPlessis et al. [82]. Analcime is noted to have a lower CEC than zeolite P due to analcime having a lower Al content.

2.4.1.7 Considerations for Zeolitised Ash as a Product

The synthetic zeolite produced in the zeolitisation process has been noted to have an affinity for K, Ca and NH_4 in solution. Such zeolitised ashes, if used to capture nutrients from agricultural run off to prevent eutrophication could be used as a soil treatment agent in order to improve the CEC of the soil and slowly release the captured K, Ca and NH_4 back to the soil, whilst also increasing the pH of acidic soils [5, 25]. In an attempt to neutralise the alkalinity of NaOH-rich solutions from the zeolitisation process Xie et al. [59] added $FeCl_3$ to the solution after the zeolite synthesis steap in order to obtain: a zeolitised-CFA-Fe_2O_3 composite material which has demonstrated an affinity for NH_4 and phosphates; and a leachate with a pH of 6.6. This Fe-laden material has demonstrated a higher surface area than the zeolitised ash from which it was made (161 vs 28.7 m^2/g), and is apt for use in stopping eutrophication from agriculture by adsorbing NH_4 and fixating phosphates from agricultural run-off. Due to the fine, powdery nature of CFA, it can be difficult to handle. Amrhein et al. [25] suggested pelletisation of zeolitised CFA as a solution to handling difficulties.

2.4.2 In-Situ Zeolitisation of Ash With a Fusion Step

The incorporation of a fusion step prior to the crystallisation step has been shown to increase the solubility of the CFA. Using this method, CFA is mixed with an alkali, and fused at a high temperature. The fusion process forms water soluble products such as sodium silicate and sodium aluminosilicate [39–41, 44, 57]. The product of this fusion process is dissolved in water, and this process is shown in Figure 2.9.

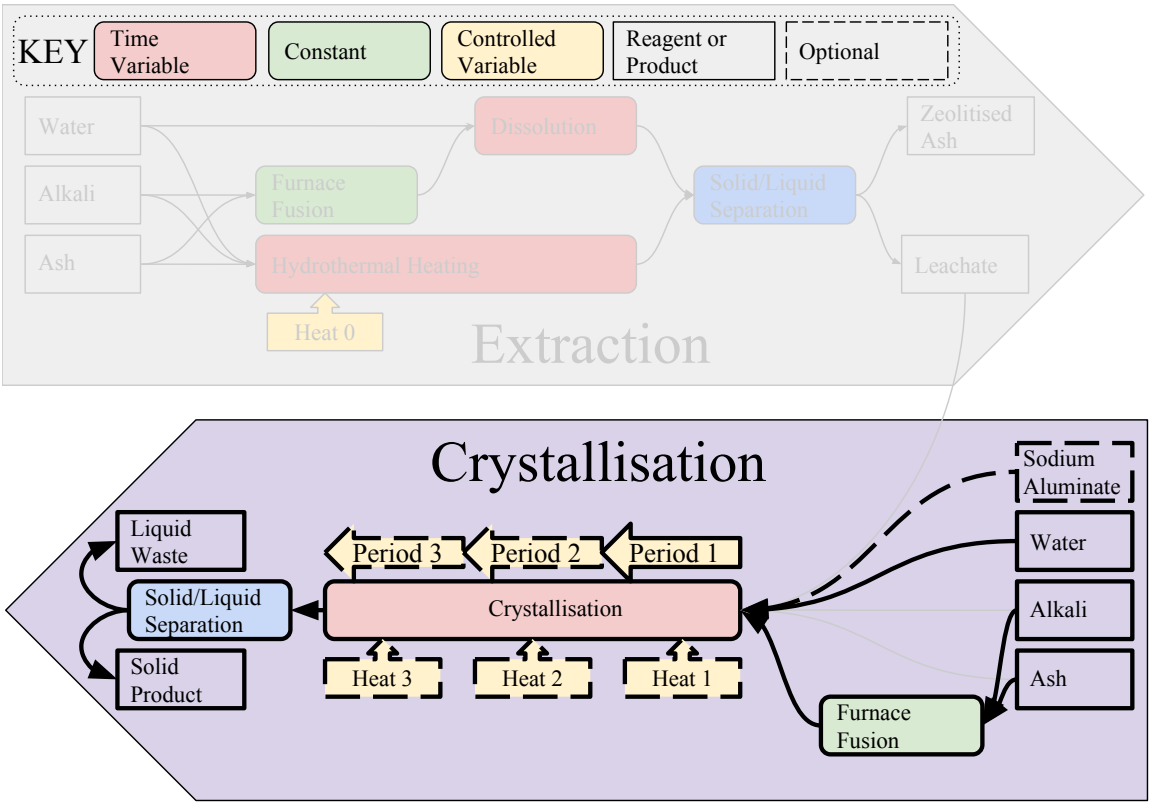

Figure 2.9: Block diagram of process for hydrothermal zeolitisation of ash with fusion step described by literature

The most common method for the fusion process is to mix CFA and NaOH at a ratio of 1:1.2, grind the mixture and fuse it in a Ni crucible at 550°C for 1-2 hours [6, 7, 35, 38, 39, 41, 44, 53, 54, 57, 85–87]. The product is then crushed and dissolved under a variety of conditions.

2.4.2.1 Dissolution Solution and Solids Loading

Various authors dissolved the products of fusion at RTP for 12-24 hours, or overnight [6, 39, 44, 53, 57]. Many authors used distilled water, however the use of seawater rather than distilled water in the synthesis of zeolites can be a cost saving measure, and literature indicates the addition of NaCl aids in the crystallisation process [60, 73] (see sections 2.3.5.6 and 2.4.1.5).

Experiments by Belviso et al. [38] compared dissolution followed by crystallisation in distilled water and dissolution followed by crystallisation in seawater. Later experiments [39] used distilled water and synthetic seawater as the dissolution media for the fusion product. The synthetic seawater was made following the method of Kester et al. [88]. The dissolution step took place overnight, however the authors did not disclose the proportion of seawater to ash used in either publication. Zeolites synthesised using seawater were zeolite X, sodalite, and zeolite ZK-5, whilst zeolites synthesised in distilled water included zeolite A as well as zeolite X, sodalite and zeolite ZK-5. The use of seawater resulted in synthesis of zeolites at lower temperatures when compared to synthesis with distilled water. The use of seawater also appears to have hindered or inhibited the synthesis of zeolite A, which was not present in pure form under any conditions, but intermixed with other zeolite phases. The experiments with synthetic seawater and distilled water [39] investigated the cation content of the crystallisation solution over time. The crystallisation process sequestered all of the Mg from the synthetic seawater, and 90 % of the Ca. In a control experiment conducted with distilled water (also at 25°C) no zeolite crystallised under the same conditions. This led the authors to conclude that Mg and Ca were involved in the synthesis of zeolite X. This supports the idea of the structure-directing role of cations in the synthesis of zeolites as mentioned in literature [30, 60].

Izidoro et al. [54] managed to achieve complete conversion of two different ashes. The complete conversion was determined by a lack of quartz and mullite in the XRD patterns, and no apparent extraneous material in the SEM images. Each ash was used to synthesise zeolite X and zeolite A by varying solids loading, Si/Al ratio and crystallisation time. In

order to synthesise zeolite X, the fly ash and NaOH were fused for 1 hour following the method described earlier. The Si/Al ratio was adjusted to 1.2 through addition of $NaAlO_2$, and dissolved in water at solids loadings of 50 g CFA/L for 16 hours at room temperature. The temperature was then raised to 100°C for 24 hours in order to synthesise zeolite X, which was filtered from the solution, washed and dried. In order to synthesise zeolite A, the fly ash and NaOH were fused for 1 hour following the method described earlier. The Si/Al ratio was adjusted to 1.0 through addition of $NaAlO_2$, and dissolved in water at solids loadings of 100 g CFA/L for 16 hours at room temperature. The temperature was then raised to 100°C for 7 hours in order to synthesise zeolite X, which was filtered from the solution, washed and dried. In short, zeolite A was synthesised with more Al, in shorter crystallisation periods, and at higher solids loadings compared to zeolite X.

Experiments by Molina and Poole [6] compared fusion to hydrothermal extraction in experiments with varied ratios of NaOH:CFA. It was found that the CEC of CFA that had undergone fusion was higher than the CEC of hydrothermally leached CFA following the same dissolution or ageing process followed by crystallisation. The fusion product was mixed in distilled water for 24 hours at RTP, before being heated to 90°C for 6 hours. The hydrothermal experiments are discussed in section 2.4.1. The highest CEC was observed at a NaOH:CFA ratio of 1.2:1 for both the fusion and hydrothermal processes. At the lowest NaOH content, where the NaOH:CFA ratio was 1:1 (equivalent to 2.94 M NaOH), zeolite X was formed. As the NaOH content increased to NaOH:CFA = 1.2:1, more crystalline zeolite X was formed, followed by a mixture of zeolite X and sodalite, and then just sodalite at ratios 1.6:1 and 2:1. In comparison, the equivalent hydrothermal experiments had a lower CEC for all values of NaOH, produced no zeolitic materials at the lowest NaOH content, and produced zeolite X XRD patterns of a much lower intensity at a NaOH:CFA ratio of 1.2:1. It was noted that reducing the content of magnetic material in the CFA through magnetic separation improved the CEC under all conditions.

2.4.2.2 Temperature

The experiments dissolved in seawater, synthetic seawater, and distilled water mentioned in section 2.4.2.1 were heated to 35-90°C to produce different zeolites. The experiments with seawater and distilled water [38] synthesised zeolite X and sodalite in both dissolution media at 90°C, with a decreasing sodalite content as temperatures decreased. At 35°C zeolites formed for only two of the four CFA samples used, both formed zeolite X, albeit poorly crystalline. As temperature increased, zeolite X was formed in all CFA samples, with crystallinity increasing with temperature, except when competing with another phase such as zeolite ZK-5, sodalite or zeolite A, where crystallinity of zeolite X was notably decreased.

Berkgaut and Singer [44] compared the effect of a 12 hour ageing step at room temperature and pressure with no ageing step. Both experiments were then heated to 100°C for several hours (with no reaction after 4 hours). The unaged experiment produced zeolite P, the aged experiment made zeolite X.

Chang and Shih [57] synthesised Faujisite and zeolite P from the same source ash by heating to 60°C for 5 days and 90°C for 4 days respectively. Zeolite X is a form of Faujisite [57].

Experiments by Molina and Poole [6] found that a 6 hour crystallisation at 90°C produced the most crystalline yield of zeolite X, when compared to crystallisation at 60 or 40°C for 6 hours at a NaOH/CFA ratio of 1.2.

Soong et al. [86] dissolved the fusion product in distilled water for 24 hours, before heating under hydrostatic conditions to 100°C for 48 hours. This resulted in a 75 % conversion to zeolite P. This method was compared with crystallisation of zeolites from the leachate, and is discussed in section 2.4.4.

2.4.2.3 Time

The dissolution step for the experiments by Belviso et al. [38] took place overnight in a stirred vessel. This was followed by a crystallisation step that lasted for 4 days. The

zeolites synthesised were zeolite X, zeolite ZK-5, sodalite and zeolite A. In the experiments conducted with synthetic seawater [39], the dissolution step also took place overnight in a stirred vessel, however the duration of the crystallisation step was varied from 0.5-192 hours. The authors observed the preferential formation of zeolite A over zeolite X for the first 96 hours, and more zeolite X than zeolite A for the longer (>96 hour) experiments. This supports Ostwald's rule of successive transformations, with zeolite A being metastable with respect to zeolite X.

Berkgaut and Singer [44] synthesised high purity zeolite X and zeolite P from the same fused ash by either ageing the leachate at room temperature for 12 hours (to make zeolite X) or not (to make zeolite P).

Experiments by Molina and Poole [6] dissolved the fusion product in distilled water for 24 hours at RTP, and then heated the solution to 90°C. At 30 minutes, only amorphous material was detected by XRD. At 1 hour, zeolite X was detected, which increased in intensity to a maximum at 2 hours, before decreasing in intensity by 6 hours. No traces of other crystalline material such as quartz or mullite were detected in the products from the fusion process, further supporting the argument that fusion improves the dissolution of crystalline phases from CFA.

2.4.2.4 Additional Reagents

Belviso et al. [40] added kaolin to the ash in varied proportions prior to fusion. Experiments consisting solely of CFA synthesised zeolite X, whilst experiments consisting solely of kaolin synthesised zeolite A. Experiments where the two starting materials were mixed produced a mixture of zeolite A and X, with all experiments producing traces of sodalite and zeolite ZK5 at different times. The materials have a slightly different Si/Al ratio, with Kaolin being richer in Al (Si/Al = 1.01) than CFA (Si/Al = 1.46).

In order to change the Si/Al ratio, additional aluminium is often added to the crystallisation process. Sodium aluminate solution is commonly the preferred method for the addition of aluminium [35, 41].

Chang and Shih [53] synthesised two zeolites from various ashes under similar conditions through addition of Al. The authors synthesised zeolite X by crystallising at 60°C for 20 days, and synthesised a higher proportion of zeolite A than zeolite X in some ashes by adding aluminium hydroxide hydrate and then crystallising at 60°C for 3 days. 2 of the 3 ashes used as a starting material synthesised zeolite X as well as zeolite A in experiments with added Al.

Experiments by Musyoka et al. [41] synthesised zeolite A and zeolite X from the same ash by changing the Al content. Crystallisation at 80°C for 9 hours without additional Al resulted in the synthesis of zeolite X, whilst addition of Al and crystallisation at 100°C resulted in the synthesis of zeolite A. Both approaches were preceded by a 2 hour dissolution step at RTP.

2.4.2.5 Other Considerations

Work by Berkgaut and Singer [44] has shown that dissolution of Si and Al from ash can be improved by wetting the NaOH and ash mixture and mixing to form a paste prior to fusion in order to achieve more intimate contact, and thus better dissolution of the glassy products.

Calcium, which has been noted to interfere with zeolite synthesis, was observed to precipitate as calcite by Belviso et al. [40] during the leaching of fusion products for the synthesis of zeolites.

Carlos A. Ríos R. [87] noted that using KOH instead of NaOH resulted in the synthesis of no zeolite products.

2.4.3 Zeolitisation of Leachate Without Fusion

By separating the ash from the leachate prior to the crystallisation step, a pure zeolite can be formed that is not contaminated with unreacted fly ash [57]. Whilst the zeolitisation of ash can sometimes result in complete conversion of ash, the removal of ash from the leachate guarantees a product free from ash, which will also be whiter than the zeolitised

ash, which often has a grey hue [44].

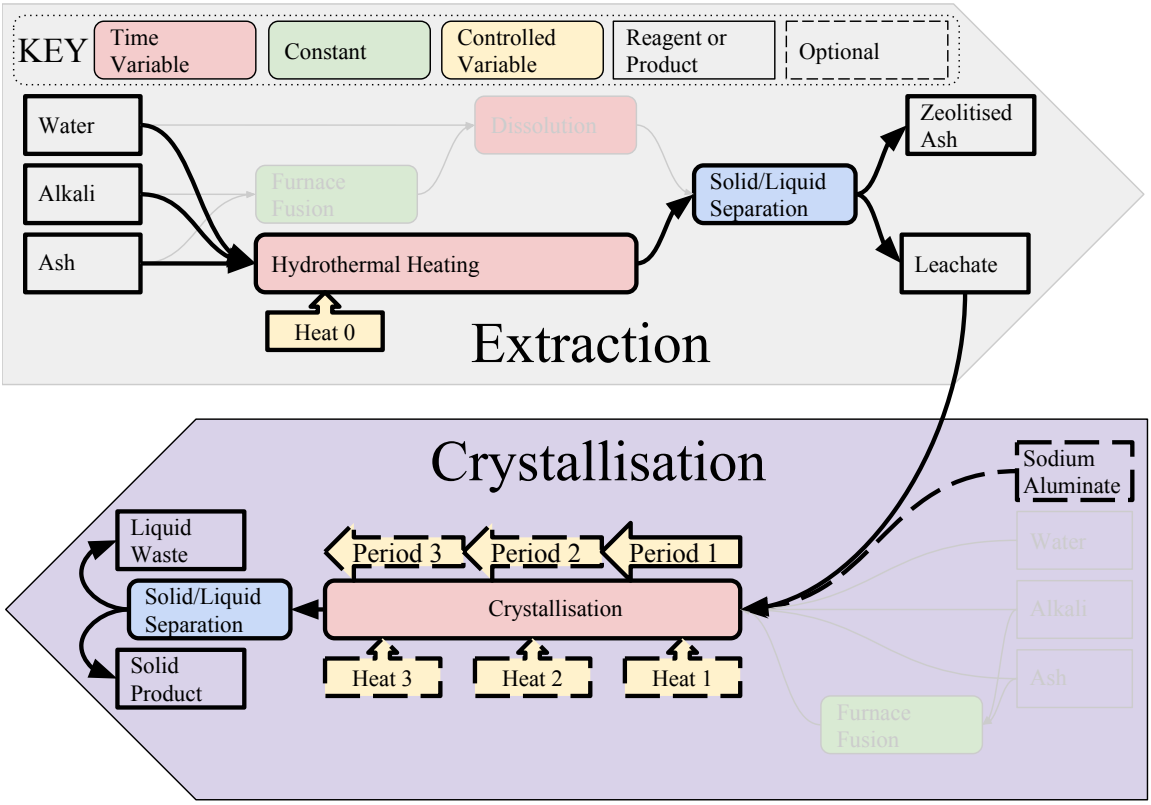

Figure 2.10: Block diagram of process for hydrothermal zeolitisation of leachate derived from ash described by literature

2.4.3.1 Extraction Methods

Analysis of the Si and Al content of crystallisation solutions from the in-situ zeolitisation of ash experiments by Hollman et al. [26] mentioned in section 2.4.1 found that the Si content of the solution was highest at 6 hours. Observing this, Hollman et al. [26] conducted an experiment under the same conditions, heating 400g CFA/L in 2 M NaOH at 90°C, and filtered out the ash at 6 hours to get a solution rich in Si. The leachate was then utilised in the synthesis of various zeolites, depending on the quantity of added Al, and is discussed in section 2.4.3.2. Synthesis without filtration of ash made zeolite P, and is discussed in section 2.4.1.

Fukui et al. [66] hydrothermally leached 40 g CFA/L in 2 M NaOH at 100°C for 1 hour. The undissolved ash was then separated from the leachate by filtration. Hui and

Chao [32] used similar conditions, but used a solids loading of 100 g CFA/L for 2 hours. After the undissolved ash was filtered out the Si content of the solution was 11.49 g Si/L, which was estimated to be an extraction of 40-50 % of the Si.

Kim and Lee [68] hydrothermally leached CFA in highly alkaline conditions with a high solids loading, before diluting for the crystallisation step. The extraction conditions utilised 1-5 M NaOH and 250 g CFA/L for 1-8 hours at 100°C. The leachate was then separated from the undissolved ash and the molar ratio was adjusted using NaOH, sodium aluminate and distilled water. The leaching step was conventionally heated, and compared to microwave-assisted heating. The highest Si and Al yield for 5 M NaOH extraction was found to be at 2 hours for the hydrothermal method, and at 5 hours for the microwave assisted extraction method. The yield of Si and Al in solution was significantly higher for microwave extraction than it was for the conventionally heated extraction process, with a maximum extraction of ~35 % Si for the microwave process, and ~10 % extraction for the conventional process. Al values were ~10 % and ~20 %. By varying the concentration of NaOH between 1 and 5 M for the conventionally heated extraction method, XRD analysis of the ash shows synthesis of zeolite P and sodalite, with the intensity of the zeolite P patten peaking at 2-3 M NaOH, and decreasing in intensity as NaOH concentration increases, and sodalite intensity increasing from 3-5 M NaOH. For microwave assisted extraction, the intensity of the zeolite P XRD patterns are significantly lower at all concentrations of NaOH, whilst the sodalite concentrations peak at 2 M NaOH, and decrease with increasing NaOH. The peak in intensity of sodalite at 2 M is of a rather low intensity. This experimental data supports the argument that microwave assisted heating inhibits nucleation of zeolites, and increases the dissolution of Si and Al from CFA, and that higher concentrations of NaOH encourage the formation of sodalite in place of zeolite P.

2.4.3.2 Additional Reagents

Fukui et al. [66] added RHA or silica powder to the leachate prior to crystallisation. These additives increase the quantity of available Si in solution, changing the Si/Al ratio. 9 hour crystallisation experiments with no added Si produced sodalite, with some phillipsite ($|(Na,K,Ca_{0.5})_x(H_2O)_{12}|$ $[Al_xSi_{16-x}O_{32}]$ x = 3.7 – 6.7) [89]. The sodalite content decreased and the phillipsite content increased as additional silica was added to the crystallisation step. RHA and silica were found to perform similarly as a source of silica for this purpose. The addition of more silica to a system which was already low in Al compared to Si resulted in a system with a high Si/Al ratio, resulting in the synthesis of phillipsite and sodalite rather than zeolites A, X and P, which have a significantly higher Al content.

Hollman et al. [26] crystallised leachate at 90°C for 48-72 hours with added aluminate solution. Depending on the Si/Al ratio, different zeolites were synthesised. A ratio of 2:1 synthesised zeolite P in 48 hours, 1.8:1 synthesised zeolite X in 48 hours, and a ratio of 1.2:1 synthesised zeolite A with some sodalite in 67 hours. The yields of zeolite were 50, 75 and 85 g/kg CFA respectively. After the zeolite was filtered from the crystallisation solution, the undissolved ash from the leaching step was reintroduced to the leachate. The crystallisation solution was still sufficiently alkaline to synthesise zeolite P zeolitised ash from the waste solution and solid residue.

Experiments by Tanaka et al. [43] adjusted the Si/Al ratio of the leachate though addition of sodium aluminate. The experiments showed an increase in yield of zeolitic materials proportional to the Si/Al ratio as the ratio increased from 5 to 1. The results shows that with more added Al and at shorter crystallisation times, zeolite A was formed, but with less added Al and longer crystallisation durations, zeolite X formed. Other experiments by the same authors [8] synthesised zeolite A at Si/Al ratios of 0.9-4.3, and zeolite X from ratios 1.7-4.3. Traces of zeolite X formed at ratio 1.7, and increased in intensity to the detriment of the intensity of zeolite A till zeolite X is the dominant phase at ratio 4.3, with traces of zeolite A present. As with the previous work, the authors noted an increase in yield as more Al was added to the crystallisation solution, with the

Si/Al ratio of 0.9 having the highest yield of zeolitic materials.

2.4.3.3 Additional Extraction Methods

An experiment by Tanaka et al. [8] suspended CFA in a semipermeable membrane in a NaOH solution of unspecified concentration. This solution was heated to 85°C for 24 hours in order to leach Si and Al from the CFA. The semipermeable membrane of ash was then removed and the leachate utilised in a crystallisation process discussed in section 2.4.3.2. It was noted that no crystalline material had formed on the surface of the ash.

2.4.3.4 Temperature And Heating Method

After producing a leachate from CFA and adding RHA, Fukui et al. [66] took two approaches to the crystallisation step: conventional heating and microwave heating. Both heating methods maintained a temperature of 100°C through feedback temperature control and a reflux condenser, being stirred at 250 rpm. Results showed that microwave assisted crystallisation increased the proportion of sodalite formed, and hindered phillipsite formation in comparison to conventional heating methods. This is attributed to the sodalite absorbing microwaves better than phillipsite during control tests with sodalite, phillipsite and RHA and phillipsite mixed with *n*-octane. The control test indicated that sodalite absorbs almost 10 times as much energy as phillipsite does. The increased temperature of the sodalite promotes growth of sodalite crystals, as crystal growth is proportional to temperature.

Hui and Chao [32] added aluminium solution and then aged leachate for 30 minutes at RTP. The crystallisation solution was then heated to an intermediate temperature of 80-90°C for 1.5 hours to induce nucleation, then heated to a higher temperature of 90-95°C for 0.5-8 hours to hamper nucleation and encourage crystal growth. The optimal results with regards to crystallinity, zeolite form and narrow PSD were from intermediate heating at 90°C and higher heating at 95°C [32, 45, 49]. With reference to Figure 2.10, this would be represented by "Heat 1", "Heat 2" and "Heat 3" being room temperature,

90°C and 95°C, and periods 1, 2 and 3 being 30 minutes, 90 minutes and 60 minutes, respectively. The paper discusses other works where high temperatures lead to zeolite A transforming to sodalite in keeping with Ostwald's rule of successive transformations.

The Si, Al, and alkalinity of the leachate from the extraction process of Kim and Lee [68] was adjusted through the addition of sodium aluminate, distilled water and NaOH. Conventional heating showed a linear increase in the crystallinity of zeolite A for hours 1-3, with a further, smaller increase by 4 hours to reach a maximum of approximately 76 %. This was accompanied by a decrease in the crystallinity of sodalite from 50 % to 20 % over 4 hours. In another experiment, the leachate was conventionally heated for 1 hour, and then heated using a microwave for 0-3 hours. The crystallinity of zeolite A increased from 20 % after the 1 hour conventional heating to 80 % after 30 minutes of microwave heating, and reached a maximum of ~90 % at 1-1.5 hours before decreasing to 80 % for 2-3 hours. The crystallinity of sodalite was inversely proportional to the crystallinity of zeolite A, reaching a minimum at 1-1.5 hours. It was noted that the particle size of the zeolite A synthesised from the microwave-assisted process was finer than the particle size of the conventionally heated process. This data supports the idea that nucleation is hindered by microwave assisted heating, but that microwave assisted heating can speed up crystal growth to improve crystallinity and purity in comparison to conventional heating methods if applied to a seed-rich crystallisation solution.

2.4.4 Zeolitisation of Leachate with a Fusion Step

Improving the dissolution of silica and alumina from CFA resulted in better conversion of ash to zeolites. Solubility of Si and Al from CFA has been shown to be improved in section 2.4.2 through the inclusion of a fusion step prior to the zeolitisation of ash. Similarly, the fusion step can be included in the zeolitisation of leachate method and the insoluble ash residue removed to leave a pure zeolite product free from contamination by undissolved ash.

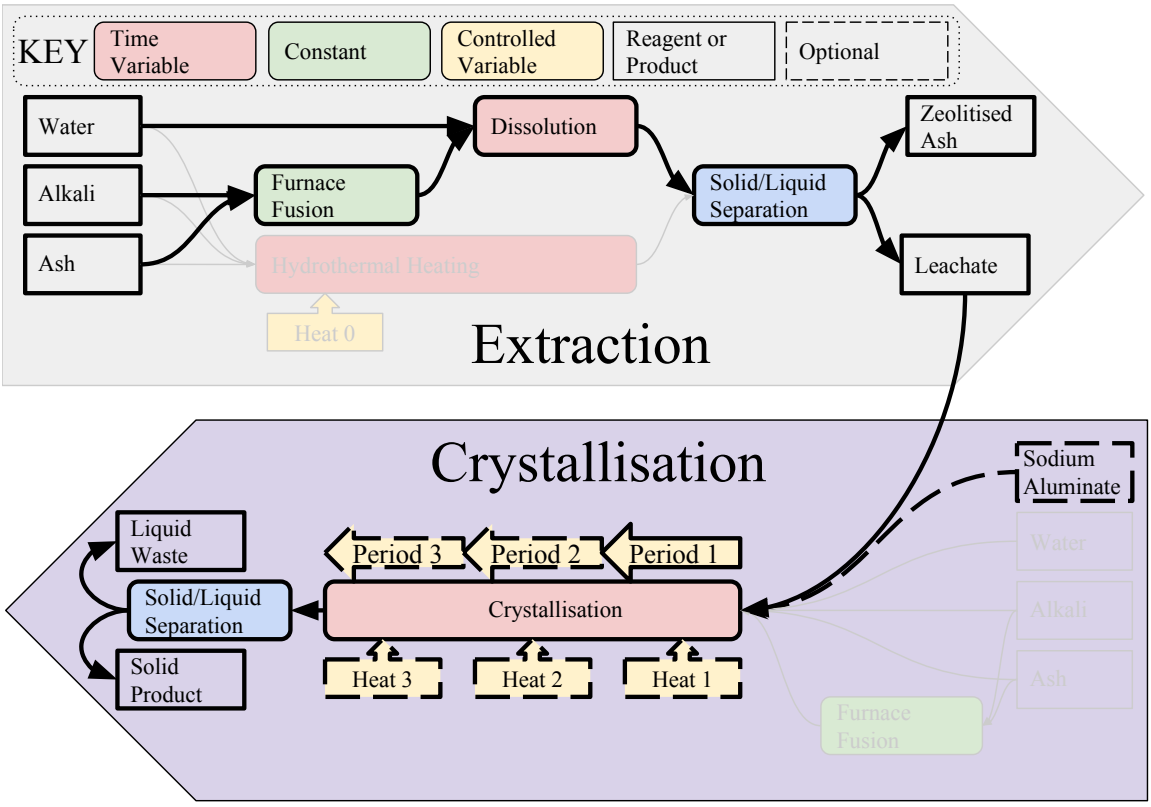

Figure 2.11: Block diagram of process for hydrothermal zeolitisation of leachate derived from fused ash described by literature

2.4.4.1 Extraction Methods

The fusion process and dissolution of the fusion products is often the same as was mentioned in section 2.4.2. After the dissolution process, the undissolved ash is separated from the fusion product by filtration. Du Plessis et al. [7] fused ash and NaOH at a ratio of 1:1.2. The fusion product was dissolved in ultrapure water at a quantity equivalent to 2.72 M NaOH and 91 g CFA/L for 2 hours, mixed at 1400 rpm. The ash was then separated from the leachate by filtration. Chang and Shih [57] fused ash and NaOH at a ratio of 1:1.2 and dissolved the fusion product in distilled water at a quantity equivalent to 2.79 M NaOH and 93 g CFA/L. The undissolved ash was separated from the leachate with a centrifuge.

Yaping et al. [90] used sodium carbonate instead of NaOH in the fusion step, at a ratio of 1.5:1 sodium carbonate:ash rather than the usual ratio of 1.2:1 sodium hydroxide:ash. The fusion step also took place at a higher temperature of 830-850°C for 1 hour rather

than the usual 550°C. It is noted that sodium carbonate decomposes to sodium oxide and carbon dioxide as shown in equation 2.2 upon reaching its melting point at 850°C [91].

$$Na_2CO_{3(l)} \rightarrow Na_2O_{(s)} + CO_{2(g)} \tag{2.2}$$

The fusion product was noted to be green, as has been observed to be the case for other fusion products [85, 86]. XRD patterns of the fusion products showed the presence of water-soluble Na_2SiO_3 and alkali-soluble $NaAlSiO_4$. The dissolution process also differed from other fusion processes, and the process depicted in Figure 2.11 in that the solution was stirred and heated, rather than just stirred at RTP. The ash was separated from the leachate via filtration. The ash from this process was then hydrothermally leached with NaOH, resulting in a total extraction of 70 % of the Al and 75 % of the Si using a 2 M NaOH solution.

A slightly altered extraction process was also used by Musyoka et al. [35], where the ratio of NaOH:ash fused was 2:1. The fusion took place for 1.5 hours at 550°C and the fusion product was dissolved in demineralised water for 2 hours at a solids loading equivalent to 3.3 M NaOH and 66.6 g CFA/L. The undissolved fly ash was separated from the leachate using a centrifuge.

2.4.4.2 Additional Reagents

Du Plessis et al. [7] added sodium aluminate to the leachate at a concentration equivalent to 3400 g/kg CFA and heated the solution to 100°C for 2 hours to produce zeolite A at a yield of 314 g / kg FA. Chang and Shih [57] were able to synthesise zeolite A by adding $Al(OH)_3$ to leachate and heating the solution to 60°C for an unspecified duration. Soong et al. [86] added $Al(OH)_3$ and noted the product of crystallisation was white, rather than the green or grey of products synthesised without removal of the CFA.

The leachate derived by Yaping et al. [90] was adjusted to a pH of 13 using HCl or CO_2. Solutions with a starting Si/Al ratio of 0.9-0.95 were heated to 100°C and structure directing agents were added. Addition of zeolite A crystal seeds resulted in the synthesis

of zeolite A within 5 hours at a yield of 314-368 g/kg CFA and CEC of 3.75-4.47 meq/g. Addition of a different structure directing agent resulted in the synthesis of zeolite X within 5 hours at a yield of 398-518 g/kg CFA and CEC of 3.19-3.15 meq/g. For solutions with a higher Si content (1.1-2) zeolite P was synthesised within 10-13 hours with no structure directing agents. The synthesised zeolite P was at a yield of 508-560 g/kg FA and CEC of 4.56-4.32 meq/g.

Musyoka et al. [35] added aluminate solution to the leachate and heated the crystallisation solution to 80°C for 6 hours. Before crystallisation, the solution was aged at room temperature for 0 hours, 6 hours, 12 hours, or 17.5 hours prior to heating. All solutions synthesised zeolite A, with XRD detecting zeolite A from 220 minutes, and SEM showing the growth of cubes with chamfered edges from 200 minutes. SEM images of zeolites derived from leachate were compared to zeolites derived from the zeolitisation of ash. The leachate-derived zeolite sample showed clean, chamfered edged cubes, whilst the zeolitised ash sample showed zeolite cubes mixed with extraneous material.

2.4.5 Other Methods

Experiments conducted by Park et al. [78] used a molten salt process to make sodalite and cancrinite from CFA without utilising any water. The experimental conditions were at a much higher temperature than other synthesis processes discussed at 350°C, and these high temperatures were maintained for 3 h to 3 days [92]. The zeolites produced were considered less desirable than zeolites A, X or P due to their lower CEC, and the extreme conditions would raise the cost of synthesis considerably. Such solid-state conversions were therefore not thoroughly investigated.

2.5 Zeolitisation Methods Investigated

From the literature analysed, a method was developed in order to synthesise zeolites from RockTron's Delta product. An overview of this method is shown in Figure 2.12. It was

decided that high pressure processes would be excluded, as industrial synthesis of zeolite A is not conducted at high pressure, and the majority of literature covers zeolitisation conditions at atmospheric pressure. It was also decided that the synthesis of pure zeolites, with no remaining ash product was desired, thus methods similar to those described in sections 2.4.3 and 2.4.4 were the basis of this experimental design. The experimental work is discussed in two parts. The extraction experiments (grey area in Figure 2.12) are discussed in section 4, and the crystallisation experiments (purple area in Figure 2.12) are discussed in sections 5, 6 and 7. In order to increase the yield, additional Al was to be added to the crystallisation solution in the form of sodium aluminate. Without the addition of sodium aluminate, literature indicates that the potentially low Al content of the leachate could be a yield limiting reagent [57].

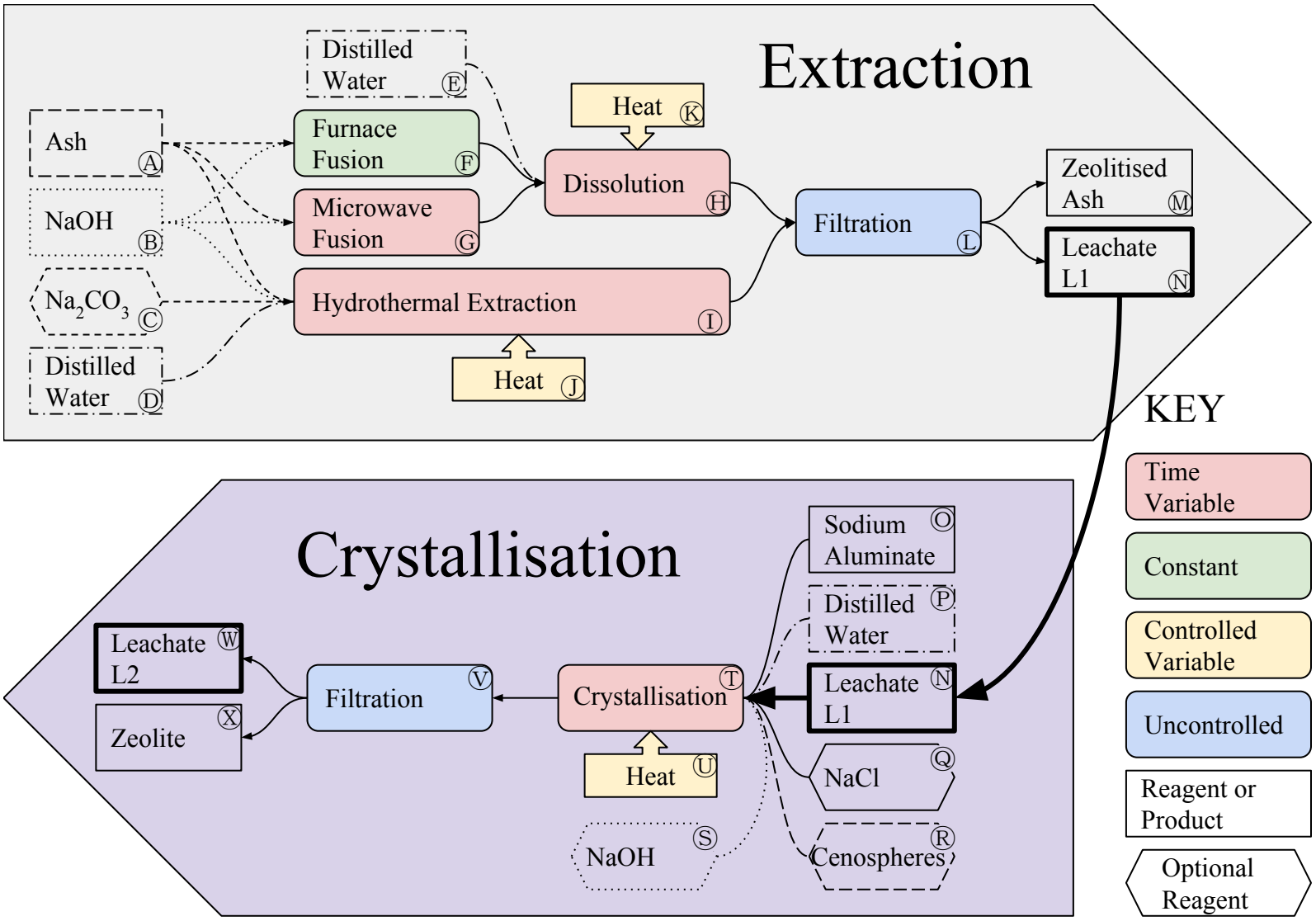

Figure 2.12: Block diagram of extraction and crystallisation processes investigated

2.6 Summary

Zeolites are negatively charged three-dimensional aluminosilicate structures counterbalanced by positively charged cations within voids. In aqueous systems, the cations within the zeolite can be exchanged for cations in the aqueous system. This property makes zeolites useful for a variety of applications, including reducing the heavy metal content of acid mine drainage, as a soil treatment agent, and as a builder for powdered detergents. Coal fly ash is a material rich in amorphous silica and alumina, a property that makes CFA well suited as a feedstock for the synthesis of zeolites. Utilising CFA in the manufacture of synthetic zeolites provides and opportunity to improve the environment by cleaning up acid mine drainage and reducing eutrophication whilst consuming an material which would otherwise be considered a pollutant [45]. Such applications provide an added-value material from a waste product.

Zeolites can be synthesised under a variety of conditions, however one of the more common and facile approaches is the hydrothermal synthesis method. The hydrothermal synthesis method mixes silica and alumina in an alkaline solution. This solution is then heated to precipitate zeolites, which are separated from the solution by filtration or centrifuging. Alkaline solutions will dissolve silica and alumina from CFA, the resulting silica and alumina rich solution can then be heated to precipitate synthetic zeolites. The heterogeneous composition of CFA results in a solution with a content that will vary depending on the coal the ash was derived from and the conditions under which the coal was burnt.

A mechanism to describe the synthesis of zeolites was developed by Cundy and Cox [60]. According to this method: amorphous material forms an equilibrium with anions and cations in solution; a small area of local order forms (nucleation occurs); this area of local order grows, consuming anions and cations from solution; the equilibrium between amorphous phase and dissolved anions and cations results in dissolution of the amorphous phase to replenish the equilibrium between amorphous phase and dissolved species. Nucleation describes the formation of a structure from which a crystal lattice

can grow. The presence, form, and concentration of nuclei in a crystallisation system can have a decisive influence on the final product and it's properties, thus the conditions of the crystallisation solution during the nucleation process are very important. Addition of nuclei to a solution can change which zeolite forms. A crystallisation solution with a large number of nuclei will result in a finer product, and the particle size distribution of the final product can be heavily influenced by the number and size of nuclei present prior to the crystal growth phase. Crystal growth follows nucleation, but the conditions of crystal growth are far more tolerant to variation than the nucleation process. Ostwald's rule of successive transformations describes how intermediate phases will form before the most thermodynamically stable form of zeolite. The desired product is often not the most thermodynamically stable form, thus the duration of the crystallisation process must be closely monitored. The dissolution and recrystallisation of one zeolite form to a more thermodynamically stable phase (according to Ostwald's rule of successive transformations) will be expedited by the presence of the more thermodynamically stable phase.

The parameters which influence the synthesis of zeolites include: temperature, alkalinity, Si/Al ratio, cation content, and time. High temperatures encourage dissolution of Si and Al from CFA, and speed up crystal growth. Nucleation at higher temperatures can encourage the formation of sodalite. Nucleation is also highly influenced by the alkalinity of the solution. A solution with a high NaOH content will synthesise sodalite, rather than zeolites A, X or P. Similarly, the increased solubility accelerates Ostwald's rule of successive transformations, accelerating the transformation of one zeolite form to the next, or bypassing them entirely to form sodalite. Altering the Si/Al ratio of the crystallisation solution can result in the synthesis of different zeolite forms from the same crystallisation solution. Zeolites with the highest CEC will have a ratio of Si:Al of 1:1, thus addition of Al to the crystallisation solution can increase the yield, as the Si content of leachates is often significantly higher than the Al content. Excess Al also increases the rate of crystallisation of zeolite A. The presence and concentration of cations in the crystallisation solution has been shown to govern which zeolites form, and to influence the crystallinity

of the zeolites that do form. The duration of the crystallisation process effectively decides at which point Ostwald's rule of successive transformations is interrupted. If the process is stopped too early, the expected product would be amorphous aluminosilicate. As the experiment duration increases, zeolite A could form, which would in turn be replaced by zeolite X and/or zeolite P, which in turn would be replaced by sodalite, depending on the conditions.

Manipulating temperature and time has been successfully employed to shorten the crystallisation process. Heating the crystallisation solution to 90°C to encourage nucleation, followed by a temperature increase to 95°C to encourage crystal growth was an approach utilised by Hui and Chao [32] and Hui et al. [45] to synthesise zeolite A. Other authors have utilised microwave-assisted heating to encourage crystal growth after a conventionally heated nucleation period, resulting in the synthesis of zeolite A in a shorter time period than would have been achieved in a conventionally heated crystallisation process [68]. A more rapid synthesis process is preferable, as extended high-temperature processes are expensive [45, 76].

Chapter 3

Material Overview

3.1 Coal Fly Ash Composition

Coal fly ash is an abrasive, grey, refractory powder, made of fine particles, mostly spherical, consisting of predominantly silica, alumina, iron oxide, calcium oxide, and unburnt carbon [2, 5, 38, 43, 82]. CFA is mostly an amorphous aluminosilicate glass [38, 39, 43, 72], with the majority of particles appearing smooth and round under SEM analysis [42]. Elemental composition and loss on ignition (LOI) is shown in Table 3.1. Untreated ashes analysed in this study were FB7, an unprocessed fly ash from the Ferrybridge power station in the UK, and Lagoon, an ash retrieved from a CFA storage pond at RockTron's Gale Common site. Elemental composition was determined through X-ray fluorescence spectroscopy (XRF). Samples were prepared using a lithium borate fused bead method. The standard reference material CANMET-SY-4 was used to assess the accuracy of the method and to check for matrix interferences [93]. LOI was conducted at 900°C for 2 hours. It is noted that the Lagoon ash (an ash from a holding pond) has a lower calcium content than the FB7 ash (an ash acquired straight from a power plant), as calcium from the Lagoon ash would leach in to the water the ash is subjected to. Heavy metals are concentrated in the finest size ranges of CFA [11, 94].

Table 3.1: Bulk chemistry of coal fly ash. Results in wt % (from Blissett [1]).

Ash	Lagoon	FB7	Alpha	Delta
SiO_2	48.4	44.7	49.2	52.2
Al_2O_3	25.5	25.2	27.8	26.2
Fe_2O_3	10.5	9.0	6.6	7.3
CaO	2.6	4.0	3.2	3.2
K_2O	1.6	2.2	1.6	1.7
MgO	0.5	0.5	0.7	0.5
TiO_2	2.8	2.5	3.0	2.9
Na_2O	1.0	1.0	1.0	1.0
P_2O_5	0.1	0.1	0.1	0.1
MnO	0.3	0.4	0.4	0.3
LOI	6.8	10.3	6.4	4.7

Whilst coal fly ash is mostly an amorphous aluminosilicate glass, crystalline phases do occur, the most common of which are mullite and quartz [5, 6, 8, 38, 39, 43, 67, 72, 77, 82] followed by hematite (Fe_2O_3) and magnetite (Fe_3O_4) [5, 6, 43, 72, 77, 82]. Calcium sulphite, calcium oxide and perliclase have also been detected [5]. The crystalline phases of two untreated fly ashes are shown in Figures 3.2 (Lagoon ash) and 3.3 (FB7 ash). Both samples show prominent peaks for mullite and quartz, with smaller peaks for maghemite (γ-Fe_2O_3) and calcite ($CaCO_3$). The broad humps from 15-30 2Θ can be attributed to the amorphous glassy material in the CFA.

Upon contact with water, CFA can increase the pH of the water. The alkalinity depends on ratio of MgO, CaO, Na_2O, K_2O to SO_2, SO_3. CaO is the most varied component, and is more common in lignite coals than bituminous coals [5]. The amorphous glassy phase dissolves more readily than crystalline material in alkaline environments [43]. Heavy metals are concentrated in the finest size ranges of CFA [11]. The particle size distribution of the Lagoon ash is compared to 23 European CFAs and shown in Figure 3.1,

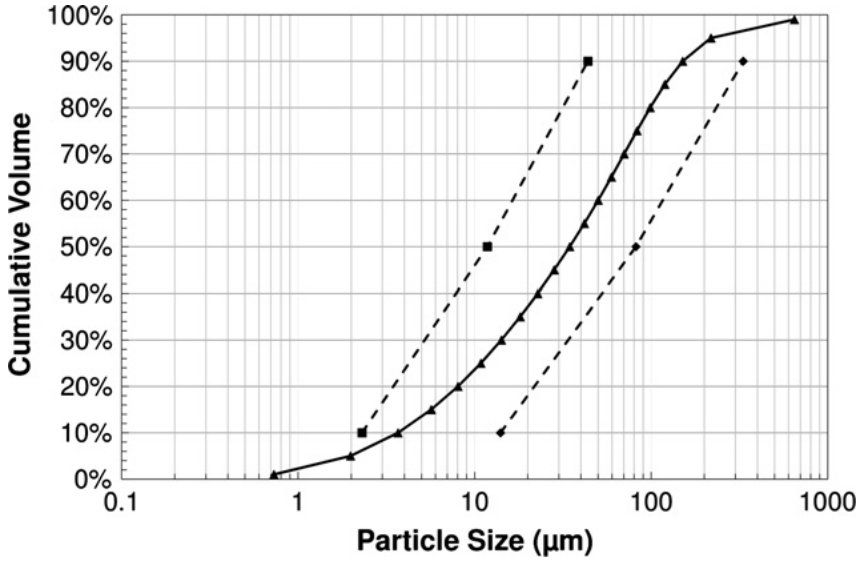

Figure 3.1: PSD of Lagoon ash (▲) in comparison to upper (♦) and lower (■) ranges from 23 European CFAs (from Blissett and Rowson [13]).

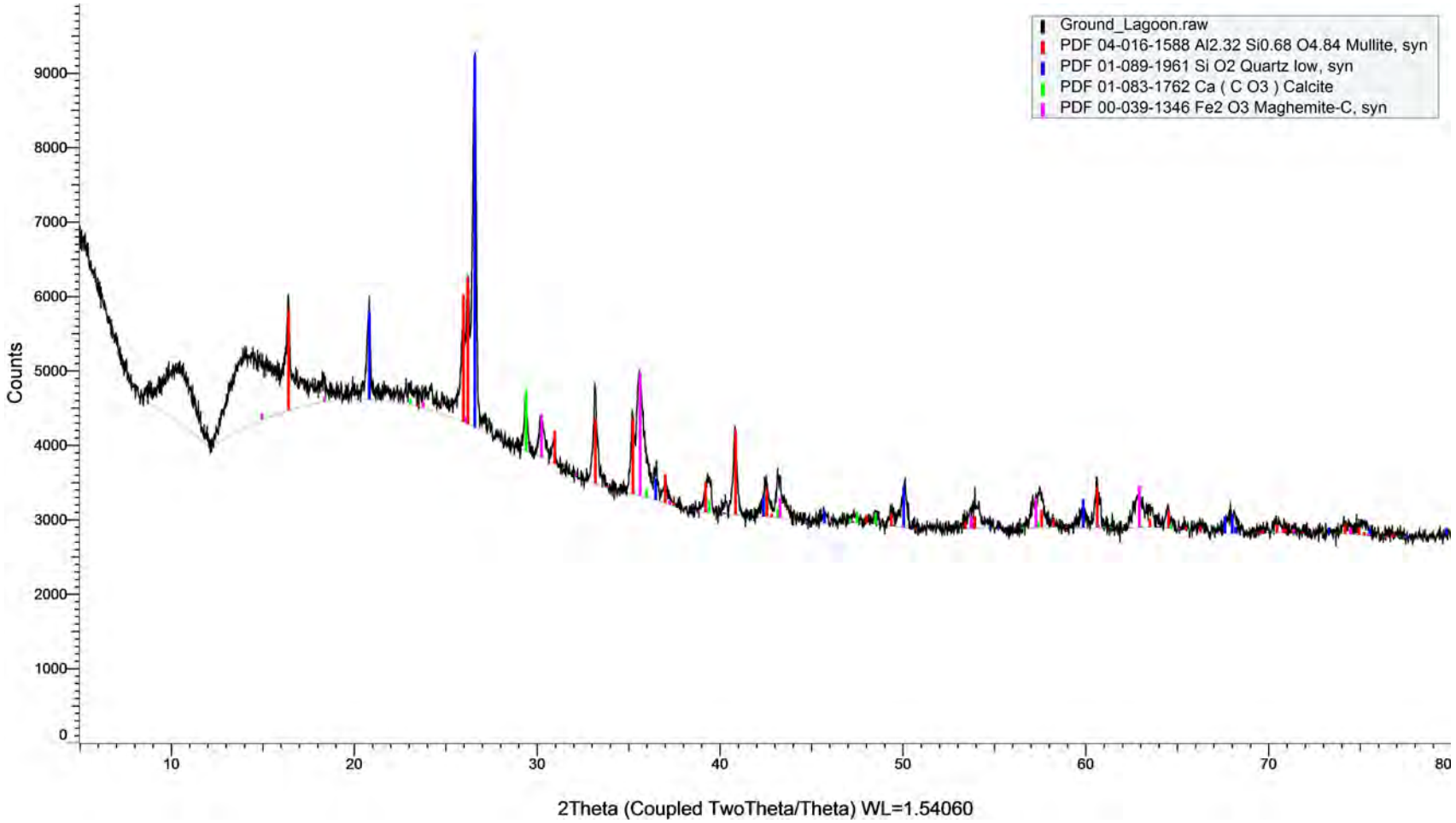

Figure 3.2: XRD Pattern of Lagoon ash. $\lambda = 1.5406$ Å

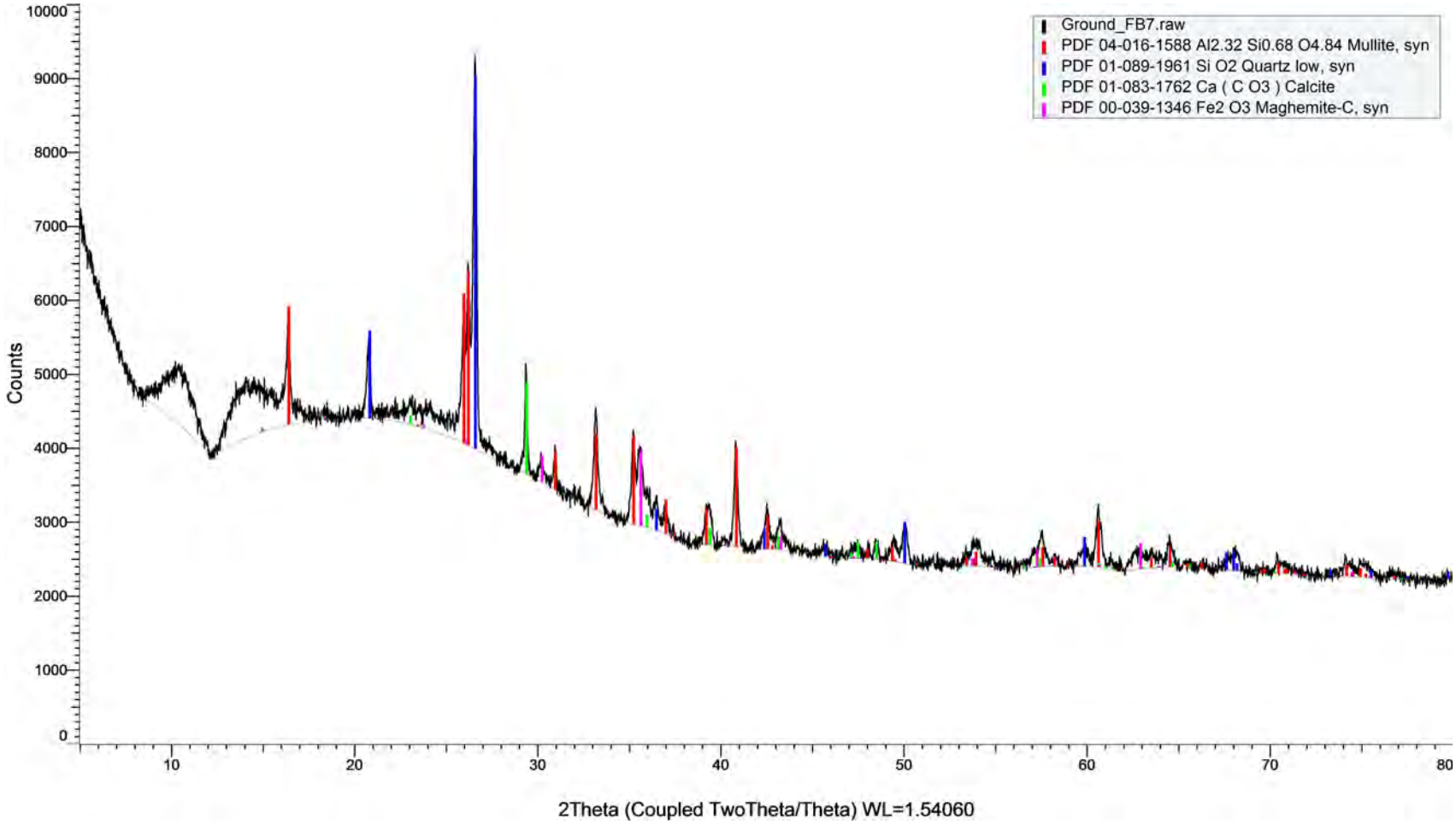

Figure 3.3: XRD Pattern of FB7 ash. $\lambda = 1.5406$ Å

3.2 RockTron Process

RockTron Mineral Services Ltd was a UK based company that owned a proprietary beneficiation process for CFA. The company utilised this process to isolate various separable components from CFA, which have applications in multiple industries. RockTron went into receivership in early 2016.

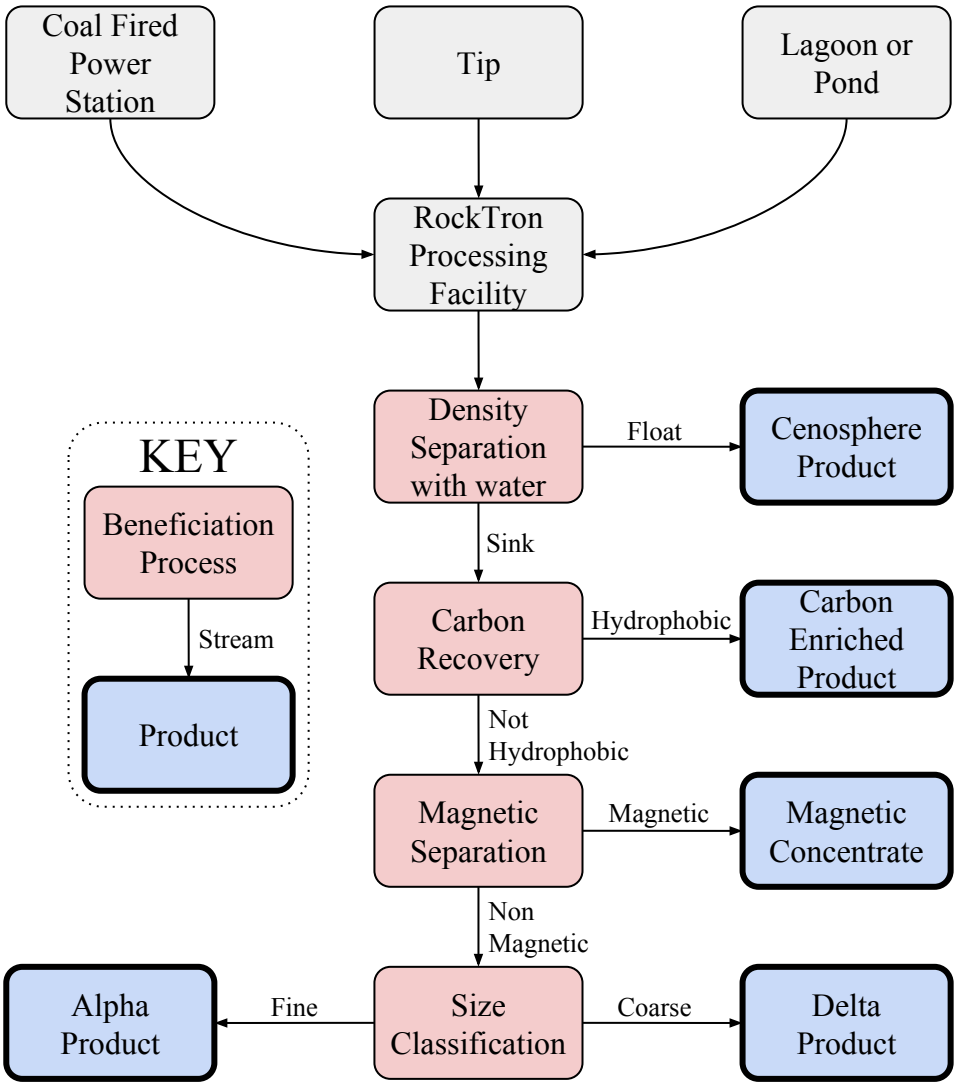

Figure 3.4: Summary of the RockTron process [95, 96]

3.2.1 Cenospheres

Cenospheres are hollow ceramic spheres formed during the combustion process. Definitions for cenospheres vary in literature, however a common definition describes ceno-

spheres as having a relative density <1. Cenospheres are formed as air is trapped within the spheres. Smaller spheres can be trapped within the hollow spheres, forming plenospheres, which will often be of a higher density and thus not be considered cenospheres. Cenospheres vary in size from 40-250 μm, and are more prevalent in coarser size fractions. Cenospheres are commonly separated from CFA by flotation in water [3, 10, 13, 38]. Some material that floats on water will not consist of hollow ceramic spheres. Such material could be non-spherical or porous, however such material is considered part of the cenosphere product [13]. The cenosphere content of any given fly ash will depend on the combustion conditions and ash content of the coal [97].

Cenospheres have applications in composite materials. These exploit the sphericity, low density and low thermal conductivity of the cenospheres. Cenospheres can be used in the manufacture of metal composites. Addition of cenospheres reduces density, decrases thermal conductivity, and improves shrinkage and warpage [14, 98]. Cenospheres can also be used in low density polymers, resulting in improved properties or reduced cost. Use of cenospheres in cement maintains consistency by limiting component separation whilst reducing density. The high mullite content of cenospheres makes them apt for use in cementitious applications where durability is necessary. Their use in heat-insulating refractory products has also been studied [10, 98, 99]. Metal coated cenospheres have applications as fillers for conductive polymers [100], or microwave absorbing materials [101]. Cenospheres have also been investigated as a substrate for the synthesis of TiO_2 coated floating photocatalysts [1, 102–106]. SEM images of cenospheres are shown in Figure 3.5.

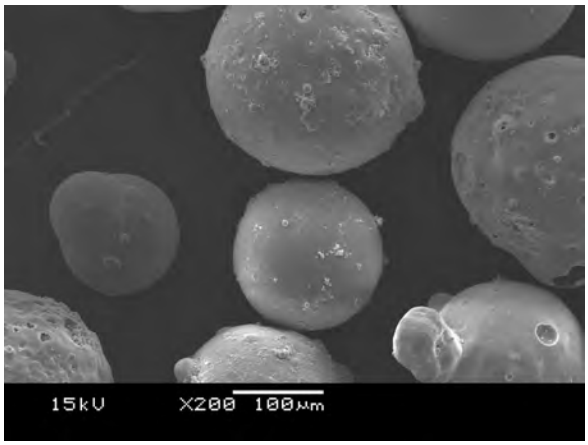

(a) Untreated Cenosphere sample 1 x200

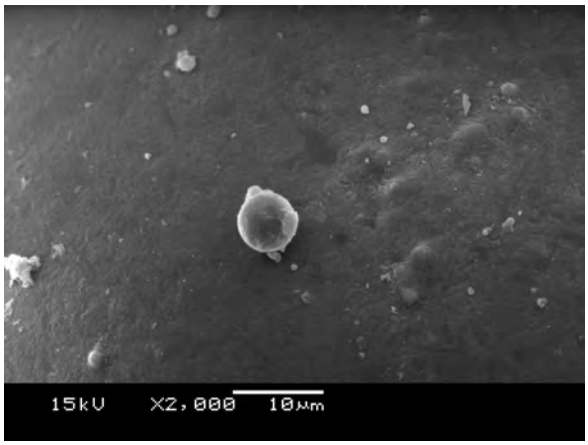

(b) Untreated Cenosphere sample 1 x2000

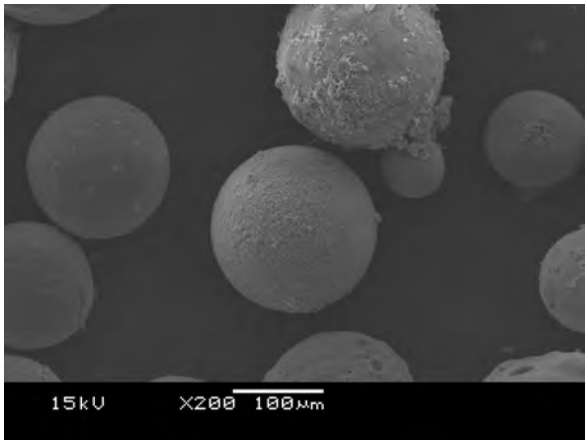

(c) Untreated Cenosphere sample 2 x200

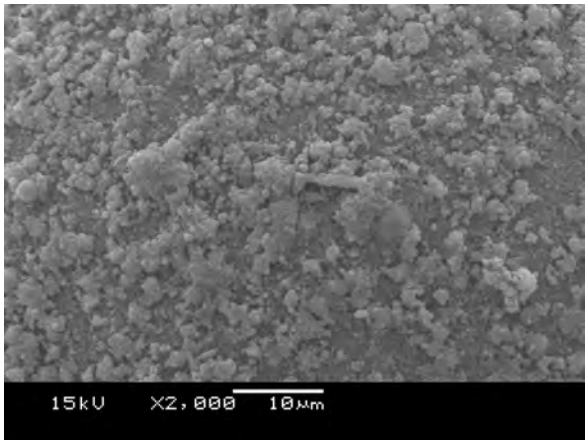

(d) Untreated Cenosphere sample 2 x2000

Figure 3.5: SEM images of untreated cenospheres

3.2.2 Unburnt Carbon

The 1990 Clean Air Act Amendments in the US set limits on NO_x emissions. Directive 2010/75/EU is the latest pollution control legislation for NO_x emissions in the EU, which replaces earlier directives [15, 107, 108]. In order to satisfy these regulations, low NO_x burners have been retrofitted to many coal combustion facilities. Combustion conditions that were hot and oxygen rich have been superseded by cooler, longer combustion conditions rich in fuel, combustion conditions which favour lower NO_x emissions [2, 15]. Such fuel-rich conditions lead to the incomplete combustion of the coal, and carbon content of the ash can increase up to 20 wt %. The carbon content of the CFA will also be influenced by coal. The increased carbon content of some CFAs raises the LOI above the 6 wt % permitted by the ASTM limits for use in cement. An excessive carbon content can adversely affect the properties of the cement as carbon can adsorb reagents added to cement to entrain air, without which cracks can form. The carbon content can be reduced through beneficiation in order to satisfy the necessary standards, and is concentrated in coarser size fractions [15, 86, 96, 109].

Carbon concentrates have a high surface area due to the porous nature of the carbon. Carbon concentrates are an inferior adsorbent when compared to activated carbon, however the cost relative to activated carbon can make carbon concentrates retrieved from CFA an attractive option for use in adsorption applications such as cleaning organic compounds from waste water [1]. Carbon concentrates that have been activated can be used as an adsorbent for NO_x, or could be coated in Rh to act as a catalyst and break down NO_x [14, 86]. The high calorific value of the carbon concentrates (5000-6000 kcal/kg) makes them suitable for use as a fuel, and they have potential applications as fillers, pigments and as a feedstock for the manufacture of activated carbon or the manufacture of graphite [1, 109].

Froth flotation can be used to separate carbon from the CFA. Froth flotation operates by introducing air bubbles to an aqueous suspension of ash. The hydrophobic nature of the carbon particles is exploited as they attach to air bubbles and float to the top of

the flotation vessel. Frothing agents can be used to maintain the froth, facilitating easy retrieval of a carbon concentrate. Due to the hydrophobic nature of the carbon particles, the quantity of frothing agent required is very low. Froth flotation is a commonly used in the processing of pulverised coal to reduce the ash content. Other forms of beneficiation include tribo-electrostatic separation and density separation [1, 11, 110, 111].

3.2.3 Magnetic Fraction of Fly Ash

The quantity of magnetic material in a CFA can vary from 0.5-18 wt % depending on the coal source and the combustion conditions [1, 109, 112–114]. Mineral phases present include maghemite, hematite, and Fe-spinel [109, 112]. The iron content of the magnetic concentrate can be 26-61 wt %, is enriched in trace elements and tends to consist of finer particles [109]. The thermal stability, relative chemical inertness and magnetic properties of the magnetic concentrate can be exploited for use in functional magnetic materials [109, 114], whilst the spinel structure of magnetospheres, combined with the presence of various transition metals, provides a potential application as a catalyst [112, 114]. The high density of the magnetic concentrate can be utilised in the form of a filler for high density concrete, whilst the high density and electromagnetic properties can be used as a filler for composite materials imparting with EM and radiation shielding properties [109, 112, 114].

3.2.4 Alpha Product

The fine inorganic fraction from RockTron's Alpha beneficiation process has a reduced alkali salt, cenosphere, carbon and iron content, with a LOI below 5 % and 5-6 % retention on a 45 μm sieve [115]. The low LOI and PSD satisfy ASTM standards and BS EN450, the latter of which requires <10-12 wt % retained on a 45 μm sieve. The reduced LOI allows for a greater quantity of ash to be substituted for Ordinary Portland Cement, and the reduction in impurities improves the pozzolanic properties of the cement thus improving the strength gain [115]. The chemical composition of the Alpha product is shown in Table

3.1. The XRD analysis of Alpha is shown in Figure 3.6.

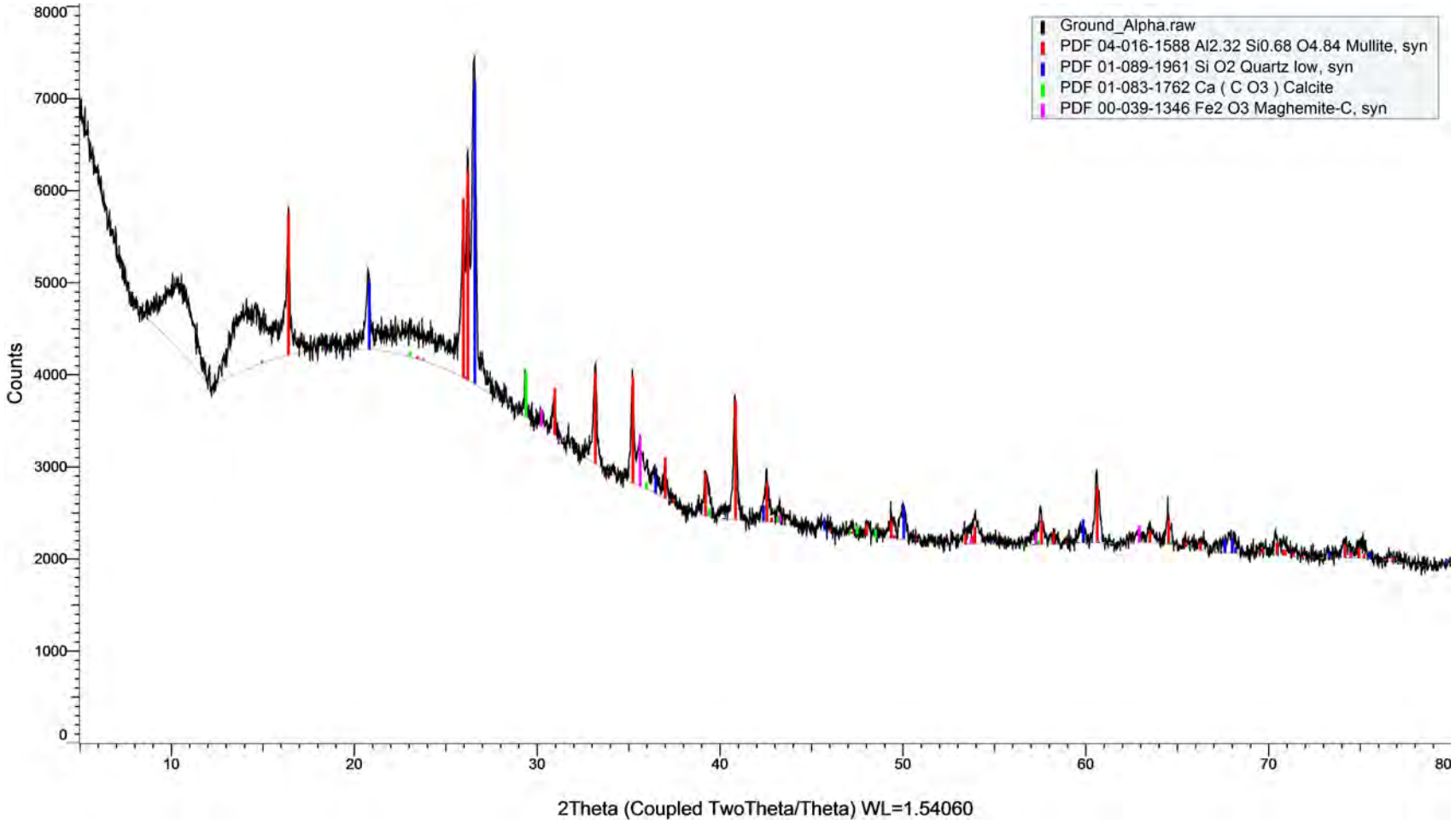

Figure 3.6: XRD Pattern of Alpha ash

3.2.5 Delta Product

As with the Alpha product, the Delta product has been through the same processes to reduce the alkali salt, cenosphere, carbon and magnetic content, leaving a material consisting of mostly aluminosilicates. The chemical composition is shown in Table 3.1. The main applications of Delta are as an aggregate or filler. Due to the coarser particle size, Delta is considered too inert to be used to replace Ordinary Portland Cement. Figures 3.7 and 3.8 show the Delta ash at various magnifications. Of note are Figure 3.7b, which shows a broken cenosphere on the right; Figures 3.7c, 3.7e and 3.7f, which show amorphous material; Figures 3.7b, 3.7d, 3.7e and 3.8b, which show smooth surfaced spheres; and Figures 3.7d and 3.8a, which show a plenosphere. These images are similar to other images of CFA in literature [38]. The PSD is shown in Figure 3.9, which is supported by the SEM images. The XRD pattern shown in Figure 3.10 shows prominent peaks for mullite and quartz, with smaller peaks for calcite and maghemite. Due to the high aluminosilicate content, the Delta ash is deemed suitable for use as a feedstock for zeolitisation, and is used in the majority of experiments in this thesis.

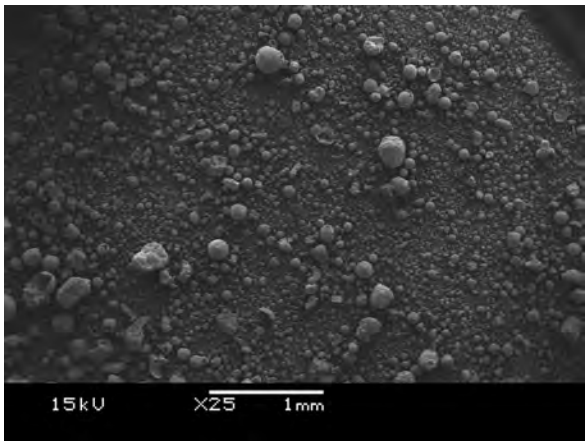

(a) Delta Example 1 x25

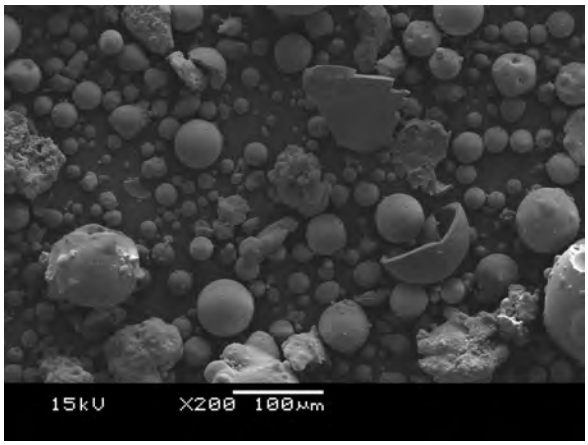

(b) Delta Example 1 x200

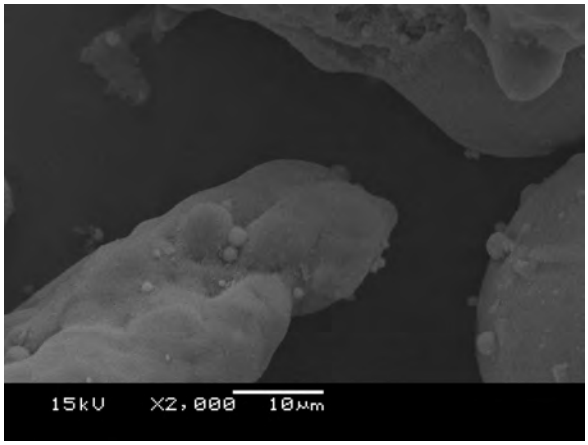

(c) Delta Example 1 x2000

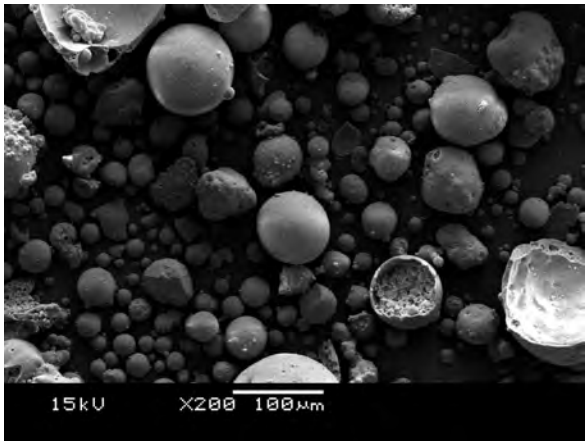

(d) Delta Example 4 x200

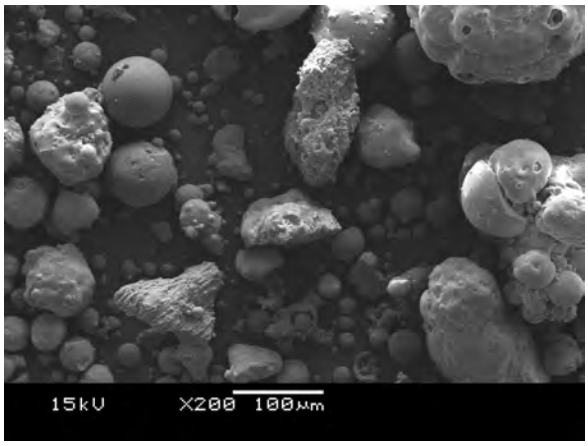

(e) Delta Example 5 x200

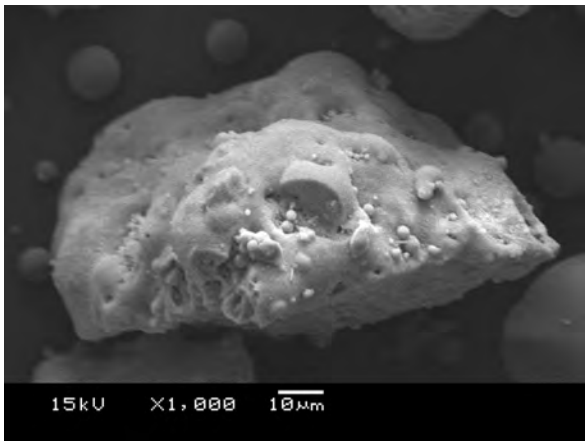

(f) Delta Example 5 x1000

Figure 3.7: SEM images of Delta product

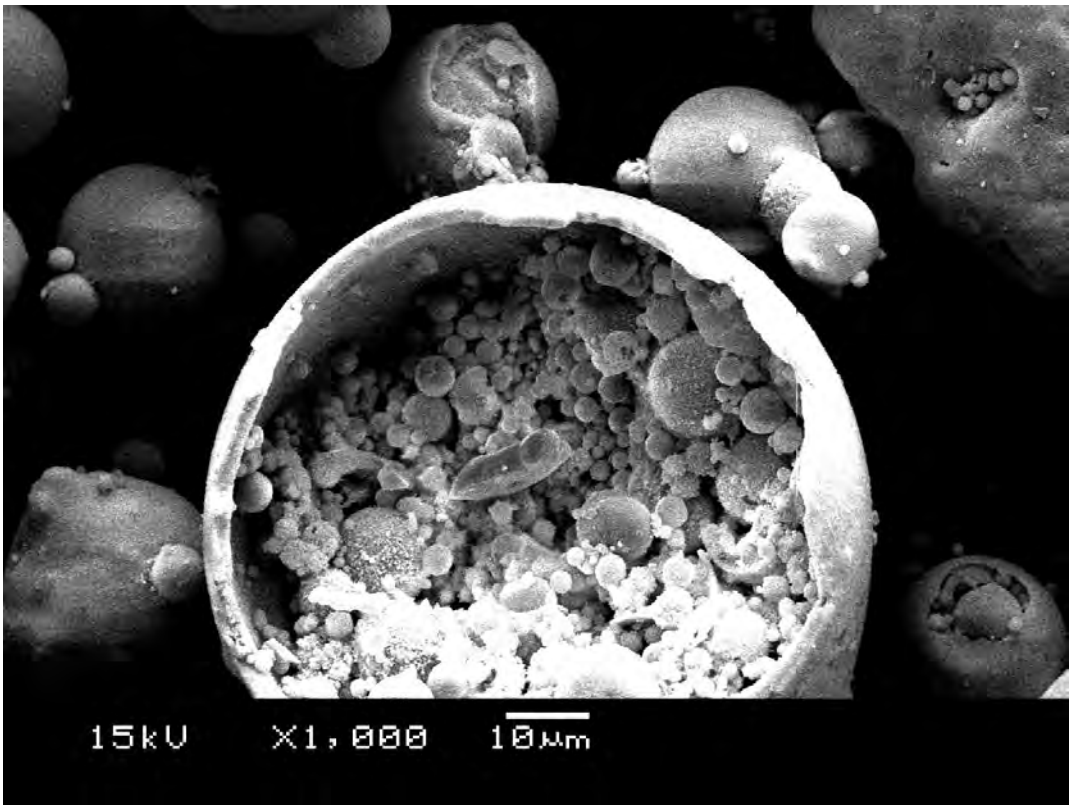

(a) Delta Example 3 x1000

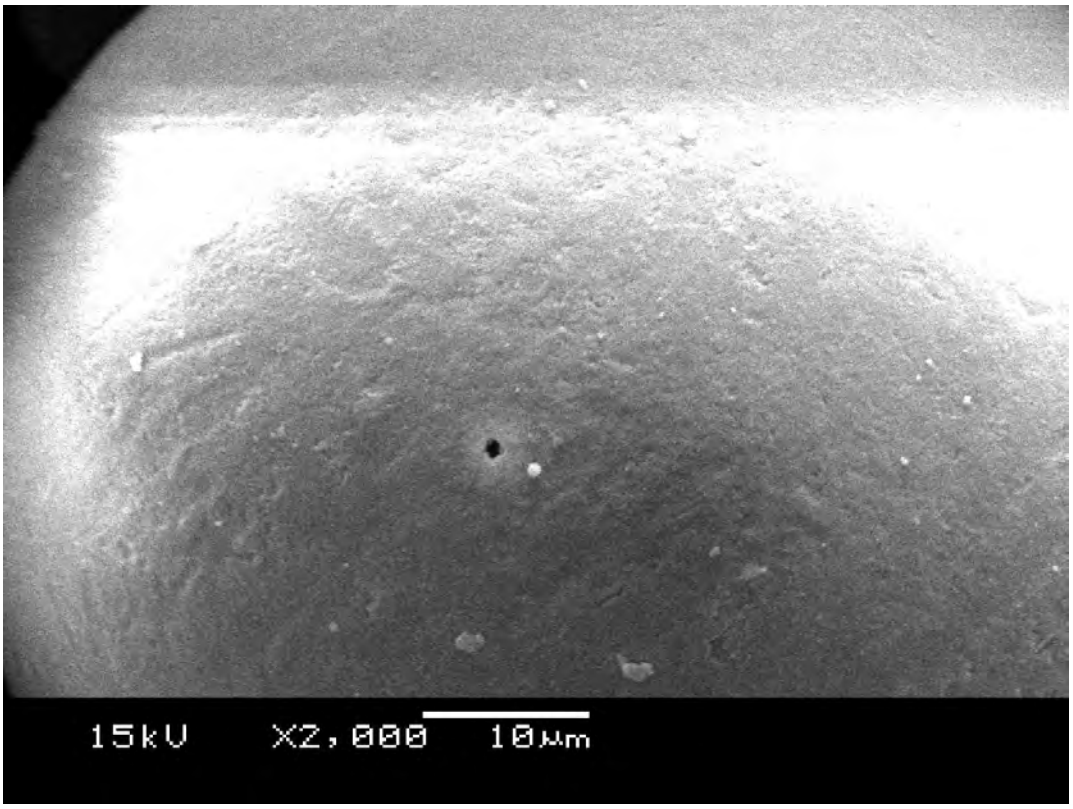

(b) Delta Example 4 x2000

Figure 3.8: Larger SEM images of Delta product

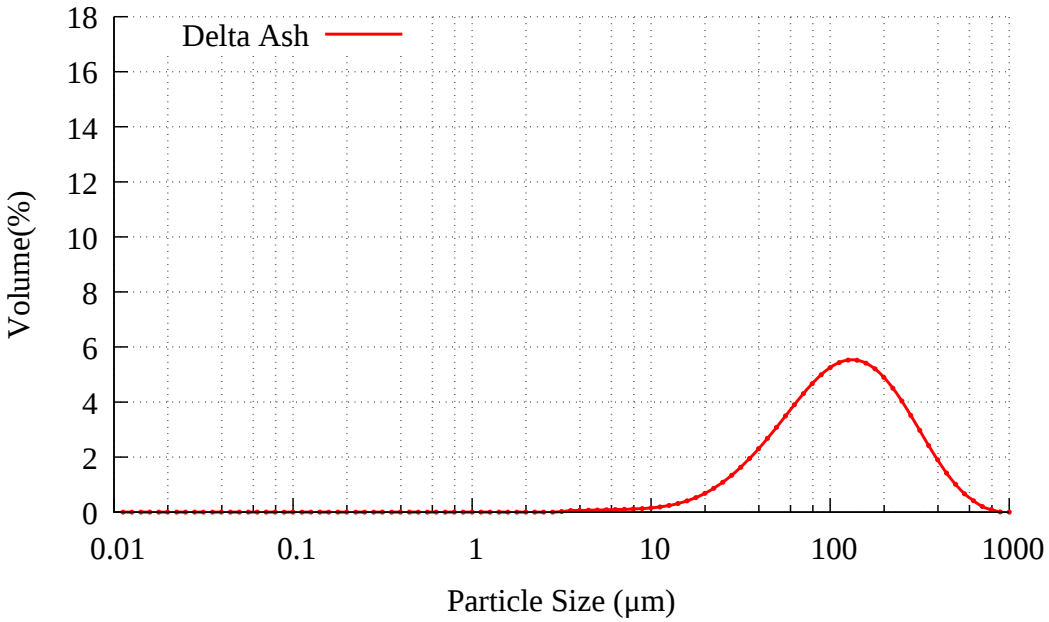

(a) PSD of Delta ash

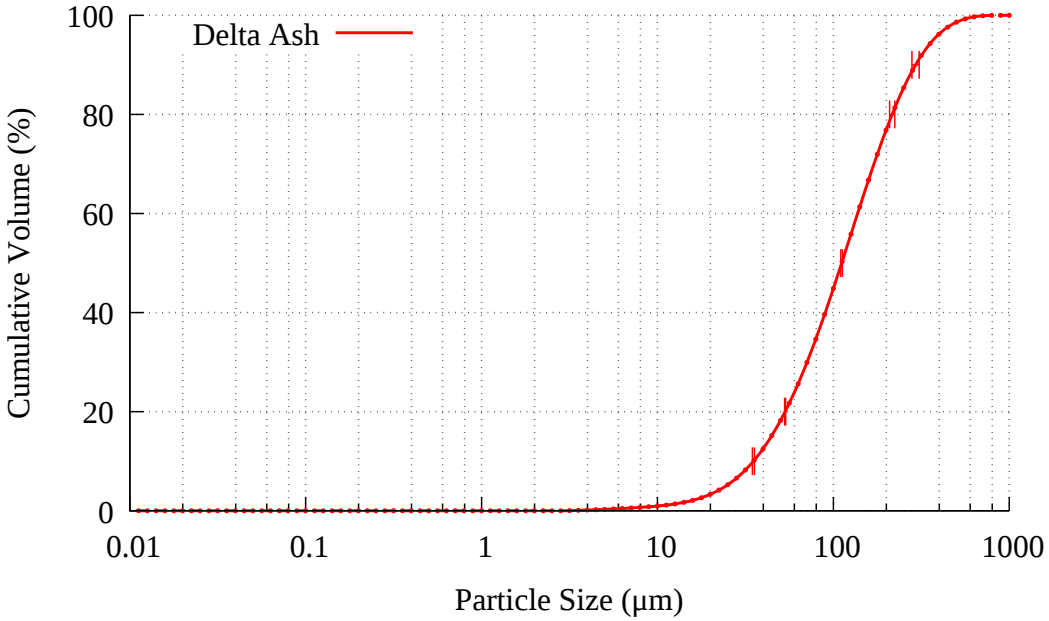

(b) Cumulative PSD of Delta ash

Figure 3.9: PSD and cumulative PSD of Delta ash

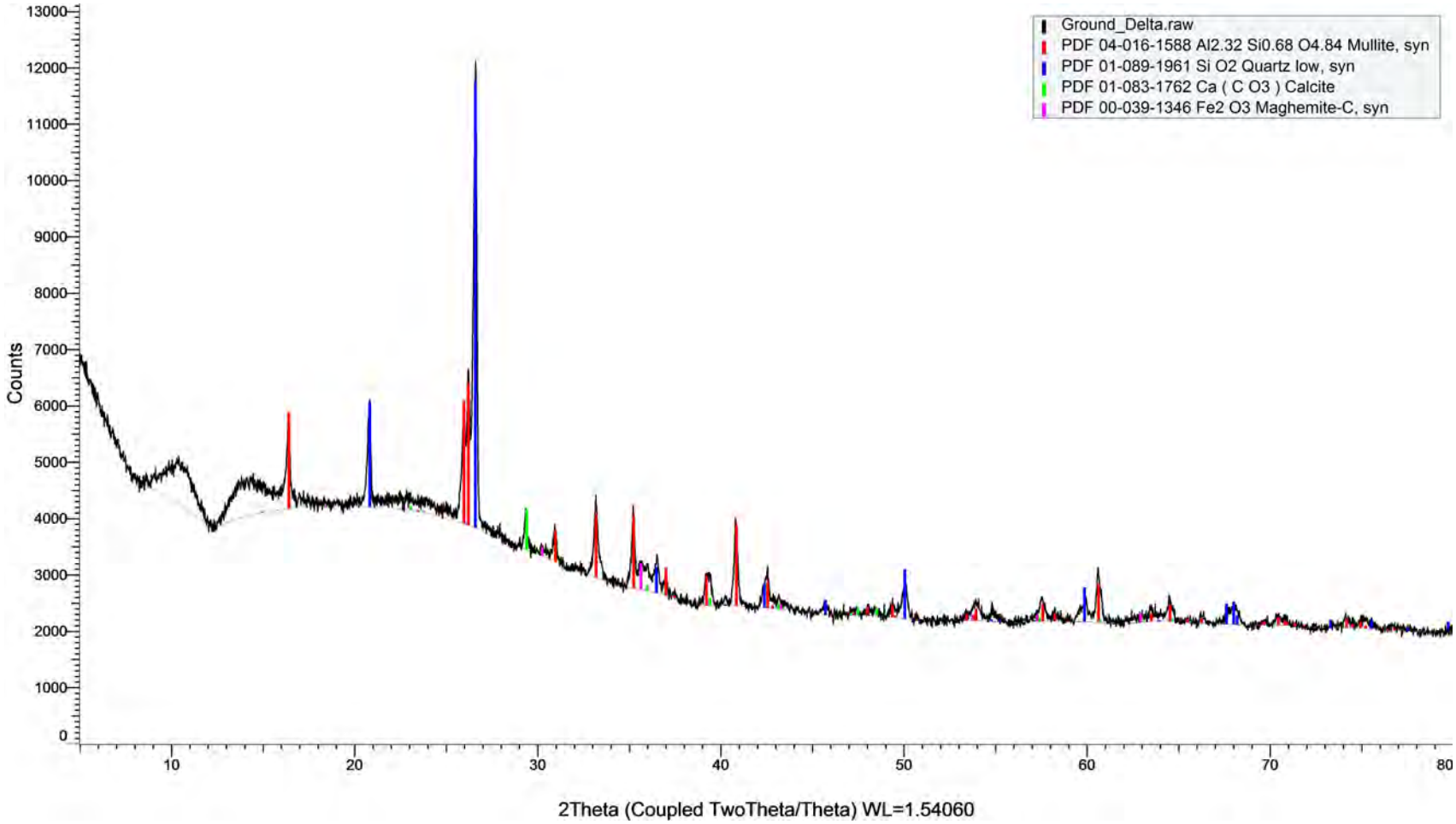

Figure 3.10: XRD Pattern of Delta ash. $\lambda = 1.5406$ Å

3.3 Rice Husk Ash (RHA)

Rice producing countries such as those in South, East and Southeast Asia, as well as Brazil and the US have a plentiful supply of rice husks, which is an agricultural waste product. Using rice husks as a biomass fuel is a CO_2 neutral solution to the energy requirements of these regions [116]. Rice husks form approximately 30 % of the mass of a rice kernel and are approximately 20 % silica. The ash produced from the burning of rice husks is mostly amorphous silica, with some carbon and various trace elements depending on combustion conditions [116–119]. RHA has potential applications as a filler [120–122], as an adsorbent material for heavy metals and dyes in waste water streams [123], catalyst support [122], and as a stabilisation agent for soils [124]. The fine nature of the RHA along with the amorphous nature of the silica make it suitable for use as a pozzolanic material, improving the properties of concrete it is incorporated into [116, 119, 122, 125]. RHA can be used as a reagent in lieu of amorphous silica for the synthesis of mesoporous silica for carbon capture [126]. Such applications of RHA as a reagent in place of amorphous silica are broad, and discussed by Pode [116] and Chandrasekhar et al. [122]. As with CFA, the amorphous silica can be dissolved in alkaline environments for the synthesis of zeolites [66, 118, 127].

Six RHA samples supplied by Torftech Ltd. were characterised. LOI, XRF, XRD and PSD were measured and SEM images were taken. The six samples were produced using Torftech's TORBED reactor technology, with bed temperatures from 700-950°C. LOI indicates a slightly raised carbon content under 700°C combustion conditions, shown in Figure 3.11 and table 3.2. Higher combustion temperatures would be expected to result in a higher combustion efficiency, so a slightly elevated LOI for the lowest bed temperature is not unreasonable, however the LOI for all bed temperatures is very low at >2 %. The bulk chemistry is shown in Table 3.3. This shows a silica content of over 95 % for all conditions, with potassium, phosphorous and calcium being the next most prevalent elements. The XRD patterns in Figure 3.12 show cristobalite detected at the highest temperatures. Crystalline silica such as cristobalite is undesired as it is

less soluble than amorphous silica, and fine, respirable silica is hazardous due to the potential for silicosis. This is in agreement with literature sources, which indicate that cristobalite/ crystalline material formation begins at temperatures between 700 and 900°C [116, 125, 128]. SEM images in Figures 3.13 and 3.14 show similarities to the parboiled husk starting material shown in Figure A.1 on page 364. The PSD shown in Figure 3.15 indicates a very slight coarsening of the PSD as temperature increases. This could be attributed to silica becoming cohesive at higher temperatures resulting in agglomeration, as indicated in literature [116].

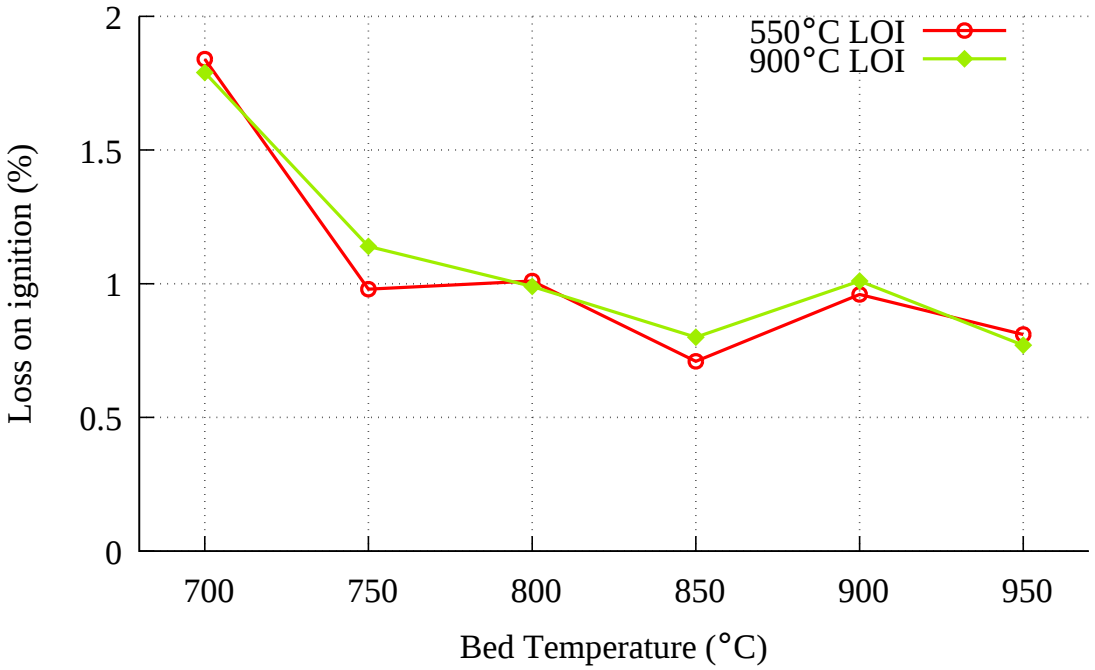

Figure 3.11: LOI of 6 RHA samples at 2 ignition temperatures

Table 3.2: LOI of 6 RHA samples at 2 ignition temperatures

LOI	700°C	750°C	800°C	850°C	900°C	950°C
550°C	1.8%	1.1%	1.0%	0.8%	1.0%	0.8%
900°C	1.8%	1.0%	1.0%	0.7%	1.0%	0.8%

Table 3.3: Bulk chemistry of rice husk ash. Results in wt %.

Sample	700°C	750°C	800°C	850°C	900°C	950°C
LOI	1.8	1.1	1.0	0.8	1.0	0.8
SiO_2	95.2	96.3	96.0	96.0	95.7	96.7
K_2O	0.8	0.6	0.7	1.1	1.0	0.7
P_2O_5	0.5	0.5	0.6	0.6	0.7	0.6
CaO	0.5	0.3	0.4	0.6	0.6	0.4
Fe_2O_3	0.3	0.3	0.3	0.4	0.4	0.3
MgO	0.3	0.3	0.2	0.2	0.2	0.2
Other	0.6	0.6	0.7	0.4	0.5	0.3

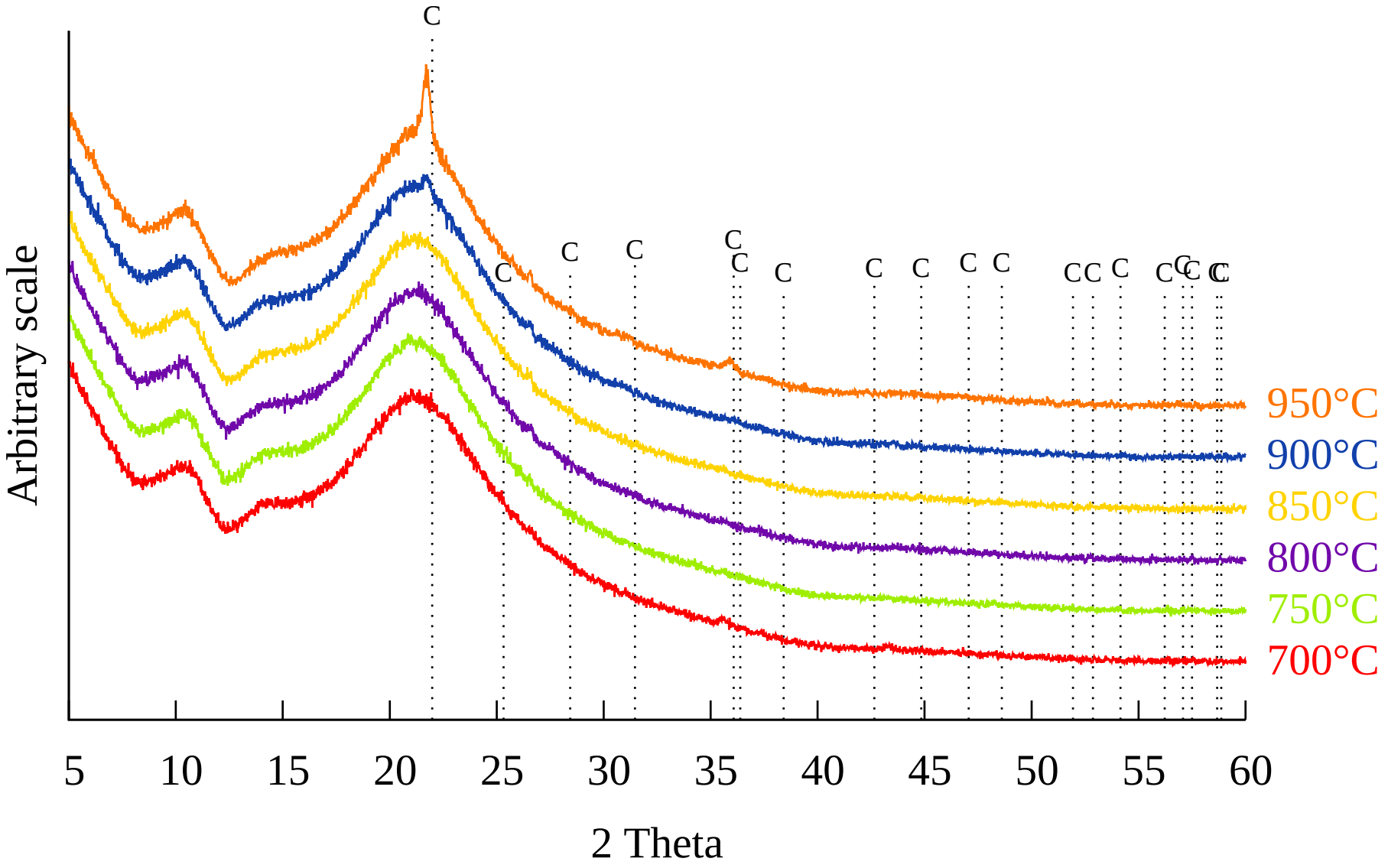
C
C
C

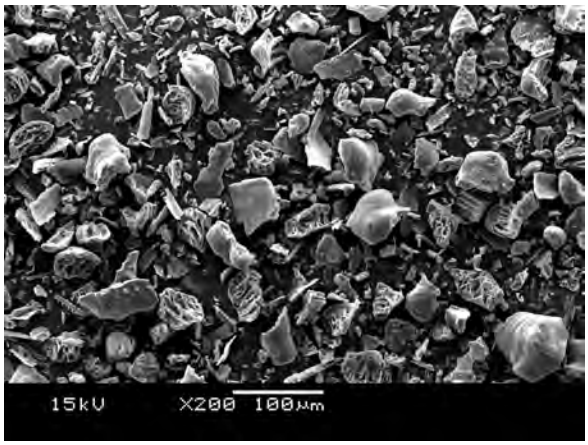

(a) 700°C

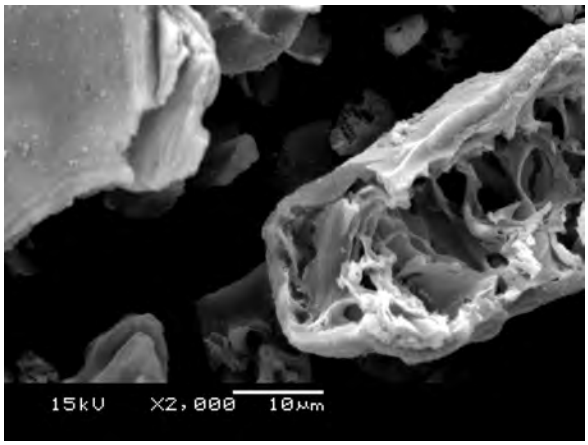

(b) 700°C

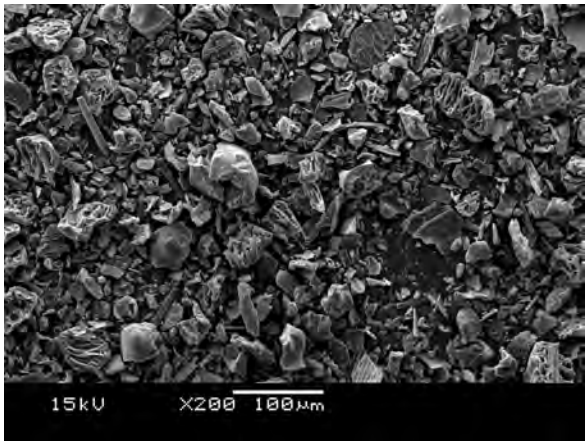

(c) 750°C

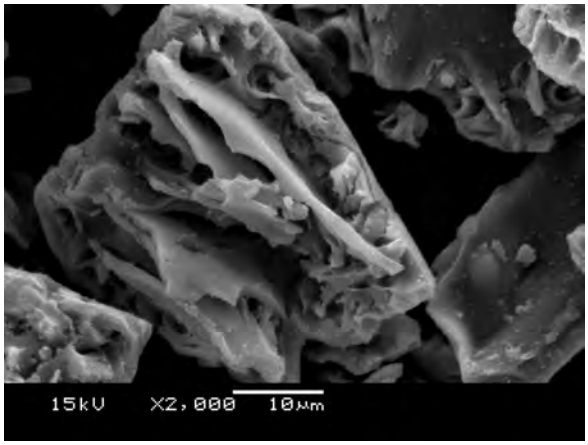

(d) 750°C

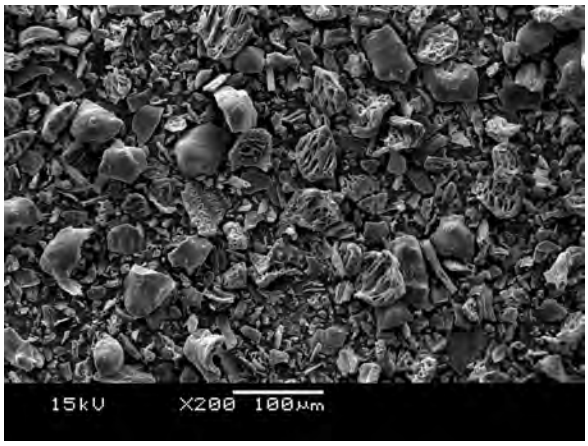

(e) 800°C

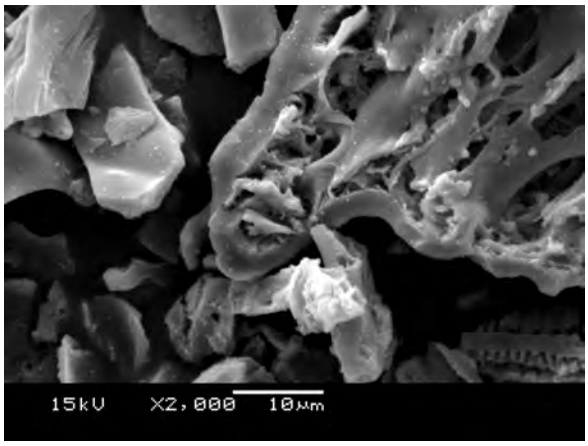

(f) 800°C

Figure 3.13: SEM images of RHA from 3 bed temperatures

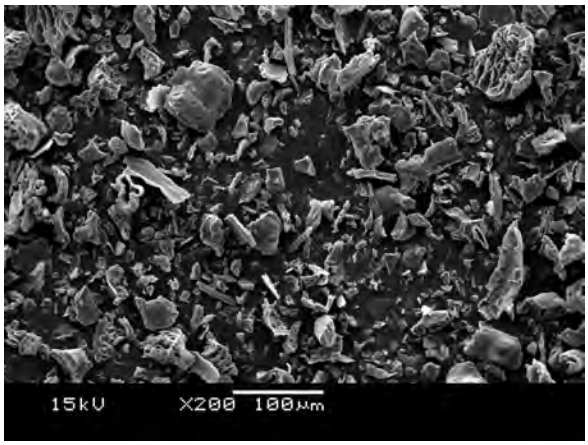

(a) 850°C

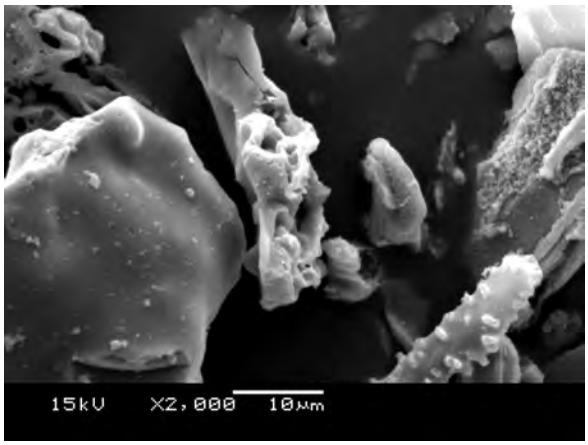

(b) 850°C

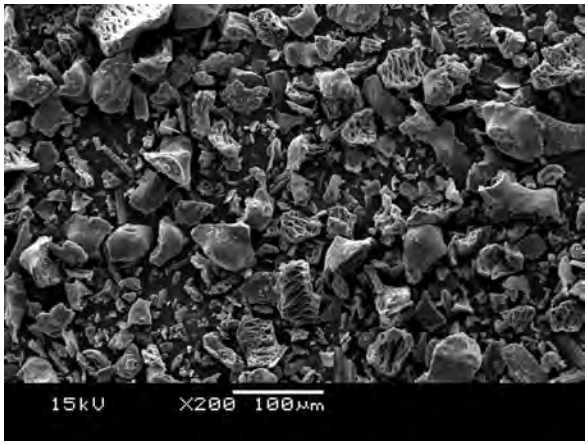

(c) 900°C

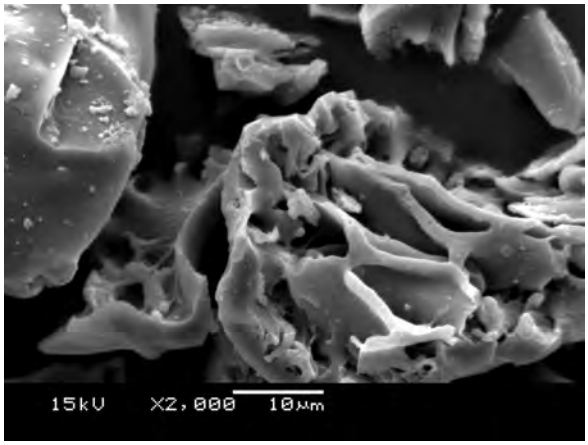

(d) 900°C

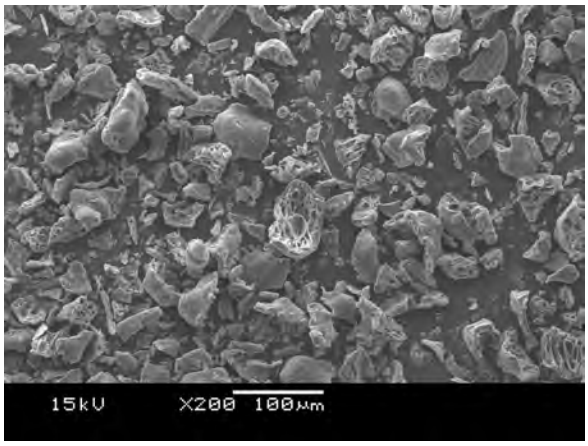

(e) 950°C

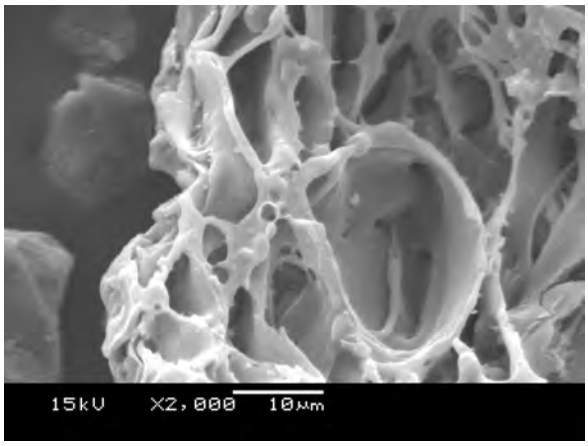

(f) 950°C

Figure 3.14: SEM images of RHA from 3 further bed temperatures

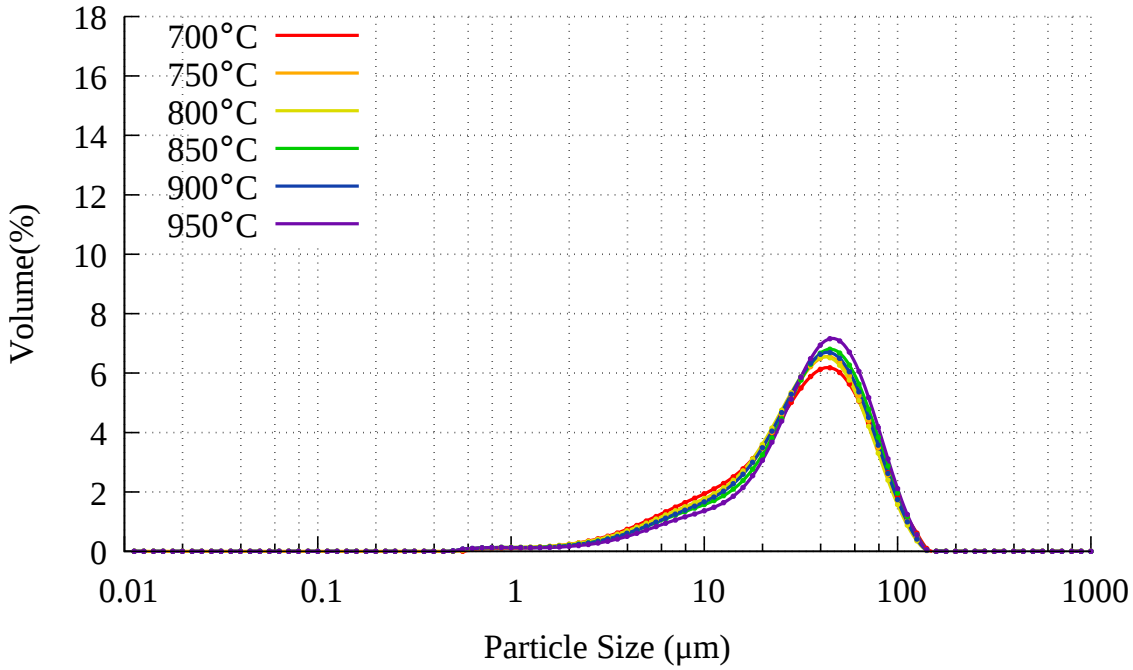

(a) PSD at various bed temperatures

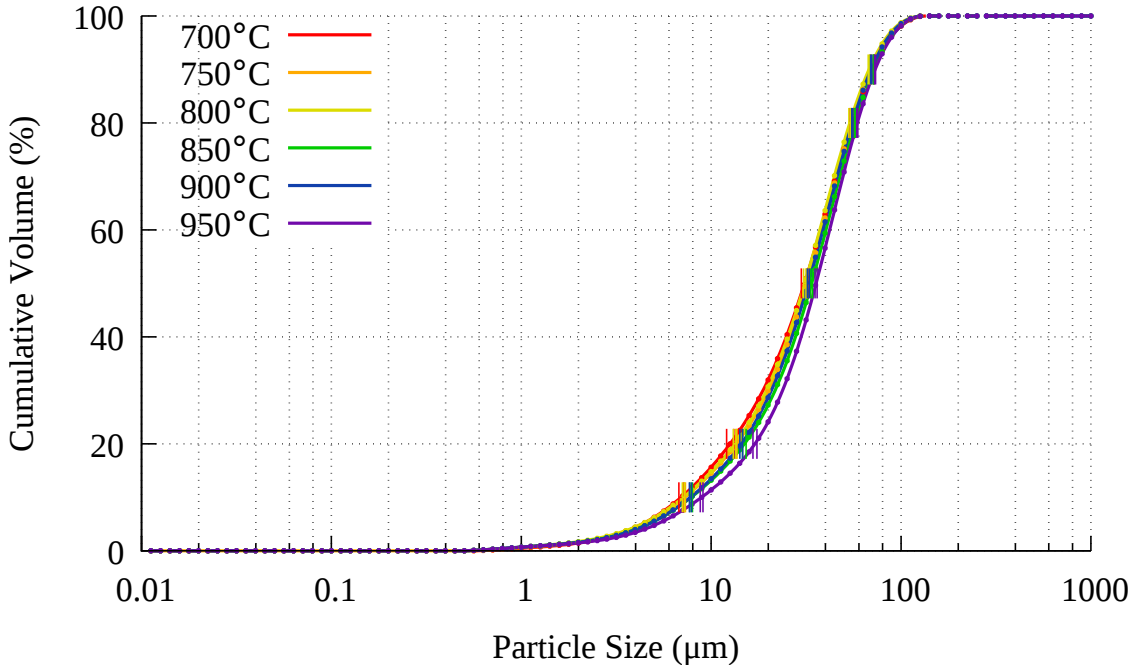

(b) Cumulative PSD at various bed temperatures

Figure 3.15: PSD and cumulative PSD of RHA at various bed temperatures

3.4 Reagents

AR grade (Ph. Eur, BP) sodium hydroxide (NaOH) pellets were supplied by Fisher Scientific (cat No. S/4920/60), CAS number 1310-73-2. AR grade sodium carbonate (Na_2CO_3) was supplied by Fisher Scientific (cat No. S/2920/60), CAS number 497-19-8. Technical grade sodium aluminate (SA) was supplied by Sigma Aldrich (cat No. 13404-5KG-R), CAS Number 11138-49-1, comprising Al (as Al_2O_3) 50-56 %, Na (as Na_2O) 40-45 %, with $\leq$ 0.05 % Fe (as Fe_2O_3). "Salt" used was supermarket table salt. "Sea salt" used was coarse supermarket sea salt, without anti-caking agents. Sea salt was used in lieu of generating synthetic seawater for simplicity and convenience.

3.5 Analysis Techniques

3.5.1 AAS

Atomic Absorption Spectrometry (AAS) analysis of alkaline leachate was conducted using a Perkin Elmer AAnalyst 800.

3.5.1.1 Principles of Operation

AAS uses the Beer-Lambert Law (equation 3.1) to determine the concentration of an element in solution [129, 130].

$$A = log_{10}\left(\frac{I_0}{I}\right) = \varepsilon bc \tag{3.1}$$

Where:

- A = absorbance
- I_0 = irradiance of a beam entering a sample (W)
- I = irradiance of a beam leaving a sample (W)
- c = molar concentration (mol L^{-}1)

- ε= absorptivity (L mol$^-$1 cm$^-$1)
- b = path length (cm)

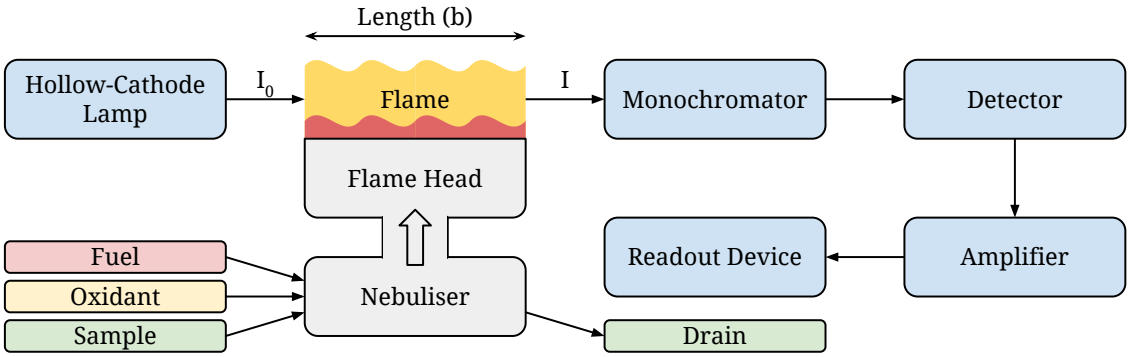

Figure 3.16: Atomic Absorption spectrometer diagram

An atomic absorption spectrometer works by measuring the amount of light of a specific frequency absorbed by an atomised sample in the flame as shown in figure 3.16. As the concentration of the element in the flame increases, the irradiance of the light leaving the flame decreases. This change in concentration can be compared to a set of standards of known concentration and the concentration of the element in the sample can be quantified.

3.5.2 CEC

The Cation Exchange Capacity (CEC) is a measure of the exchangeable material in the zeolite, measured in equivalents of charge, thus one equivalent is equal to one mole of Na^+ or half a mole of Ca^2+. The CEC of samples was analysed using an ammonium acetate method based on similar methods in literature [6, 25, 54, 76, 90]. 2.00 g of sample was added to 100 ml of 1.0 M sodium acetate and stirred at 300 rpm for 20 minutes, the sample filtered and washed with 1.0 L of distilled water, then mixed with 100 ml of 1.0 M ammonium acetate and stirred at 300 rpm for 20 minutes. The sample was then filtered and the filtrate retained for AAS analysis of the Na content.

The CEC is calculated from this using equation 3.2, where CEC is the Cation Exchange Capacity of the zeolite in milliequivalents per gram (meq/g), $[Na]$ is the concentration of sodium in the 100 ml ammonium acetate solution (g/L), RAM is the relative atomic mass of sodium (23), S is the scaling factor of the ammonium acetate solution (0.1), Z is the mass of zeolite (g).

$$CEC = 1000 \left(\frac{\left(\frac{[Na]}{RAM} \right) S}{Z} \right) \tag{3.2}$$

3.5.3 LOI

Loss On Ignition (LOI) for RHA was conducted on 2.00 g samples in a Carbolite ELF furnace for 2 hours at 900°C or for 4 hours at 500°C.

3.5.4 PSD

The Particle Size Distribution (PSD) was analysed using a Malvern Mastersizer 2000. Samples were dispersed in distilled water using a Hydro 2000SM dispersion unit.

3.5.4.1 Principles of Operation

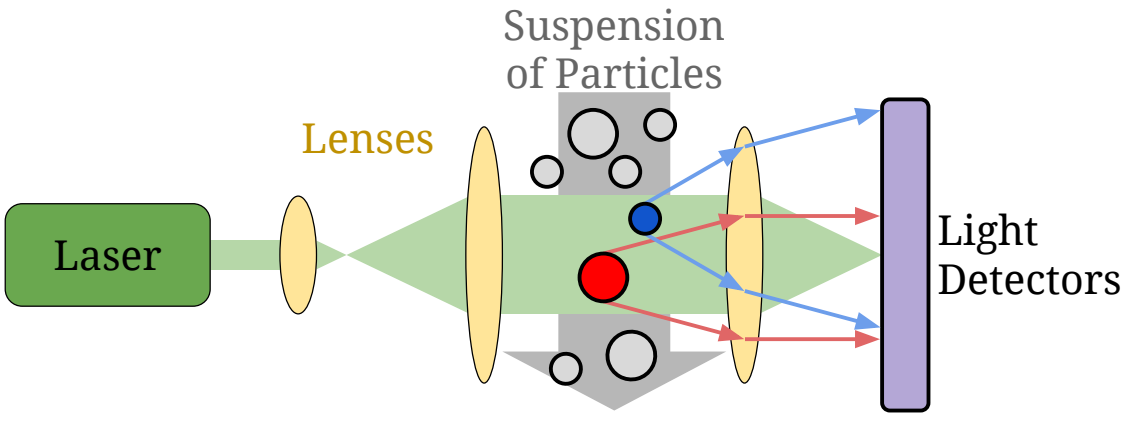

Figure 3.17: Use of laser diffraction in PSD analysis

Particles of light suspended in a solution will diffract light. Smaller particles will diffract light more than larger particles. The particle size distribution can be ascertained

by passing a suspension of a sample through a laser beam as shown in figure 3.17. The scattering of the light can be measured in order to determine the particle size distribution. Mie theory requires knowledge of the refractive indices of the solid and solution. It is noted that this method is sensitive to anisotropic particles [131].

3.5.5 SEM

Samples for Scanning Electron Microscopy (SEM) analysis were sputter coated with gold using an Emscope SC500 sputter coater and analysed with a Jeol JSM-6060LV scanning electron microscope.

3.5.5.1 Principles of Operation

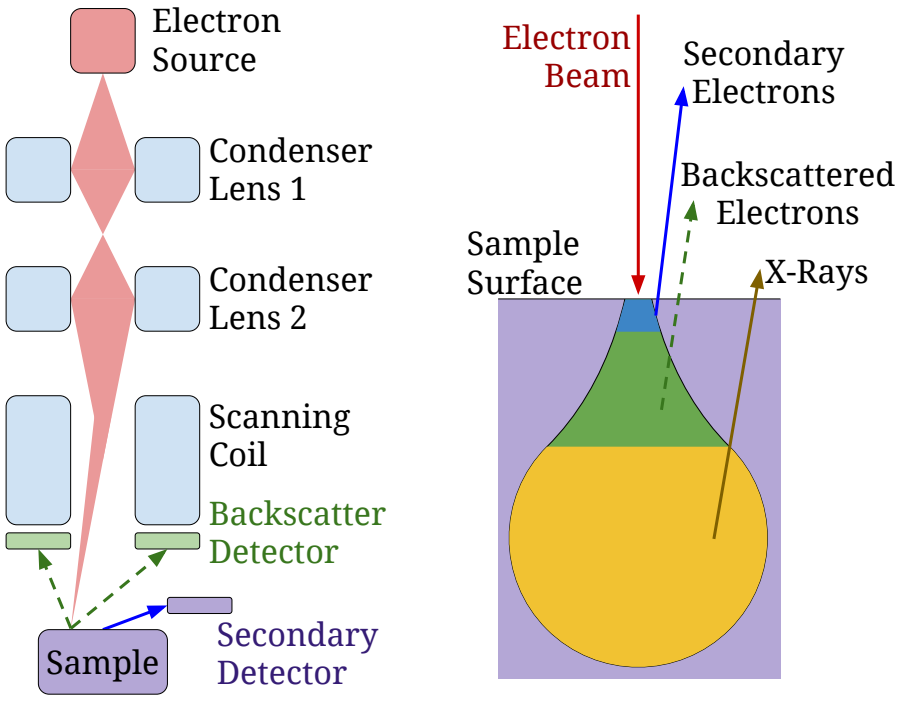

Figure 3.18: Scanning Electron Microscopy Principles of Operation

Scanning electron microscopy works by firing an electron beam at a sample in a raster pattern. The electrons interact with the sample as shown in figure 3.18. When the electron beam hits the sample, electrons from the sample are displaced, and can leave the sample in the form of secondary electrons. These are low energy electrons and therefore can not

travel far through the sample before being absorbed. This makes secondary electrons highly suited for analysing the topography of a sample, as the only secondary electrons which can escape the sample come from the surface of the sample. The electrons from the electron beam leave the sample as backscattered electrons, and X-rays are released by the sample through x-ray fluorescence. This can be utilised in energy dispersive x-ray fluorescence to analyse the elemental composition of a sample [132–134].

3.5.6 XRD

X-Ray Diffraction (XRD) analysis was carried out using two instruments. Figures 3.2, 3.3, 3.6, 3.10, 3.12, 4.23, 4.24 and 7.25 were analysed using a Bruker D8 reflection X-ray diffractometer with Cu-Kα radiation (1.5406 Å). All other XRD analysis was conducted using a Brucker D8 transmission diffractometer with Cu-Kα radiation (1.5406 Å).

3.5.6.1 Principles of Operation

XRD exploits Bragg's law (equation 3.3 to measure the distance betweeen atomic nuclei in crystalline materials. This is shown in figure 3.19. An x-ray of known wavelength λ is fired at a crystalline sample. A detector 2θ degrees away from the x-ray source measures the intensity of the x-rays leaving the sample, as shown in figure 3.19. For some values of θ, constructive interference will occur with the x-rays which leave the sample, resulting in a large increase in the intensity of x-rays measured by the detector [135].

$$\lambda = 2d \sin \theta \tag{3.3}$$

- λ = wavelength
- d = lattice spacing (Å)
- θ = angle of incidence

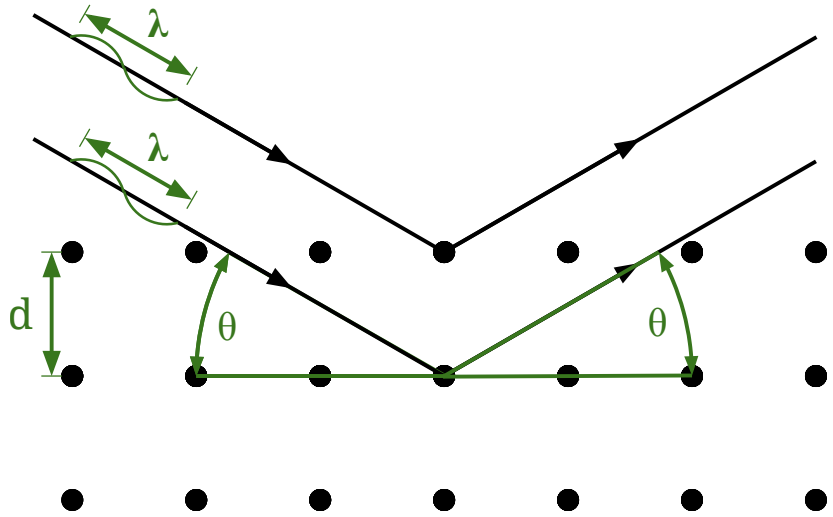

Figure 3.19: XRD Principles of Operation

3.5.7 XRF

X-Ray Fluorescence (XRF) analysis of RHA was conducted using a Bruker S8 Tiger wavelength dispersive X-ray fluorescence spectrophotometer with a rhodium source. Samples were formed into pressed pellets for XRF using 0.50 g of RHA and 0.10g of Chemplex SpectroBlend binder.

3.5.7.1 Principles of Operation

The chemical composition of a sample can be determined using x-ray fluorescence. An incident x-ray beam excites electrons in low orbitals to a higher orbital. Electrons from higher orbitals then descend to lower orbitals. As they descend, they release x-rays of a frequency characteristic to the element they were released from, and the shells between which they moved, as shown in figure 3.20. This technique is not effective at detecting elements lighter than sodium, due to the limited number of electron shells [136, 137].

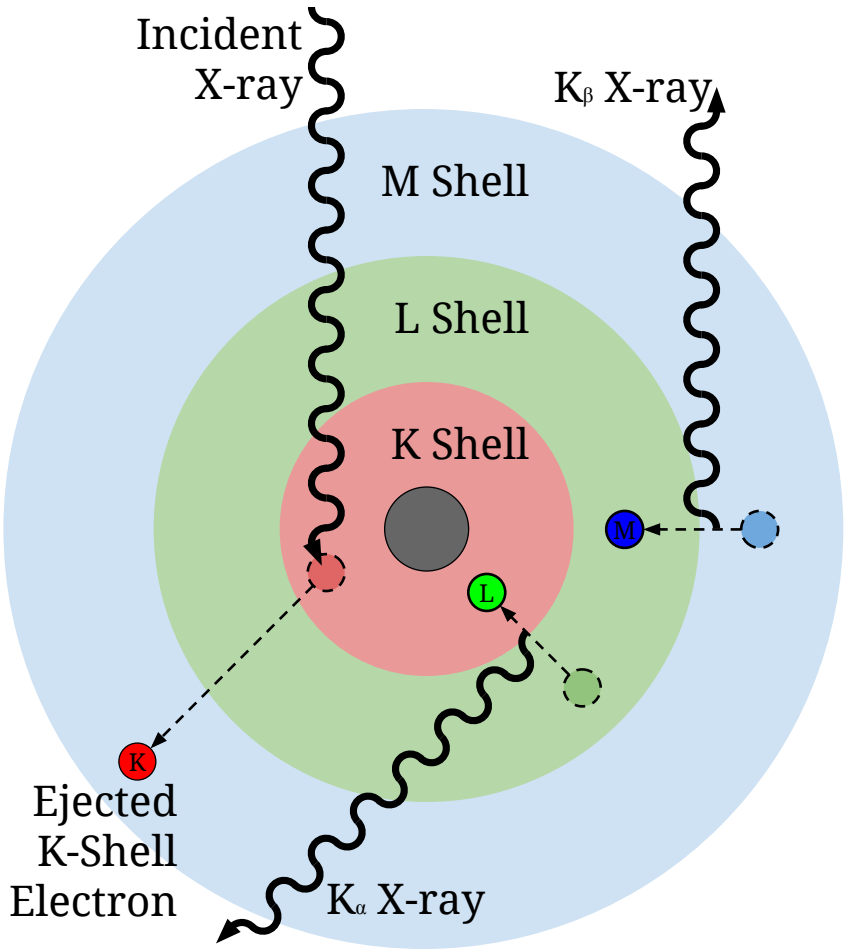

Figure 3.20: XRF Principles of Operation

Chapter 4

Extraction of Si and Al from Processed Coal Fly Ash

4.1 Introduction

In order to achieve the highest efficiency in the production of synthetic zeolites from processed coal fly ash, the extraction of Si and Al must be optimised. To attain a high yield of synthetic zeolite, a high Si content in the leachate is desired. The Si and Al content of the leachate must be known, in order to add the appropriate quantity of sodium aluminate so that a constant Si:Al ratio can be maintained. Ideally, sufficient Al would be extracted from the fly ash so that addition of sodium aluminate is not necessary, however such additional expenditure is not prohibitive, and grants flexibility in the extraction process. A variety of extraction conditions were investigated, and the Si and Al content of leachates from these experiments were analysed using AAS.

4.1.1 Experimental Approach

The statistical design of experiment approach was considered for the subsequent experiments. Such an approach would make the experimental workload lighter, but provide a less comprehensive set of data. It was decided that a more comprehensive data set was

preferable, and thus the statistical design of experiment approach was not used.

4.1.2 Experimental Conditions Investigated

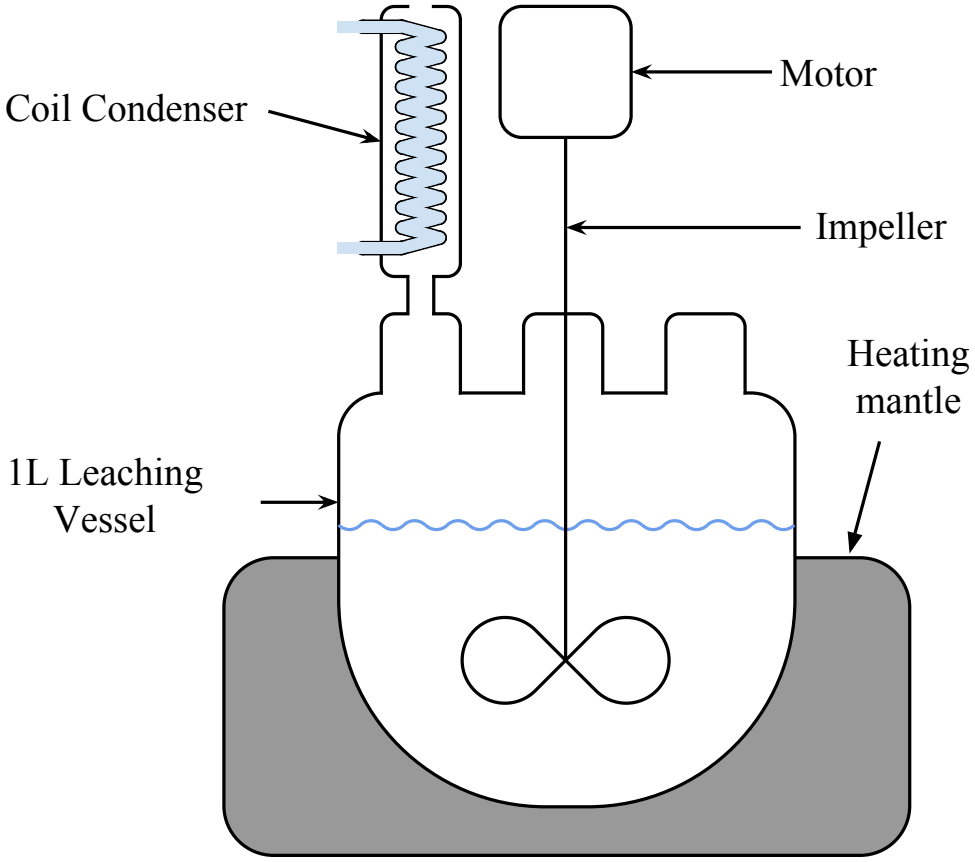

Figure 4.1: Diagram showing equipment setup for reflux reactions (not to scale)

Extraction conditions investigated were:

- NaOH (2-4 M) concentration of hydrothermal extraction.
- Substitution of 0-50 % of NaOH with Na_2CO_3, maintaining constant [OH] during hydrothermal extraction.
- Conventional fusion with ground NaOH and ground processed fly ash.
- Conventional fusion without grinding.
- Water temperature during dissolution of fusion products: ambient and reflux.

Figure 4.2: Photograph showing equipment setup for reflux reactions depicted in Figure 4.1

- Microwave fusion.
- Solids loading.

- Re-use of ash that has already undergone extraction.
- Different source ashes.

The hydrothermal extraction apparatus is shown in Figures 4.1 and 4.2. The hydrothermal extraction process described by Hollman et al. [26] where the ash is filtered out to produce a leachate from which a pure zeolite is crystallised, was combined with a fusion extraction process adapted from Belviso et al. [38], and a novel microwave fusion process. Conditions for fusion and dissolution of the fusion product were varied. In an attempt achieve complete dissolution of the ash, acid was used to wash off the zeolite coating formed on the ash surface during hydrothermal leaching prior to re-leaching in order to increase Si yield from ash.

4.1.3 Microwave Fusion

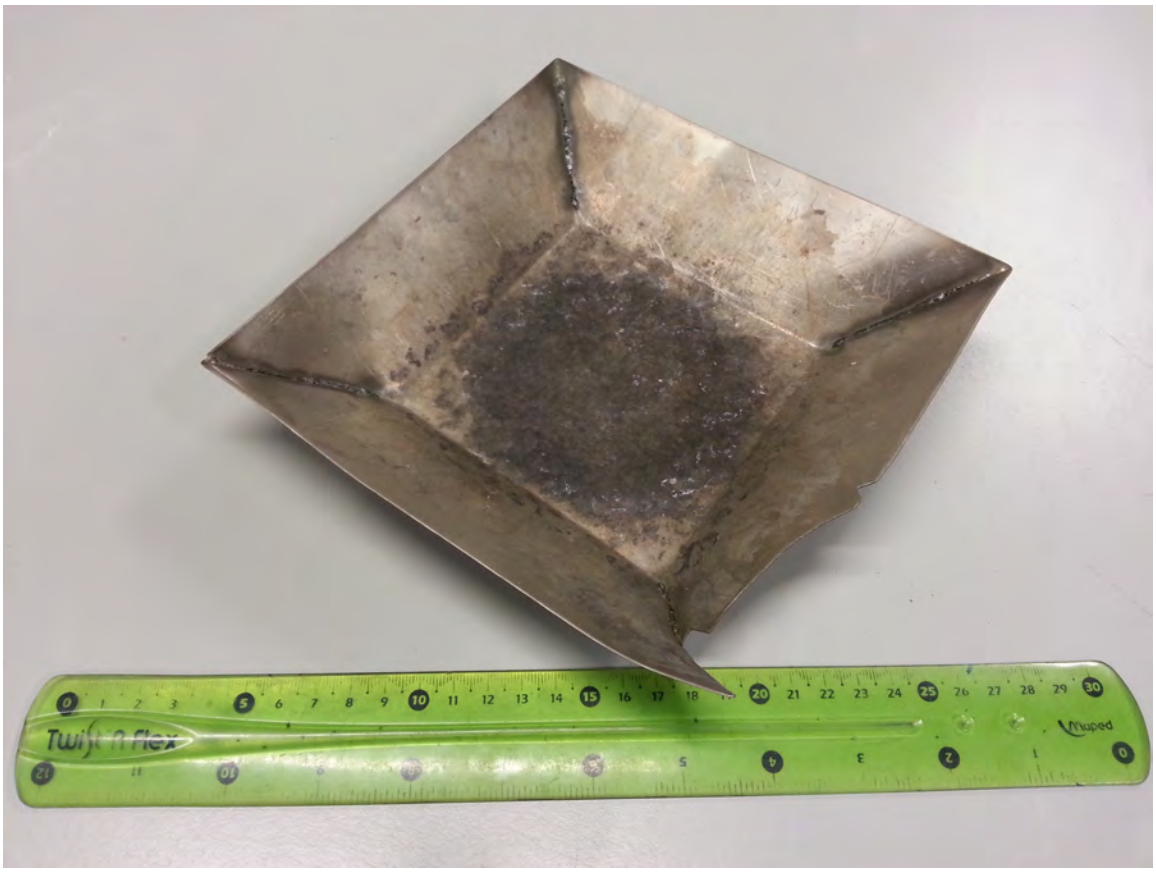

Figure 4.3: Vessel manufactured for microwave fusion

Microwave fusion was first explored as an alternative to using a muffle furnace as a heat source. A 700 W 2.45 GHz domestic microwave was used due to availability and cost. Challenges were presented in the choice of reaction vessel. The first vessel chosen was a PTFE beaker. The melting point of PTFE (327°C) is higher than that of NaOH (318°C), but not by much. At first this vessel was sufficient to prove that a microwave was capable of melting NaOH mixed with ash. This required the microwave to not be set on full power, and the contents of the beaker required frequent stirring to minimise hot pockets forming. The beakers used became deformed after multiple uses. It was decided that a new reaction vessel would be necessary. Attempts using a large nickel crucible were less effective, as only the top and centre most parts of the sample were melted. It is believed that the sides of the crucible were blocking microwaves from interacting with the bulk of the sample, as the rim of the crucible was significantly higher than the level of the sample. In order to avoid blocking microwaves from reaching the bulk of the samples a new vessel was desired, one with low sides, but a sufficient volume to carry the quantities of ash and NaOH used. A new fusion vessel was fabricated from sheet nickel. Nickel was selected due to its resistance to molten sodium hydroxide [138]. As well as low sides, the vessel was designed to have obtuse angles where possible to minimise possibility of arcing. The fabricated vessel is shown in Figure 4.3, blackened after repeated use.

4.1.4 Error and Repeatability

Error bars provided on AAS plots account for variation between the 3 measurements (unless otherwise stated) taken by the AAS, and the expected error introduced through inaccuracies of pipettes and volumetric flasks used in the dilution process. Ideally each experiment would be carried out and measured in triplicate, however such an approach would be prohibitively time consuming and costly, and was deemed outside of the remit of this work.

Two data sets have been compiled for repeatability: the most commonly used extraction method (see Figure 4.31) and the preferred crystallisation conditions (figure 6.83a)

which take averages of 44 and 5 samples respectively. In light of this, experiments that have not been repeated are used for their qualitative value, rather than providing any quantitative results. For most data points, the error bars are quite small, and so could be considered superfluous, however some AAS results were not as closely grouped as the rest, introducing significant errors, thus requiring error bars.

4.1.5 Dissolution of Glassware

Hot alkaline solutions resulted in "frosting" and thinning of glassware. An experiment was carried out in a previous work [102] to quantify Si gained from the reaction vessels. The experiment leached the pyrex vessels for 4 hours using a 4M NaOH solution to produce a yield of 0.82 g/L Si. From this result, any extraction experiments with prolonged contact between hot NaOH solutions and the Pyrex reaction vessels have had their lower error bar elongated to account for a possible accumulation of vessel-derived Si (rather than ash-derived Si). Pyrex dissolution was modelled as 0.05 g/L of Si per Mole of OH^- per hour. The quantity of Al derived over the aforementioned 4 hour experiment was 0.05 g/L, and considered small enough to be ignored.

4.2 Influence of Hydroxide Content and Source

4.2.1 Concentration of NaOH

Hydrothermal leaching experiments were carried out using the equipment in Figure 4.1. The experimental method is described as follows, with reference to Figure 2.12. 2, 3 or 4 moles of NaOH (B) were placed in the round-bottomed flask of the leaching vessel (I), 800 ml of distilled water (D) was added, and the mixer was set to 300 rpm. The heating mantle (J) and condenser were turned on and the solution brought to boil. Upon boiling, 100 g of Delta ash (A) was added to the NaOH solution, and washed in with the remaining 200 ml of distilled water (D) and the timer started. A 25 ml aliquot was then immediately taken as a 0 minute sample. Samples were taken using a 25 ml syringe and flexible tube. The

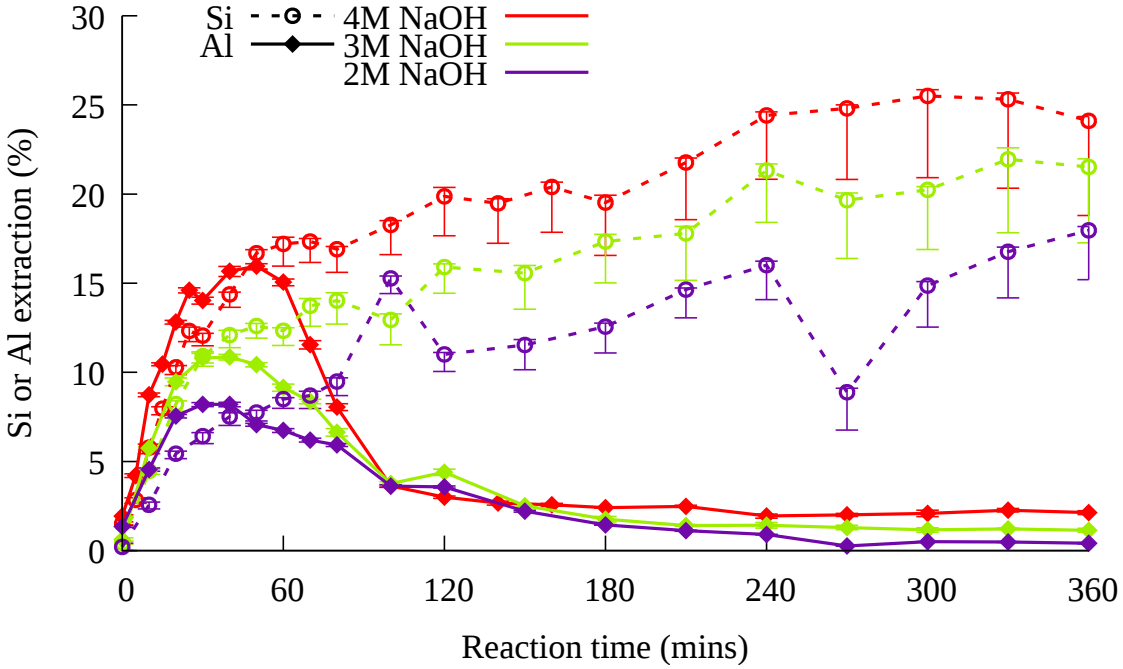

Figure 4.4: Si and Al extraction of processed coal fly ash with increasing concentrations of NaOH.

contents of the syringe was emptied into a sintered glass Büchner funnel (L), the leachate (N) retained for later analysis, and the ash washed with distilled water and retained (M) for later analysis. The filter apparatus was then washed with distilled water, and the receiving flask left inverted to encourage drying.

The 25 ml leachate samples were analysed using AAS and the data are presented in Figure 4.4. The data shows increased Si content with increasing concentration of NaOH, and a rapid increase in Si concentration for the first 30 minutes, before the Si content becomes more stable. This is consistent with literature [74, 75]. Experiments by Hui and Chao [32] leached 100 g CFA/L with 2 M NaOH for 2 hours under hydrostatic conditions to get a Si concentration of 11.49 g/L. The highest yield of Si achieved by experiments shown in Figure 4.4 was 6.09 g/L at 5 hours using 4 M NaOH, whilst the the Si yields at 2 hours were 2.63, 3.80 and 4.75 g/L for 2, 3 and 4 M NaOH respectively. The disparity in the yields of these experiments, compared to the yields produced by Hui and Chao [32] can be attributed to the crystallinity of the material. The most soluble part of the CFA is the amorphous, glassy fraction, which forms during the combustion

process, whilst quartz and mullite are significantly less soluble. Thus the proportion of amorphous material to crystalline material will be heavily influenced by the combustion conditions of the CFA. It is noted that whilst aluminium content first increases, it peaks at between 30 and 40 minutes and then starts to decrease. This is also consistent with literature [74]. It is postulated that the Al concentration decreases as Al is consumed by the crystallisation process which produces a coat on the surface of the ash particles, limiting further dissolution of Si and Al [72, 84]. Al content is considered the limiting reagent for crystallisation of zeolites during extraction experiments. Crystallisation is discussed in greater depth in section 5. No SEM images are available for these experiments, however SEM images of a similar hydrothermal extraction experiment with 2M NaOH and half the ash content are shown in Figure 4.11. Experiments in literature frequently use 2 M NaOH to synthesise zeolites, due to the trade-off between dissolution of CFA and increased alkalinity promoting synthesis of sodalite or zeolites with a lower CEC [25, 32, 49, 58, 73, 74].

4.2.2 Effect of Replacing NaOH with Na_2CO_3 on Si and Al Extraction

This experiment follows the preceding method in section 4.2.1, however an effort was made to keep the concentration of OH^- constant at 4M. Varying quantities of NaOH were replaced with half the equivalent molar concentration of Na_2CO_3. Only half the Na_2CO_3 was used because each mole of NaOH produces 1 mole of OH^-, as shown in equation 4.1, whilst 1 mole of Na_2CO_3 will produce 2 moles of $[OH]^-$, as shown by equation 4.2.

$$NaOH_{(s)} \rightarrow Na^+_{(aq)} + OH^-_{(aq)} \tag{4.1}$$

$$Na_2CO_3 + H_2O \rightarrow 2Na^+_{(aq)} + H_2CO_3 + 2OH^-_{(aq)} \tag{4.2}$$

Due to the production of carbonic acid in the latter equation, this substitution is imperfect, however it is deemed sufficient for this study. The AAS results in Figure 4.5

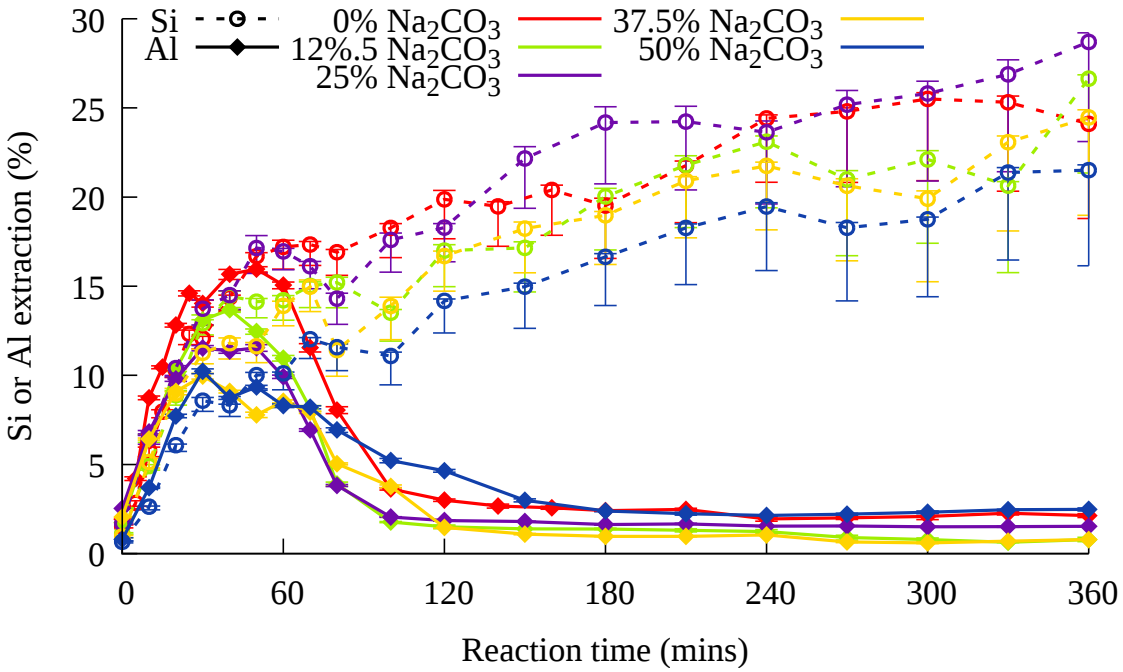

Figure 4.5: The effect of replacing NaOH with Na_2CO_3. Legend describes Na_2CO_3 content.

show a general trend of decreasing yield of Si in solution as NaOH content decreases, in keeping with results in literature [68, 74, 75]. The low Al content is consistent with consumption through crystallisation as is the case in Figure 4.4. The extraction of Si and Al is generally less effective as more NaOH is replaced with Na_2CO_3. This is as expected, due to the carbonic acid. This experiment was conducted out of a desire to produce a leachate with a decreased calcium content, as further discussed in section 5.2.

4.3 Hydrothermal Extraction Efficiency in Comparison with Fusion Extraction Efficiency

4.3.1 Grinding

The hydrothermal method described in section 4.2.1 was compared with a fusion method adapted from one commonly used in literature [38, 39, 54, 85]. In the aforementioned papers, the ash and NaOH were ground prior to fusion, and the ash was not filtered out

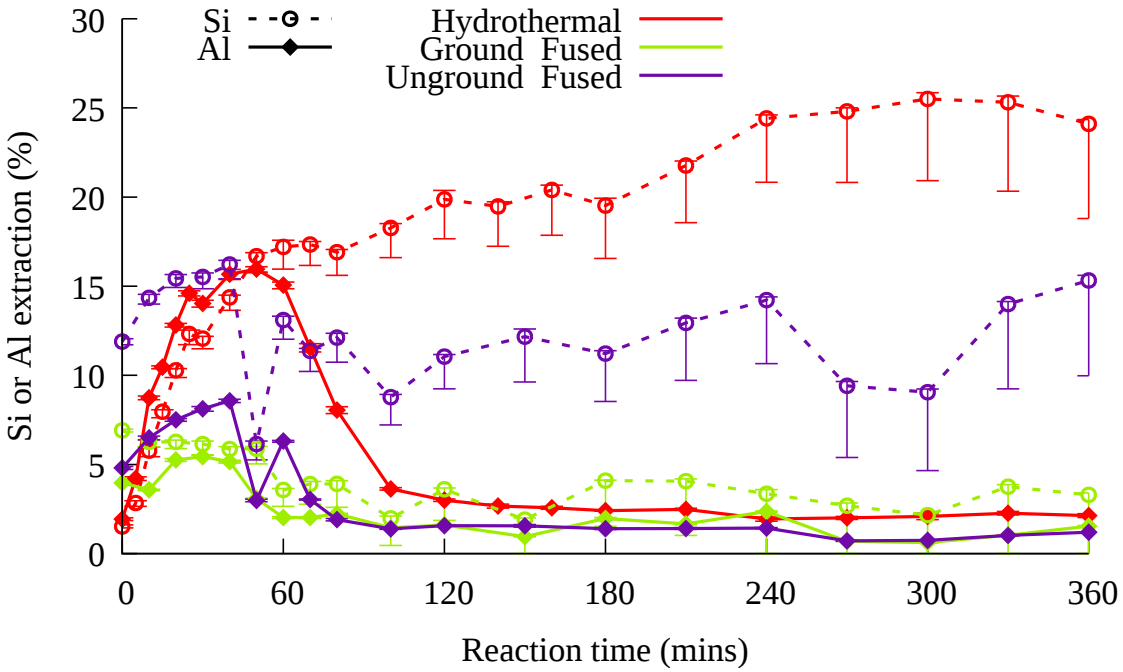

Figure 4.6: Comparison of hydrothermal extraction technique and conventional fusion of ground Delta ash, and conventional fusion of unground Delta ash

prior to crystallisation of zeolites. Other parameters also vary. In these experiments the grinding of the ash and NaOH prior to fusion was investigated. With reference to Figure 2.12, two samples were prepared, consisting of 100 g of Delta ash (A) and 4 moles of NaOH (B). One sample was ground, the other was not. Both samples were put in a nickel crucible and heated in a muffle furnace (F) to 550°C for 2 hours, left to cool, and then broken up in a pestle and mortar. The fused product was put in the leaching vessel in Figure 4.1, 1L of distilled water was added, and the mixer set at 300 rpm (H). The heater was turned on (K) and when boiling temperature was achieved the timer was started. It is noted that some dissolution will have occurred in the time taken to raise the liquid to boiling temperature, however adding ash and NaOH to boiling distilled water was deemed unsafe. AAS results for leachates gathered are shown in Figure 4.6. A dilution error is noted at 50 minutes for the unground sample, due to the sudden dip in both Al and Si values. Due to the "head start" the fusion products had in partially dissolving as the heating mantles reached boiling point, the 0 minute samples are higher than the hydrothermal experiment. The unground experiment continues to rise slowly up to 40 minutes. The

ground sample produces results that are consistently lower than the unground sample, decreasing from a maximum at 0 minutes. Given that the samples were ground prior to fusion, the dissolution may have been significantly more rapid, resulting in a much earlier availability of Si and Al, providing conditions suitable for crystallisation during the heating up period. Further dissolution of Si and Al could have been outstripped by the rate of consumption of Si and Al in the crystallisation of aluminosilicate that forms on the surface of ash particles, inhibiting further dissolution of Si and Al. Dissolution is inhibited as the aluminosilicate blocks $[OH]^-$ from getting to the surface of the ash. This position is supported by literature [42, 70, 72, 75]. The data indicates that under these conditions, grinding does not aid in the extraction process, however grinding may be of use if samples are taken before the extraction process reaches boiling point. Wałek et al. [70] argues that grinding of ash speeds dissolution, however such a difference was not observed in these experiments, quite possibly due to the unrecorded ramp-up period.

4.3.2 Influence of Temperature During Dissolution of Fusion Product

An experiment was conducted to investigate the influence of the temperature of the dissolution process. If the dissolution process yielded a similar Si content without heating, savings could be made. An experiment was designed comparing the unground fusion product dissolved in hot water from section 4.3, to the same unground fusion product dissolved in ambient temperature water (i.e: without (K) in Figure 2.12). The 4M hydrothermal experiment from section 4.2.1 was used as a control. An experiment with the correct NaOH:ash ratio is included, but using 2M NaOH instead of 4M. The AAS data is presented in Figure 4.7. The Hydrothermal experiment (4 M NaOH, 100 g ash) is shown in red, the fusion experiment extracted under reflux conditions (4 M NaOH, 100 g ash) is shown in green. The first fusion experiment dissolved in ambient temperature water (4 M NaOH, 50 g ash) is shown in yellow, and the second fusion experiment dissolved in ambient temperature water (2 M NaOH, 100 g ash) is shown in purple.

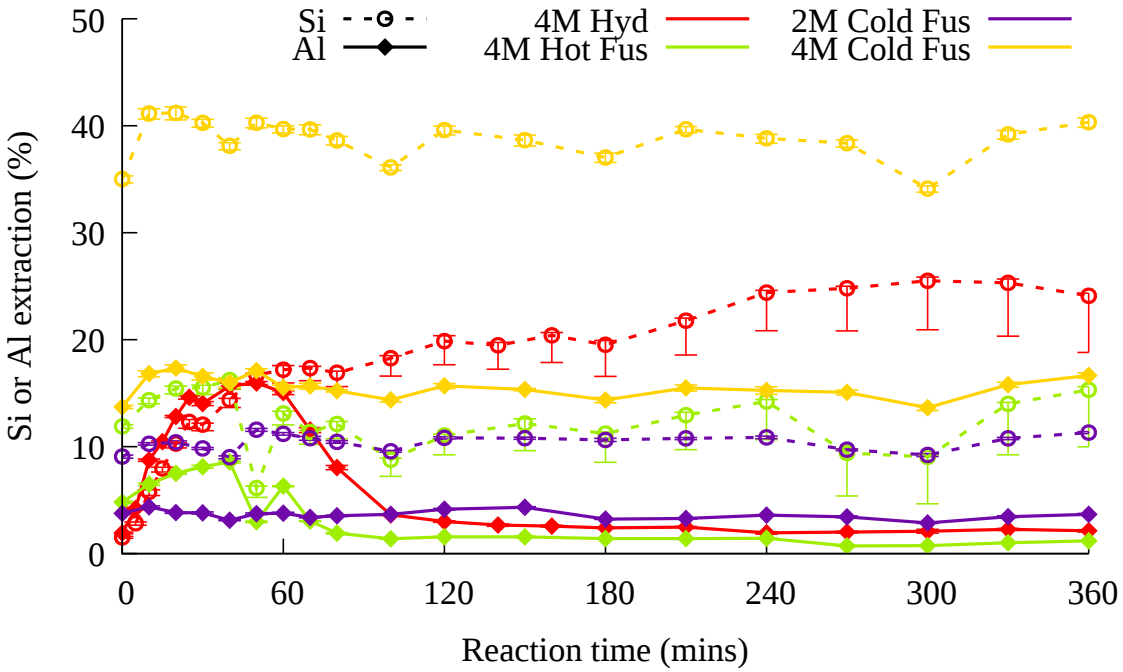

Figure 4.7: Comparison of hydrothermal extraction with fusion and dissolution at ambient temperature, and fusion and dissolution under reflux conditions on Si and Al extraction

Despite the lower solids loading, Si yield is doubled in real terms and quadrupled in as a proportion of Si extracted from ash when comparing the 4M fusion and cold dissolution experiment (yellow) to the 2M fusion and cold dissolution (purple). It is also noted that the 2M fusion (purple) has half the NaOH content of 4M Hot fusion (green) yet has similar Si and Al content after 1 hour. Si content prior to 1 hour is similar, but lower for cold water extraction. This indicates that heating water during dissolution of fusion products is unnecessary. The data does make clear two points: a lower concentration of NaOH and cold extraction conditions do not diminish Si extraction in the long term (purple vs green), and lower solids loadings combined with cold extraction conditions are similarly favourable for Si extraction. Using ambient temperatures in the extraction process also hinders the crystallisation process. This hindered crystallisation process results in Si and Al remaining in solution, and not being consumed to form aluminosilicate precipitates or crystallisation products.

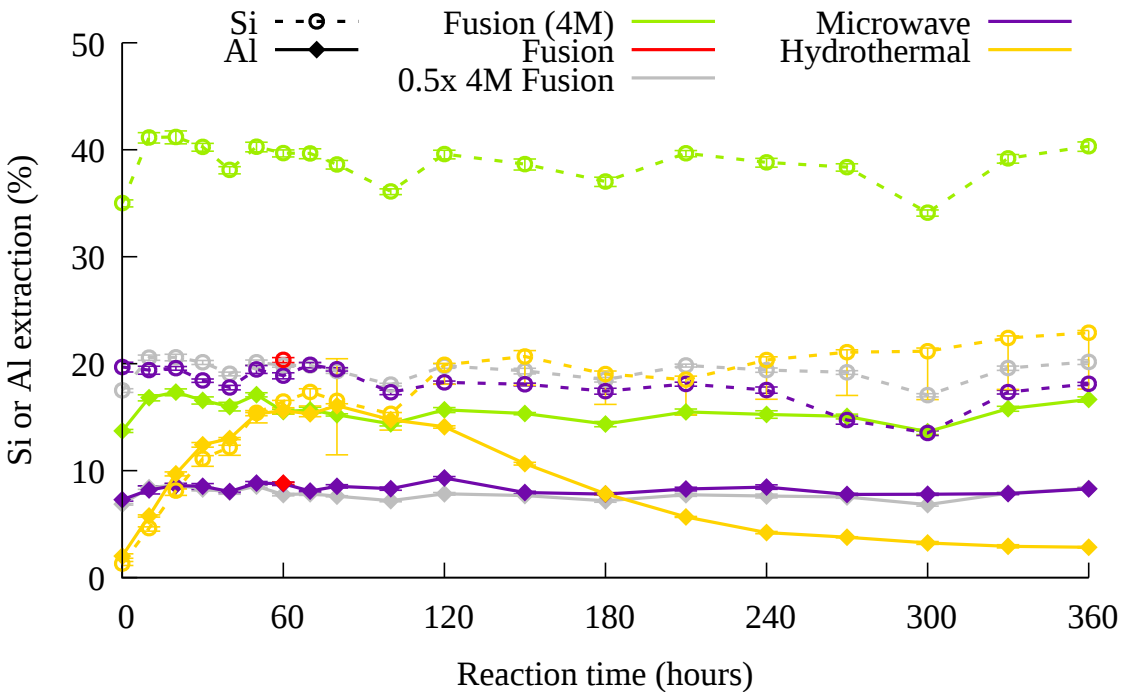

Figure 4.8: Comparison of hydrothermal extraction, conventional fusion and microwave fusion on Si and Al extraction

4.3.3 Microwave Fusion

In order to expedite the conventional fusion method, a microwave was used in lieu of a furnace to fuse the NaOH and ash. For the microwave fusion experiment, 50 g of unground Delta ash (Ⓐ from Figure 2.12) was mixed with 2 moles of NaOH Ⓑ. These were put in the microwave fusion vessel shown in Figure 4.3, and put in the microwave Ⓖ. The microwave was then run for 5 minutes at 600 W, the fusion vessel was removed using nickel tongs, and the contents mixed using nickel spatulas, and returned to the microwave. This process was repeated till the sample had been microwaved for 20 minutes. The fusion product was then treated as other fusion products, and the method follows that described in section 4.3, being dissolved in ambient temperature distilled water.

The experiments in Figure 4.8 compare hydrothermal extraction (yellow) from section 4.2.1, microwave fusion (purple) and conventional fusion (red/green/grey) from section 4.3.2 to each other. Microwave (purple) and hydrothermal (yellow) extractions were conducted with 2 M NaOH. Only one data point is available for the furnace fusion experiment using 2 M NaOH, which is provided in red at 60 minutes. The AAS data from a 4 M NaOH

furnace fusion experiment (green) was halved to present an estimation (grey) of the values a 2M experiment should have produced. This estimation is considered appropriate for two reasons. Firstly, Figure 4.4 shows increasing NaOH content in hydrothermal experiments produces similarly shaped, but proportionally larger yields of Si and Al. Secondly the 4M fusion experiment (green) produced approximately double the Si and Al as was extracted in the 2M fusion experiment (red). Halving the 4M fusion experiment data produces the grey data set which are very similar in value to the red data points.

From Figure 4.8, it is noted that Si and Al contents in hydrothermal extraction experiments decrease after peaking at 60-80 minutes, whilst fusion experiments remain relatively constant. Fusion experiments give yields of Si and Al similar to 1 hour hydrothermal extraction within short periods. It is noted that Microwave fusion produces similar yields to conventional fusion experiments, notably a high Si content faster than is procured using the hydrothermal method. It is postulated that Si and Al do not decrease over time with fusion experiments as dissolution of fusion products is conducted at ambient temperatures (due to results from Figure 4.7), which deprives the Si and Al rich solutions of the heat necessary to begin rapid crystallisation.

Comparing the image of the Delta ash in Figure 4.9a to the other 5 images of treated ash in Figure 4.9 shows that the untreated ash has a smoother surface. Further images of Delta ash showing smooth surfaces can be found in the characterisation section on page 63. Images 4.9b and 4.9c show similarly "fluffy" surfaces, indicating that microwave and conventional furnace fusion followed by dissolution in cold water have similar effects on the ash. Image 4.9d shows a surface not as smooth as the starting ash, but also lacking the "fluffyness" of fused ash. The roughness could be due to erosion by the hot alkaline solution or the precursors to crystalline aluminosilicate seen coating the ash 6 hours later in image 4.9f. Roughening of ash particles followed by deposition of gel on the surface of the ash has been noted in literature [42, 68, 75]. The formation of crystalline material on the surface of the ash is consistent with the decreasing Al content from AAS data represented in yellow in Figure 4.8, and has been observed in literature [68, 75]. From the

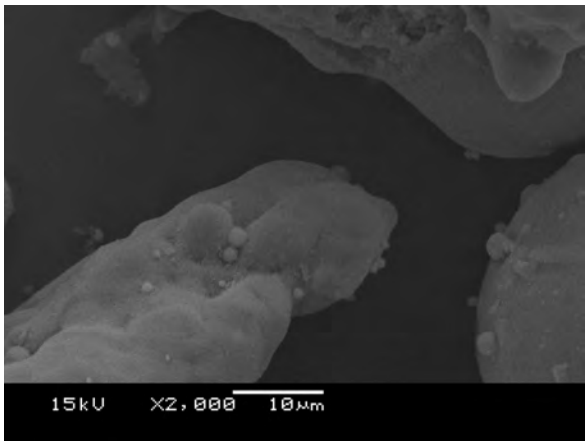

(a) Delta Example 1 x2000

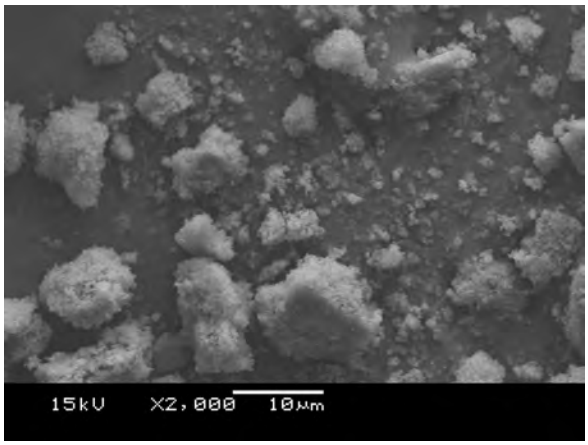

(b) Furnace Fusion Cold Dissolution, 1 h

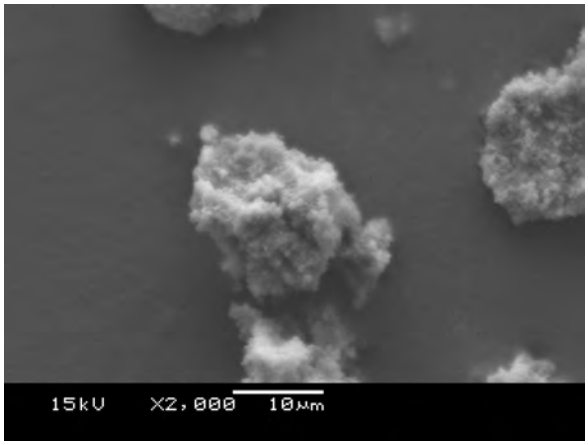

(c) Microwave fusion Cold Dissolution, 1 h

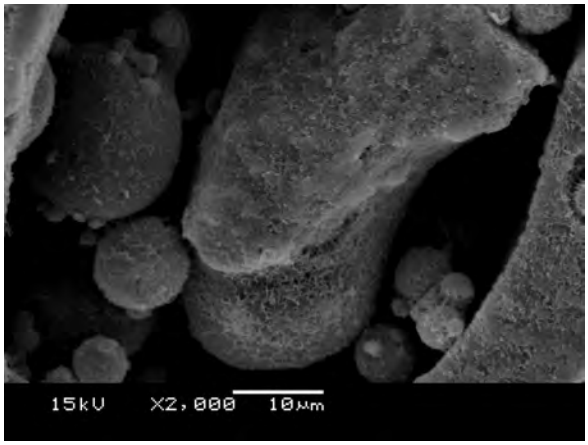

(d) Hot Hydrothermal Dissolution, 1 h

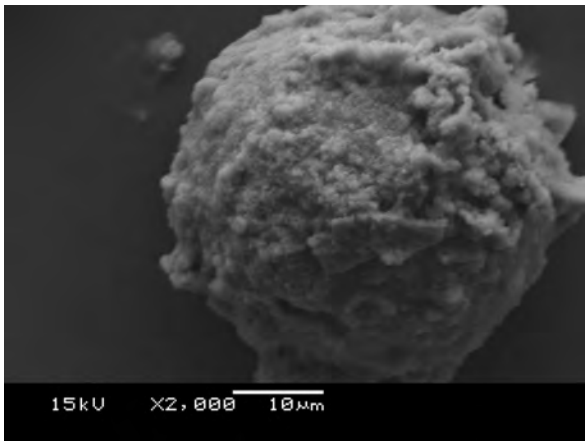

(e) Microwave fusion Cold Dissolution, 6 h

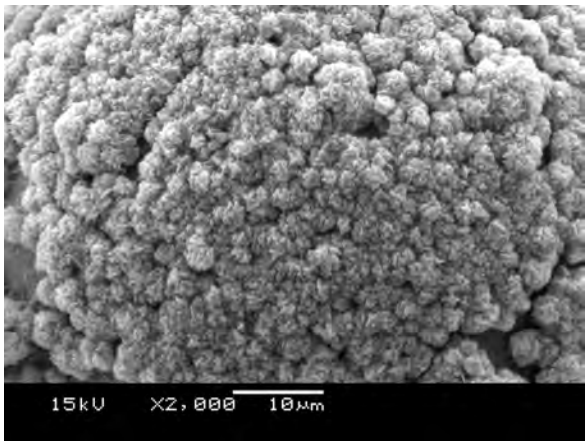

(f) Hot Hydrothermal Dissolution, 6 h

Figure 4.9: SEM images of ash, comparing extraction methods

presented data, it is believed that the rate of consumption of Al through crystallisation is higher than the rate of dissolution of Al from ash. Image 4.9e of microwave fusion ash after 6 hours seems similar to image 4.9c of ash from 1 hour in to the experiment indicating that there is little or no change during the 5 hours, which is consistent with the AAS data of the microwave fusion experiments (purple) plateauing in Figure 4.8.

4.4 Solids Loading

4.4.1 Influence of Solids Loading on Si and Al Hydrothermal Extraction

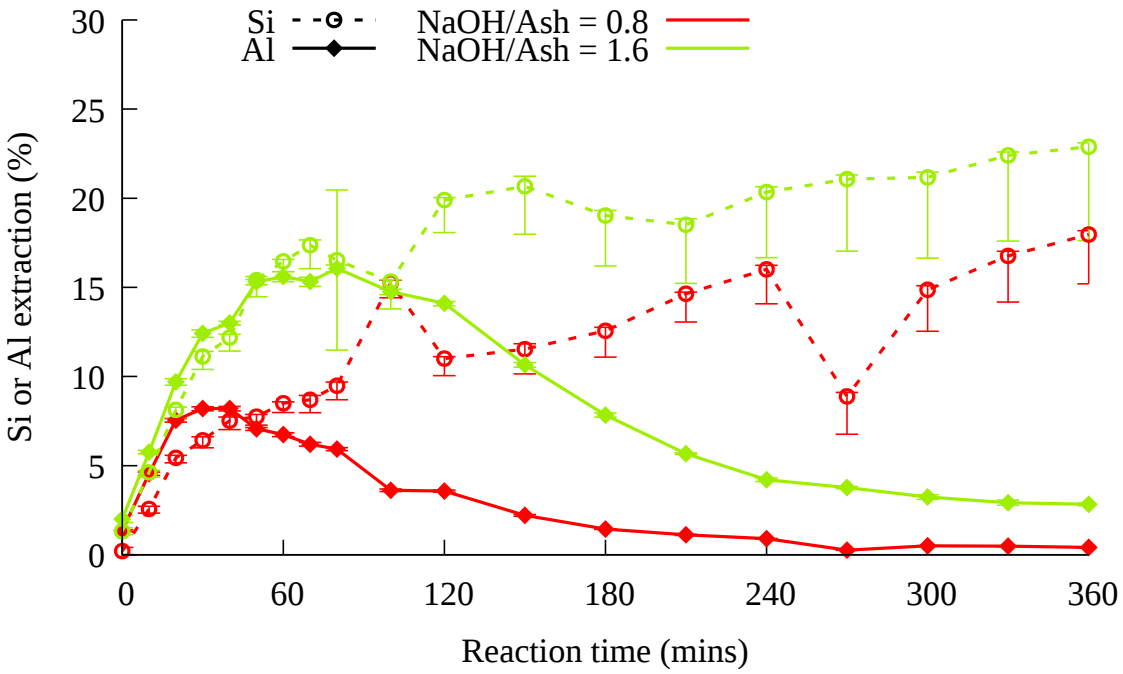

Figure 4.10: Comparison of solids loadings in hydrothermal extraction experiments. Conditions: 80 g NaOH, 100 g Delta, NaOH/Ash = 0.8; 80 g NaOH, 50 g Delta, NaOH/Ash = 1.6

An experiment was conducted following the hydrothermal method described in section 4.2.1 but using a lower ash solids loading. Figure 4.10 compares hydrothermal Si and Al extraction with two solids loadings: 100 g of ash per litre (NaOH/ash = 0.8) and 50 g/L (NaOH/ash = 1.6) referred to as high and low solids loadings respectively. The Si content

for both solid loadings is similar in real terms at 1 hour being 2.03 and 1.97 g/L for high and low solids loadings respectively. At 1 hour Al content is again similar with 0.91 g/L and 1.06 g/L for high and low solids loadings respectively. As time progresses, the Si content in real terms increases faster for high solids loading than low, giving a final Si content at 6 hours of 4.29 g/L and 2.74 g/L respectively. After an initial peak at 40-60 minutes, the Al content starts to decrease. It is postulated that this is due to Al being consumed by crystallisation of aluminosiliate on the surface of the ash at rates higher than Al is dissolved from the ash, as is shown in Figure 4.11. Smooth ash particles were observed at the start (figure 4.11a), as time progresses, the surface roughens through dissolution, or formation of a precursor to crystallisation in Figures 4.11b and 4.11c. Distinct products of crystallisation can then be observed in Figure 4.11d, which increase in size and concentration in the remaining Figures to cover the particles completely. This data indicates that for shorter extraction times, a lower solids loading may be desirable to maximise extraction efficiency, whilst for longer experiments a higher solids loading may be preferable to maximise Si yield. It is noted that these conditions are similar to hydrothermal extraction conditions utilised by Fukui et al. [66], who had a ratio of NaOH/ash = 2, and hydrothermally leached CFA at 100°C for 1 hour.

4.4.2 Mixing During Fusion

The fusion method used in the next experiments follows the method described in section 4.3, but with two differences. No samples were ground prior to fusion, and half of the samples were removed midway through the fusion process and stirred with a nickel spatula. The purpose of the stirring was to improve contact between the molten NaOH and the fly ash, hoping to improve Si extraction. Various NaOH/ash ratios were also investigated. The AAS data from the leachates is shown in Figure 4.12. The highest proportions of Si and Al were extracted at the highest NaOH/ash ratios (6.4). The Si yields in real terms are similar for the ratios 6.4 and 3.2, being 1.5 g/L and 1.45 g/L respectively, but increase as ash content increases. It is noted that the Si yields improve with mixing, however the

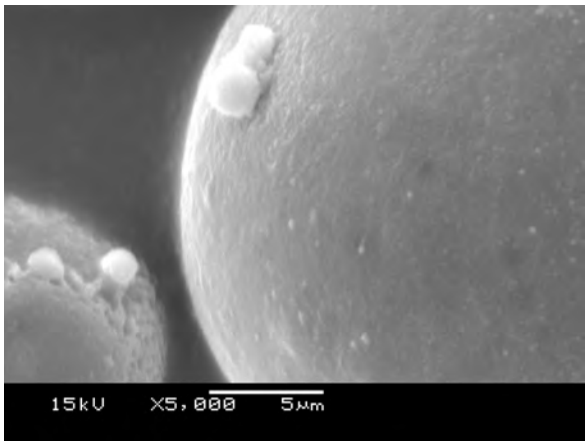

(a) Ash removed at 0 minutes

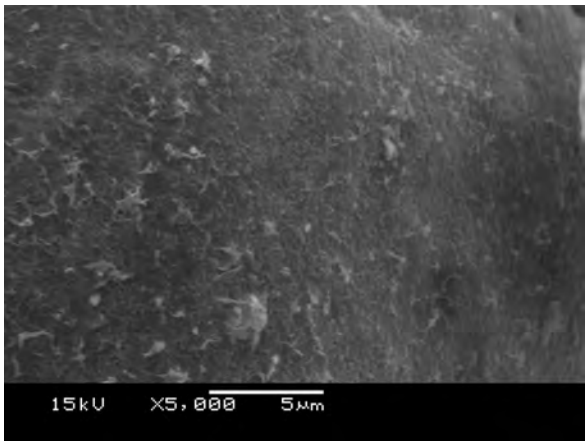

(b) Ash removed at 30 minutes

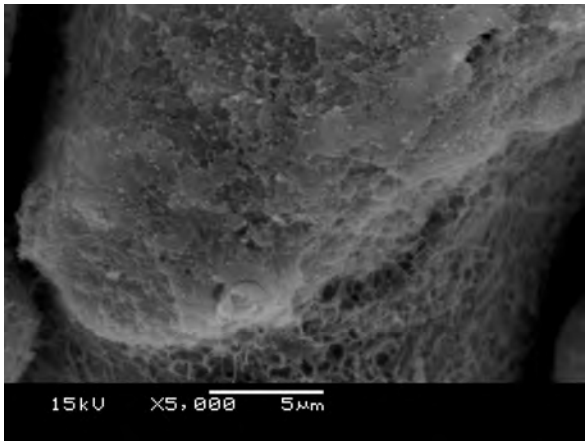

(c) Ash removed at 60 minutes

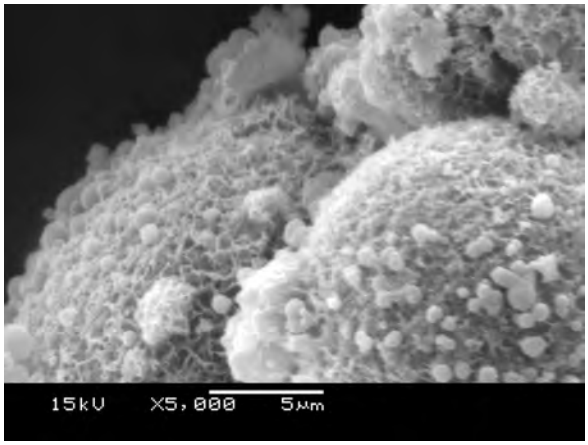

(d) Ash removed at 120 minutes

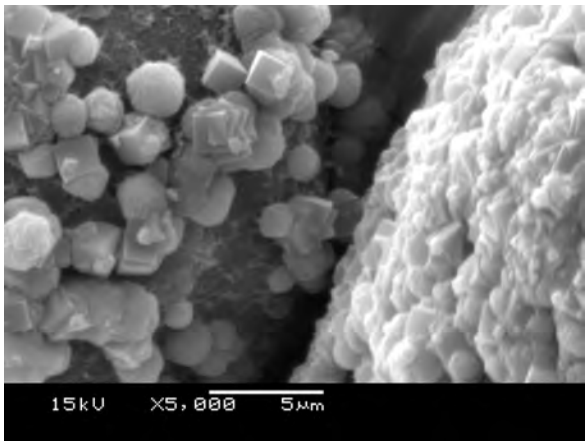

(e) Ash removed at 180 minutes

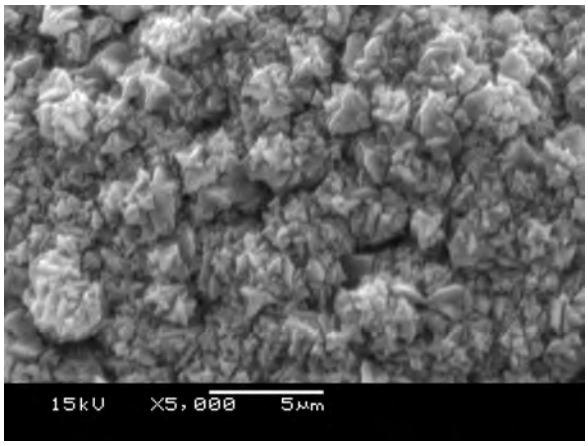

(f) Ash removed at 360 minutes

Figure 4.11: SEM images of ash, showing crystallisation on ash surface over time

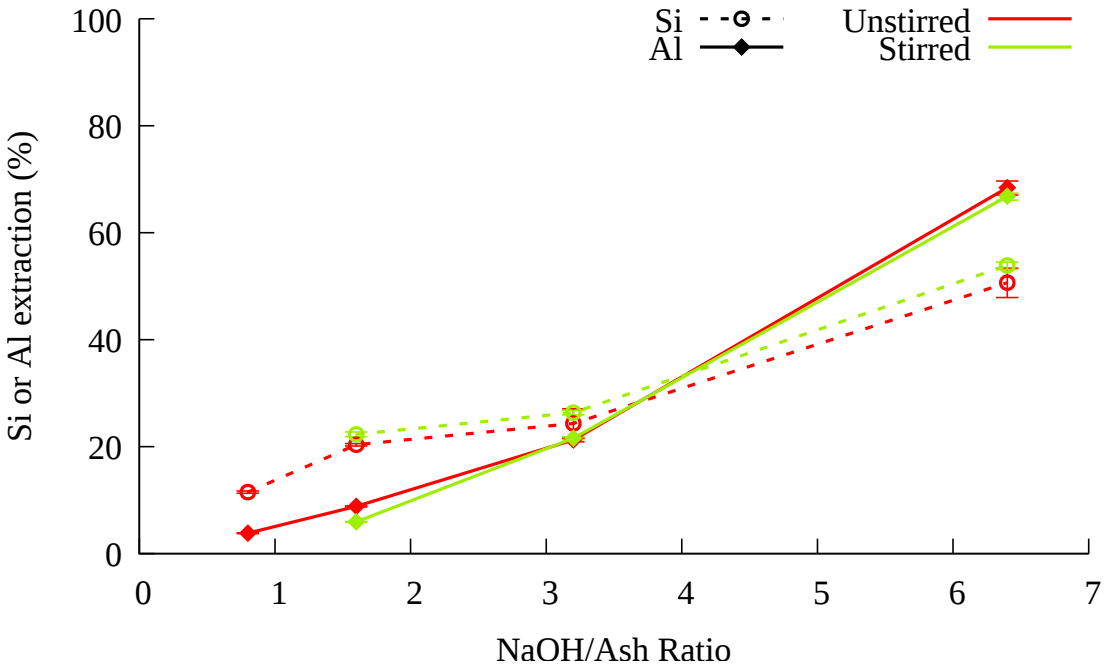

Figure 4.12: Comparison of solids loadings in conventional fusion experiments

improvement is slight. Despite the stirring the results appear consistent between the two conditions, indicating that the results are somewhat reliable. Al yields appear to surpass Si yields as the NaOH/ash ratio increases above 3.2. This is attributed to the Al content of Delta ash being lower (14 %) than the Si content (24 %) of the same ash, and a low sample size of the ash used (12.5 g). A small ash sample, combined with a low Al content means that a small change in the already low Al content produces a large relative "improvement" in Al extraction. As the quantity of NaOH necessary to produce such high yields would be prohibitive, the higher solids loadings were not to be used in later experiments, but instead provided as context.

The SEM images of ash in Figure 4.13 all show ash surfaces with similar fluffyness, despite varied NaOH/ash ratios. This would indicate that the fusion process produces the same effect on the ash, regardless of solids loading, therefore quantity of available NaOH is not a limiting factor. Alternatively, this indicates that SEM images provide no useful insight into the liberation of Si from ash by fusion.

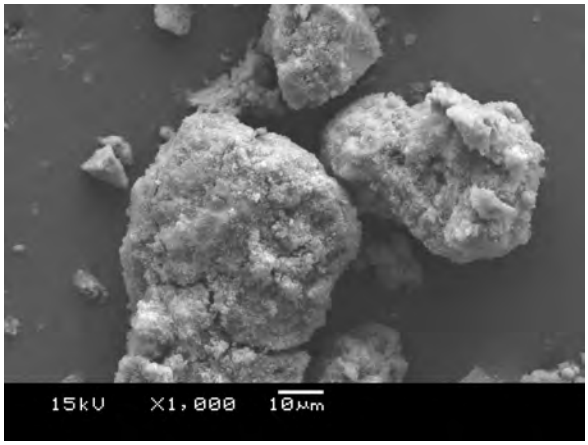

(a) NaOH/ash = 0.8

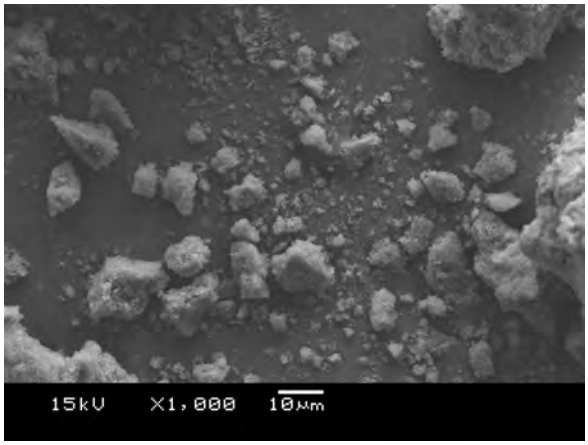

(b) NaOH/ash = 1.6

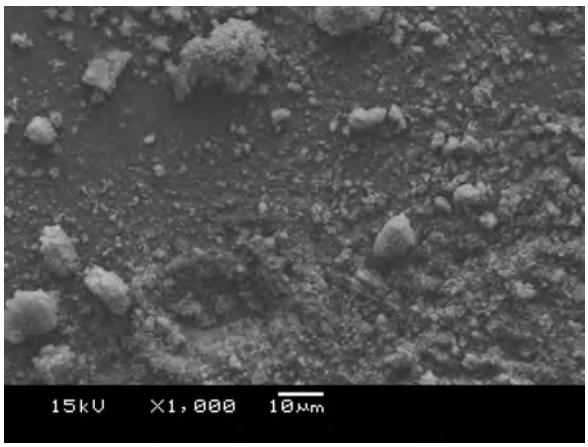

(c) NaOH/ash = 3.2

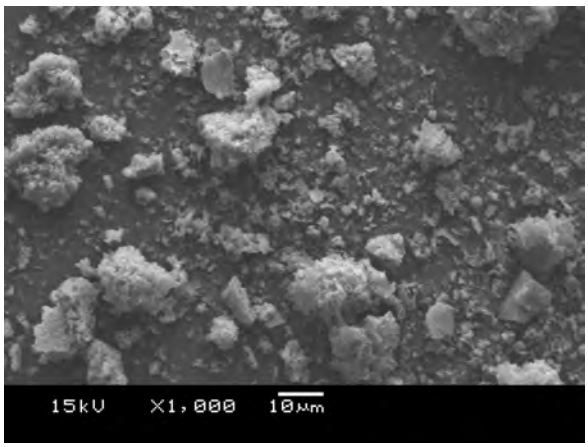

(d) NaOH/ash = 6.4

Figure 4.13: SEM images of ash, after fusion at varied solids loadings and dissolution

4.4.3 Influence of Solids Loading of Processed Ash During Microwave Fusion on Si and Al Extraction

To investigate the effects of NaOH/ash ratio on the yield of Si and Al from ash, varying quantities of ash were fused in a microwave for 10 minutes with 2 moles of NaOH (duration of microwave fusion is explored in section 4.5). The fusion time and dissolution time were both 10 minutes. In Figure 4.14a the percentage of Si and Al extracted is plotted as a function of the ratio of NaOH to ash. The percentage of Si increases from ratios 1-2, then drops slightly by ratio 3. Whilst this may appear an anomalous result, Figure 4.14b shows a straight line in the Si content between ratios 1.2 and 3, followed by an apparently distinct line from ratios 4-10. Whilst this precise experiment was not repeated, Figure

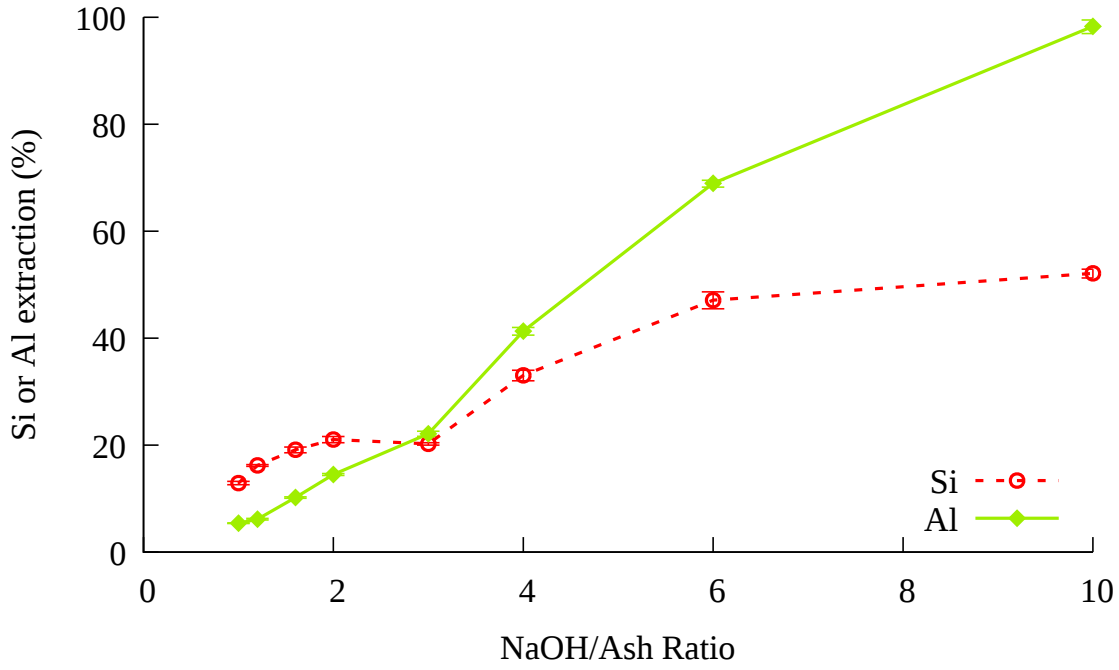

(a) Comparison of microwave fusion solids loading: relative extraction

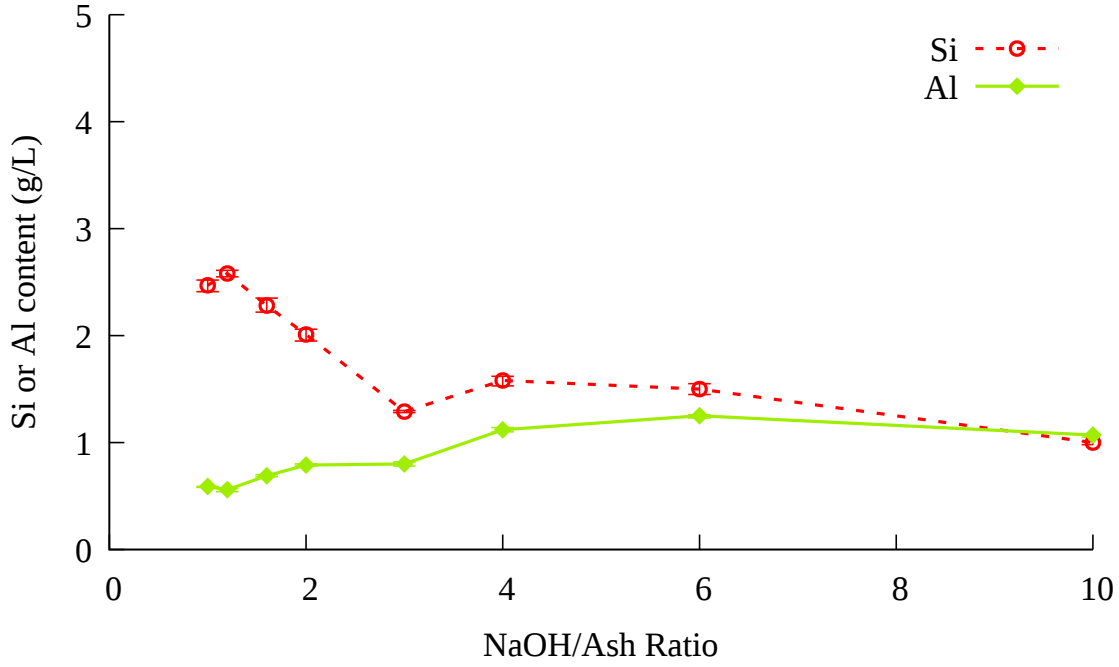

(b) Comparison of microwave fusion solids loading: absolute extraction

Figure 4.14: Comparison of solids loadings in microwave fusion extraction experiments: relative and absolute extraction

4.16 shows values at 10 minutes which are similar to results shown in Figure 4.14a, where ratios 1.6 and 3.2 show similar relative Si yields. In Figure 4.16 the microwave fusion process was 3 times as long, and the dissolution of the fusion products protracted. It is noted that the highest absolute value of Si seems to be yielded from the 1.2 ratio point. Latter experiments used this 1.2 ratio of NaOH/Ash.

4.4.3.1 Re-Fusing Used Ash

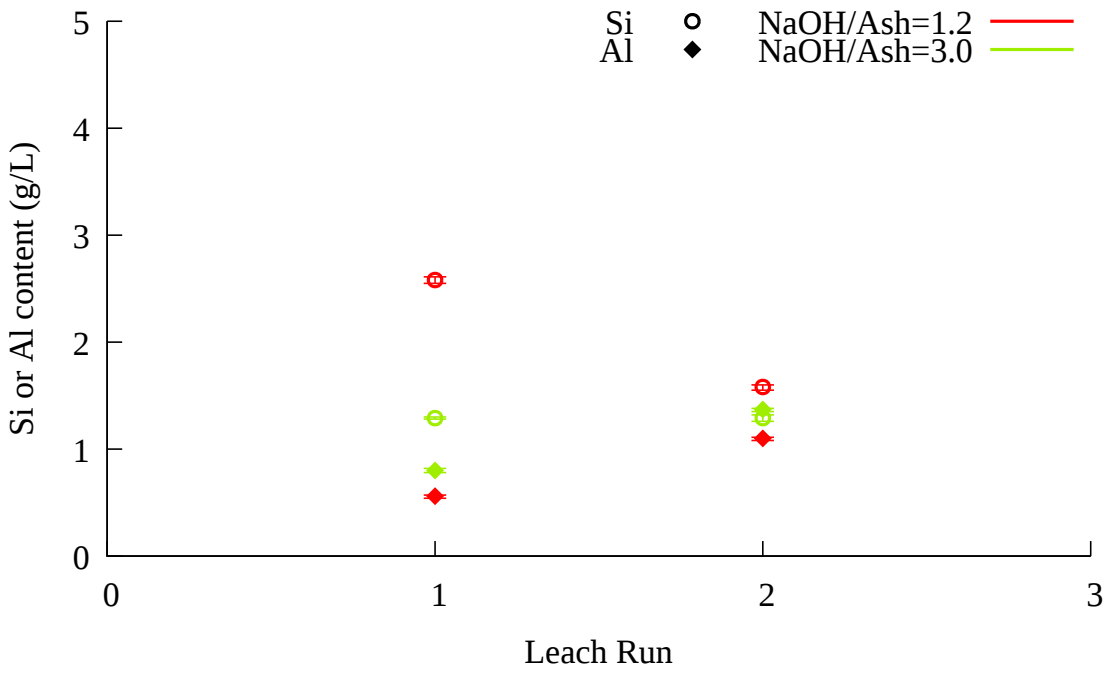

Figure 4.15: Repeated microwave fusion extractions of the same ash at different solids loadings. 80 g NaOH / 67 g ash = 1.2; 80 g NaOH / 27 g ash = 3.0

In Figure 4.15 two of the ash samples from Figure 4.14 were dried, then the fusion and leaching process was repeated. It is noted that the ash was not washed prior to drying and re-fusing, thus the NaOH ratios on the second round will be higher than their descriptions state. As expected, the Si content from the second leaching was lower for the ratio 1.2 experiment. Unexpectedly, the Si content for the second leaching of the ratio 3.0 experiment remained constant. This would indicate that for high NaOH/ash ratios, repeated leaching could be considered in order to attain better yields of Si, although this would require drying of ash, or investigation in to the efficacy of fusing moist ash.

It is noted that the Al content in the second round of experiments was higher in each case than the first round of experiments. This seems to indicate that the Al extraction is independent of Si extraction. A survey of literature has found insufficient material to support or oppose this argument, due to insufficient literature on the subject of microwave assisted fusion of ash with NaOH. The closest relevant literature by Wang et al. [84] describes how dissolution of Al is minimal in comparison to dissolution of Si (under hydrothermal conditions), and that Al in solution is consumed in the formation of, and limited by, a layer of zeolite.

4.4.3.2 Long Dissolution of Microwave Fused Ash

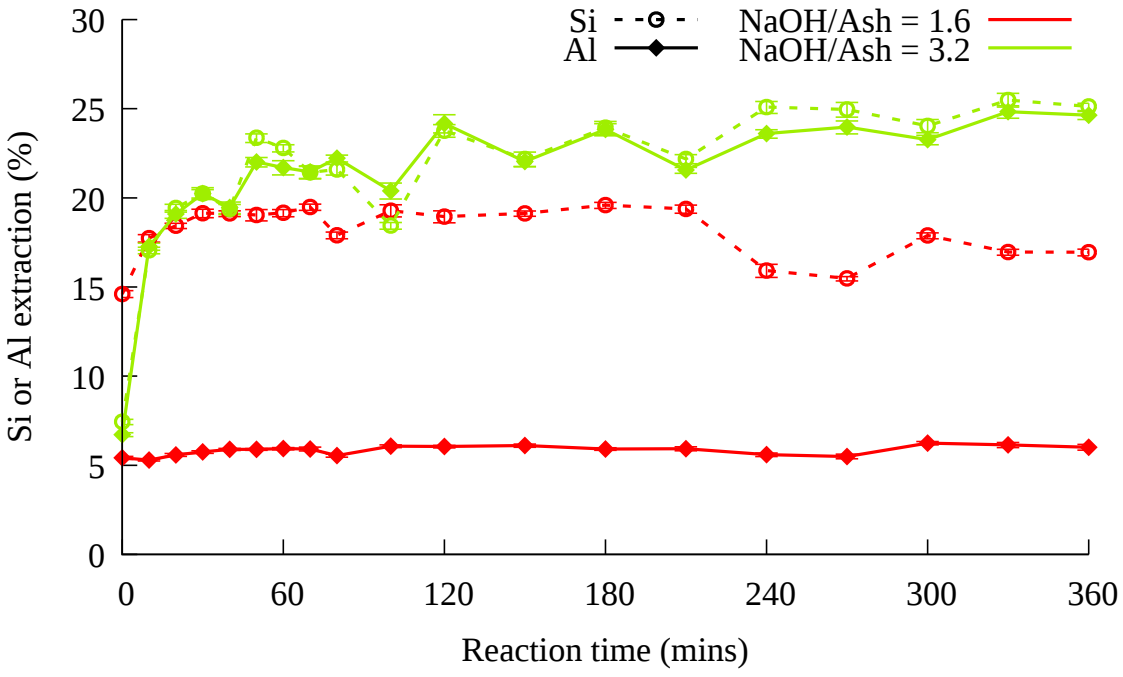

Figure 4.16: Effect of solids loading on extended dissolution of microwave fused ash. 80 g NaOH / 50 g ash = 1.6; 80 g NaOH / 25 g ash = 3.2

Two quantities of ash were fused with 2 moles of NaOH in a microwave for 30 minutes. Each sample was dissolved in water of ambient temperature for 6 hours, with samples taken regularly. Figure 4.16 shows the resulting Si and Al extraction. It is noted that relative Si extraction is similar for both ash contents for the first 40 minutes, after which the experiment with less ash (ratio 3.2) shows a higher proportional extraction, however

the higher ash content (ratio 1.6) gives a higher absolute Si yield. Whilst Si extraction also increases for the ratio 1.6 experiment after 40 minutes, there is a dip in the Si content between 210 and 300 minutes. As the Al content for this period is also slightly depressed, this could be attributed to errors in dilution. The Al content for the ratio 3.2 experiment seems to closely follow the relative quantity of Si extracted, and is significantly higher than the ratio 1.6 Al values, which, along with the Si values is consistent with earlier data in Figure 4.14a which indicates that higher ratios of NaOH/ash extract a higher proportion of the Al from the ash. This consistency between Figure 4.14a and the 10 minute measurements of Figure 4.16 seems to indicate that a longer microwave fusion time has not increased the quantity of Si or Al liberated from the ash via dissolution. Figure 4.17 shows images of ratio 1.6 ash which have been partially dissolved. Both images seem similar, except for the particle size, with the ash sample which has been in solution for longer being smaller. This reduction in size is attributed to random deviation in ash particle sizes.

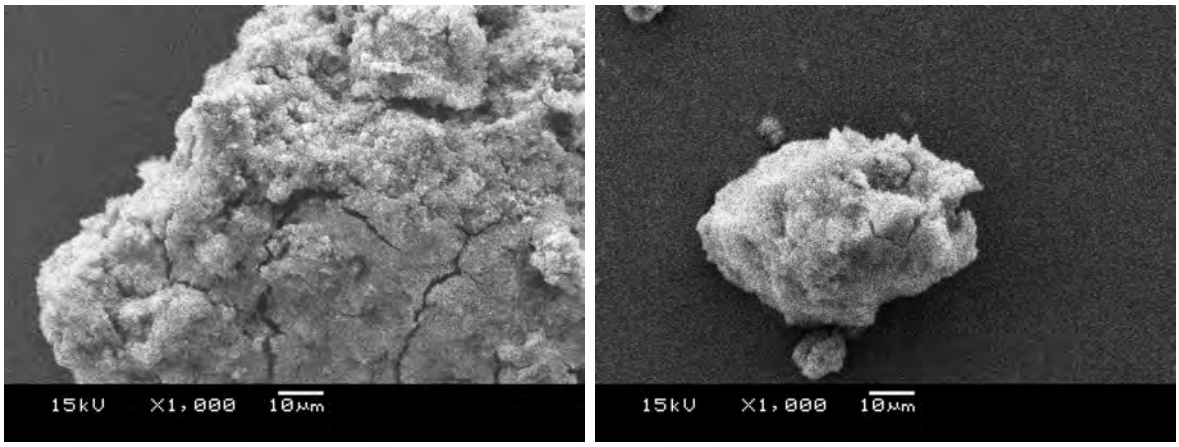

(a) Ash removed at 0 minutes (b) Ash removed at 330 minutes

Figure 4.17: SEM images of partially dissolved ash after 30 minutes of microwave fusion

4.5 Influence of Microwave Fusion on Extraction of Si and Al from Ash

4.5.1 Fusion Duration

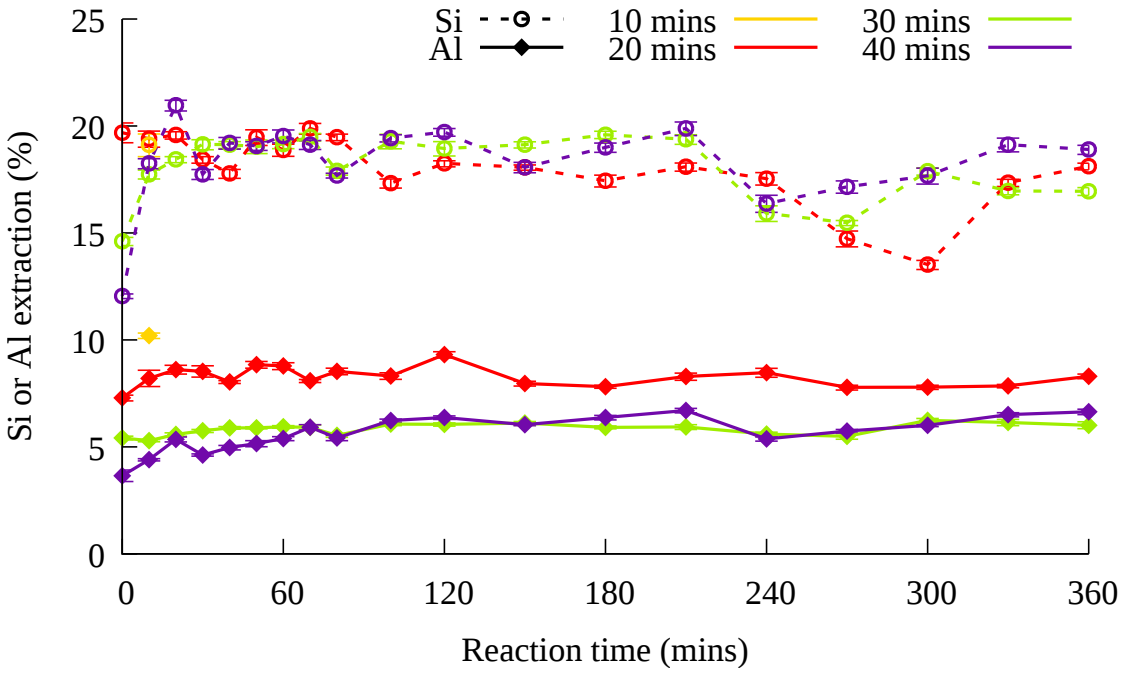

Figure 4.18: Effect of fusion duration on extraction

Figure 4.18 shows the effects of the duration of the microwave fusion process on the proportion of Si and Al extracted from the ash over 6 hours of dissolution. For these experiments, 2 moles of NaOH and 50 g of ash (NaOH/ash = 1.6) were fused in a microwave for a specified time, the fusion product was broken up in a pestle and mortar, and the fusion product mixed with ambient temperature distilled water and stirred at 300 rpm for 6 hours, in keeping with the method of previous experiments. For the 10 minute fusion experiment, there is only one data point at 10 minutes. All the Si extraction values appear to be around 20 % for the first 210 minutes, irrespective of fusion duration. The Si values appear to dip after this, but recover later. The Al extraction appears to be higher for shorter fusion durations, with the one 10 minute data point giving the highest value of 10 % extraction, whilst 30 and 40 minute fusion experiment Al yields appear to

be very similar. The steady levels of Si and Al are expected, as the dissolution process is carried out at ambient temperature, which does not provide sufficient heat or time for crystallisation of aluminosilicate on the surface of the ash to consume Si or Al.

Figure 4.19 shows a sample from each fusion length at the start and end of the dissolution process. They look quite similar, indicating little change is made by increasing the length of the fusion process. For the 20 minute fusion sample the measurement is taken at 330 minutes (figure 4.19d) rather than 360, because the image taken at 360 minutes is of poor quality (this also applies to Figure 4.17b).

Figure 4.20 shows the proportions of Si and Al extracted as microwave fusion time was varied, with a control experiment which was not microwaved. In this experiment, 16 g of NaOH and 10 g of ash (NaOH/ash = 1.6) were fused in the 700 W microwave for a specified time. The fusion product was then broken up in a pestle and mortar and dissolved in 200 ml of distilled water which was stirred at 2000 rpm for 10 minutes, after which the ash was filtered out using a sintered glass Büchner funnel. The microwave wattage divided by the mass of NaOH and ash was 27.0 W/g. These results were compared to the results from Figure 4.18 which had been dissolved for 10 minutes. These experiments used 80 g of NaOH and 50 g of ash in the same 700 W microwave, and thus wattage per gram was 5.4 W/g.

As with Figure 4.18, little change is noted as microwave fusion time is increased. The results at 10 and 20 minutes which were conducted under both power to weight ratios show similar extraction efficiencies for Si. This indicates that the power to weight ratio has little effect on the extraction efficiency of Si within the range examined. The yield of Al in solution appears to be slightly higher when the power to weight ratio is higher.

4.5.2 Effect of Different Source Ashes on the Extraction Process

Figure 4.21 compares the 10 minute microwave fusion method with 4 different ashes. Alpha and Delta are processed ashes from the RockTron process, whilst Lagoon and FB7 are untreated ashes. Ashes are characterised in section 3. In these experiments, the

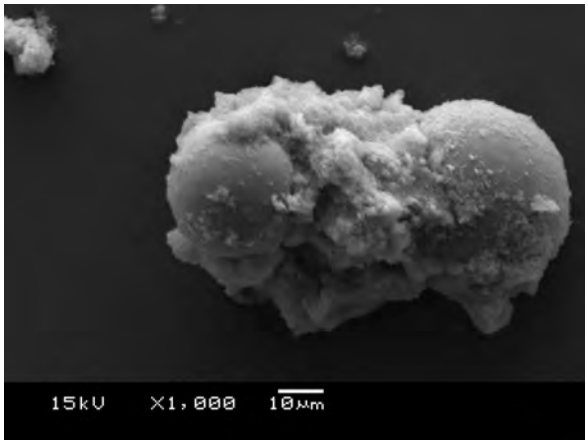

(a) 20 minute fusion Ash: 0 minutes

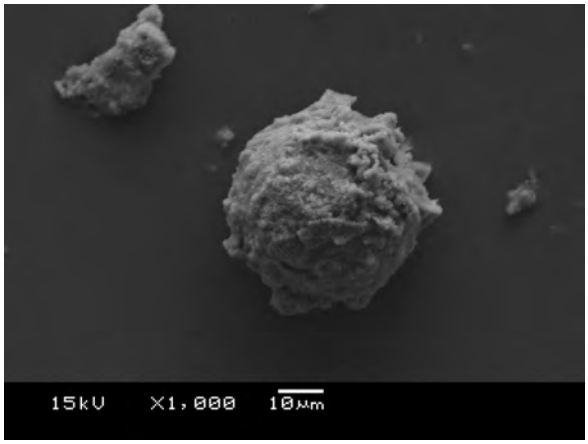

(b) 20 minute fusion Ash: 360 minutes

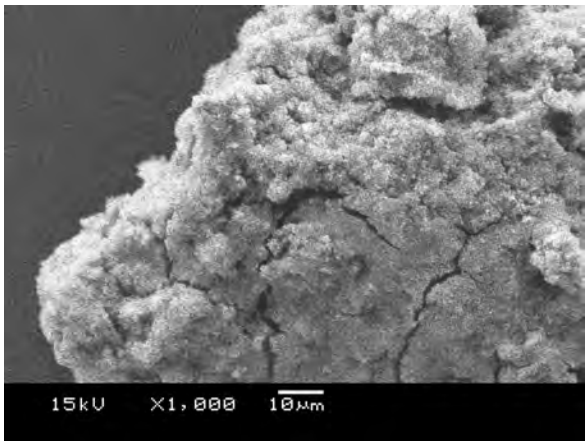

(c) 30 minute fusion Ash: 0 minutes

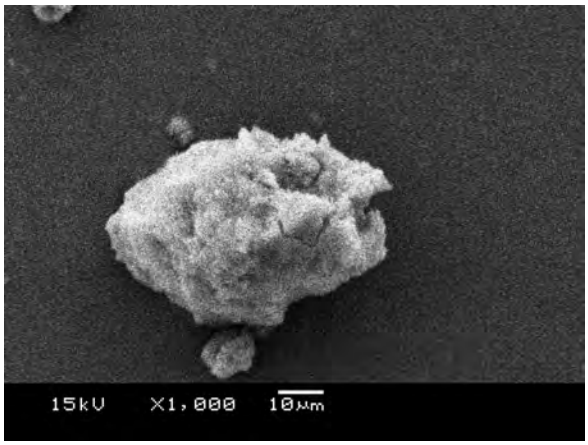

(d) 30 minute fusion Ash: 330 minutes

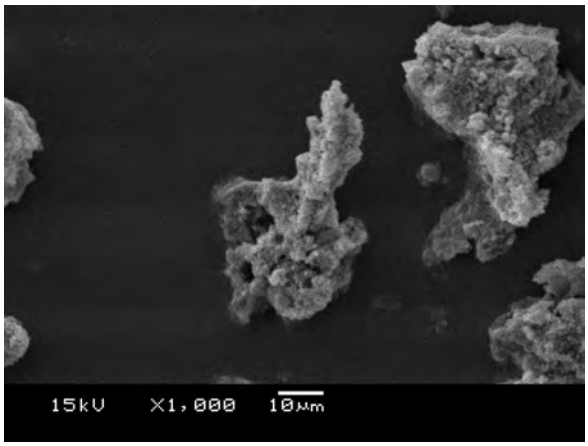

(e) 40 minute fusion Ash: 0 minutes

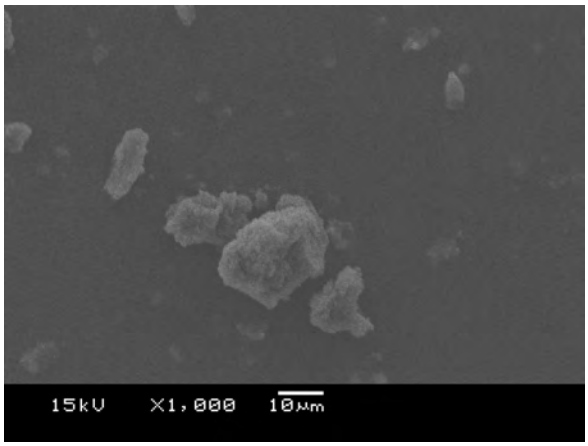

(f) 40 minute fusion Ash: 360 minutes

Figure 4.19: SEM images of ash, showing effects of microwave fusion followed by specified minutes of dissolution

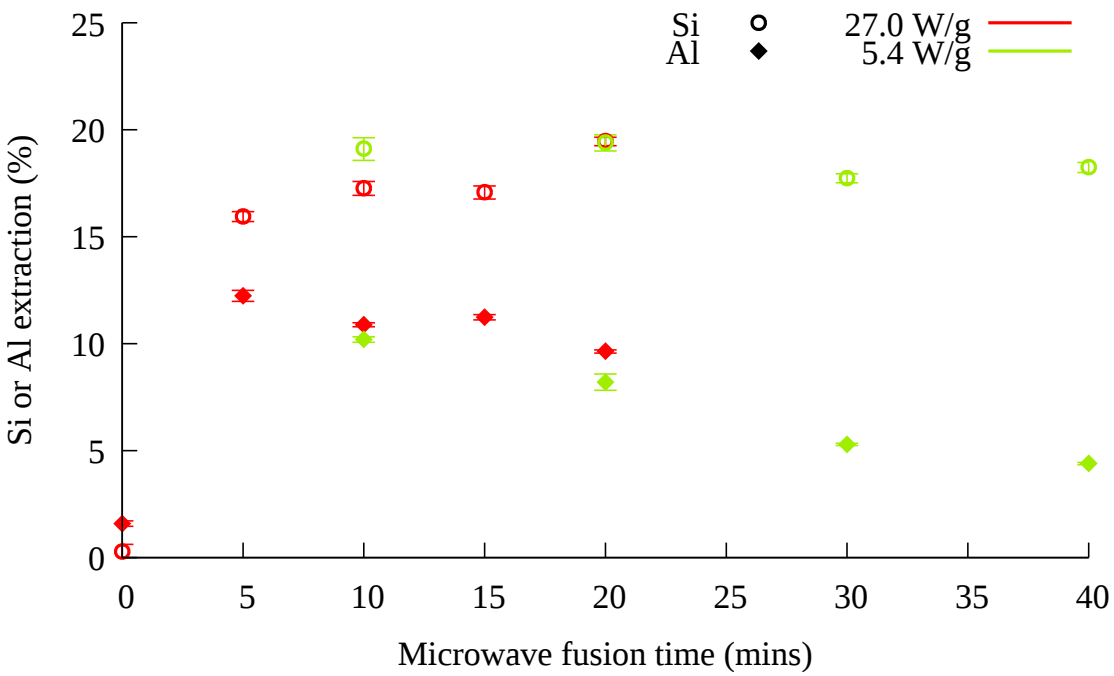

Figure 4.20: Effect of fusion duration on Si and Al yield of leachate at different loadings: 16 g NaOH + 10 g ash = 27 W/g; 80 g NaOH + 50 g ash = 5.4 W/g

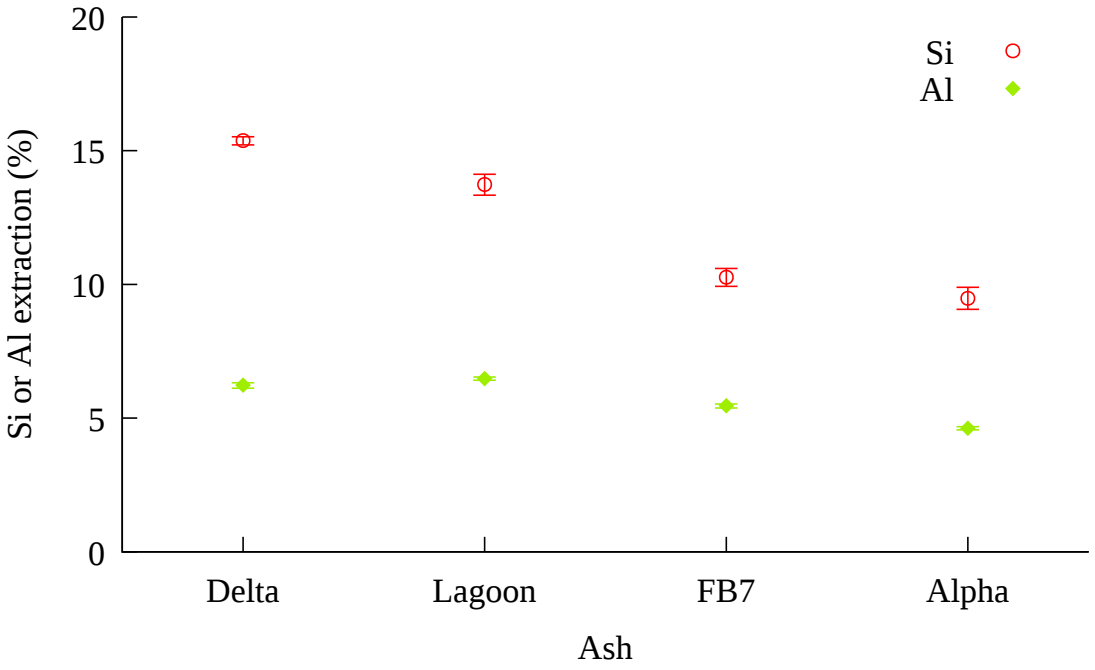

Figure 4.21: 10 minute microwave fusion and extraction of 4 ashes

NaOH/ash ratio was 1.2. Ash and NaOH were fused in a microwave for 10 minutes, then leached with distilled water and mixed for 10 minutes before being filtered, in keeping

with methods previously used. It is noted that the highest Si extraction is achieved with the Delta ash, and the lowest with Alpha ash.

The finer particle size of the Alpha ash could be expected to deliver a higher yield of Si in solution due to the increased surface area, however this is not the case. This is due to the microwave fusion process. Early work on dielectric heating of granular materials found that the heating rate increases with an increase in particle size [139]. Later works found that the relationship between heating rate and particle size was was not quite as simple, and that heating rate could also decrease with an increase in particle size. Experimental works by Harrison [140] demonstrated that minerals could be divided into groups based on how they behave when subjected to 2.45 GHz microwave radiation. Quartz and calcite were described as showing little change in temperature, whilst hematite showed a slight change and magnetite a large change in temperature when exposed to microwave radiation. This would make the Fe content of the ashes a much more important parameter, but for the fact that CFA is highly amorphous. Literature on the effect of particle size of amorphous glass on absorption of microwave radiation is scant, with the closest article describing coarser particles than are pertinent to this discussion [141]. Cursory experiments on melting NaOH in a microwave with no CFA indicated minimal adsorption. The difference in the yield of Si in solution between the various CFA samples is therefore attributed primarily to the variation in particle size resulting in a variation in the amount of microwave energy adsorbed by the CFA samples. This is supported by the behaviour or the ashes during the mixing steps of the fusion process, as the Delta and Lagoon ash samples glowed red after 10 minutes, whereas the Alpha ash sample did not glow as much. This would indicate that the Delta ash sample achieved a higher temperature during the microwave fusion process than the Alpha ash sample achieved.

The Al yields reflected the changes in Si yields, except for the Delta yield, which was slightly lower. This data indicates that the processing of ash into Delta and Alpha products affects the yield of Si which can be derived from the ash, and that the Delta product is an improvement in terms of Si yield compared to untreated ash.

4.5.3 Re-Leaching Ash for Extraction Maximisation

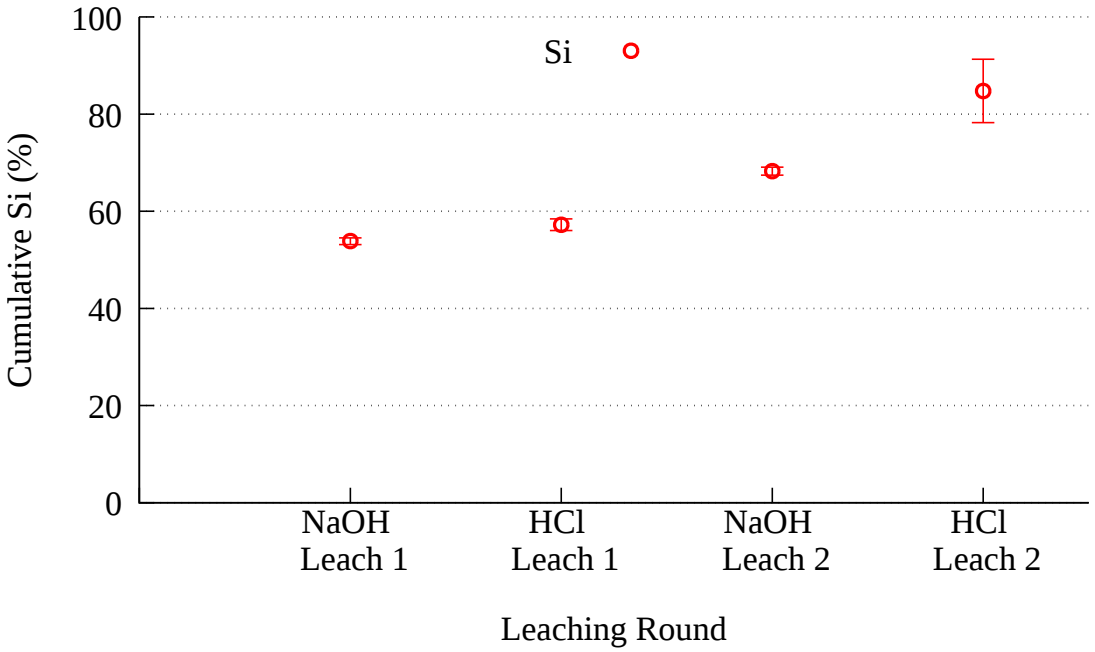

Figure 4.22: Repeated extractions of fly ash

In an attempt to extract a high proportion of Si and Al from one sample, NaOH and ash (NaOH/ash = 6.4) was fused in a furnace for 2 hours. The fusion product was broken up, and then dissolved for 1 hour at ambient temperatures in keeping with methods previously mentioned. The ash was filtered out and resulting leachate was used, in combination with 10 g of sodium aluminate (800 g/kg FA) to form 7 g of synthetic zeolite (560 g/kg FA). The leachate from this process then had sufficient NaOH added to it to bring it back to the 2M concentration desired, and was used in a hot hydrothermal leaching process with the ash from the first round. This second extraction produced a minimal increase in Si content, as can be seen in Figure 4.22. It was proposed that the ash was coated with a stable layer of zeolite which inhibited further dissolution, a stable layer that perhaps could be removed with a wash of HCl. As such, this ash sample was washed with 6M HCl, and then hydrothermally leached with the previous leachate which had been adjusted to 2 M NaOH. As can be seen from the graph, this provides a slight improvement in Si yield. The ash was then dried, and fused in a furnace for 2 hours

and leached with distilled water a final time, to gain a slight improvement in Si yield. It is noted that the Si lost in the acid wash is not included in the graph representing Si extraction. Whilst this Si may have been extracted from the ash, it was not usable in any process, and as such is not counted towards the Si extracted. With such a high ratio of NaOH to ash, and repeated extractions, it was hoped that a higher proportion of the Si could be made available. This does not seem to have been the case.

4.5.4 Fusion Product Analysis

The products of the microwave fusion process were analysed using XRD, and the results are presented in Figures 4.23 and 4.24 (see Appendix section C.1 on page 380 for presentation inconsistency discussion). Delta ash prior to fusion is shown in Figure 3.10 on page 66. The phases present in untreated Delta with the clearest peaks are Mullite and Quartz, with weaker peaks for calcite and maghemite-C. After the ash undergoes fusion, the aforementioned phases do not appear to be present, or are obscured by the greater relative intensity of the phases now detected in Figure 4.23. The hygroscopic nature of the product made grinding and preparation prior to XRD analysis more challenging. Water-soluble phases such as natrite ($Na_2CO_3 \cdot H_2O$, which is also noted to be hygroscopic) and sodium silicate are shown, as well as iron phases such as maghemite (γ-Fe_2O_3). These results are in line with literature, with XRD analysis of conventional fusion products having detected water-soluble phases such as sodium silicate and sodium aluminosilicate [39, 40, 44, 57]. These water soluble phases are no longer detected after dissolution in water, shown in Figure 4.24, which is also in line with literature [39, 40, 57]. The phases originally detected in Delta ash are present, notably quartz and mullite, as well as new phases such as sodalite, observed to form during crystallisation processes, and thermonatrite, which is an evaporite of sodium carbonate.

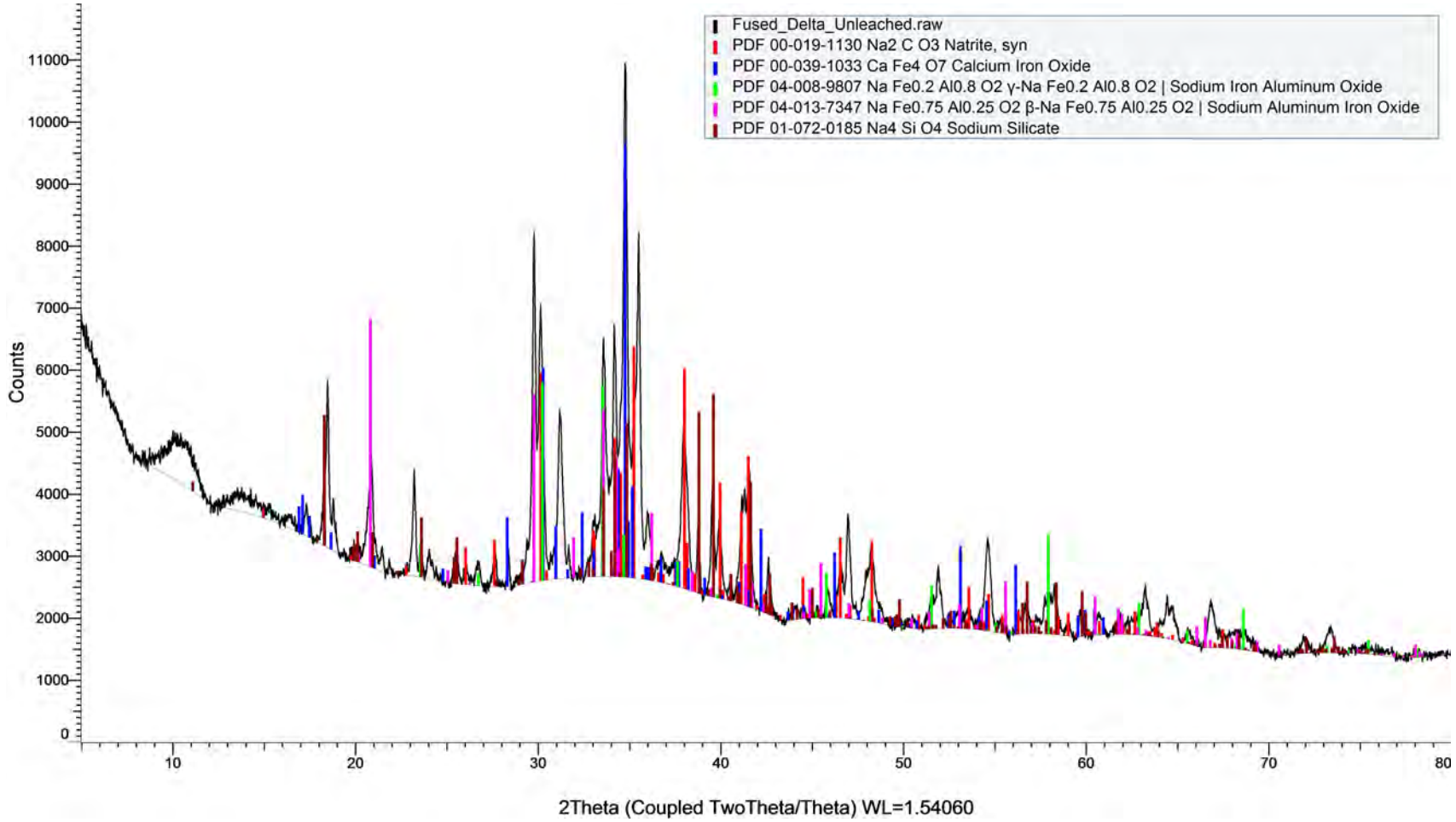

Figure 4.23: XRD Pattern of Delta ash after microwave fusion. $\lambda = 1.5406$ Å

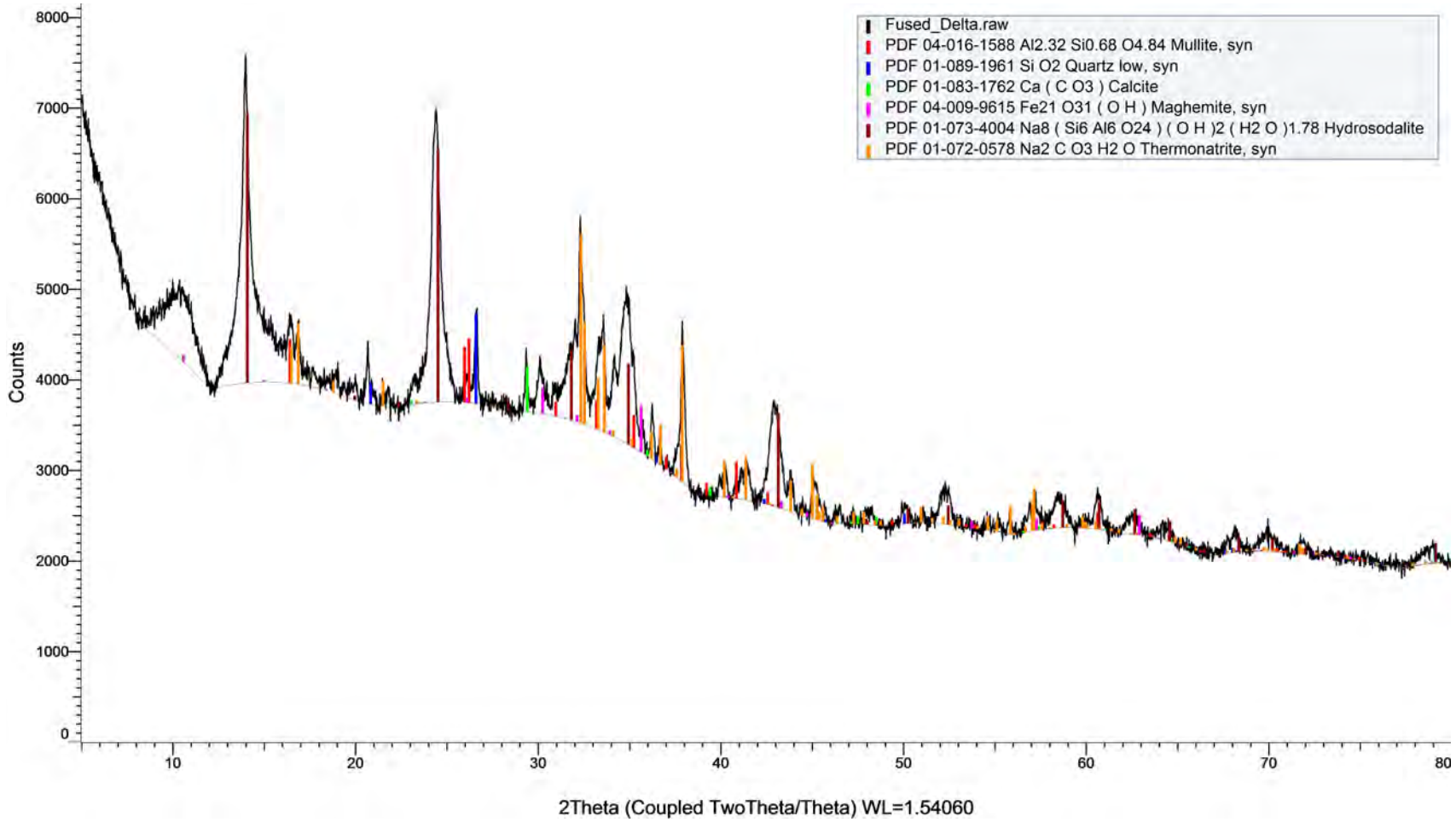

Figure 4.24: XRD Pattern of Delta ash after microwave fusion and leaching. $\lambda = 1.5406$ Å

Sodium hydroxide reacts with atmospheric carbon dioxide to form sodium carbonate as described by equation 4.3.

$$2NaOH_{(s)} + CO_2 \rightarrow Na_2CO_3 + H_2O \tag{4.3}$$

The formation of sodium carbonate from sodium hydroxide would happen regardless of the microwave fusion process due to the sample being exposed to air, however the melting and mixing of molten NaOH would increase the surface area of the NaOH and presumably increase the rate of absorption of carbon dioxide. Sodium hydroxide itself would not appear on the XRD patterns due to it not being crystalline. The sodium carbonate and sodium silicate are then dissolved. Were the ash sample to have been washed after leaching prior to XRD analysis the thermonatrite content would undoubtedly have been lessened or removed. The fusion process turns the ash sample green as shown in Figure 4.25, and as described by Musyoka et al. [85], Soong et al. [86], Yaping et al. [90]. The colouring is attributed to iron (II) hydroxide. The leachate derived from the fusion product is initially green, as shown in Figure 4.26, but turns yellow/ brown over time, as the iron (II) is oxidised to the more thermodynamically stable iron (III), shown in equation 4.4. The fusion product after leaching had a brown tinge, and was distinctly more granular.

$$4Fe(OH)_2 + O_2 + 2H_2O \rightarrow 4Fe(OH)_3 \tag{4.4}$$

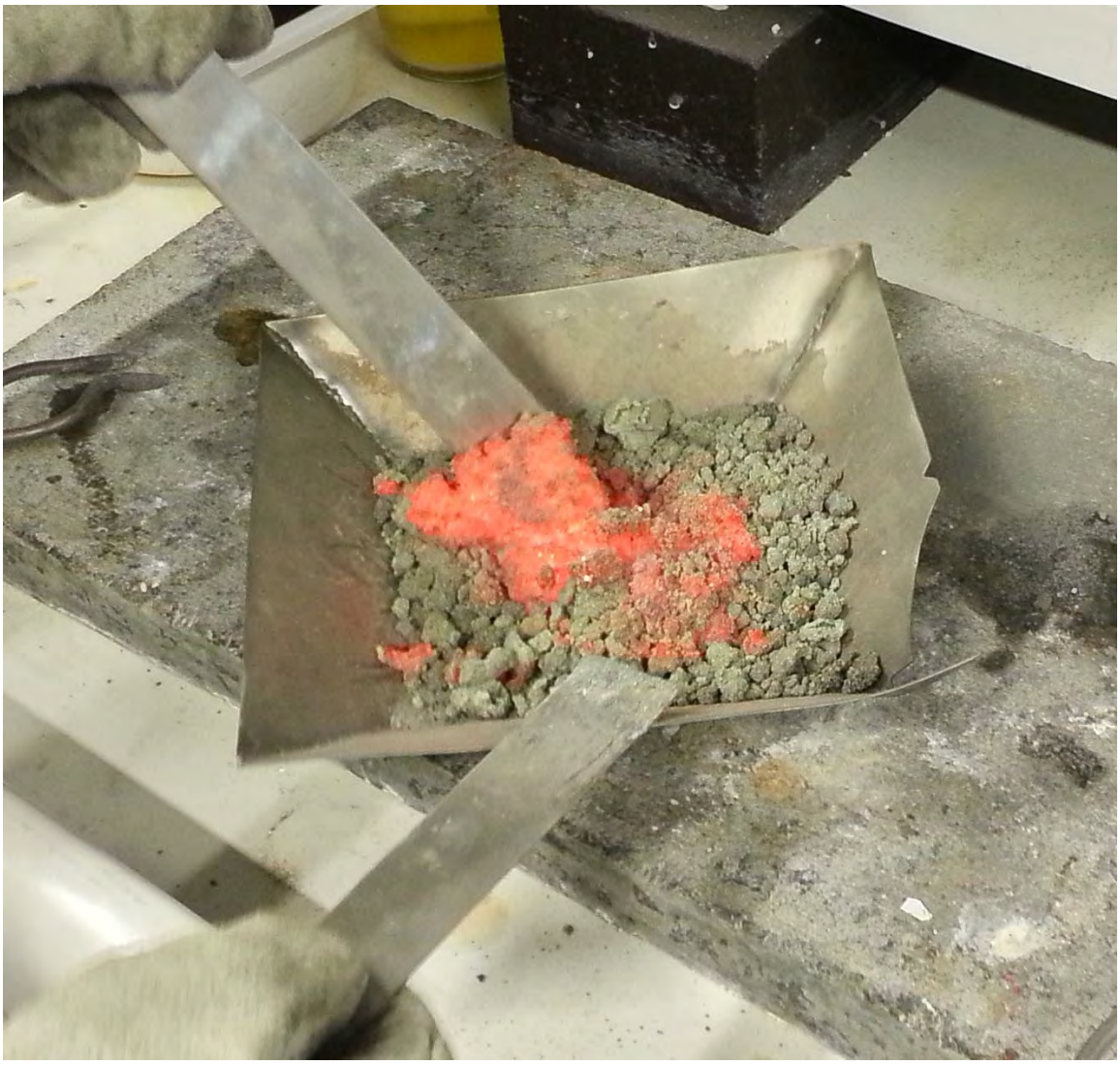

Figure 4.25: Photograph depicting ash after 10 minutes of microwave fusion with NaOH

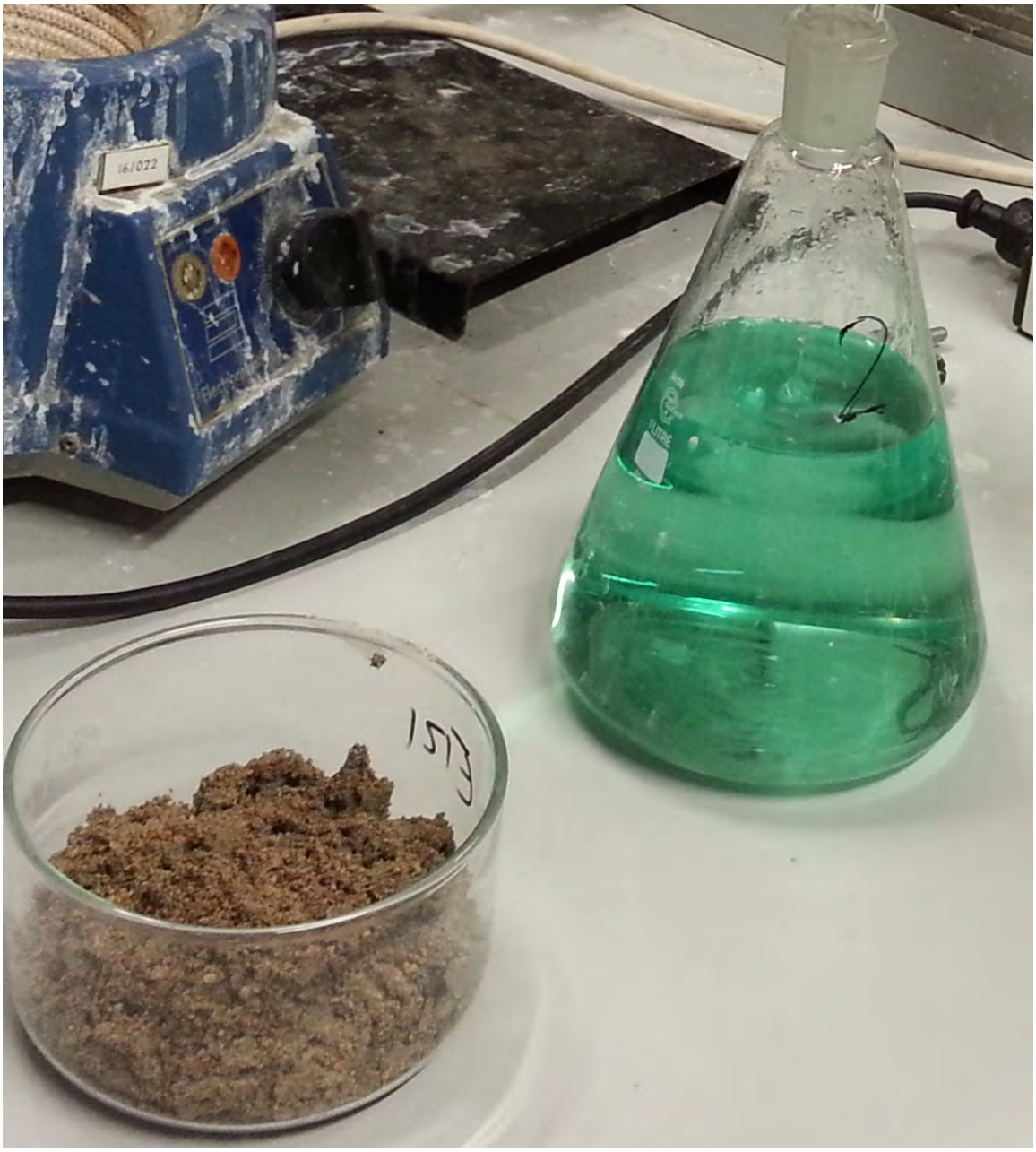

Figure 4.26: Photograph depicting green leachate on the right, and fused ash after leaching on the left

4.6 Effect of Acid Washing Ash on Si and Al Extraction

4.6.1 Hot Vs Cold Acid Wash

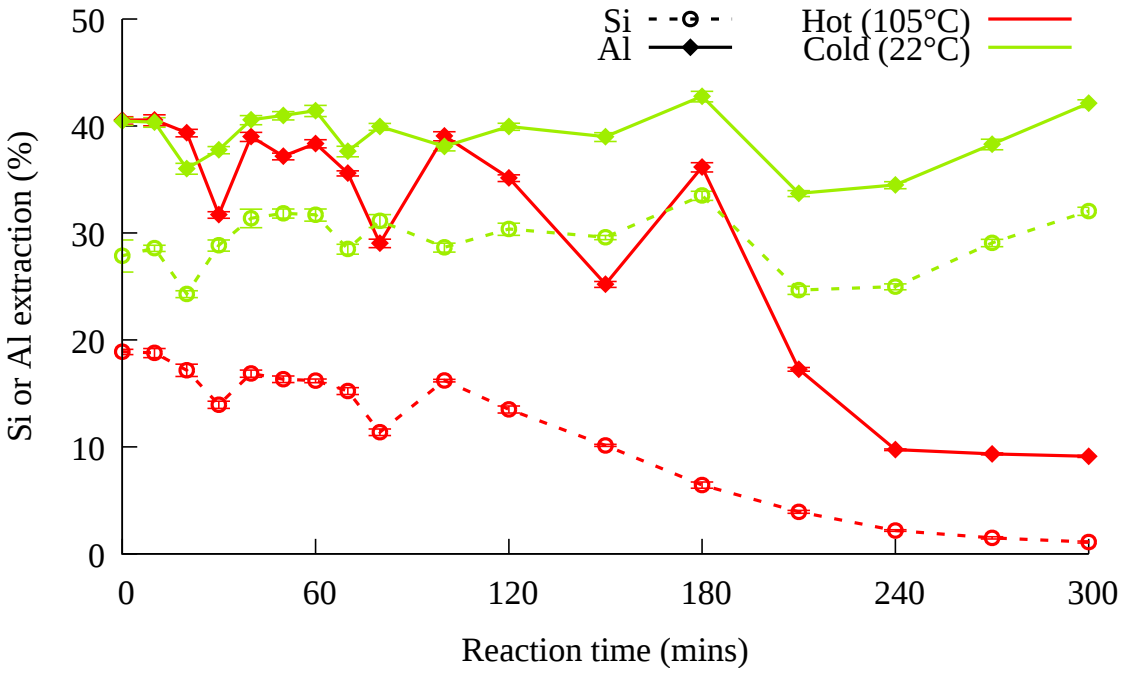

Figure 4.27: Hot (105 °C) vs cold (22 °C) HCl wash of zeolitised ash

A 100 g sample of Delta ash which had previously been hydrothermally leached with 4M NaOH for 1 hour, then washed and dried was mixed with 1L of 2M HCl in two experiments. One experiment was conducted at ambient temperature, and one under reflux conditions at 105 °C. The AAS data of the resulting leachate is shown in Figure 4.27. It shows that the Si extraction was more effective when conducted at ambient temperatures. Al extraction for the first 100 minutes seemed to be similarly effective for reflux conditions and ambient temperature extraction. It is believed that the reflux experiment provided conditions conducive to crystallisation or precipitation of Si, and possibly also Al from solution, based on the steady decrease of the Si content from 100 minutes. As time progressed, the ash became progressively harder to filter, indicating fine particles becoming entrained in the sintered glass filter. This could be because the ash

became finer, or because of new precipitates clogging up the filter.

As can be seen from Figure 4.28, the 3 images 4.28a, 4.28b, and 4.28c of zeolitised ash show a rough, crystalline surface. None of the images of acid-washed ash show this coating to still be present. It is noted that the image 4.28d seems to show long thin crystal structures below the smooth surface of the ash which are not dissimilar to crystals of mullite [42]. The ash which has been in hot acid for 6 hours (figure 4.28e) appears pocked, or coated in lumps. The ash sample which was exposed to ambient temperature acid for even a short period (figure 4.28f) appears to have had the crystalline material removed, revealing the mostly smooth surface of the ash particle. From this, it can be concluded that the heated acid is unnecessary in order to remove the zeolite coating, and that even a quick wash with ambient temperature acid is sufficient to remove the zeolite coating.

4.6.2 Repeated Acid Washes

Ash which had previously been hydrothermally leached and washed was mixed with four successive 250 ml aliquots of 2 M HCl at ambient temperature. Two different ash samples were used, one Delta ash sample which had been leached with 4 M NaOH for 1 hour and another Delta ash sample which had been leached with 3.5M NaOH and 0.25 M Na_2CO_3 for 1 hour. After the ash was filtered from the alkaline leachate, the Büchner funnel was washed with distilled water, and then concentrated HCl, in order to avoid clogging the funnel's pores with aluminosilicate precipitate when the pH was reduced. After the acid wash, the ash was returned to the funnel, and the first aliquot of HCl was added, the air flow in the Büchner funnel was reversed and the ash and acid mixture was sparged for 2 minutes. After 2 minutes, the air flow was returned to normal, and the first 250 ml aliquot of acid was saved for later analysis. This process was repeated with three more 250 ml aliquots of HCl. In Figure 4.29 the Si and Al content of the alkaline leachate is shown on the Y axis at "0 ml HCl", followed by the Si and Al contents of each 250 ml aliquot of HCl which followed washing. The Si and Al content appears highest in the first 250 ml aliquot

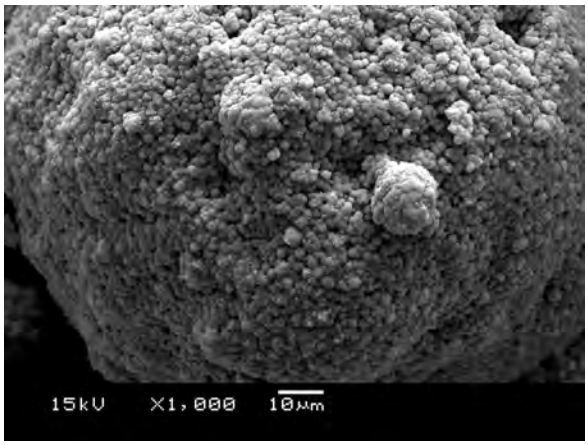

(a) Zeolitised Ash Sample 1

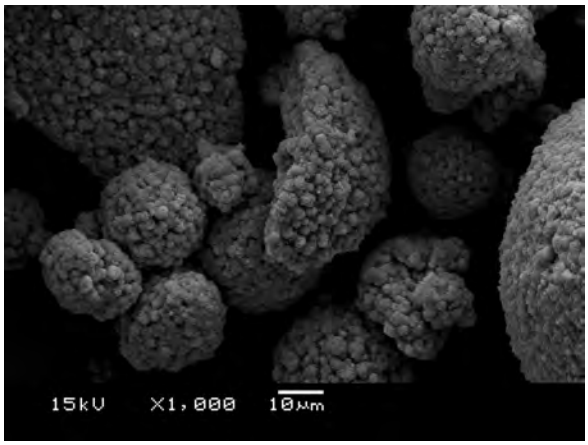

(b) Zeolitised Ash Sample 2

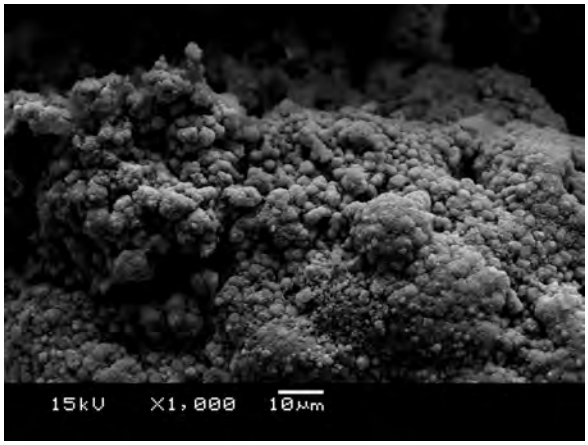

(c) Zeolitised Ash Sample 3

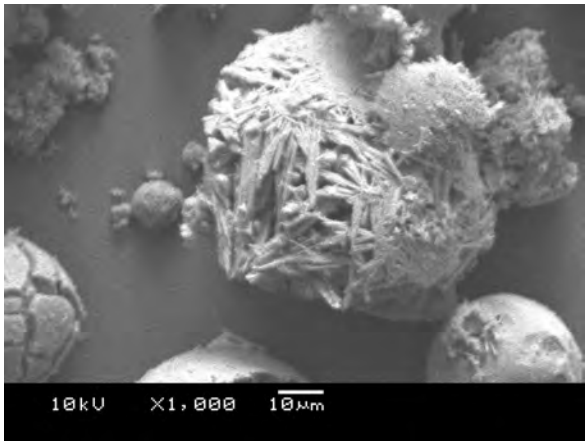

(d) Hot acid Washed at 0 minutes

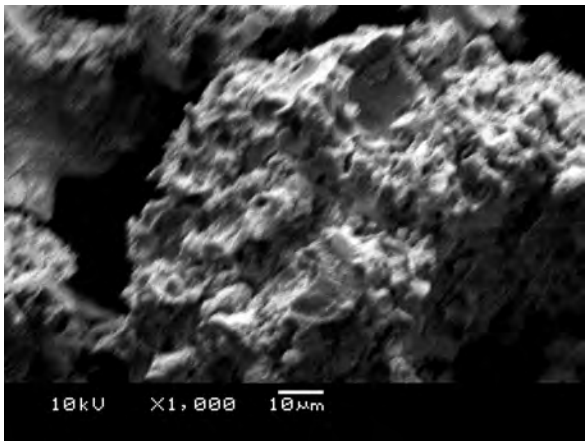

(e) Hot acid washed at 6 h

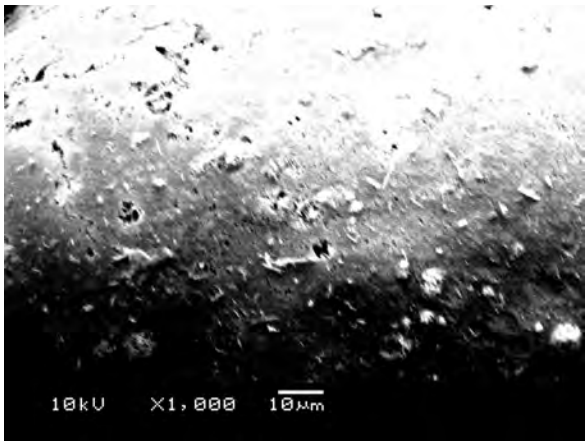

(f) Cold acid wash at 0 minutes

Figure 4.28: SEM images of ash, showing effects of dissolving zeolite coating in 2M HCl

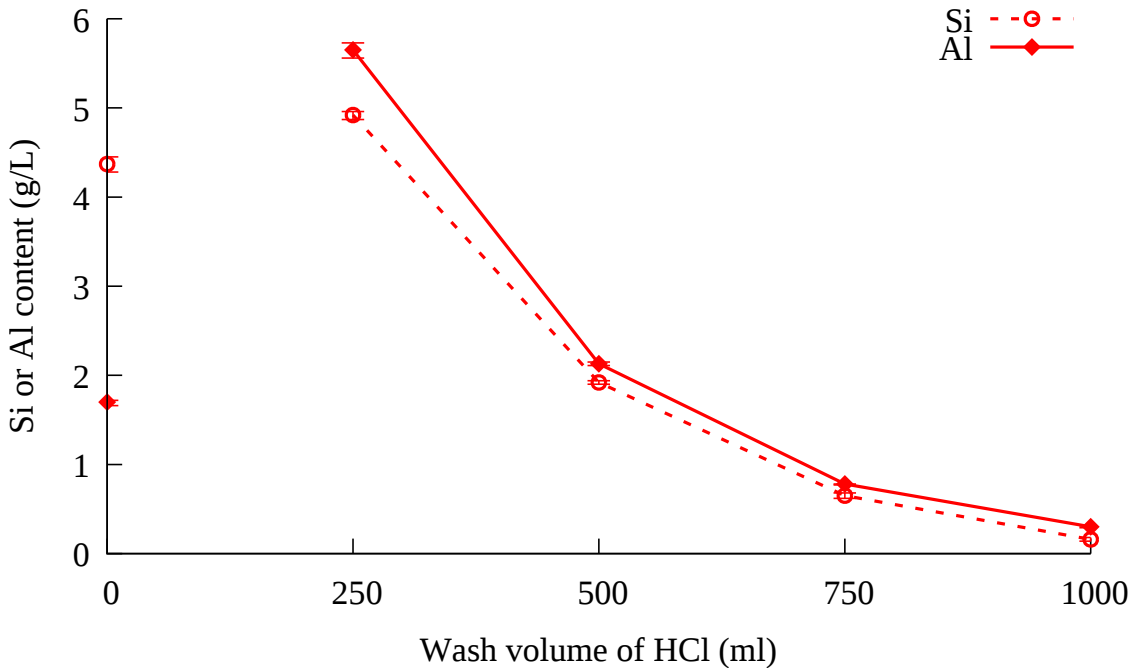

Figure 4.29: Si and Al content of HCl following repeated washes with 250 ml HCl

of HCl, and then decreases in each successive washing. The general trend indicates that the aluminosilicate coating on the surface of the ash particles is easily dissolved in acid, and that further washing with more than four 250 ml aliquots is unnecessary.

4.6.3 Acid Washing Alkaline Ash

Ash was hydrothermally leached with 1 L of 3.5 M NaOH and 0.25 M Na_2CO_3 for 1 hour. One sample was then washed with 1L of distilled water, and the other was not. Both ashes were mixed with ambient temperature 2 M HCl for 24 hours, with samples taken every hour for 12 hours, and then a final sample taken at 24 hours. The HCl samples were then analysed for their Si and Al contents, the results are shown in Figure 4.30. The unwashed ash (green) has a higher Si content in the first sample. This is believed to be due to dissolved Si from the alkaline hydrothermal leaching not being washed away in the distilled water. The Si content then increases to a maximum at 1 hour, before decreasing and becoming stable at 4 hours. This indicates that previously dissolved Si precipitates out of the solution over the first 4 hours. The washed ash (red) appears to follow a similar

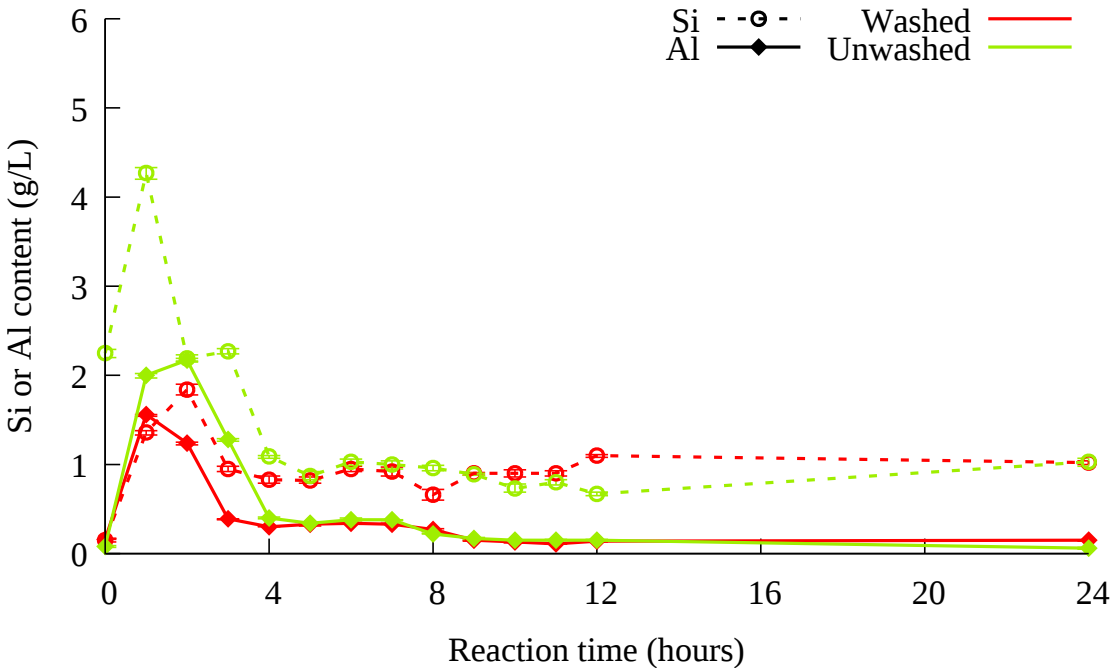

Figure 4.30: Si and Al content of HCl from alkaline zeolitised ash, and washed zeolitised Delta ashes

process, but from a lower starting point. The maximum Si and Al yields are at 2 and 1 hours respectively before decreasing and reaching a stable plateau from 3 hours.

4.7 Long Term Extraction Average

In order to conduct experiments on crystallisation conditions, multiple extractions of Si and Al were carried out on the Delta ash using the same method. The method used was a 10 minute fusion of NaOH and ash in a microwave, on full power, stirred at 5 and 10 minutes. 10 minutes was chosen based on Figure 4.20. 2 moles of NaOH and a NaOH/ash ratio of 1.2 were used, based on results from Figure 4.14b. This fusion product was then added to 1L of ambient temperature distilled water and stirred at 2000 rpm for 10 minutes (based on results from Figure 4.16), after which the ash was filtered out using a sintered glass Büchner funnel. It is noted that the fusion product and post-filtration leachate were green in colour, as noted in literature [85, 86, 90]. This green colouring was attributed to the iron(II) hydroxide content. It was noted that the fusion product was heated to the

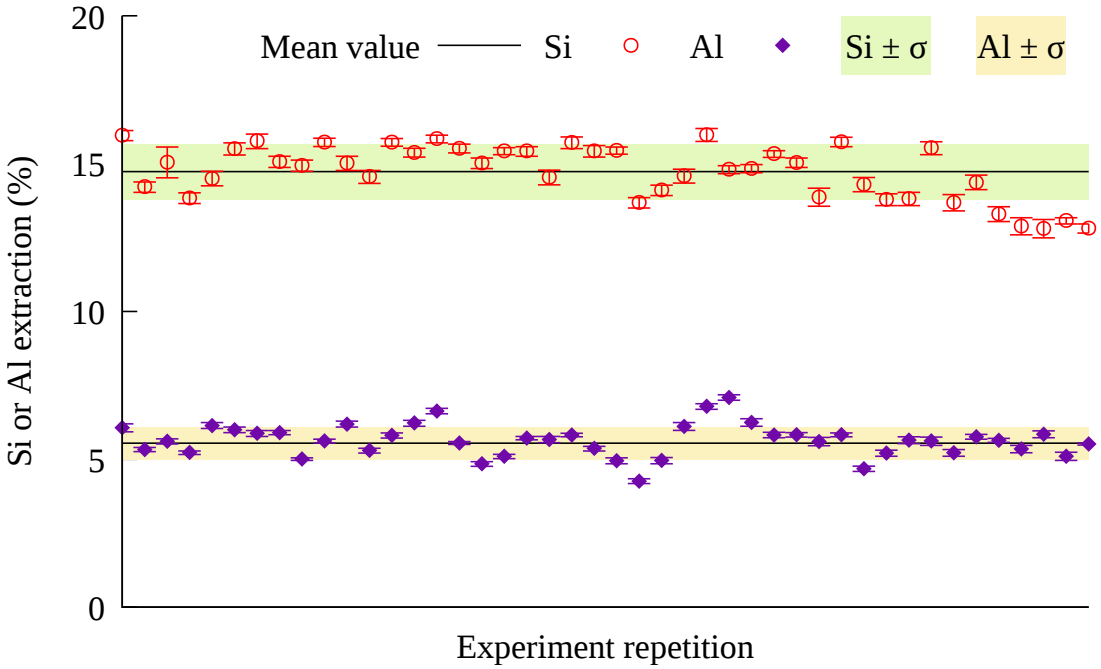

Figure 4.31: Average Si and Al content of 44 identical extraction experiments

point that some parts glowed red hot by the end of the fusion process. The data in Figure 4.31 shows the AAS results for Si and Al content of the leachate, mean values for these results, and a highlighted area 1 standard deviation either side of the mean. The relative standard deviation (RSD) for the Si is values is 6 % and the RSD for the Al values is 10 %. This variation is put down to a combination of factors listed below.

- Ash is a heterogeneous material, the Si and Al content of each ash sample is unlikely to be the same.
- Ash and NaOH were not perfectly mixed during microwave fusion
- Microwave fusion heating was not even due to the limitations of the microwave oven. The centre most parts of the NaOH/ash mixture glowed red hot, outer parts did not.

As a proportion of Si and Al extracted from ash, these mean values represent 14.7 % of the Si and 5.6 % of the Al. Whilst these values may be considered low, the extraction process is very rapid at only 20 minutes plus filtering time.

4.8 Use of Rice Husk Ash as a Starting Material

4.8.1 Rice Husk Ash Heat Treatment Temperature

Multiple samples of rice husk ash (RHA) were available as a source material for zeolitisation. The difference between the samples was the temperature at which they were processed. The temperatures varied between 700 and 950°C, four of these RHA samples were leached with NaOH, and compared to the Delta ash. The method used was the hydrothermal extraction method discussed in section 4.4.1. Following the process diagram shown in Figure 2.12, 800ml of distilled water (D) and 80 g of NaOH (B) were added to the extraction vessel (I) depicted in Figure 4.1. The condenser, mixer and heater were turned on, and the solution brought to the boil. 50 g of Delta ash or RHA (A) were then added to the vessel, and washed in with 200 ml of distilled water (D) and the timer started. AAS results for the leachate (N) are shown in Figure 4.32. The coal fly ash is 24 % Si, whilst the RHA is 44 % Si. By 60 minutes, 16 % of the Si from the Delta ash is in solution, whilst 50-69 % of the the Si has been extracted. In absolute terms, the Si content of the RHA leachate is approximately six times greater than the Delta ash sample.

Between the four RHA samples analysed, the 700°C sample appears to have the highest solubility, producing the highest Si extraction within the 40 minutes. As RHA treatment temperature increases, the solubility decreases, with the 950°C sample being distinctly less soluble than the other three RHA samples for the first 80 minutes. There is minimal increase in Si extraction after 1 hour for the 700-800°C RHA, and the 950°C RHA similarly plateaus after 2 hours. The increased solubility of the lower temperature RHA is attributed to lower temperature ashes containing less crystalline material such as cristobalite. Figure 3.12 shows the XRD patterns for six RHA samples. The prominent crisobalite peak is at 22°2Θ, with a smaller peak at 36°2Θ. Other peaks greater than 36°2Θ are 4 % or less of the intensity of the 22°2Θ peak, and are thus unlikely to be detected due to signal noise. Due to the broadening of the 22°2Θ peak, peaks between 25 and 30°2Θ would be difficult to detect, even if their relative intensity were not very low.

These RHA XRD patterns come from a reflection diffractometer and were analysed for 1 hour. Most other XRD patterns in this work were analysed in a transmission diffractometer for 10 minutes. The longer time in the different instrument was necessary, as the 950°C ash peak was not detected in the transmission diffractometer.

Due to the highly heterogeneous nature of the RHA, observing the progress of the dissolution process through SEM images of the ash is equivocal. The broad trend appears to demonstrate a pitting and roughing of smooth surfaces as shown in the differences between Figures 4.33a and 4.33d; and between Figures 4.34a and 4.34e.

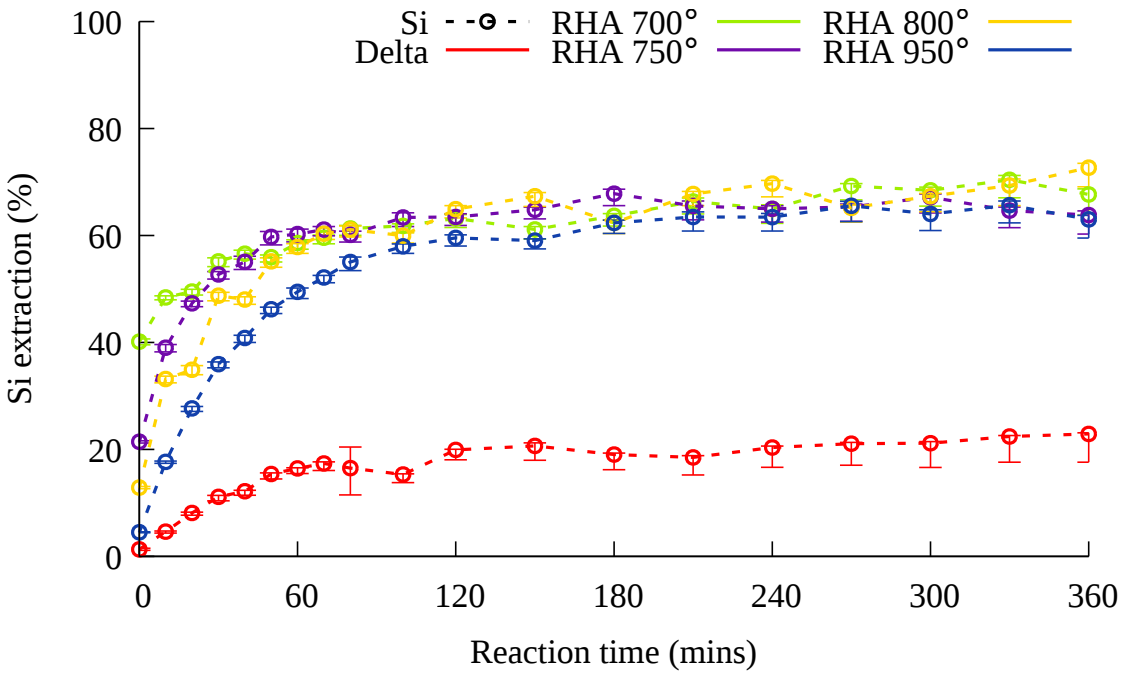

Figure 4.32: Si content of leachate from Delta ash Vs Rice Husk Ash

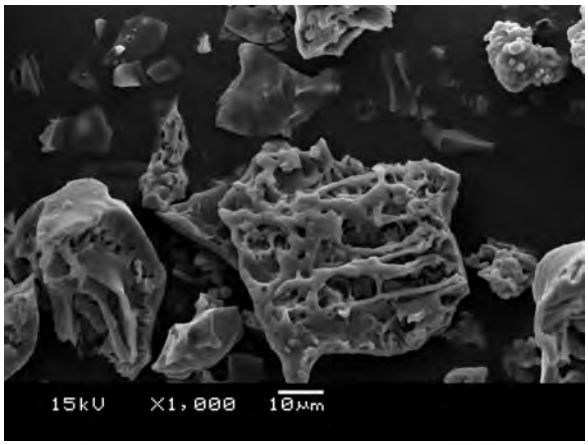

(a) 0 minutes

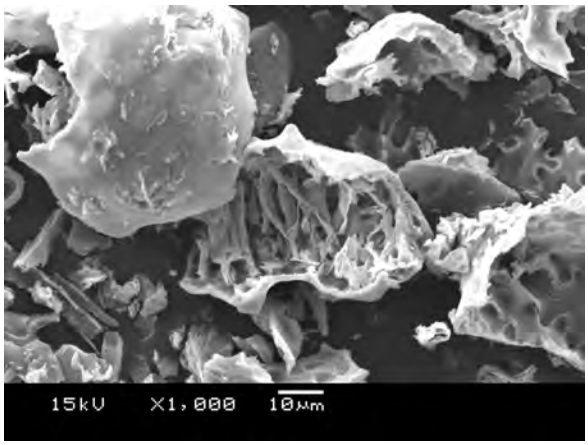

(b) 10 minutes

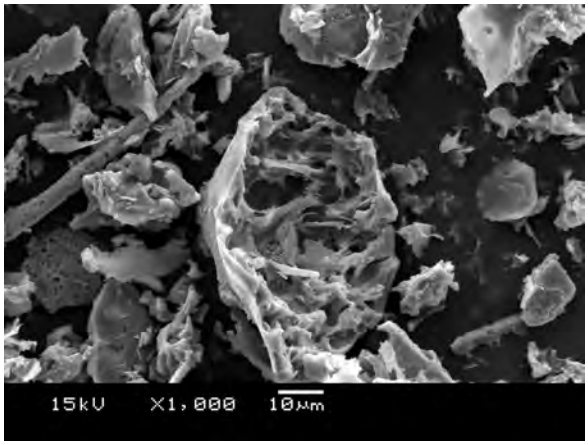

(c) 30 minutes

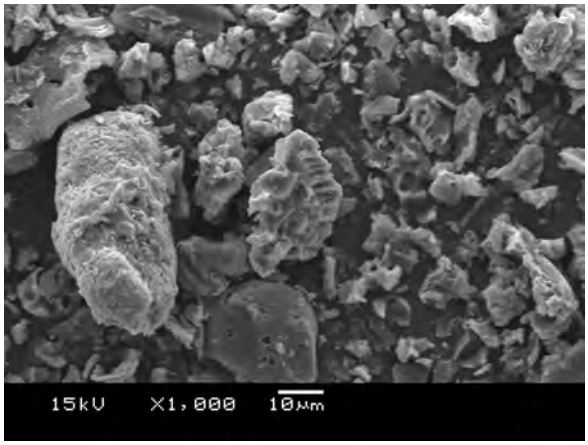

(d) 60 minutes

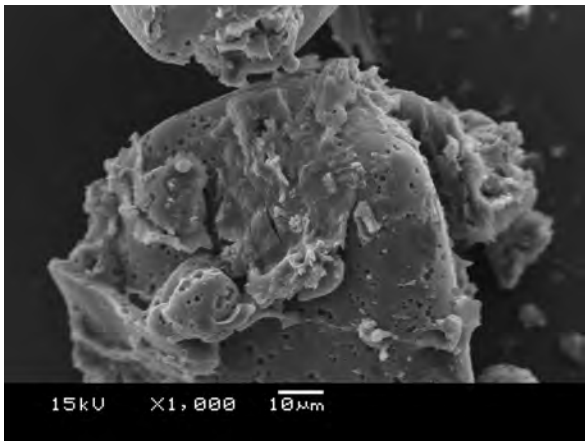

(e) 2 hours

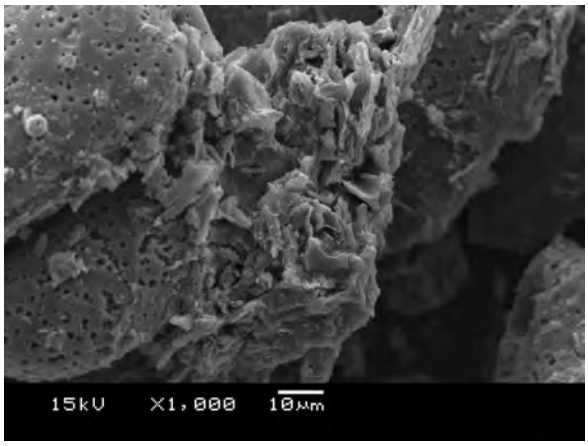

(f) 6 hours

Figure 4.33: SEM images of leached RHA treated at 700°C

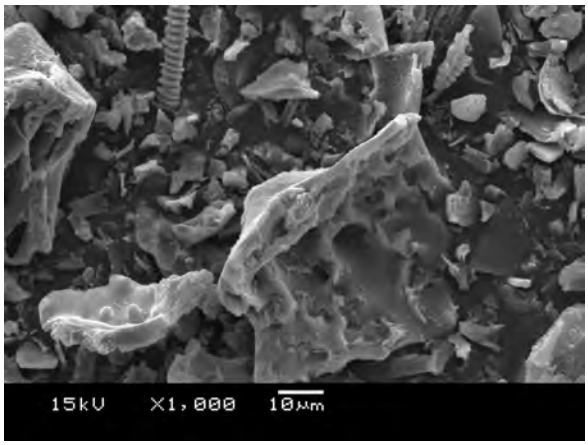

(a) 0 minutes

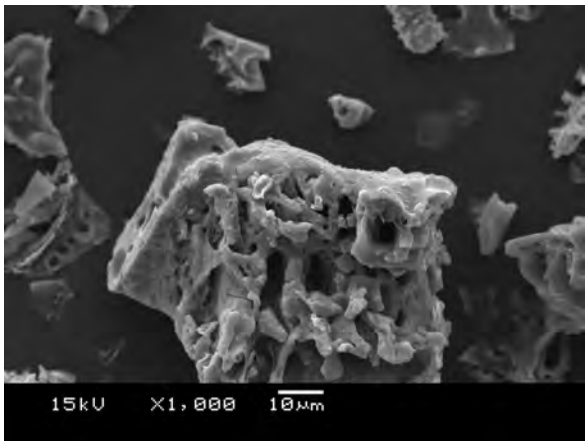

(b) 10 minutes

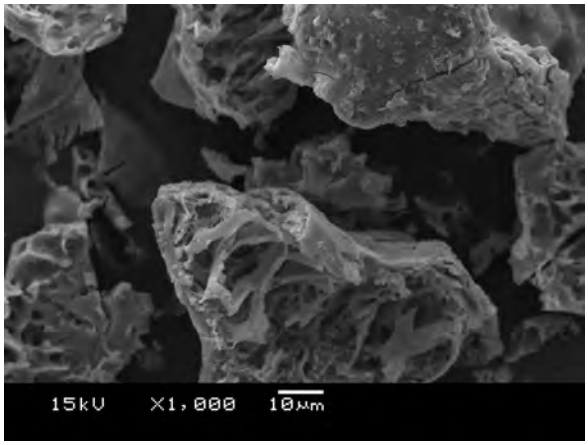

(c) 30 minutes

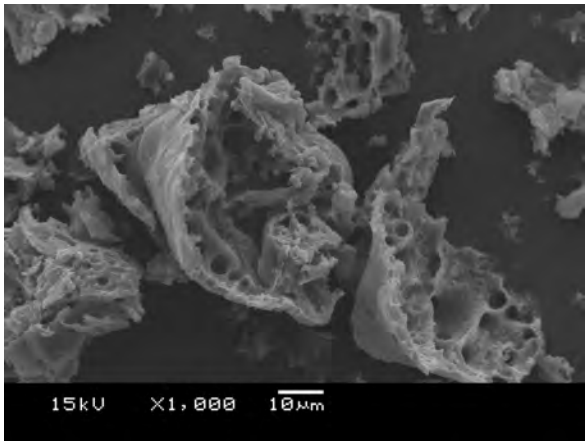

(d) 60 minutes

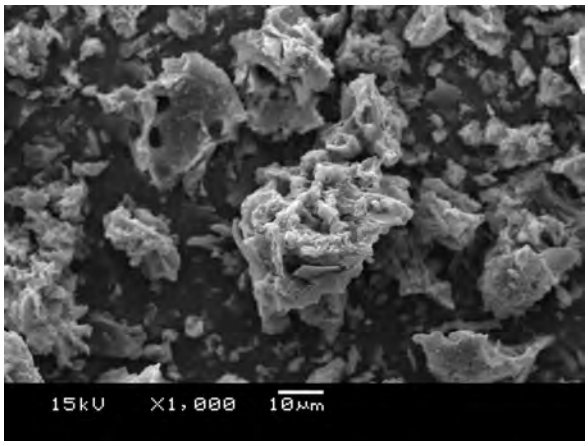

(e) 2 hours

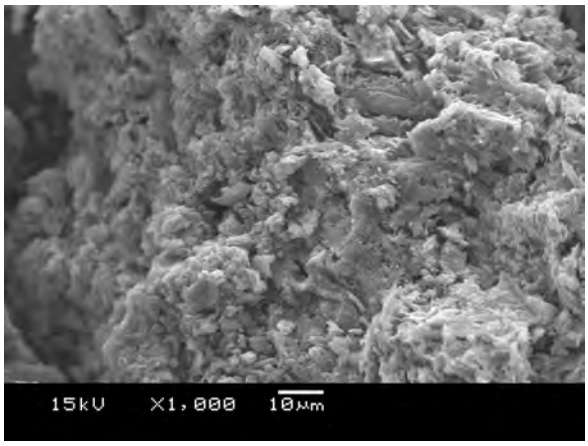

(f) 5.5 hours

Figure 4.34: SEM images of leached RHA treated at 950°C

4.8.2 RHA Solids loading

Si extraction appears to plateau after 1 hour for the 700-800°C RHA samples in Figure 4.32. For this reason, subsequent Si extraction experiments from RHA were carried out for 1 hour. The next experiment conducted investigated the effect of solids loading on hydrothermal extraction of Si from RHA. From Figure 2.12: NaOH (B) and liquid content (D) were kept constant, but the quantity of RHA (A) used was reduced from 50 g to 25 and 12.5 g, all from the same 700°C RHA sample. The experimental protocol was otherwise consistent with the previous section. Figure 4.35 shows the AAS results of leachate from the three different solids loadings. As the quantity of RHA decreases, the percentage of Si extracted increases slightly. The exception to this is the 0 minute sample for the lowest RHA dosage, which is slightly lower than the other two results. The slightly decreased value for Si extraction for the lowest solids loading (NaOH/RHA = 6.4) at 0 minutes is attributed to the time taken to add ash to the leaching vessel; it took longer to add 50 or 25 g of ash to the vessel than it did to add 12.5 g of ash, resulting in the higher solids loading experiments having a slightly longer contact time prior to the experiment start. From this data, it would appear that the three solids loadings presented had minimal effect on the solubility of the ash, resulting in a Si yield of approximately 50 % after 10 minutes, and 60 % by one hour.

4.8.3 Effect of NaOH Concentration on Si Extraction from RHA

Complete dissolution of RHA was desired, thus an experiment was designed with a higher NaOH content to investigate if 8M NaOH would yield more Si in solution. The experimental conditions were the same as in the previous conditions, however 8M of NaOH were used in lieu of 2M. Figure 4.36 shows the result of this experiment. Again the experiment was conducted for 1 hour, as the increase in yield observed in other experiments after 1 hour was minimal. The data shows that varying the NaOH concentration between 2 and 8 M does not significantly affect the results.

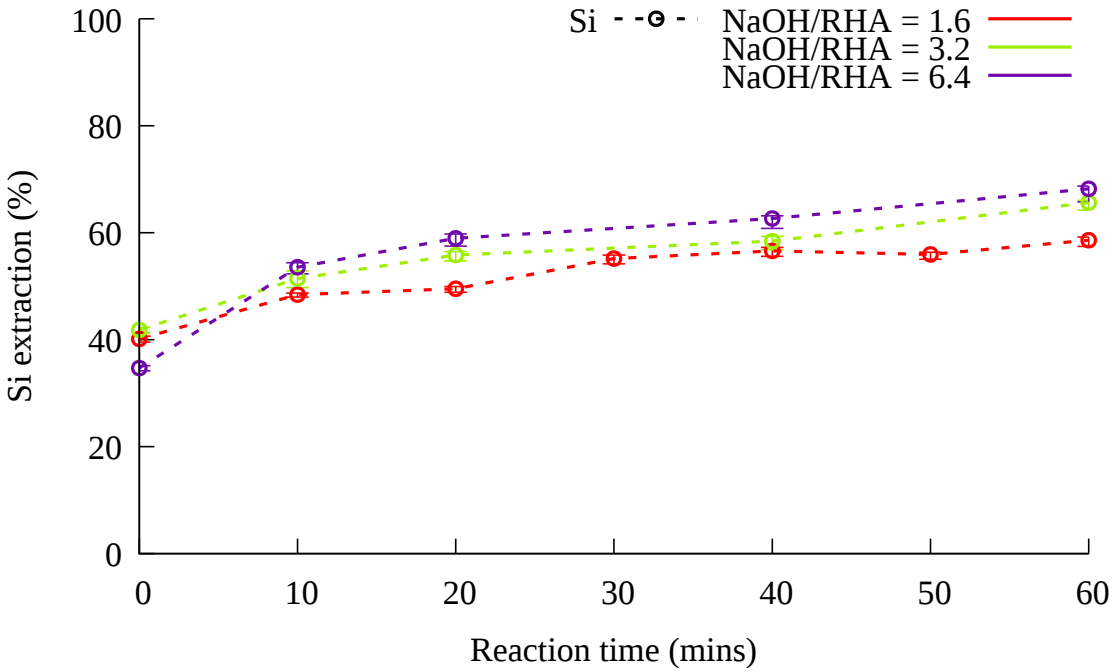

Figure 4.35: Si content of leachate at various solids loadings. 80 g NaOH/ 50 g RHA = 1.6; 80 g NaOH/ 25 g RHA = 3.2; 80 g NaOH/ 12.5 g RHA = 6.4

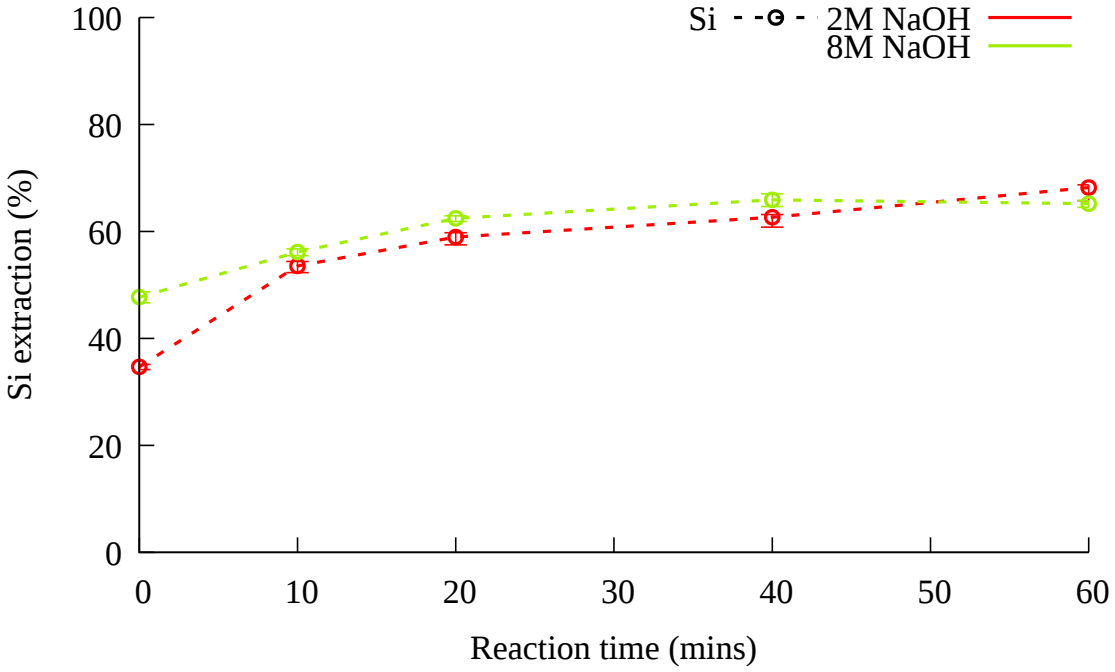

Figure 4.36: Si content of leachate of RHA at two NaOH concentrations

4.8.4 Extraction Method

In another attempt to increase the yield of Si in solution, the hydrothermal extraction method was compared to the furnace fusion extraction method. For the fusion method,

12.5 g of 700°C RHA was mixed with 80 g of NaOH (NaOH/ash ratio = 6.4) and put in a nickel crucible and heated to 550°C, left to cool and broken up with a pestle and mortar before being dissolved in 1 litre of distilled water under reflux conditions. Removing the fusion product from the nickel crucible proved challenging, and it was not possible to remove the entirety of the sample, thus AAS results shown in Figure 4.37 for the fusion method should be taken as a slightly lower estimate of potential Si yields. The decreased value for Si at 0 minutes for the fusion sample in comparison to the hydrothermal sample can be attributed to the fusion product still being in lumps, compared to the loose powder of the RHA in the hydrothermal method. With the exception of the 0 minute sample, all other sample points seem broadly similar, and the fusion method appears to offer no improvement in yield from the hydrothermal method.

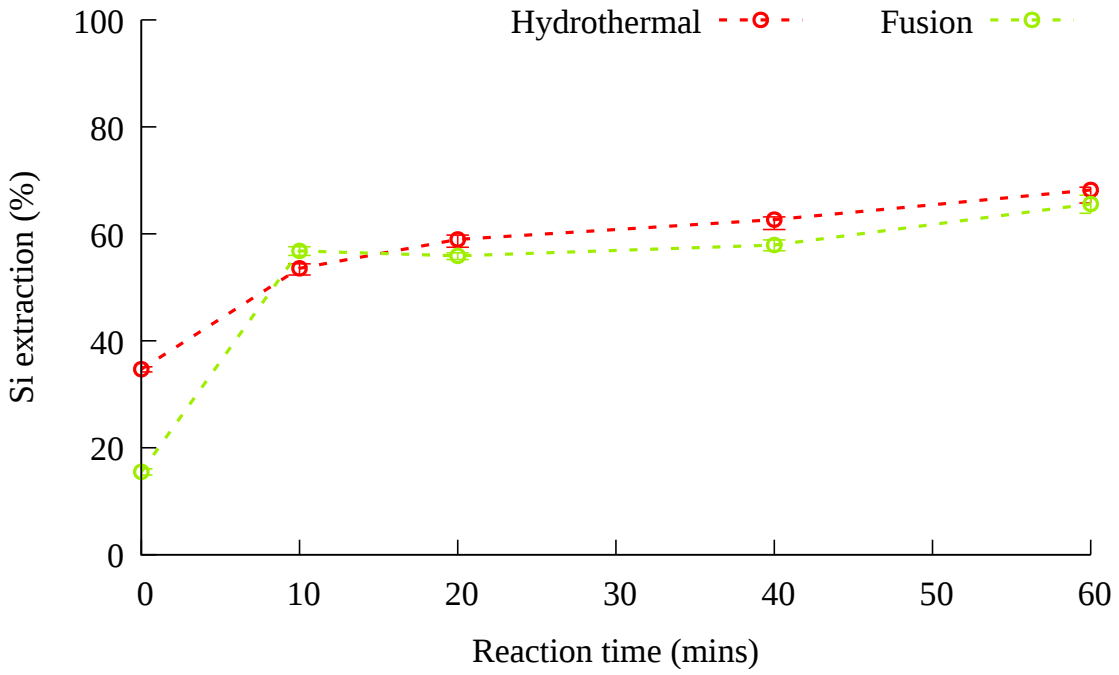

Figure 4.37: Si content of leachate from different extraction methods

4.9 Summary of Extraction Experiments

4.9.1 Hydrothermal extraction

Hydrothermal alkaline extraction produces a greater yield of Si as NaOH concentration increases. There is minimal increase in Si yield from 1-6 hours, and Al content peaks at 30-40 minutes before decreasing due to consumption through formation of a zeolite coat on ash particles.

Replacing NaOH with a quantity of Na_2CO_3 during hydrothermal extraction results in a slightly decreased yield in Si content and a minimal increase in Si yield between hours 1 and 6. A similar consumption of Al from 30-40 minutes is also observed.

4.9.2 Fusion and Dissolution

Hot dissolution of fusion products showed preferable results for samples which were not ground. This counter intuitive result is attributed to dissolution during the unsampled heating phase of the experiment. The samples which were not ground produced a Si yield which was comparable to the hydrothermal extraction method. Further dissolution experiments at ambient temperatures produced yields of Si comparable to the hydrothermal extraction methods. Al was noted to not decrease during ambient temperature extractions due the conditions not being as favourable for zeolite crystallisation.

Microwave fusion experiments were found to produce similar yields of Si and Al to dissolution of fusion products or hydrothermal extraction experiments. Both conventional and microwave fusion were noted to produce yields of Si and Al which did not vary greatly between 10 minutes and 6 hours, providing scope to speed up the extraction process through a faster fusion method and a shorter dissolution process.

Optimisation of the NaOH/Ash ratio for the microwave fusion process found that a 1.2 ratio of NaOH/ash produced the highest yield of Si in solution. No obvious improvement in Si extraction was observed by extending the microwave fusion process from 5 to 40 minutes. Experiments with a low power to fusion product ratio produced similar

extraction efficiencies to higher power to fusion product ratios, indicating that the process could be optimised by microwaving larger batches at once.

Comparison of the microwave fusion experiment with different starting CFA's produced the highest yields for the Delta processed fly ash, and the poorest yields for the the FB7 ash and the Alpha processed fly ash.

4.9.3 Extraction Maximisation

Re-leaching of zeolitised ash in order to maximise Si and Al extraction showed a minimal improvement in Si yield. Al-rich acid solutions did not provide a viable feedstock for the crystallisation process and this extraction maximisation method was not pursued further.

4.9.4 Rice Husk Ash

Rice husk ash provides a promising feedstock as a Si-rich material which is well suited to hydrothermal extraction as it lacks a significant Al content. Yields of Si show minimal improvement between 1 and 6 hours, but show a yield three times higher than that of the Delta processed fly ash. Hydrothermal extraction of Si from RHA appears to be unaffected by solids loading within the range tested, and appears similarly unaffected by increasing the alkalinity of the hydrothermal extraction process. RHA also appears to be suited to fusion and dissolution as an extraction method.

Chapter 5

Crystallisation of Zeolites: Effect of Leachate & Temperature

5.1 Introduction

5.1.1 Apparatus

For crystallisation experiments conducted under reflux conditions, the apparatus shown in Figures 4.1 and 4.2 was used. For crystallisation experiments conducted at specified temperatures, two IKA C-MAG HS 7 magnetically stirred hot plates with feedback temperature controls from IKA ETS-D5 temperature probes were used. This apparatus is shown in Figures 5.1 and 5.2

5.1.2 Experimental Conditions

A variety of experimental conditions are explored in this chapter. These are itemised below:

- Leachate from Na_2CO_3 leached Delta ash with a potentially reduced Ca^{2+} content.
- Crystallisation at 100°C on a hot plate with variation in sodium aluminate content.

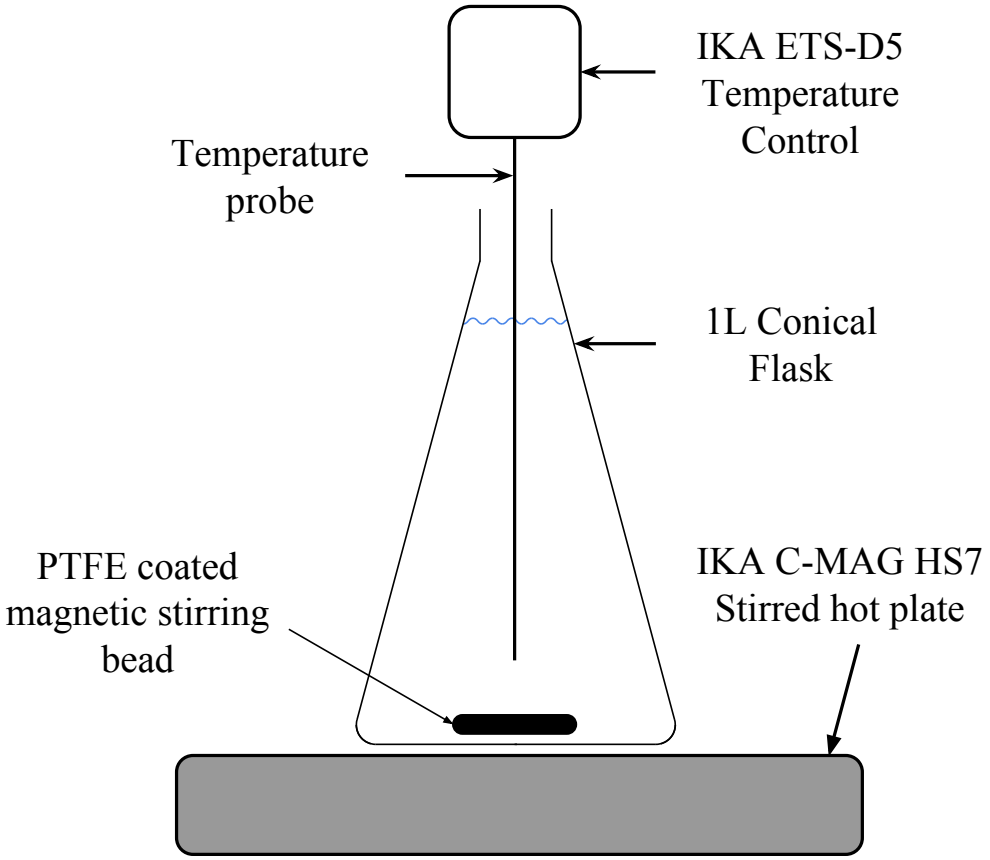

Figure 5.1: Diagram showing equipment setup for set temperature crystallisation reactions

- Crystallisation with variation in sodium aluminate content and experiment temperature.
- Influence of NaOH on crystallisation.
- Influence of Na^+ source on crystallisation.
- Influence of additional NaCl on crystallisation.
- Influence of NaCl with varied sodium aluminate on crystallisation.
- 95°C constant temperature on crystallisation.
- Influence of NaCl Vs sea salt on crystallisation.
- Influence of sea salt with varied sodium aluminate on crystallisation.
- Influence of source ash (Delta, Alpha, FB7, Lagoon and RHA ashes).

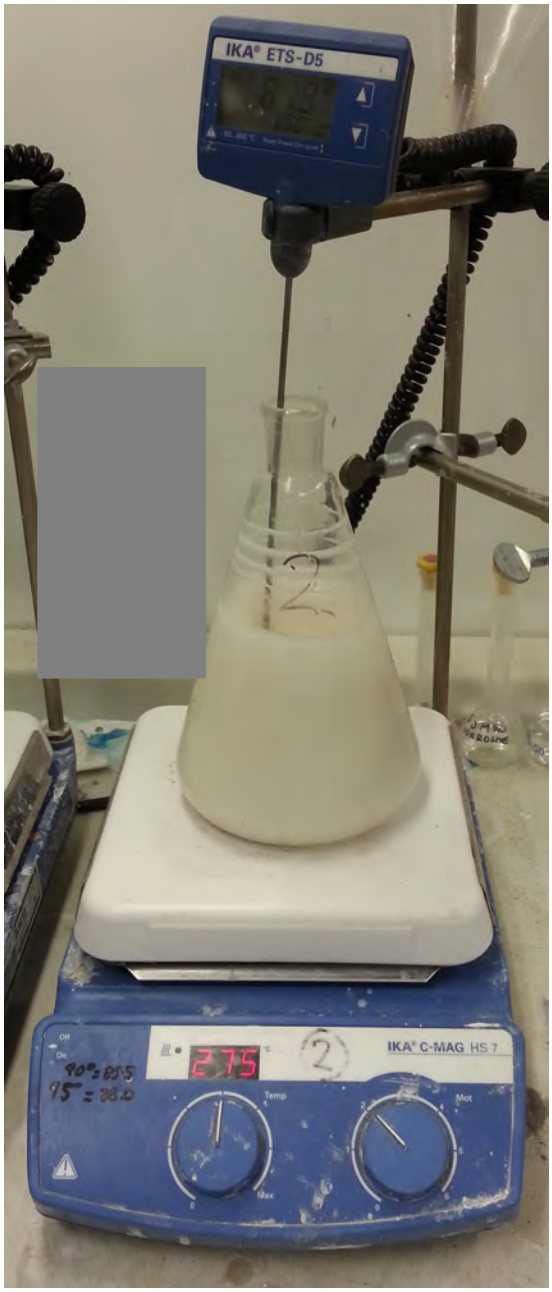

Figure 5.2: Photograph showing equipment setup for set temperature crystallisation reactions shown in figure 5.1

- Manufacture of zeolites on a buoyant substrate.

5.2 Synthesis of Zeolites from Na_2CO_3 Leached Ash

It was noted by Catalfamo et al. [5] that excess CaO may inhibit crystallisation of zeolites.

XRD spectra of zeolites produced by Murayama et al. [75] using 1-3 M Na_2CO_3 show a

mixture of zeolite P, mullite quartz and $CaCO_3$. It was hypothesised that by leaching with a mixture of NaOH and Na_2CO_3, the $[CO_3]^{2-}$ could react with any calcium present in the ash to produce $CaCO_3$, and possibly improve the yield of zeolite. Three pairs of experiments were carried out to investigate substitution of NaOH for Na_2CO_3, with increasing amounts of sodium aluminate added to the crystallisation process. The total concentration of OH^- was kept constant at 4 M.

5.2.1 Experimental Method

For the extraction process, The NaOH (Ⓑ from Figure 2.12, page 46) was added to the reflux vessel Ⓘ depicted in Figure 4.1. Na_2CO_3 Ⓒ, if applicable was then added, followed by 800 ml of distilled water Ⓓ, and the heater Ⓙ, mixer and condenser turned on and the solution brought to boiling point. 100 g of Delta ash Ⓐ was then added and washed in with 200 ml of distilled water, and the timer was started. The hydrothermal extraction proceeded for 60 minutes, before being filtered Ⓛ, with the leachate Ⓝ retained for crystallisation.

For the crystallisation process, 500 ml of leachate Ⓝ was placed in the reflux vessel shown in Figure 4.1 Ⓣ, followed by 300 ml of distilled water Ⓟ. The condenser, and heater Ⓤ were turned on, and the mixer set to 300 rpm. A quantity of sodium aluminate (160, 200 or 240 g sodium aluminate /kg FA) Ⓞ was added to the remaining 200 ml of distilled water and dissolved with the aid of an ultrasonic bath. The clear sodium aluminate solution was added to the clear leachate mixture when the leachate mixture reached its boiling point. This formed an opaque, "milky" solution, which is consistent with observations in literature [7]. 25 ml samples were taken with a syringe and tube and emptied into a sintered glass Büchner funnel Ⓥ. The leachate Ⓦ was retained for later analysis, while the zeolite sample Ⓧ was washed with excess distilled water, and the sample dried in an oven.

5.2.2 Results

The AAS results for 0 hours are theoretical values, based on the Si and Al contents of the first leachate (L1), the proportions of leachate and distilled water used, and the Al content of sodium aluminate added. There is an immediate precipitation upon addition of sodium aluminate to hot, Si-rich solutions, and starting points for the Si and Al contents of the crystallisation solution were desired. AAS analysis of leachates shows a general trend of Si and Al content of the solutions decreasing over time as shown by Figures 5.3, 5.4, 5.5 and 5.6. The XRD analysis showed little or no crystalline material at first, with zeolite A and sodalite forming as the experiments progressed, as shown by Figures 5.7-5.11. Figures containing more data are available in the Appendix Figures B.1-B.4 beginning on page 372. Comparing the AAS results with literature experiments show similar results. Belviso et al. [40] showed a decreasing Si and Al content from 1-24 hours for in-situ conversion experiments. Whilst the experimental conditions were not the same, both data sets show Si and Al being consumed to synthesise zeolites.

SEM images show cubes (zeolite A has a cubic structure [38, 40]) surrounded by rough spheres (likely sodalite). From Figures 5.5 and 5.6 it is noted that increasing the sodium aluminate content from 80 g/kg FA or 100 g/kg FA to 120 g/kg FA reduces the amount of available Si in solution. Replacing NaOH with Na_2CO_3 does not seem to have produced a noticeable effect, other than decreasing the quantity of available Si at the start of the crystallisation process. This decrease in available Si in the starting solution is attributed to Na_2CO_3 being a less effective leaching agent than NaOH. The decrease in available Si with increasing sodium aluminate is attributed to Si being consumed in the crystallisation process, leaving less Si in solution.

XRD patterns show sodalite forming in all instances, and the formation appears to be concurrent with the formation of zeolite A, based on SEM analysis. This indicates that the crystallisation conditions favour the formation of both zeolite A and sodalite, and this is not an example of Ostwald's law of successive transformations, where zeolite A formed first, and is then transformed into sodalite, but that zeolite A and sodalite formed

concurrently and are both stable forms for these conditions, within this time frame [60].

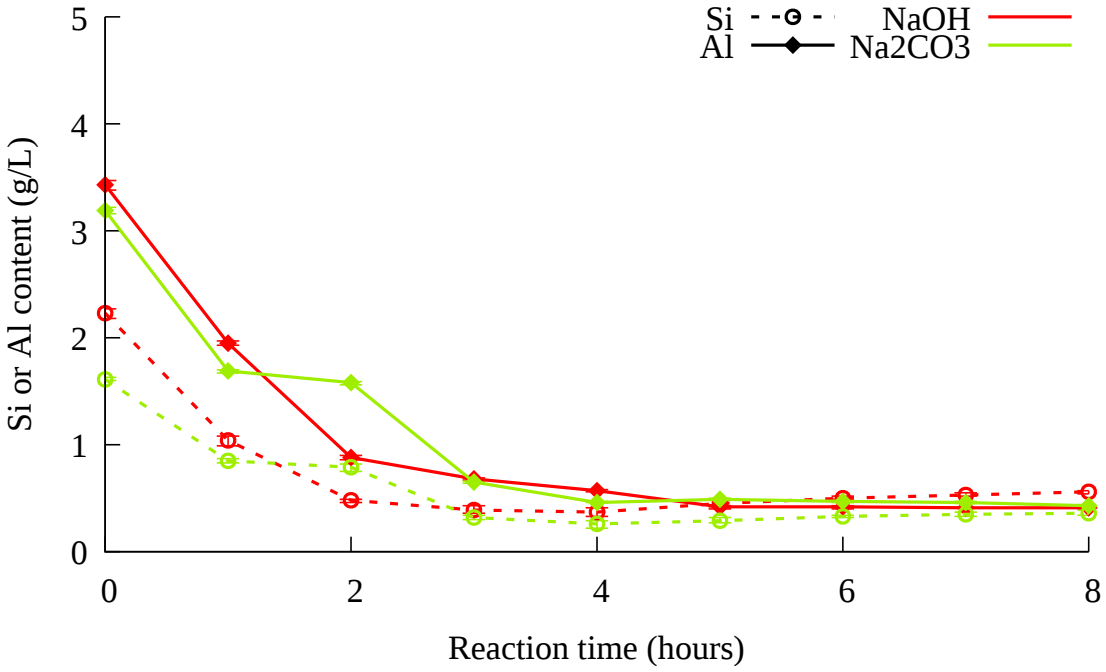

Figure 5.3: AAS results for substituting NaOH with Na_2CO_3, crystallised with 160 g of Sodium aluminate/kg FA

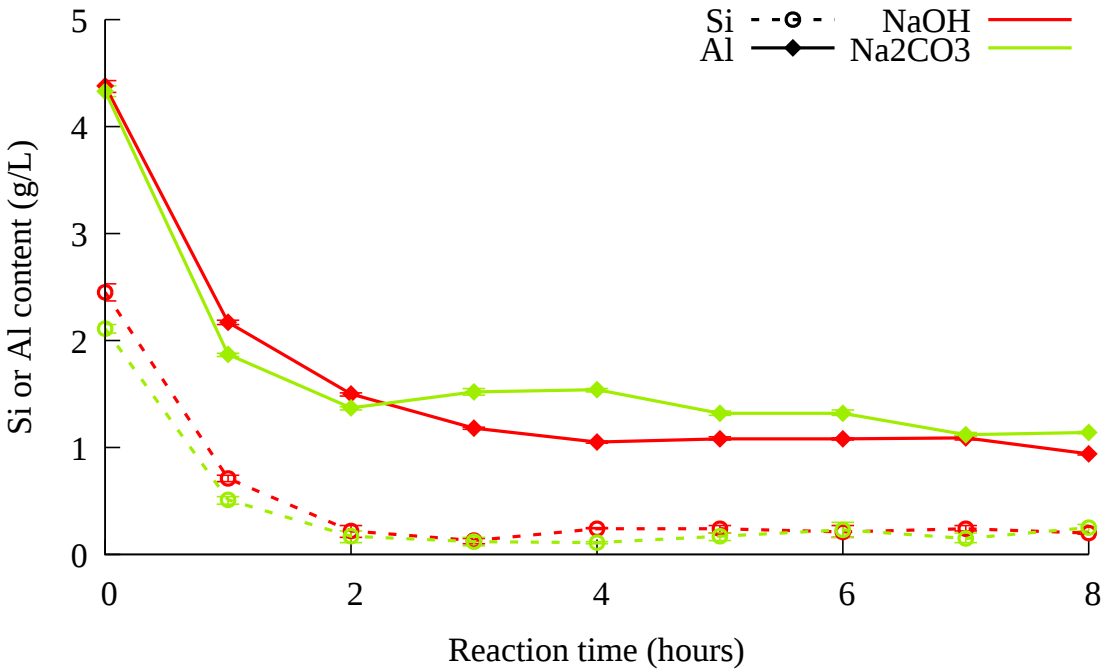

Figure 5.4: AAS results for substituting NaOH with Na_2CO_3, crystallised with 240 g/kg FA of sodium aluminate/kg FA

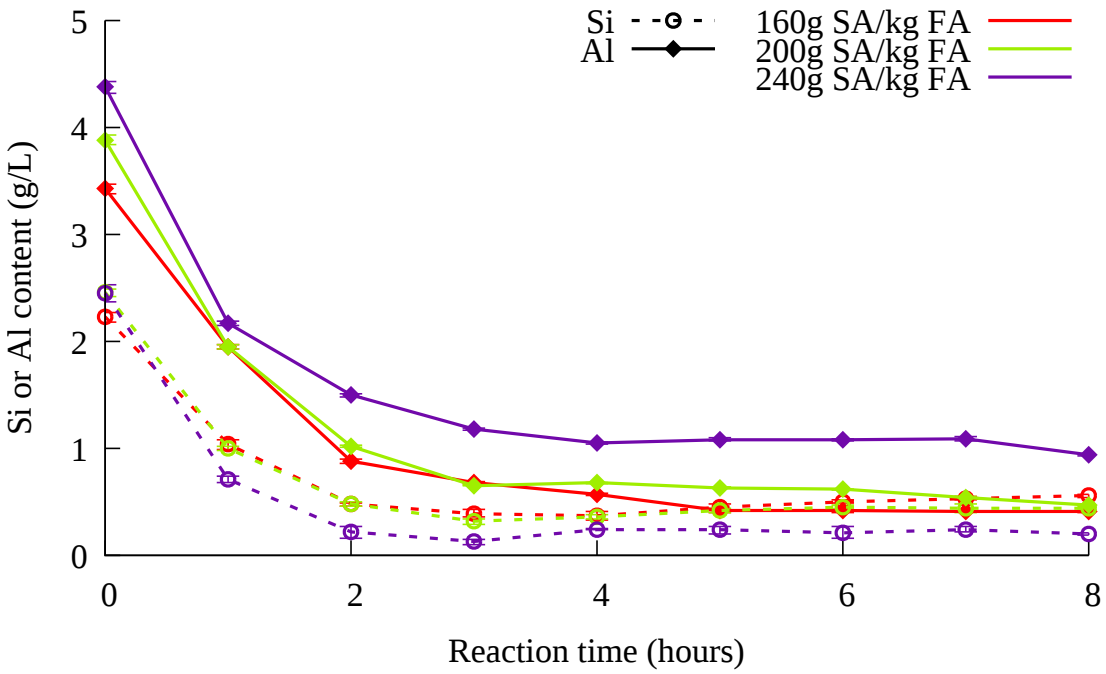

Figure 5.5: AAS result for NaOH extraction, crystallised with 160, 200 and 240 g sodium aluminate/kg FA

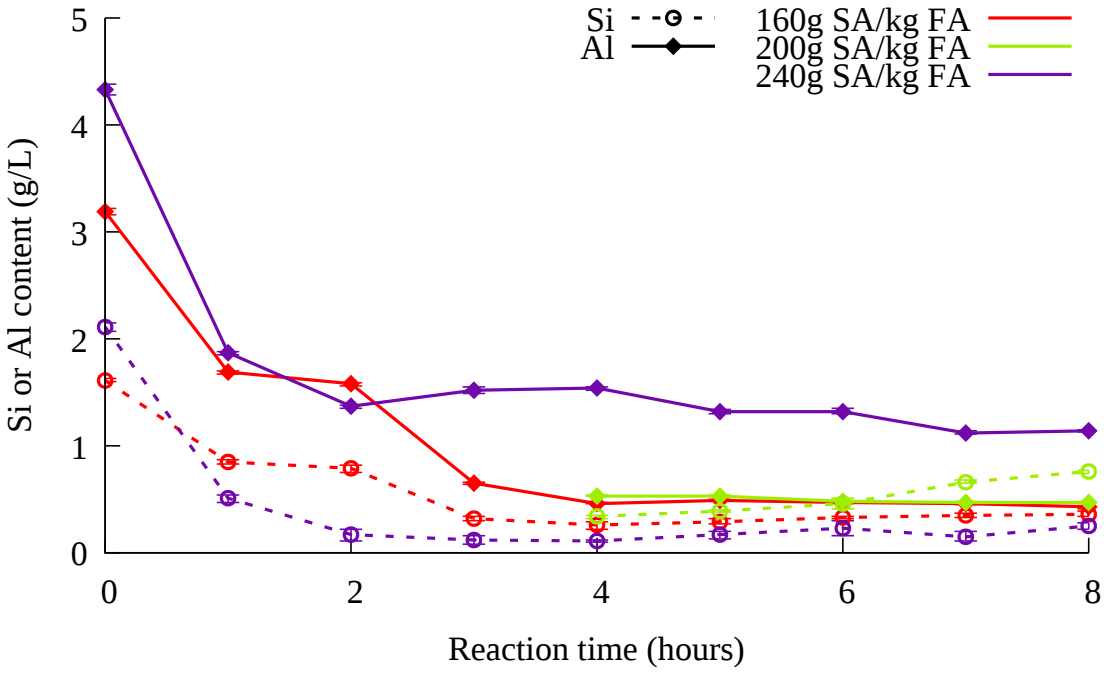

Figure 5.6: Na_2CO_3 extraction, crystallised with 160, 200 and 240 g sodium aluminate/kg FA

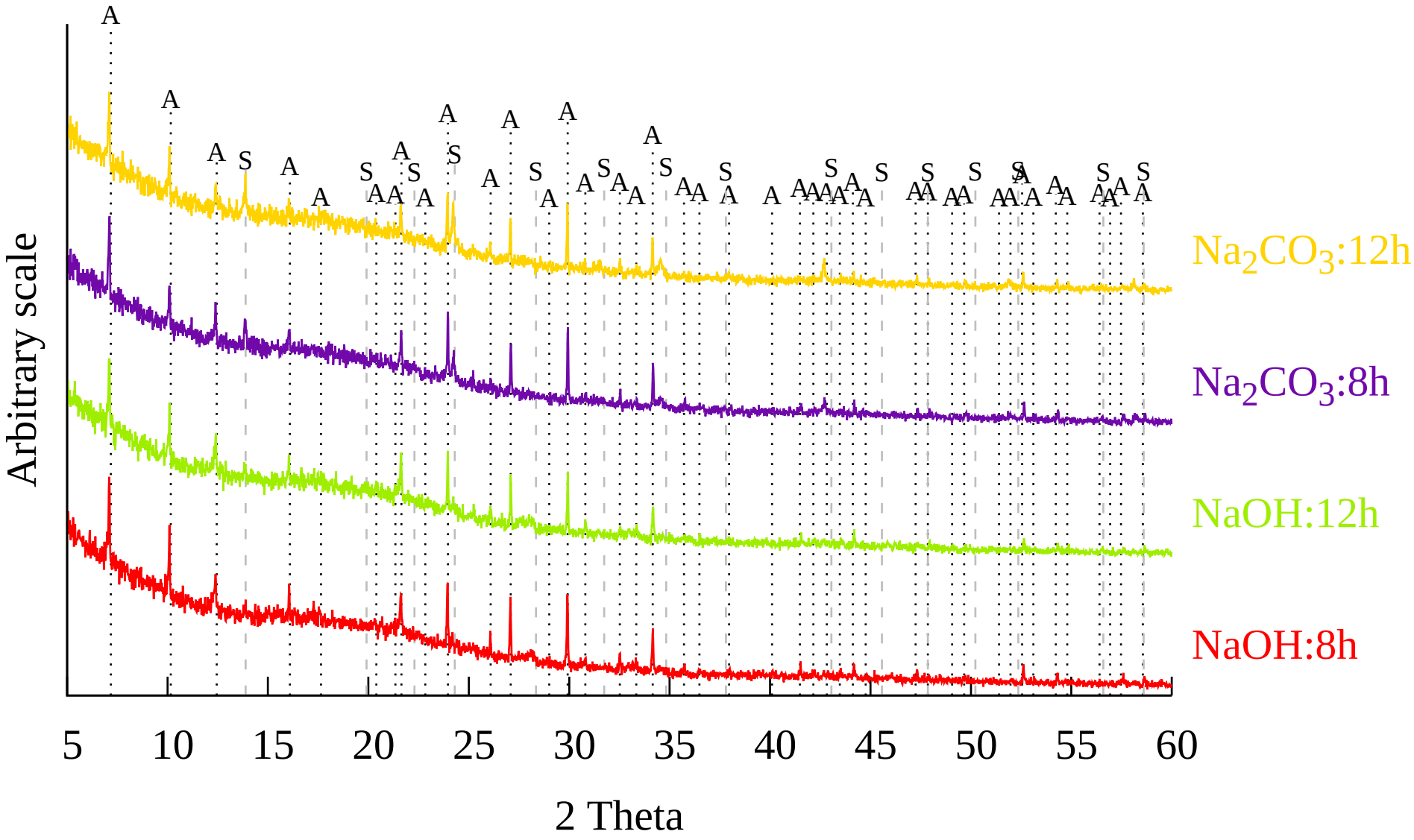

Figure 5.7: XRD patterns of NaOH Vs Na_2CO_3 extraction with 160 g sodium aluminate/kg FA added during crystallisation. A: Zeolite Na-A, S: Sodalite. $\lambda = 1.5406$ Å

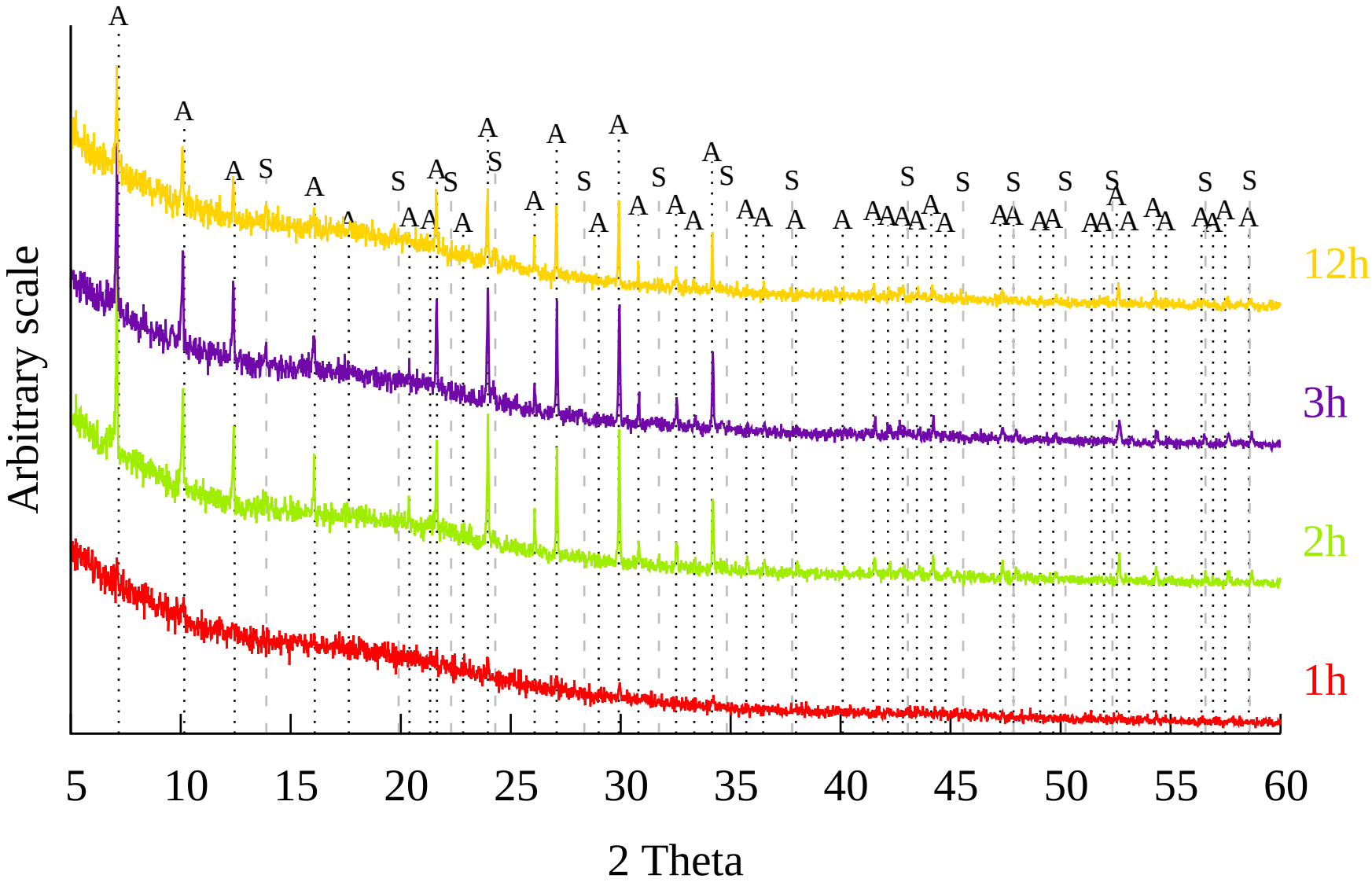

Figure 5.8: XRD patterns of NaOH extraction with 200 g sodium aluminate/kg FA added during crystallisation. A: Zeolite Na-A, S: Sodalite. $\lambda = 1.5406$ Å

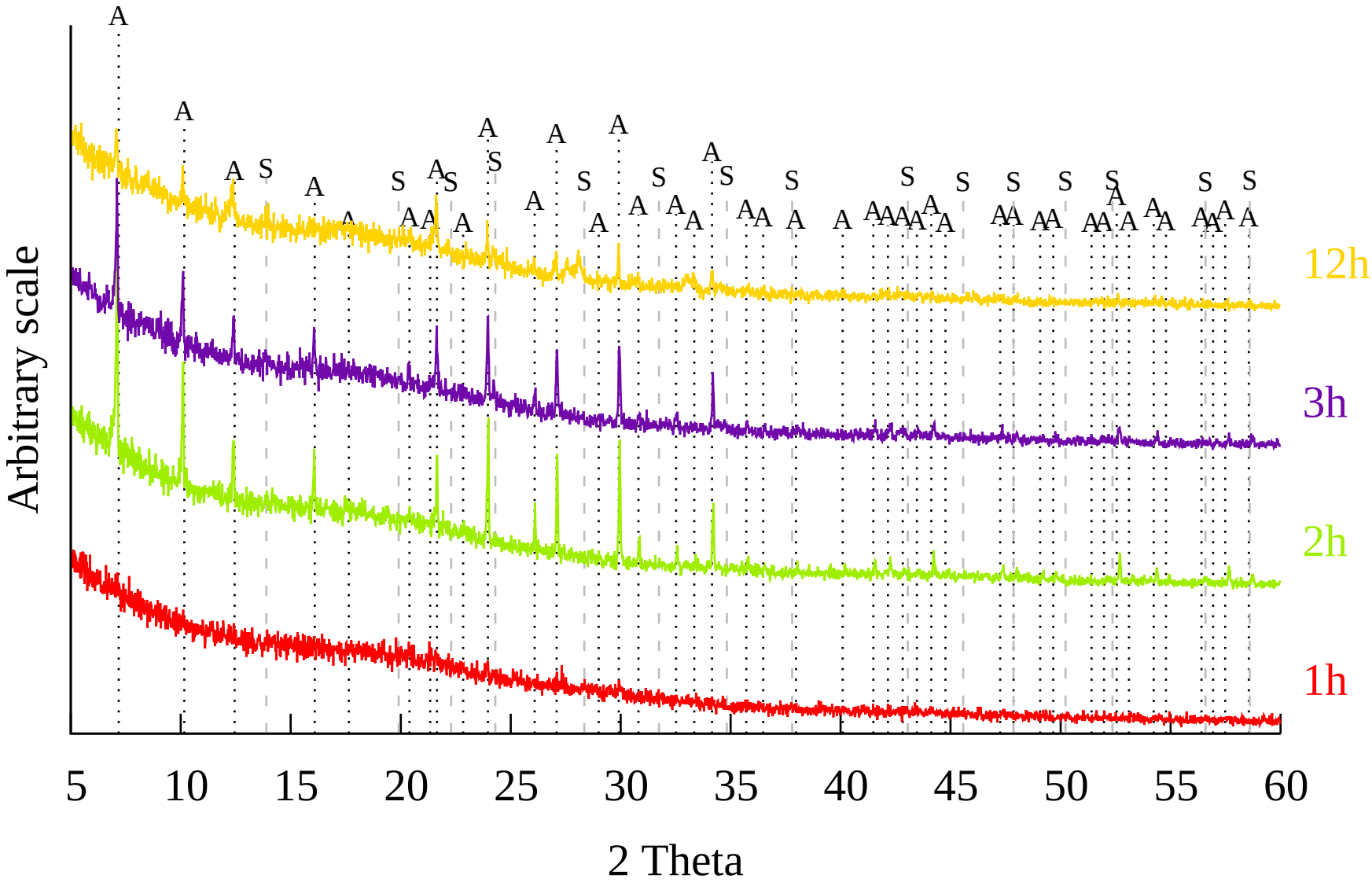

Figure 5.9: XRD patterns of Na_2CO_3 extraction with 200 g sodium aluminate/kg FA added during crystallisation. A: Zeolite Na-A, S: Sodalite. $\lambda = 1.5406$ Å

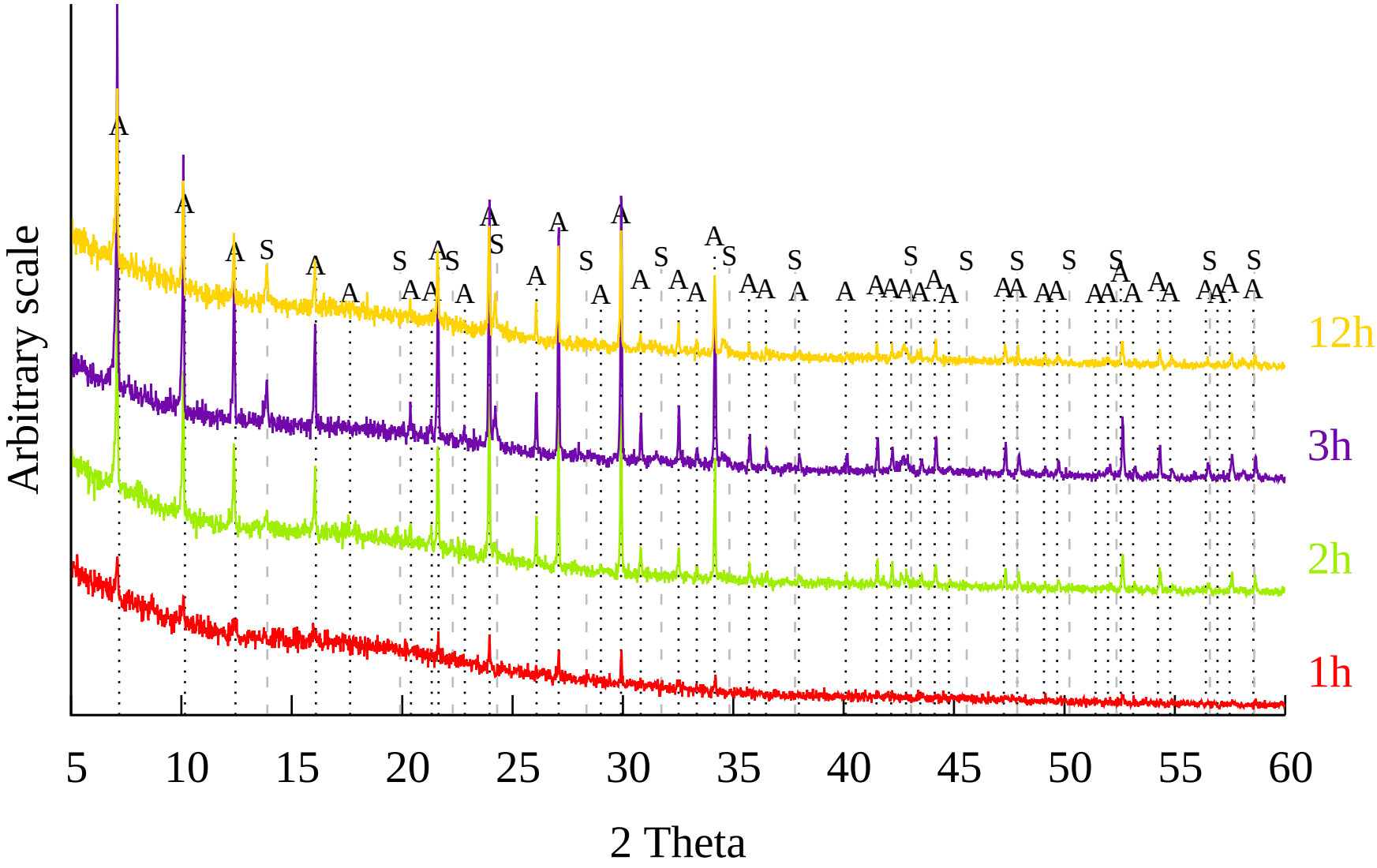

Figure 5.10: XRD patterns of NaOH extraction with 240 g sodium aluminate/kg FA added during crystallisation. A: Zeolite Na-A, S: Sodalite. $\lambda = 1.5406$ Å

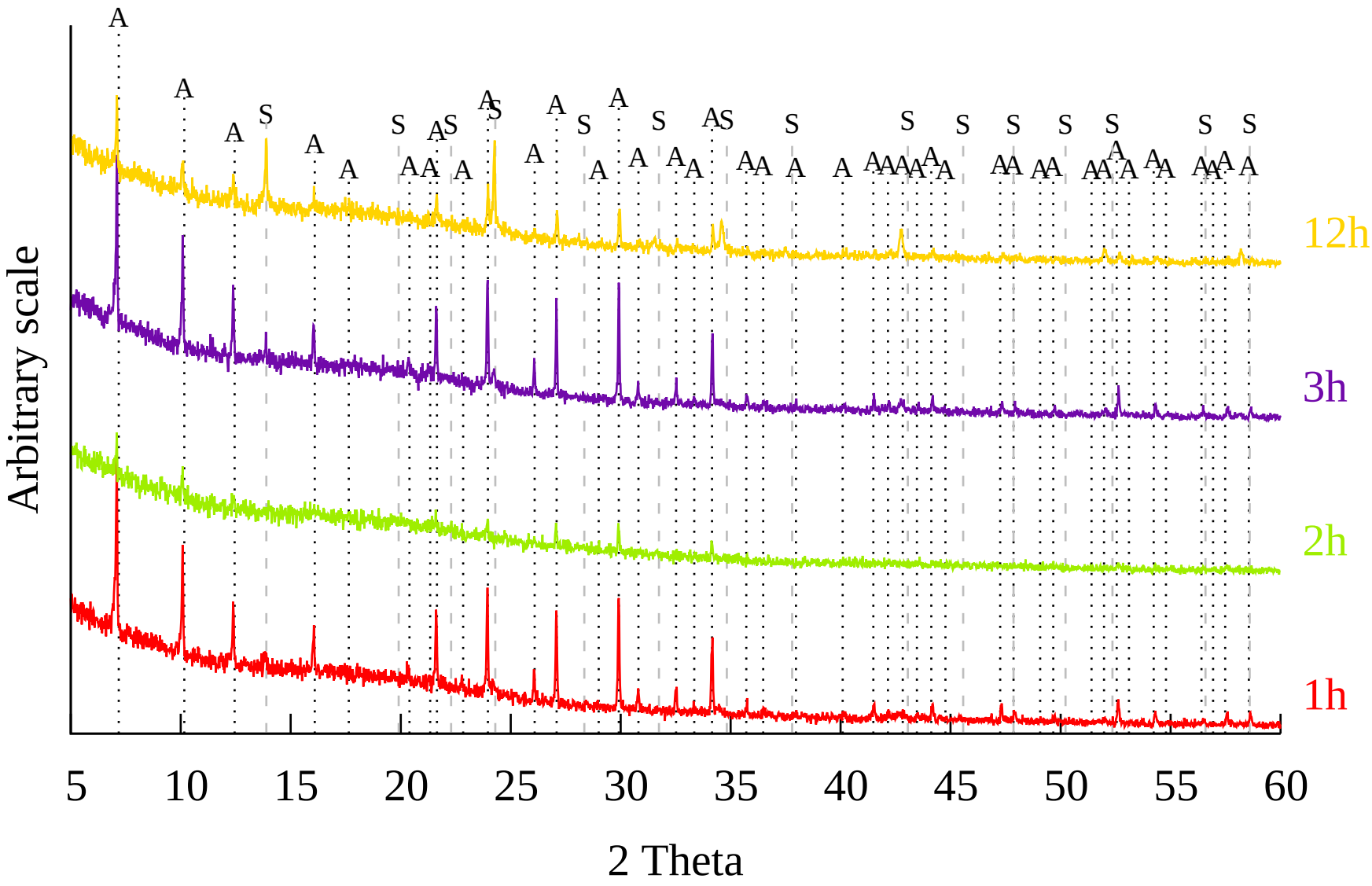

Figure 5.11: XRD patterns of Na_2CO_3 extraction with 240 g sodium aluminate/kg FA added during crystallisation. A: Zeolite Na-A, S: Sodalite. $\lambda = 1.5406$ Å

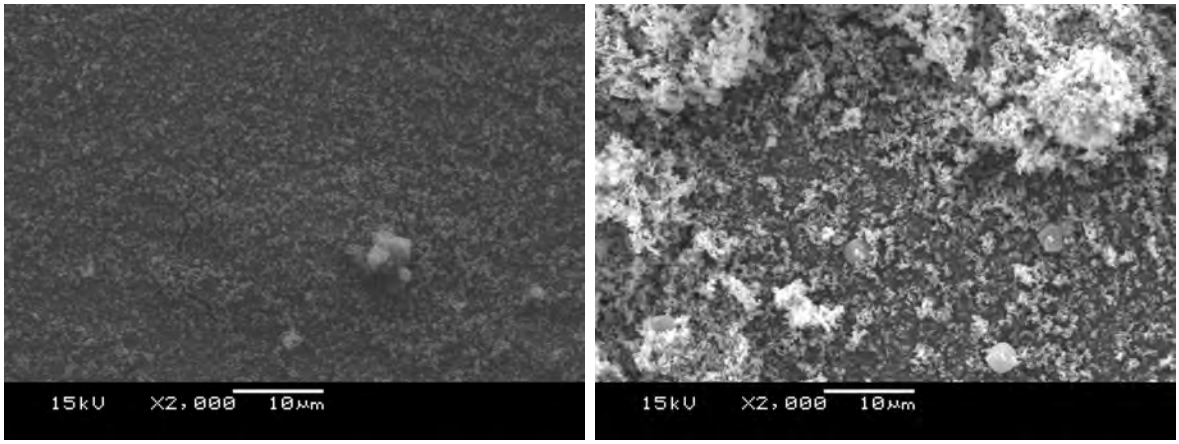

(a) 0 h (b) 1 h

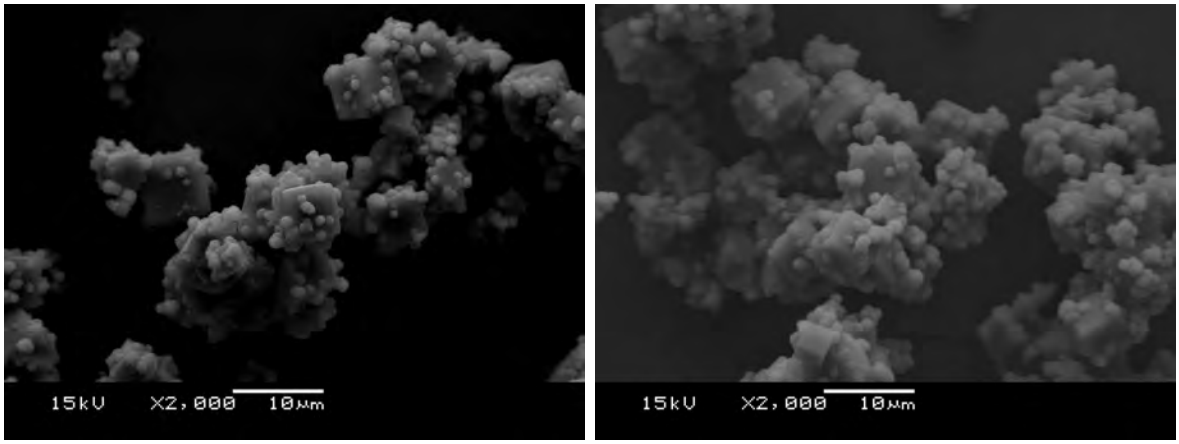

(c) 2 h (d) 3 h

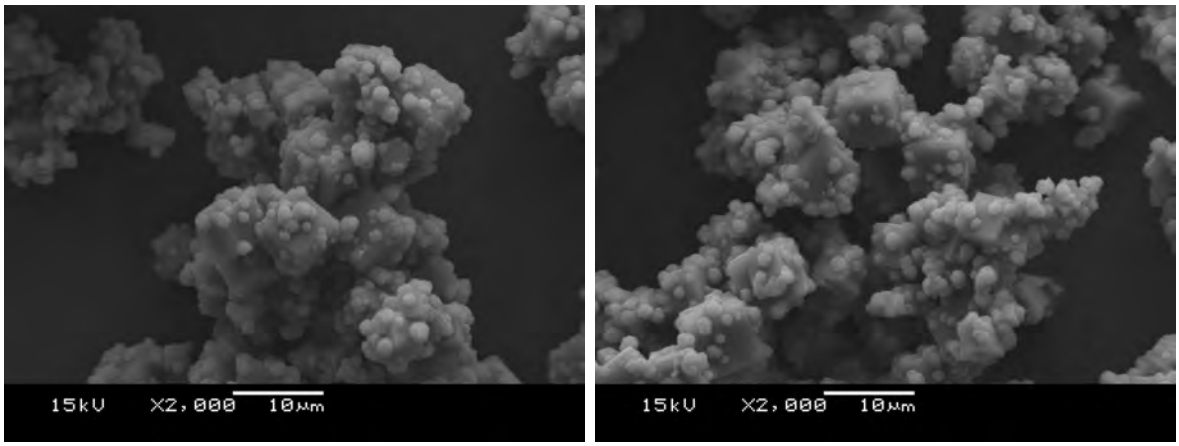

(e) 4 h (f) 5 h

Figure 5.12: SEM images of zeolites from ash leached with NaOH, crystallised with 200 g of sodium aluminate/kg FA, 0-5 h

(a) 6 h

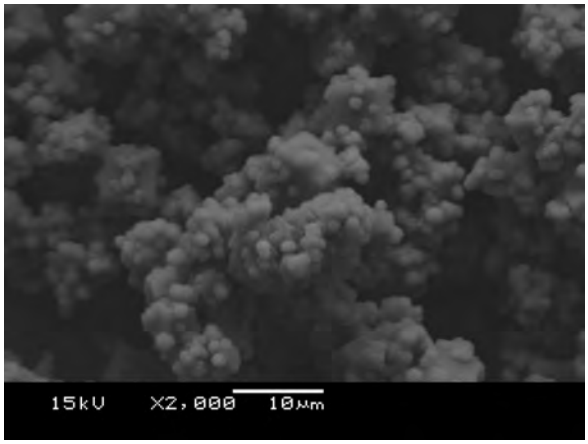

(b) 7 h

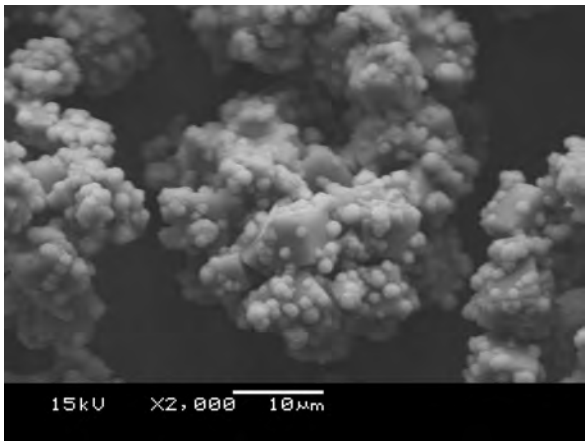

(c) 8 h

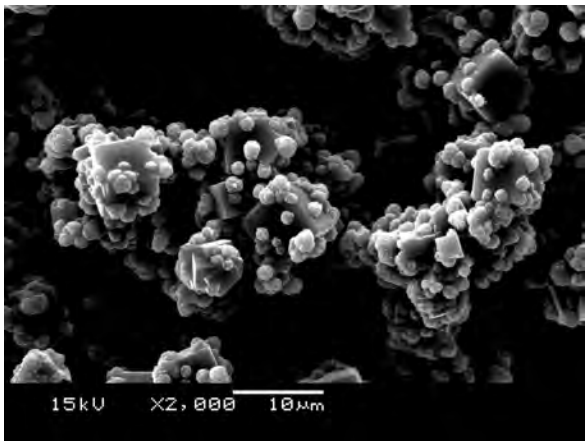

(d) 9 h

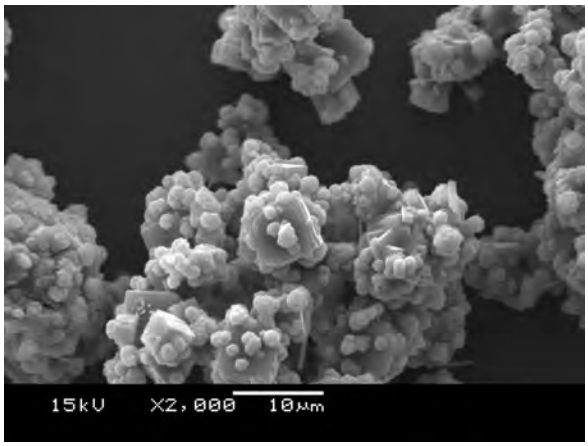

(e) 10 h

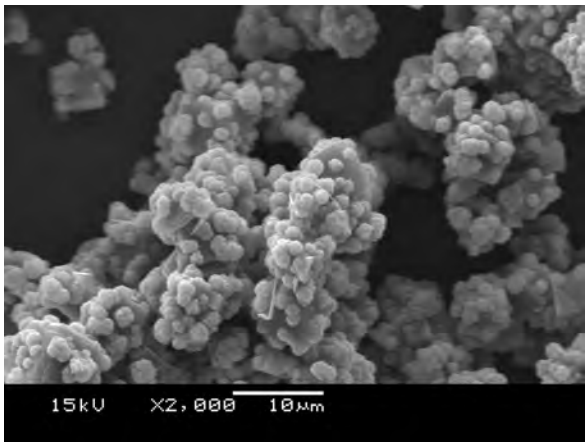

(f) 11 h

Figure 5.13: SEM images of zeolites from ash leached with NaOH, crystallised with 200 g of sodium aluminate/kg FA, 6-11 h

5.3 Crystallisation at 100°C Using a Stirred Hot Plate

It was not possible to accurately control the temperature using the apparatus shown in Figure 4.1. For this reason, the apparatus shown in Figure 5.1 was used. This apparatus provided feedback temperature control.

5.3.1 Experimental Method

900 ml of leachate (Ⓝ from Figure 2.12, page 46) produced using the method described in section 4.7 was placed in the conical flask Ⓣ depicted in Figure 5.1, the stirring bead was added, the conical flask was placed upon the hot plate and the equipment turned on. The stirrer was set to "2", which was found to be near 300 rpm using a laser tachometer, and the temperature probe set to 95°C Ⓤ. 100 ml of distilled water Ⓟ and a set quantity of sodium aluminate Ⓞ were both put in a duran bottle, which was put in an ultrasonic bath to expedite the dissolution of the sodium aluminate. When the temperature probe on the hot plate read 95°C, the sodium aluminate was added, the timer started, and a sample taken. As with previous experiments, the sample was filtered using a sintered glass Büchner funnel Ⓥ, the leachate Ⓦ was retained for later analysis, the zeolite sample Ⓧ was washed with excess distilled water, and the sample dried in an oven. Whilst the 0 hour samples were saved and analysed by AAS, the results were not used. Instead, the 0 hour results provided are theoretical as explained in section 5.2.2. A later test of the equipment found that the calibration of the temperature probe was incorrect, and that the experiments had been conducted at 100°C, rather than the intended 95°C.

5.3.2 Results

The AAS results shown in Figure 5.14 show similar values for Si at T0 for all six experiments. There is a noticeable drop between 0 and 1 hour, which is to be expected, as Si and Al combine in solution. The higher the dose of sodium aluminate provided, the greater the drop between the starting value of Si at T0, and the value of Si at T1.

Si concentrations then remain comparatively level after this first drop. A further slight decrease in Si concentration is noted in each experiment at a different time, with the trend showing drops in Si content earlier with increased sodium aluminate dosages. The Al values at T0 in Figure 5.14b show a noticeable separation due to the incremental dosages of sodium aluminate raising the Al content. These measurements also show the sharp drop between hours 0 and 1, then remain comparatively constant, but for a smaller decrease later on. This small decrease observed later also occurs earlier as sodium aluminate dosage increases, and coincides with the small decreases in concentration of Si. These drops are most obvious in the higher dosages of sodium aluminate such as 222 g/kg FA (drop between 3 hours and 4 hours, blue lines) and 266 g/kg FA (drop between 2 hours and 3 hours, orange lines Figure 5.14). This small, simultaneous drop in Si and Al also coincides with a marked decrease in the quantities of amorphous material (described by Shoumkova and Stoyanova [42] as amorphous gel) in SEM images, as shown in Figures 5.15-5.20. The XRD patterns in Figures 5.21-5.25 show crystalline material appearing at the start of the drop.

The XRD patterns show little or no crystalline material for early samples, but show peaks for zeolite A at the start of the aforementioned drop point of Si and Al values. None of the XRD patterns appear to show sodalite traces, however, the XRD scans were not run for long periods, and low peaks could be hidden within the noise. This indicates that the non-cube shaped matter present in the SEM images could either be sodalite that was not detected by the XRD, or more likely is the amorphous material from which zeolite crystals grow [42]. Literature has multiple examples of zeolites (such as zeolite A) forming from amorphous material or geopolymers [38–40]. The lack of sodalite detected by XRD in these 100°C experiments in comparison to prior reflux experiments is consistent with higher temperature or reflux crystallisation processes promoting sodalite synthesis [42, 70]. The quantity of extraneous material appears to be lower for the hot plate experiments than for the reflux experiments, thus indicating that conducting crystallisation at a temperature even a few degrees lower improves the product. Whilst the question of crystallinity and

amorphous material could be answered through Rietveld refinement, the XRD patterns are not of sufficiently high quality and are numerous. Due to the complexity of Rietveld refinement and the quantity of XRD patterns produced, Rietveld refinement was deemed beyond the remit of this work. A brief discussion on Rietveld refinement is in appendix C.2 on page 381.

The yield of zeolite after 6 hours is shown in Figure 5.26. These yield calculations are slightly lower than would have been the case were 6 samples not taken in the preceding hours. It is assumed that when the hourly samples are taken, the crystallisation solution is well mixed, therefore sampling will not influence the composition of the final result. It is also assumed that all samples taken are of approximately the same quantity, and therefore all final yields are similarly diminished, allowing for qualitative comparisons of how experimental conditions influence yield. There is a clear linear trend of increased yield with increased sodium aluminate dosage from 44 g SA/kg FA to 177 g SA/kg FA. This trend is reflected in literature [43].

Further increases in SA dosage from 177 g/kg FA to 266 g/kg FA do not seem to yield significant increases in zeolite yield. The yield graph 5.26 combined with the Si content at 6 hours in Figure 5.14a indicates that Si content may be the yield limiting factor. Si content at 6 hours as a function of sodium aluminate addition decreases as sodium aluminate content increases from 44-133 g/kg FA, as shown by Figure 5.14a, however for 177-266 g SA/kg FA, the Si content for hours 1, 2, 5 and 6 is very similar, indicating that the additional Al introduced by higher sodium aluminate dosages does not result in more Si being consumed in crystallisation. It is also noted that the Si content at 6 hours is low for the aforementioned high dosages of sodium aluminate. The CEC graph shown in Figure 5.27 shows a broadly similar but not entirely consistent CEC for all dosages but 222 g SA/kg FA, which appears lower than the other results. The CEC multiplied by the yield compares the effectiveness of the zeolite with the effectiveness of the crystallisation process. The decreased CEC for 222 g SA/kg FA is clearly shown in Figure 5.28, however dosages 177 and 266 g SA/kg FA appear equally effective.

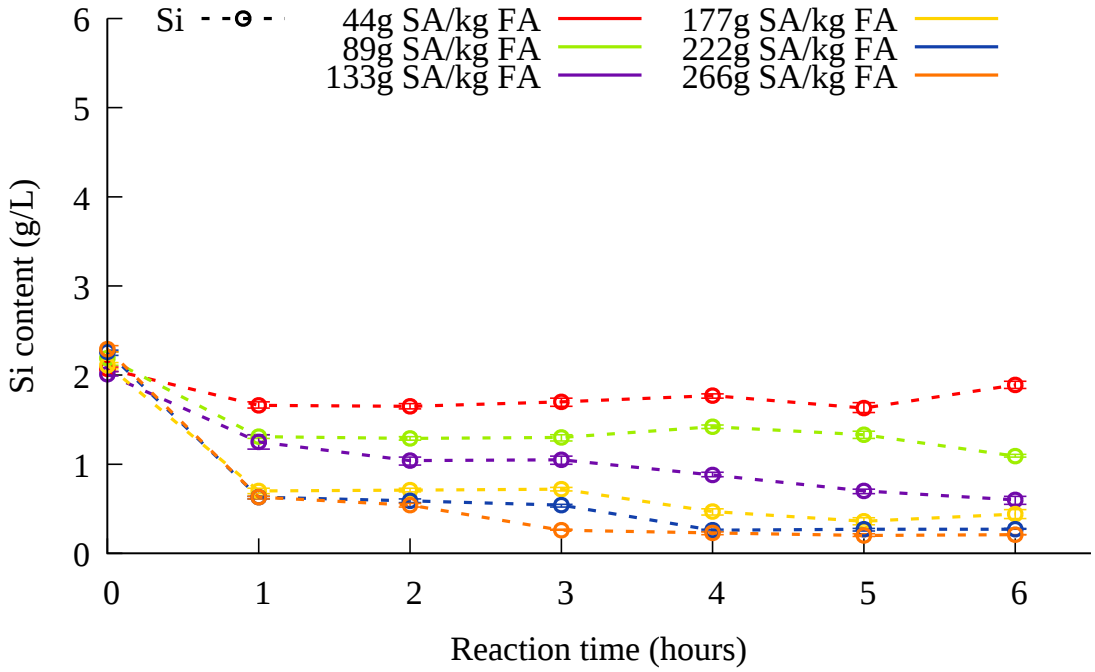

(a) Hot Plate: Si

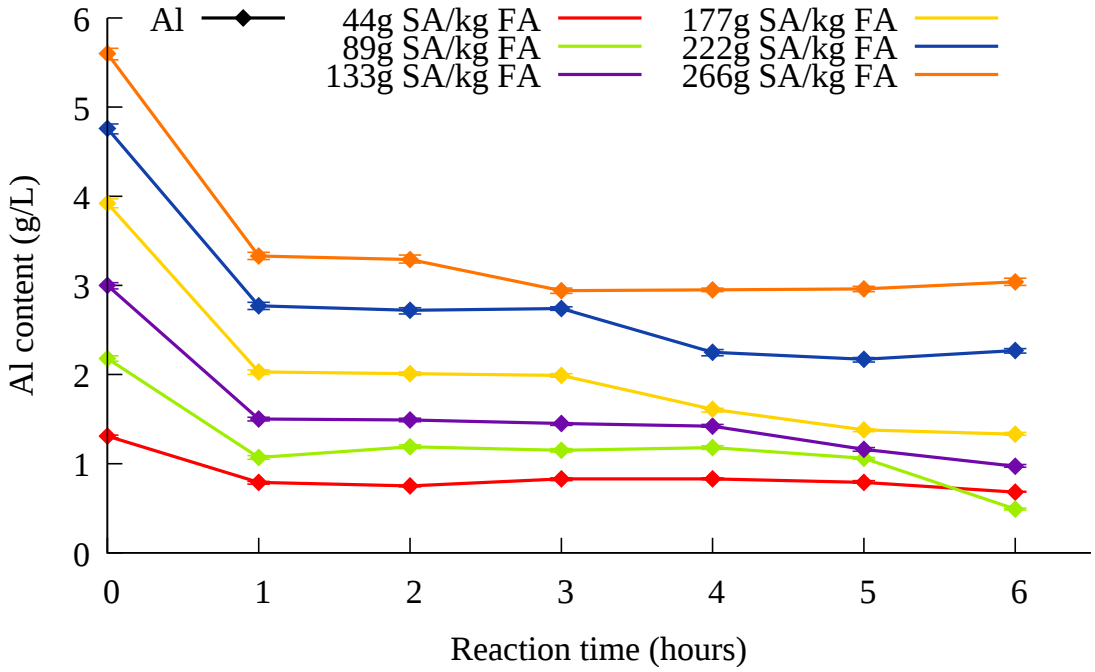

(b) Hot Plate: Al

Figure 5.14: The effect of SA loading on Si and Al content

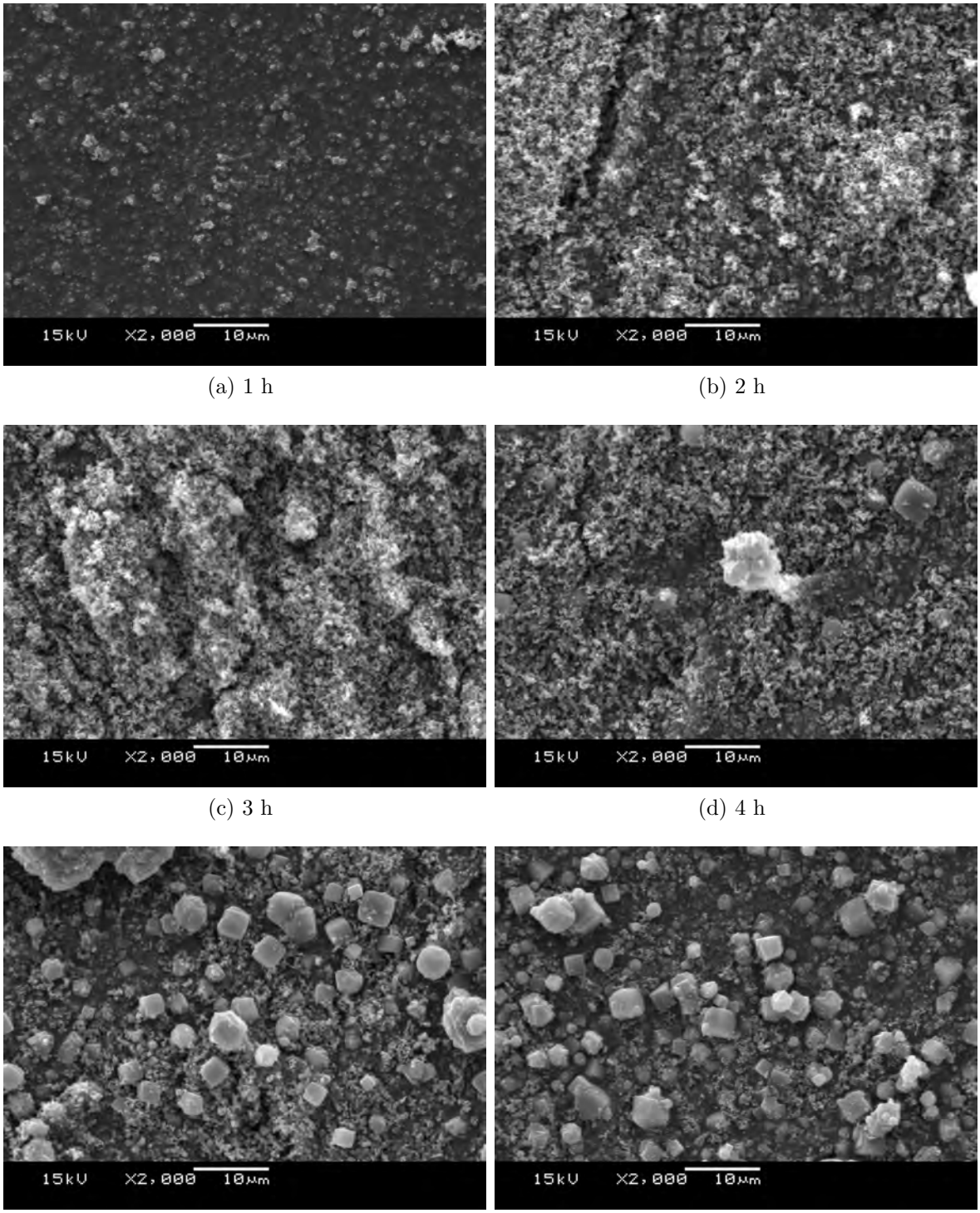

(a) 1 h (b) 2 h

(c) 3 h (d) 4 h

(e) 5 h (f) 6 h

Figure 5.15: SEM images of zeolites from ash leachate crystallised with 44 g of sodium aluminate/ kg FA on a stirred hot plate at 102-103°C

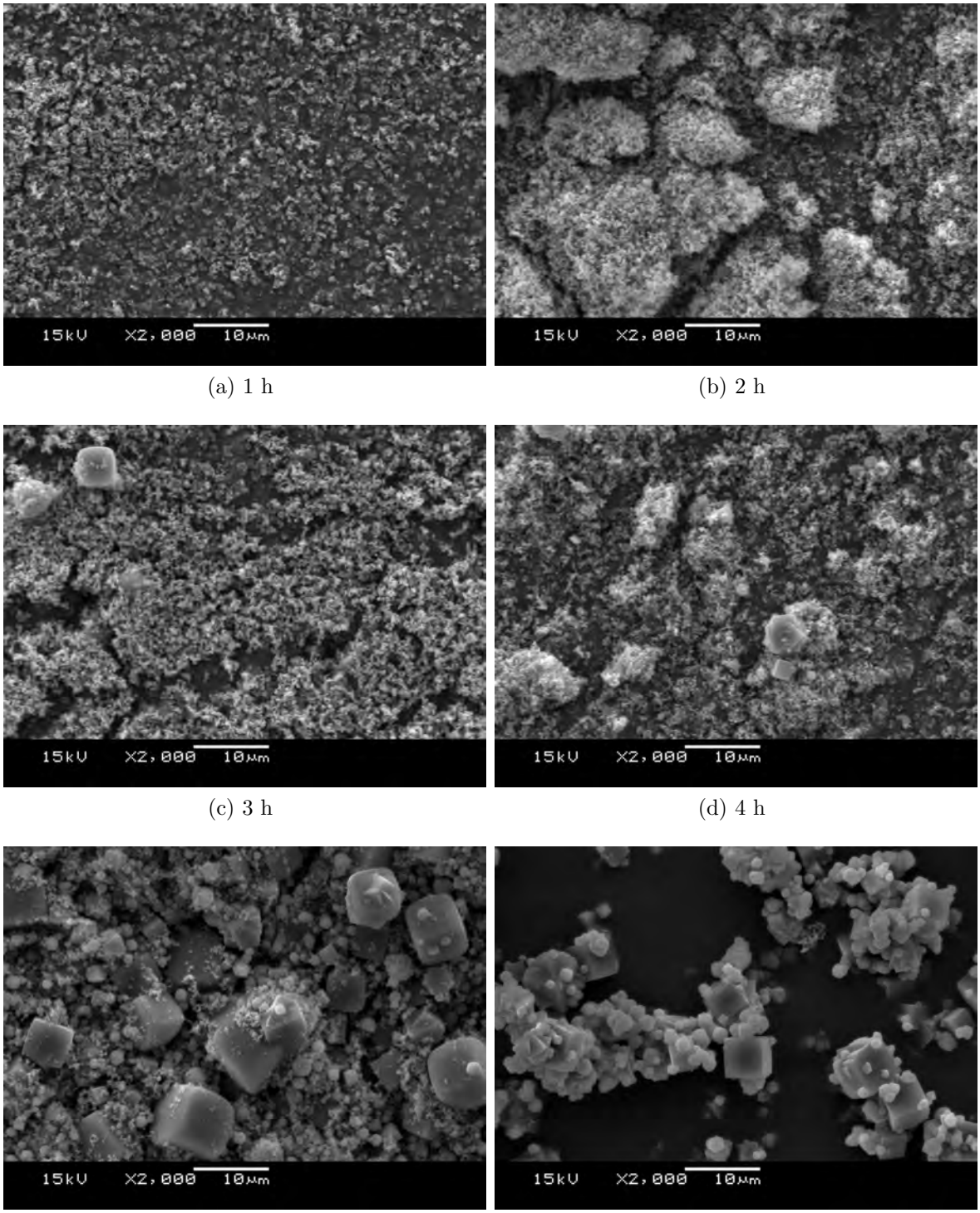

(a) 1 h (b) 2 h

(c) 3 h (d) 4 h

(e) 5 h (f) 6 h

Figure 5.16: SEM images of zeolites from ash leachate crystallised with 89 g of sodium aluminate/kg FA on a stirred hot plate at 102-103°C

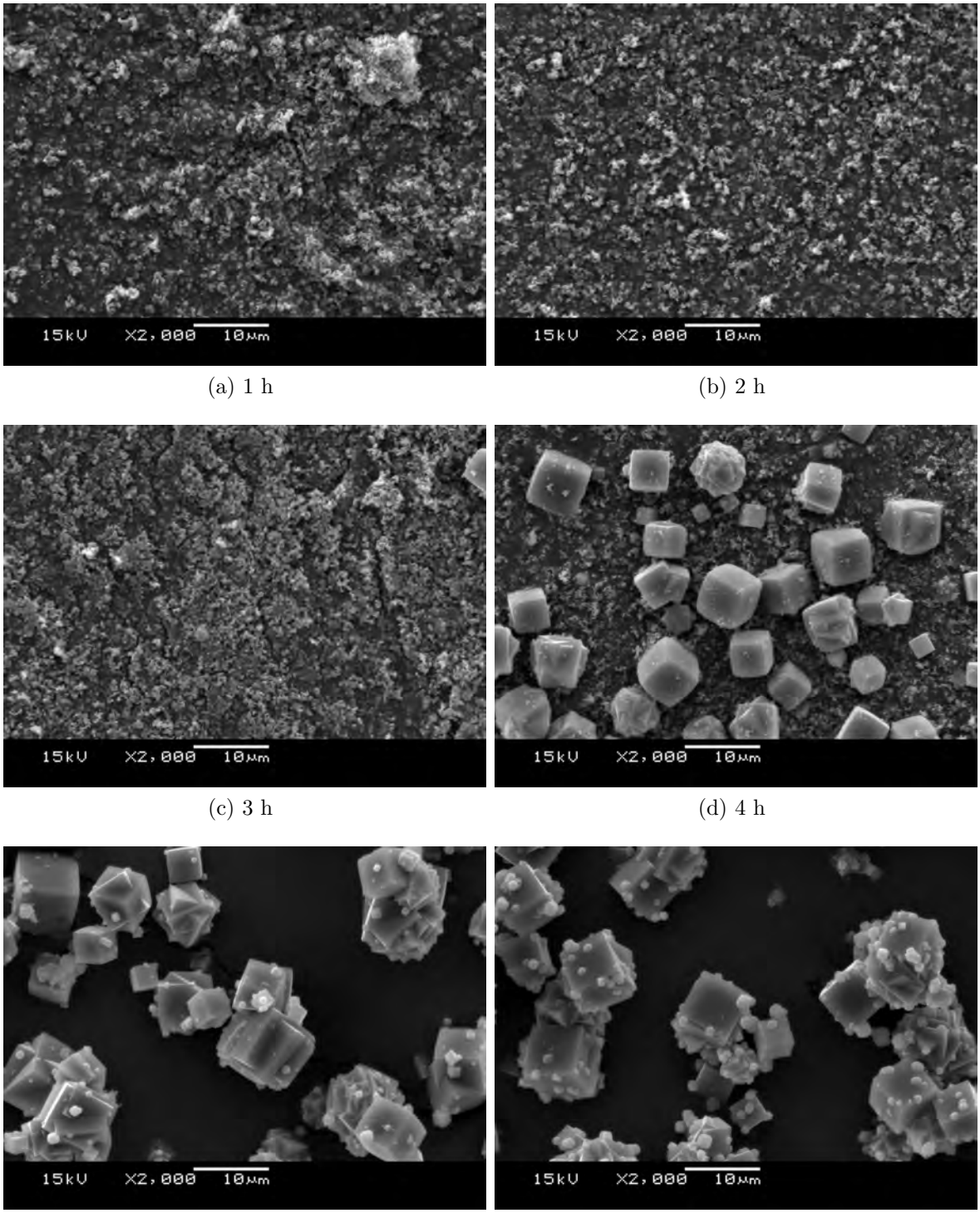

(a) 1 h (b) 2 h

(c) 3 h (d) 4 h

(e) 5 h (f) 6 h

Figure 5.17: SEM images of zeolites from ash leachate crystallised with 133 g of sodium aluminate/kg FA on a stirred hot plate at 102-103°C

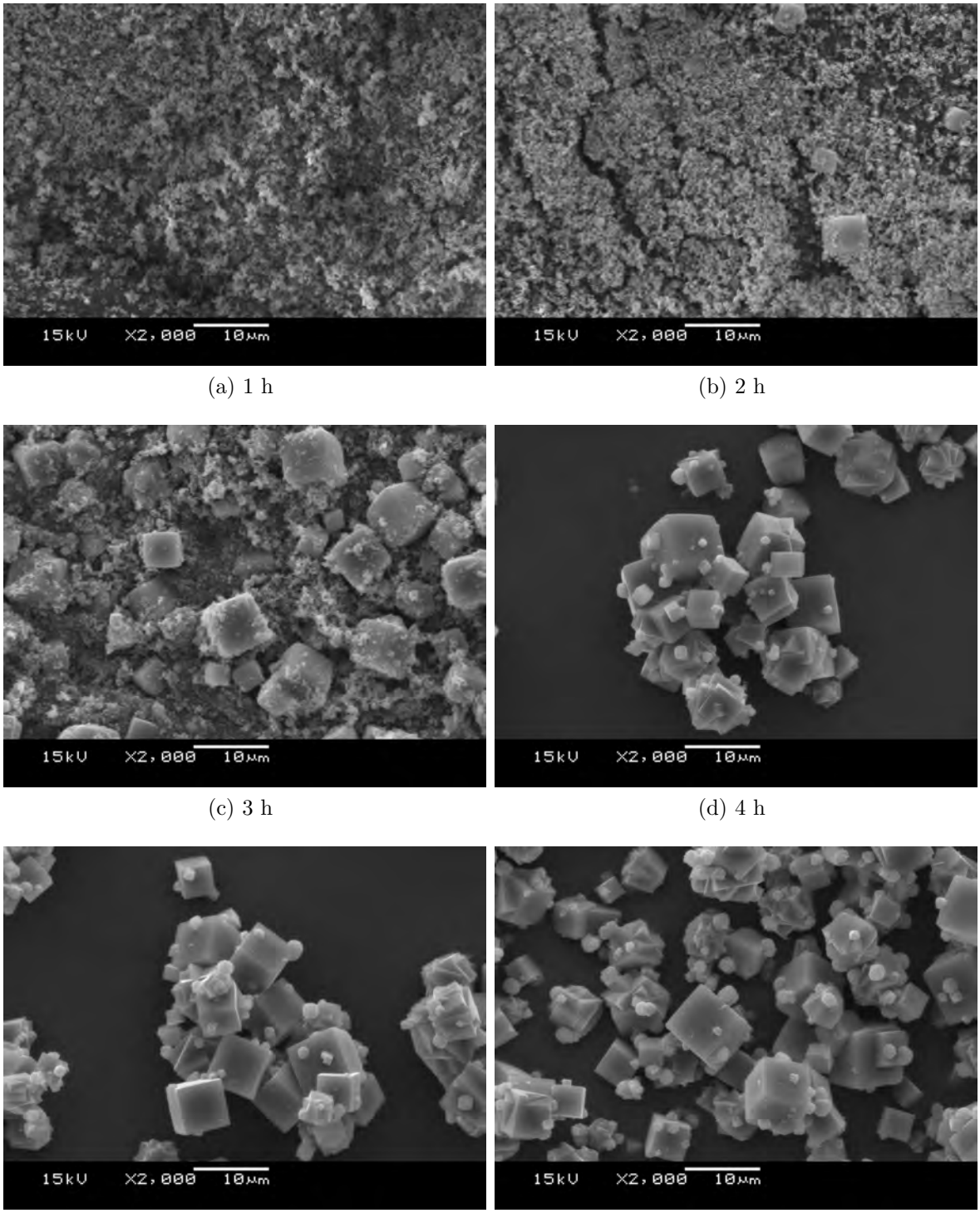

(a) 1 h (b) 2 h

(c) 3 h (d) 4 h

(e) 5 h (f) 6 h

Figure 5.18: SEM images of zeolites from ash leachate crystallised with 177 g of sodium aluminate/kg FA on a stirred hot plate at 102-103°C

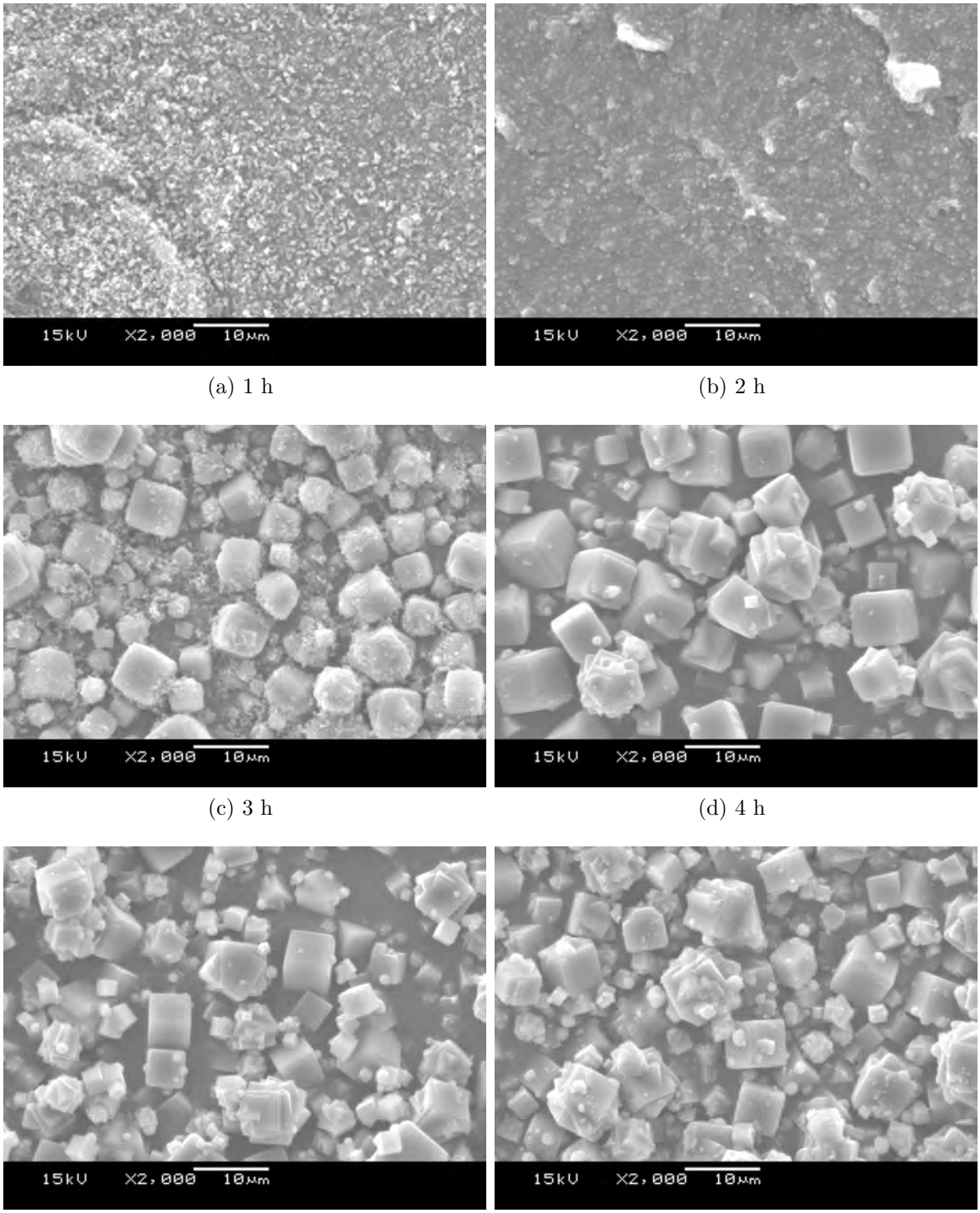

(a) 1 h (b) 2 h

(c) 3 h (d) 4 h

(e) 5 h (f) 6 h

Figure 5.19: SEM images of zeolites from ash leachate crystallised with 222 g of sodium aluminate/kg FA on a stirred hot plate at 102-103°C

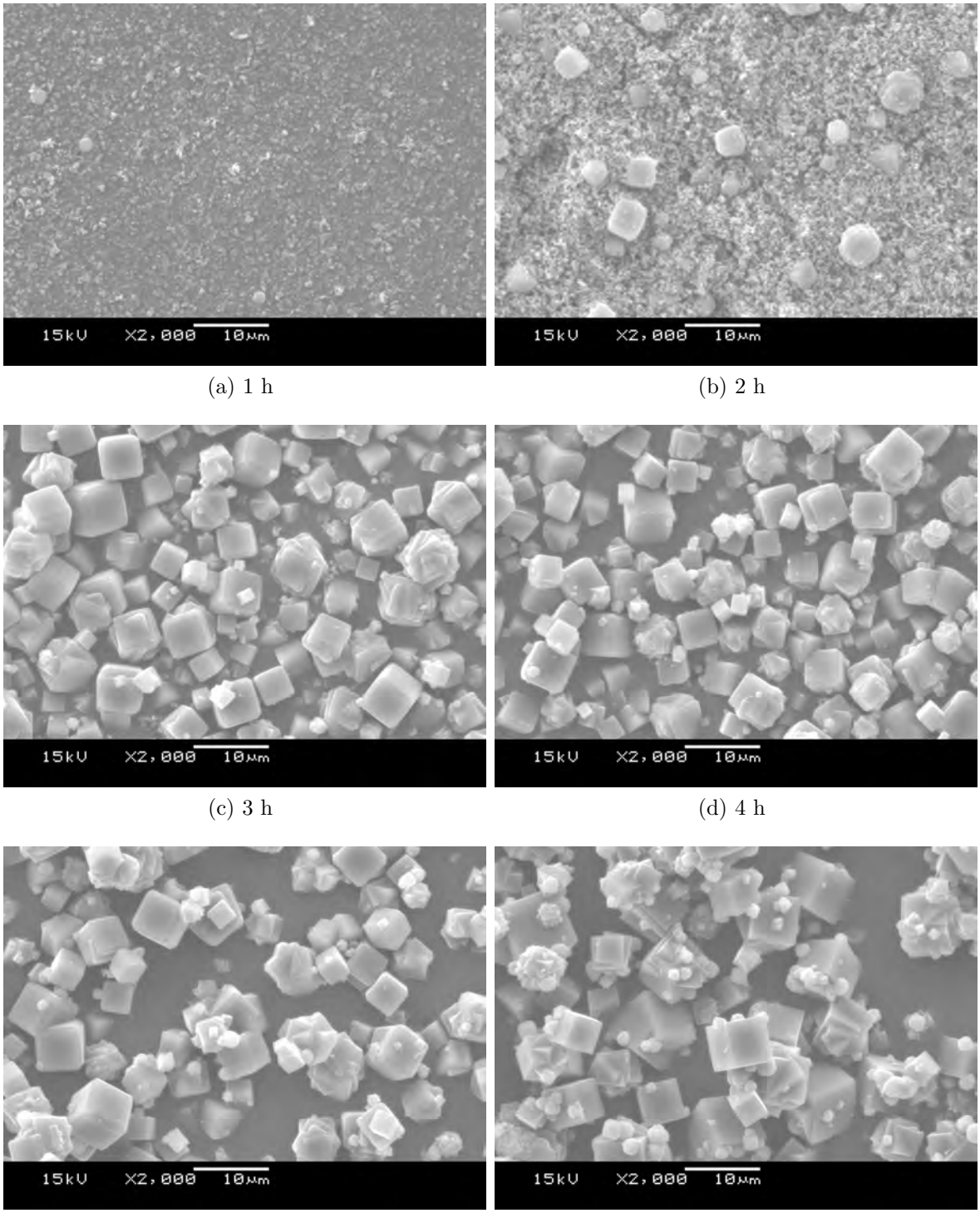

(a) 1 h (b) 2 h

(c) 3 h (d) 4 h

(e) 5 h (f) 6 h

Figure 5.20: SEM images of zeolites from ash leachate crystallised with 266 g of sodium aluminate/kg FA on a stirred hot plate at 102-103°C

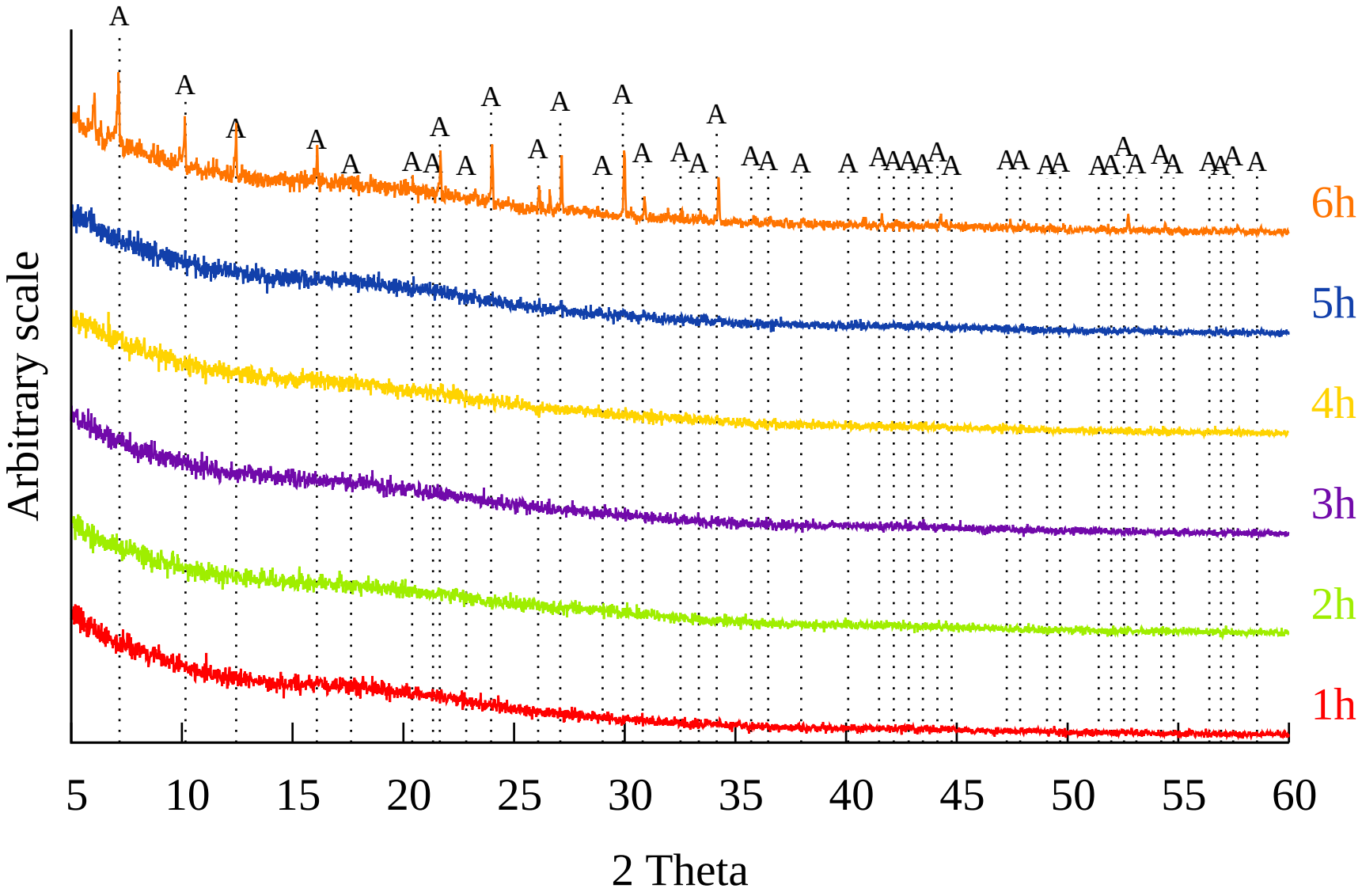

Figure 5.21: XRD patterns of controlled temperature crystallisation with 44 g sodium aluminate/kg FA. A: Zeolite Na-A. $\lambda = 1.5406$ Å

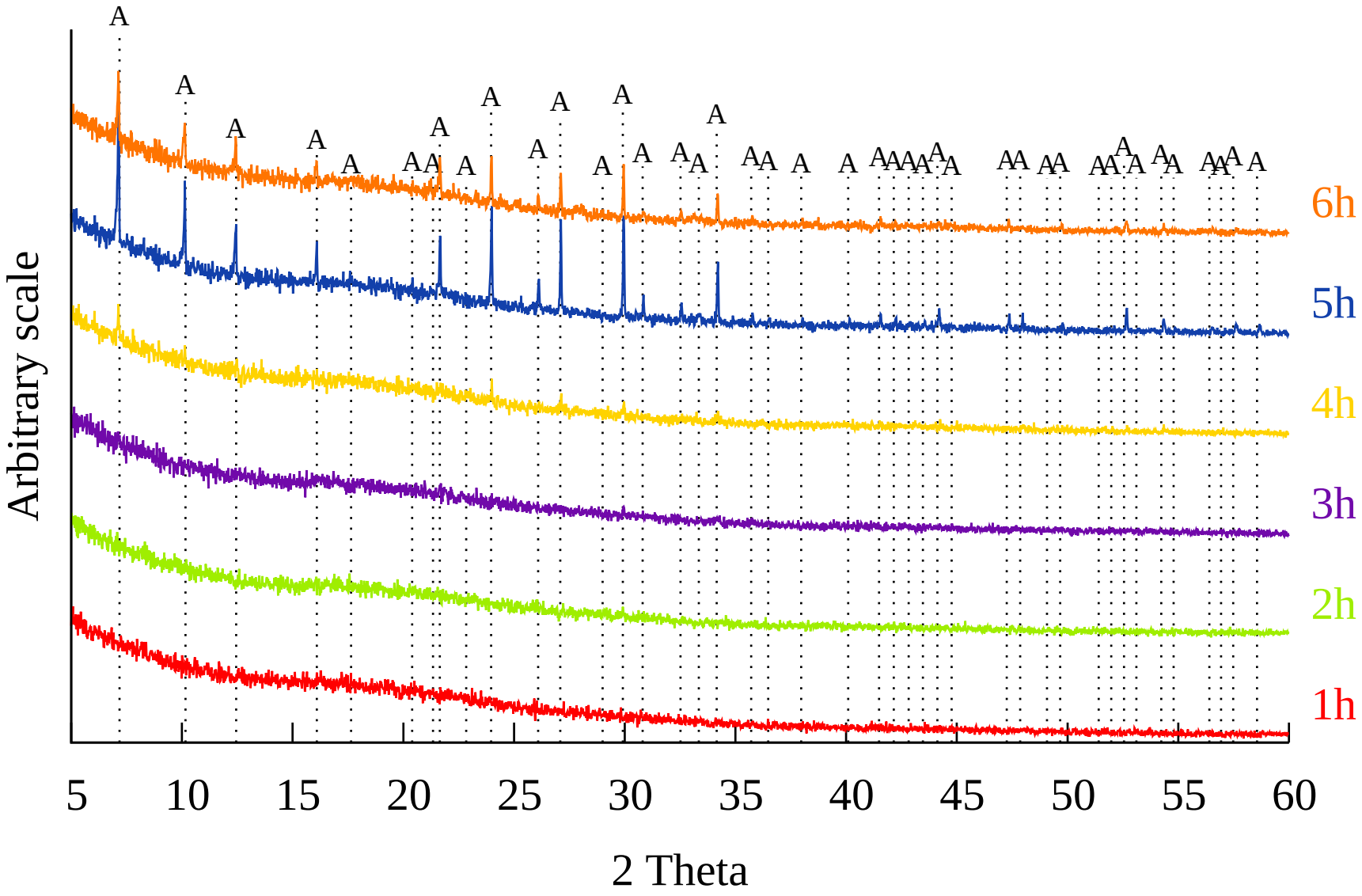

Figure 5.22: XRD patterns of controlled temperature crystallisation with 89 g sodium aluminate/kg FA. A: Zeolite Na-A. $\lambda = 1.5406$ Å

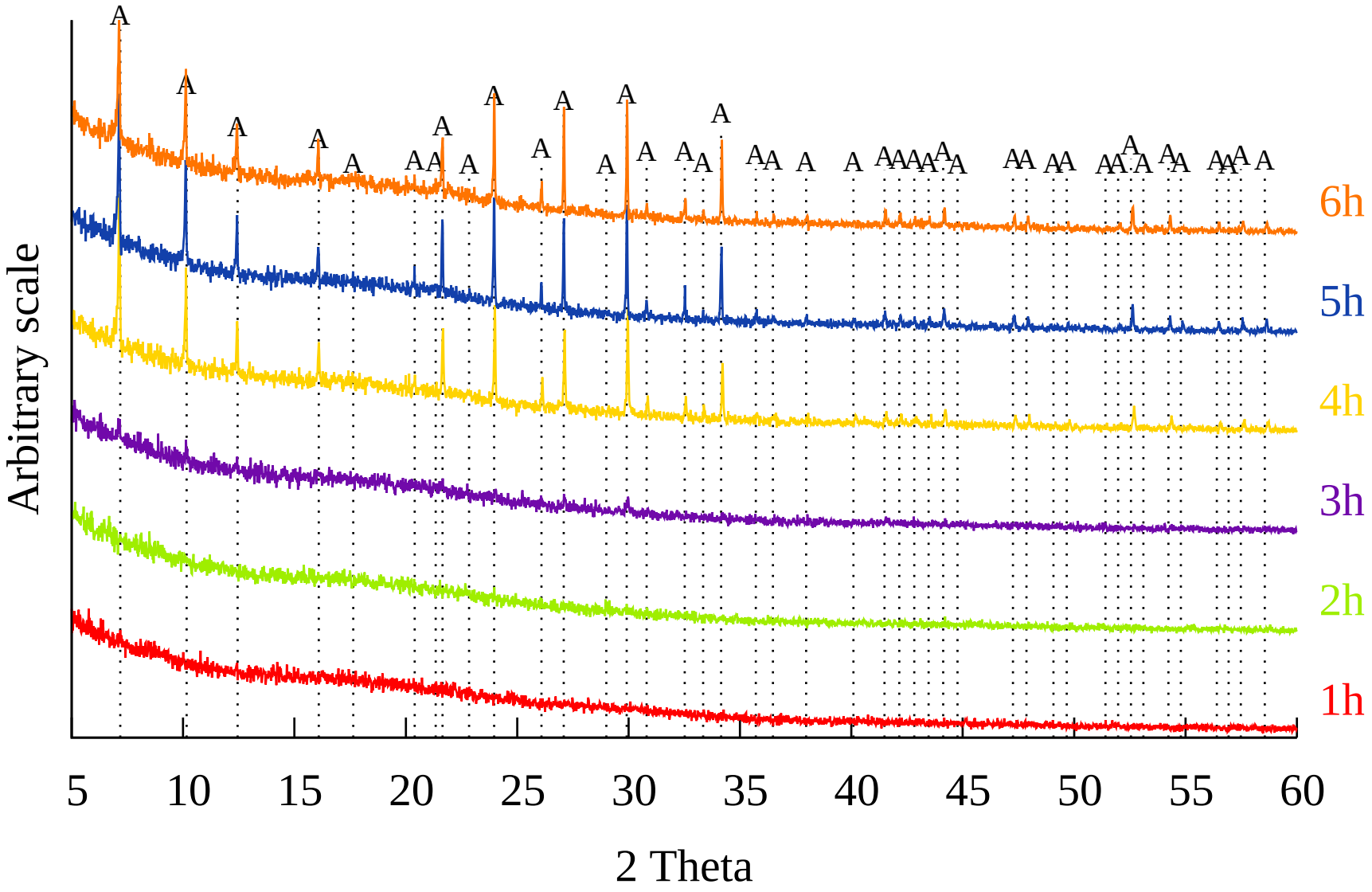

Figure 5.23: XRD patterns of controlled temperature crystallisation with 133 g sodium aluminate/kg FA. A: Zeolite Na-A. λ = 1.5406 Å

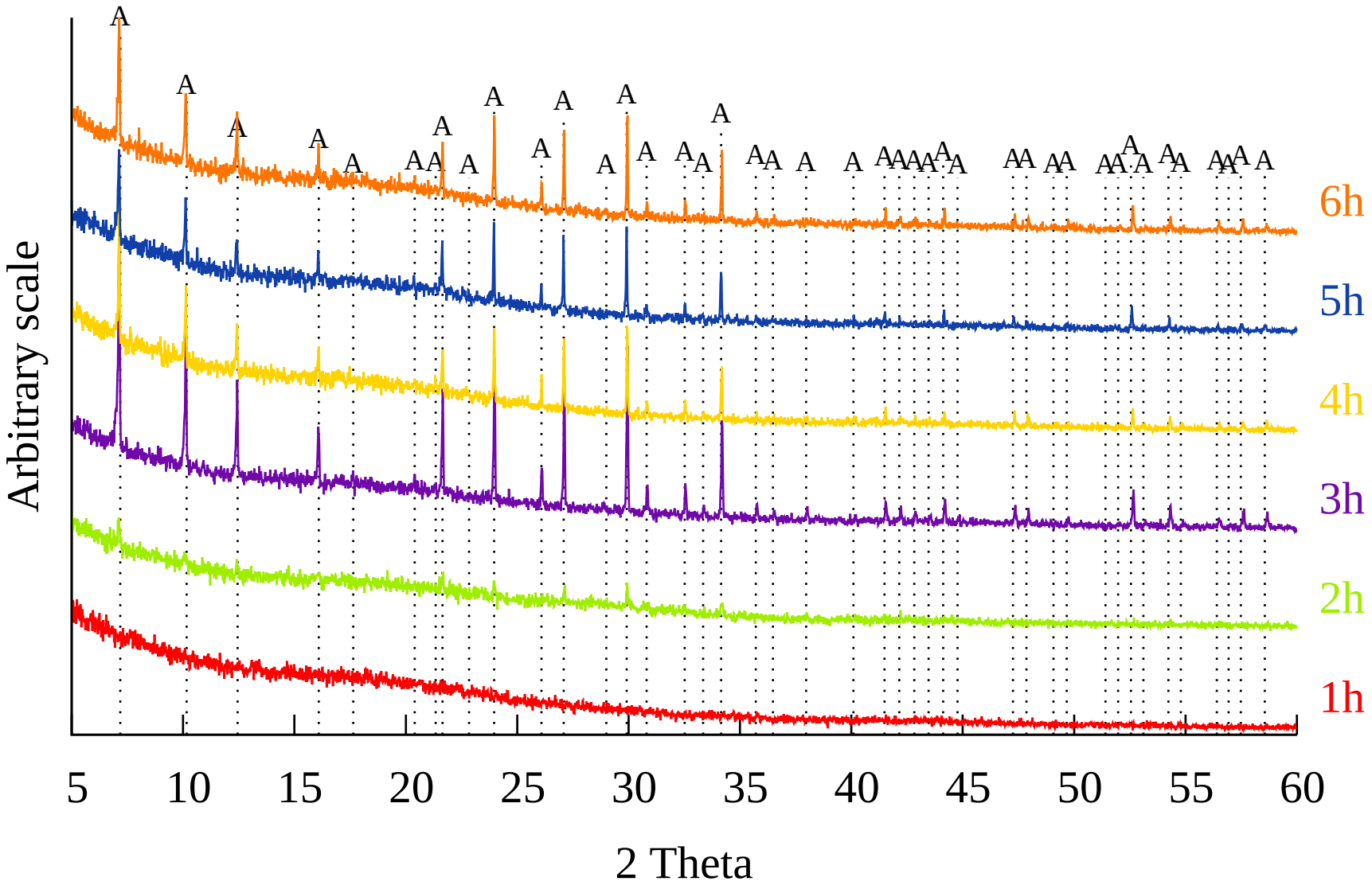

Figure 5.24: XRD patterns of controlled temperature crystallisation with 177 g sodium aluminate/kg FA/kg FA. A: Zeolite Na-A. $\lambda = 1.5406$ Å

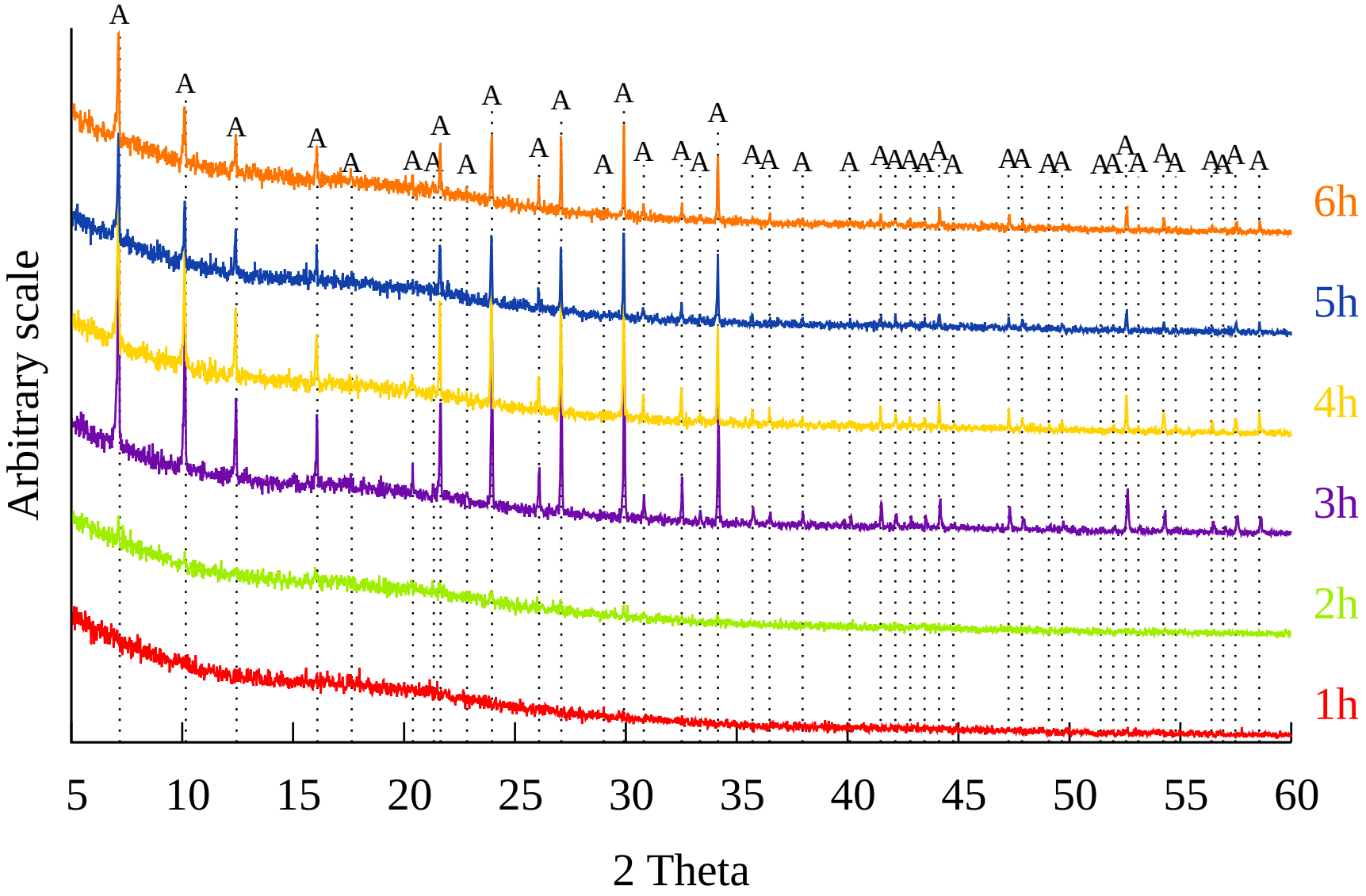

Figure 5.25: XRD patterns of controlled temperature crystallisation with 222 g sodium aluminate/kg FA. A: Zeolite Na-A. λ = 1.5406 Å

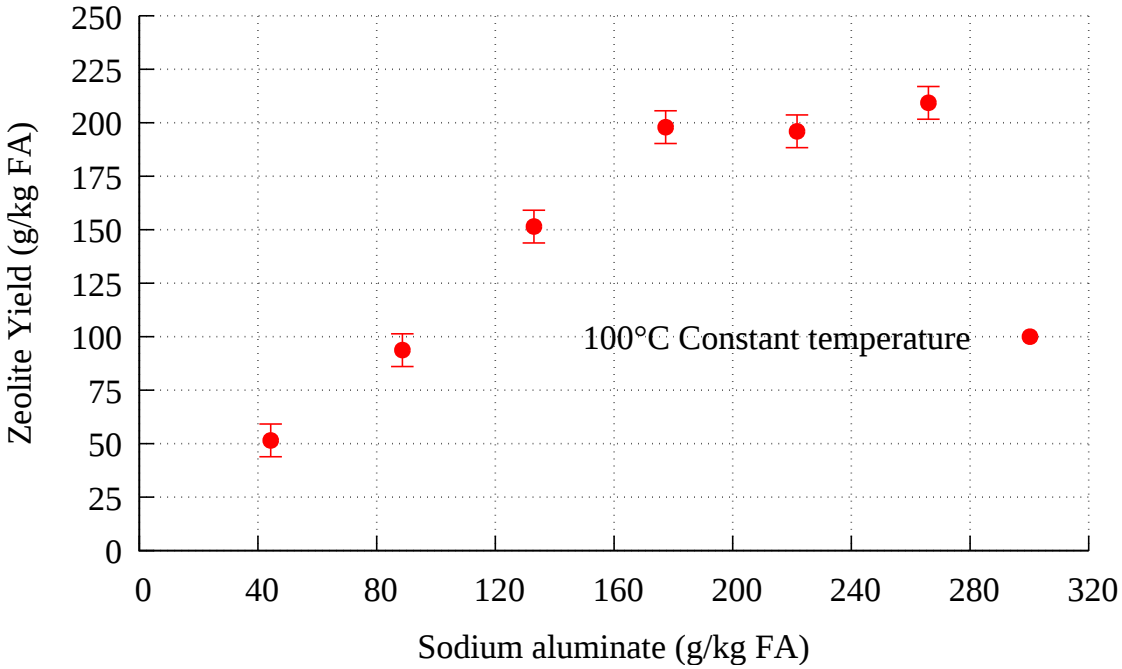

Figure 5.26: Yield of zeolite compared to mass of sodium aluminate addition

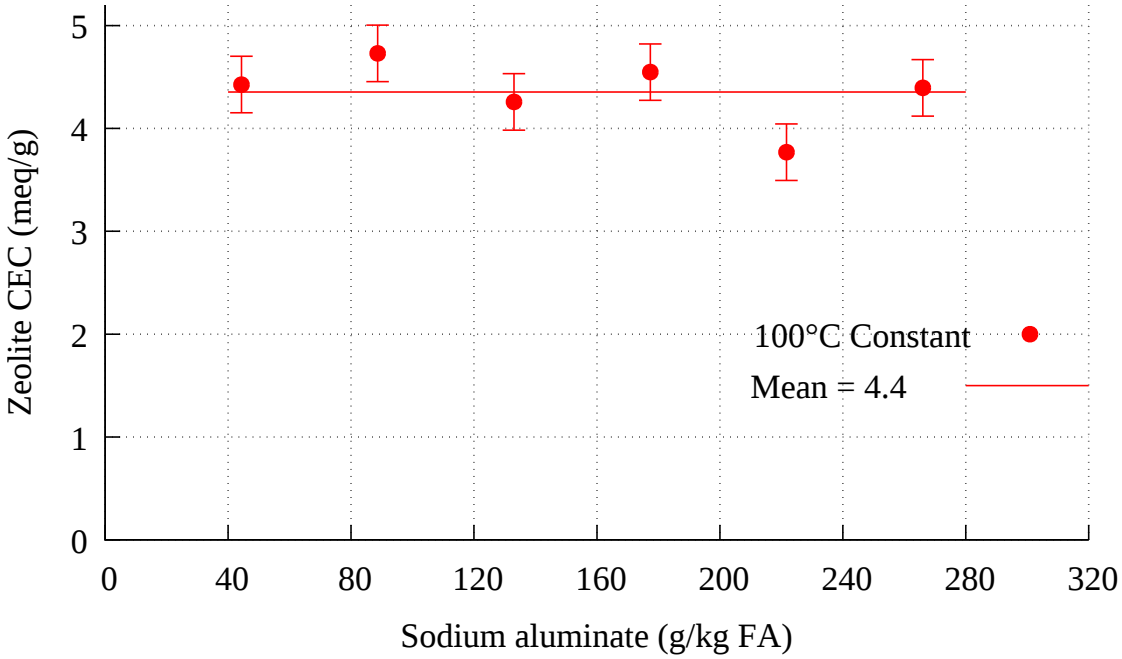

Figure 5.27: CEC of zeolite compared to mass of sodium aluminate addition

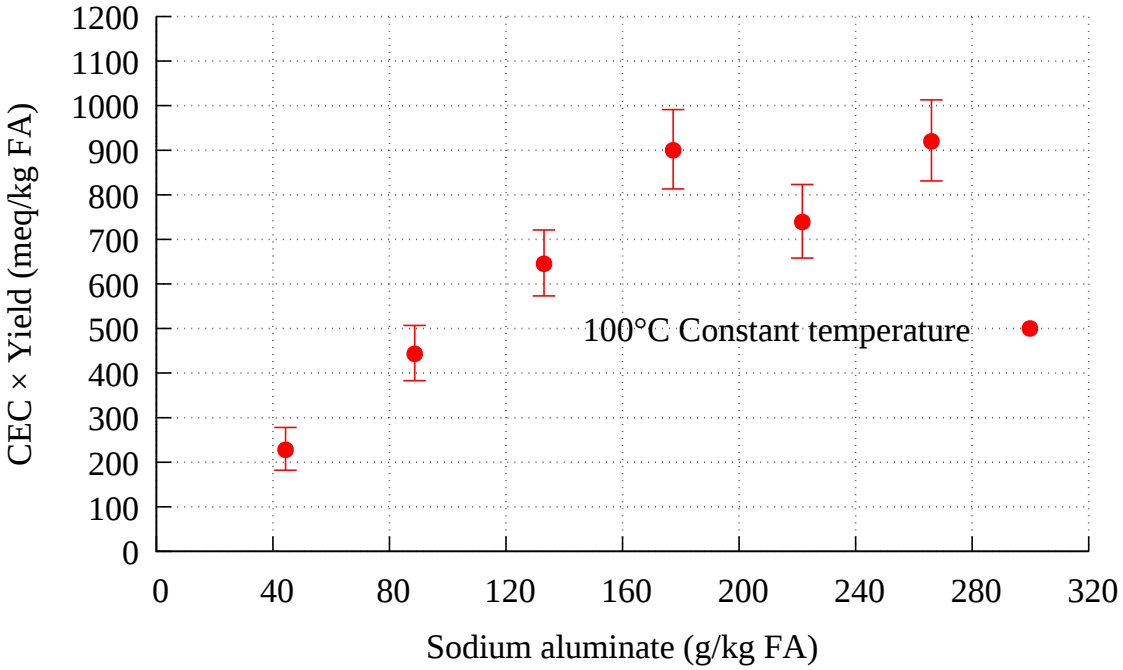

Figure 5.28: CEC × yield of zeolite compared to mass of sodium aluminate addition

5.4 Effect of Changing the Temperature of the Hot Plate During Crystallisation

Hui and Chao [32] discussed a step change in temperature during the crystallisation process. Nucleation occurs at the start of the reaction, with zeolite A nuclei forming preferentially to sodalite nuclei at lower temperatures. Raising the temperature once the system is seeded with zeolite nuclei is argued to result in rapid crystallisation around the seeds that have already formed, rather than seeding new nuclei, thus producing a purer yield of zeolite A than would have been formed at a constant, higher temperature.

5.4.1 Experimental Method

In the previous 100°C hot plate experiments it was noted that the secondary leachate (Ⓦ from Figure 2.12, page 46) remained quite hot for a time after filtering. The sample needed to reach ambient temperatures in order for an accurate volumetric sample to be taken for dilution for AAS analysis. Hot temperatures are conducive to crystallisation, and it was feared that further crystallisation or precipitation could occur during this cooling time. In order to account for this, the 6 hour sample was taken in the same manner as the previous 6 samples, and the entire conical flask Ⓣ then placed in a bath of cold water for 30 minutes prior to filtration Ⓥ. This allowed for:

- The contents of the flask to reach ambient temperatures, making filtration more convenient.
- Any further precipitates to form and add to the yield of the final product.
- The precipitates which had formed to sink to the bottom of the crystallisation vessel allowing for faster filtration of the majority of the leachate due to a lack of filter cake.
- The leachate samples to not be contaminated with solids, which may potentially block AAS equipment and produce erroneous results.

Other than the 30 minute extension in the water bath, the experimental method followed the method used in section 5.3 with one further alteration: the temperature of the hot plates was set at 90°C at the start and raised to 95°C when the 2 hour sample was taken. For these experiments, the hot plates had been re-calibrated to improve their accuracy, and the stated temperatures of 90 and 95°C are considered correct.

5.4.2 Results

As with the previous controlled temperature experiments in section 5.3 each experiment has a noticeable point where Si and Al content decreases slightly, which is concurrent with increases in crystallinity from XRD patterns, and an increase in the quantity of cubes and decrease in presumed amorphous material visible in SEM images. This data set also includes particle size distribution data which shows an increasing particle size as time progresses.

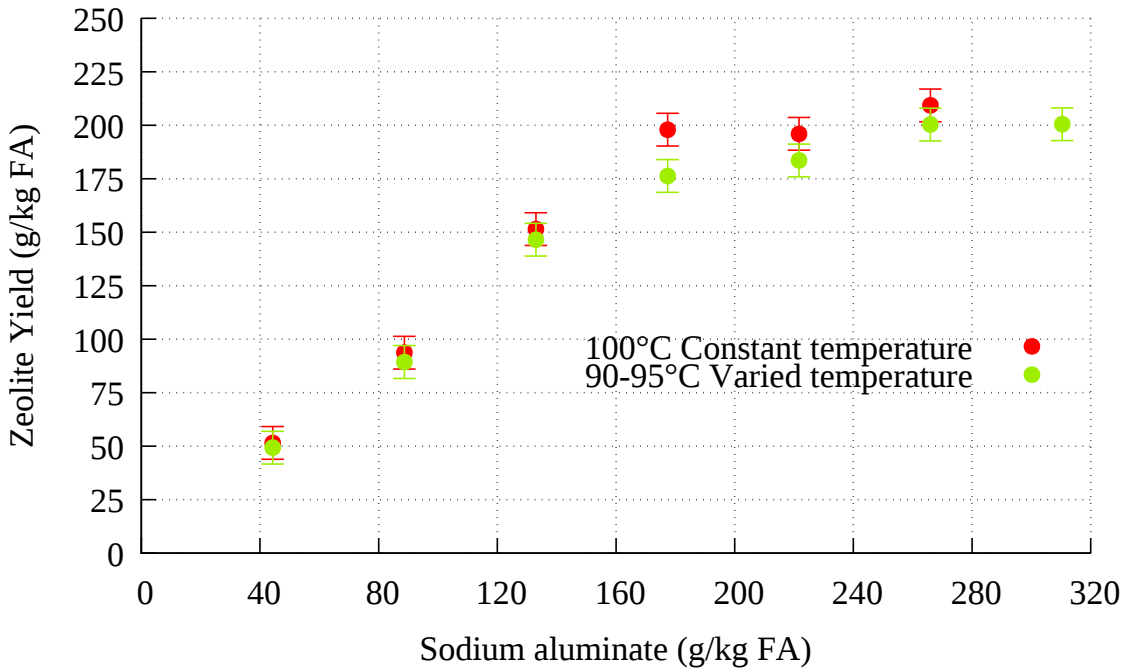

Figure 5.29: Yield of zeolite compared to sodium aluminate addition

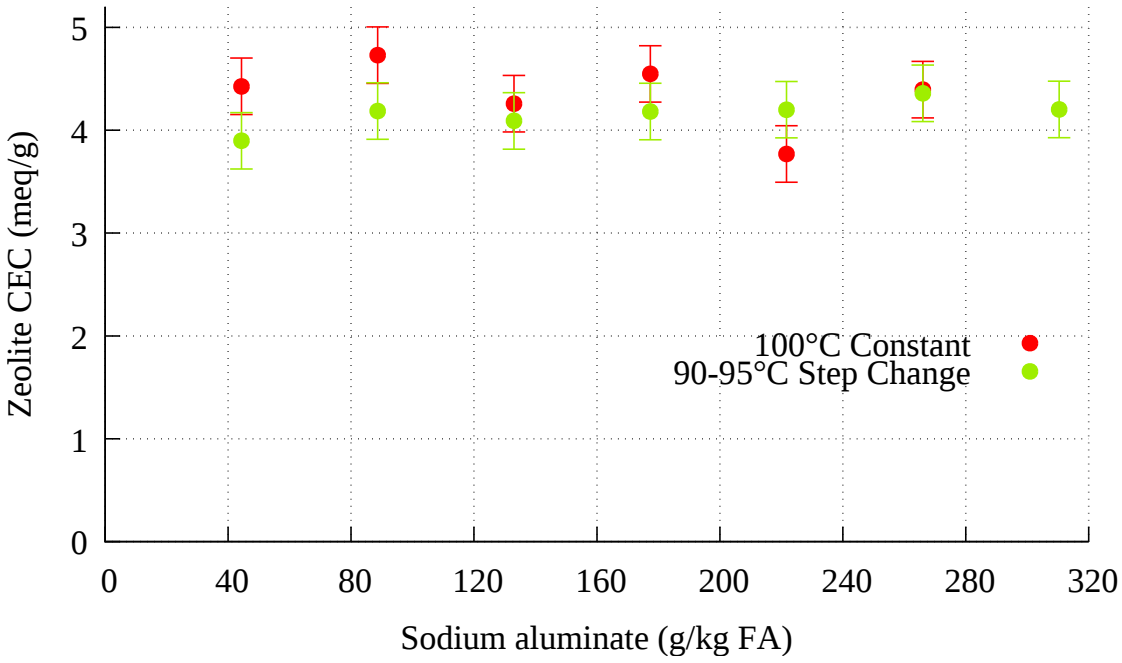

Figure 5.30: CEC of zeolite compared to sodium aluminate addition

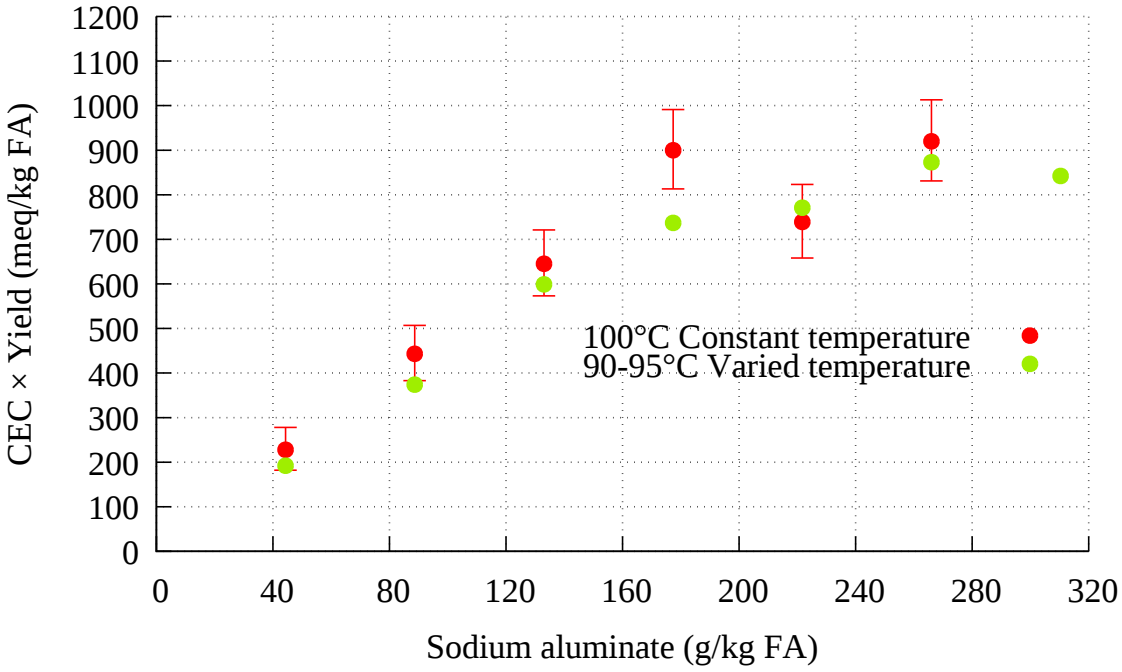

Figure 5.31: CEC × yield of zeolite compared to sodium aluminate addition

5.4.2.1 Dosage of 44 g SA/kg FA

For the lowest dosage of sodium aluminate (44 g/kg FA), crystalline material is not visible in the XRD pattern till 6 hours (figure 5.34), and even then the signal is not strong, with

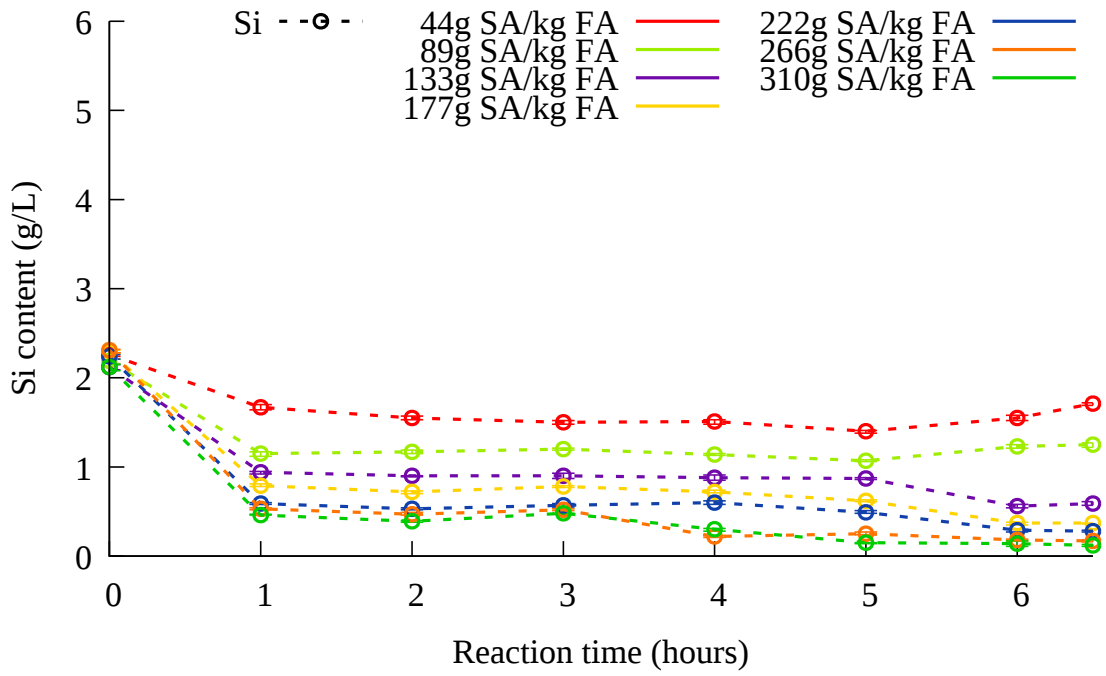

(a) 90-95°C: Si

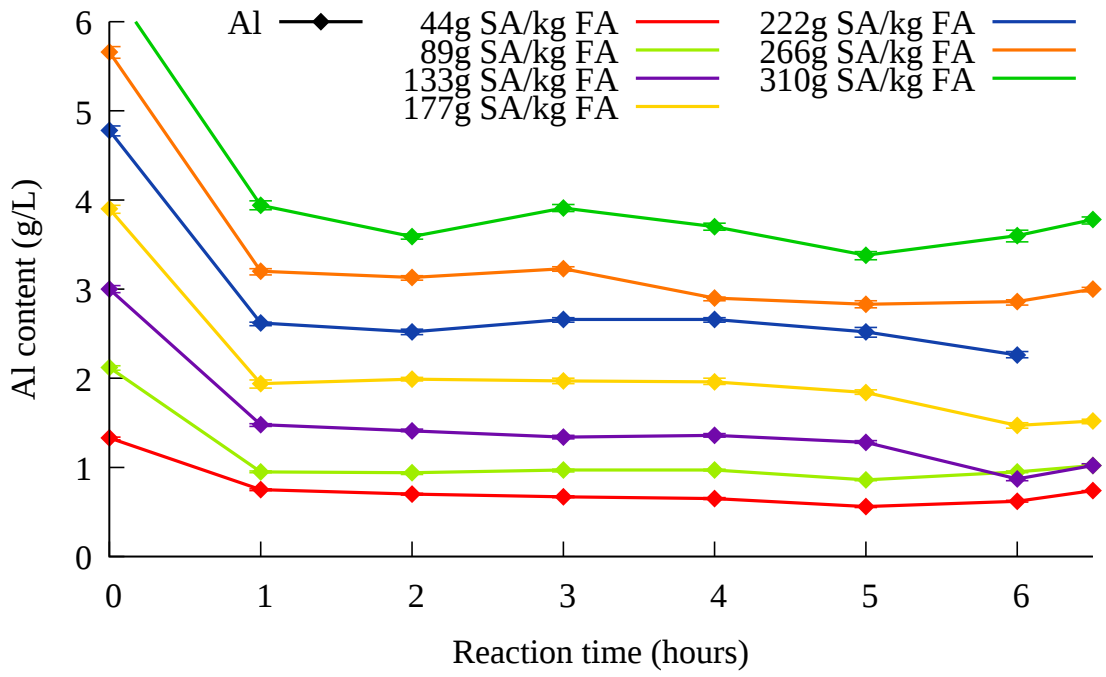

(b) 90-95°C: Al

Figure 5.32: AAS results for 90-95°C crystallisation process with increasing sodium aluminate dosage

the strongest peak visible at 30°2Θ. The SEM image of Figure 5.33f shows scant small cubes, of a similar grain size to the presumably amorphous material surrounding it. The other SEM images of Figure 5.33 do not appear to show any conspicuously crystalline material.

The PSD data in Figure 5.35a shows a broad particle size distribution for the early measurements. The 1 hour PSD is noted to have two small humps at ~8 μm and ~14 μm. These are attributed to errors in analysis, either due to bubbles in the dispersion medium, or agglomerated particles being insufficiently dispersed. The standard deviation of the d_{80} and d_{90} of the 1 hour sample in Figure 5.35b shows a significantly larger error when compared to other results in the same Figure. This indicates that there was inconsistency between the 6 measurements from which the average and standard deviation were drawn. Similarly, the 6.5 hour sample also has a larger standard deviation indicating the same problems. A bimodal distribution of particle sizes is shown for the first 5 hours, with the 6 hour measurement showing a narrower distribution, peaking at ~3 μm.

The sphere in the middle of Figure 5.33e is believed to be cross contamination from an ash sample, rather than the formation of a spherical precipitate. The AAS results in Figure 5.32 do not seem to show much of a dip in Si or Al to indicate sudden crystallisation as in prior experiments. As expected, the lowest dosage of sodium aluminate provides the lowest yield of zeolite, as shown in Figure 5.29. This yield appears to be similar to, but fractionally lower than, the constant temperature crystallisation experiments in section 5.3. The CEC, shown in Figure 5.30 and therefore CEC yield of Figure 5.31 are also lower than the constant temperature experiments.

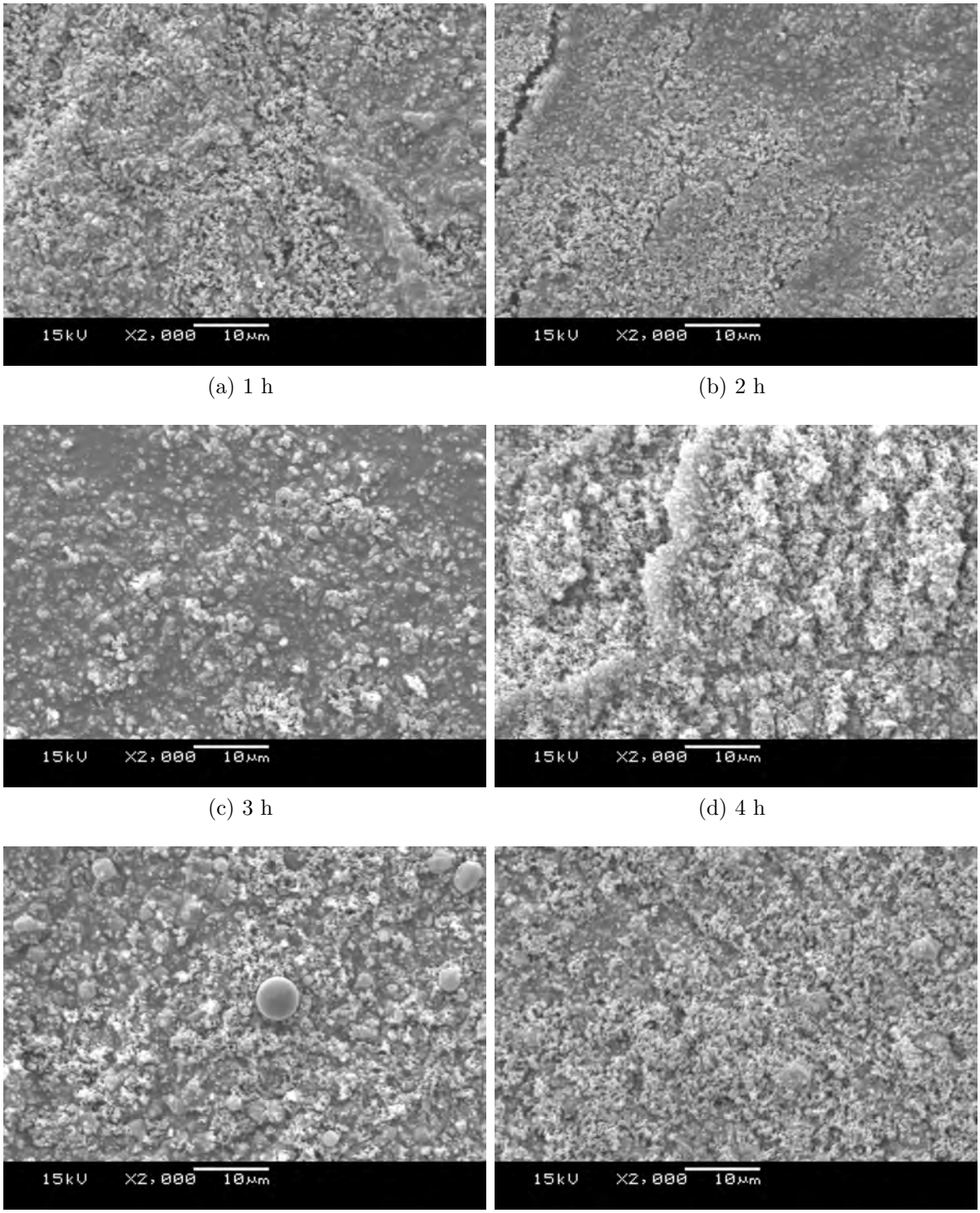

(a) 1 h (b) 2 h

(c) 3 h (d) 4 h

(e) 5 h (f) 6 h

Figure 5.33: SEM images of zeolites from ash leachate crystallised with 44 g of sodium aluminate/ kg FA on a stirred hot plate at 90-95°C

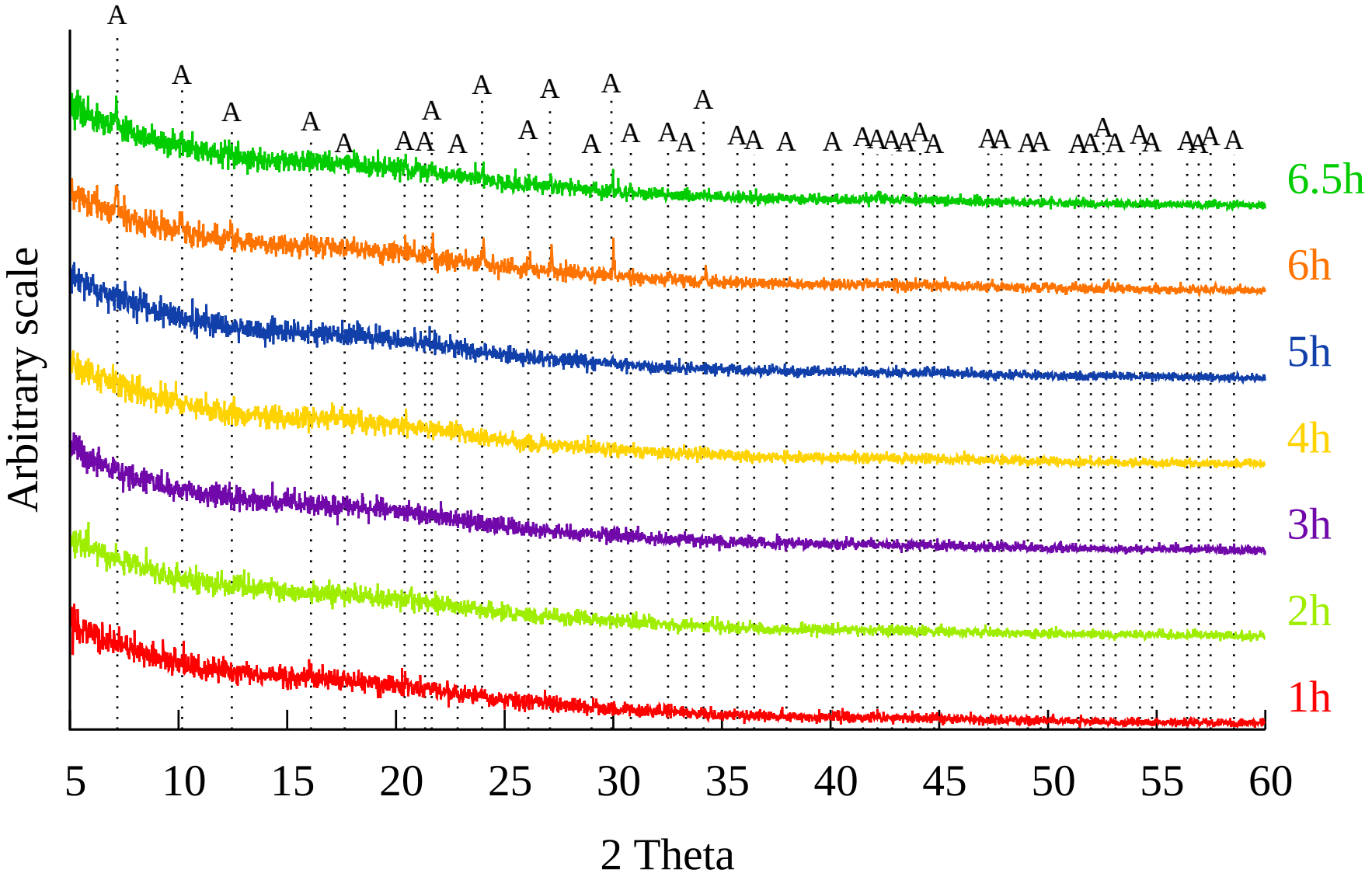

Figure 5.34: XRD patterns of 90-95°C crystallisation with 44 g sodium aluminate/kg FA. A: Zeolite Na-A. $\lambda = 1.5406$ Å

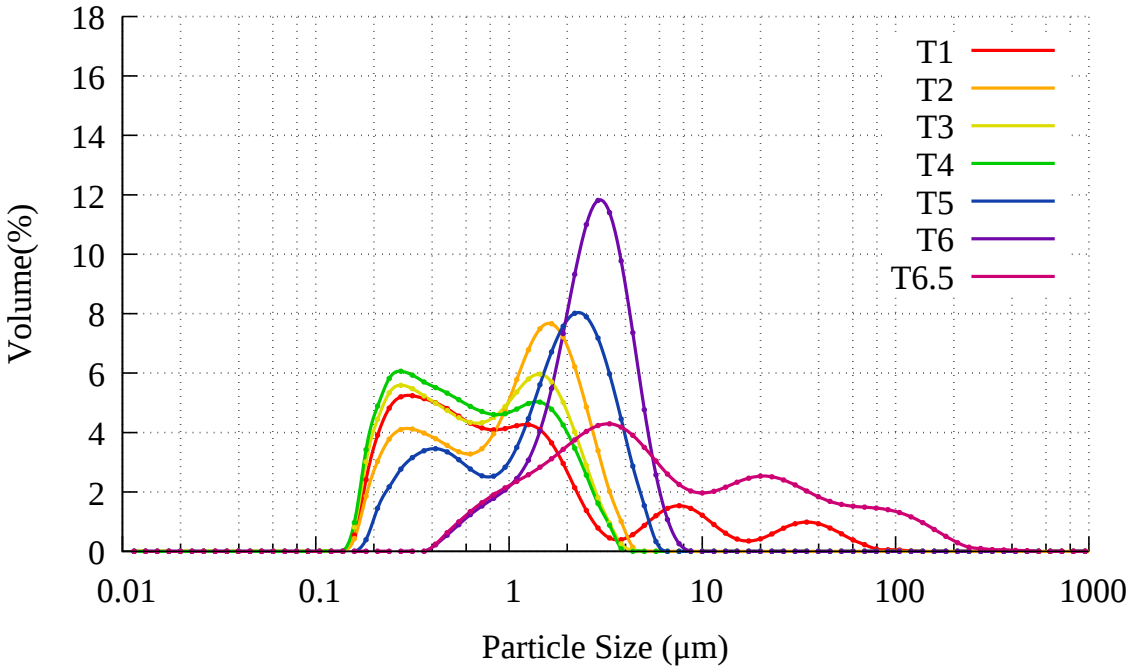

(a) PSD

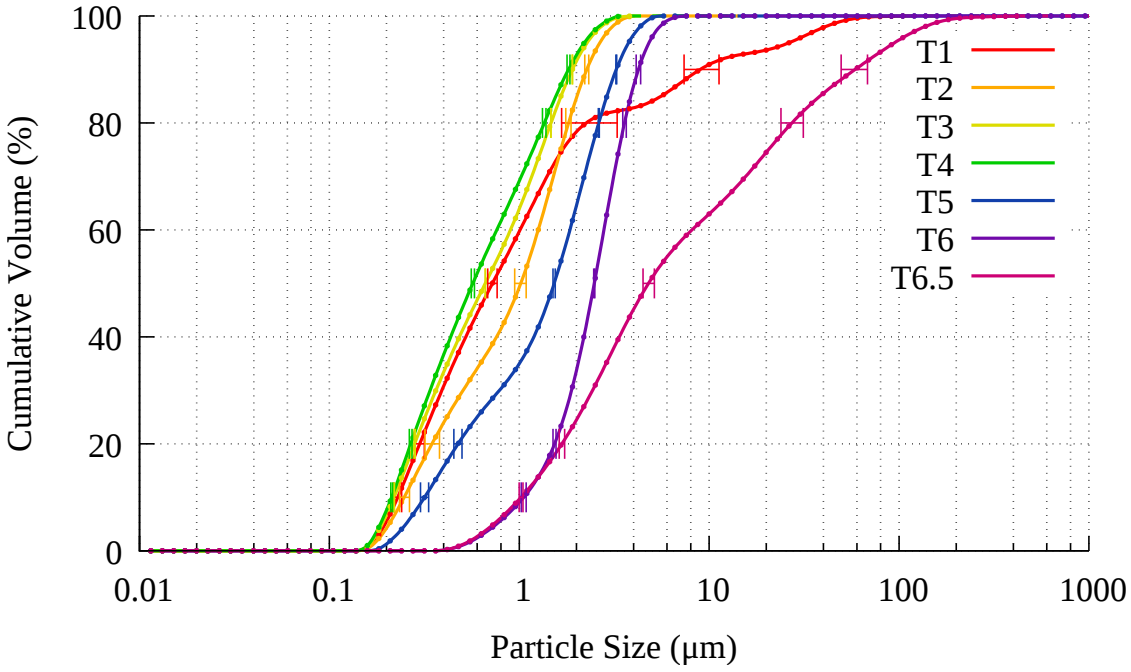

(b) Standard deviation in PSD

Figure 5.35: 90-95°C crystallisation process with 44 g SA/kg FA

5.4.2.2 Dosage of 89 g SA/kg FA

SEM images in Figure 5.36 of crystallisation products from the experiment with the next highest dosage of sodium aluminate (89 g/kg FA) show sporadic cubes at 5 and 6 hours. The XRD results in Figure 5.37 show zeolite A detected at 6 hour, with no obvious signs of crystalline material in prior samples. The AAS results in Figure 5.32 show Si and Al results similar in shape to the 44 g SA/kg FA dosage, but with a higher consumption of Si in the first hour.

The results in Figure 5.38a show a wide PSD for the first 3 hour, before showing a bimodal distribution develop from 4 hours onward, with the peak representing the smaller particle sizes diminishing in size, and moving to the right, indicating a growth in particle size. The peak representing larger particles, which at first appears at around 4 μm, overtakes the smaller particle size peak at 5 hours. At 6 hours, the peak representing larger particles is narrower, and reaches its apex at around 6 μm. The 6.5 hour sample has a larger standard deviation for most points, as seen in Figure 5.38b, again indicating air entrainment during analysis. The bimodal distribution in the PSD is not attributed to anisotropic particles, as the SEM confirms the particles are cube-shaped.

The increased dosage of sodium aluminate results in an increase in yield, as shown by Figure 5.29. The yield is again similar, but fractionally lower than the yield of section 5.3. This yield is comparable to a similar experiment by Du Plessis et al. [7], which added 80.7 g SA/g FA to leachate derived from fused fly ash to produce 78.4 g zeolite A/kg FA. The CEC, shown in Figure 5.30 and therefore CEC yield of Figure 5.31 are again lower than the constant temperature experiments of section 5.3.

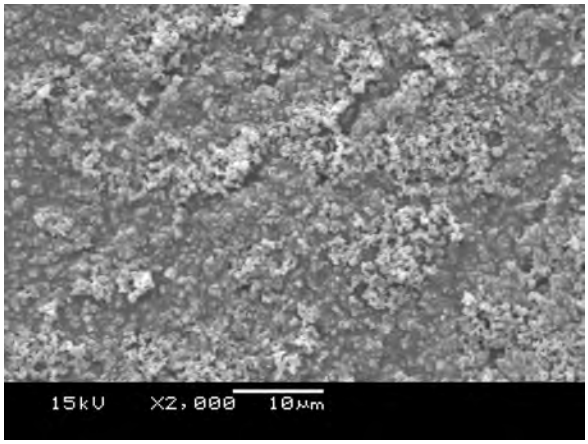

(a) 1 h

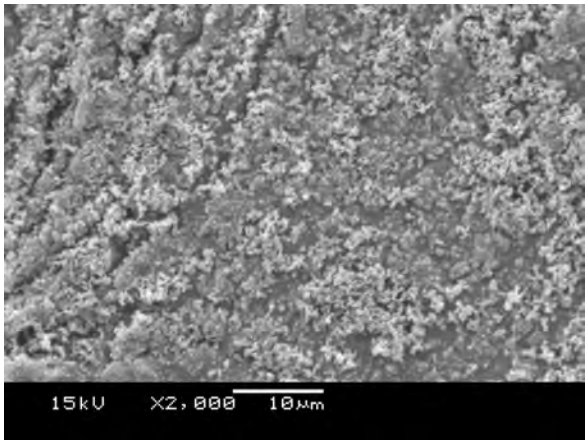

(b) 2 h

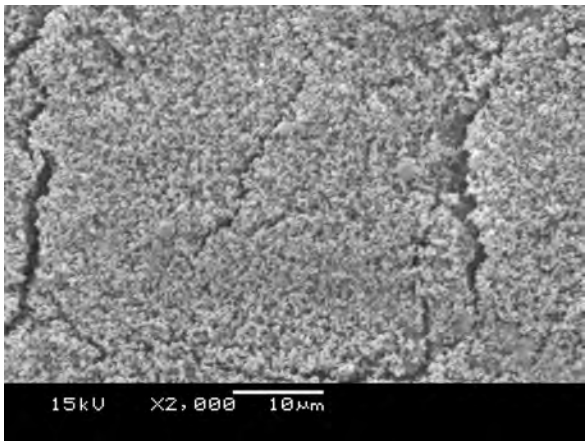

(c) 3 h

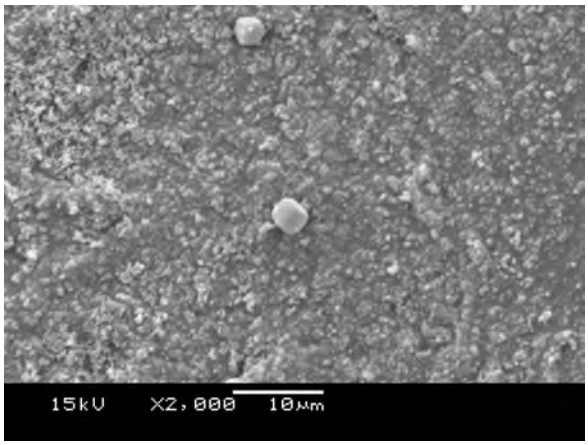

(d) 4 h

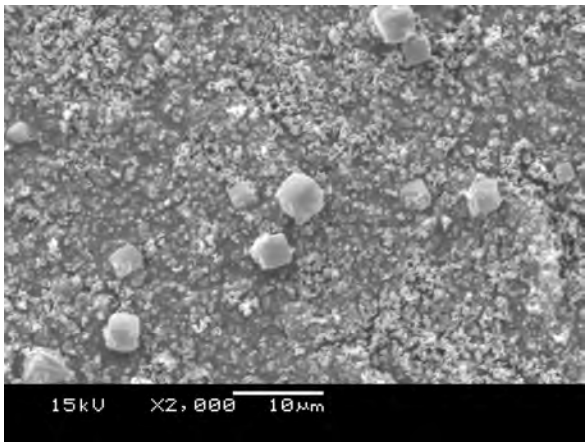

(e) 5 h

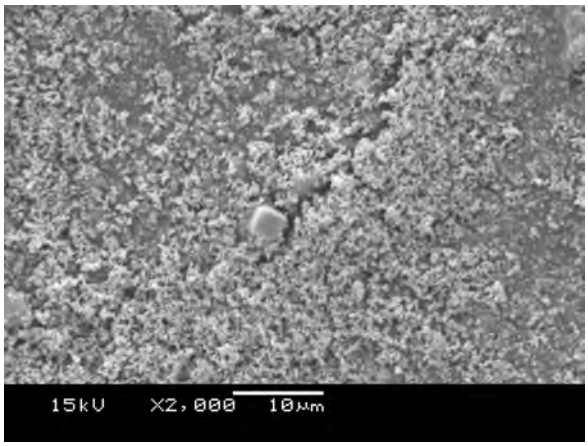

(f) 6 h

Figure 5.36: SEM images of zeolites from ash leachate crystallised with 89 g of sodium aluminate/kg FA on a stirred hot plate at 90-95°C

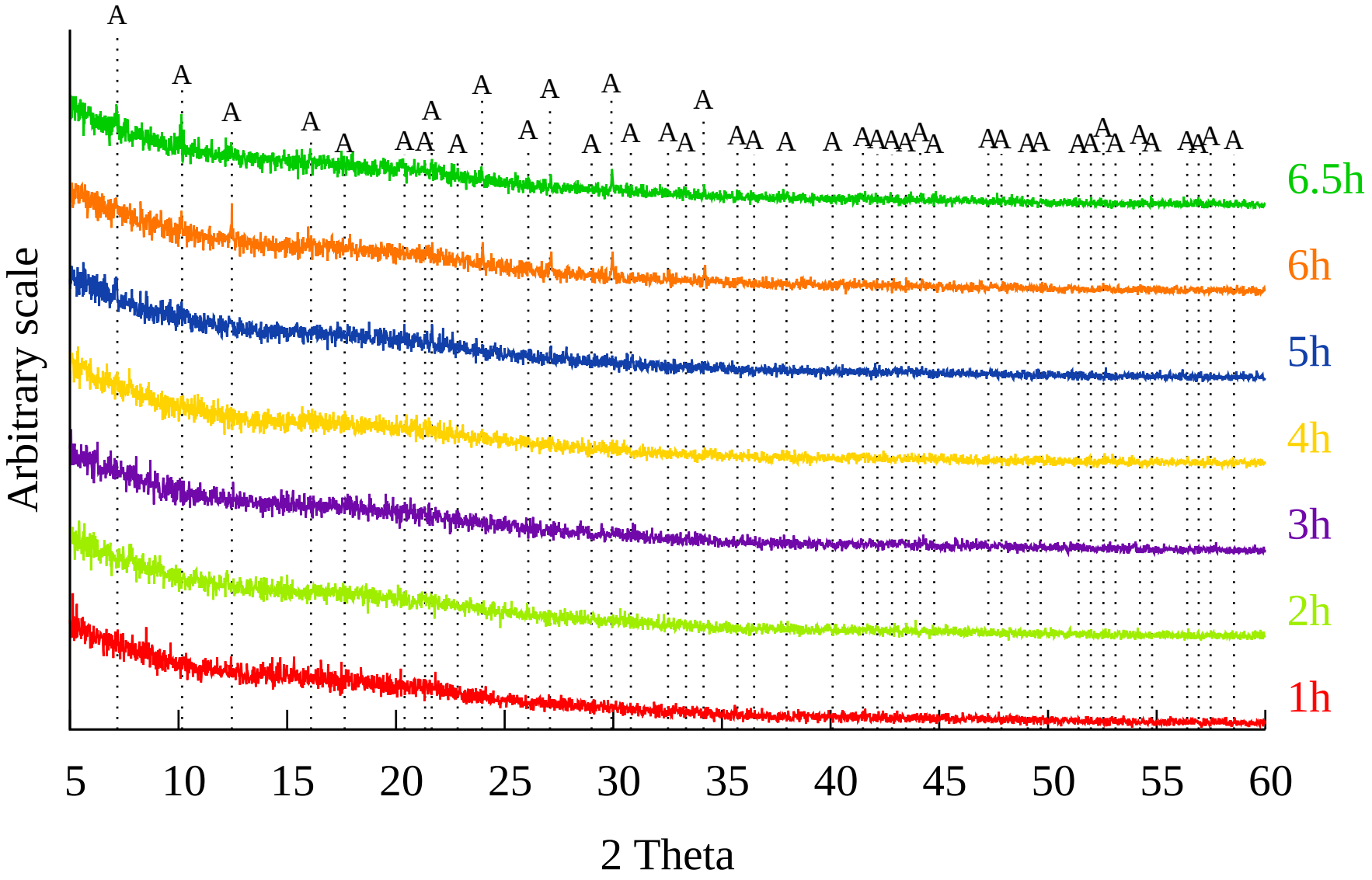

Figure 5.37: XRD patterns of 90-95°C crystallisation with 89 g sodium aluminate/kg FA. A: Zeolite Na-A. $\lambda = 1.5406$ Å

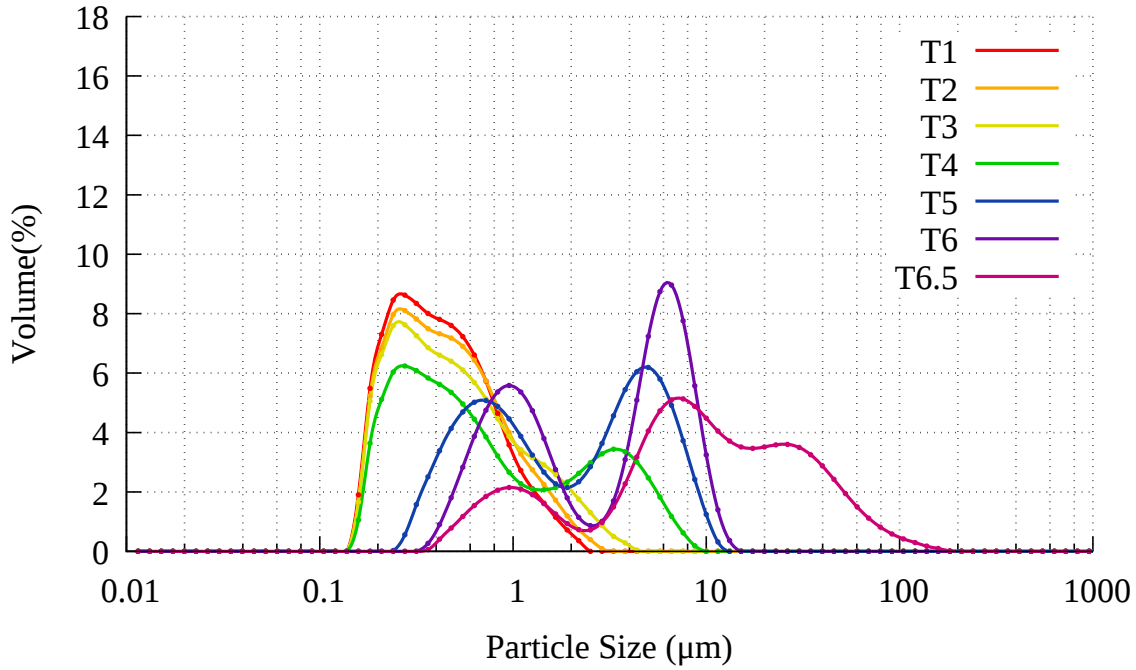

(a) PSD

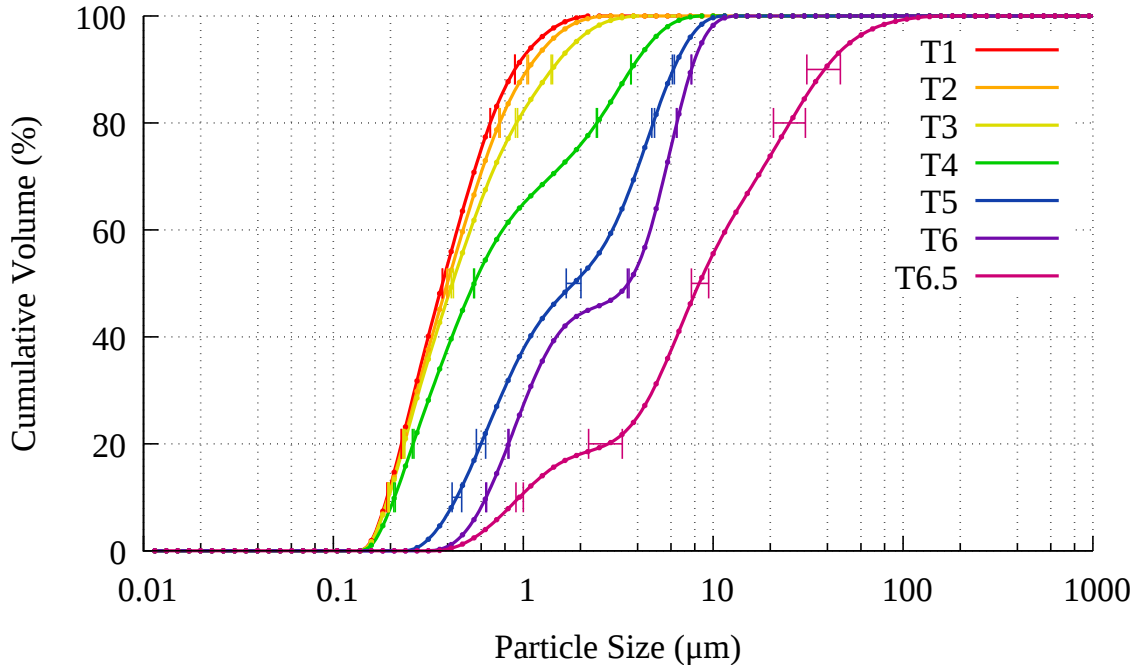

(b) Standard deviation in PSD

Figure 5.38: 90-95°C crystallisation process with 89 g SA/kg FA

5.4.2.3 Dosage of 133 g SA/kg FA

The first SEM images with a conspicuous crop of cubes are Figures 5.39e and 5.39f from experiments with 133 g SA/kg FA. Whilst there is still much amorphous material in Figure 5.39e, the cubes are clearly visible, and zeolite A is detected in the XRD pattern of Figure 5.40, with prominent peaks starting from 5 hours. It is noted that these peaks are significantly clearer than any peaks for lower dosages of sodium aluminate. The AAS results of Figure 5.32 again show a higher consumption of Si in the first hour compared to lower dosages of sodium aluminate. The AAS results show the anticipated drop in Si and Al between 5-6 hours, which coincides with the disappearance of amorphous material between 5 hours in Figure 5.39e and 6 hours in Figure 5.39f. This drop in Si and Al during the disappearance of amorphous material can also be seen in SEM images and ICP-AES data of Musyoka et al. [35], where zeolite A was crystallised from the leachate of a fusion product at similar concentrations of NaOH and at similar solids loadings. Work by Belviso et al. [39] also shows SEM images where amorphous material decreases as crystalline material develops, however such samples are also intermixed with undissolved fly ash.

As with previous dosages of sodium aluminate, the PSD in Figure 5.41a starts quite broad, before showing a bimodal distribution at 3 hours, with both peaks heading to the right, and the right hand peak overtaking the left hand peak in height at 4 hours. The PSD for 6 hours shows a narrower particle size range for the right hand peak, and a shorter range on the left hand side. The standard deviation values in Figure 5.41b show very little variation. The d_{50} of the first 3 hours are quite similar, and the d_{50} increases as time progresses.

As with previous dosages of sodium aluminate, the yield shown in Figure 5.29 shows an increase in yield similar, but slightly lower, than the yield of experiments from section 5.3. The CEC, shown in Figure 5.30 is slightly lower than the constant temperature equivalent, thus the CEC yield of Figure 5.31 is lower than the equivalent constant temperature experiment of section 5.3.

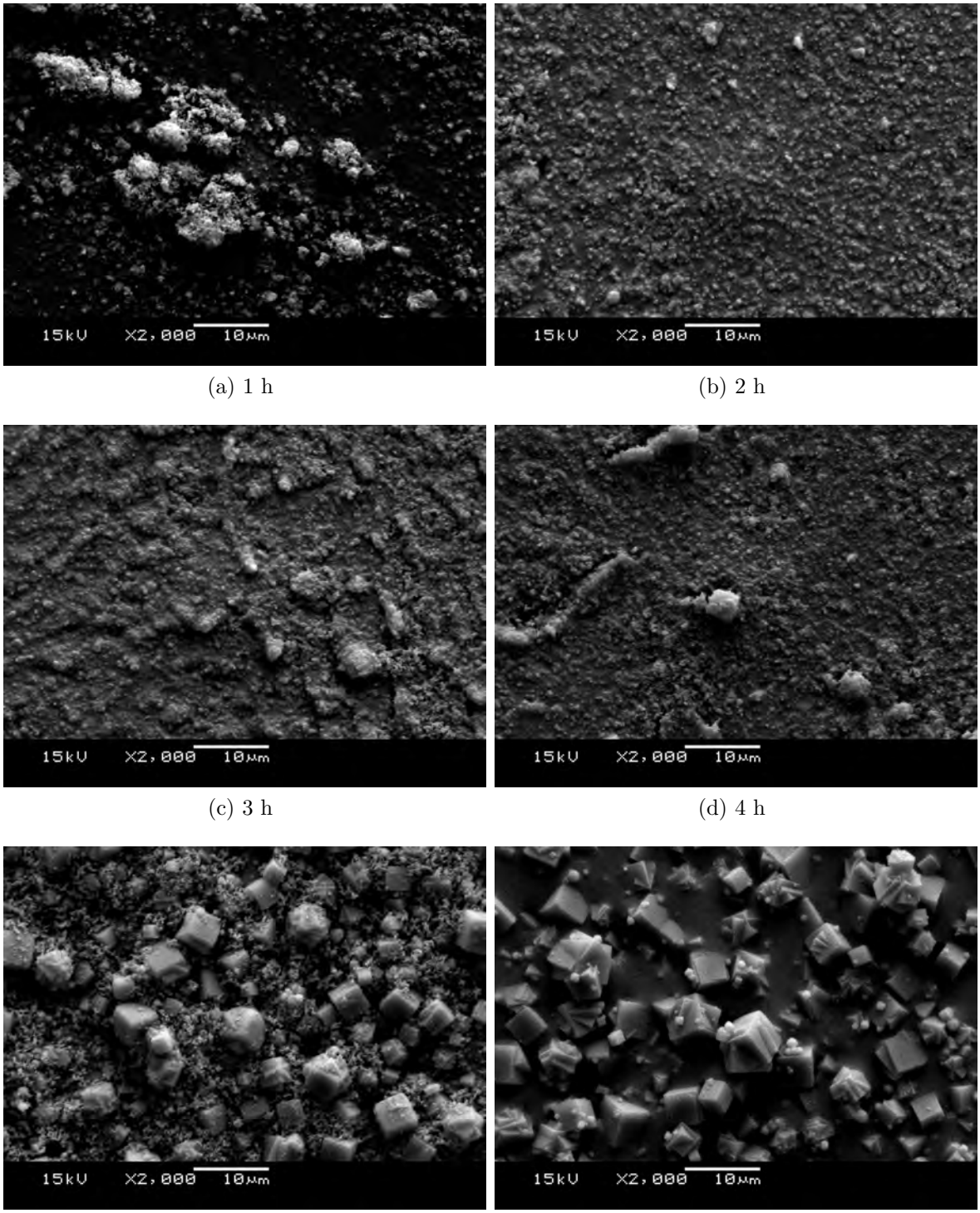

(a) 1 h (b) 2 h

(c) 3 h (d) 4 h

(e) 5 h (f) 6 h

Figure 5.39: SEM images of zeolites from ash leachate crystallised with 133 g of sodium aluminate/kg FA on a stirred hot plate at 90-95°C

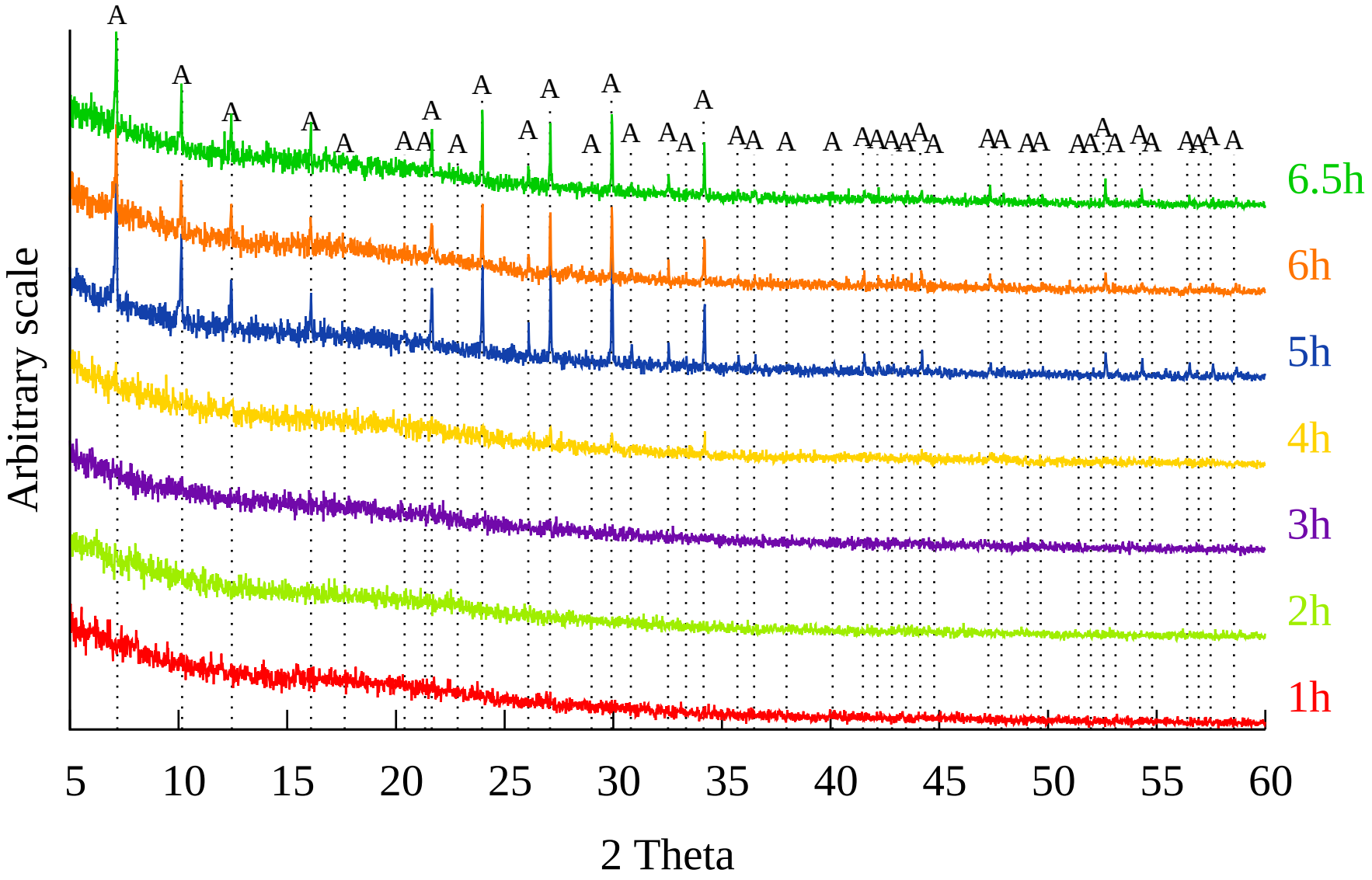

Figure 5.40: XRD patterns of 90-95°C crystallisation with 133 g sodium aluminate/kg FA. A: Zeolite Na-A. $\lambda = 1.5406$ Å

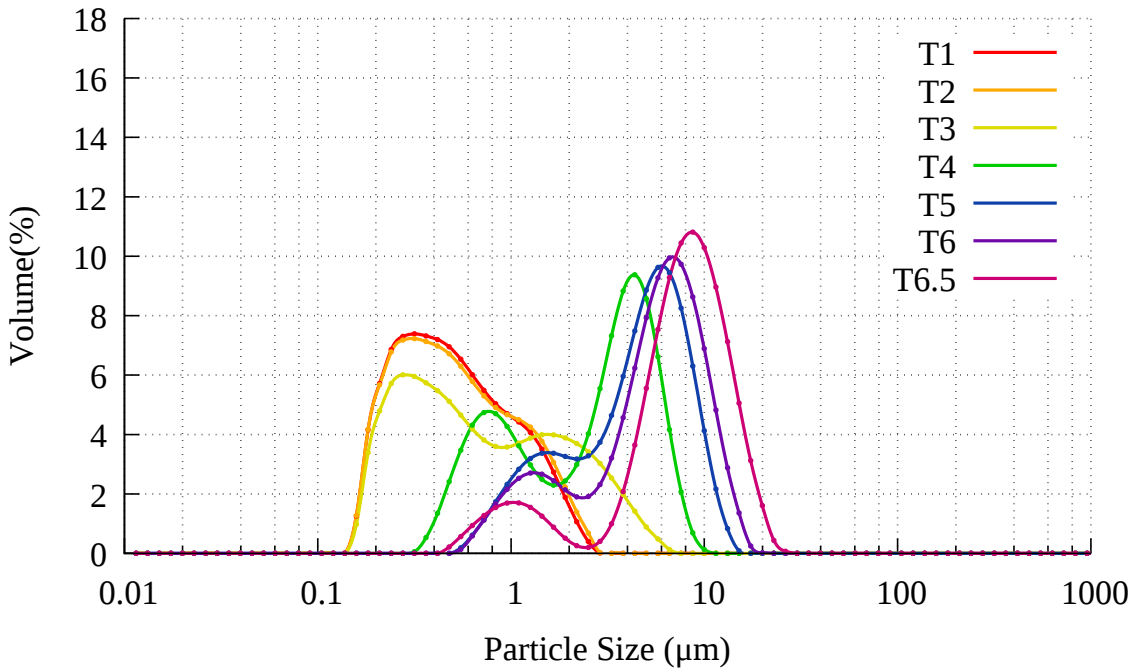

(a) PSD

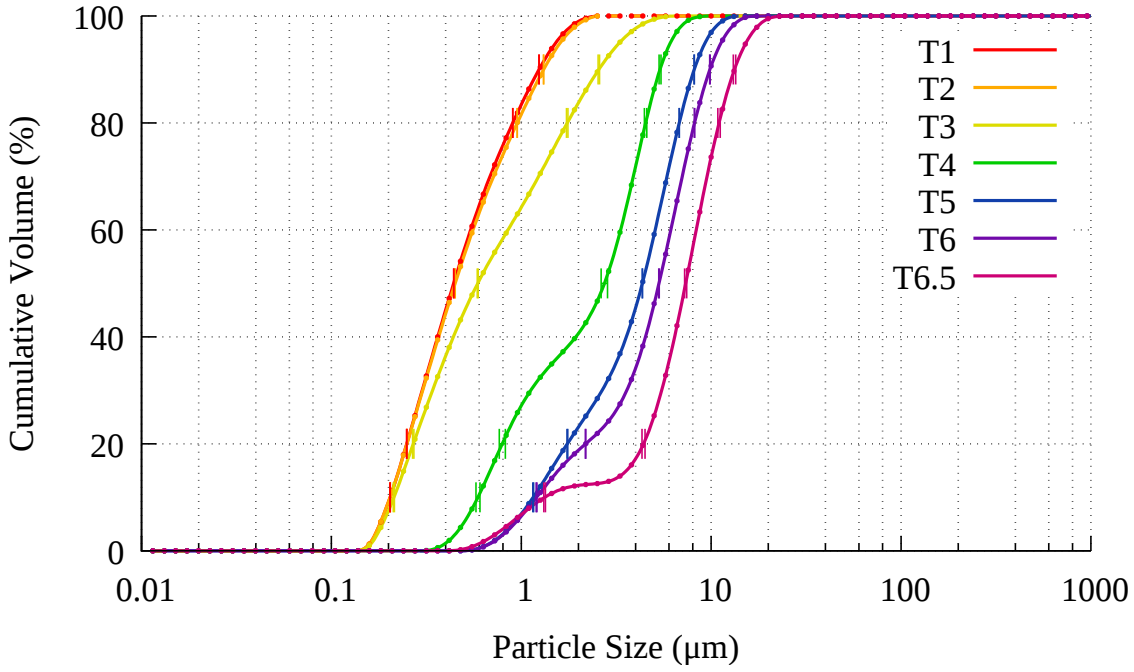

(b) Standard deviation in PSD

Figure 5.41: 90-95°C crystallisation process with 133 g SA/kg FA

5.4.2.4 Dosage of 177 g SA/kg FA

The 177 g SA/kg FA dosage shows cubes with chamfered edges at 4 hours (figure 5.42d) onward. The XRD results in Figure 5.43 show small peaks for the 4 hour sample, with peaks of greater intensity for later samples. In the AAS results of Figure 5.32, there is a drop in Si and Al content that starts between 4 and 5 hours, but drops further between 5 and 6 hours. This is consistent with much of the amorphous material being consumed between 4 and 5 hours, with consumption continuing till 6 hours. The PSD at the first hour shown in Figure 5.44a is narrower than previous PSD results at 1 hour. As time increases, this peak shortens and moves to the right, and a right hand peak develops, which grows in height whilst moving to the right.

The SEM image 5.42d of cubes at 4 hours, shows cubes smaller than 10 μm surrounded by smaller particulates, this is reflected in the PSD at 4 hours, where a peak is shown at 6 μm (indicating the most common size of particle) and the Figure 5.44b shows a d_{50} of 4 μm. There is a smaller peak of the left hand side with a peak at 0.8 μm, which may represent the surrounding material. This surrounding material decreases significantly by the 5 hour SEM image, and the right hand PSD peak increases in height, and moves to 8 μm. The left hand peak decreases significantly and moves up to peak at 1 μm. As there are two distinct peaks in the PSD, this would indicate that the smaller particles visible in the SEM images are not attached to the cubes, but are merely intermixed with them.

XRD analysis does not detect more than one phase. This indicates that the small particulates are either zeolite A, amorphous material undetected by XRD, or of such a low concentration that their peaks are obsured by the signal noise. The standard deviation for the PSD results seem acceptable, but the d_{20} of the 5 hour sample appears to have a higher standard deviation than other results in this data set. This would indicate a variation in the 6 results analysed for the 5 hour PSD. The variation would be localised around the left hand peak, as the d_{50} and higher appear consistent. This variation could be attributed to agglomeration of finer particles. Comparison of these SEM images with PSD data in Figure 5.44 shows that the SEM images appear to be a good representation of

the bulk of the sample. The yield of zeolite shown in Figure 5.29 does not conform to the trend of being slightly lower than the yield of zeolite produced in constant temperature experiments, but is significantly lower, whilst still being higher than the previous SA dosage of 133 g/kg FA. This would indicate that the yield is starting to plateau. The CEC, shown in Figure 5.30 is very similar to previous values for this experiment set, being slightly lower than the constant temperature CEC. The CEC yield of Figure 5.31 is again lower than the constant temperature experiments, but higher than previous CEC yield values.

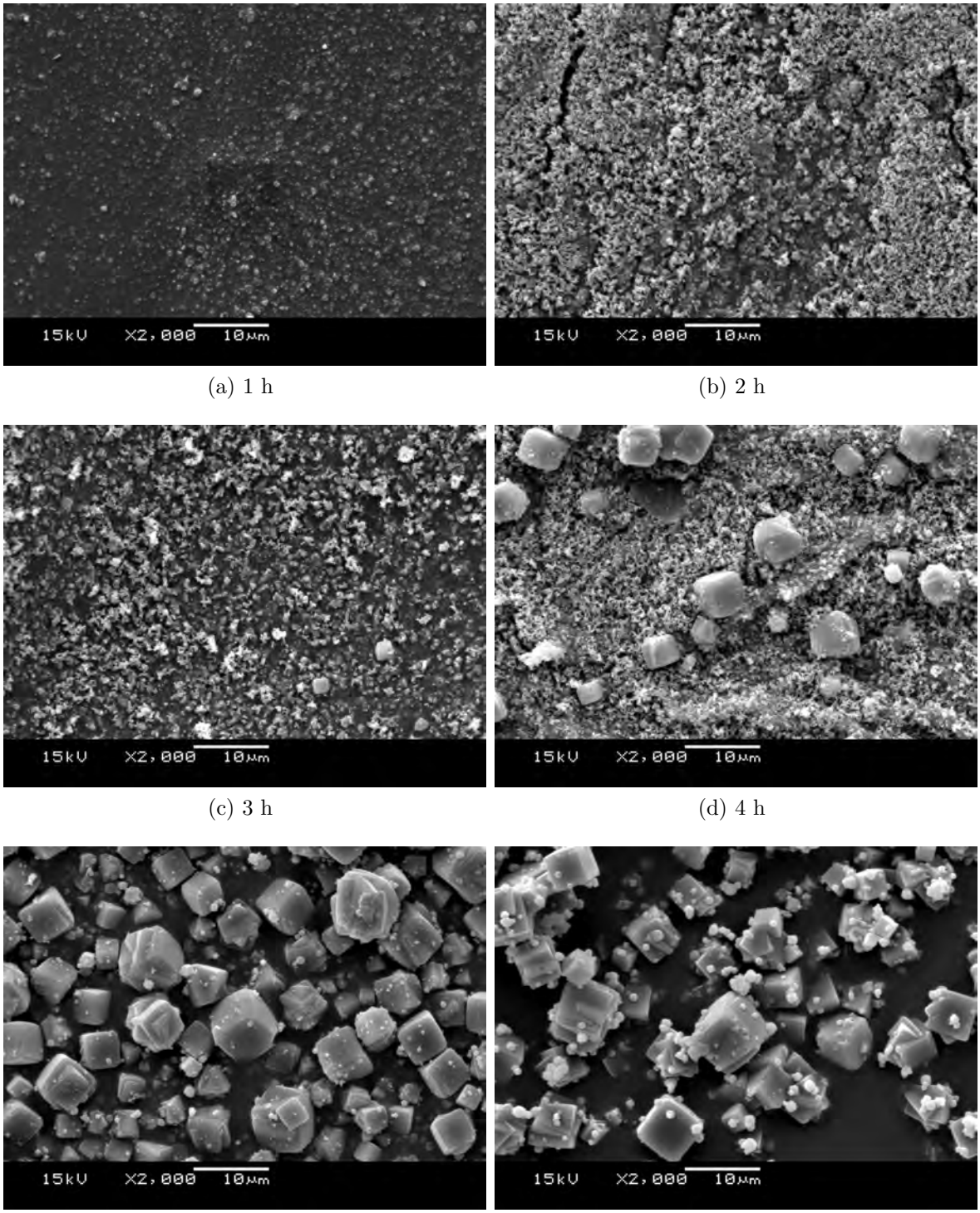

(a) 1 h (b) 2 h

(c) 3 h (d) 4 h

(e) 5 h (f) 6 h

Figure 5.42: SEM images of zeolites from ash leachate crystallised with 177 g of sodium aluminate/kg FA on a stirred hot plate at 90-95°C

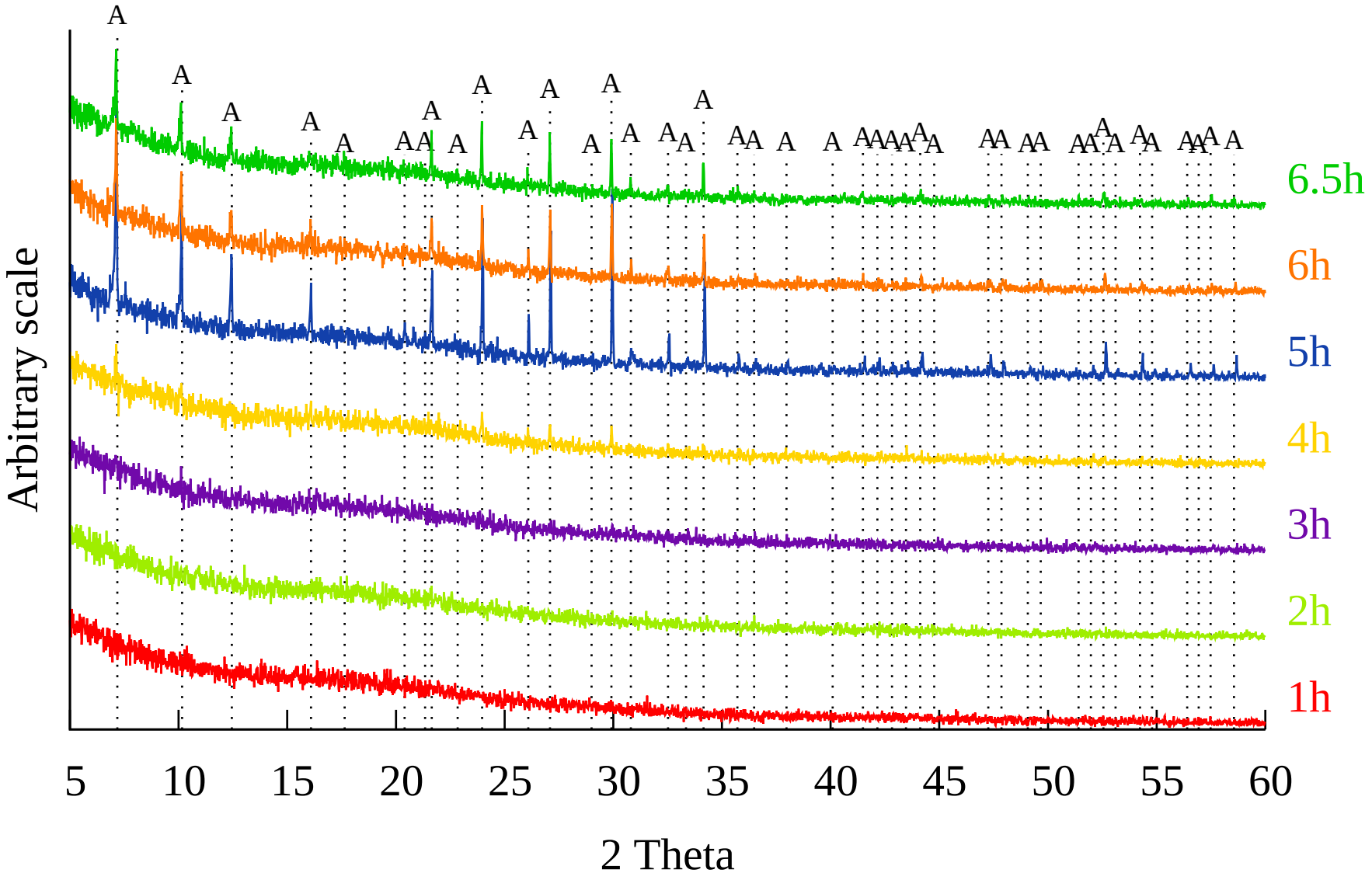

Figure 5.43: XRD patterns of 90-95°C crystallisation with 177 g sodium aluminate/kg FA/kg FA. A: Zeolite Na-A. $\lambda = 1.5406$ Åv

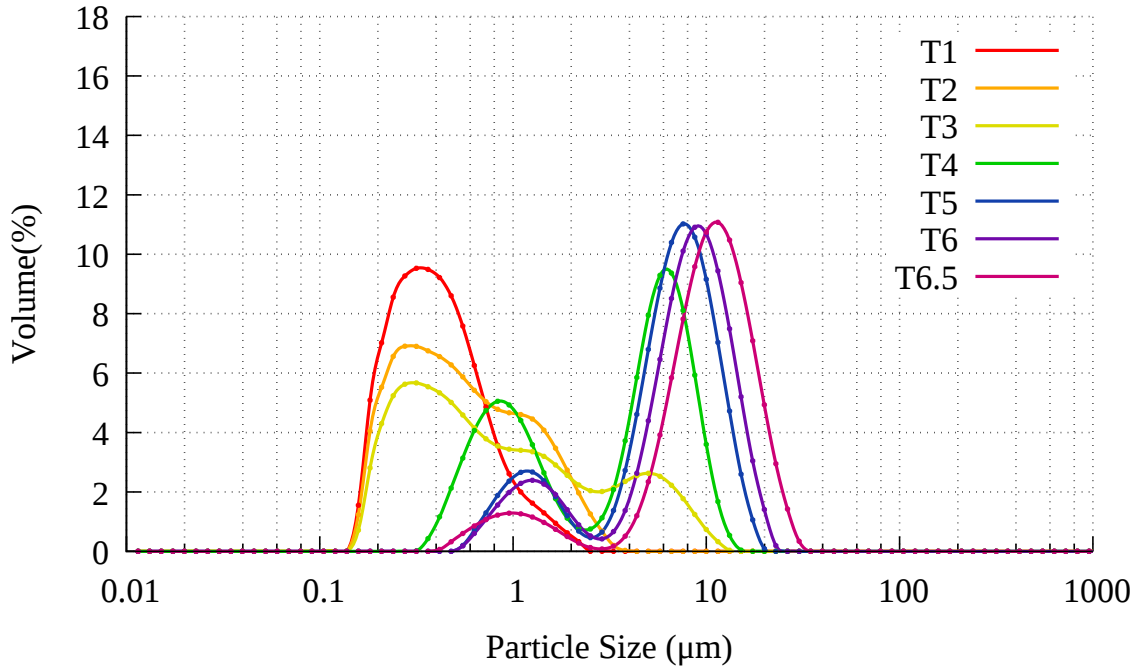

(a) PSD

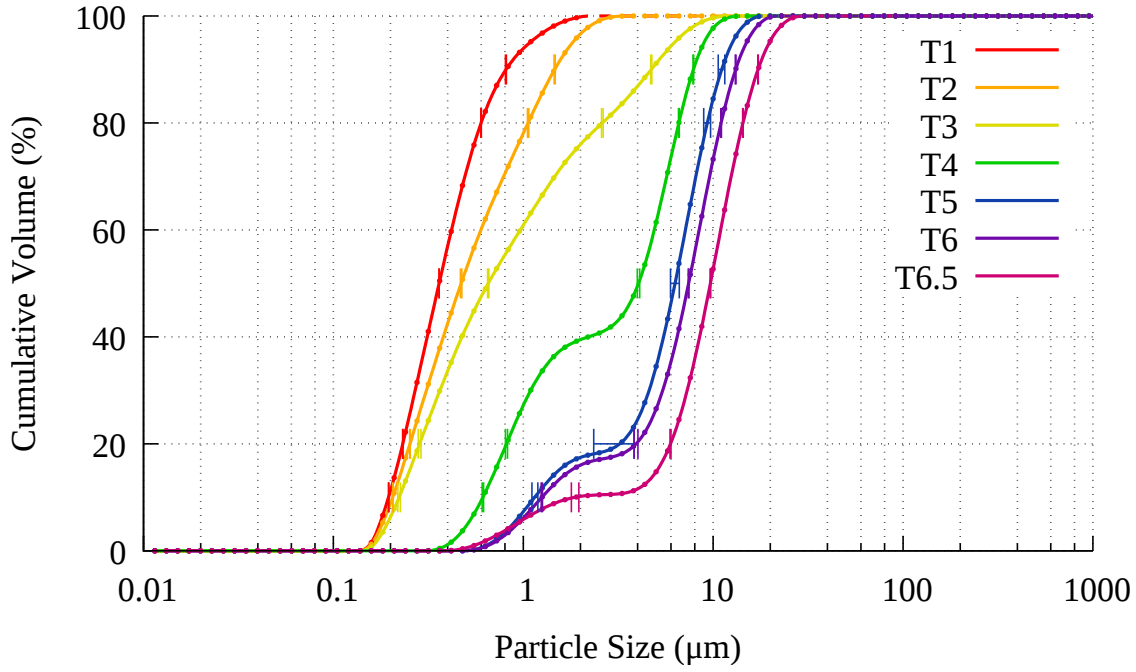

(b) Standard deviation in PSD

Figure 5.44: 90-95°C crystallisation process with 177 g SA/kg FA

5.4.2.5 Dosage of 222 g SA/kg FA

The 222 g SA/kg FA dosage of sodium aluminate shows a significant concentration of cubes at 5 hours (figure 5.45e), which coincides with high intensity peaks for zeolite A at 5 hours in Figure 5.46. Low intensity peaks are visible at 4 hours in the XRD pattern, which would correspond to the sparse cubes visible in Figure 5.45d. The zeolite sample in Figure 5.45f shows chamfered cubes with fewer 1 μm fine particulates than in previous SA dosages. AAS analysis shows a steady decline in Si and Al between hours 4 and 6. The PSD shown in Figure 5.47a shows low, broad humps for smaller particle sizes at 1-3 hours, with 4 hours showing a bimodal distribution, and hours 5 and 6 showing very high similarity, with a peak at around 10 μm, which coincides with the cubes shown in Figure 5.45f.

The smaller materials seen in Figure 5.45f would be represented by the left hand peak at 1 μm in Figure 5.47a at 6 hours. The standard deviation of the d_{80} for the 2 hour result as shown in Figure 5.47b is larger than most, however the d_{90} has a relative standard deviation of ~140 %. This high error in the d_{90} is attributed to bubbles in the dispersion medium, and is significant enough to also influence the d_{80}. The increase in particle size between 6 and 6.5 hours (during the cooling and filtration process) is attributed to agglomeration, as no discernible change is visible in the size of the cubes in SEM images. See Appendix Figures A.2 and A.3. This agglomeration during the cooling phase would be possible if precipitates or zeolites grow between individual zeolite cubes, bonding them together into larger agglomerates.

As with previous dosages of sodium aluminate, the yield has increased, but is lower than the yield from section 5.3. The increase in yield is small, which is consistent with the yield reaching a plateau. The CEC, shown in Figure 5.30 is similar to previous values for this experiment set. The CEC yield of Figure 5.31 is higher than the constant temperature experiment, due to the lower CEC for that particular experiment. The AAS results in Figure 5.32 show a decrease in Si and Al between 4 and 6 hours, which coincides with the disappearance of amorphous material in the SEM images. The lower Al value for the

6.5 hour measurement is not reflected in the Si result for 6.5 hours. This value is also noted to not follow the slight upward trend between 6 and 6.5 hours noted in all Si and Al measurements, whilst being conspicuously similar to the 6.5 hour Al result for 177 g SA/kg FA. It is possible this result was not measured, and the 177 g dosage analysed again in error.

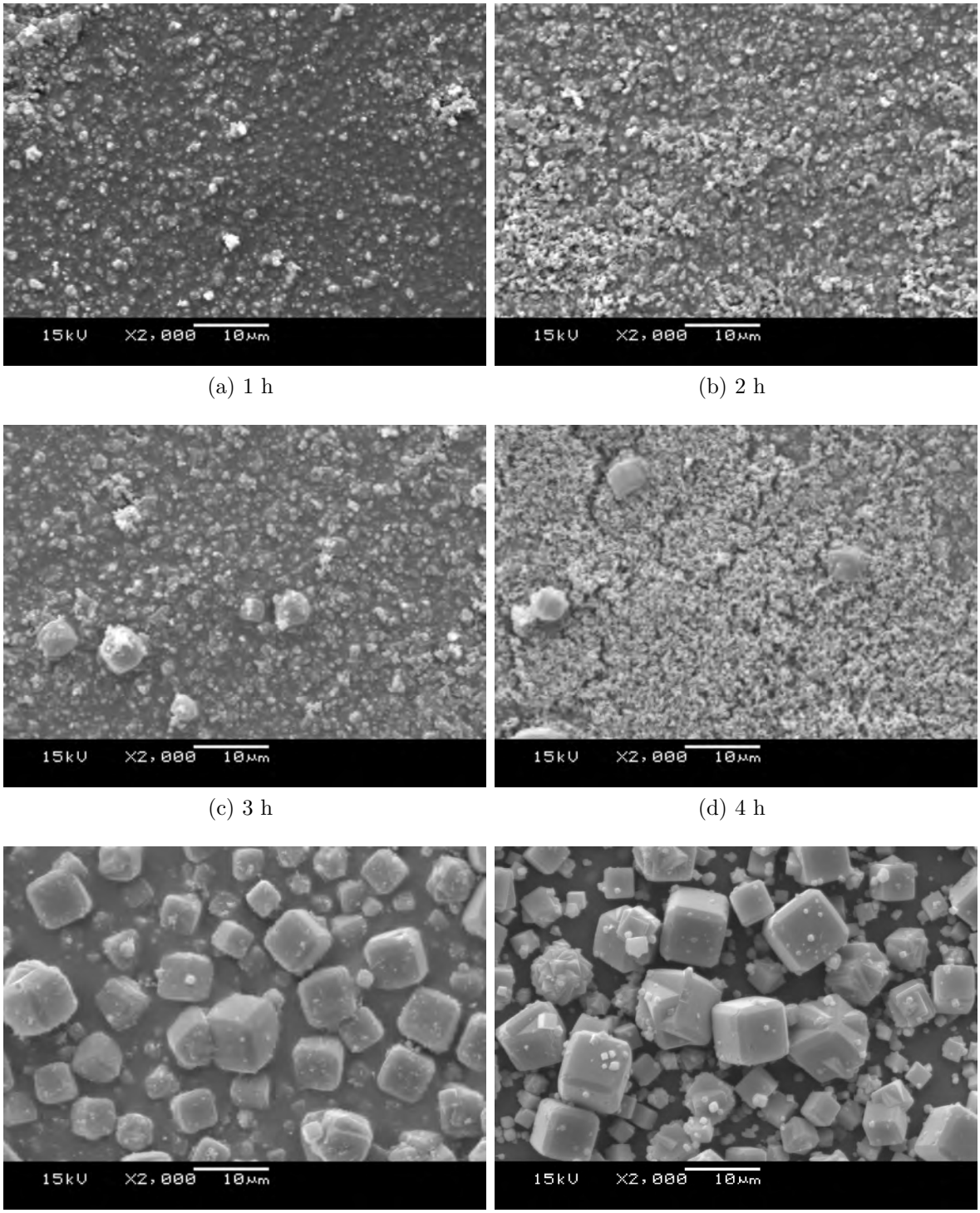

(a) 1 h (b) 2 h

(c) 3 h (d) 4 h

(e) 5 h (f) 6 h

Figure 5.45: SEM images of zeolites from ash leachate crystallised with 222 g of sodium aluminate/kg FA on a stirred hot plate at 90-95°C

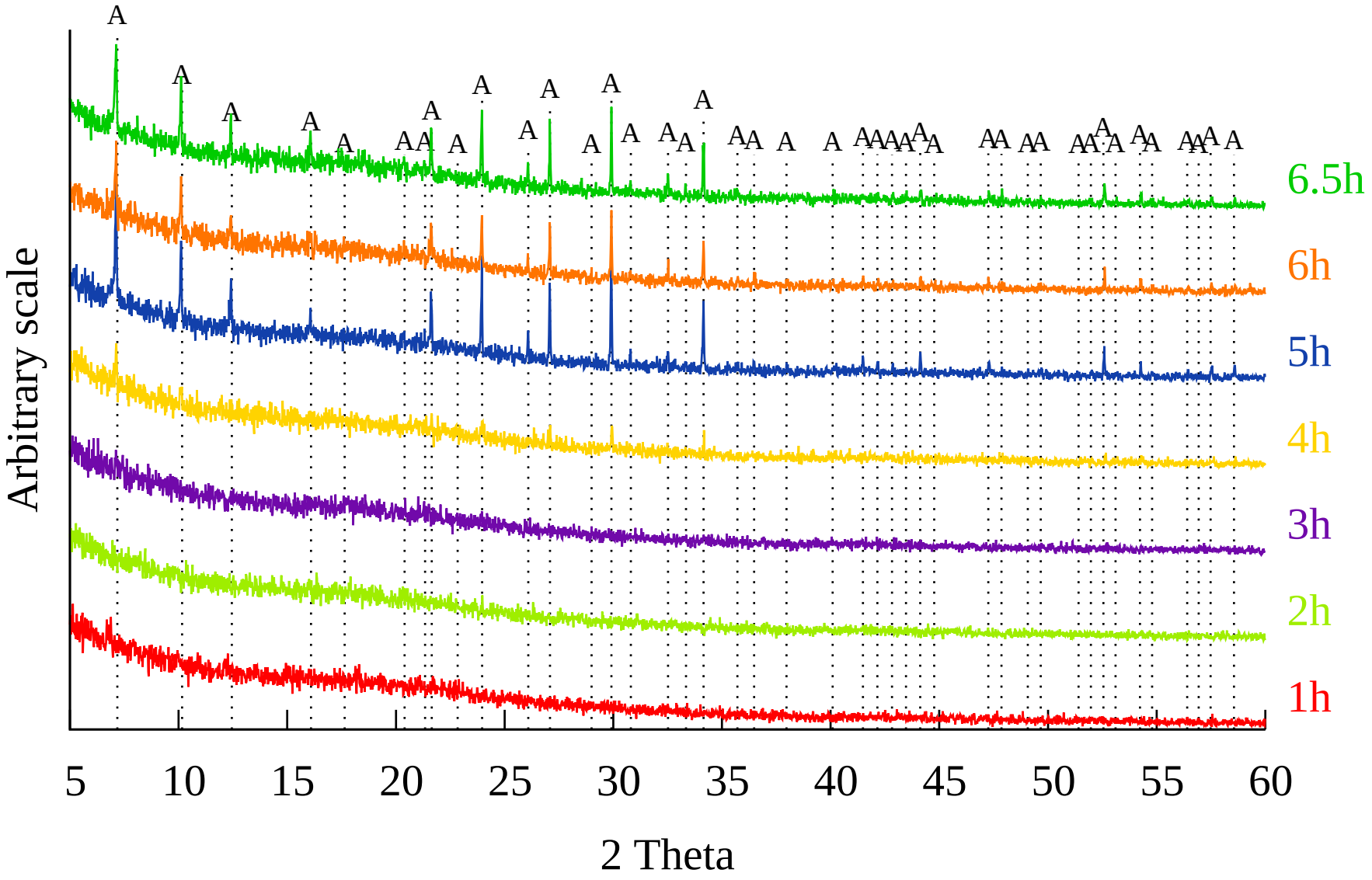

Figure 5.46: XRD patterns of 90-95°C crystallisation with 222 g sodium aluminate/kg FA. A: Zeolite Na-A. $\lambda = 1.5406$ Å

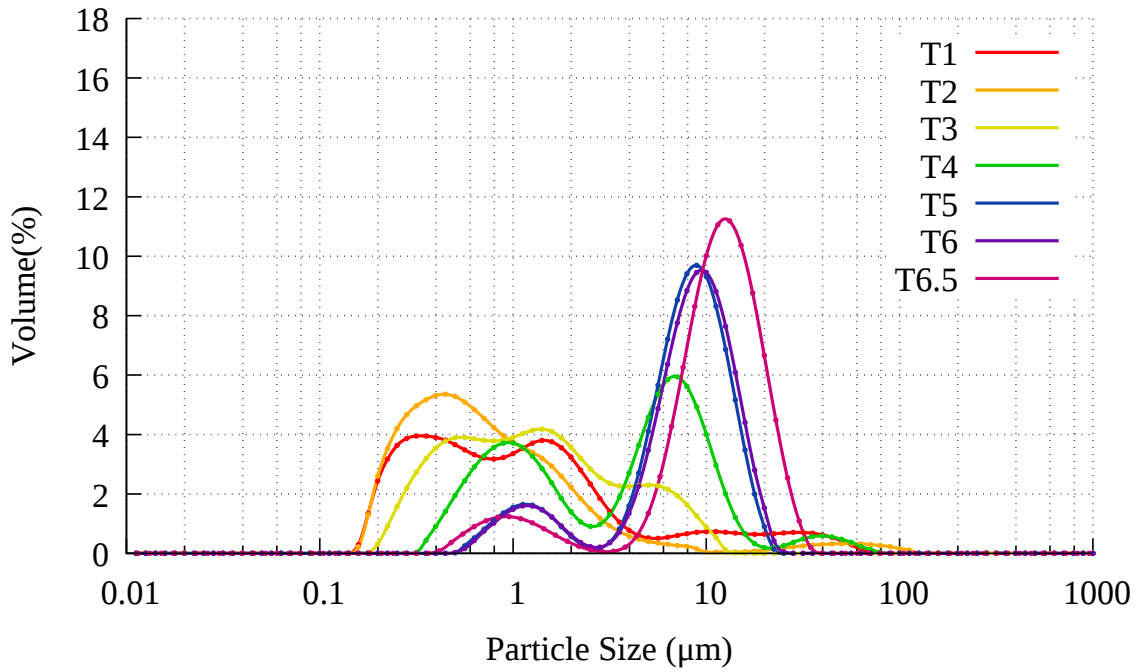

(a) PSD

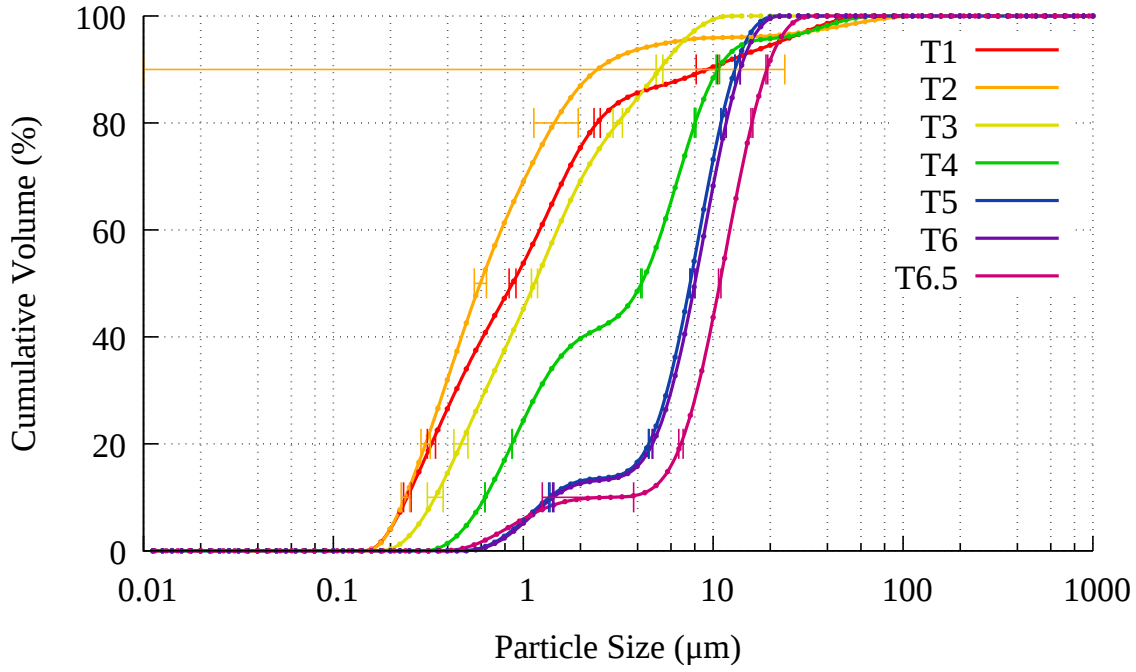

(b) Standard deviation in PSD

Figure 5.47: 90-95°C crystallisation process with 222 g SA/kg FA

5.4.2.6 Dosage of 266 g SA/kg FA

Chamfered cubes are shown in the 5 and 6 hour SEM images 5.48e and 5.48f. The smaller particulates that often appear alongside the larger ~10 μm cubes are also cube shaped. The XRD patterns shown in Figure 5.49 display zeolite A from 3 hours onward. The AAS results presented in Figure 5.32 show a similar consumption of Si in the first hour compared to the 222 g SA/kg FA dosage.

The yield shown in Figure 5.29 follows the trend of being slightly higher with the increase in sodium aluminate, whilst still being lower than the yield produced in section 5.3. The CEC appears to be very similar to the CEC for the constant temperature expermients. The CEC yield shown in Figure 5.31 is only slightly lower than the constant temperature experiments. The limited increase in yield, combined with the similar consumption of Si from 1-2 hours, and the low value of Si at 6 hours indicates that Si content of the leachate may be a more yield limiting factor than the Al content. The AAS shows a drop in Si and Al between 3 and 4 hours, which coincides with the disappearance of much of the material that is not cube shaped between Figures 5.48c and 5.48d.

The PSD shown in Figure 5.50a shows a bimodal distribution from 2 hours, and almost no change from 4 to 6 hours. The 4-6 hour peak is highest at around 6 μm, and a d_{50} of 5.4-5.6 μm. The peak representing the smaller particles peaks at a little over 1 μm, as shown by the d_{10} of 1.1 μm. During the cooling and filtration process the peak of the larger particle size group moves up to around 12 μm. The standard deviations of the d_{50}, d_{80} and d_{90} are all quite small, so this is accepted to be a reliable measurement. This doubling in the most common size could be attributed to agglomeration of particles, as SEM images do not show a drastic change in particle sizes between the two samples, as shown in Appendix Figures A.4 and A.5.

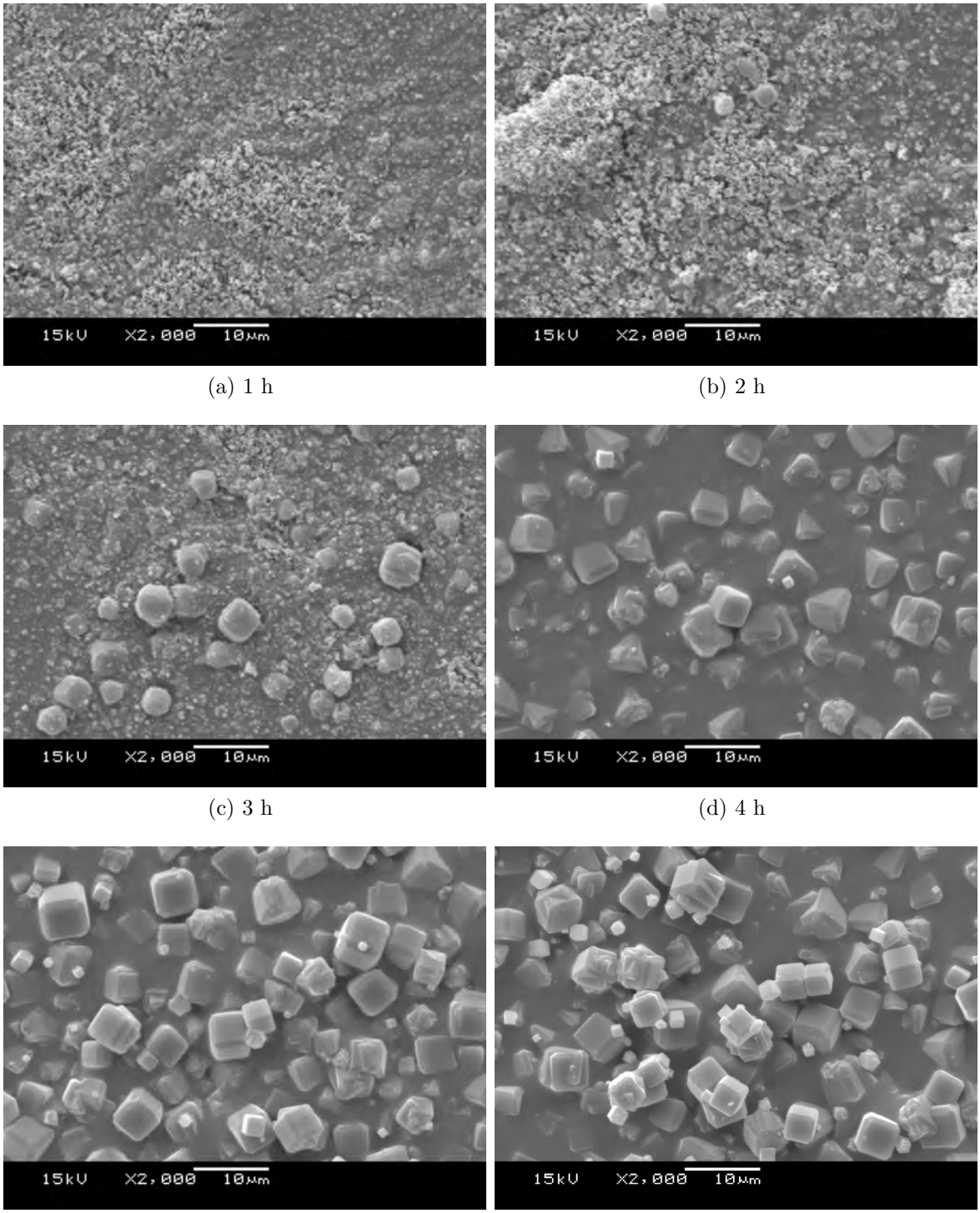

(a) 1 h (b) 2 h

(c) 3 h (d) 4 h

(e) 5 h (f) 6 h

Figure 5.48: SEM images of zeolites from ash leachate crystallised with 266 g of sodium aluminate/kg FA on a stirred hot plate at 90-95°C

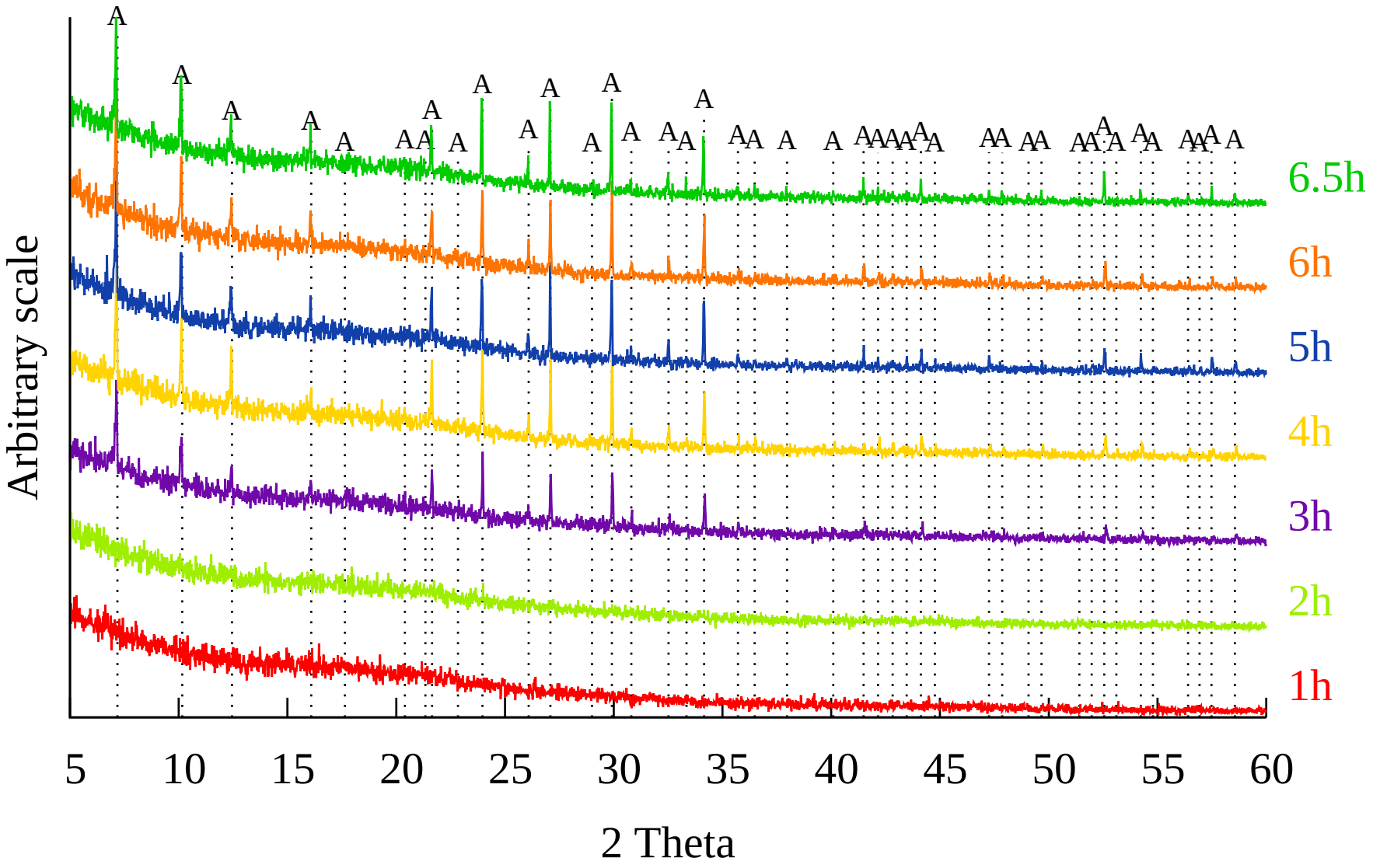

Figure 5.49: XRD patterns of 90-95°C crystallisation with 266 g sodium aluminate/kg FA. A: Zeolite Na-A. $\lambda = 1.5406$ Å

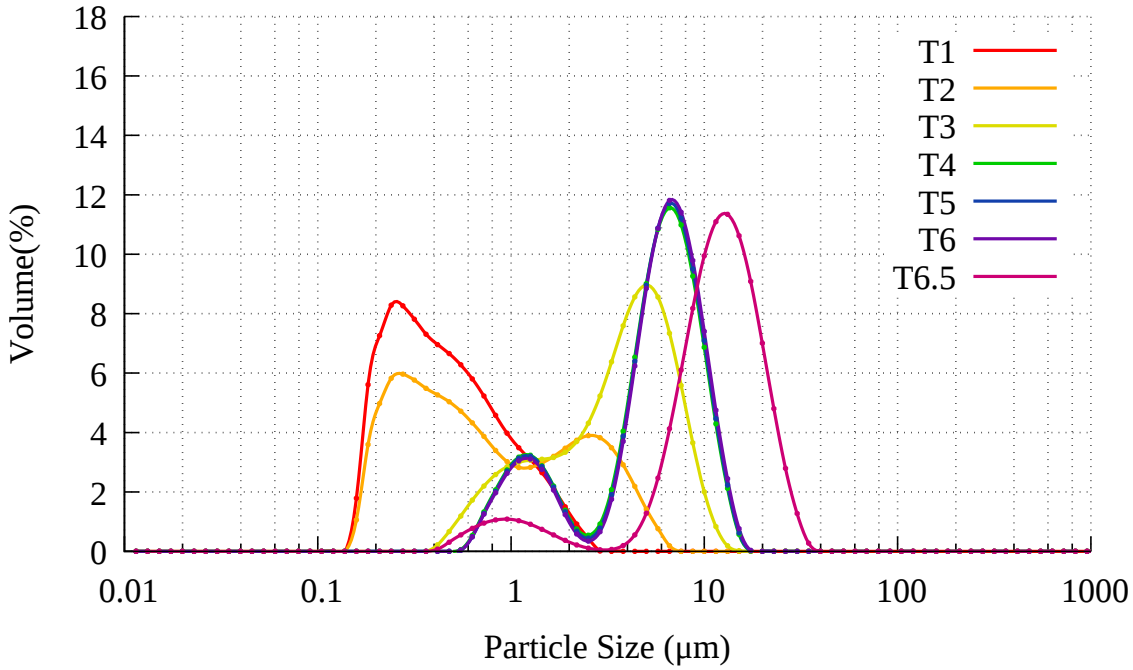

(a) PSD

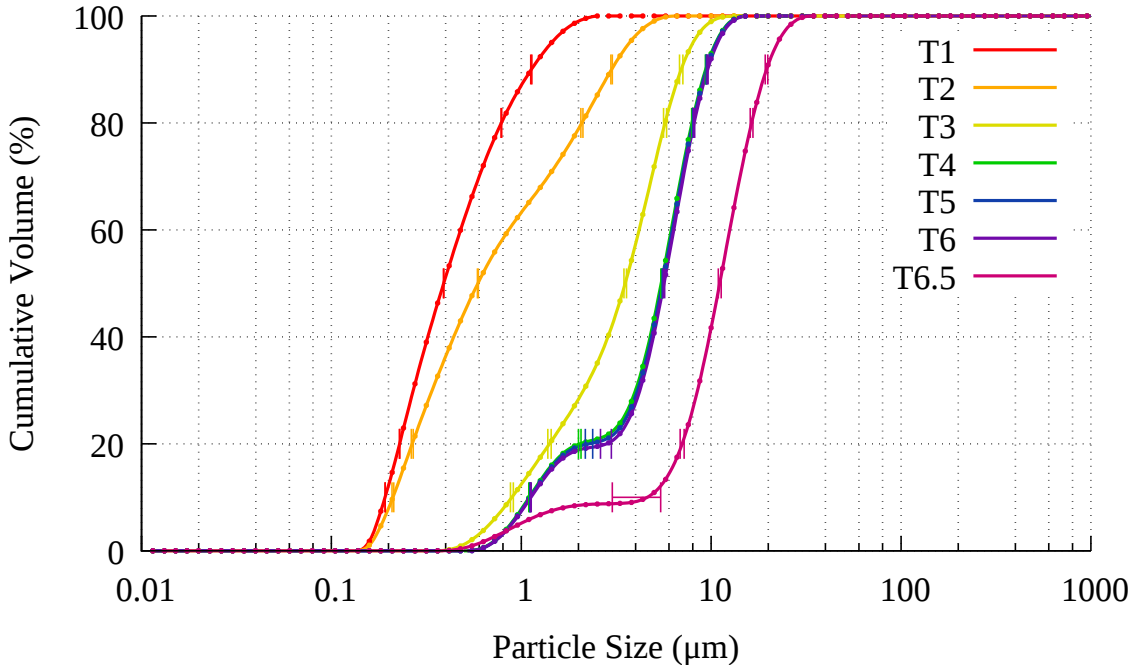

(b) Standard deviation in PSD

Figure 5.50: 90-95°C crystallisation process with 266 g SA/kg FA

5.4.2.7 Dosage of 310 g SA/g FA

For the highest dosage of sodium aluminate at 310 g/kg FA, XRD shows zeolite A detected at 4 hours, with some possible small peaks at 3 hours, however the signal to noise ratio is too high to be certain. The SEM images in Figure 5.51 corroborate the XRD patterns, showing sparse cubes at 3 hours in Figure 5.51c, and then a far greater abundance at 4 hours, with chamfered cubes shown at 4 hours and in subsequent samples. The amorphous material in Figure 5.51c is no longer visible in Figure 5.51d, which coincides with a drop in the Si and Al content from the AAS analysis shown in Figure 5.32. This decrease happens during the same time period as the previous sodium aluminate dosage of 266 g/kg FA. It is also noted that the quantity of Si consumed within the first hour is similar to the previous two experiments, and that the Si content at 6 hours is also similarly low. Figure 5.29 depicts no increase in yield from the 266 g SA/kg FA dosage. These conditions are closest to the conditions used by Hui and Chao [32], who synthesised zeolite A. SEM images appear quite similar, however the PSD measured by Hui and Chao [32] appears slightly finer. This can be attributed to the 30 minute 25°C ageing step that took place prior to heating to 90-95°C. During this ageing step, the amorphous aluminosilicate gel would have some time to equilibrate with the dissolved silica and alumina and allow for more rapid nucleation.

The CEC is similar to previous results, but slightly lower, thus the CEC yield of Figure 5.31 is also lower than the 266 g SA/kg FA value. The Si AAS results, combined with the yield data again indicates that Si is the yield limiting factor in this experiment. The AAS results show an incongruous drop in Al between 1-2 hours. This decrease is not reflected in the Si results. This decrease is also inconsistent with the pattern of stable Al and Si values between 1 hour and the formation of cubes. As this result conflicts with the Si, SEM and pattern of other results, it is attributed to experimental error, but lacking repetition cannot be completely ruled out. The PSD in Figure 5.53a shows results of very high similarity. The 4 hour results are a close approximation, but slightly to the left, indicating finer particles. The standard deviation of the d_{90} for the 1 hour measurement

in Figure 5.53b is slightly higher than other results, indicating that the right hand hump in Figure 5.53a may be slightly inaccurate, however the standard deviations for the 4, 5 and 6 hour results all appear to be minimal.

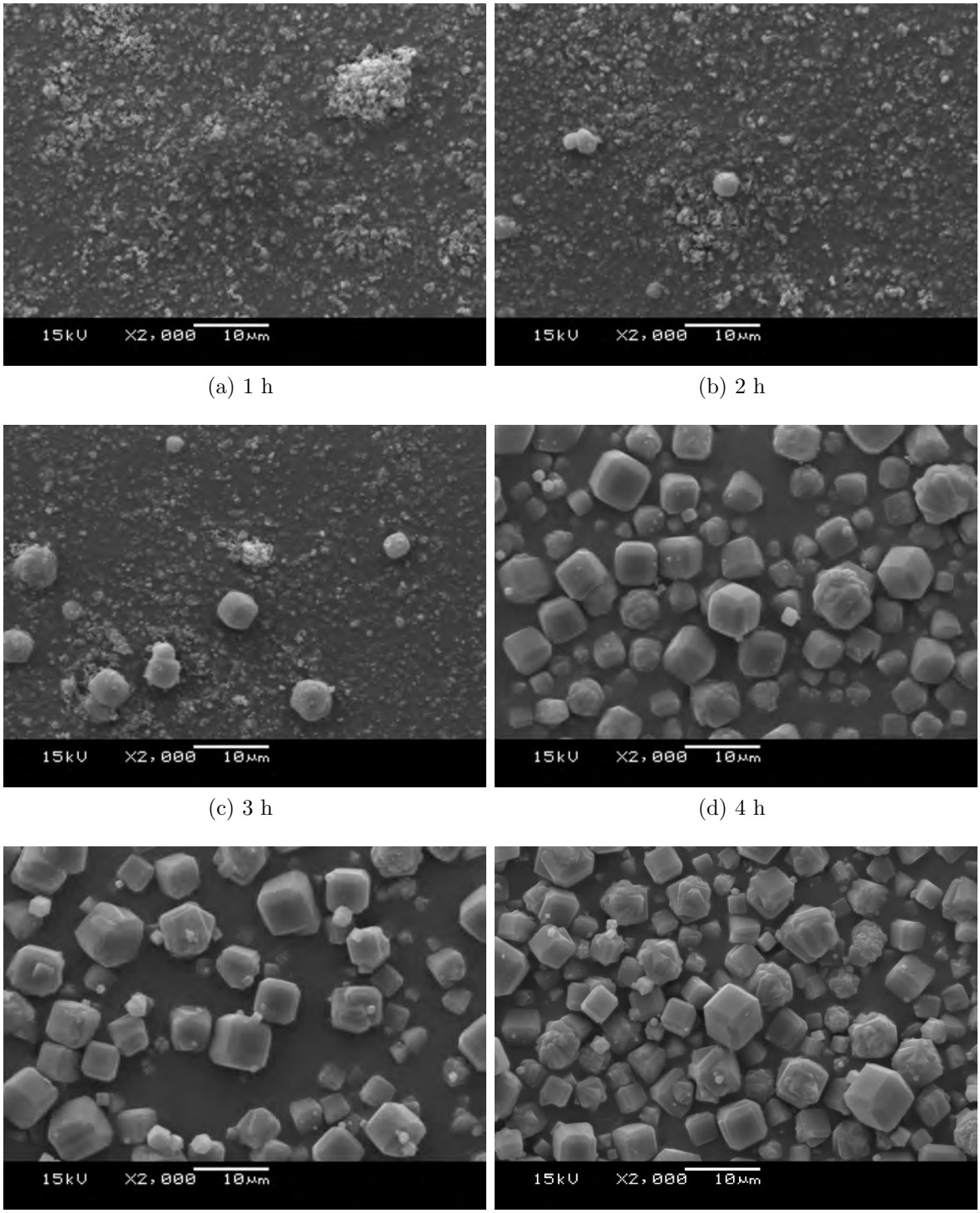

(a) 1 h (b) 2 h

(c) 3 h (d) 4 h

(e) 5 h (f) 6 h

Figure 5.51: SEM images of zeolites from ash leachate crystallised with 310 g of sodium aluminate/kg FA on a stirred hot plate at 90-95°C

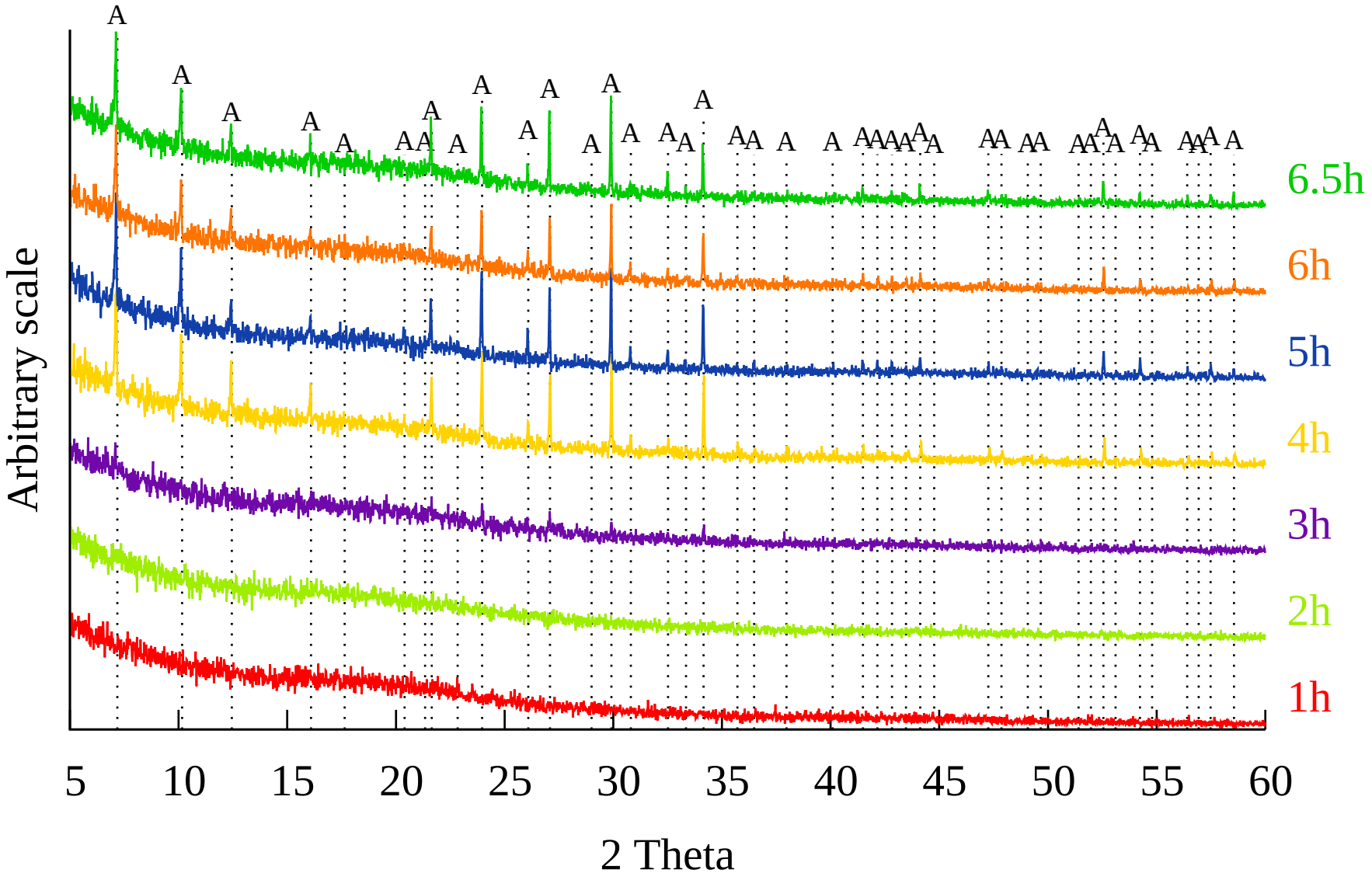

Figure 5.52: XRD patterns of 90-95°C crystallisation with 310 g sodium aluminate/kg FA. A: Zeolite Na-A. $\lambda = 1.5406$ Å

5.4.2.8 Effect of Sodium Aluminate on Crystallisation

All yield values for the temperature step change experiment are lower than their counterpart values in the constant temperature experiment, however the constant temperature experiment yield results were taken at 6 hours, whilst the yield results for the step change experiment were taken on the sample after the 6 hour measurement, thus this small decrease in yield may be attributed to the additional measurement. Despite the step change results being slightly lower, they are quite similar for the lowest three SA dosages. These lower dosages also follow the constant temperature pattern of increasing linearly with sodium aluminate addition, before starting to plateau between 177 and 266 g SA/kg FA. The CEC of all SA dosages are similar, being slightly above 4 meq/g, except the lowest dosage of sodium aluminate. The plateauing of the yield in combination with the AAS data indicates that, despite increasing the Al content, yield is unable to increase as there is insufficient Si in solution for the Al to react with to form zeolite.

PSD graphs are presented for the final products at 6.5 hours in Figure 5.55. The larger standard deviations for the lower two dosages of sodium aluminate in Figure 5.55b are indicative of inconsistent measurements, therefore the PSD for the 6 hour measurements are provided in Figure 5.54. In both Figures, as sodium aluminate content increases, the general trend is for the particle size to become larger, and the particle size distribution to become narrower. In both the 6 and 6.5 hour measurements, the left hand peak denoting the smaller particle size group is delineated from the taller right hand peak denoting the bulk of the product by a trough at or near the 2.5 μm particle size. At 6 hours, the finer material comprises <13-22 % of the product, and at 6.5 hours the finer material comprises <9-15 %. The 89 g SA/kg FA dosage at 6 hours has 46 % of the material <2.5 μm, whilst the 44 g dosages lacks a trough, with the exception of the 44 and 89 g dosages of sodium aluminate. For the 6.5 hour measurements the data is considered unreliable.

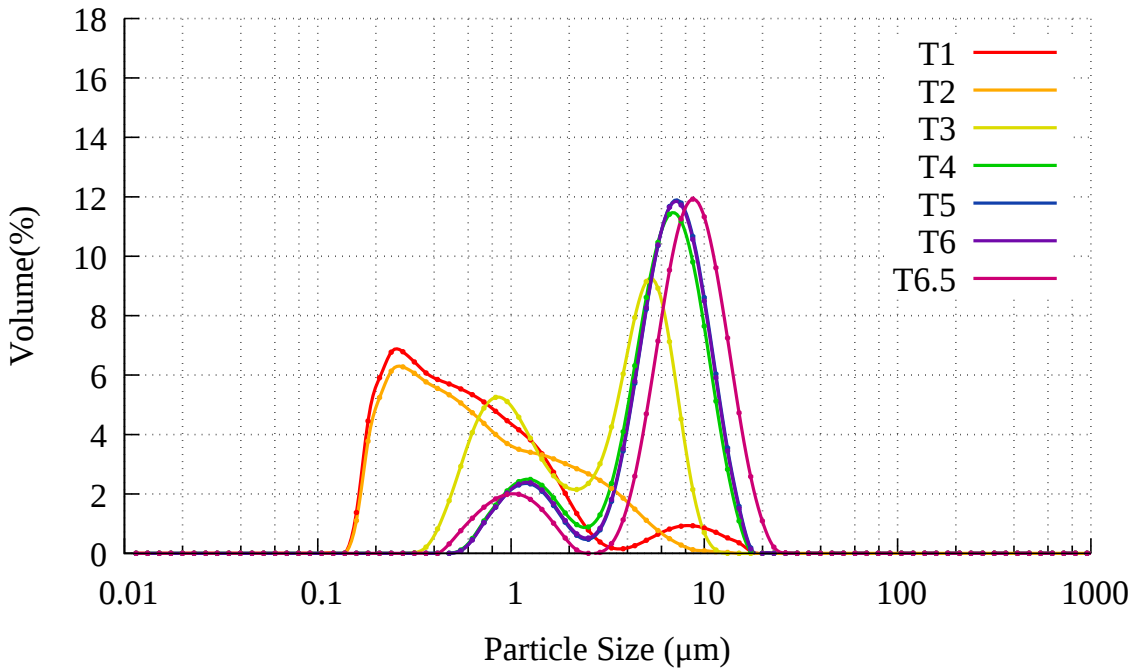

(a) PSD

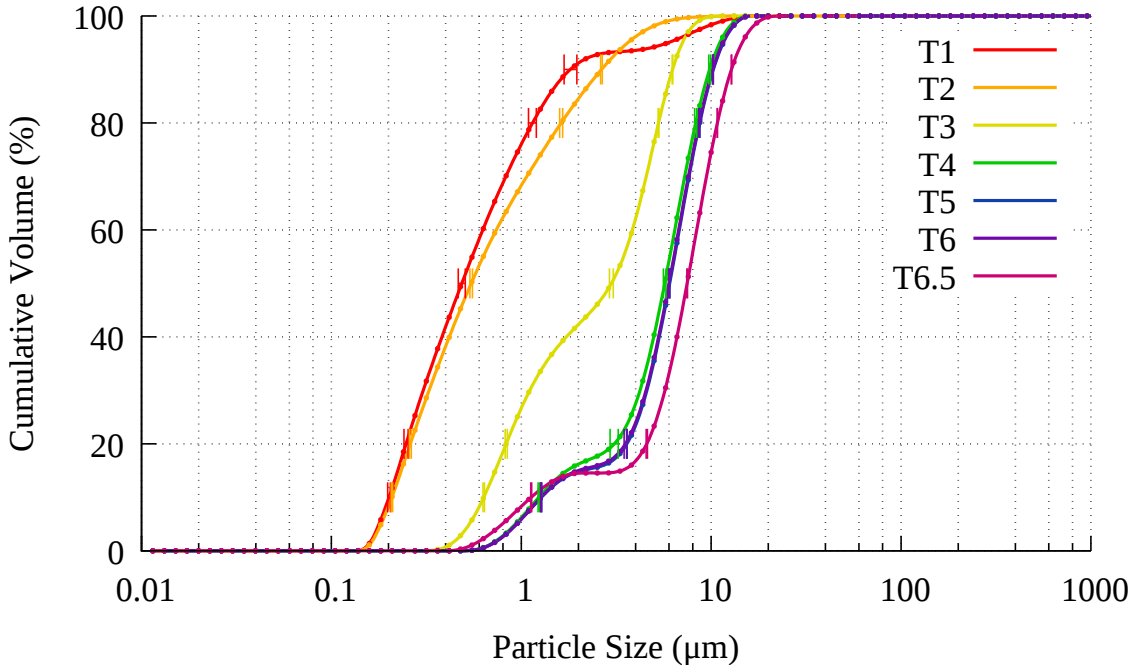

(b) Standard deviation in PSD

Figure 5.53: 90-95°C crystallisation process with 310 g SA/kg FA

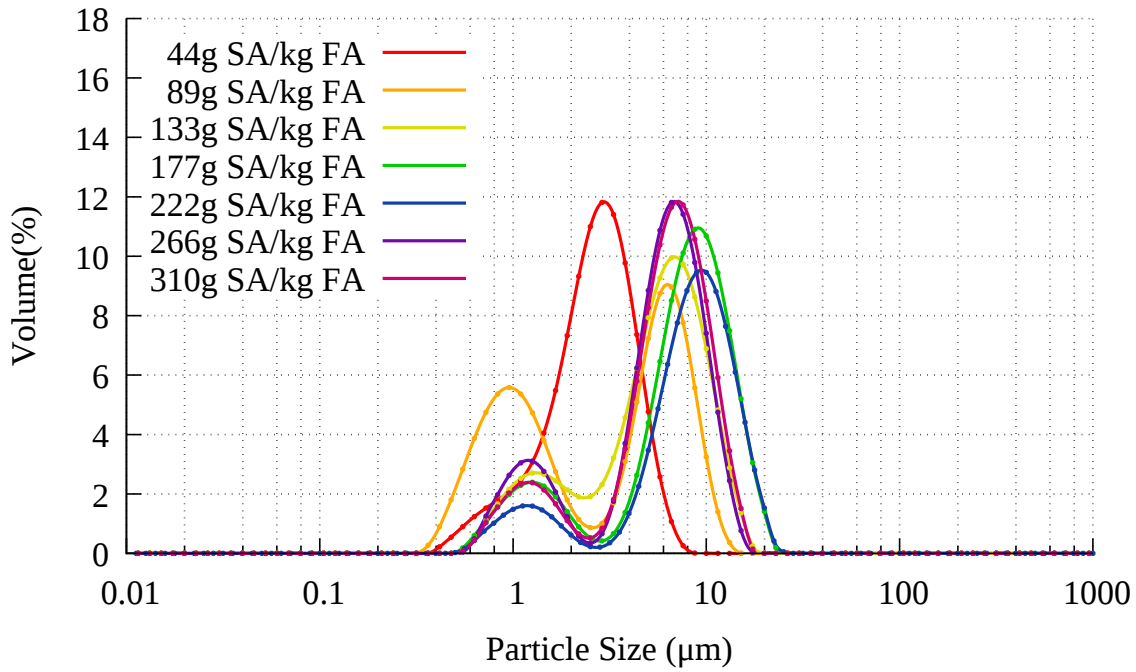

(a) PSD

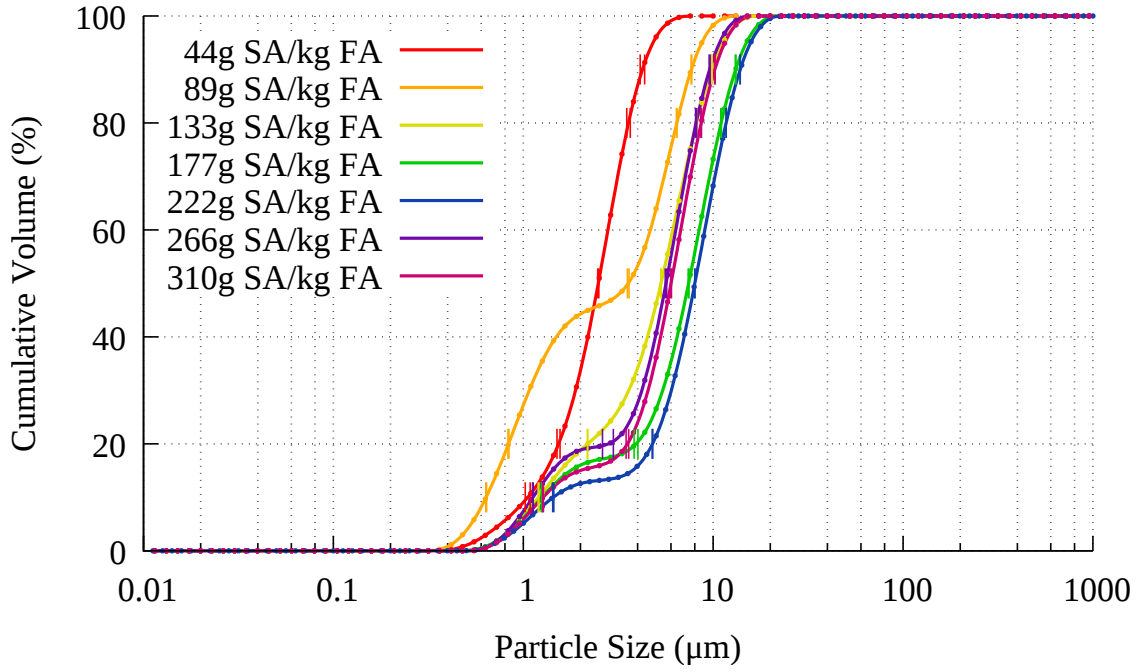

(b) Standard deviation in PSD

Figure 5.54: 90-95°C crystallisation process with varied sodium aluminate after 6 hours

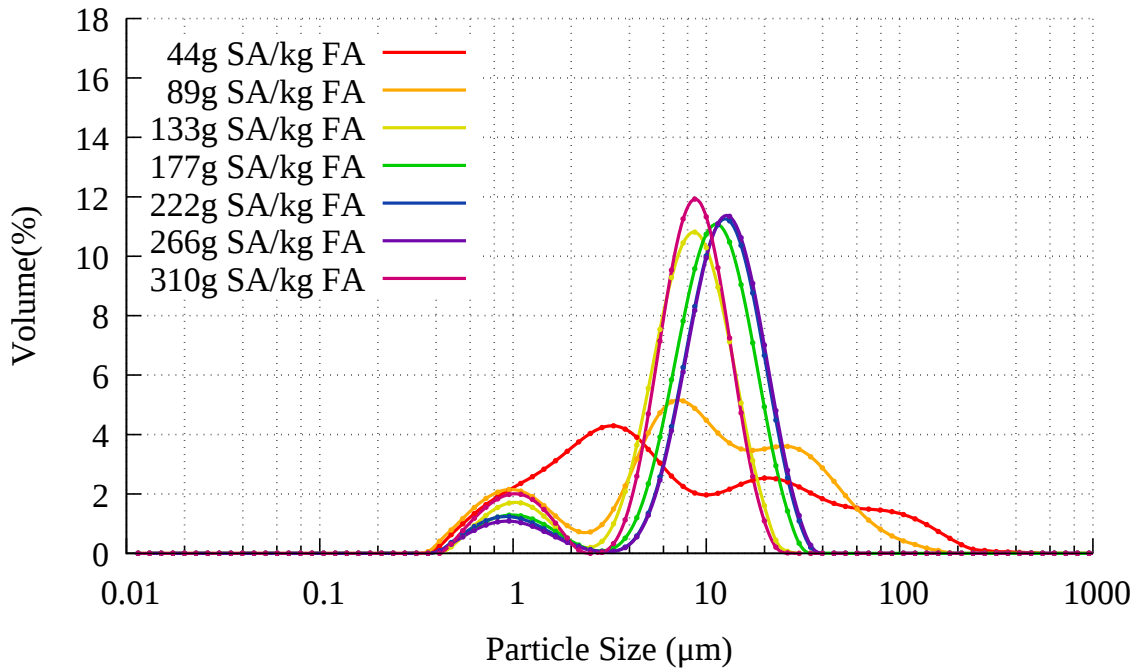

(a) PSD

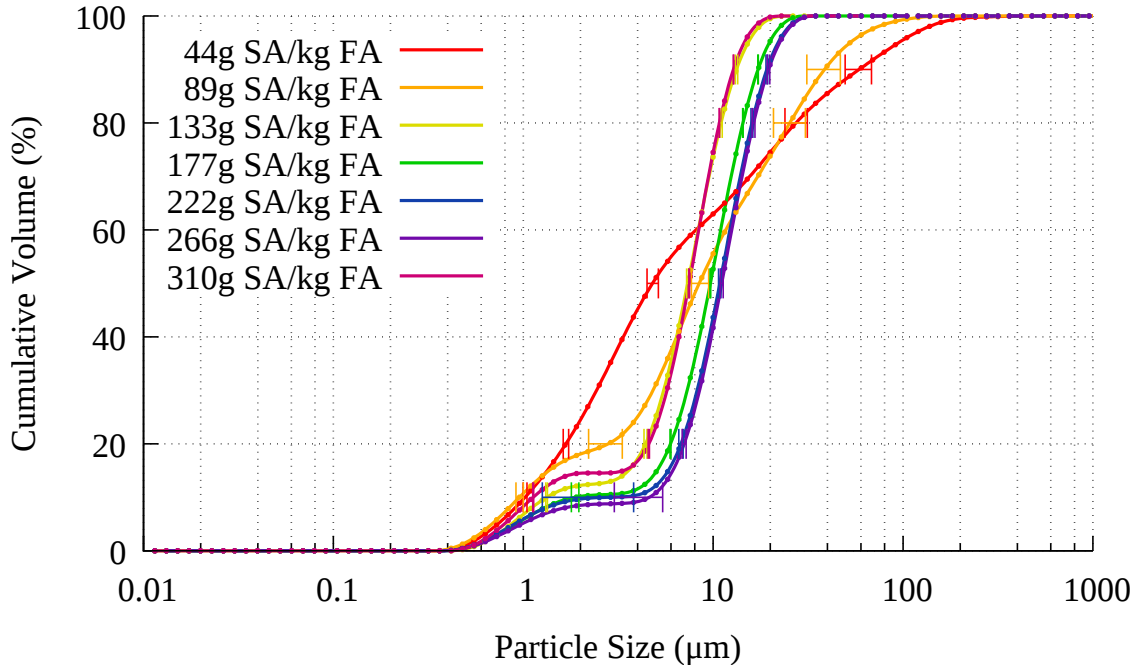

(b) Standard deviation in PSD

Figure 5.55: 90-95°C crystallisation process with varied sodium aluminate after 6.5 hours

Chapter 6

Crystallisation of Zeolties: Effect of Additional Reagents

6.1 The Effect of Adding NaOH to the Crystallisation Step

The sodium aluminate used consisted of Al (as Al_2O_3) 50-56 %, Na (as Na_2O) 40-45 %, with $\leq$ 0.05 % Fe (as Fe_2O_3). As sodium aluminate contains a significant quantity of Na_2O, which reacts with water as shown in equation 6.1, the NaOH content of a 1 L 2 M solution of NaOH increases by 2-17 % through the addition of sodium aluminate dosages described in section 5.4.

$$Na_2O + H_2O \rightarrow 2NaOH \tag{6.1}$$

It was deemed necessary to investigate the influence of additional NaOH on the crystallisation process.

6.1.1 Experimental Method

The experimental method was similar to the method described in section 5.4. The control experiment with no additional NaOH is the 222 g SA/kg FA experiment from section

5.4.2.5. The extraction process is described in section 4.7. 900 ml of leachate (N) was used in the crystallisation process. 0.5 moles or 1 mole of additional NaOH (S) were added to the 900 ml prior to heating. The rest of the experimental process was the same as that described in section 5.4, conducted at 90°C for 2 hours, then the temperature was raised to 95°C for the remainder of the experiment.

6.1.2 Results

6.1.2.1 Control experiment

See section 5.4.2.5.

6.1.2.2 Dosage of 296 g NaOH/kg FA

Yield results shown in Figure 6.2 show a slight decrease with yield as NaOH content increases, whilst the CEC results of Figure 6.3 show a slight improvement in CEC before decreasing. This is better communicated in Figure 6.4 where the changes in yield and CEC are more pronounced.

The decrease in yield comes despite AAS results in Figure 6.1 showing similar Si consumption by 6.5 hours. The decrease in Si and Al content that coincides with the disappearance of amorphous material in SEM images takes place from 4-6 hours in the control experiment. For the 296 g NaOH/kg FA experiment, the decrease in Si and Al in the AAS results takes place from 3-5 hours. The SEM image Figure 6.5b taken at 2 hours shows an abundance of amorphous material. Amorphous material is still visible at 3 hours in Figure 6.5c, and decreases further by Figure 6.5d. The reduction in amorphous material apparent when comparing the 2, 3 and 4 hour images in the SEM were expected to take place between 3, 4 and 5 hours, based on the AAS data.

The XRD data in Figure 6.6 shows zeolite A from 3 hours onward, with no obvious signs of another phase. The PSD data in Figure 6.7a shows a similar trend to experiments in section 5.4 with a broad PSD for early measurements, followed by a bimodal distribution, and heightening of the right hand peak as time progresses. With the added

296 g NaOH/kg FA, the right hand peaks in Figure 6.7a are narrower and taller than their counterparts in Figure 5.47a, except for the 6.5 hour measurement, which is slightly taller in the control experiment.

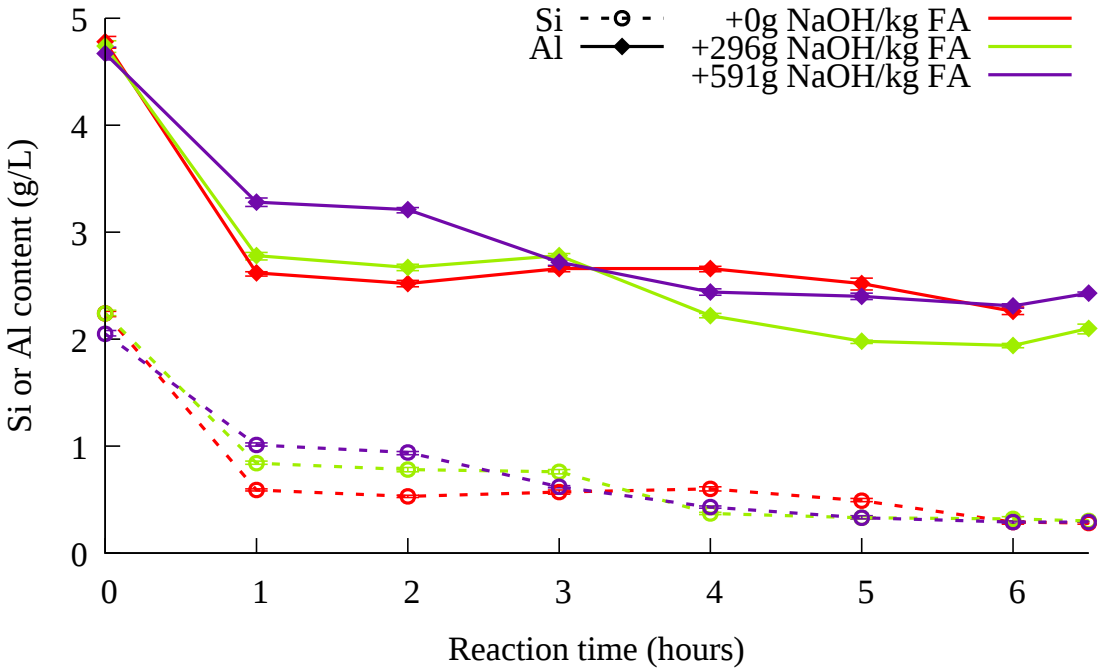

Figure 6.1: AAS results for 90-95°C crystallisation process with increasing NaOH dosage

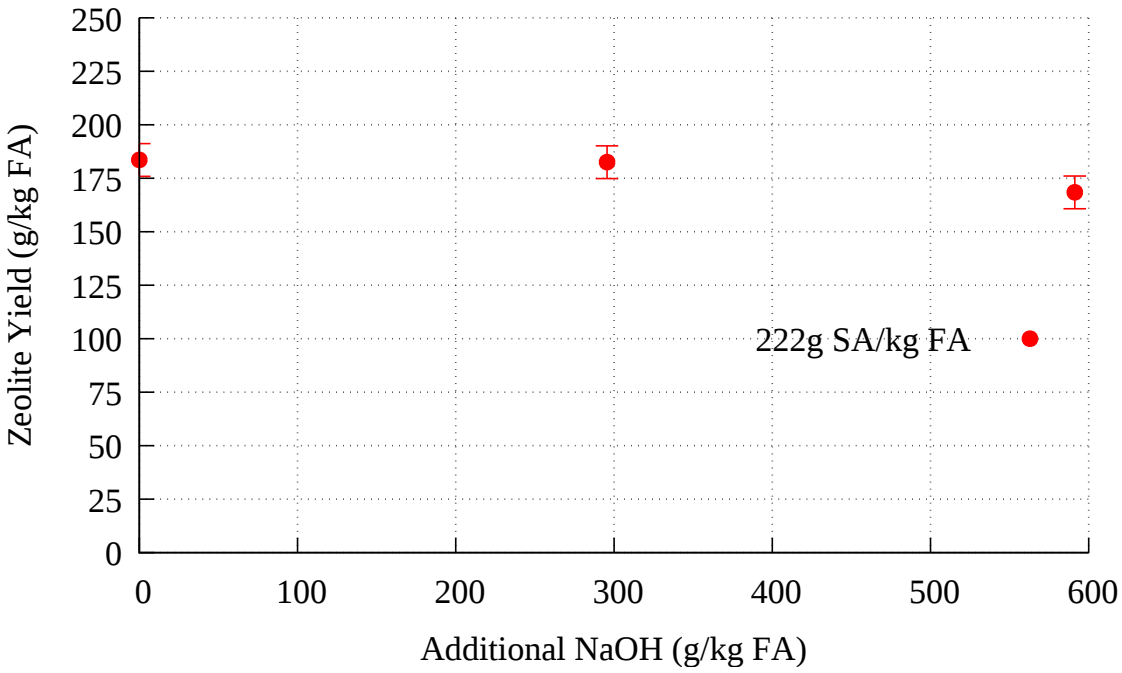

Figure 6.2: Yield of zeolite compared to NaOH addition

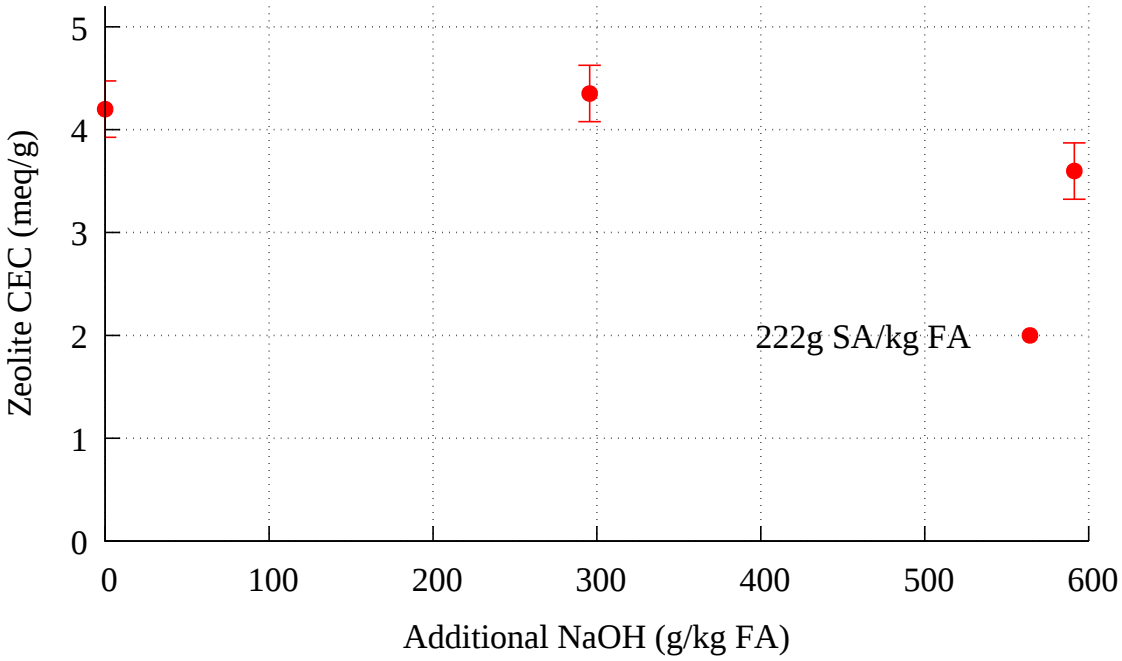

Figure 6.3: CEC of zeolite compared to NaOH addition

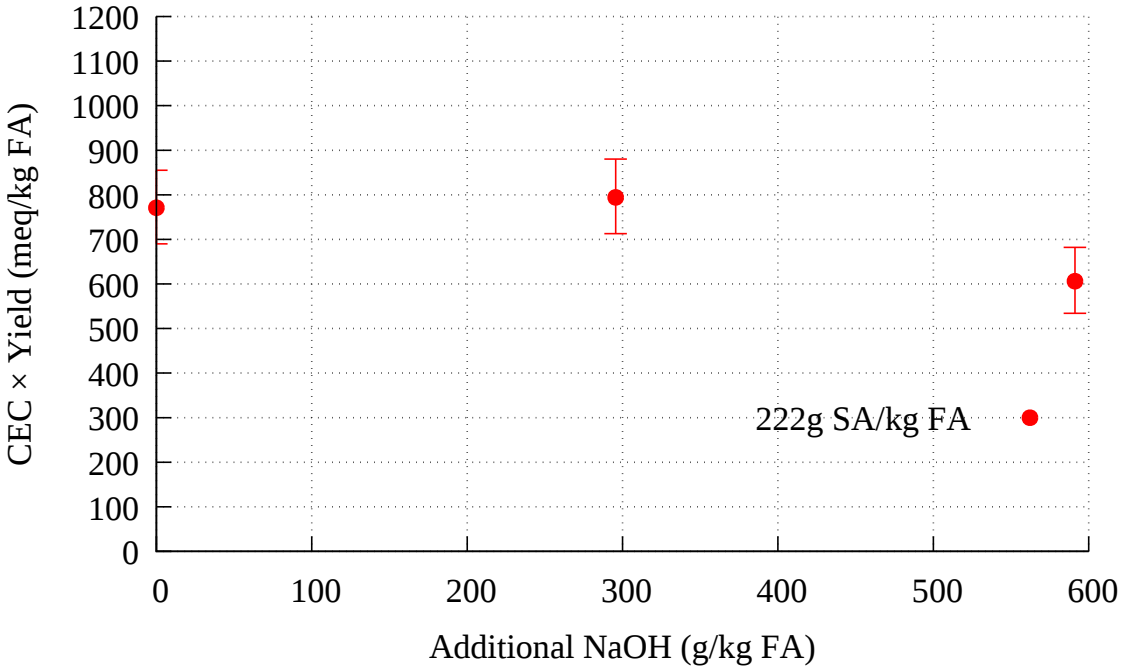

Figure 6.4: CEC × yield of zeolite compared to NaOH addition

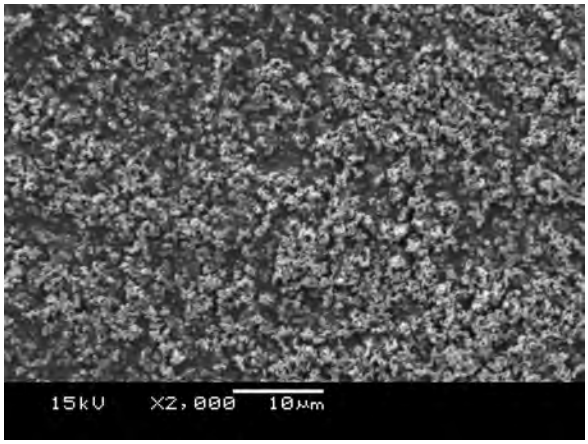

(a) 1 h

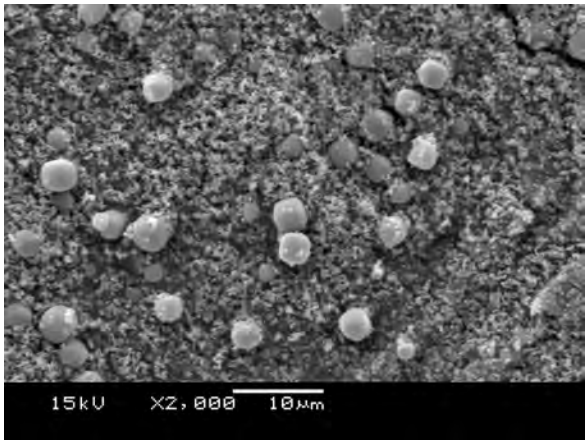

(b) 2 h

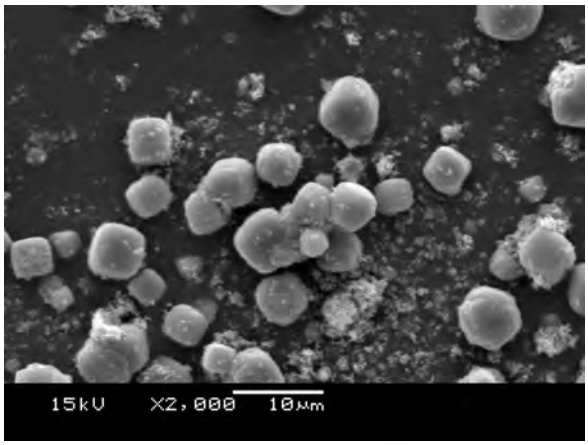

(c) 3 h

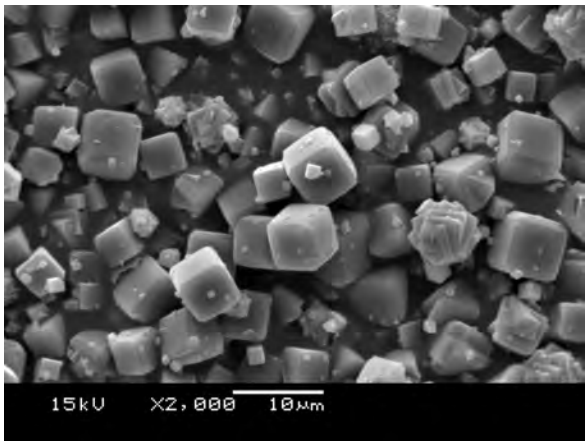

(d) 4 h

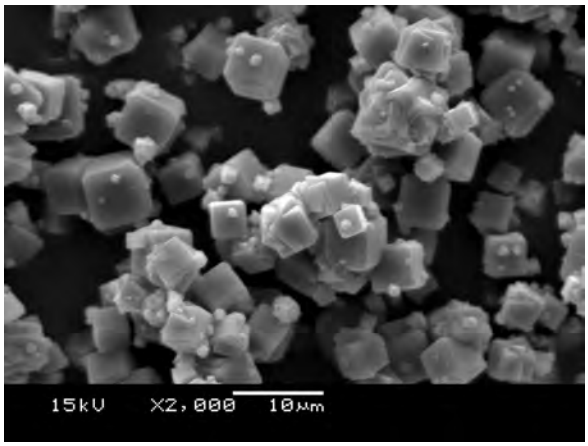

(e) 5 h

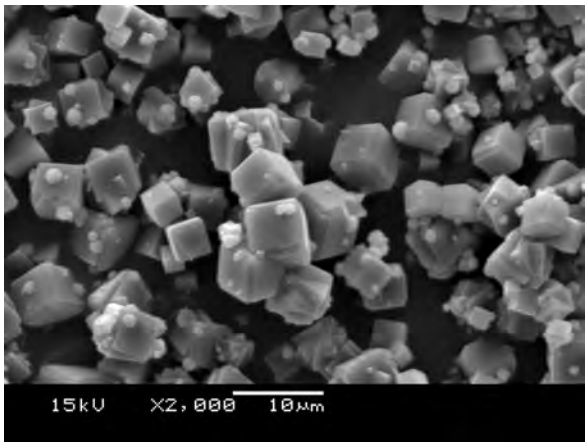

(f) 6 h

Figure 6.5: SEM images of zeolites from ash leachate crystallised with an additional 296 g of NaOH/kg FA on a stirred hot plate at 90-95°C

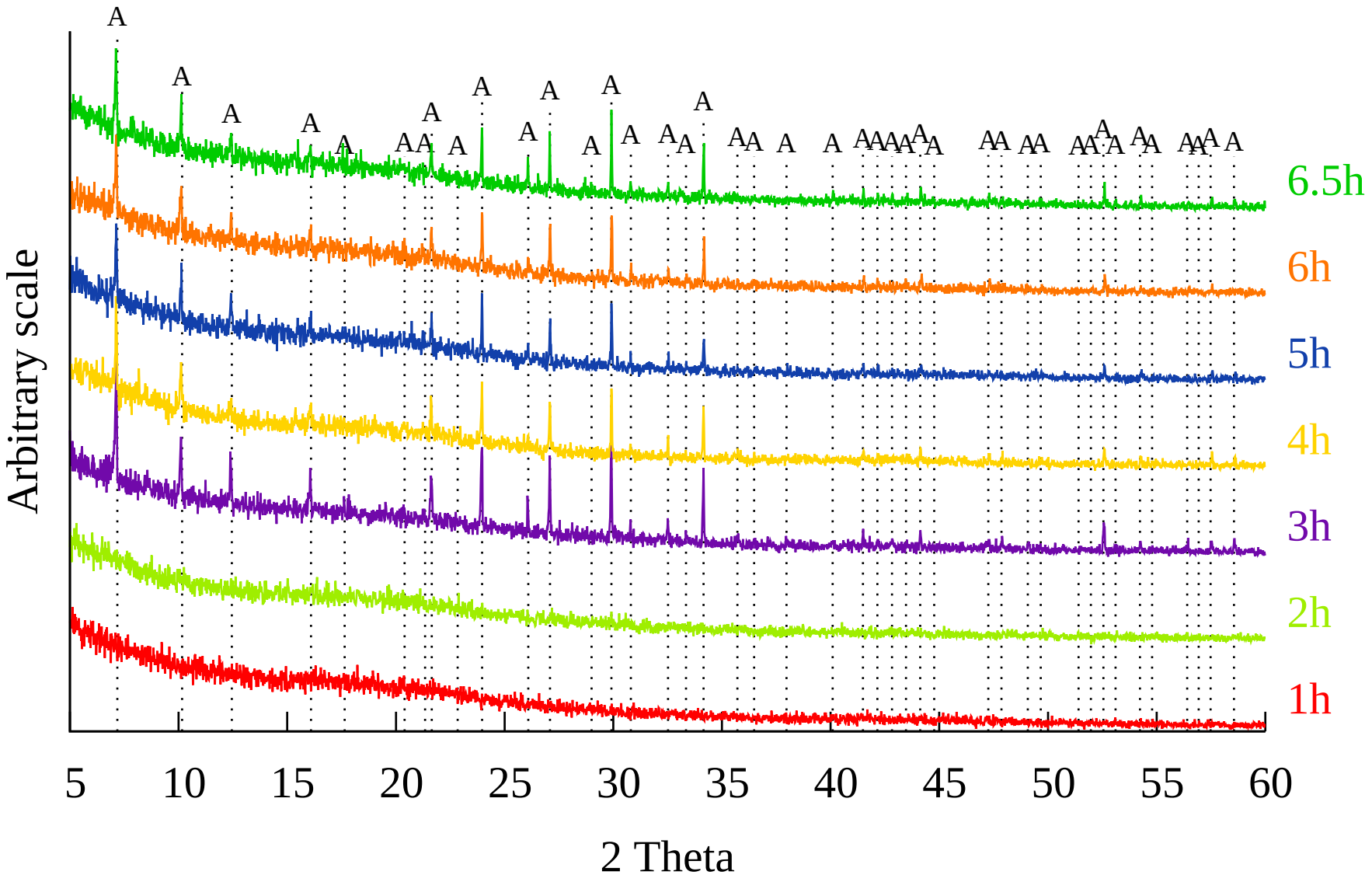

Figure 6.6: XRD patterns of 90-95°C crystallisation with an additional 296 g NaOH/kg FA. A: Zeolite Na-A. $\lambda = 1.5406$ Å

6.1.2.3 Dosage of 591 g NaOH/kg FA

With a further increase in NaOH dosage to 591 g NaOH/kg FA, the decrease in Si and Al content in Figure 6.1 runs from 2 to 4 hours. This result is reflected in SEM images of Figure 6.8, showing the appearance of cubes, and a disappearance of the presumably amorphous material around the cubes, followed by smoothing of cube surfaces and sharpening of edges. The AAS results in Figure 6.1 also show a change in the initial decrease in concentration of Si and Al from the theoretical 0 hour value to the first measurement at 1 hour. The experiment with no added NaOH has the largest change in Si and Al between 0 and 1 hours. This change is slightly lower for both Si and Al with the introduction of 296 g NaOH/kg FA, and is further decreased with the introduction of 591 g NaOH/kg FA. This change in the initial drop could be attributed to better stability of Al and Si ions in the more alkaline environments. The 5-6.5 hour values for Si are quite similar, however the Al content at 5-6.5 hours for 296 g NaOH/kg FA is noticeably lower than the other NaOH value. This slightly higher consumption of Al corroborates the higher CEC of the 296 g NaOH/kg FA dosage shown in Figure 6.3, and the higher yield shown in Figure 6.2.

The PSD in Figure 6.10a does not show the broad peak for the first few results noted in the lower dosage of NaOH or the control experiment, instead forming a tall peak. The following results then demonstrate the bimodal distribution and narrowing of the peak demonstrated in the 296 g dosage, but to a lesser extent. The 6.5 hour measurement is again taller in the control experiment. The change in particle size during the filtration process could be attributed to rapid crystallisation during the cooling process joining cubes together. It is noted that separate cubes are more common in the control experiment, whilst the experiments with added NaOH appear to consist mostly of clumps of cubes. The XRD results in Figure 6.9 show zeolite A detected from 3 hours onward again, with no obvious signs of other crystalline phases. In the control experiment with no additional NaOH, the first traces of zeolite A are noticeable at 4 hours, and strong measurements can be found only from 5 hours onward, as shown in Figure 5.46.

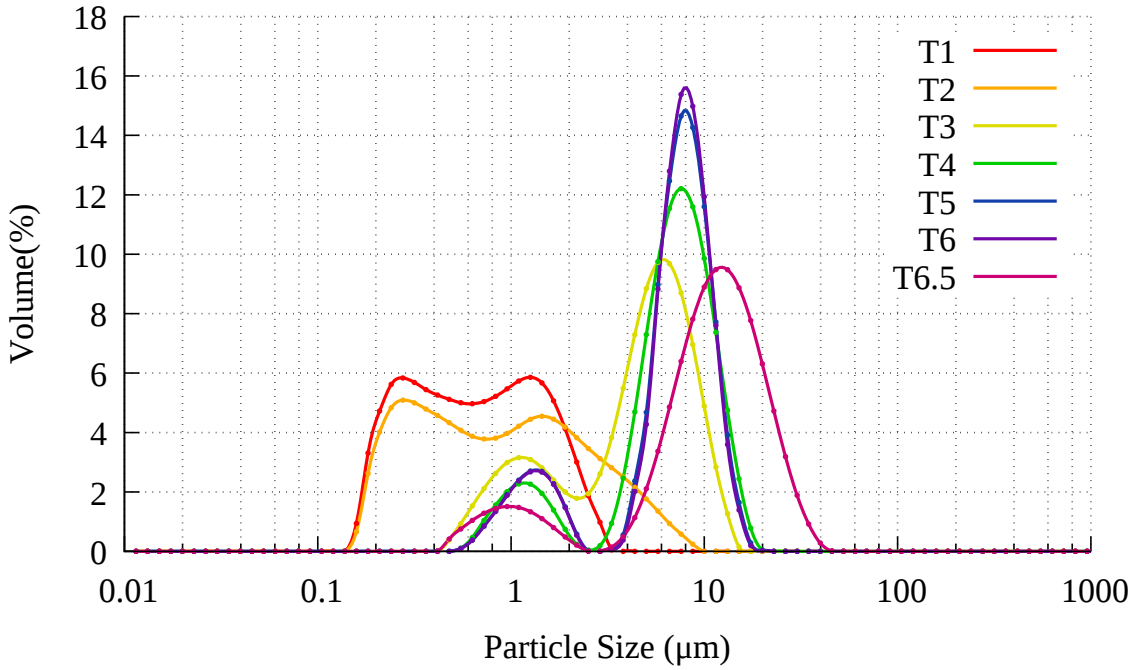

(a) PSD

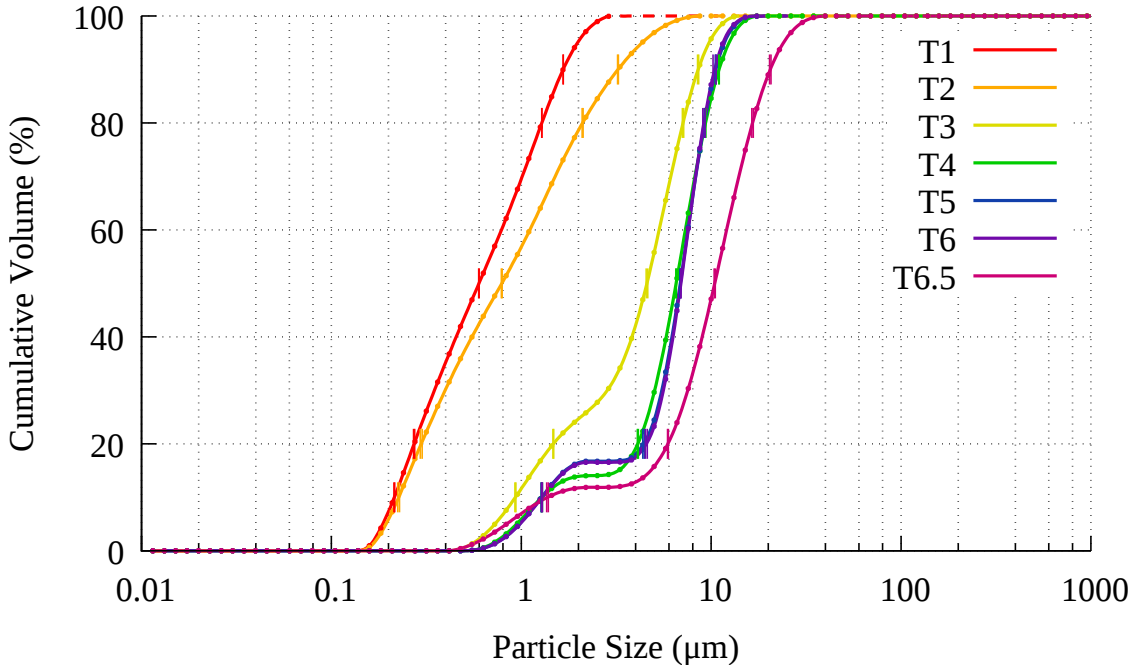

(b) Standard deviation in PSD

Figure 6.7: 90-95°C crystallisation process with 296 g NaOH/kg FA added

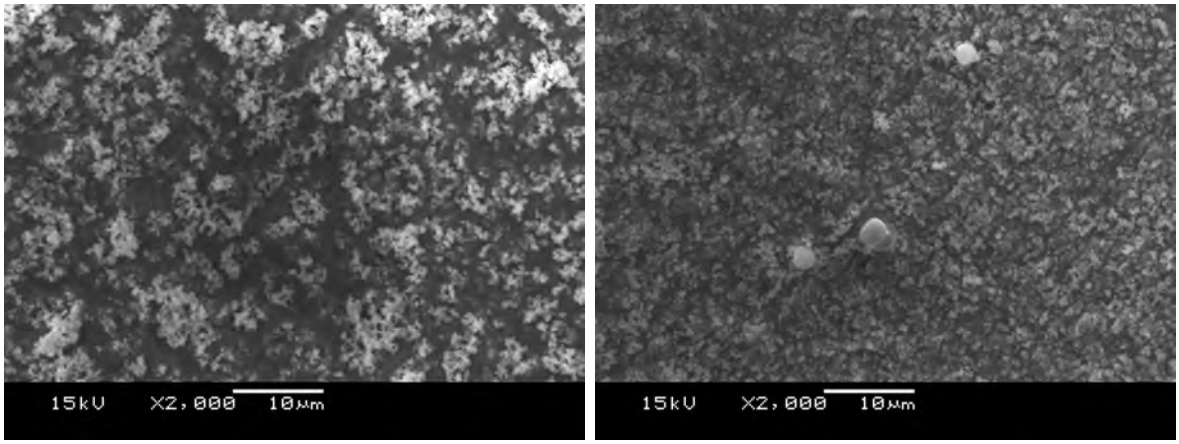

(a) 1 h (b) 2 h

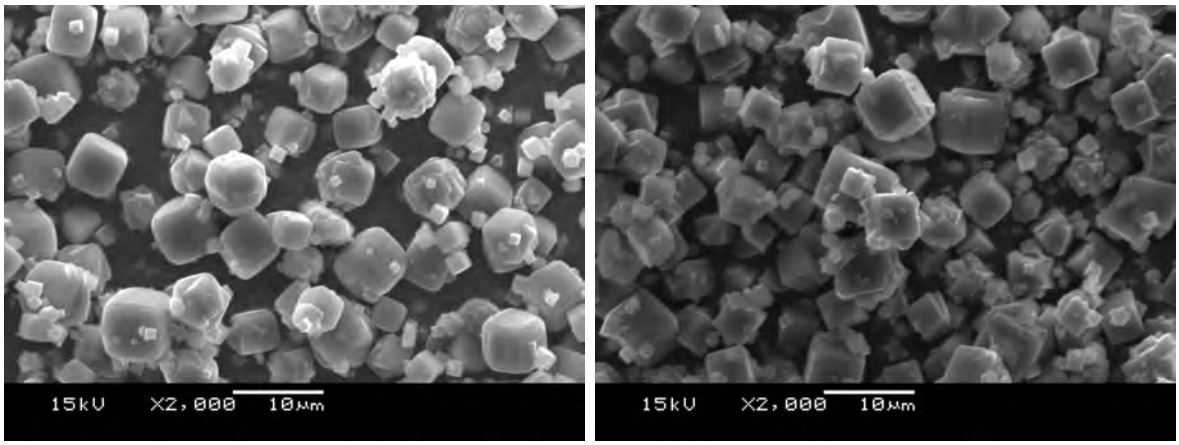

(c) 3 h (d) 4 h

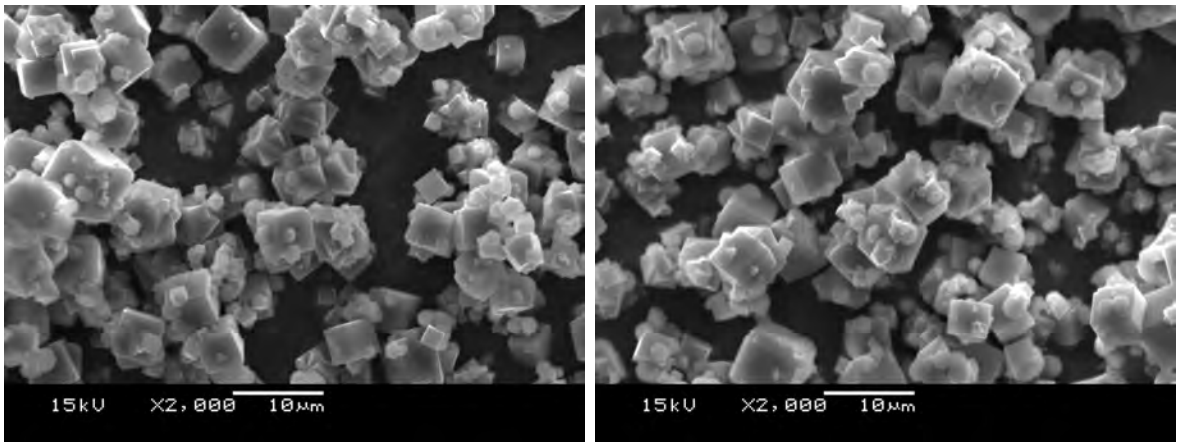

(e) 5 h (f) 6 h

Figure 6.8: SEM images of zeolites from ash leachate crystallised with an addition of 591 g of NaOH/kg FA on a stirred hot plate at 90-95°C

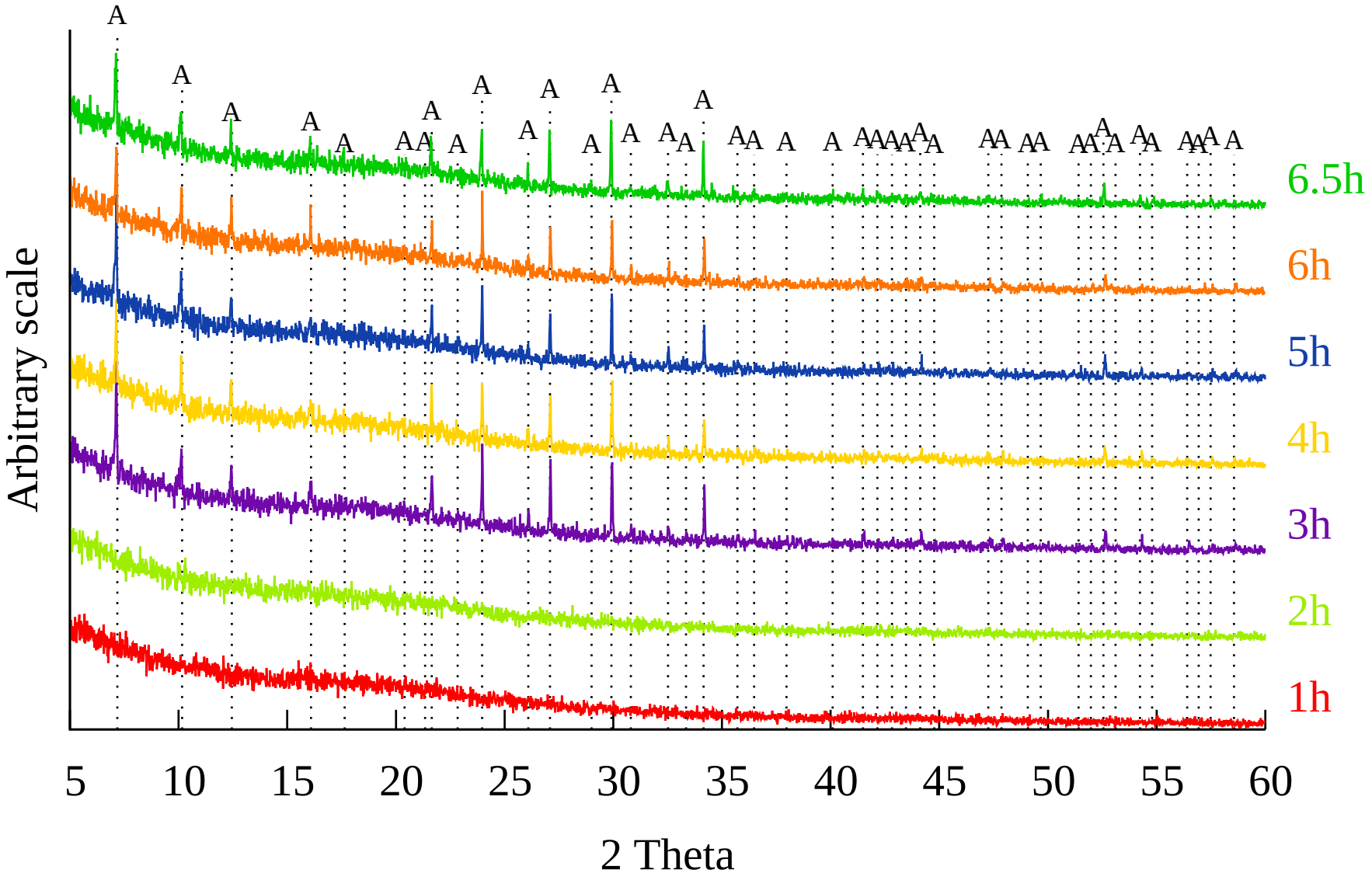

Figure 6.9: XRD patterns of 90-95°C crystallisation with an addition of 591 g NaOH/kg FA. A: Zeolite Na-A. $\lambda = 1.5406$ Å

If a small loss of yield, and agglomerated particles were acceptable, this data would indicate that additional NaOH would be beneficial, as it induces faster crystallisation, however, an inspection of SEM images of a higher resolution shows that this may not be the case. As a comparison, two images of x10,000 magnification are shown in Figure 6.11. These are SEM images from section 5.4, one of which is the control, with a sodium aluminate dosage of 222 g/kg FA and the other is the highest dosage of sodium aluminate: 310 g/kg FA. It is noted that the cubes in these images show few particulates or surface structures, and the few contaminants present appear to be amorphous, rather than cube or disc shaped. It was not possible to attain clear images at higher magnification using this SEM, and the blurry surface particles do bear a similarity to the amorphous materials which are present in SEM images prior to zeolite A formation. The small particulates or surface structures in Figure 6.12 consist of cubes and round clusters of intersecting discs. These clusters of intersecting discs are very similar to the 1-2 μm structures in Deng et al. [142] Figures 2a, 2b and 2c, which consist of cancinite/ sodalite structures, and sodalite/ LTA (zeolite A) structures; and Carlos A. Ríos R. [87] which has various well-labelled SEM images. They are also similar to the zeolite P structures in Molina and Poole [6] in Figure 11. This similarity in structure has been noted by Shoumkova and Stoyanova [42]. It is possible that these are early seeds of zeolite P or A following Ostwald's law of successive transformations, as both zeolite P and sodalite are noted to be more thermodynamically stable than zeolite A, and conversion of zeolite A to P or sodalite has been observed [5, 6, 53, 60, 65].

The sodalite-like structures do not appear to be present in the XRD patterns of Figure 6.6 or Figure 6.9. A prominent sodalite peak, such as peaks in Figure 5.8 would appear at $2\Theta = 13.886$. The lack of peaks could be attributed to low concentrations of sodalite. The relatively low concentration of sodalite would result in shorter peaks which would be obfuscated by the noise of the XRD pattern, said noise being of higher intensity due to the fast scan time of 10 minutes. This problem could be rectified through re-analysis with a longer scan time, which would decrease the signal:noise ratio.

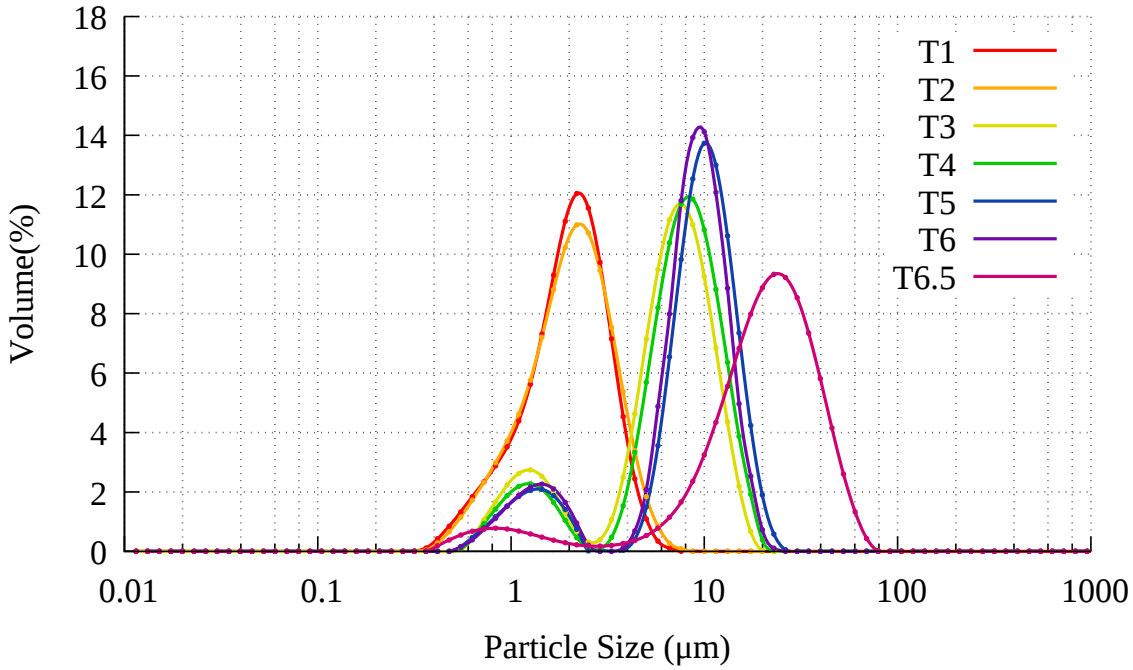

(a) PSD

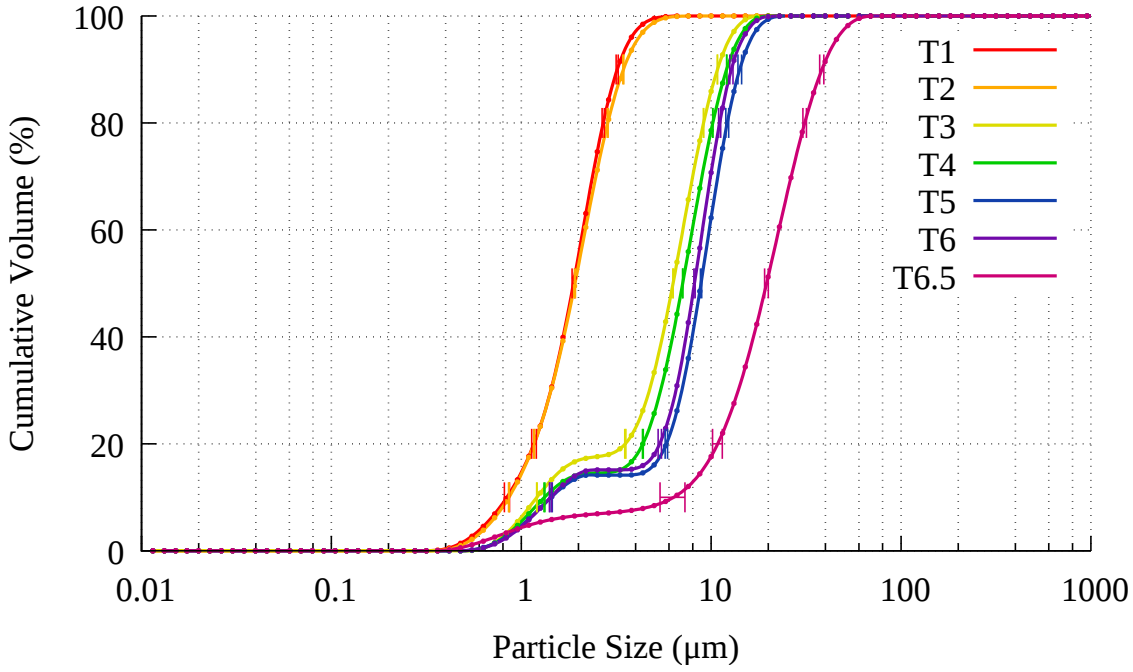

(b) Standard deviation in PSD

Figure 6.10: 90-95°C crystallisation process with 591 g NaOH/kg FA added

Figure 6.13 shows the PSD of samples taken at 6 hours. The 296 g NaOH/kg FA dosage has a narrower size range for the right hand peak, a d_{50} of 7 μm, whereas the control experiment has a d_{50} of 8 μm, and has a wider peak. The highest dosage of NaOH also has a d_{50} of 7 μm. The 6.5 hour measurements in Figure 6.14 show broader PSD's for all right hand peaks, with the highest NaOH dosage peaking above 20 μm. This broadening of the PSD and move to the right is consistent with the idea of particles becoming attached to each other during the cooling and filtration process. Figure 6.14b shows a wide standard deviation for the d_{10} of the control and 591 g NaOH/kg FA experiments. This would indicate that the smaller left hand peaks are of limited accuracy.

The cation exchange capacity is diminished with the highest dosage of NaOH, as seen in Figure 6.3. This, along with the decrease in yield results in a more pronounced decrease in the cation exchange capacity yield shown in Figure 6.4. This decrease in CEC can be attributed to the larger particle size shown in Figure 6.14a as well as the potential inclusion of sodalite. With the higher magnification SEM images, it is argued that increasing the NaOH content of the crystallisation process hastens the crystallisation process of zeolite at the expense of introducing sodalite and causing agglomeration of particles.

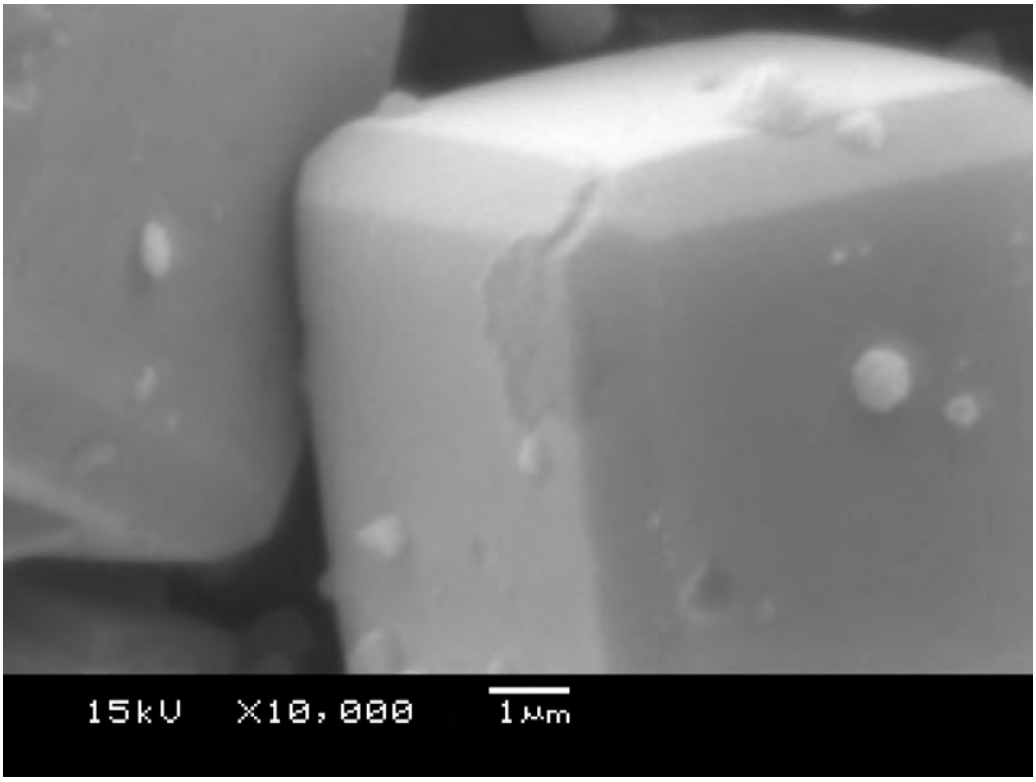

(a) 6 h +0 g NaOH/ kg FA, + 222 g SA/ kg FA

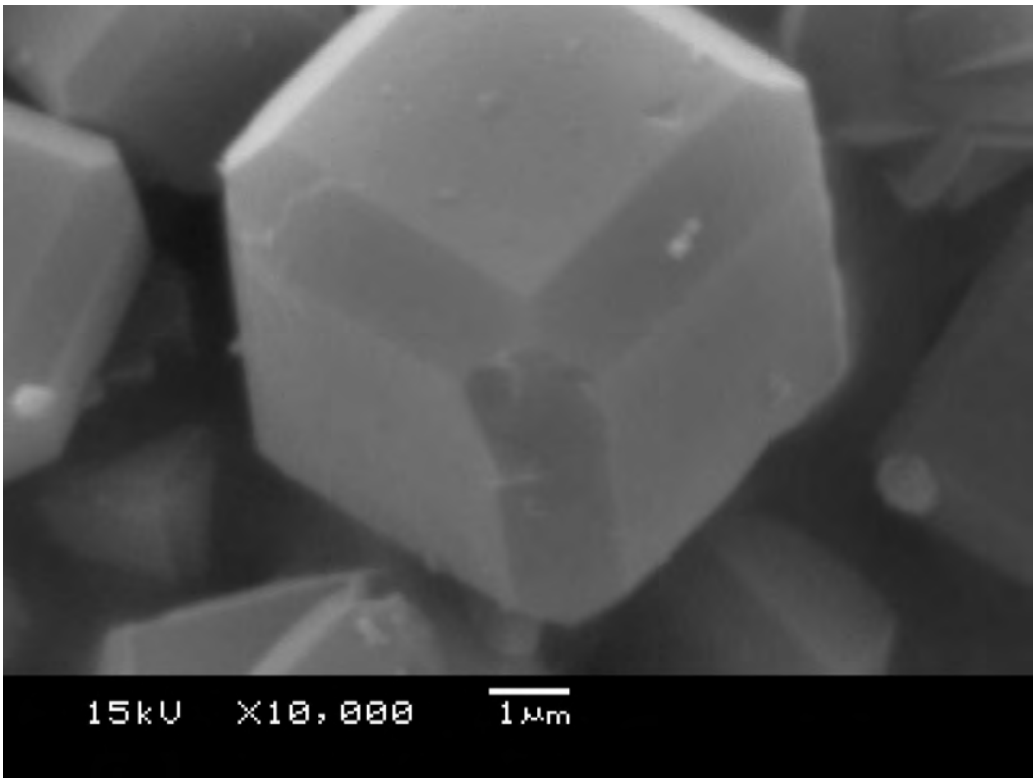

(b) 6 h +0 g NaOH/ kg FA, + 310 g SA/ kg FA

Figure 6.11: SEM images of zeolites from ash leachate crystallised with increasing sodium aluminate/kg FA on a stirred hot plate at 90-95°C

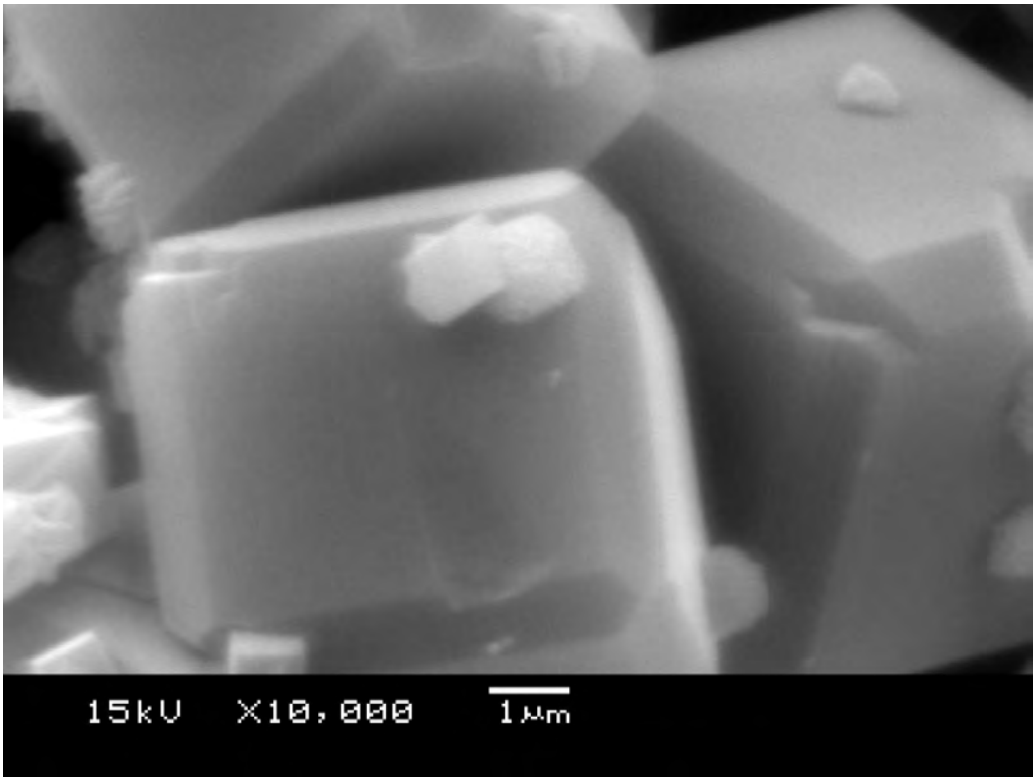

(a) 6 h +296 g NaOH/ kg FA

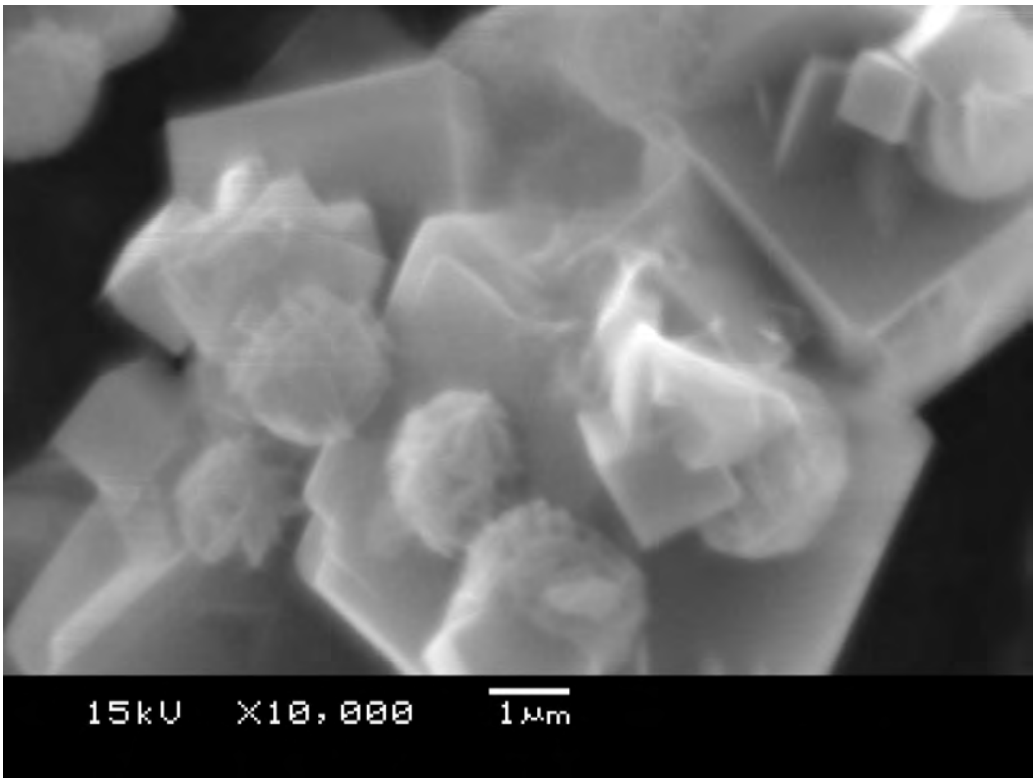

(b) 6 h +591 g NaOH/ kg FA

Figure 6.12: SEM images of zeolites from ash leachate crystallised with increasing NaOH/kg FA on a stirred hot plate at 90-95°C

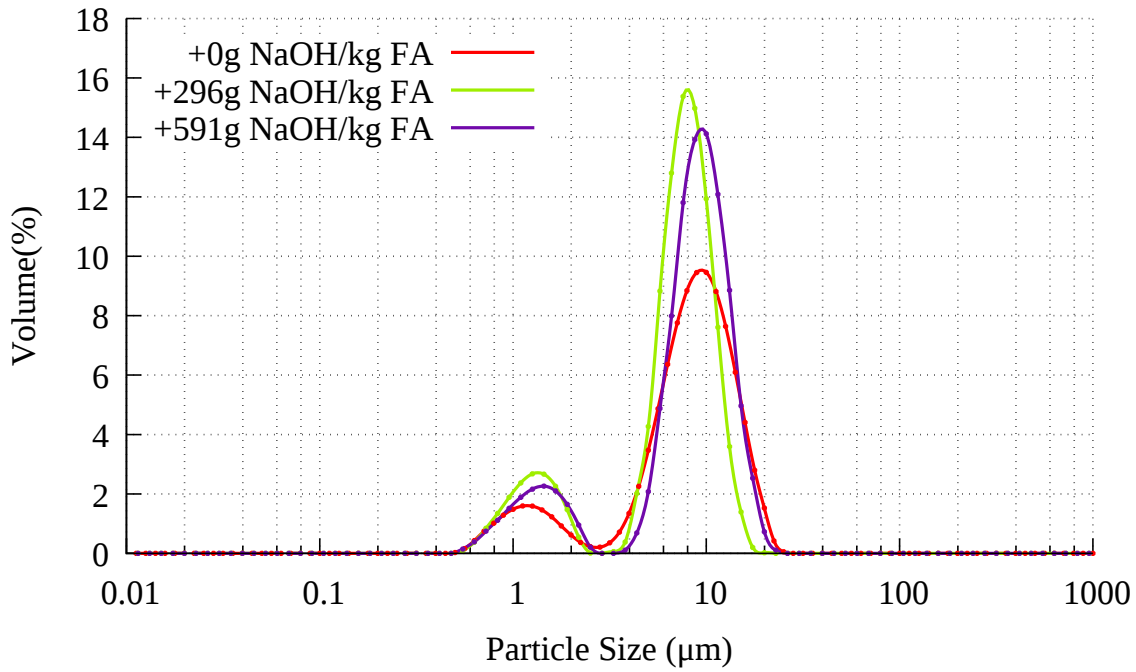

(a) PSD

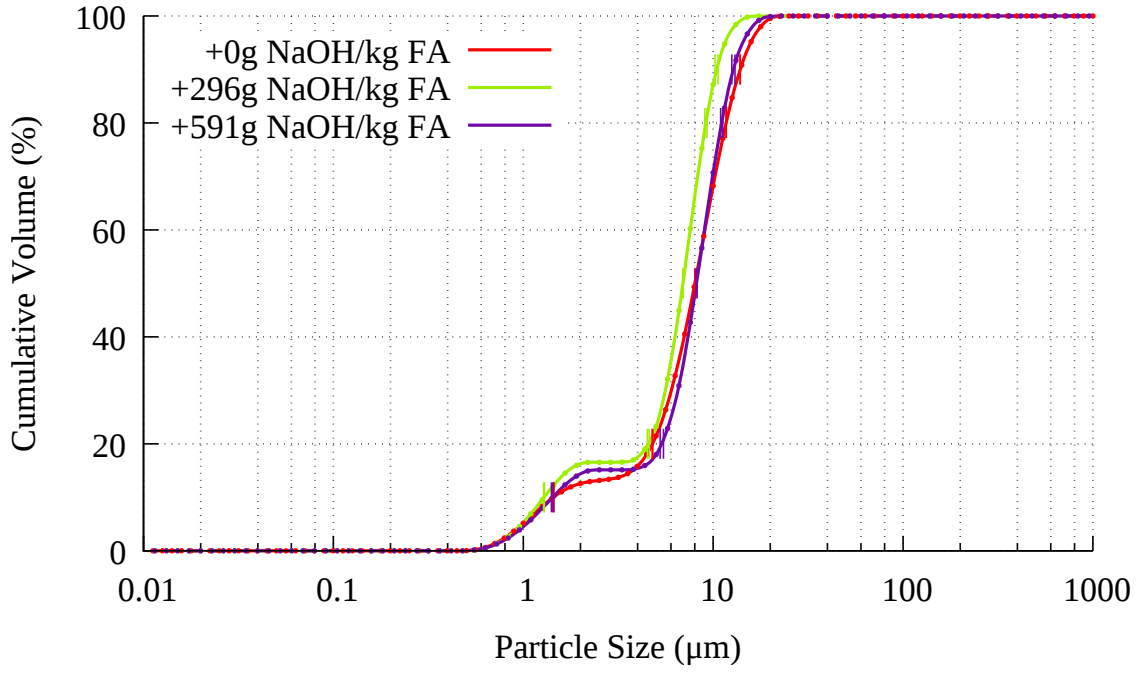

(b) Standard deviation in PSD

Figure 6.13: 90-95°C crystallisation process with added NaOH at 6 hours

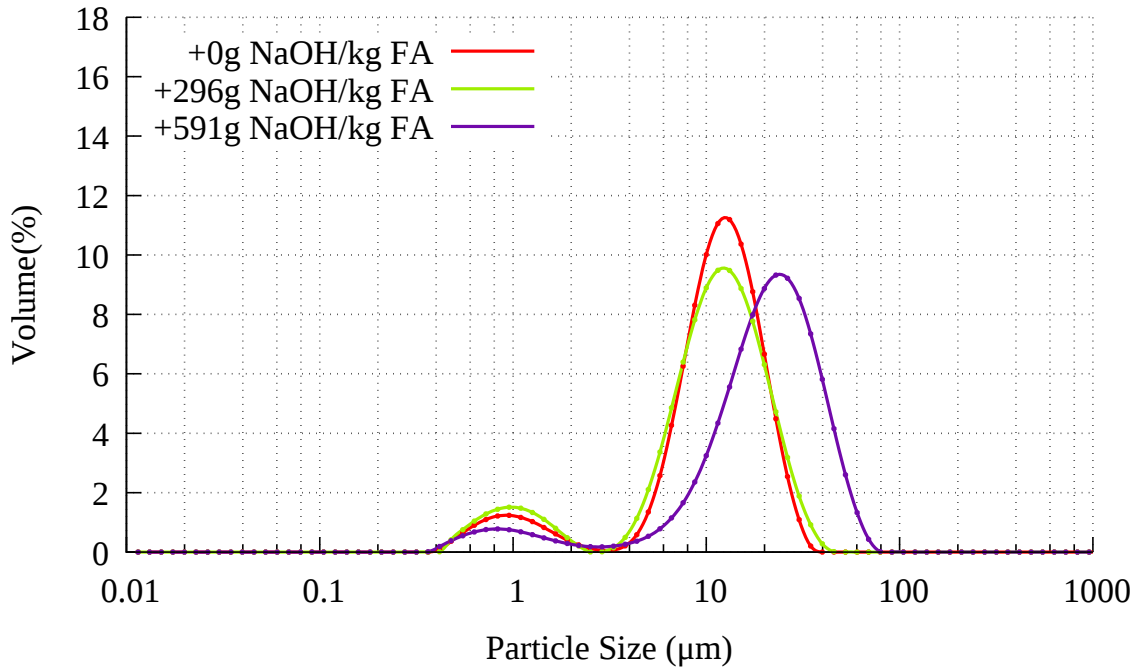

(a) PSD

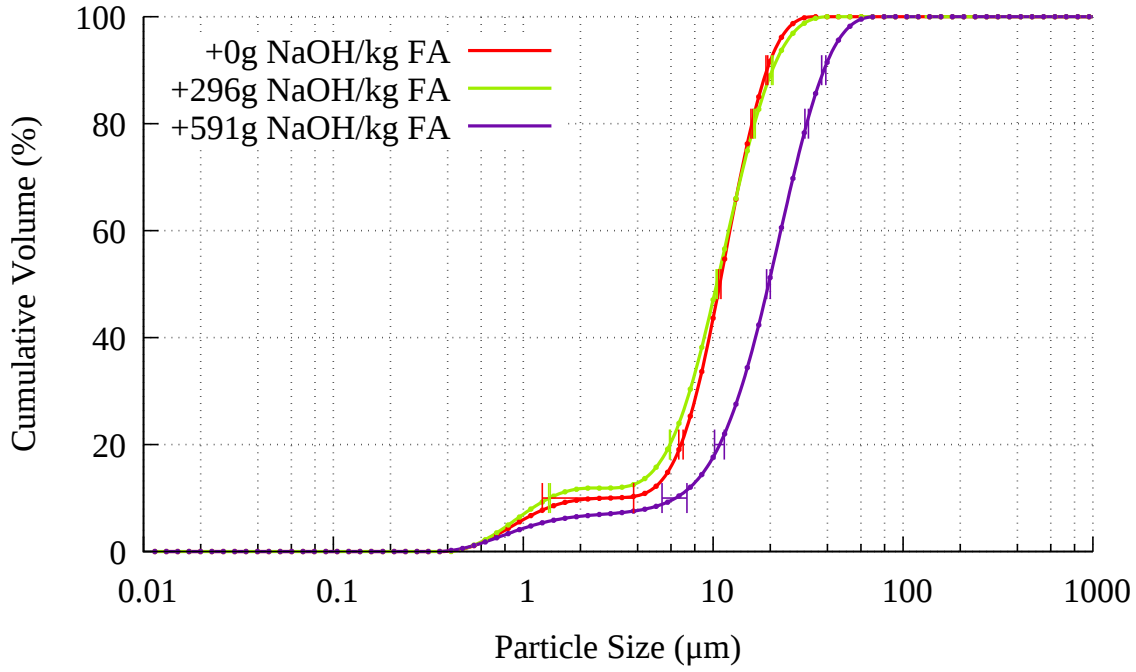

(b) Standard deviation in PSD

Figure 6.14: 90-95°C crystallisation process with added NaOH at 6.5 hours (after filtration)

6.2 Effect of Various Sources of Na on the Crystallisation Process

As mentioned in the previous section, the NaOH content increases with sodium aluminate dosage. Increasing the NaOH content not only increases the alkalinity of the crystallisation process, but also increases the Na^+ content. Sodium cations form a significant part of the LTA structure, as described in Figure 2.1. NaOH is not the only possible source of Na^+. Sodium can be introduced as NaCl, in order to investigate the influence of additional Na^+.

6.2.1 Experimental Method

The control experiment used was the 222 g SA/kg FA experiment from section 5.4.2.5 and the NaOH experiment was the 591 g NaOH/kg FA experiment from section 6.1.2.3. The experimental method used in the NaCl experiment follows the method described in section 6.1, replacing the 1 mole of NaOH with 1 mole of NaCl.

6.2.2 Results

6.2.2.1 Control Experiment

See section 5.4.2.5

6.2.2.2 Adding NaOH to the Crystallisation Step

See section 6.1.2.3

6.2.2.3 Adding NaCl to the Crystallistaion Step

Yield results shown in Figure 6.16 show that whilst adding NaOH decreases the yield slightly, NaCl appears to have the inverse effect, increasing the final yield of zeolite. The CEC in Figure 6.17 shows similar results, and are emphasised in Figure 6.18.

The AAS results in Figure 6.15 show an increase in Si and Al consumption by the sixth hour for the experiment with added NaCl, which agrees with the increased yield. The similar Si and Al consumption in the context of differing yield is attributed to the formation of phases other than zeolite A. The sample with added salt shows a larger drop in Si and Al between 0 and 1 hours, than is observed in the control experiment or the NaOH experiment. This is followed by a decrease in Si content between 3 and 4 hours which coincides with crystallisation of zeolite in SEM images in Figure 6.20. It is noted that the Al content shows a significant drop between 2 and 3 hours, and a less significant drop between hours 3 and 4. This disparity between the Si and Al results is not observed in other experiments with varied NaCl dosages in Figure 6.25. Analysis of XRD patterns shown in Figure 6.21 shows the presence of zeolite A at 3 hours, but the signal becomes clearer from 4 hours onward. The Si and Al content of experiment with added NaCl follows a similar shape as the experiment with added NaOH from hour 1.

Analysis of the SEM image from 6 hours at 10,000x magnification shows small cubes intermixed. This single SEM image may not be representative of the entire sample, so it can not be used to rule out the possibility of that sodalite has been produced in this sample, but none appears present in this image. As with the previous set of experiments, this could be verified through more intensive XRD analysis.

The PSD in Figure 6.22a shows that the first two measurements are quite similar, both being broad and showing d_{50} of 0.4 μm. This abundance of small particles indicates that the introduction of NaCl may aid nucleation. Between 2 and 3 hours there is a distinct change as the PSD moves to the right, indicating a growth or agglomeration in particle sizes, with a smaller peak near 1 μm, and the taller peak near 6 μm. The measurements from 4-6.5 hours all have a $d_{50} \sim 5$ μm. During the cooling and filtration step, the formation of finer particulates bring the left hand peak more to the left and closer to the 1 μm point.

Comparing the effect various Na^+ sources have on the PSD at 6 and 6.5 hours is shown in Figures 6.23 and 6.24. For the 6 hour samples, the addition of NaCl appears to keep

the formed particles smaller, and the bimodal PSD is not as well defined as in the control experiment. Even after cooling and filtration the right hand peak for the NaCl PSD in Figure 6.24a is more to the left than the control of NaOH experiments. With the higher quantity of fine particles for the 1 and 2 hours measurements in Figure 6.22a compared to the control in Figure 5.47a or the NaOH experiment in Figure 6.10a, it is argued that NaCl aids in the seeding process.

This argument is supported by the higher consumption of Si and Al in the first hour in Figure 6.15. Given a plentiful supply of seeds, when the temperature was raised at 2 hours, the Si and Al in solution was consumed to a greater extent than in the control experiment, leading to a lower final value of Si in solution at 6 hours, and an increase in yield. The data provided from this experiment and section 6.1 is insufficient to define the roles of Na^+ and OH^- in the crystallisation of zeolites. The role of the Cl^- anion, if any, is unaccounted for, and the extent to which each ion influences the reaction is also unknown, however the data does indicate that additional NaCl is advantageous.

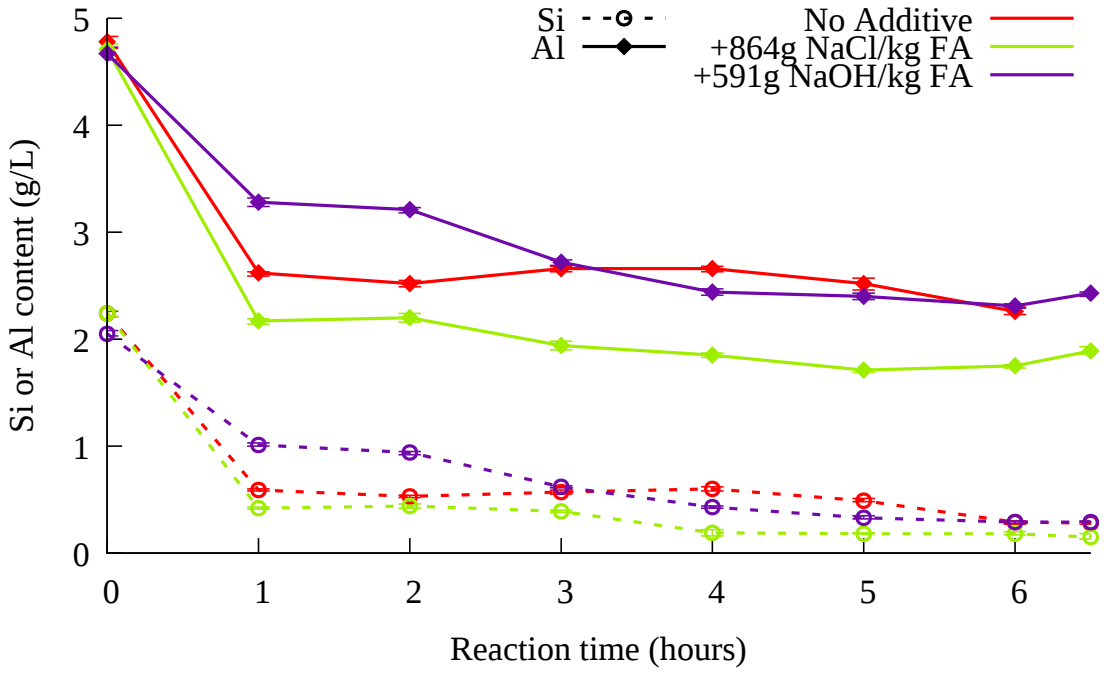

Figure 6.15: AAS results for 90-95°C crystallisation process with varied Na sources

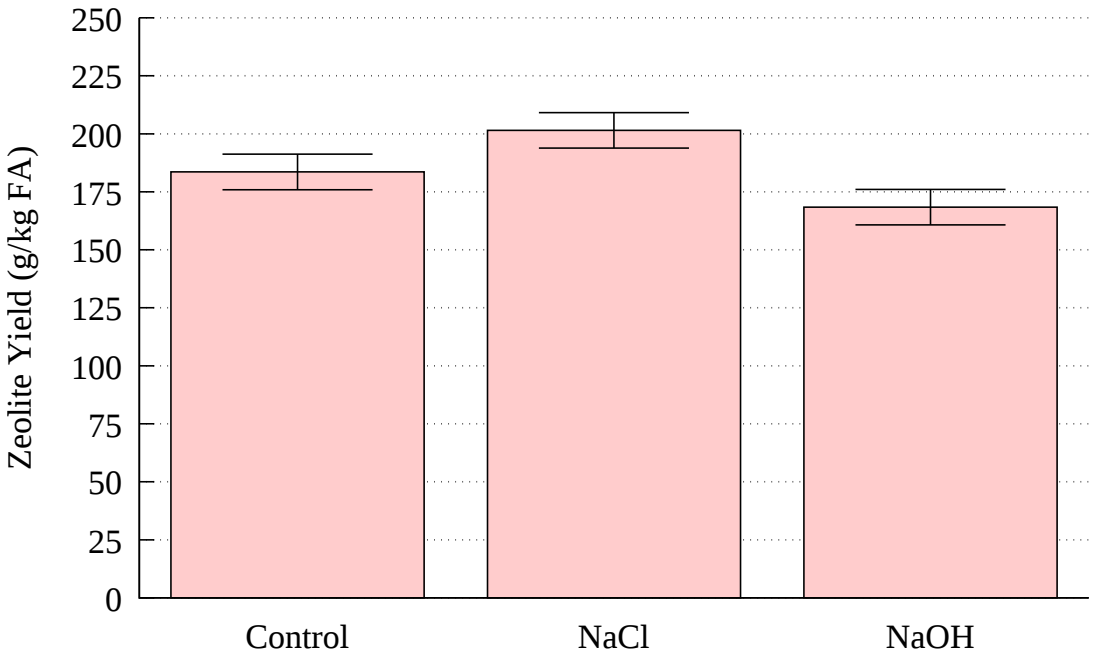

Figure 6.16: Yield of zeolite comparing Na source

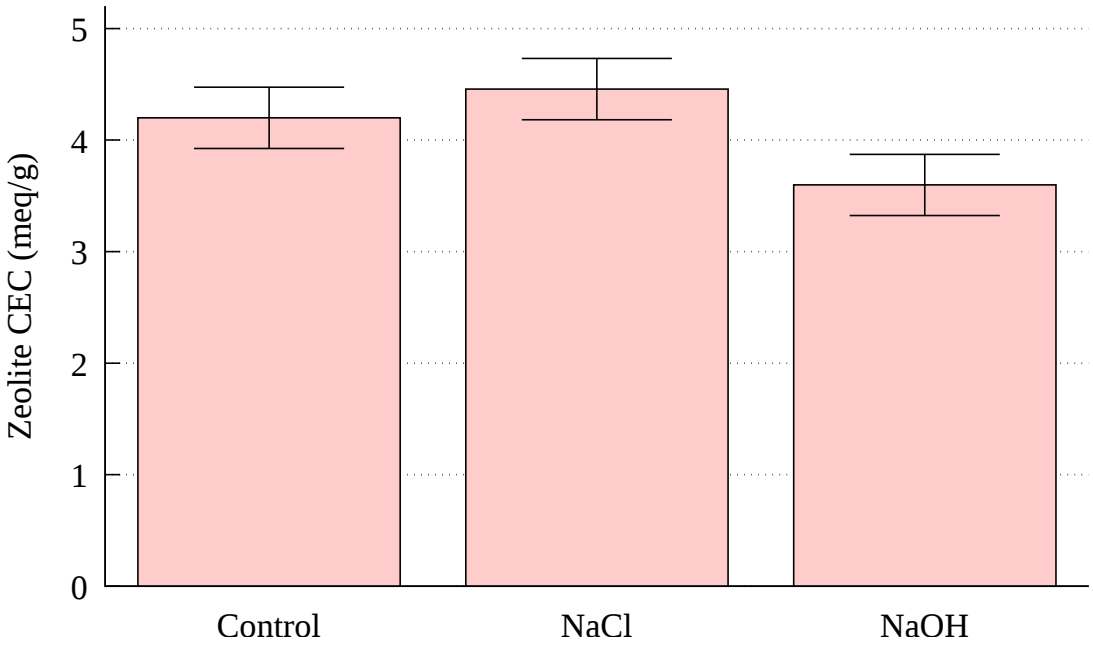

Figure 6.17: CEC of zeolite comparing Na source

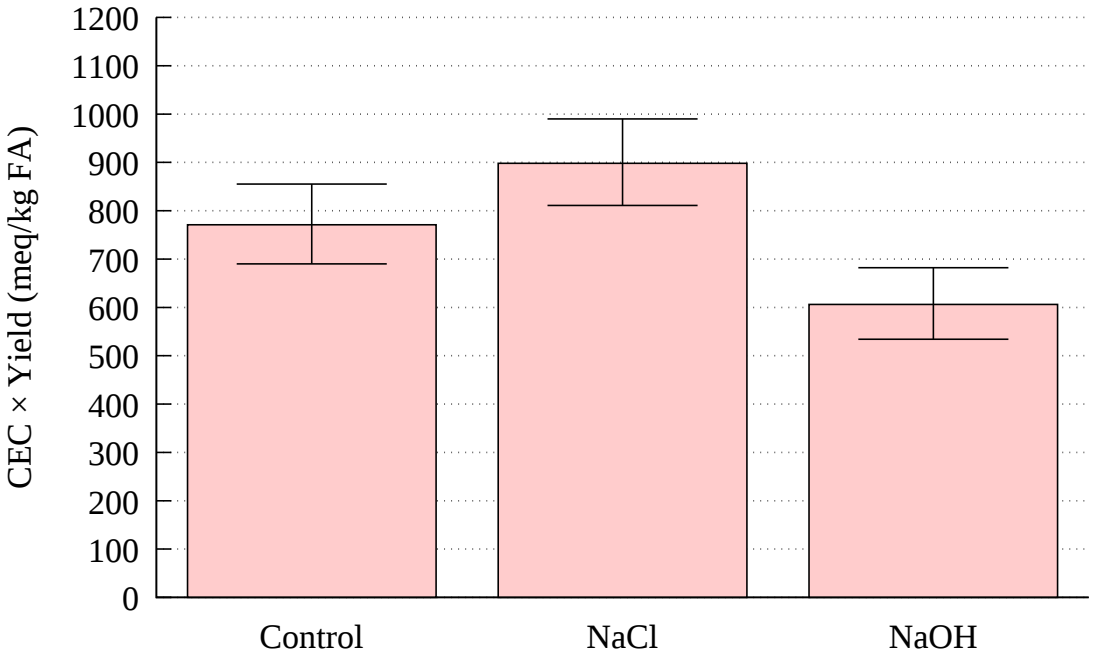

Figure 6.18: CEC × yield of zeolite comparing Na source

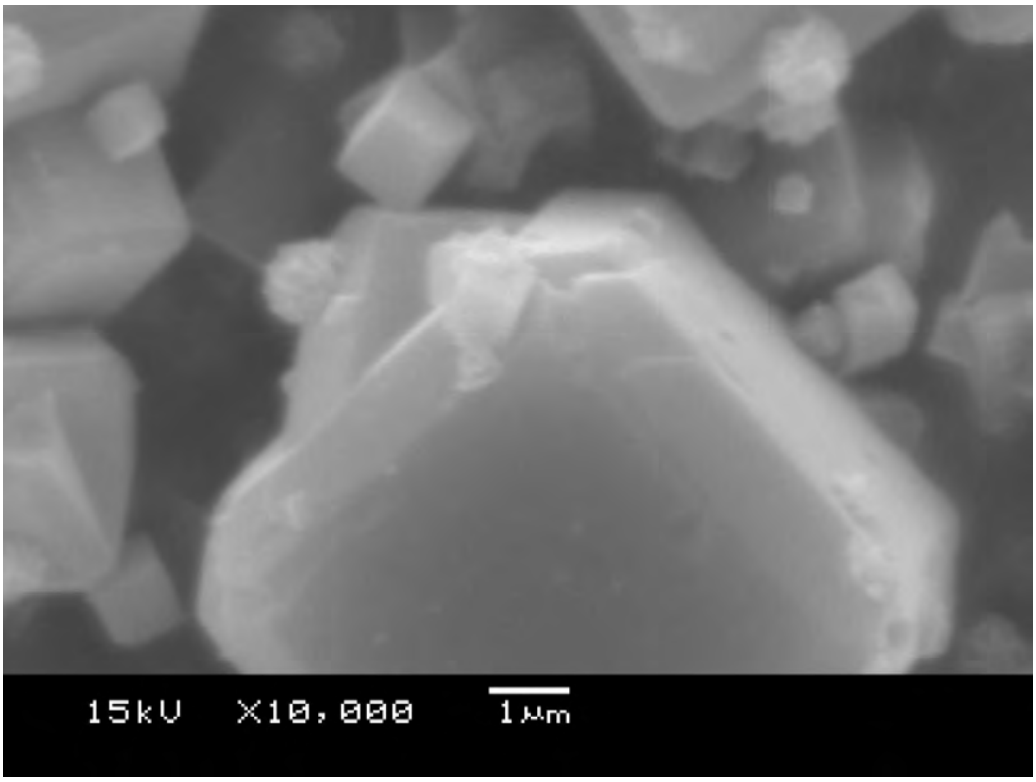

Figure 6.19: 6 h + 864 g NaCl/ kg FA, + 222 g SA/ kg FA

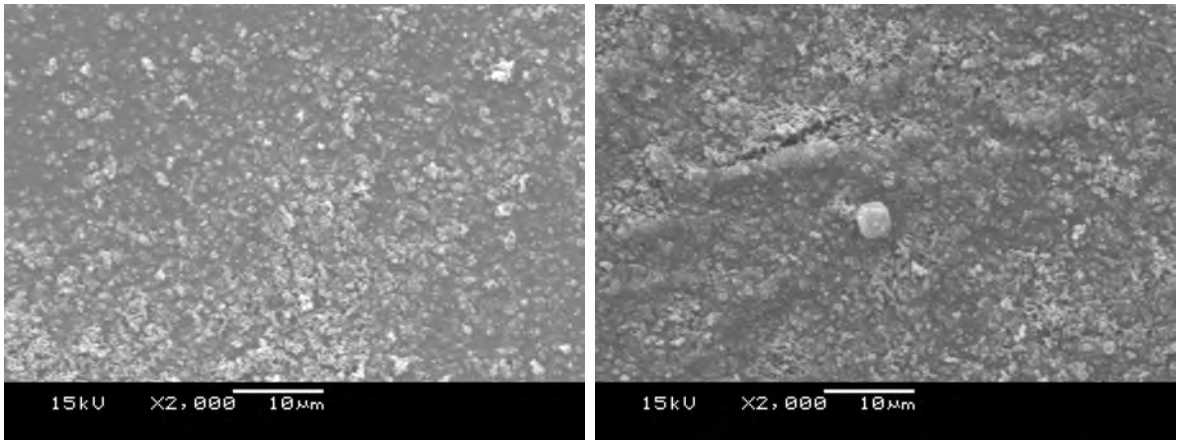

(a) 1 h (b) 2 h

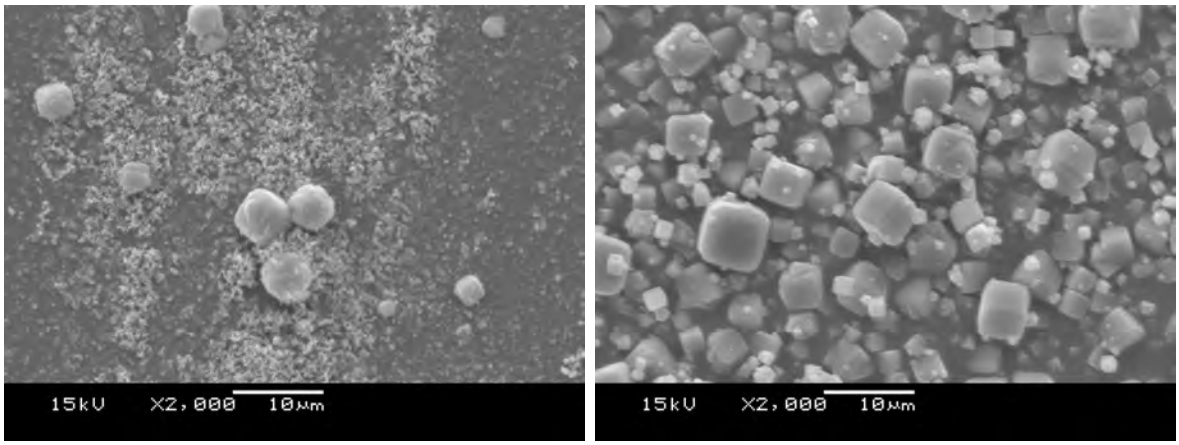

(c) 3 h (d) 4 h

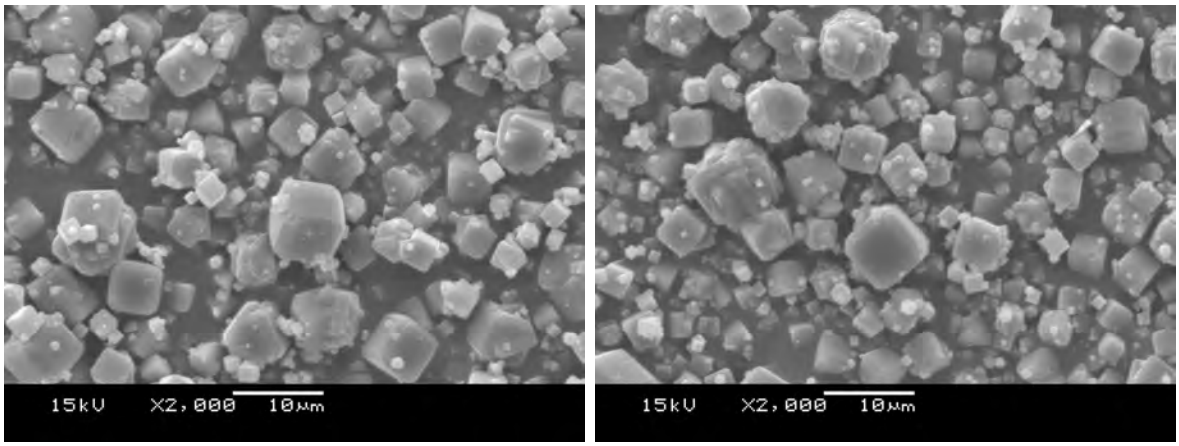

(e) 5 h (f) 6 h

Figure 6.20: SEM images of zeolites from ash leachate crystallised with an additional 864 g of NaCl/kg FA on a stirred hot plate at 90-95°C

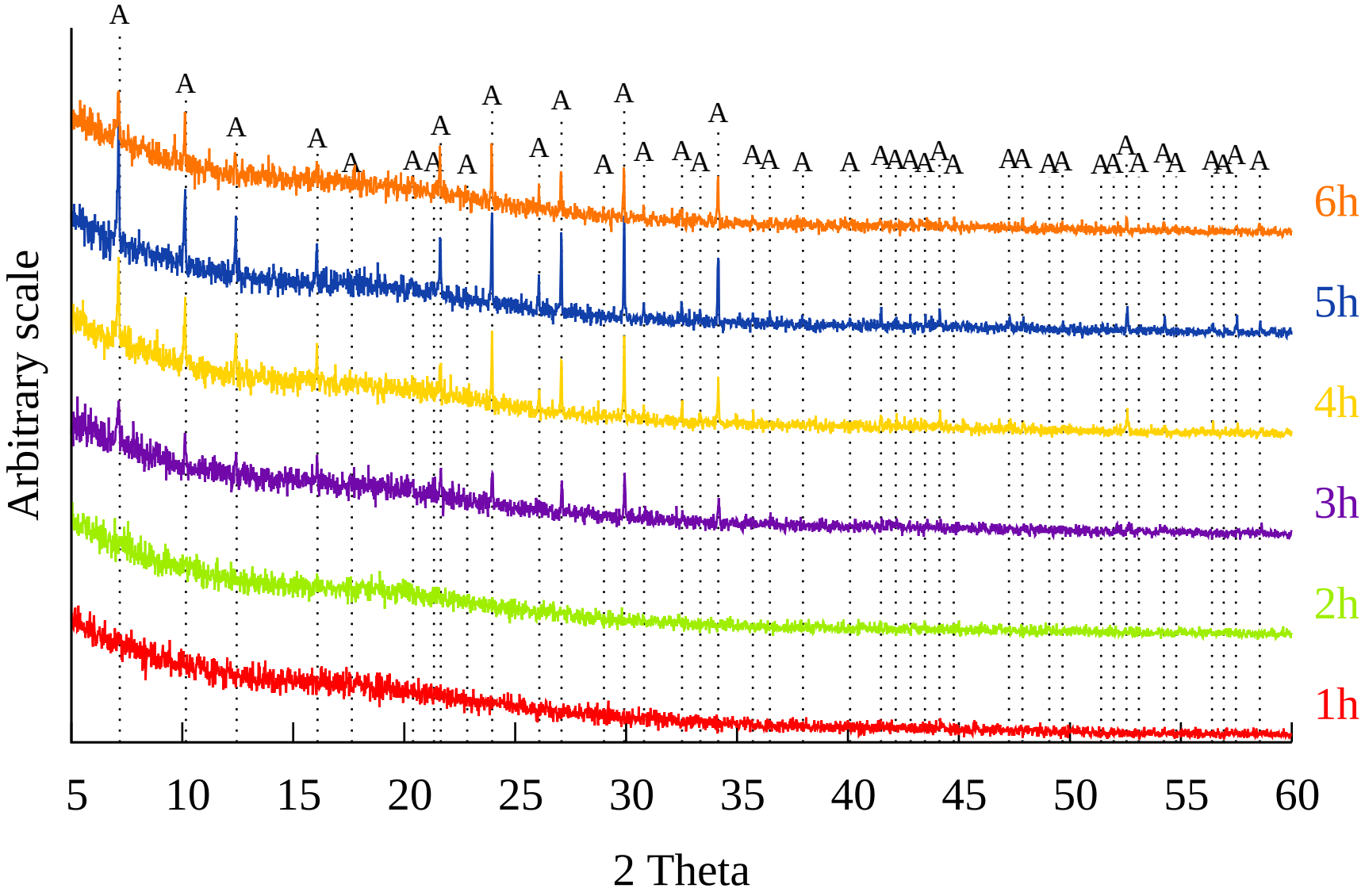

Figure 6.21: XRD patterns of 90-95°C crystallisation with an additional 864 g NaCl/kg FA. A: Zeolite Na-A. $\lambda = 1.5406$ Å

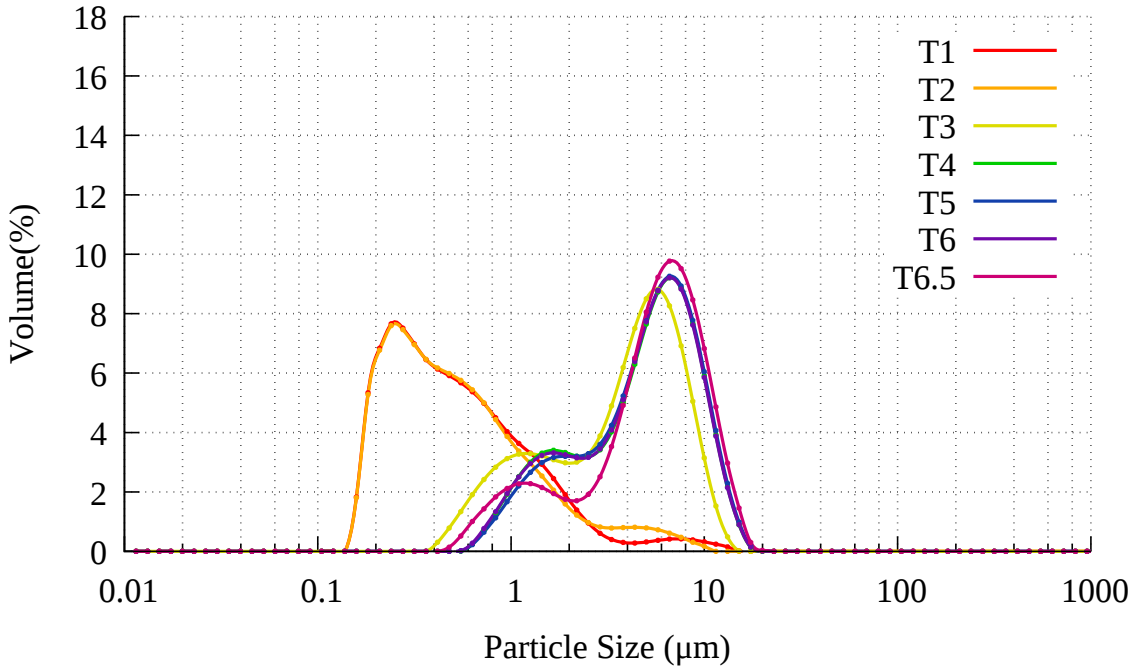

(a) PSD

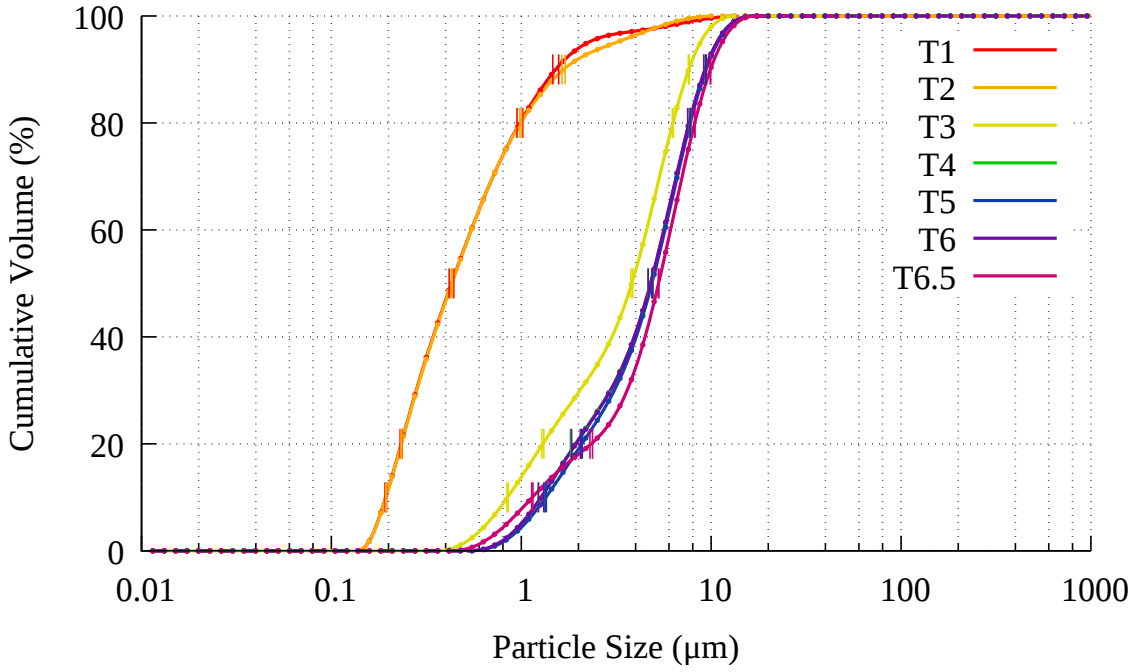

(b) Standard deviation in PSD

Figure 6.22: 90-95°C crystallisation process with 864 g NaCl/kg FA added

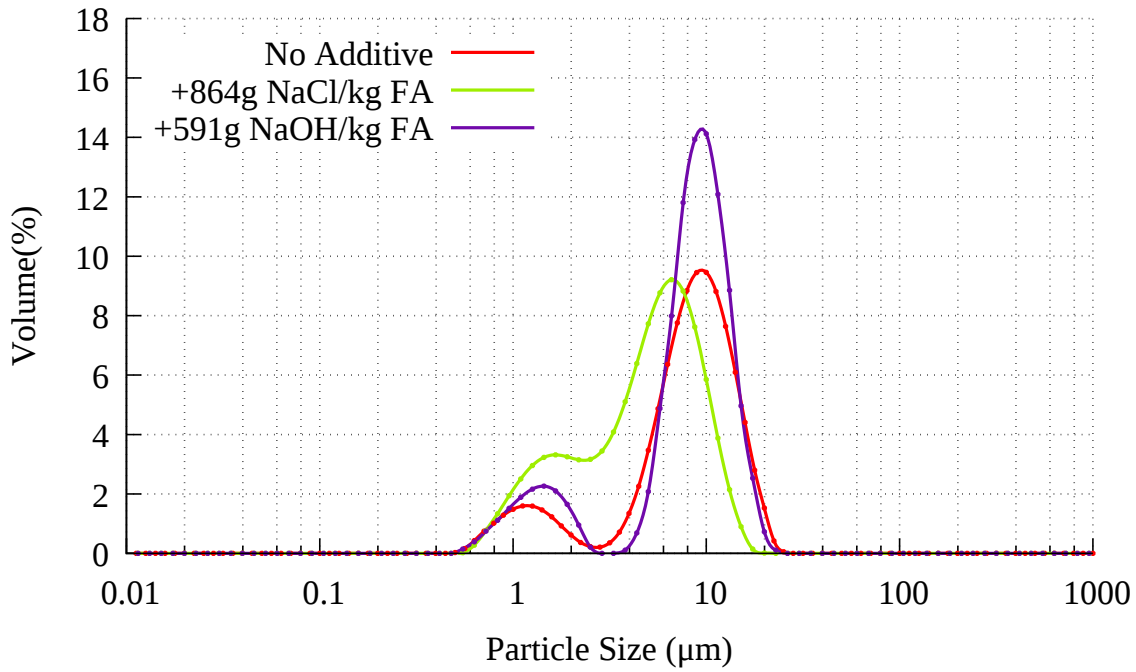

(a) PSD

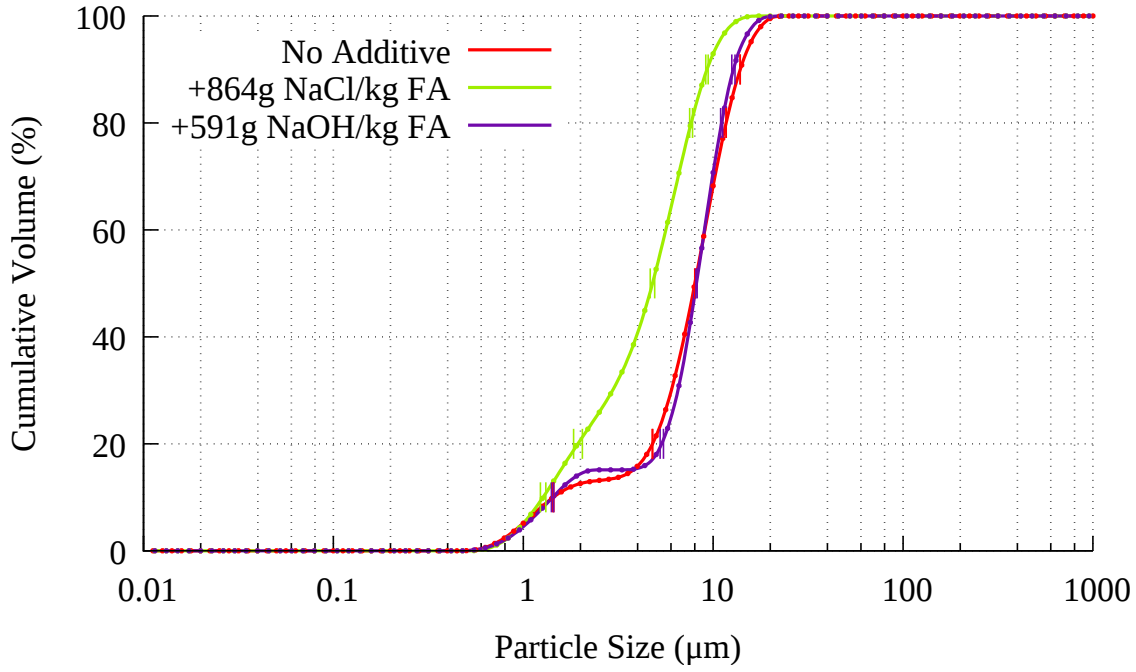

(b) Standard deviation in PSD

Figure 6.23: 90-95°C crystallisation process with added Na^+ at 6 hours

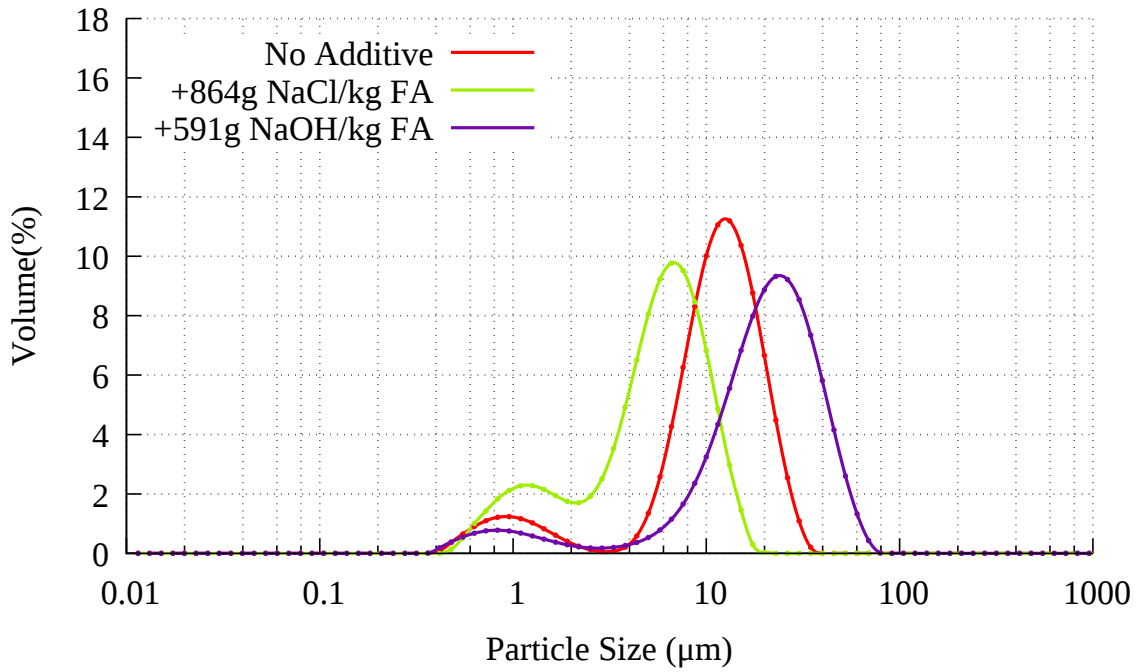

(a) PSD

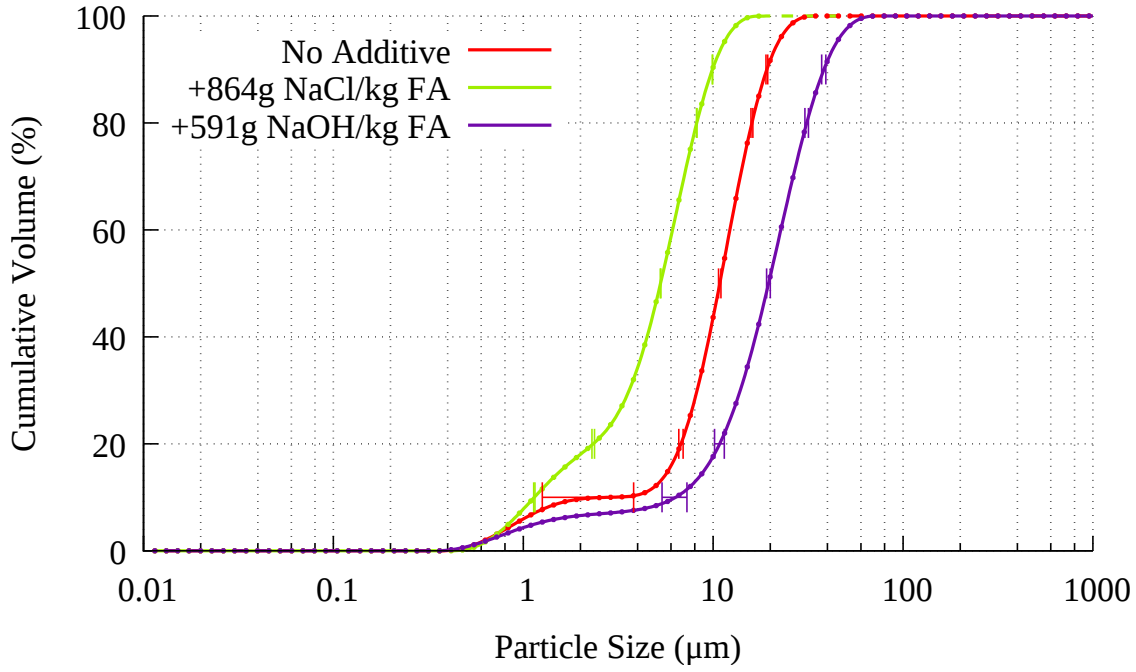

(b) Standard deviation in PSD

Figure 6.24: 90-95°C crystallisation process with added Na^+ at 6.5 hours

6.3 The Effect of Adding NaCl to the Crystallisation Process

As the previous section has shown, different Na^+ sources have different effects on the crystallisation process, with added NaCl producing preferable results in terms of yield and CEC. Thus, the effect of varied quantities of NaCl was investigated. The control experiment used that of section 5.4.2.5. Four dosages of NaCl were used, 0.5, 1, 2 and 4 M, which were 315, 864, 1728 and 3455 g NaCl/kg FA. The 1 M dosage was compared to a 1 M dosage of NaOH and described in section 6.2.

6.3.1 Experimental Method

The experimental method used in the NaCl experiment follows the method described in section 6.1, replacing the 1 mole of NaOH with varied quantities of NaCl.

6.3.2 Results

6.3.2.1 Dosage of 315 g NaCl/kg FA

The AAS results for the 0.5 M dosage of NaCl shown in Figure 6.25 show a decrease in both Si and Al between 3 and 4 hours. This decrease coincides with the disappearance of amorphous material between Figures 6.29c and 6.29d. SEM images from 4 hours onwards show chamfered edged cubes smaller than 10 μm. The XRD patterns in Figure 6.30 show clear peaks of zeolite A from 3 hours onward, with no obvious signs of any other phase present. The PSD in Figure 6.31a shows a broad asymmetric peak at the 1 hour measurement, with a peak just above 0.2 μm, followed by a bimodal distribution at 2 hours. The peaks from 3-6.5 hours all have a higher right hand peak, with a smaller left hand peak around the 1 μm point. Peaks from hours 4, 5, and 6 cannot be differentiated due to their similarity. The yield shown in Figure 6.26 shows an improvement from the control experiment, whilst the CEC shown in Figure 6.27 shows a similar, but slightly

lower CEC than the control experiment.

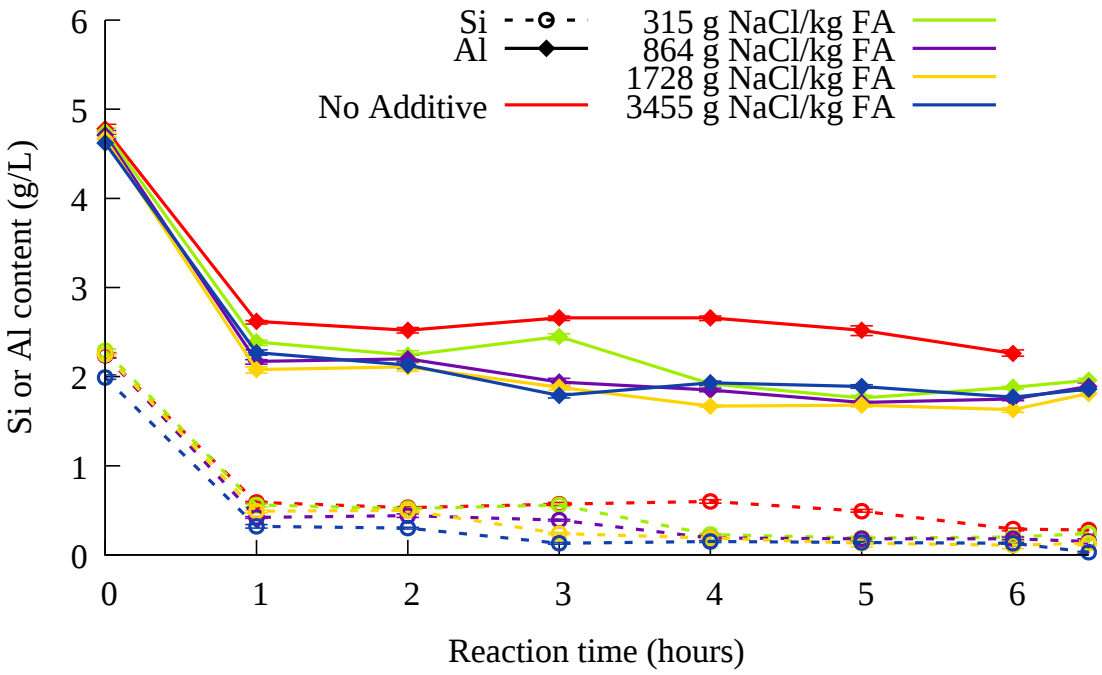

Figure 6.25: AAS results for 90-95°C crystallisation process with increasing NaCl dosage

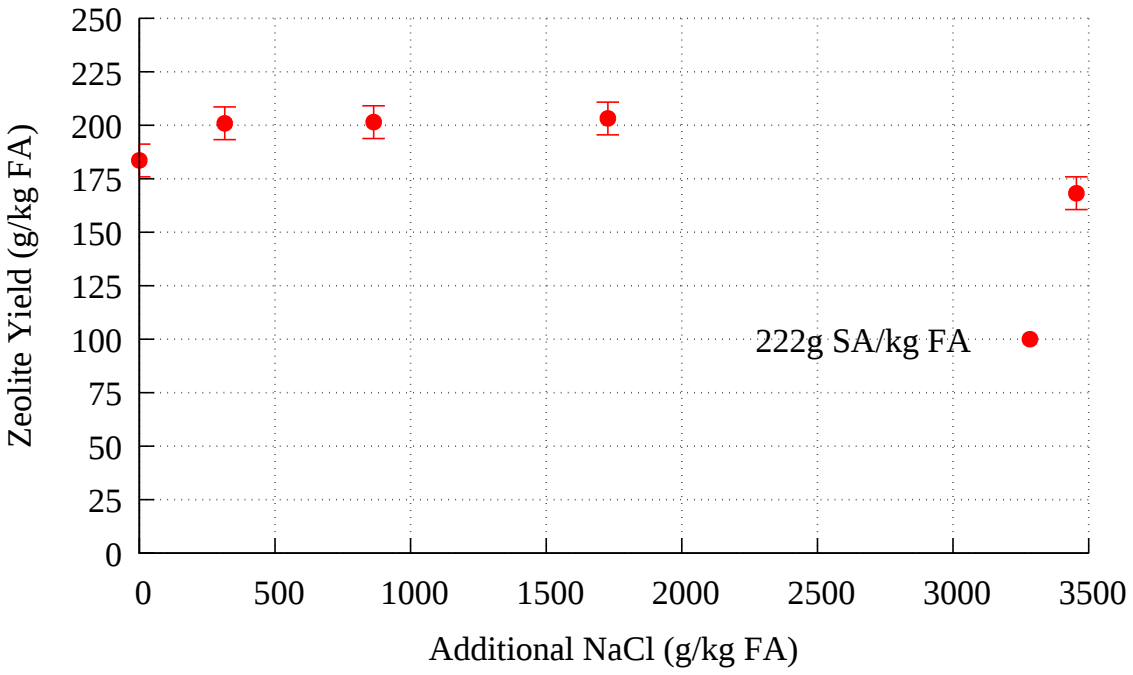

Figure 6.26: Yield of zeolite for 90-95°C crystallisation process with increasing NaCl dosage

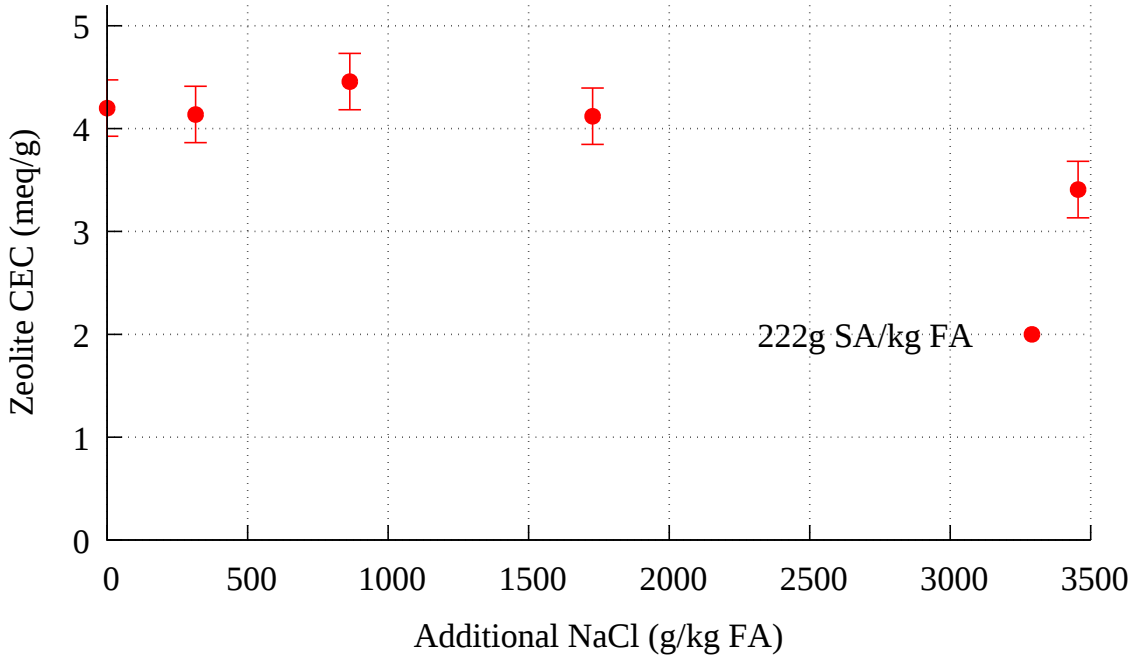

Figure 6.27: CEC of zeolite for 90-95°C crystallisation process with increasing NaCl dosage

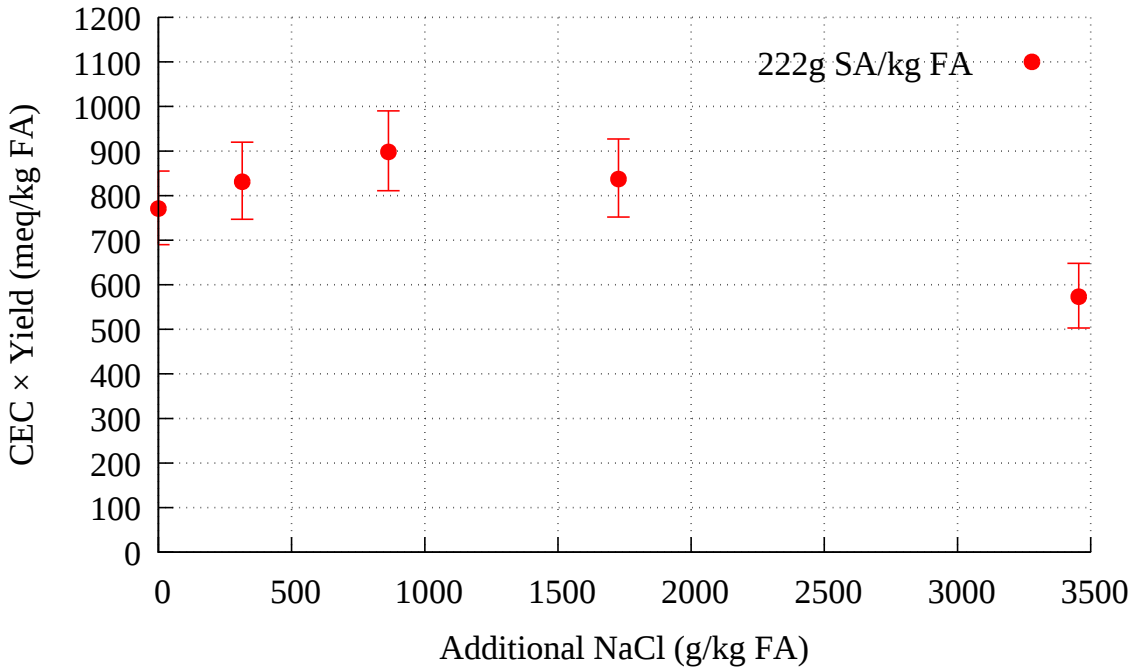

Figure 6.28: CEC × yield of zeolite for 90-95°C crystallisation process with increasing NaCl dosage

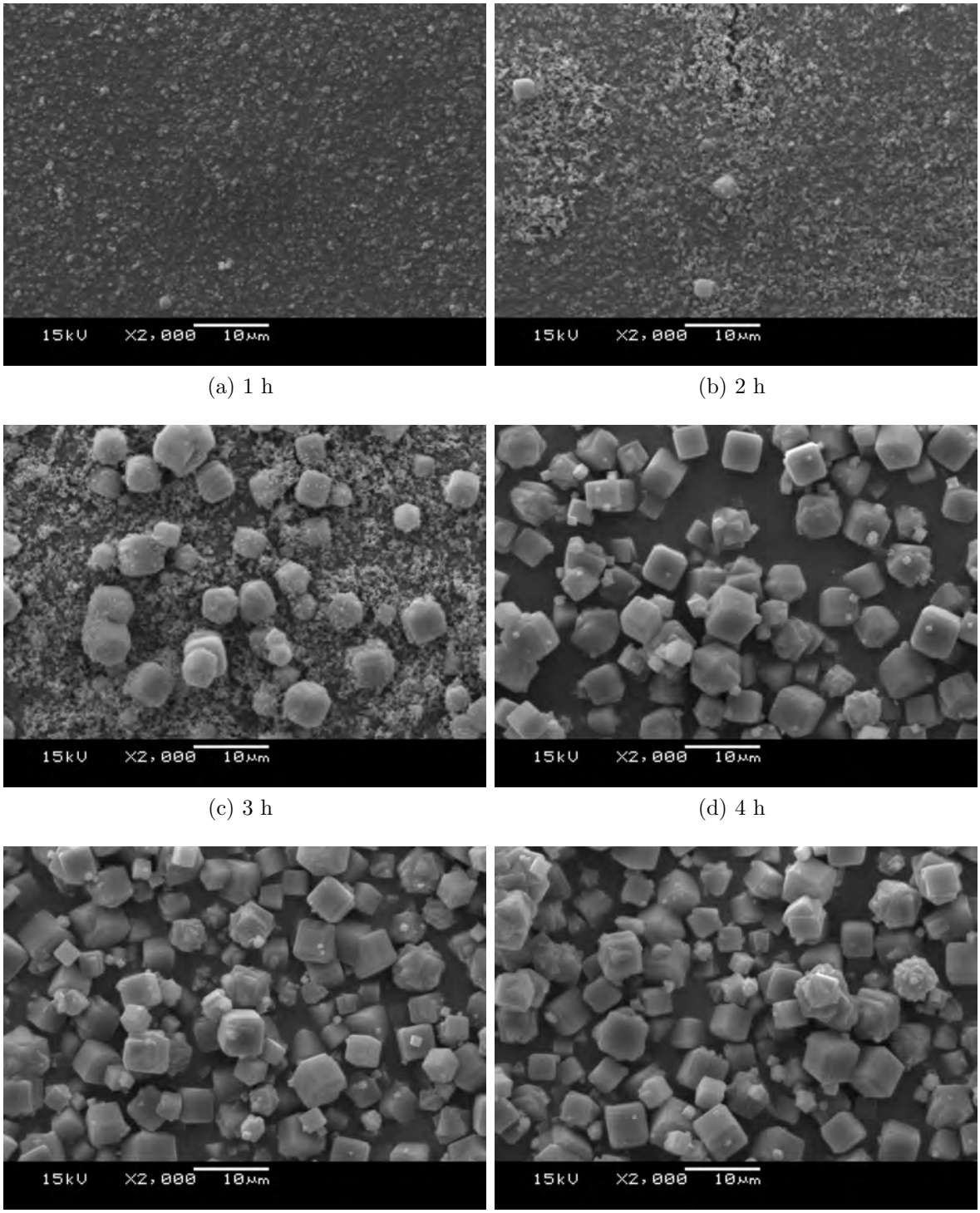

(a) 1 h (b) 2 h

(c) 3 h (d) 4 h

(e) 5 h (f) 6 h

Figure 6.29: SEM images of zeolites from ash leachate crystallised with an additional dosage of 315 g of NaCl/kg FA on a stirred hot plate at 90-95°C

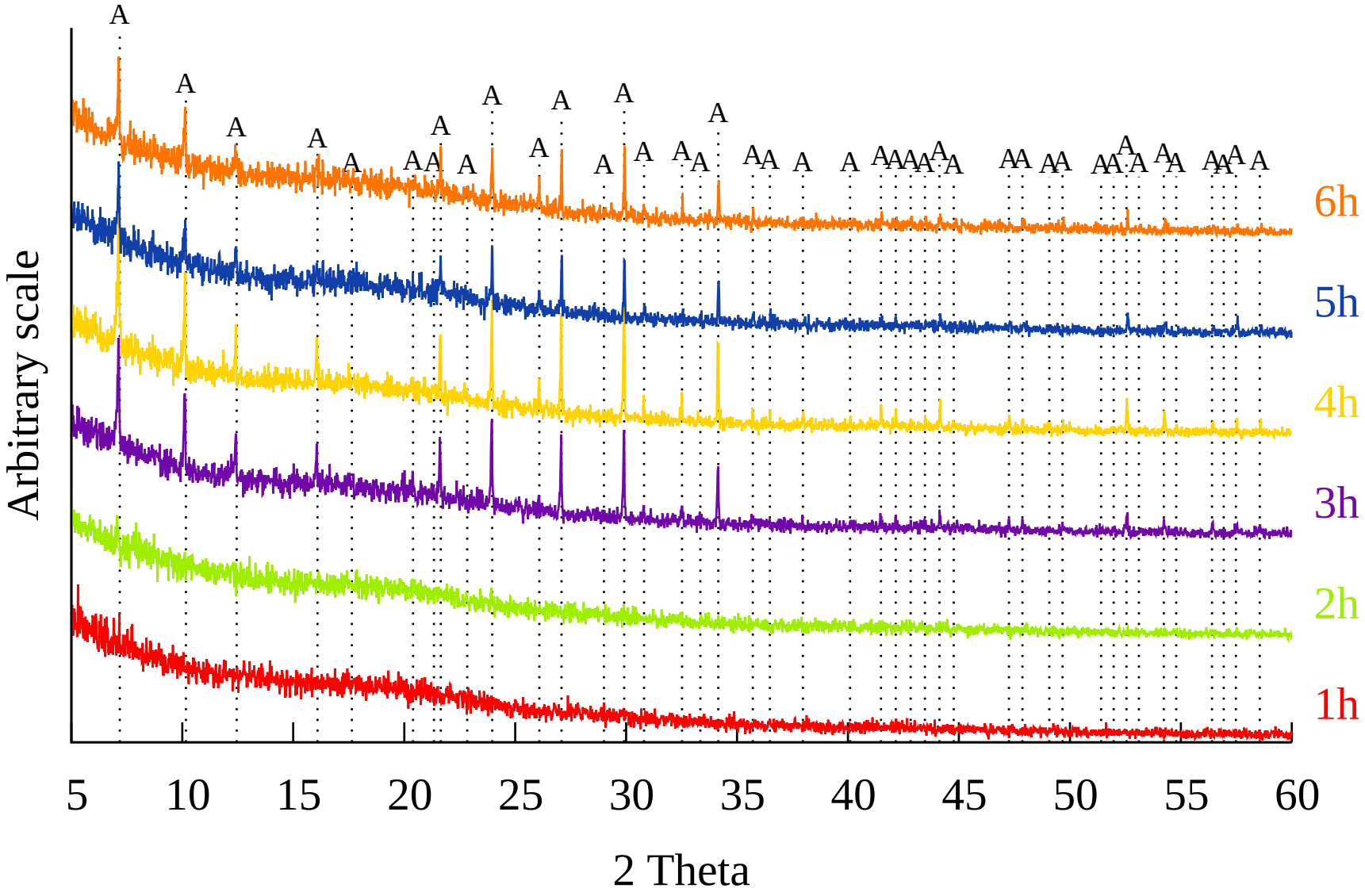

Figure 6.30: XRD patterns of 90-95°C crystallisation with an additional dosage of 315 g NaCl/kg FA. A: Zeolite Na-A. $\lambda = 1.5406$ Å

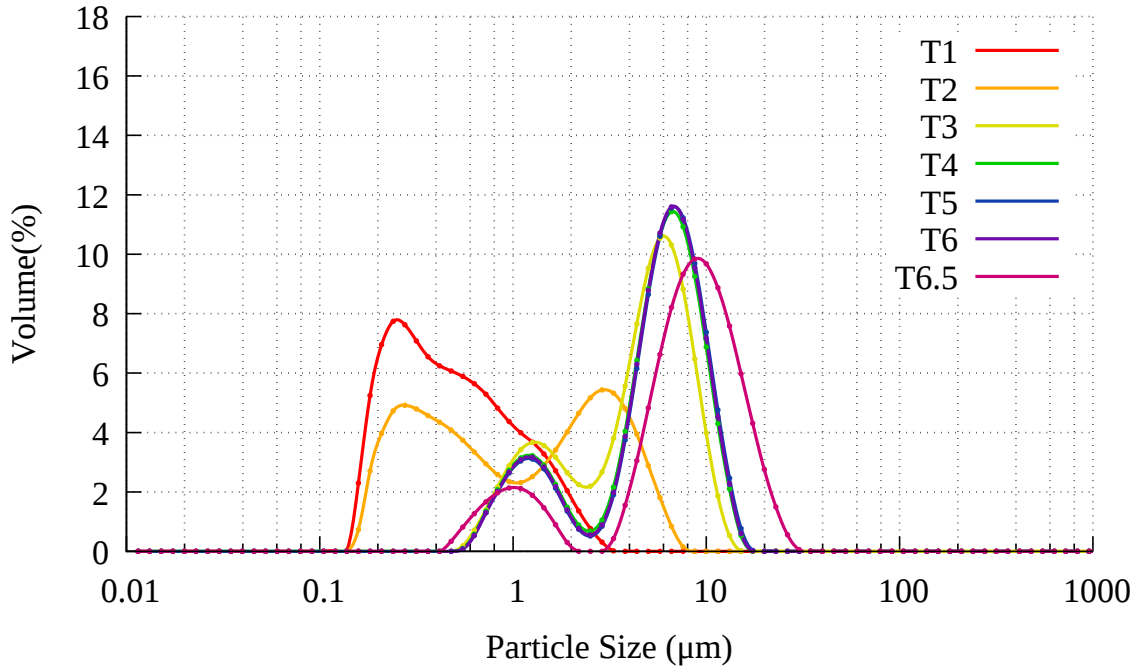

(a) PSD

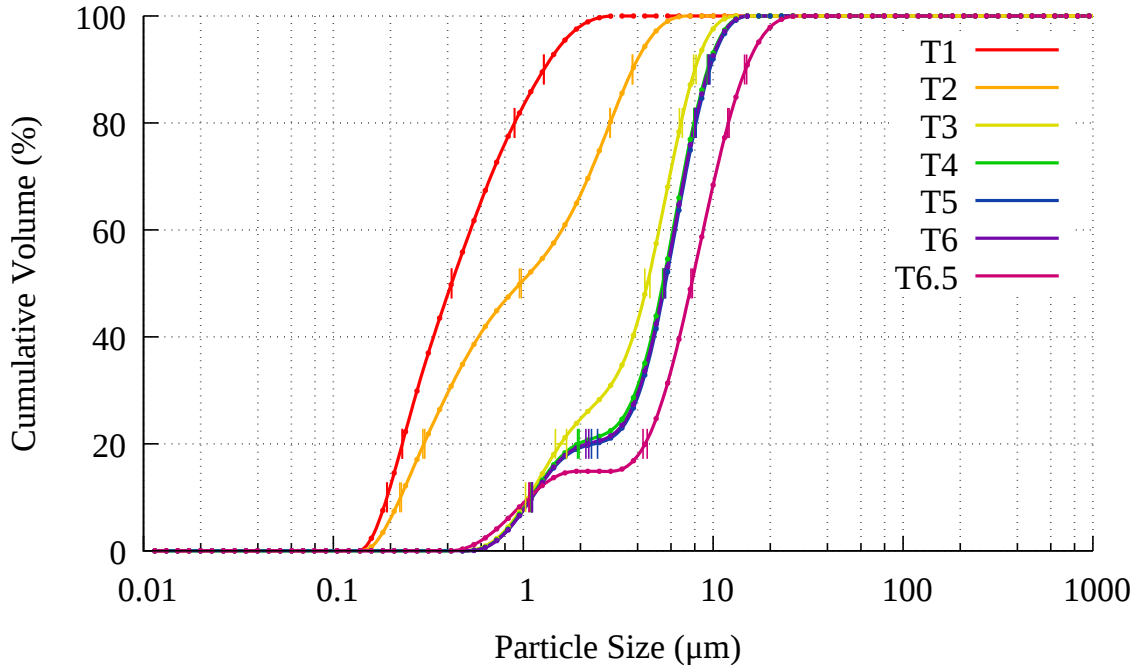

(b) Standard deviation in PSD

Figure 6.31: 90-95°C crystallisation process with a dosage of 315 g NaCl/kg FA added

6.3.2.2 Dosage of 864 g NaCl/kg FA

See section 6.2.2.3.

6.3.2.3 Dosage of 1728 g NaCl/kg FA

The AAS results for the 2 M dosage of NaCl are shown in Figure 6.25; they indicate a drop in the Si and Al content between 2 and 4 hours. This decrease coincides with the disappearance of much of the amorphous material between 2 and 3 hours in SEM images 6.32b and 6.32c. Many of the cubes formed in the SEM images of Figure 6.32 appear to have rounded edges rather than chamfered edges, being less well defined than the cubes in the previous dose of NaCl shown in Figure 6.20. It has not been possible to find literature on crystallisation processes with similarly high NaCl concentrations in order to support or oppose these findings, as literature primarily deals with concentrations similar to that of seawater. It is also noted that many of the cubes intermixed are not cube-shaped. The XRD patterns shown in Figure 6.33 show zeolite A from 3 hours onward. The PSD in Figure 6.34a shows the broad, asymmetric peak showing a d_{50} of around 0.4 μm, and a d_{80} of >0.8 μm. A bimodal distribution as noted in previous experiments is not visible in the 3-6.5 hour measurements, which all show a similar, broad PSD, with 60 % of the particles being between 2 and 6 μm. In the context of an abundance of fine material from the PSD data, followed by a broad PSD with a finer size range than lower dosages of NaCl, this leads to the impression of rapid seeding, followed by limited crystal growth. The crystal growth being limited by a lack of available Si or Al due to the prior rapid seeding. This is further supported by zeolite A cubes visible as early as 2 hours in Figure 6.32b. The yield shown in Figure 6.26 shows no noticeable change from the previous two doses of NaCl, whilst the CEC in Figure 6.27 shows a similar result to the 315 g dosage of NaCl, but a decrease from the 864 g NaCl dosage.

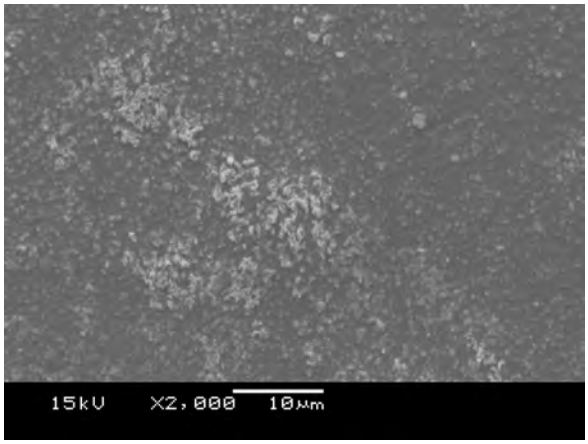

(a) 1 h

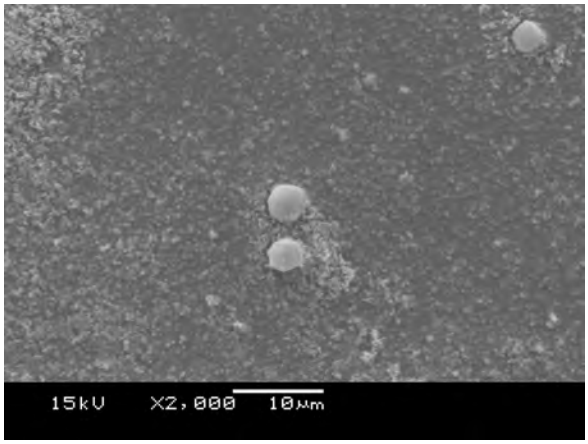

(b) 2 h

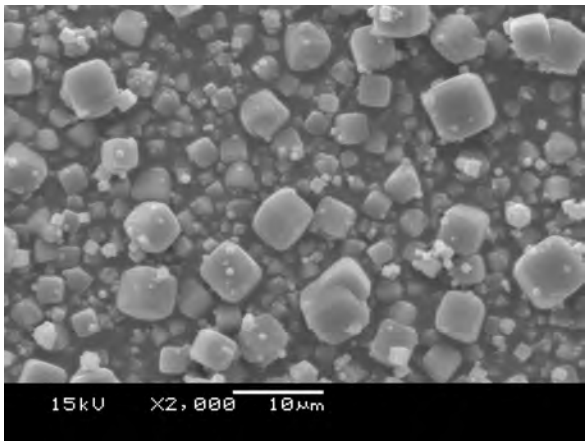

(c) 3 h

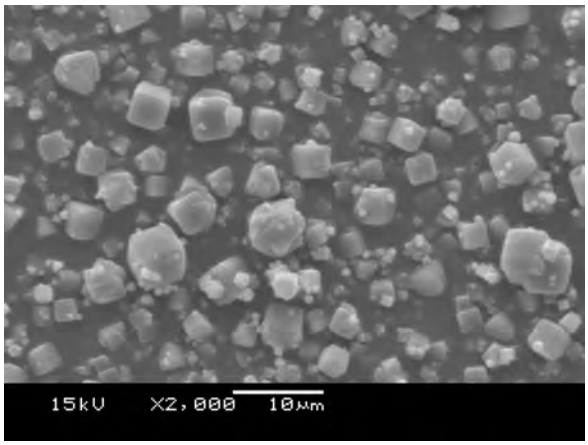

(d) 4 h

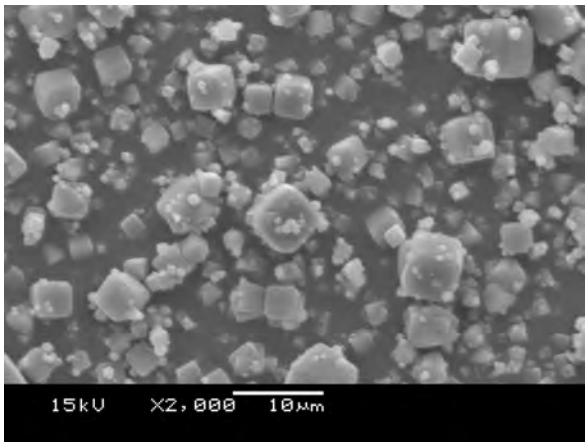

(e) 5 h

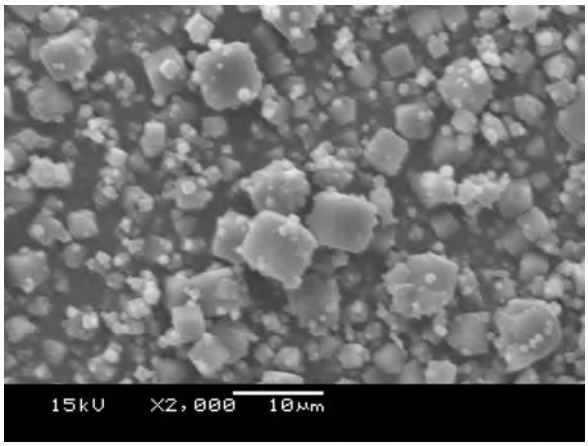

(f) 6 h

Figure 6.32: SEM images of zeolites from ash leachate crystallised with an additional 1728 g of NaCl/kg FA on a stirred hot plate at 90-95°C

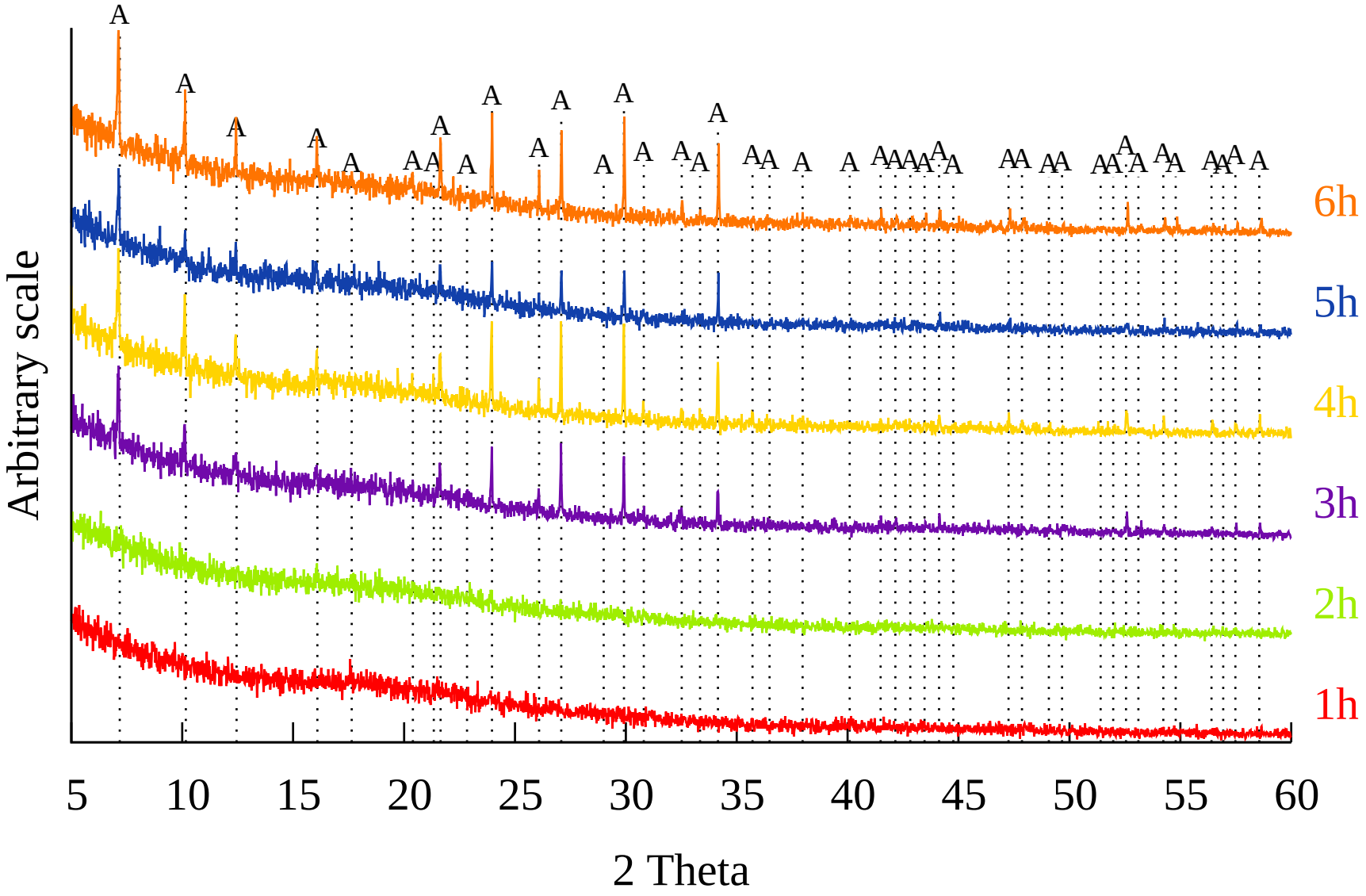

Figure 6.33: XRD patterns of 90-95°C crystallisation with an additional 1728 g NaCl/kg FA. A: Zeolite Na-A. $\lambda = 1.5406$ Å

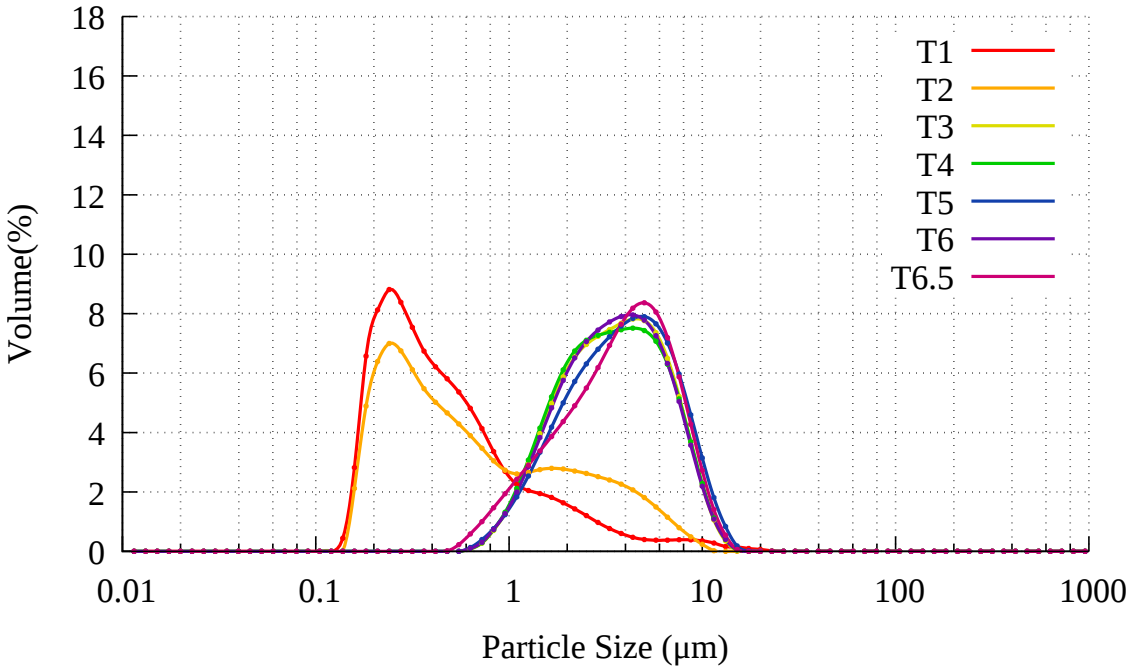

(a) PSD

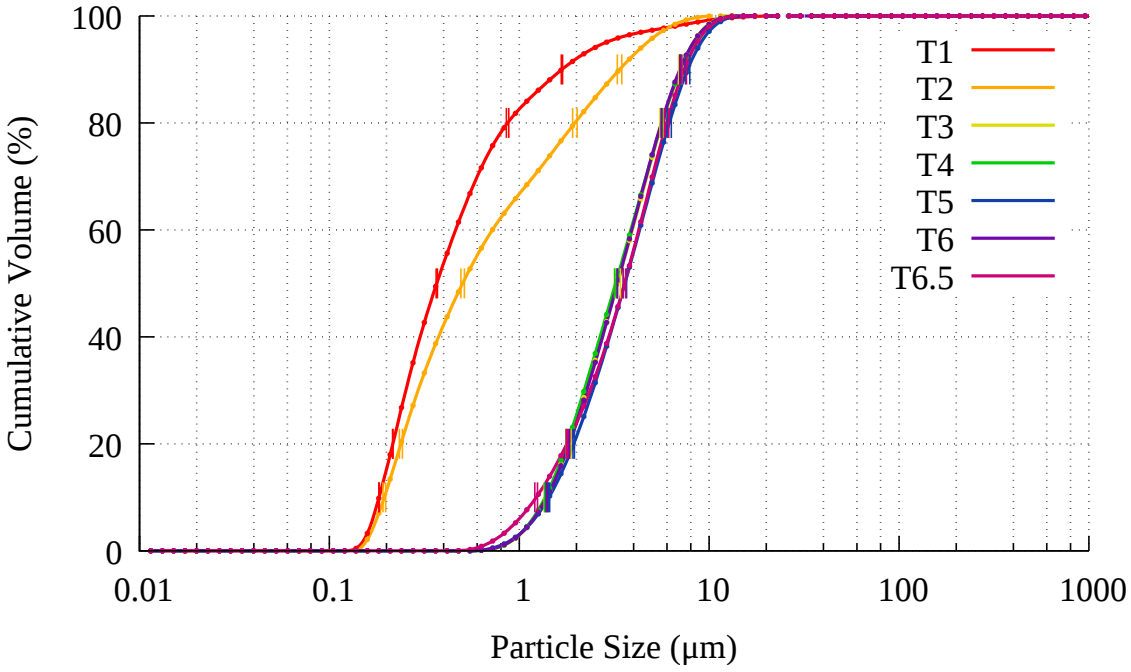

(b) Standard deviation in PSD

Figure 6.34: 90-95°C crystallisation process with 1728 g NaCl/kg FA added

6.3.2.4 Dosage of 3455 g NaCl/kg FA

The AAS in Figure 6.25 shows a decrease in the Si and Al content between 2 and 3 hours. In the SEM images of Figure 6.35 there appear to be few cubes, however sparse cubes are visible, one such is noted in the 1 hour sample in Figure 6.35a. The 2 and 3 hour images of Figures 6.35b and 6.35c appear quite different. The material in the 3 hour Figure 6.35c that is not cube-shaped is significantly coarser than in the 2 hour image. There does not appear to be any change between the 3 hour SEM image and the rest of the SEM images for this dosage of NaCl. The XRD patttern shown in Figure 6.36 shows some weak peaks at 3, 4 and 5 hours, but these are so weak as to be easily lost in the pattern noise. These samples show poor crystallinity. The PSD of Figure 6.37a shows the broad, asymmetric peak for the first hour, with >50 % of the particles being smaller than 0.6 μm. The 3-6.5 hour PSD are all similar in shape, being roughly symmetrical distributions with a d_{50} around 2 μm. The yield in Figure 6.26 shows a decrease compared to previous dosages of NaCl and the control experiment, and Figure 6.27 shows lowest CEC of all NaCl experiments, hence these conditions are the least favourable for zeolite synthesis.

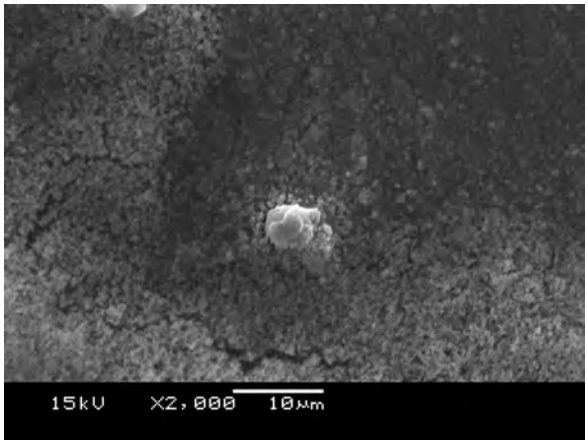

(a) 1 h

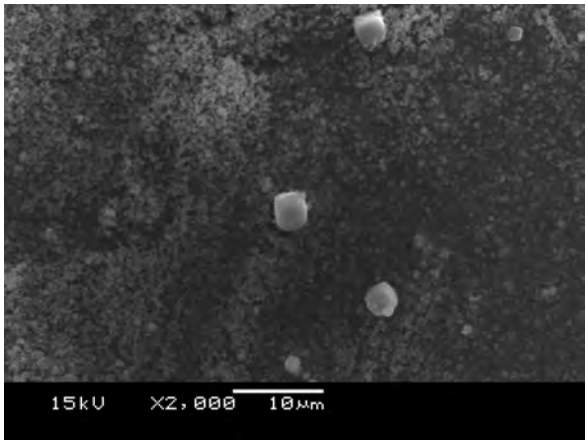

(b) 2 h

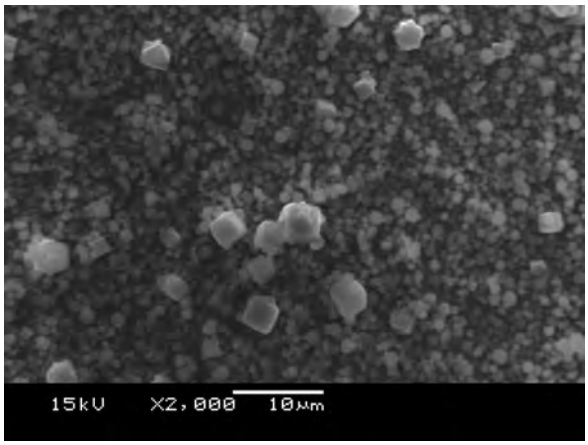

(c) 3 h

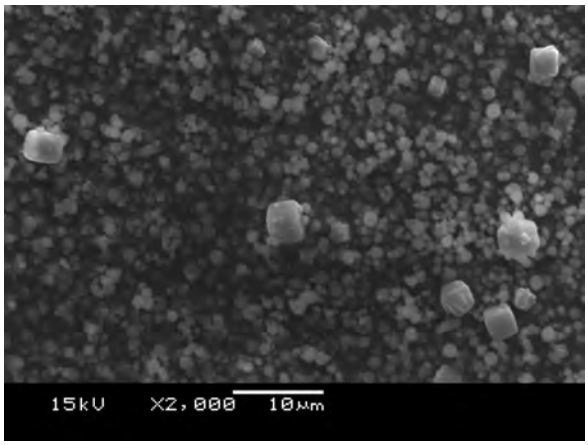

(d) 4 h

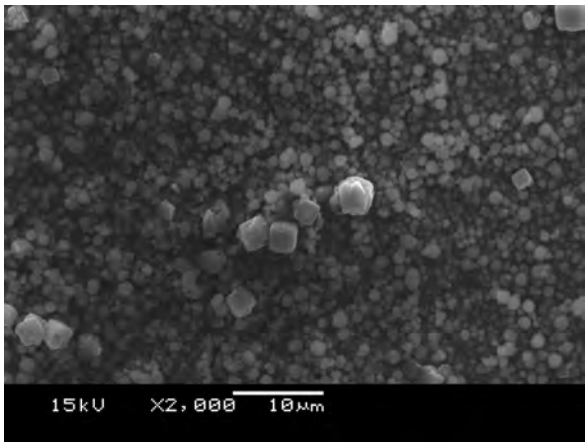

(e) 5 h

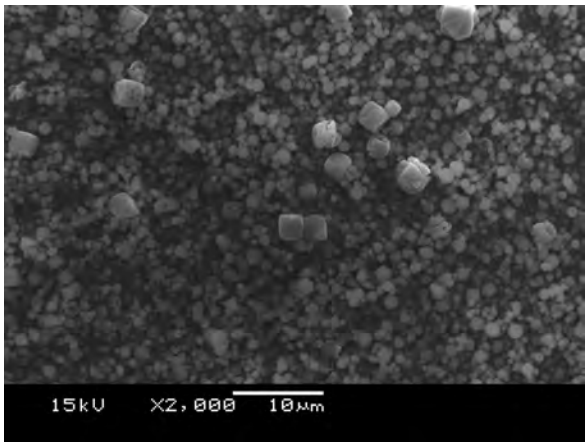

(f) 6 h

Figure 6.35: SEM images of zeolites from ash leachate crystallised with an additional 3455 g of NaCl/kg FA on a stirred hot plate at 90-95°C

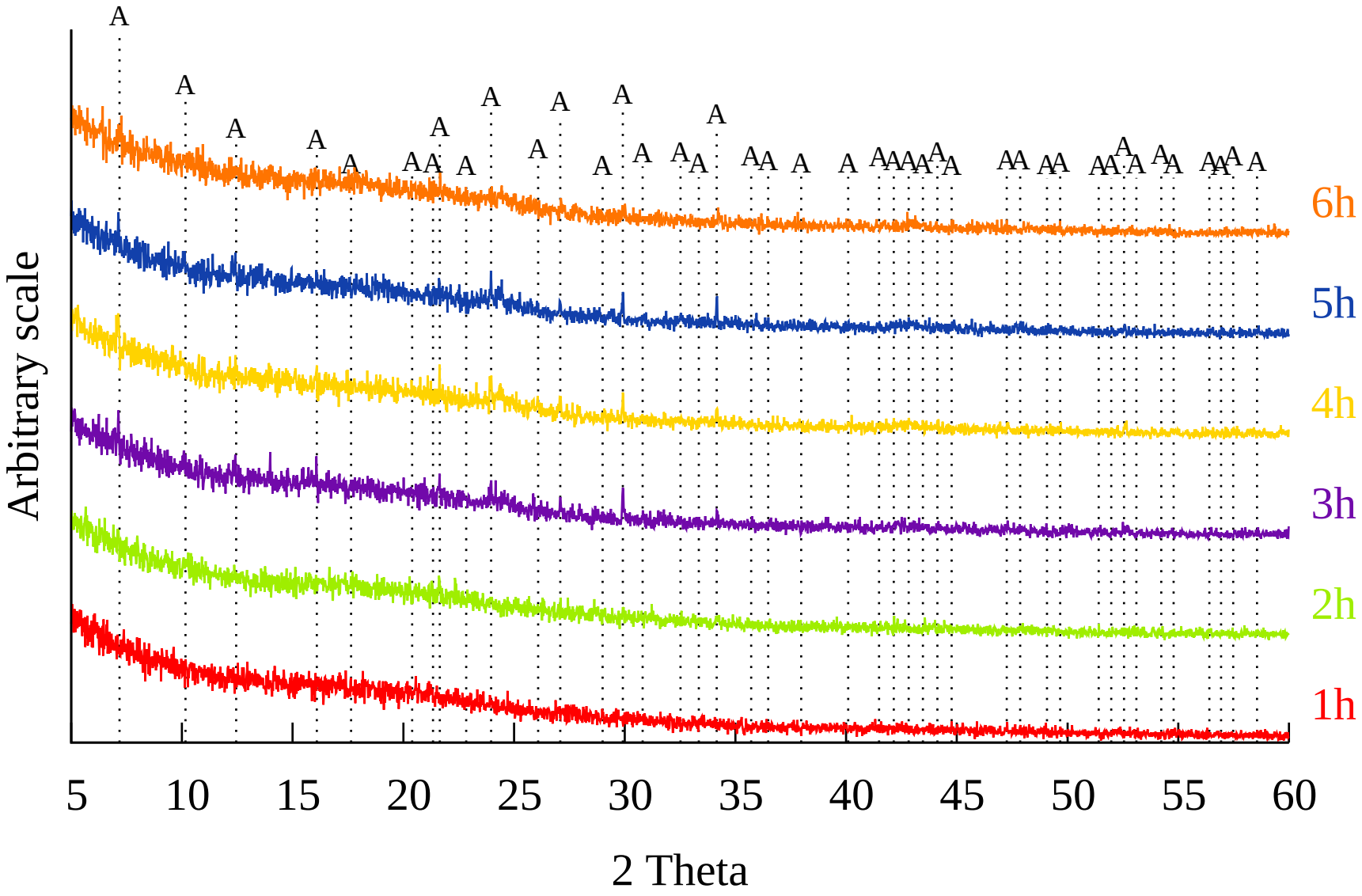

Figure 6.36: XRD patterns of 90-95°C crystallisation with an additional 3455 g NaCl/kg FA. A: Zeolite Na-A. $\lambda = 1.5406$ Å

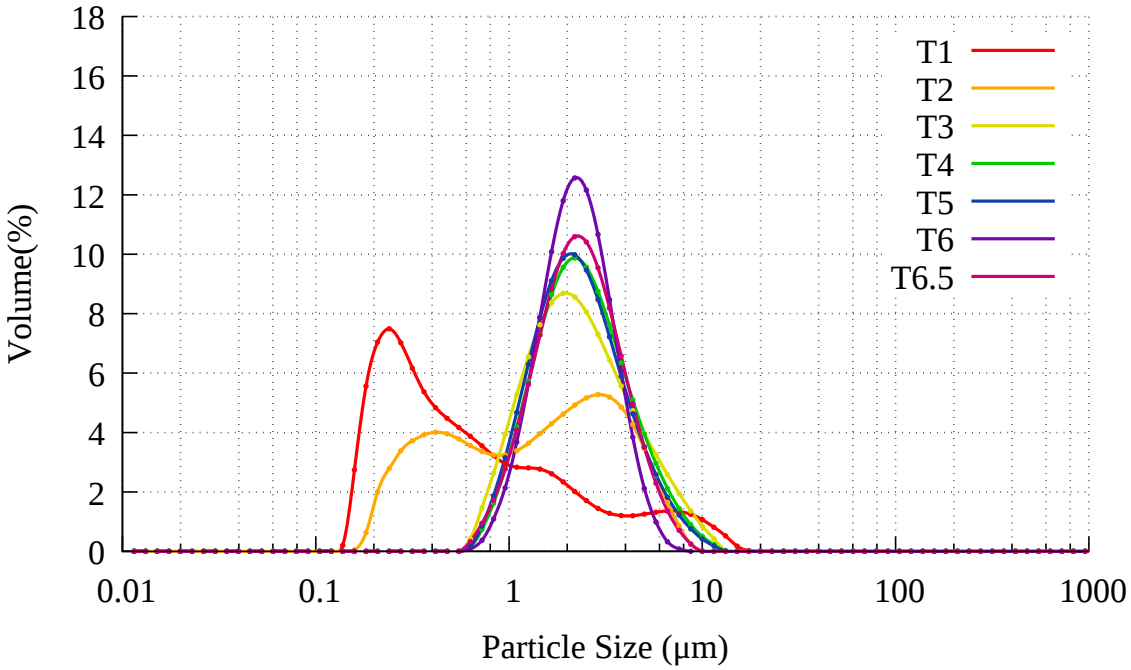

(a) PSD

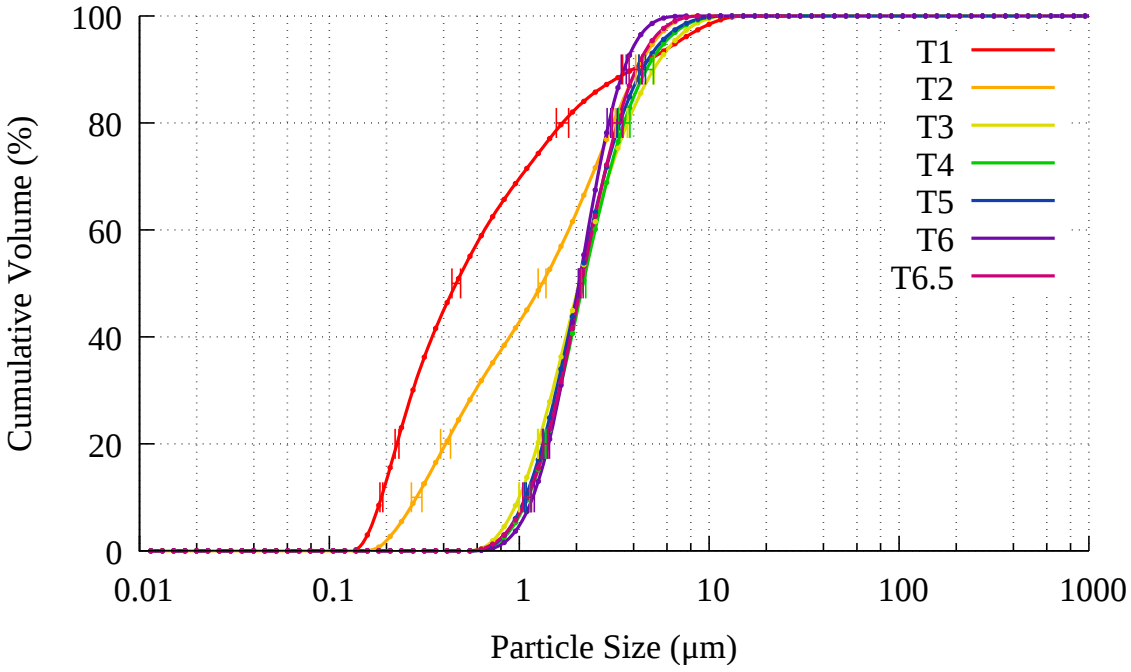

(b) Standard deviation in PSD

Figure 6.37: 90-95°C crystallisation process with 3455 g NaCl/kg FA added

6.3.2.5 Trends

The AAS results in Figure 6.25 show an increasing quantity of Si and Al consumed in the first hour as NaCl dosage increases, as well as leaving the final quantity of Si and Al in solution lower than in the control experiment. Despite this high consumption of both Si and Al, the 3455 g NaCl/kg FA dosage has the lowest yield, even compared to the control experiment. This low yield could be attributed to the fine particles (shown in Figure 6.37a) passing through the sintered glass filter, which was a 25-50 μm filter. The lack of crystallinity and low yield in the experiment with 3455 g NaCl/kg FA could be explained by the high dosage of NaCl causing much of the available Si and Al to be consumed within the first hour in the formation of zeolite nuclei, leaving little Si and Al in solution for crystalline growth after 2 hours. Parallels can be drawn between this process and the Bayer process used for refining bauxite. The Bayer process is also highly alkaline, with a high ionic strength. Al-bearing minerals are dissolved from the bauxite using a hot NaOH solution. Undissolved materials are removed via settling or filtration to give an Al rich solution. From this solution $Al(OH)_3$ is precipitated by cooling the solution and seeding it with $Al(OH)_3$. The extraction solution can then be recycled, and the $Al(OH)_3$ can then be washed and calcined to produce Al_2O_3 [143].

Figures 6.38 and 6.39 show the 6 and 6.5 hour PSD measurements for increasing quantities of NaCl. These show that as NaCl content increases, the peaks shift to the left, indicating finer particles. This is notable in Figure 6.39b, where the d_{50} changes from ~11 μm in the control experiment, to 8, 5, 4 and 2 μm, as NaCl dosage increases. As NaCl increases, seeding is increased. With an increasing supply of seeds which grow evenly as the experiment progresses, the size of each particle decreases as the limited supply of Si and Al is spread between an increasing quantity of seeds. As the NaCl dosage increases, the initial concentration of seeds increases, consuming enough of the available Si and Al to leave a solution too poor in Si and Al to enable the seeds to grow, resulting in a final product which is mostly zeolite seeds. This is supported by a decreasing CEC yield in Figure 6.28, where the CEC yield increases from the control to its apex at 864 g NaCl/kg

FA, and then decreases. Experiments were conducted where experiments were seeded with zeolite A at the start of the experiment, however the yields were not noted to have improved and such experiments were omitted.

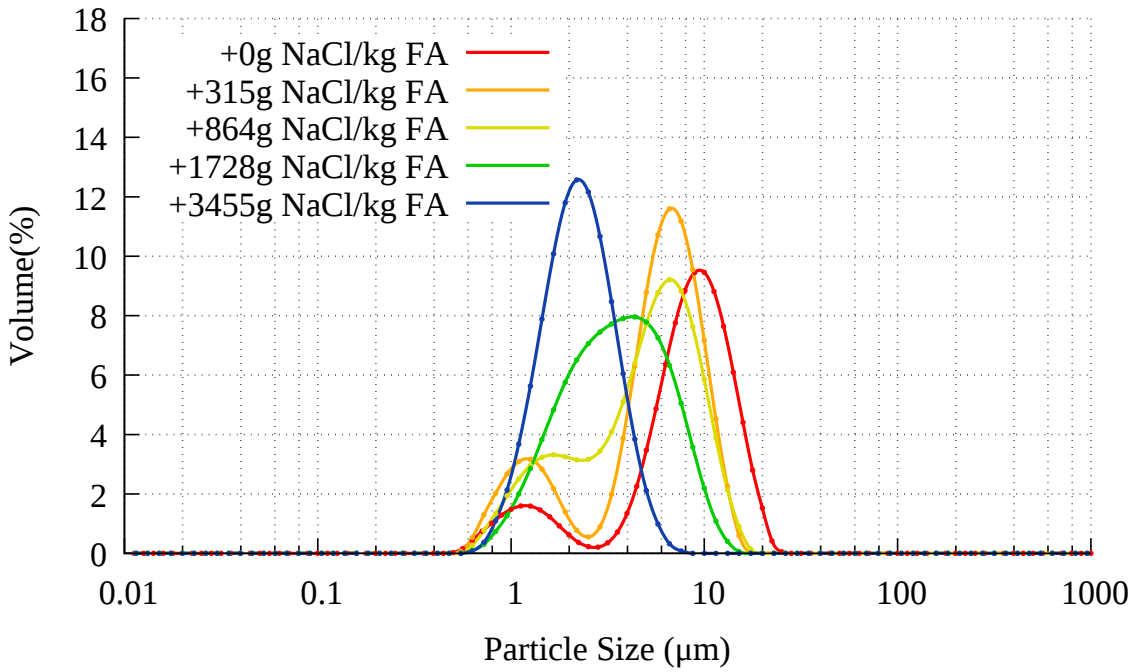

(a) PSD

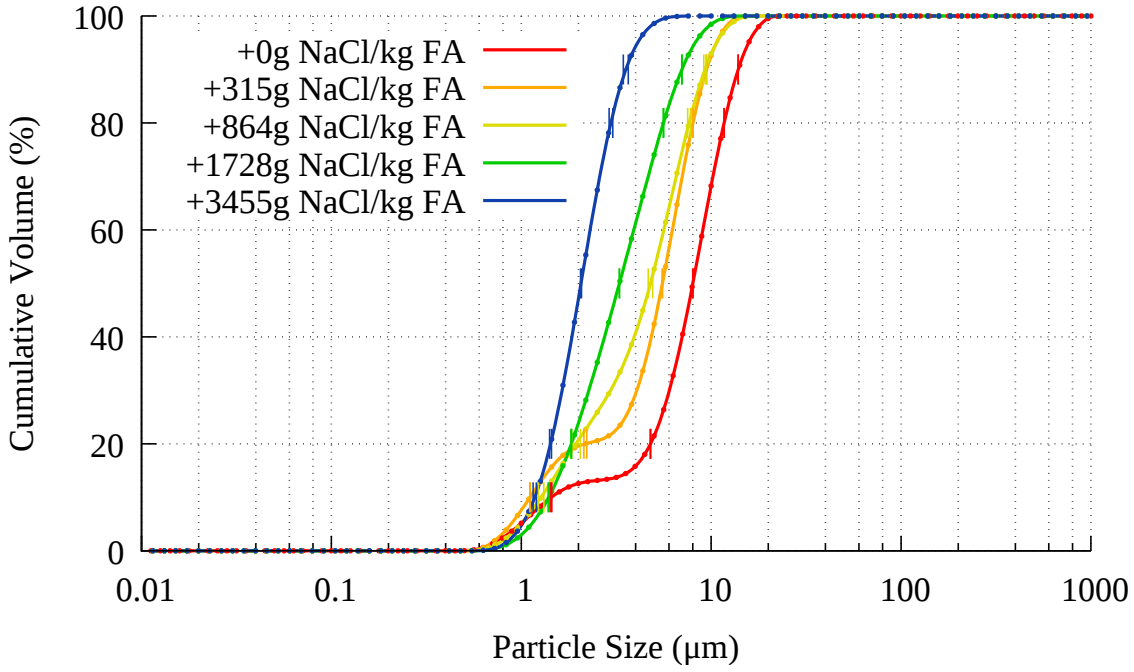

(b) Standard deviation in PSD

Figure 6.38: 90-95°C crystallisation process with added Na^+ at 6 hours

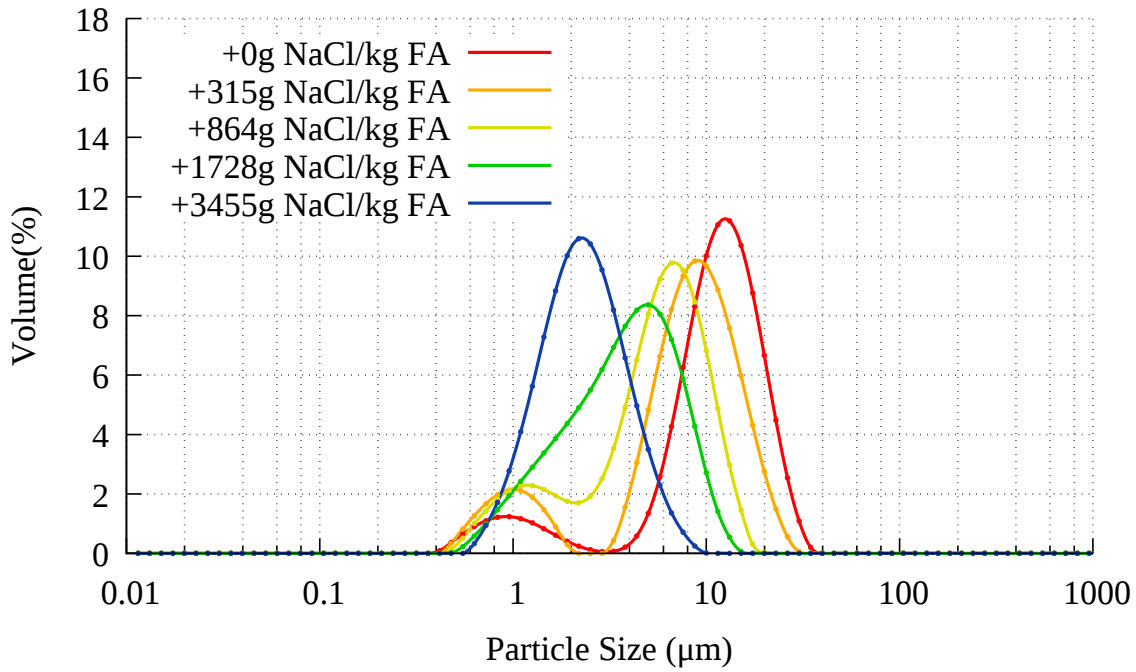

(a) PSD

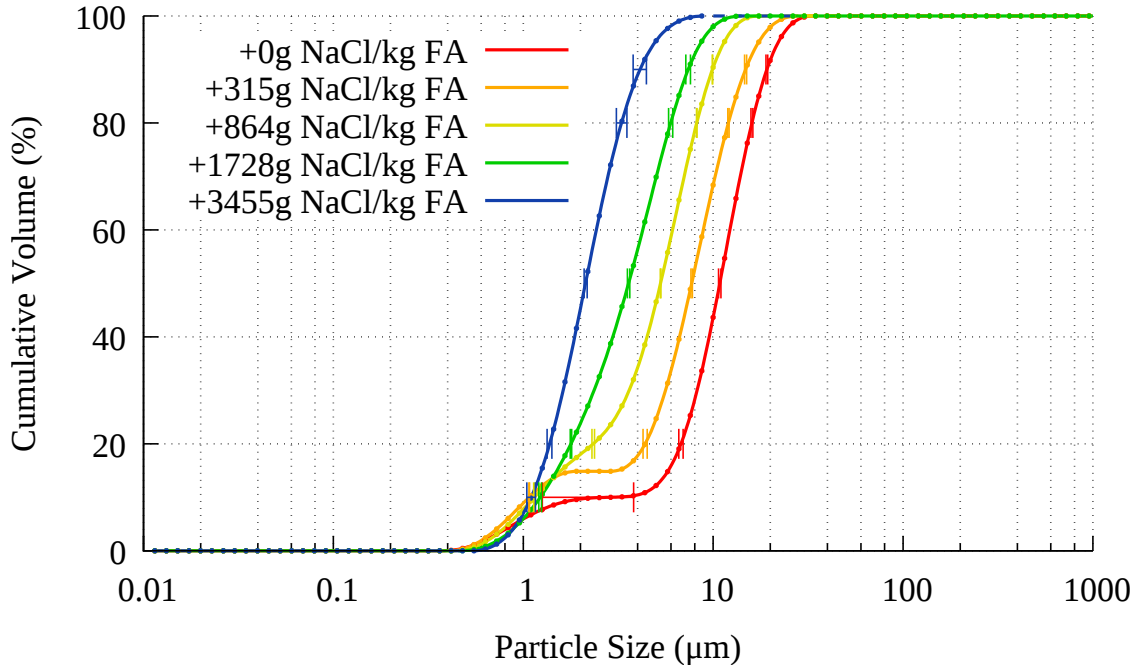

(b) Standard deviation in PSD

Figure 6.39: 90-95°C crystallisation process with added Na^+ at 6.5 hours

6.4 Increasing Sodium Aluminate with a Constant Dosage of NaCl

The effect of varied NaCl addition to a constant sodium aluminate content was explored in section 6.3. In this section, varied sodium aluminate content is explored with a constant addition of 2 M NaCl, equal to 1728 g NaCl/kg FA. The experimental method used follows the method described in section 6.1, replacing the 1 mole of NaOH with 2 moles of NaCl. Three quantities of sodium aluminate were used: 177, 222 and 266 g/kg FA.

6.4.1 Results

6.4.1.1 Dosage of 177 g SA/kg FA

The AAS data in Figure 6.40 shows a decrease in Si and Al between 3 and 4 hours. This decrease is steeper and sooner than the similar drop in Si and Al seen for the 177 g SA/kg FA experiment in Figure 5.32. The consumption of Si and Al within the first hour is greater in Figure 6.40 than in Figure 5.32. This is followed by a lower final level of Si and Al in hours 4-6.5. The disparity in the size of the decrease between Si and Al can be attributed to variations in the equilibria between Si and Al in gel, solution and zeolite, as described by Cundy and Cox [60]. The Al content at 6.5 hours is lower for the 177 g SA/kg FA experiment due to the lower value of Al at 0 hours when compared to the two 266 g SA/kg FA experiments.

SEM images in Figure 6.44 show cubes forming from 3 hours, with the amorphous material no longer present at 4 hours. For comparison, Figure 5.42 shows cubes first appearing at 4 hours, with amorphous material gone by 6 hours. The cubes from 4-6 hours in Figure 6.44 appear very similar; few large cubes with abundant small cubes. The XRD of Figure 6.45 shows that zeolite A is detected from 3 hours. The PSD in Figure 6.46 shows a d_{50} of 0.4 μm for the first 2 hours, followed by a d_{50} of 3-3.6 for 3-6 hours. In comparison, Figure 5.44 shows a d_{50} of 0.4-0.7 μm for the first 3 hours, then a d_{50} of 4.0-7.4 μm for 4-6 hours.

The yield is also increased, as shown in Figure 6.41. Without the addition of NaCl, 60 % of the particles are within 4-11 μm at 6 hours, with the NaCl, 60 % of particles are within 2-6 μm. This indicates that the addition of 2 moles of NaCl encourages nucleation for the first 2 hours, and then crystallisation in the following hour, increases Si and Al consumption to produce a higher yield with a lower particle size. The CEC is however reduced from the experiments with no added NaCl, as shown in Figure 6.42.

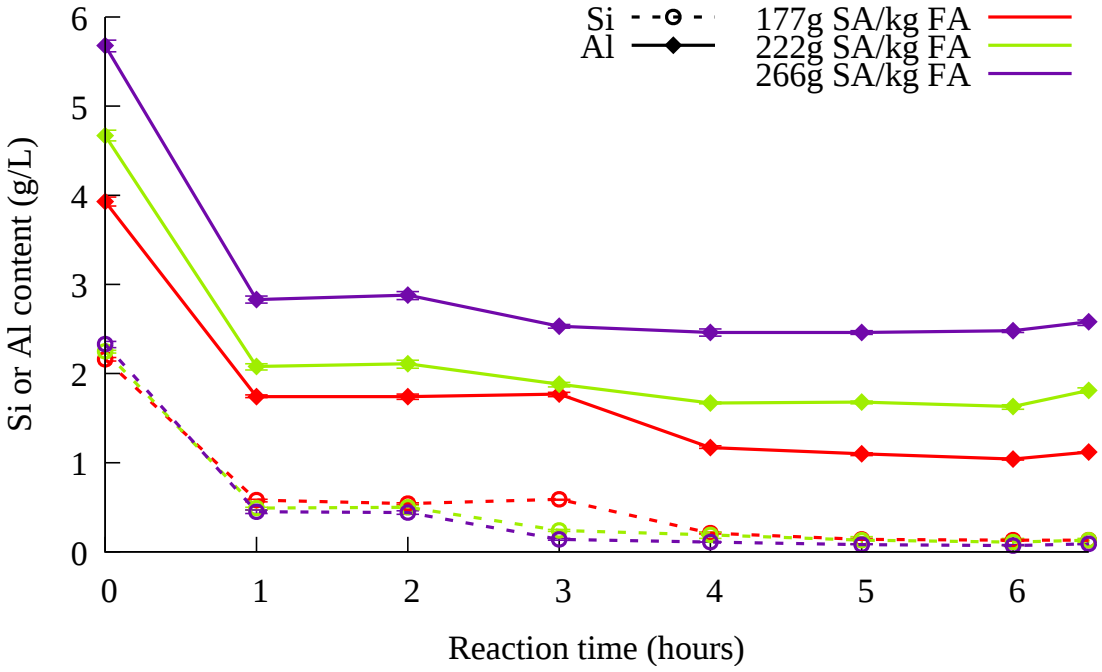

Figure 6.40: AAS results for 90-95°C crystallisation process with 1728 g NaCl and increasing varied sodium aluminate

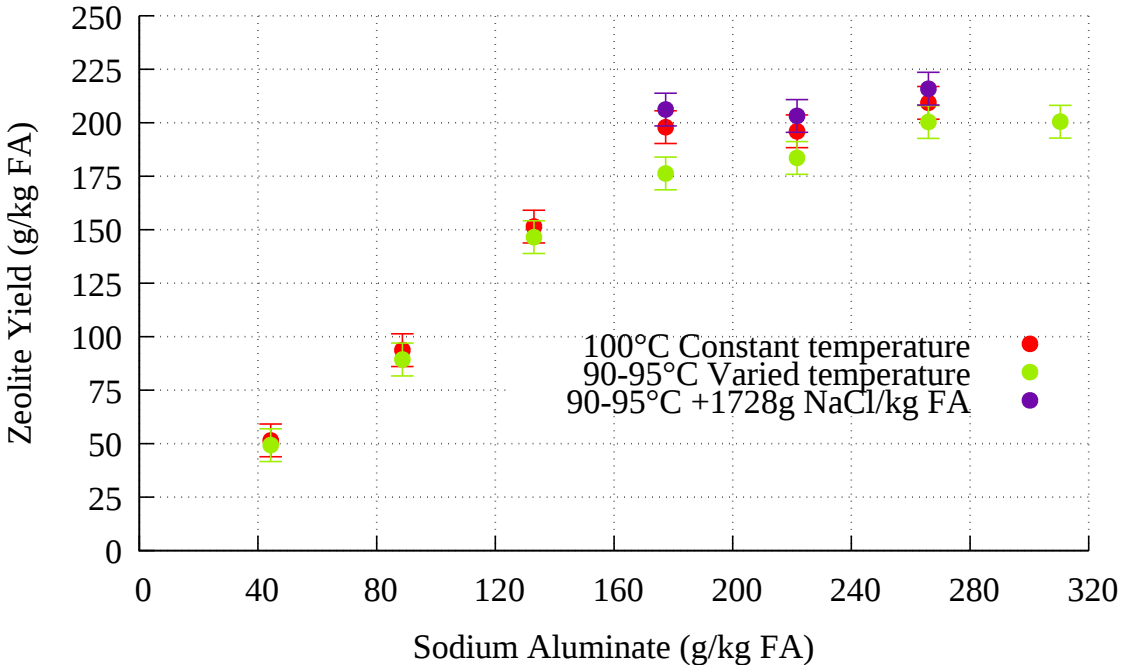

Figure 6.41: Yield results for 90-95°C crystallisation process with 1728 g NaCl and increasing varied sodium aluminate. Experiments with low dosages of sodium aluminate (<222 g SA/kg FA) omitted for brevity. Previous results from sections 5.3 and 5.4 included for context

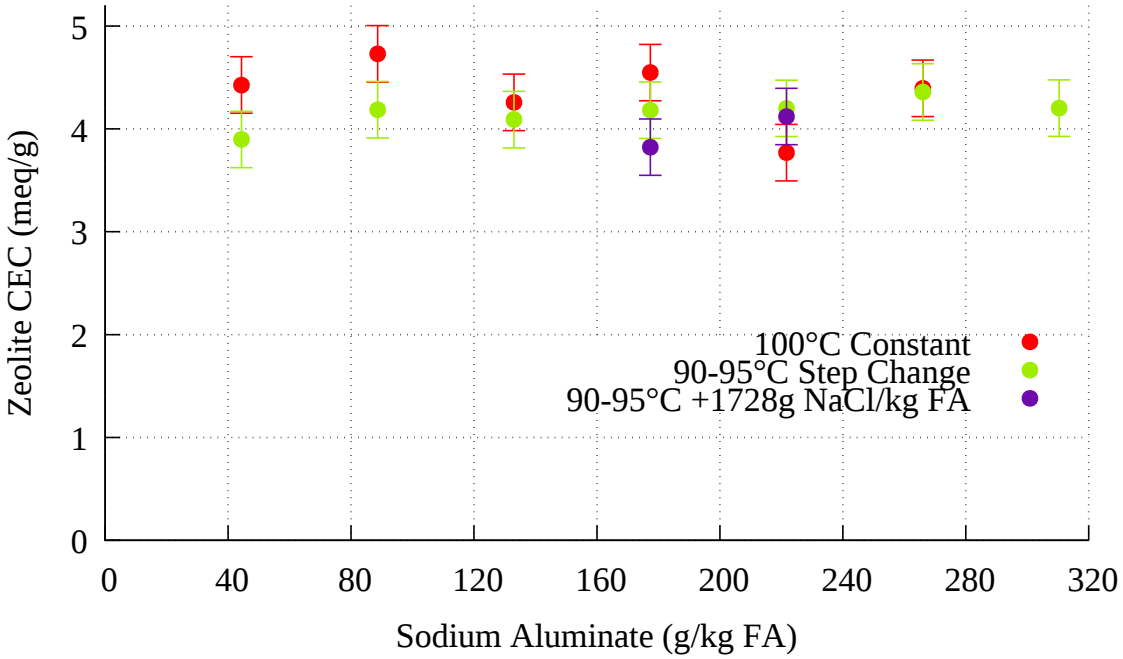

Figure 6.42: CEC results for 90-95°C crystallisation process with 1728 g NaCl and increasing varied sodium aluminate. Previous results from sections 5.3 and 5.4 included for context

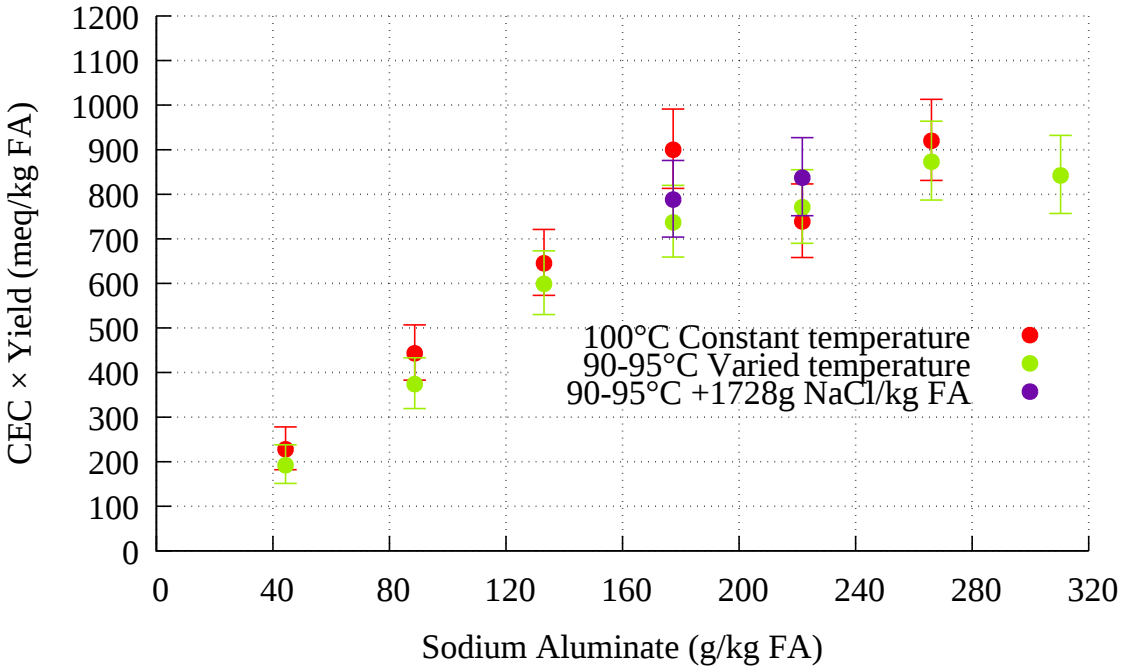

Figure 6.43: CEC × yield results for 90-95°C crystallisation process with 1728 g NaCl and increasing varied sodium aluminate. Previous results from sections 5.3 and 5.4 included for context

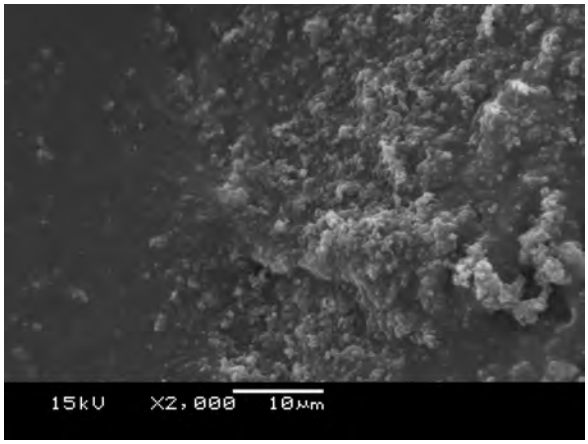

(a) 1 h

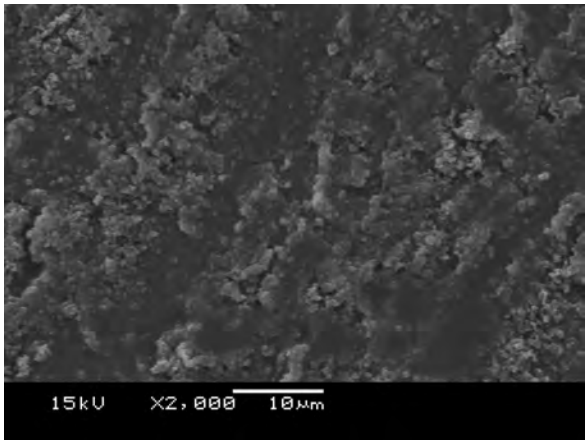

(b) 2 h

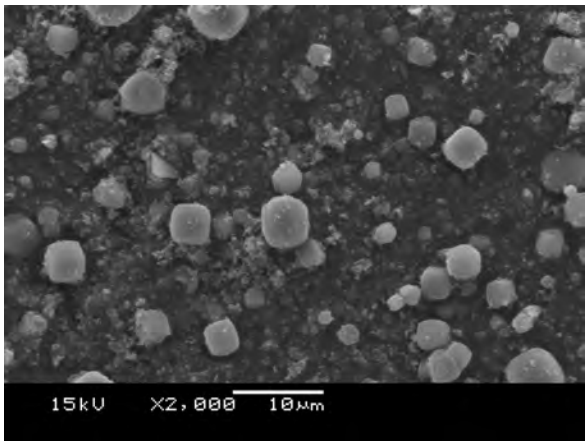

(c) 3 h

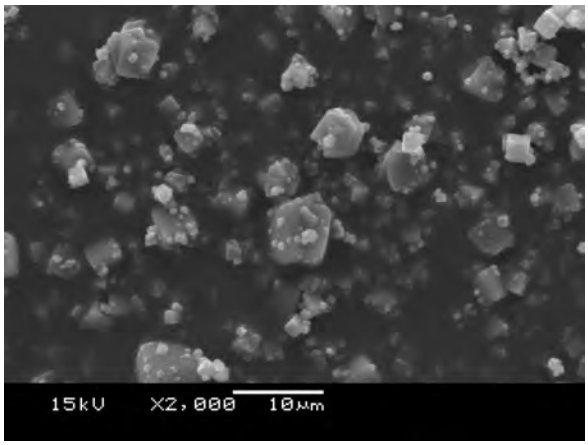

(d) 4 h

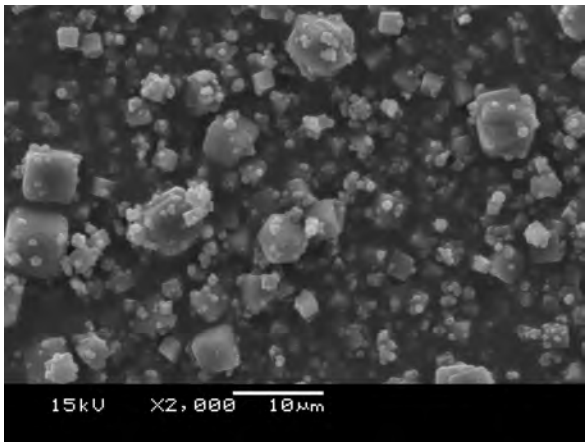

(e) 5 h

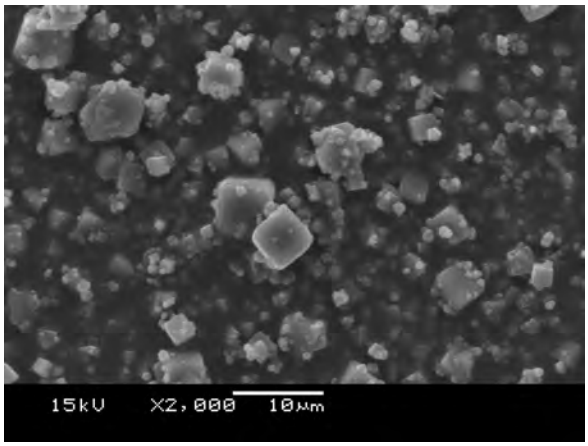

(f) 6 h

Figure 6.44: SEM images of zeolites from ash leachate crystallised with 1728 g of NaCl/kg FA and 177 g SA/kg FA on a stirred hot plate at 90-95°C

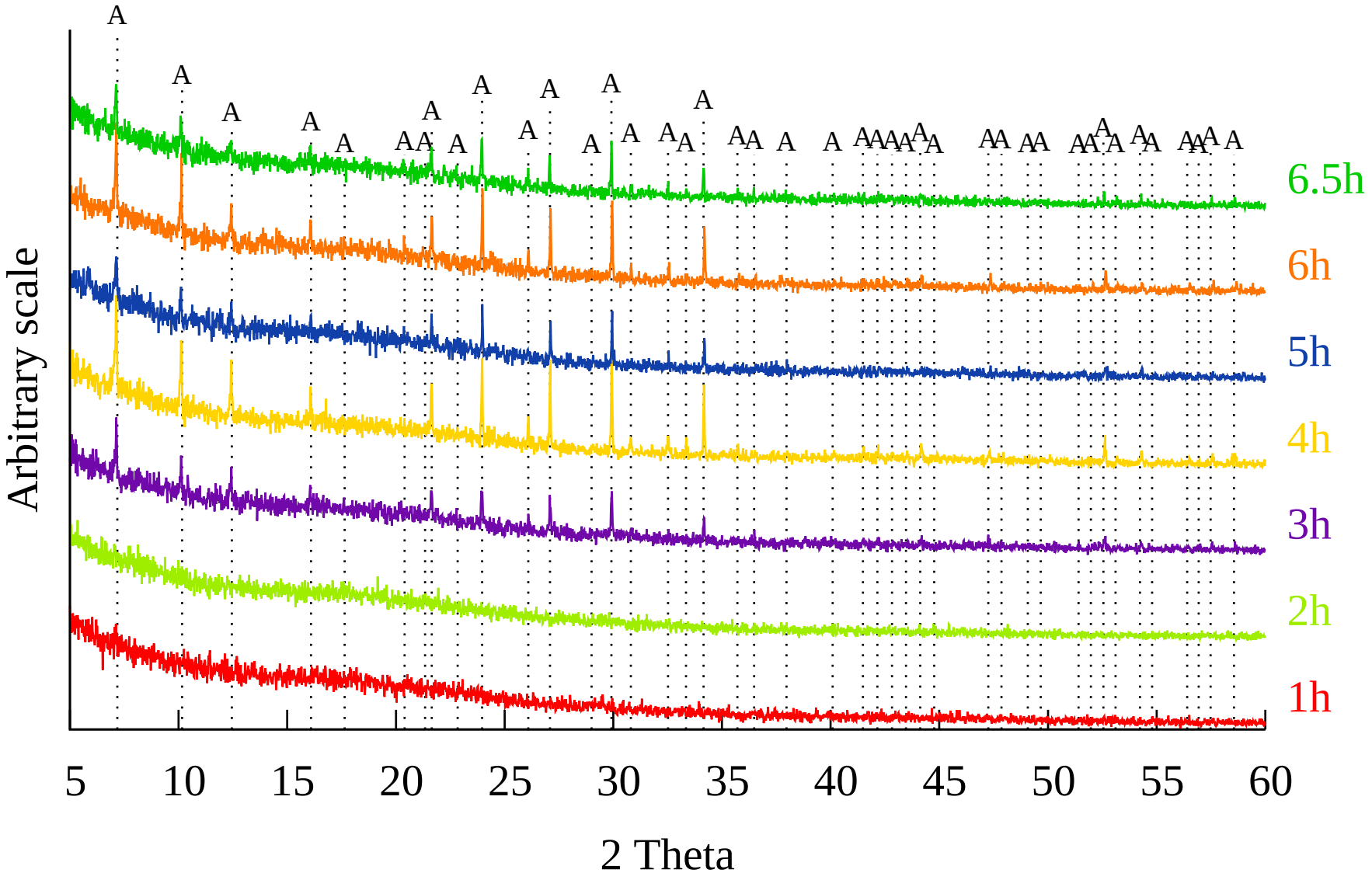

Figure 6.45: XRD patterns of 90-95°C crystallisation with 1728 g of NaCl/kg FA and 177 g SA/kg FA. A: Zeolite Na-A. $\lambda = 1.5406$ Å

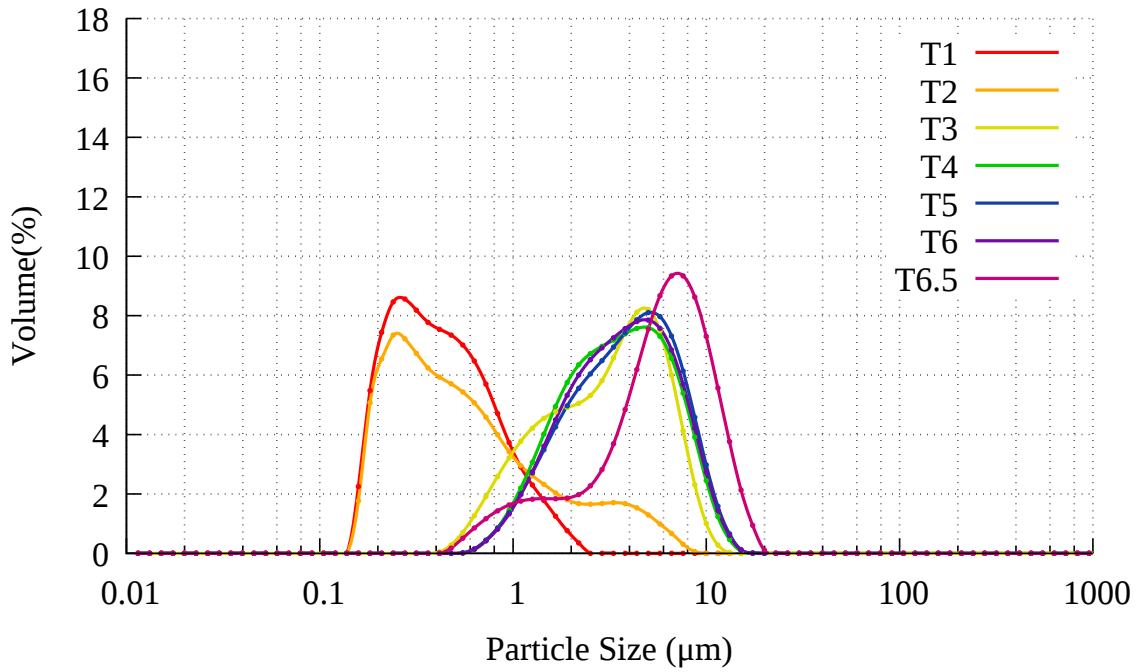

(a) PSD

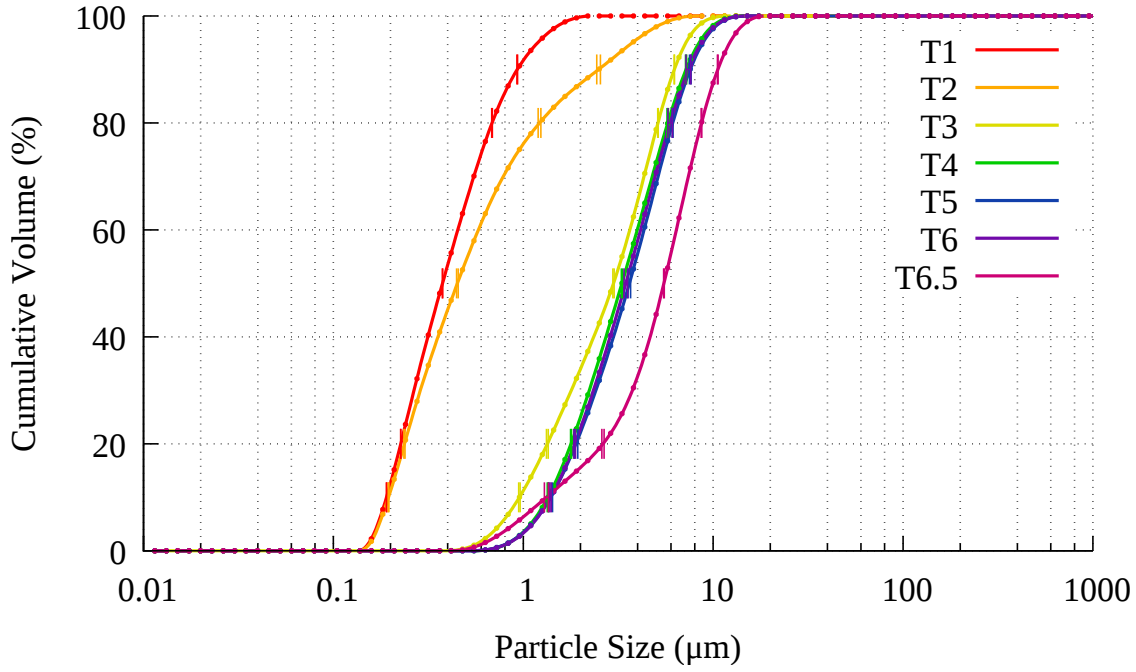

(b) Standard deviation in PSD

Figure 6.46: 90-95°C crystallisation process 1728 g of NaCl/kg FA and 177 g SA/kg FA

6.4.1.2 Dosage of 222 g SA/kg FA

See section 6.3.2.3.

6.4.1.3 Dosage of 266 g SA/kg FA

The AAS results presented in Figure 6.40 show a drop in Si and Al content between 2 and 3 hours. As with other sodium aluminate dosages in this experiment, this is preceeded and followed by steady levels of Si and Al. In comparison, the AAS results with no added NaCl shown in Figure 5.32 show a drop between hours 3 and 4. The decrease between 2 and 3 hours coincides with the decrease in amorphous material present between SEM images 6.47b and 6.47c. The cubes formed in hours 4-6 of Figure 6.47 appear to have more rounded edges, and are richer in fine particles than the same experiment without NaCl, shown in Figure 5.48.

The XRD patterns shown in Figure 6.48 show zeolite A detected from 3 hours. The PSD in Figure 6.49a shows particles >10 μm present within the first hour. This is probably due to the agglomerated sample being improperly dispersed prior to analysis, as no such reading is present at 2 hours. The PSD for 3-6 hours are very similar, with a d_{50} of 3.0 μm as shown by Figure 6.49b, whereas the d_{50} for the same experiment without added NaCl has a d_{50} of 5.5-5.6 for 4-6 hours, as shown in Figure 5.50b. As with previous dosages of sodium aluminate, this demonstrates an increase in yield, sooner, with finer particle size.

The particle size produced was of such a fineness that it was not possible to conduct a CEC test. The method for the CEC test requires excess sodium acetate to be washed from a 2 g zeolite sample that has been mixed with sodium acetate for 20 minutes. The sample is washed by filtering the zeolite from the sample using a 25-50 μm sintered glass Büchner funnel, and then further washing through with distilled water. In the filtration and washing process, the entirety of the 2 g sample passes through the filter. Separation of the zeolite from the crystallisation solution at the end of production is believed to have been possible through entrainment of zeolite particles with other zeolite particles due to the larger quantity of zeolite present. However, the yield value for this experiment is

considered unreliable due to the filtration method.

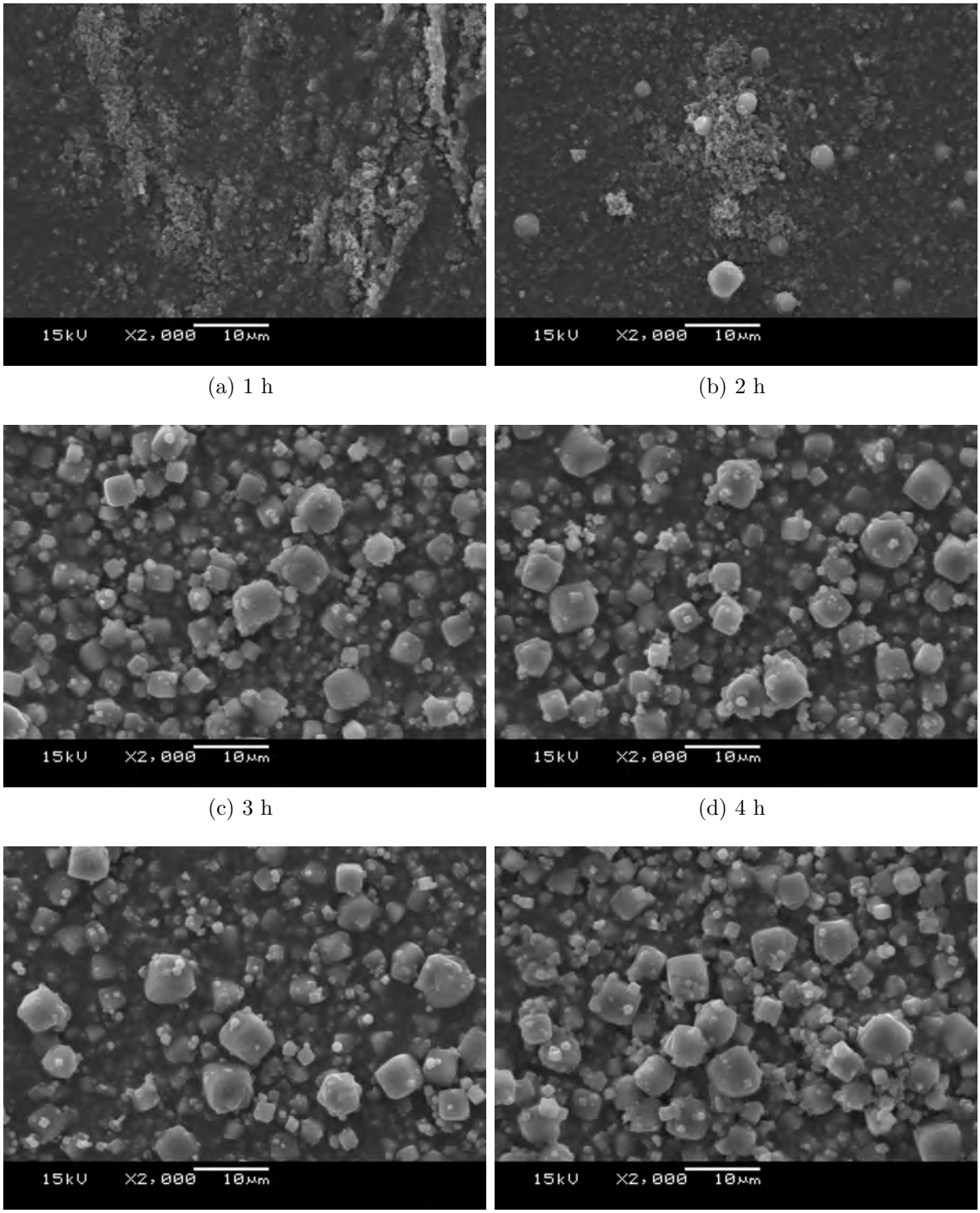

(a) 1 h (b) 2 h

(c) 3 h (d) 4 h

(e) 5 h (f) 6 h

Figure 6.47: SEM images of zeolites from ash leachate crystallised with 1728 g of NaCl/kg FA and 266 g SA/kg FA on a stirred hot plate at 90-95°C

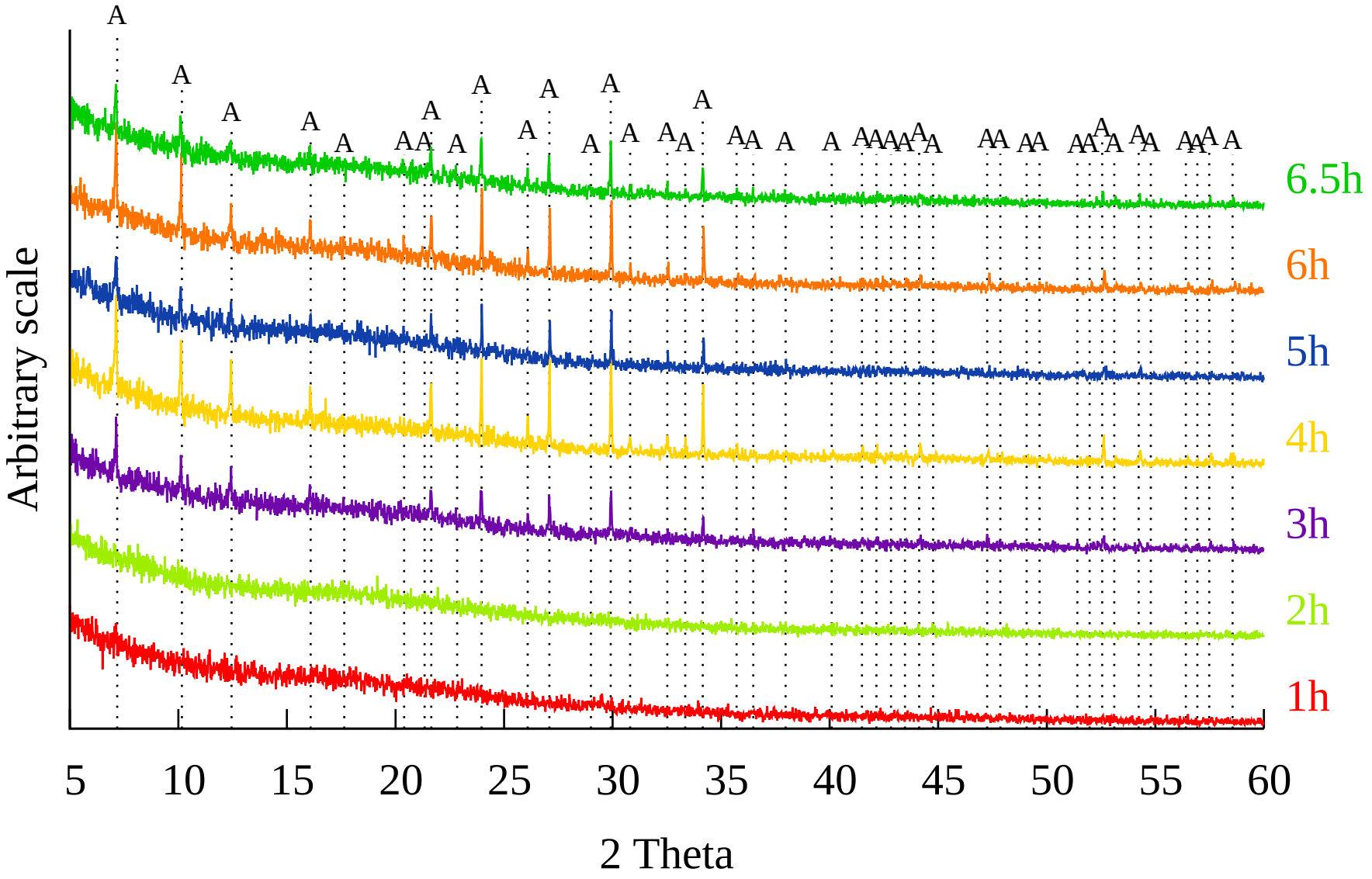

Figure 6.48: XRD patterns of 90-95°C crystallisation with 1728 g of NaCl/kg FA and 266 g SA/kg FA. A: Zeolite Na-A. $\lambda = 1.5406$ Å

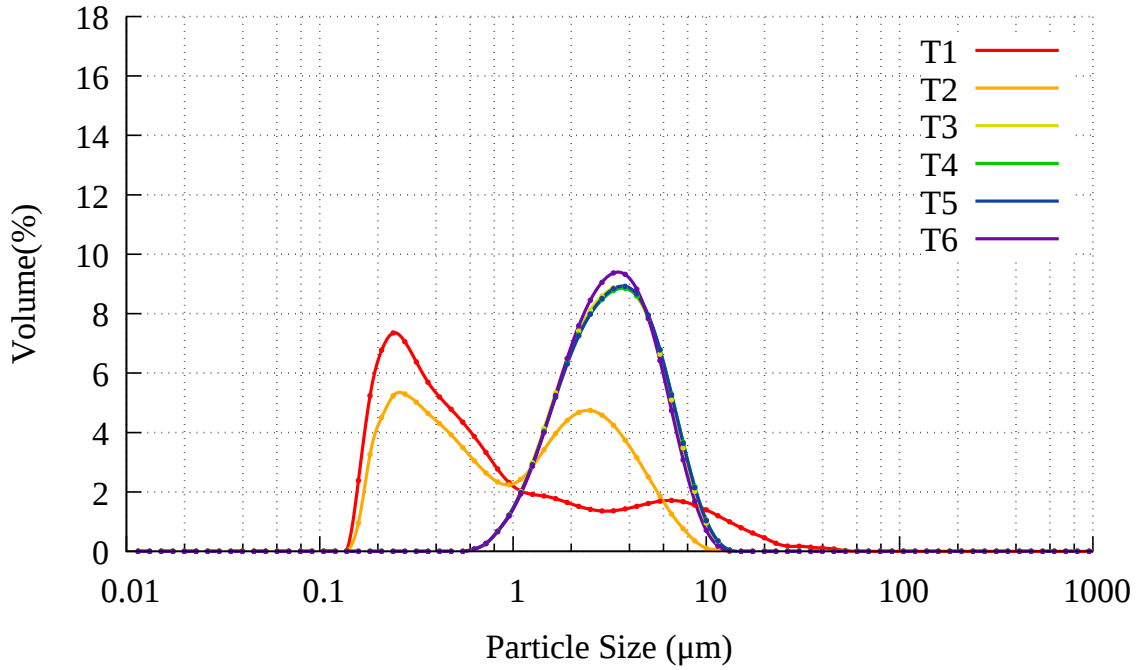

(a) PSD

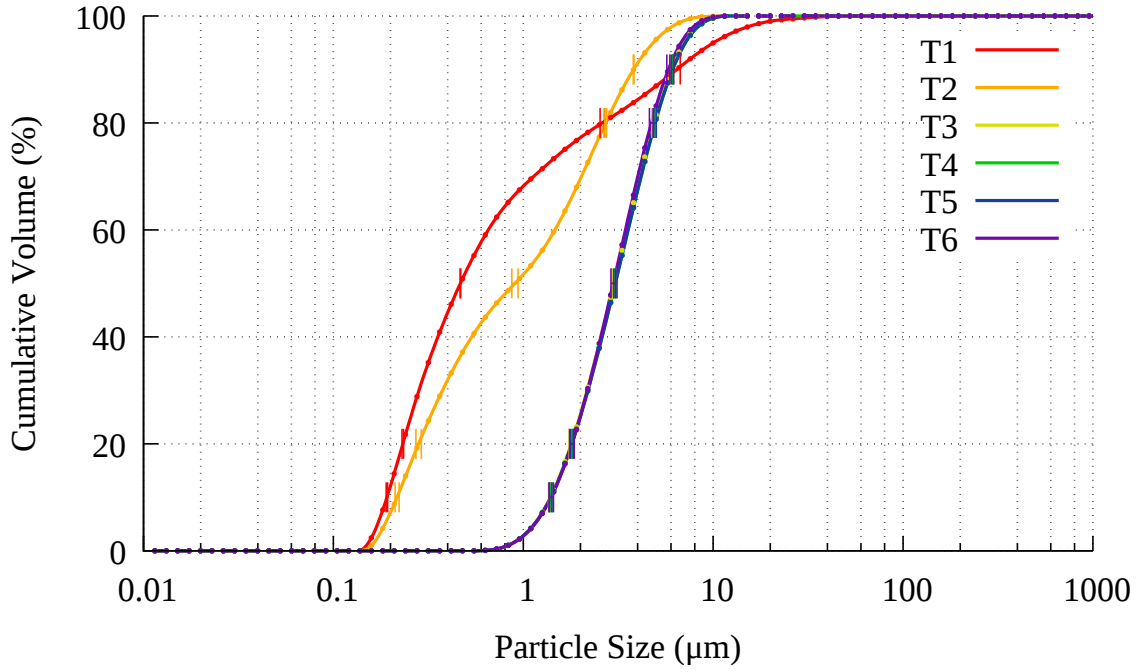

(b) Standard deviation in PSD

Figure 6.49: 90-95°C crystallisation process 1728 g of NaCl/kg FA and 266 g SA/kg FA

6.4.1.4 Trends

The PSDs shown in Figure 6.50 are quite similar, demonstrating a fine particle size, as the d_{90} ranges from 7.4 to 5.8 μm. Whilst the CEC shown in Figure 6.42 indicates that addition of NaCl at this concentration decreases the CEC, the yield shown in Figure 6.41 is improved to such an extent that the yield of CEC in Figure 6.43 supports adding NaCl.

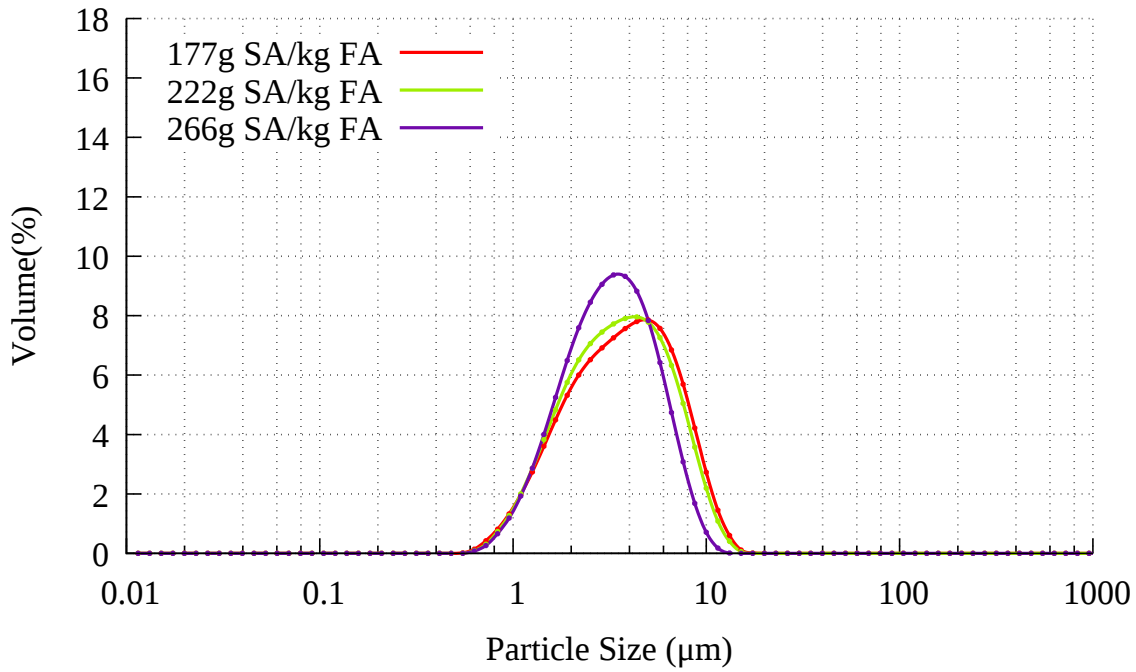

(a) PSD

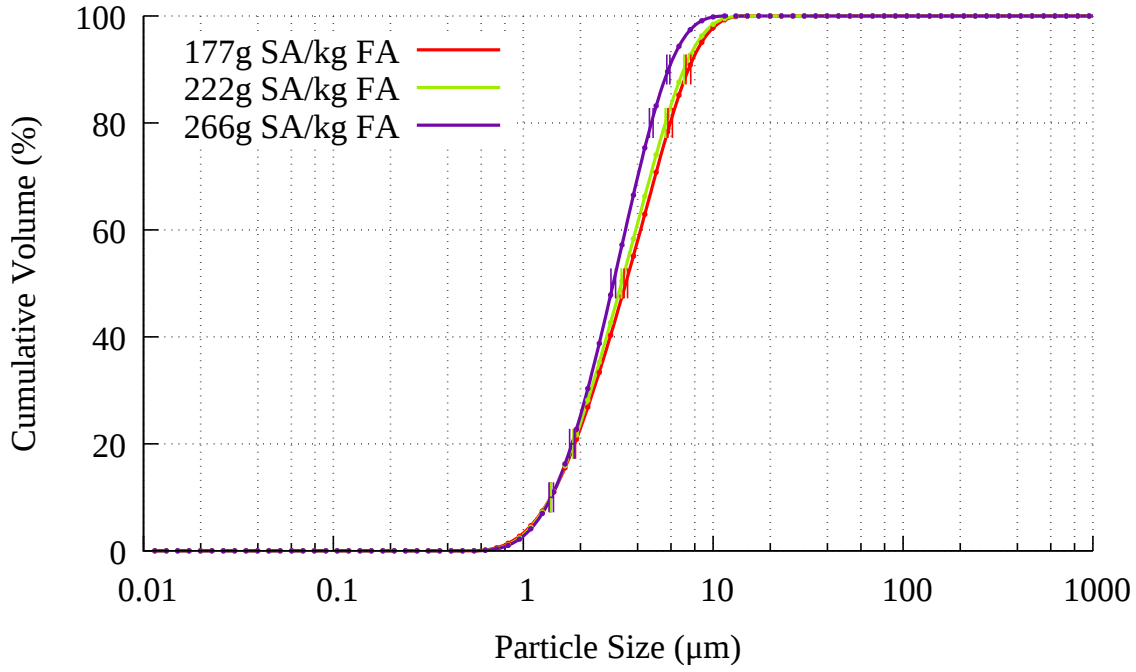

(b) Standard deviation in PSD

Figure 6.50: 90-95°C crystallisation process with added Na^+ at 6 hours

6.5 Crystallisation at a Constant Temperature of 95°C

In order to ascertain whether the step change in temperature implemented in experiments since section 5.4 has a significant influence on results, three experiments were repeated at a constant 95°C, rather than 90°C for 2 hours, followed by 95°C. The method used was the same as that used in section 6.3. Experiments repeated at 95°C consist of the experiments described in sections 5.4.2.6, 6.4.1.1 and 6.4.1.3.

6.5.1 Results

6.5.1.1 Dosage of 266 g SA/kg FA

Figure 6.51 shows the AAS results comparing each 95°C experiments to the equivalent 90-95°C experiment. The results appear very similar, and it is difficult to discern a difference in the Si values. For the Al values, it would appear the 95°C experiment has a higher Al content for all but the 0 hour value. The difference in Al values increases as time progresses. Were the higher Al content in solution also reflected in the Si values, a reduced yield would be expected, however Si values appear unaffected by the change in temperature. The yield shown in Figure 6.52 shows an increase in yield. The increase in yield is small, and is within the relative standard deviation of the new result. The slight increase in yield is offset by a decrease in CEC shown in Figure 6.53 to give a yield of CEC in Figure 6.54, which is lower than the 90-95°C experiment, but within the error limits.

The SEM images in Figure 6.55 are very similar to the images of the equivalent 90-95°C experiment shown in Figure 5.48, both showing a reduction in amorphous material between hours 3 and 4, and showing clean chamfered edged cubes from hours 4-6, in line with the XRD patterns of Figures 6.57 and 5.49, as well as the decrease in Si and Al from the AAS measurements. The PSD shown in Figure 6.56a shows a narrow right hand peak that increases in height between hours 4 and 6, whereas the equivalent 90-95°C experiment in Figure 5.50a shows a PSD that demonstrates little if any change between

hours 4 and 6. The 6 μm d_{50} for the 95°C experiment is slightly higher than the 5-6 μm d_{50} demonstrated by the 90-95°C experiment for hours 4-6.

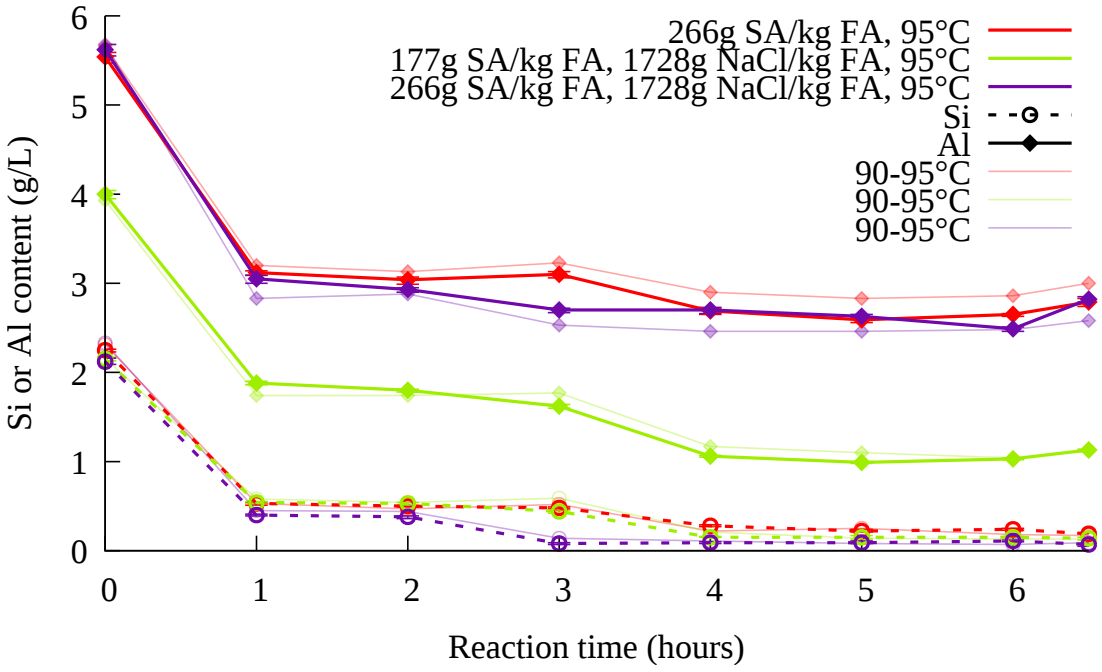

Figure 6.51: AAS results for 95°C crystallisation process compared to 90-95°C process

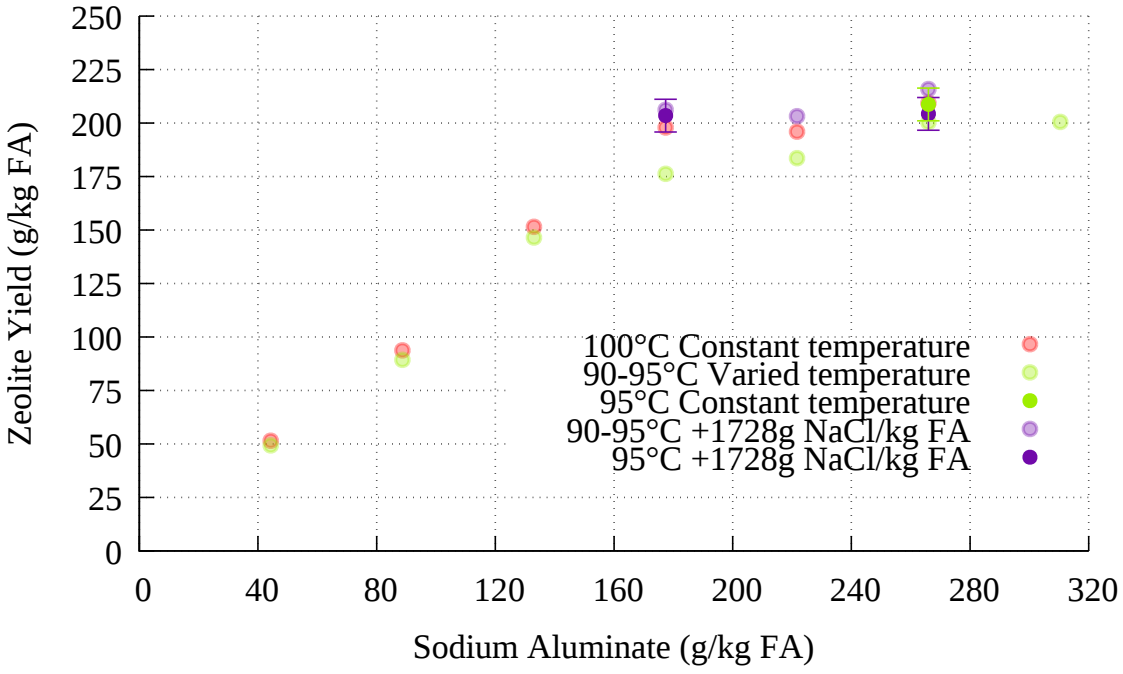

Figure 6.52: Yield results for 95°C crystallisation process compared to 90-95°C process

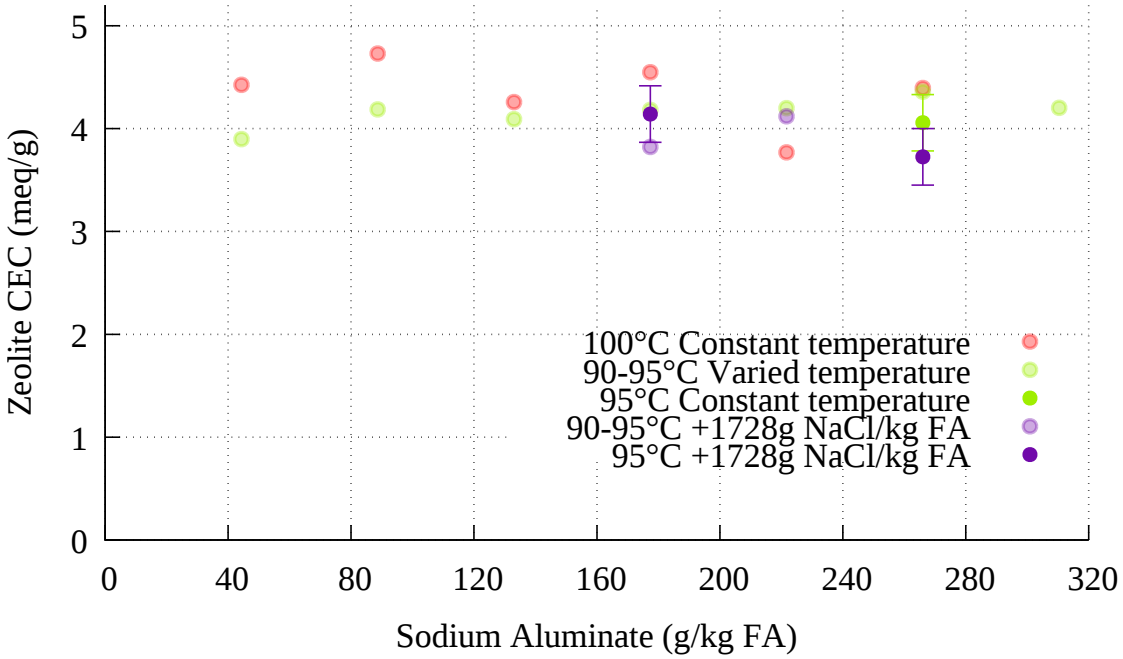

Figure 6.53: CEC results for 95°C crystallisation process compared to 90-95°C process

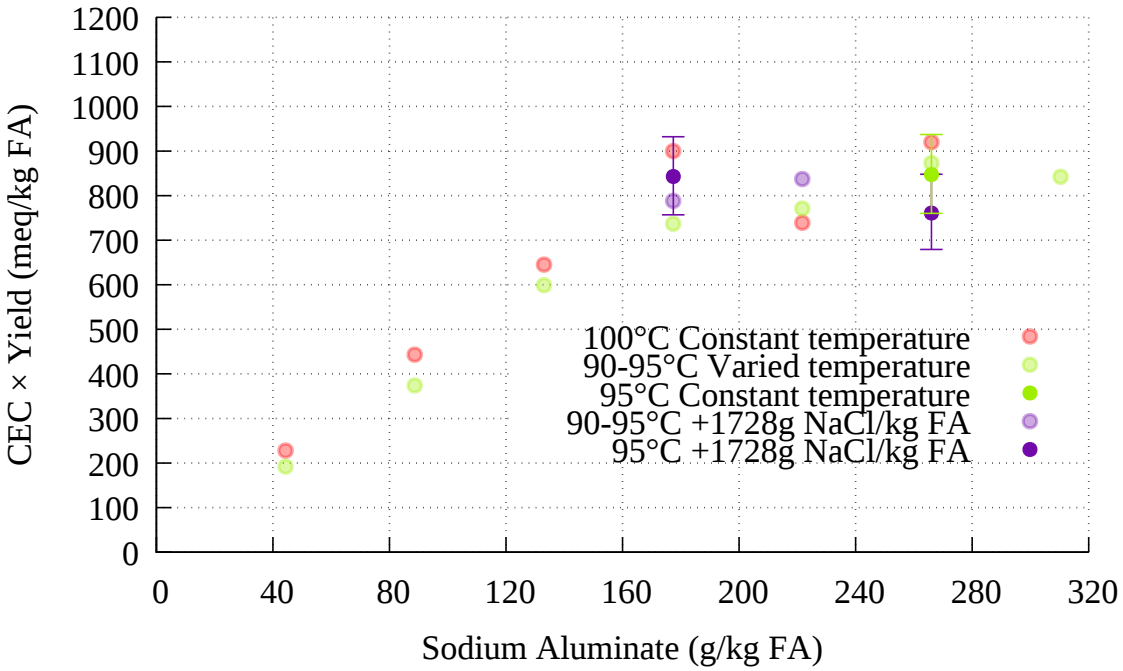

Figure 6.54: CEC × yield results for 95°C crystallisation process compared to 90-95°C process

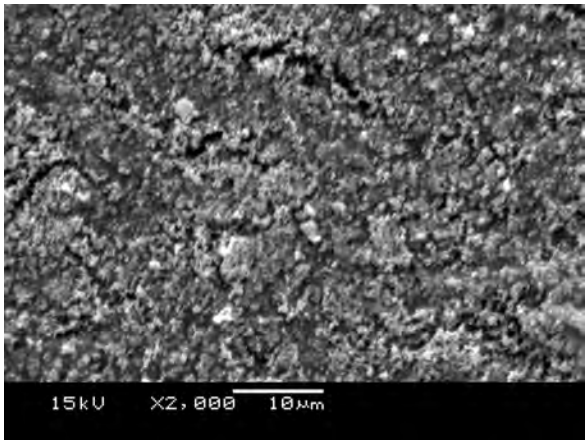

(a) 1 h

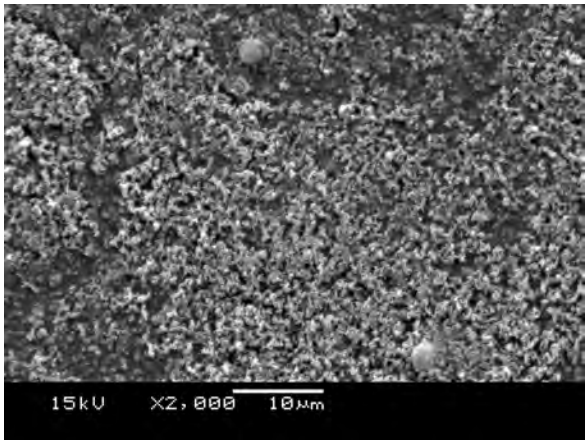

(b) 2 h

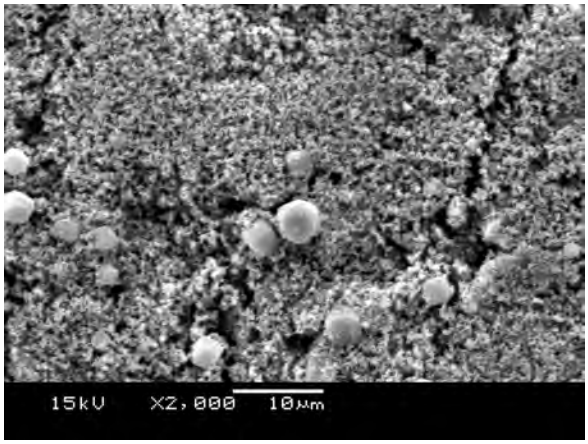

(c) 3 h

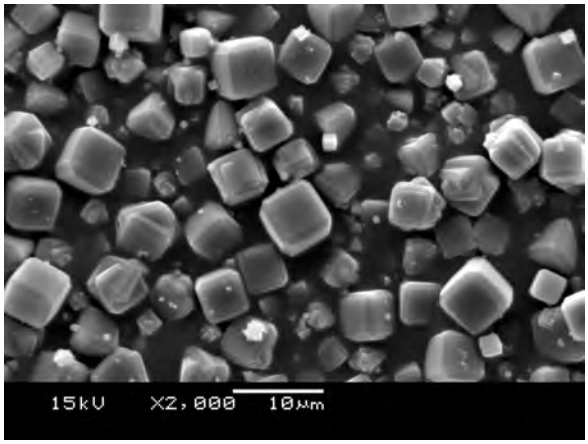

(d) 4 h

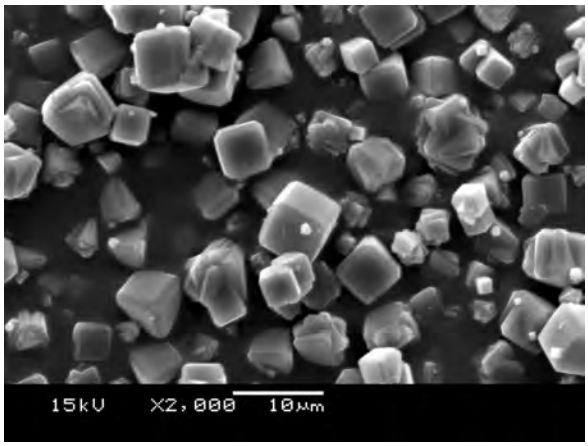

(e) 5 h

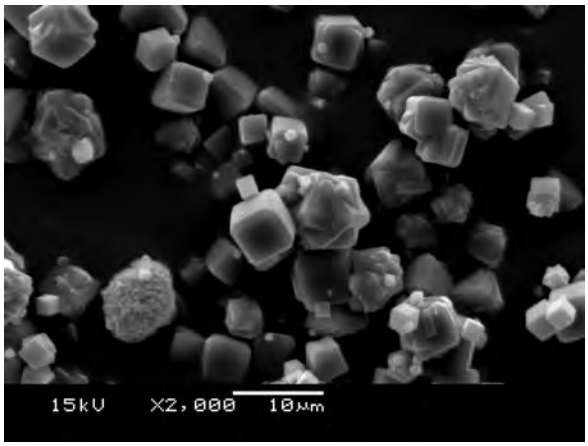

(f) 6 h

Figure 6.55: SEM images of zeolites from ash leachate crystallised with 266 g of sodium aluminate/kg FA on a stirred hot plate at 95°C

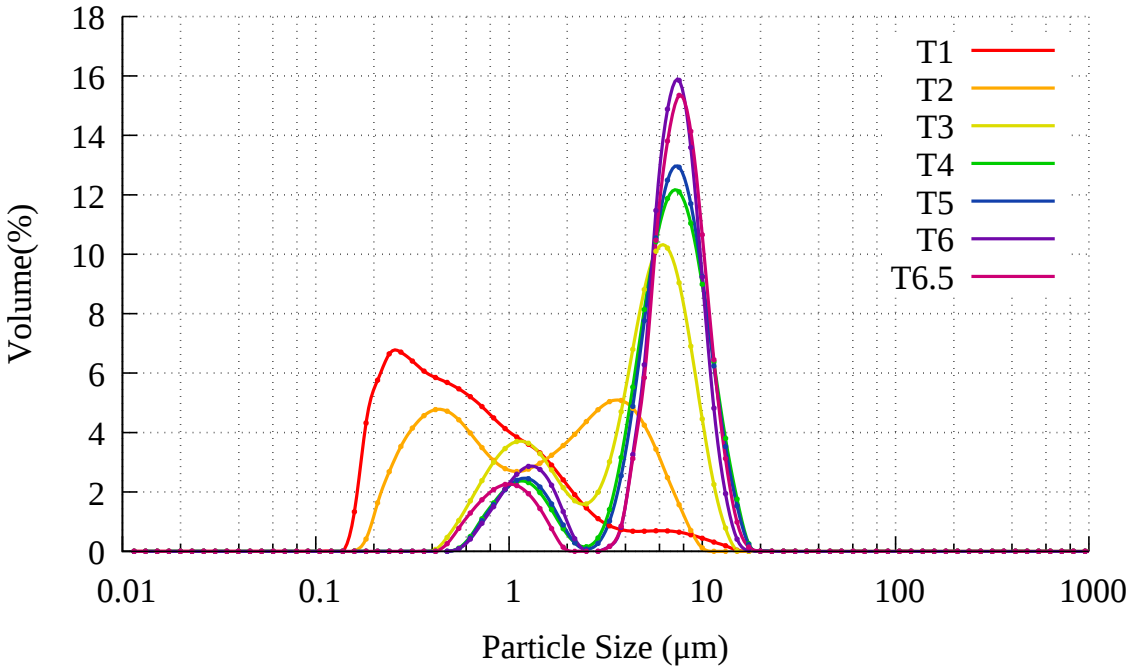

(a) PSD

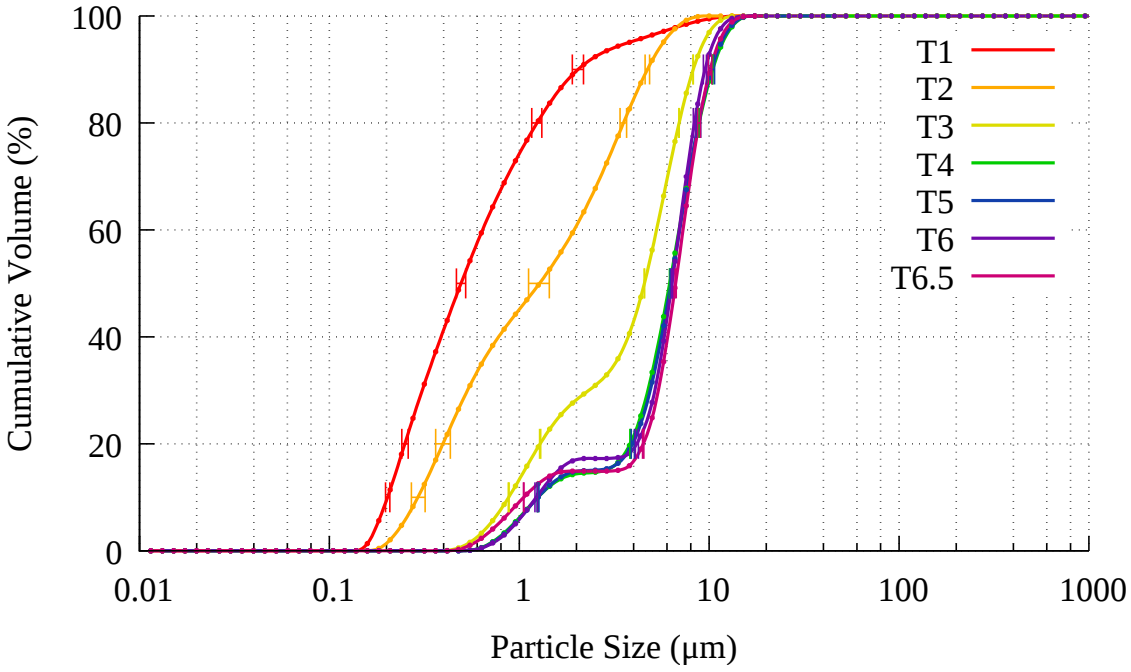

(b) Standard deviation in PSD

Figure 6.56: 95°C crystallisation process with 266 g SA/kg FA

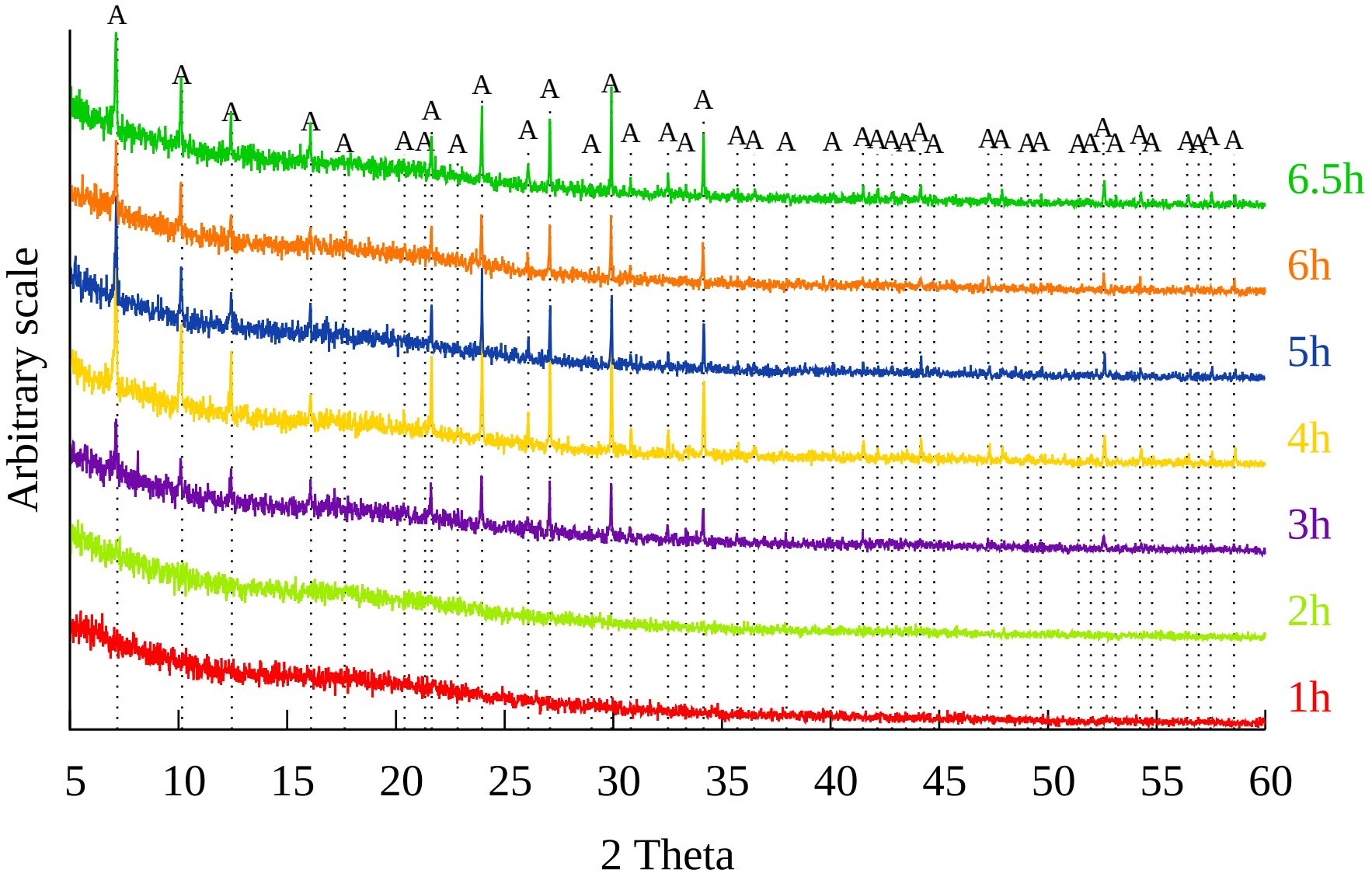

Figure 6.57: XRD patterns of 95°C crystallisation with 266 g sodium aluminate/kg FA. A: Zeolite Na-A. $\lambda = 1.5406$ Å

6.5.1.2 Dosage of 177 g SA/kg FA & 1728 g NaCl/kg FA

The AAS results shown in Figure 6.51 again show little difference in Si values, except for a slightly lower Si content for the 95°C experiment at 3 hours. There are some difference in Al values, with the difference fluctuating slightly based on the equivalent 90-95°C experiments, but there is no discernible change by 6 hours. The yield results shown in Figure 6.52 show a slight decrease in yield, still within the error limits of the corresponding 90-95°C experiment. The CEC and thus CEC yield of Figures 6.53 and 6.54 show a slight improvement, but improvements are within the error for the CEC tests. The SEM images shown in Figure 6.58 are very similar to the SEM images of the corresponding experiment in Figure 6.44, but with slightly more amorphous material noted at 3 hours in the 95°C experiment, which may be a reflection of the lower Si content in Figure 6.51. The XRD patterns in Figures 6.60 and 6.45 show no obvious differences.

The PSD shown in Figure 6.59a seems similar to the 90-95°C PSD in Figure 6.46a, albeit that the 3-6 hour measurements are more uniform in the 95 °C experiment. The d_{50} shown for the 95°C experiment in Figure 6.59b between 3 and 6 hours is ~4 μm, whilst the d_{50} shown in Figure 6.46b for the 90-95°C experiment in the same time frame is ~3 μm. This supports the idea of a fewer number of nuclei being present, which grow to a larger size in the 95°C conditions. As with other PSD results, the difference between 6 and 6.5 hour results is attributed to agglomeration through rapid crystallisation during the cooling process.

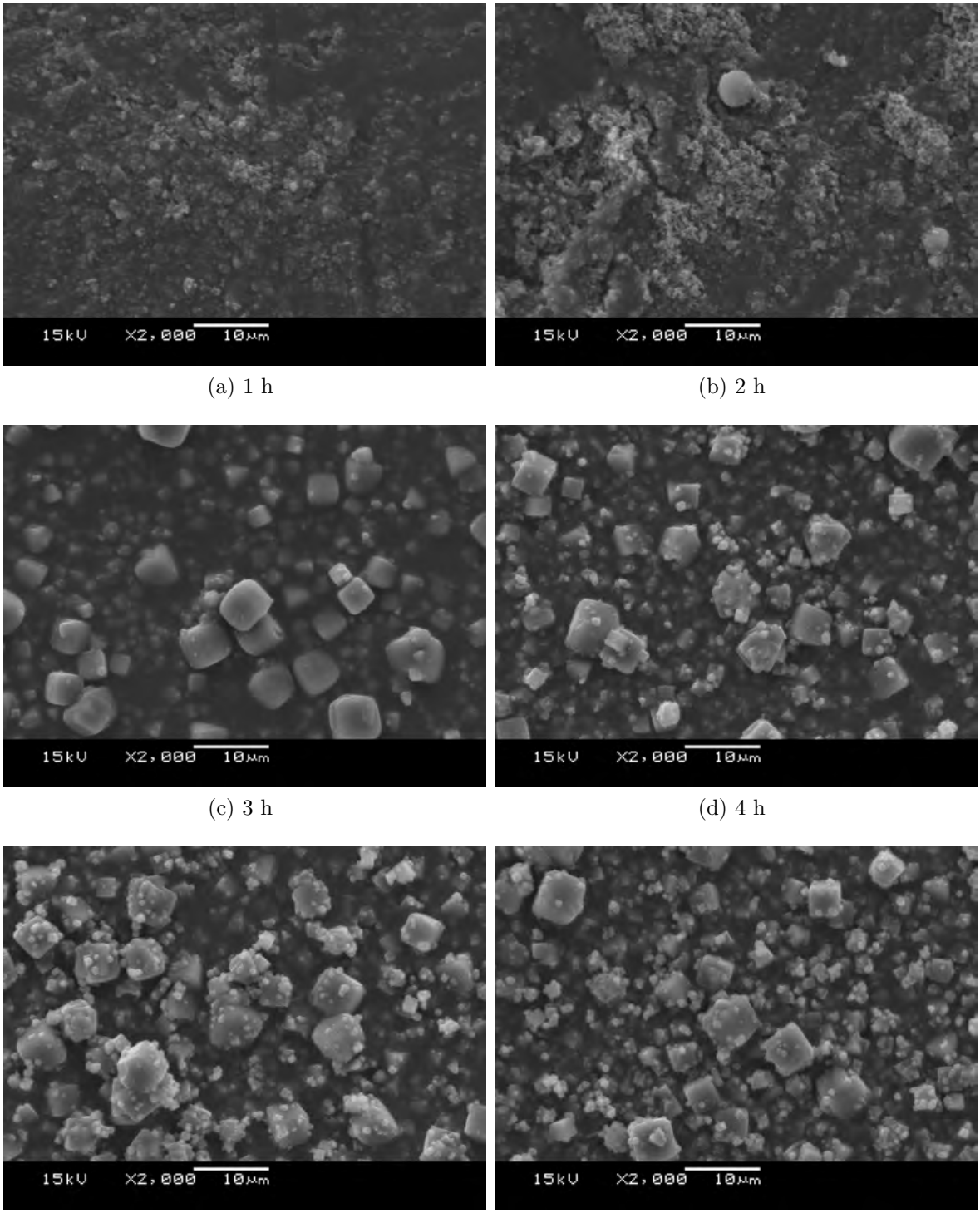

(a) 1 h (b) 2 h

(c) 3 h (d) 4 h

(e) 5 h (f) 6 h

Figure 6.58: SEM images of zeolites from ash leachate crystallised with 177 g of sodium aluminate/kg FA & 1728 g NaCl/kg FA on a stirred hot plate at 95°C

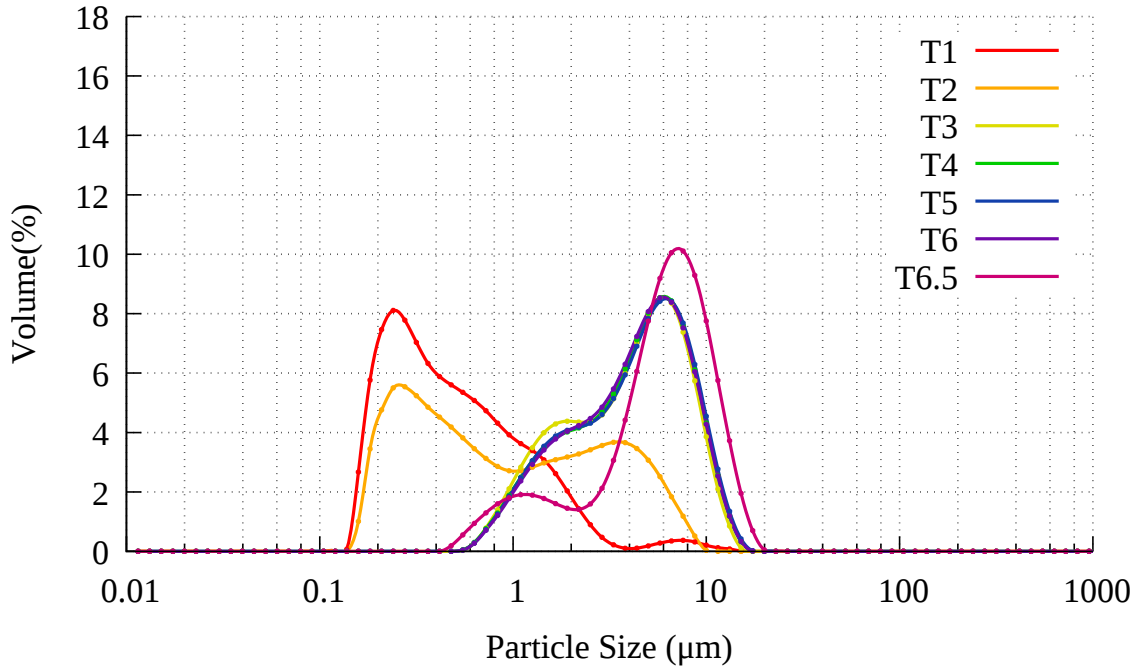

(a) PSD

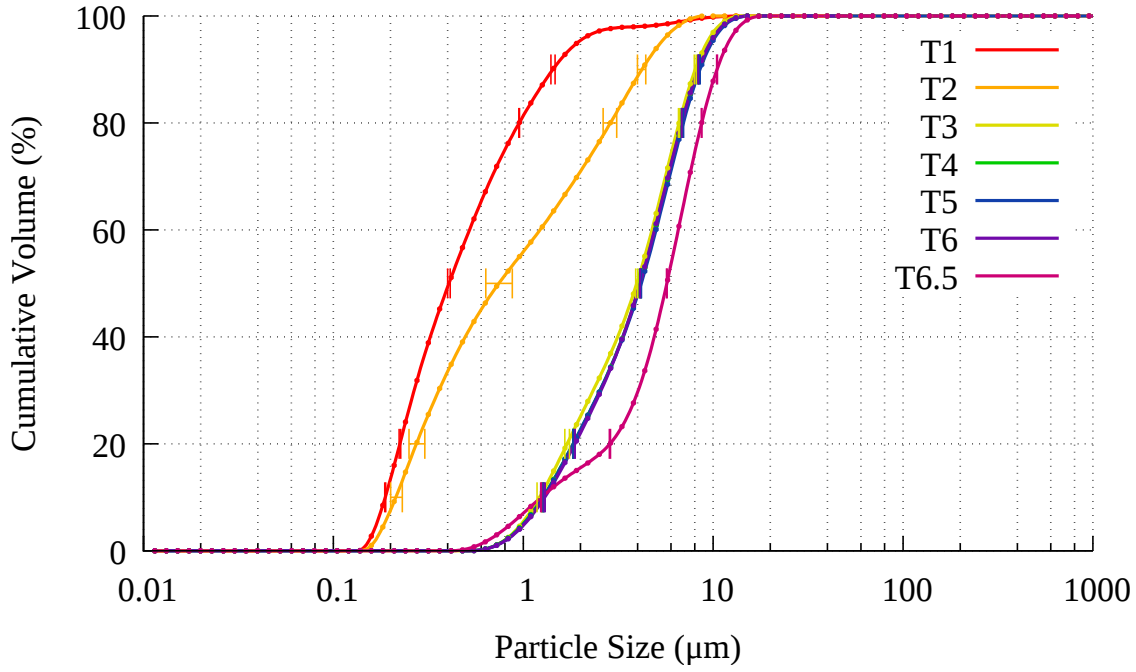

(b) Standard deviation in PSD

Figure 6.59: 95°C crystallisation process with 177 g SA/kg FA, 1728 g NaCl/kg FA

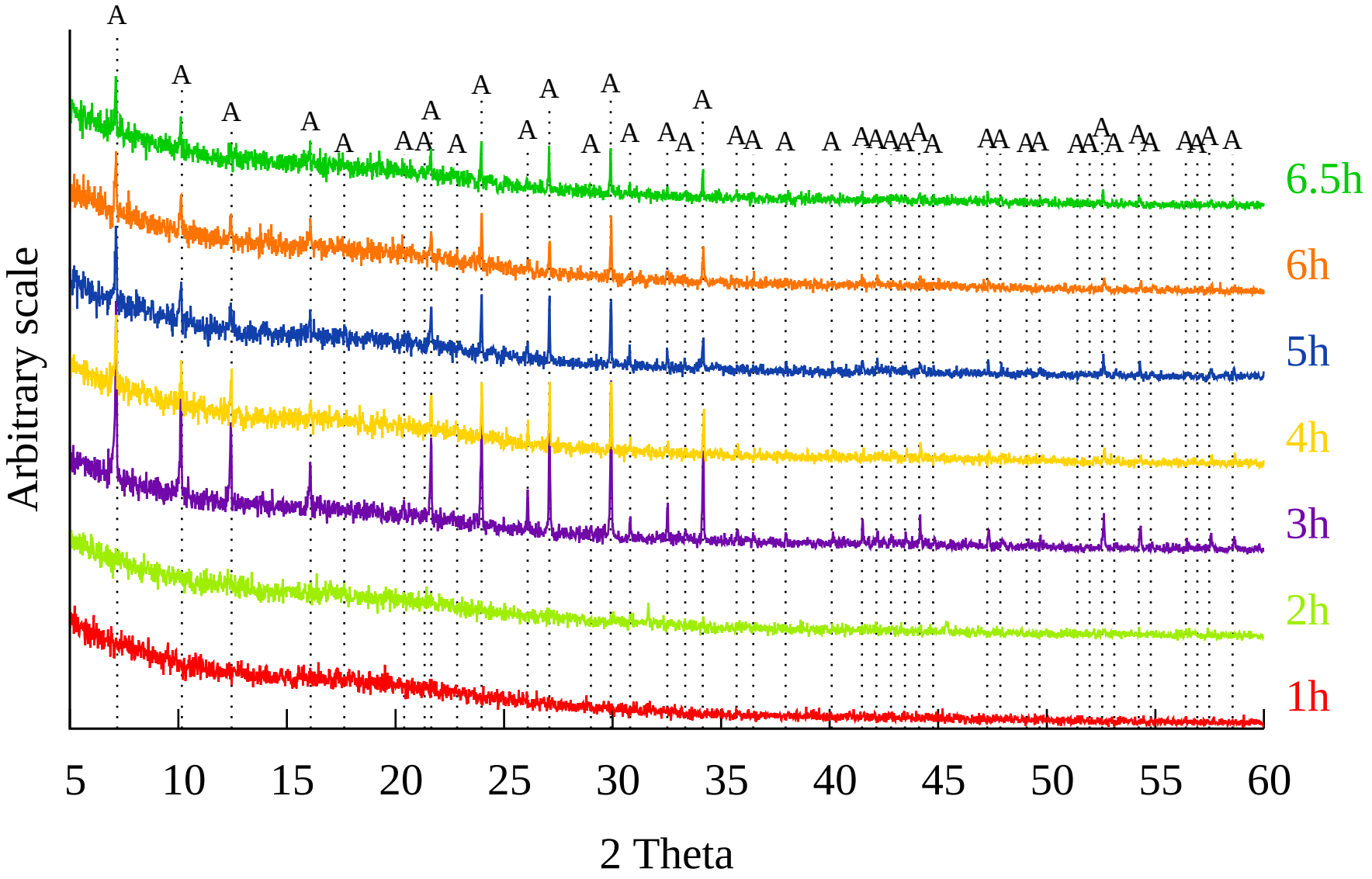

Figure 6.60: XRD patterns of 95°C crystallisation with 177 g sodium aluminate/kg FA & 1728 g NaCl/kg FA. A: Zeolite Na-A. λ = 1.5406 Å

6.5.1.3 Dosage of 266 g SA/kg FA & 1728 g NaCl/kg FA

The AAS in Figure 6.51 again shows little difference in the Si values, and only a slight variation in the Al values. The yield in Figure 6.52 again seems slightly lower, with the CEC also being lower than the previous dosage of sodium aluminate (no CEC measurement was made for the 90-95°C experiment due to the zeolite being too fine). The CEC yield in Figure 6.54 appears to have suffered with the introduction of the NaCl in comparison to the other 95°C experiment at this dosage of sodium aluminate.

The SEM images of Figure 6.61 appear similar to the corresponding SEM images on Figure 6.47, although more cubes appear present at 2 hours in the 95°C experiment. The XRD patterns of Figure 6.63 shows peaks from 2 hours, but otherwise is very similar to the 90-95°C patterns in Figure 6.48. The 95°C PSD in Figure 6.62a shows the 2 hour PSD in a similar range to the 3-6 hour patterns, with Figure 6.62b showing a d_{50} of 2.9-3.6 μm from 2-6 hours. The PSD of the 90-95°C experiment shown in Figure 6.49b has a d_{50} of 3.0 μm from 3-6 hours.

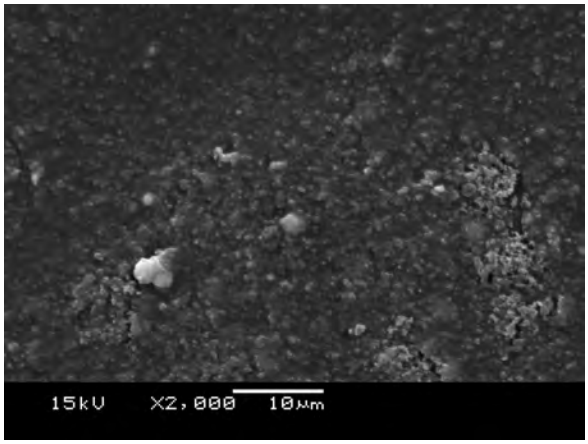

(a) 1 h

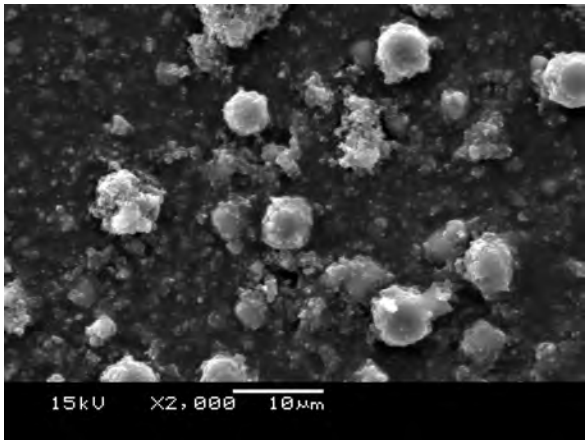

(b) 2 h

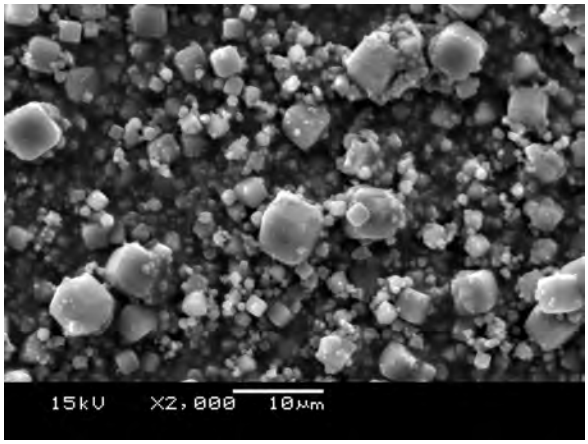

(c) 3 h

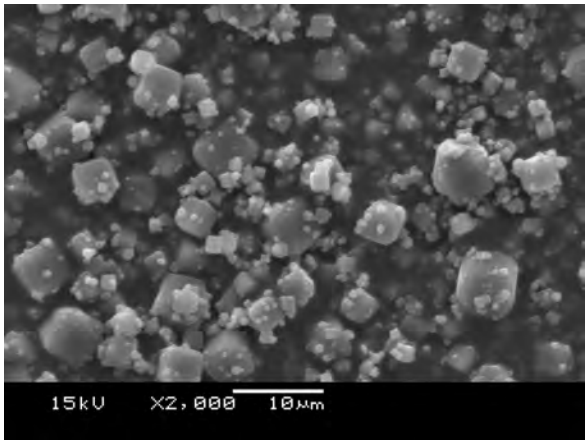

(d) 4 h

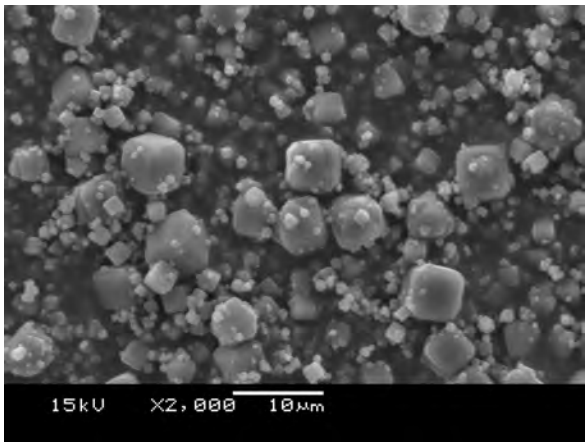

(e) 5 h

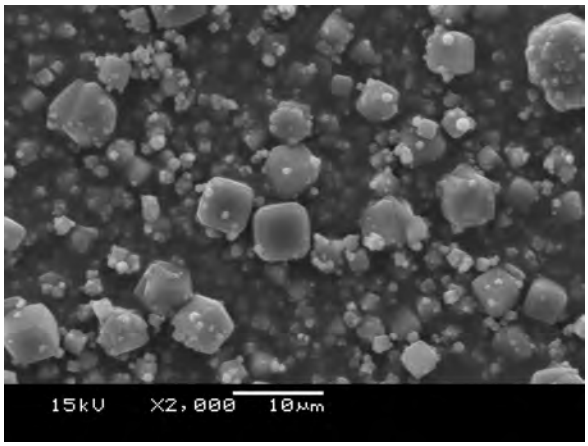

(f) 6 h

Figure 6.61: SEM images of zeolites from ash leachate crystallised with 266 g of sodium aluminate/kg FA & 1728 g NaCl/kg FA on a stirred hot plate at 95°C

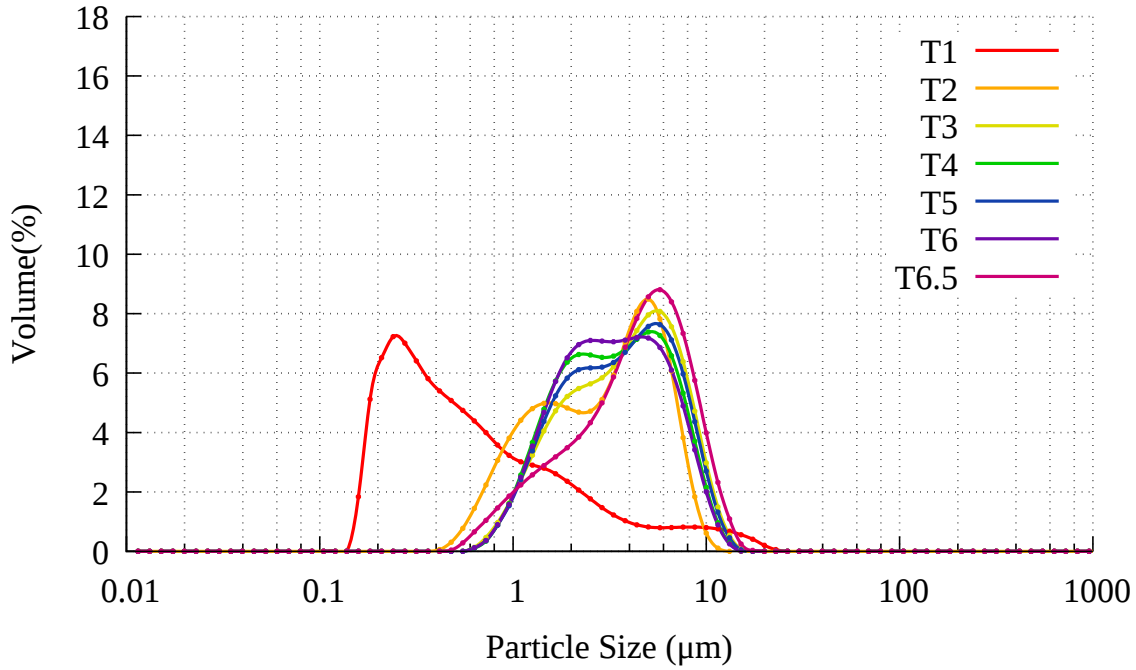

(a) PSD

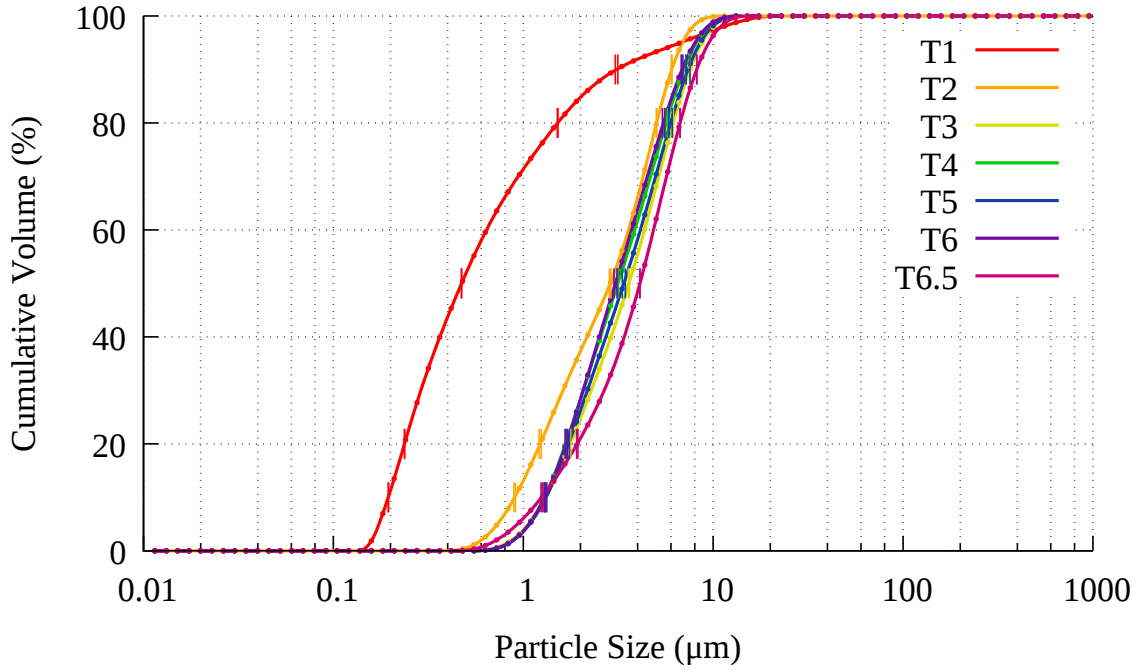

(b) Standard deviation in PSD

Figure 6.62: 95°C crystallisation process with 266 g SA/kg FA, 1728 g NaCl/kg FA

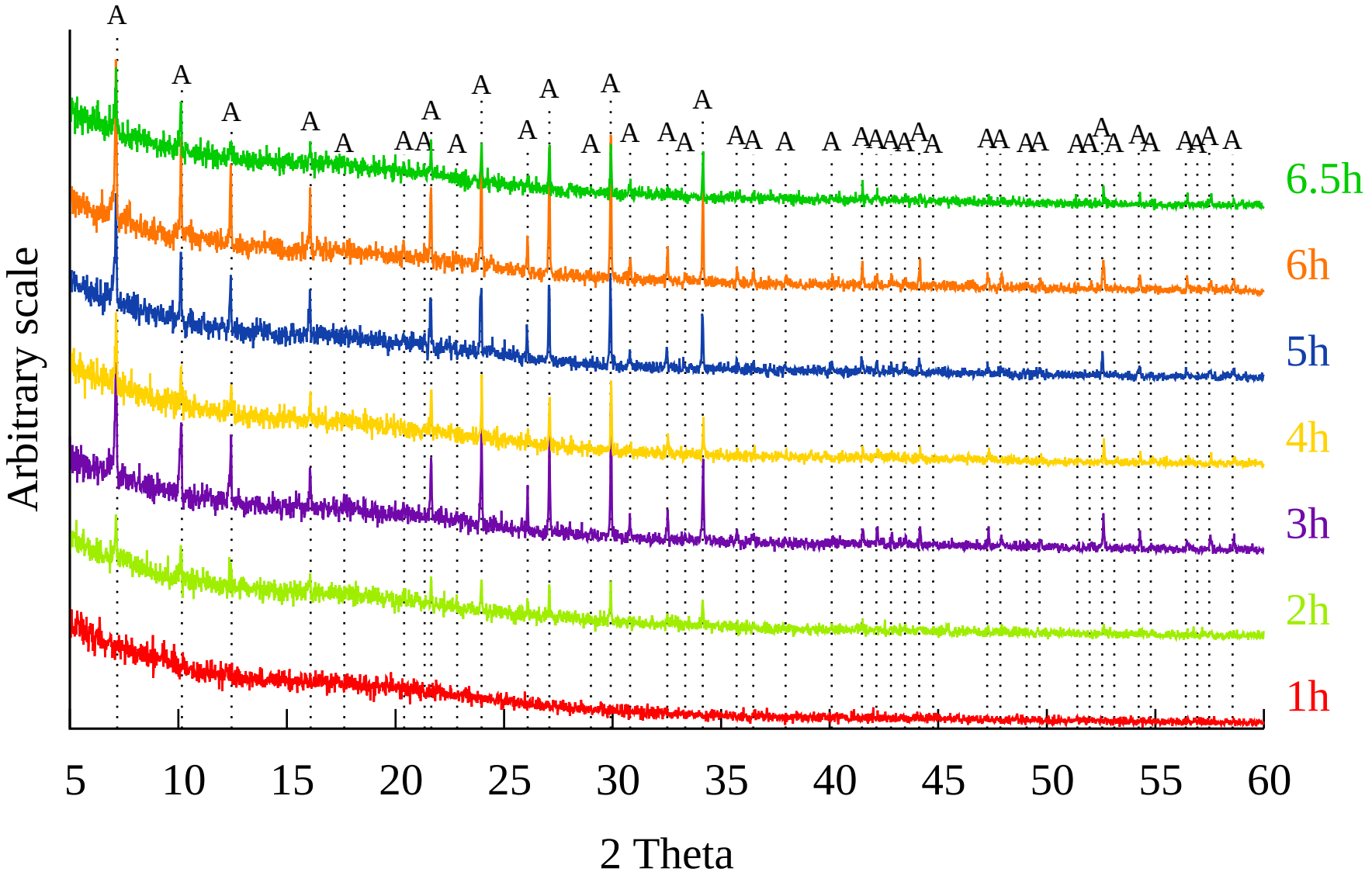

Figure 6.63: XRD patterns of 95°C crystallisation with 266 g sodium aluminate/kg FA & 1728 g NaCl/kg FA. A: Zeolite Na-A. λ = 1.5406 Å

6.5.2 Trends

From these three experiments, it would not appear that changing the 90-95°C step change to a constant 95°C experiment greatly influences results. AAS data indicates little or no difference between crystallisation at 90-95°C and crystallisation at a constant 95°C. Assuming the difference in temperature has no influence, these experiments indicate good repeatability. Yield and CEC appear to be slightly, but inconsistently changed, such changes being slight enough to be within error limits for some variables. SEM appears largely unchanged by the 90-95°C change. Figures 6.64 and 6.65 do show that operating at a constant temperature produces coarser particles. This is in keeping with literature reports that ageing at a lower temperature encourages seeding, resulting in a finer particle size [60]. In the case of these experiments, the ageing or nucleation step is the 0-2 hour step, conducted at 90°C. It was decided that subsequent experiments would continue to follow the 90-95°C experimental method as no drastic change in results other than PSD was observed by conducting experiments at a constant 95°C. Continuing with the 90-95°C method also maintains backward comparability with experiments conducted thus far, and would provide energy savings upon scale up.

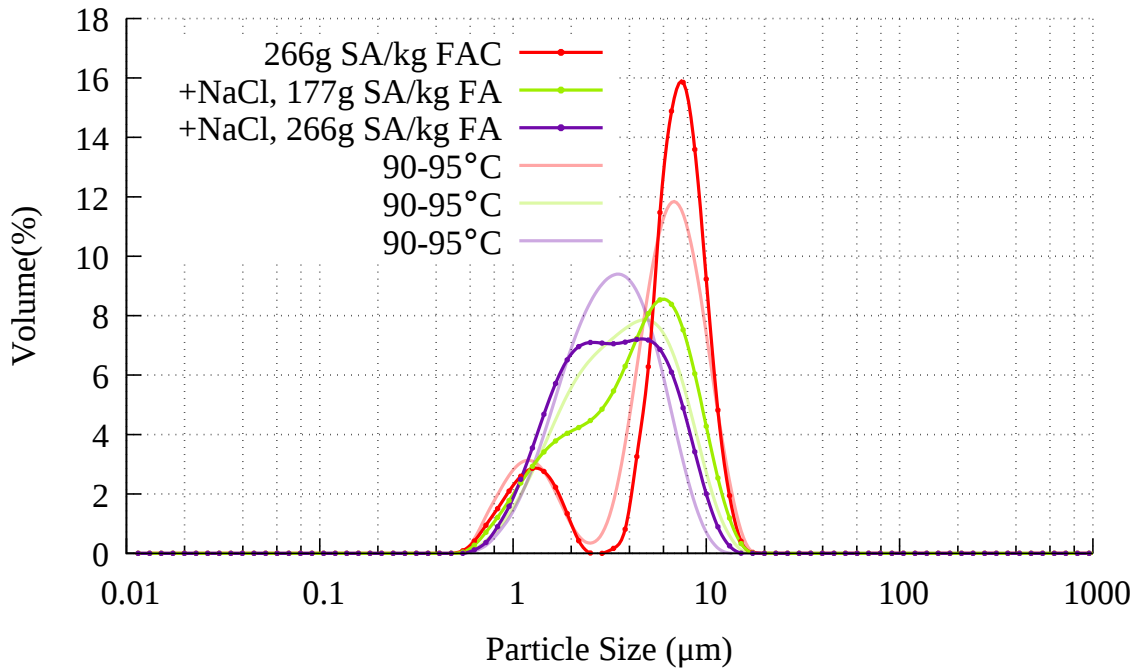

(a) PSD

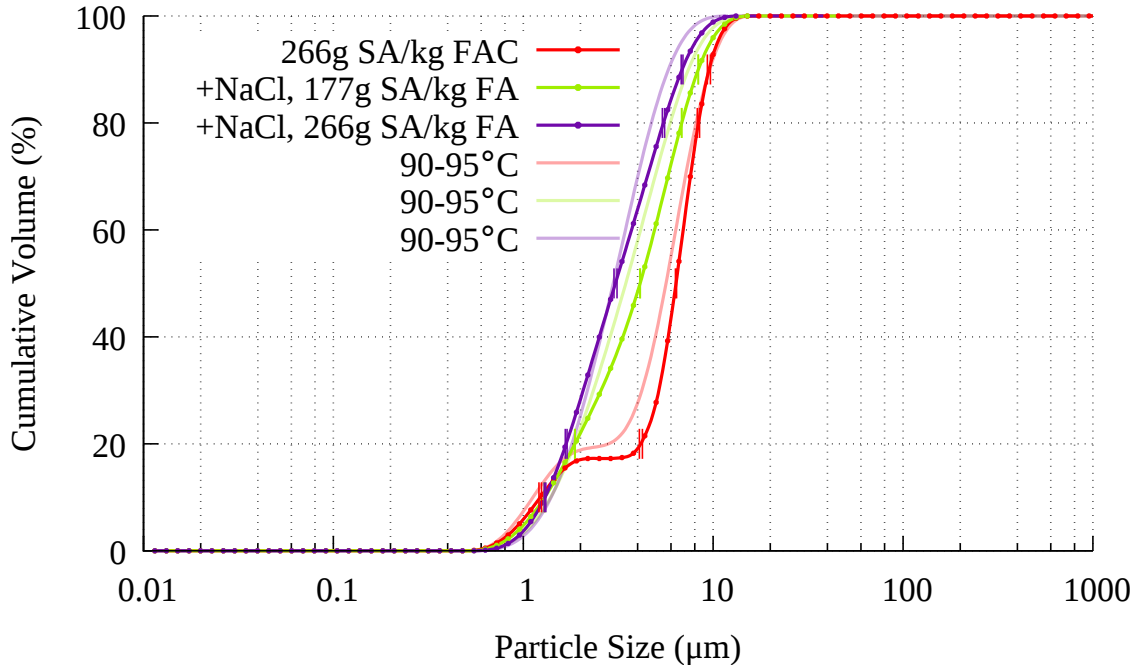

(b) Standard deviation in PSD

Figure 6.64: Crystallisation process at 95°C vs 90-95°C at 6 hours

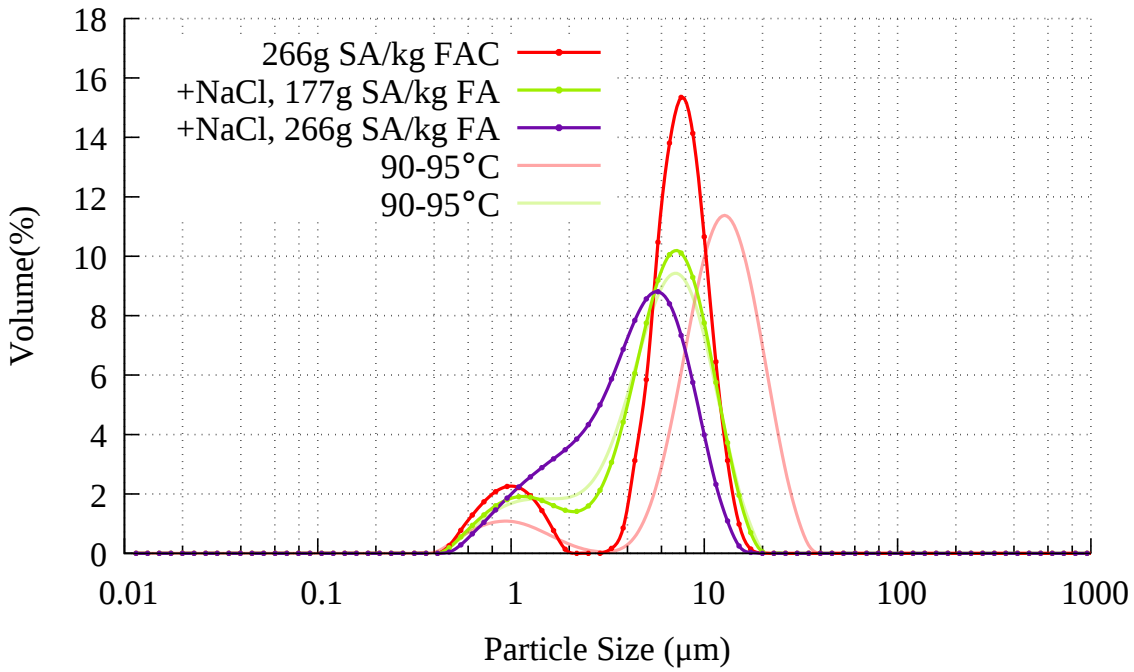

(a) PSD

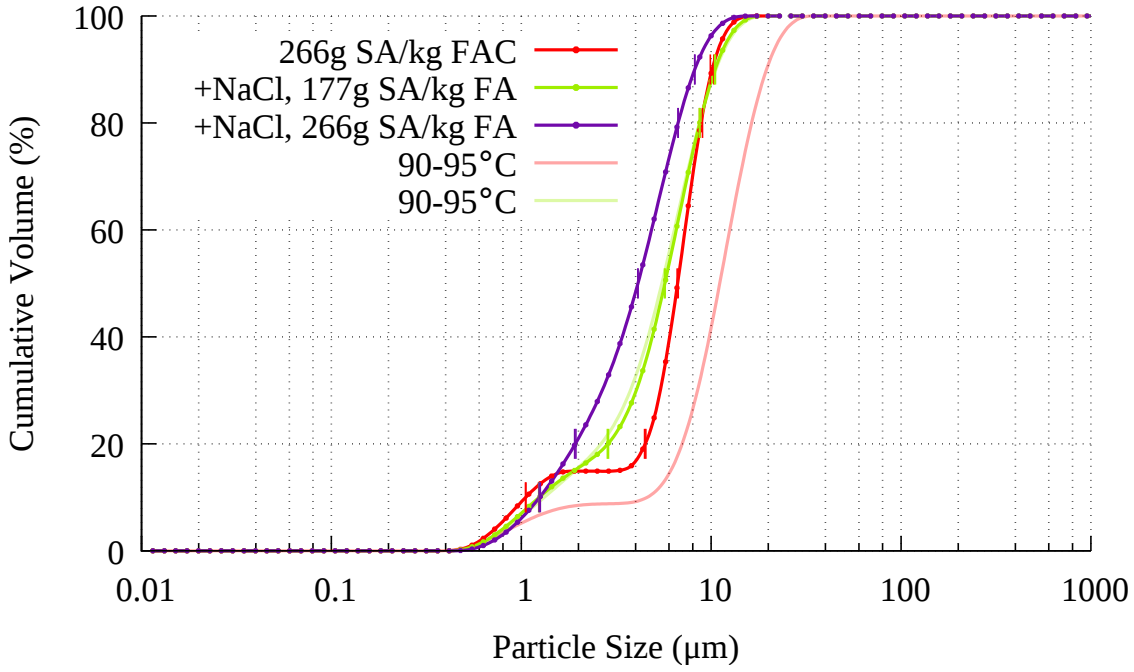

(b) Standard deviation in PSD

Figure 6.65: Crystallisation process at 95°C vs 90-95°C at 6.5 hours

6.6 Effect of Different Sources of NaCl on the Crystallisaton Process

Papers such as Belviso et al. [39] and Belviso et al. [38] have shown it is possible to use seawater in lieu of distilled water in the crystallisation process. This would be advantageous in reducing running costs. As experiments with added NaCl have shown no disadvantage, it was decided to experiment using artificial seawater. Rather than producing fresh artificial seawater for each experiment (which would have proven time consuming and costly), sea salt was added to distilled water as an approximation of seawater. Based on Kester et al. [88], 35 g of sea salt was added to each litre of distilled water. This concentration of sea salt falls between the two lowest concentrations of NaCl used in experiments so far, thus an experiment was conducted to compare a control experiment with no added NaCl, with the two experiments with the lowest concentrations of NaCl, and the 35 g quantity of sea salt. In order to maintain backward compatibility with previous experiments, this experiment was conducted at 90-95°C, and the method follows the method described in section 6.1.

AAS results are shown in Figure 6.66. The control experiment and experiments with 315 and 864 g NaCl/kg FA are taken from section 6.3 shown in Figure 6.25. Si values in Figure 6.66 show similar consumption for Si when comparing sea salt experiments with NaCl experiments, with a decrease in available Si between 3 and 4 hours. Al values shown in Figure 6.66 show a decrease in available Al from 3 to 5 hours. The Al consumption appears to be lower for the sea salt experiment than for NaCl experiments for most points, but still higher than the control experiment for all points. The yield of zeolite shown in Figure 6.67 is slightly higher for sea salt than for NaCl, however it is within boundaries of error. The CEC shown in Figure 6.68 is slightly higher for the sea salt experiment than for other NaCl experiments and it is outside of the error boundaries, thus the CEC yield show in Figure 6.69 indicates use of sea salt in the crystallisation process increases the CEC yield over using NaCl. The drop in Al and Si between 3 and 4 hours coincides with

the disappearance of the amorphous material in the SEM images of Figure 6.32. Cubes show chamfered edges and appear to be below 10 μm, which is supported by the PSD data in Figure 6.71. The samples are rich in amorphous material for 3 hours with broader bimodal distribution, before results at 4-6 hours show a consistently narrow distribution centered around ~8 μm, with a smaller peak around 1 μm. The PSD is quite narrow for the 4-6.5 hour samples with no particles in the 2-4 μm range, indicating that any zeolite particles within this range grew to the larger size range, no small particles were raised to this size range. The SEM results also support the XRD results shown in Figure 6.72, with traces of zeolite A detected from 3 hours, but much clearer peaks from 4-6.5 hours. It is noted that the XRD source was changed prior to the analysis of the data in Figure 6.72, hence patterns appear much clearer than other XRD patterns. The increases in both yield and CEC when comparing sea salt experiments with NaCl experiments indicate that using seawater rather than distilled water and salt in the crystallisation process would not only save on costs but also improve results.

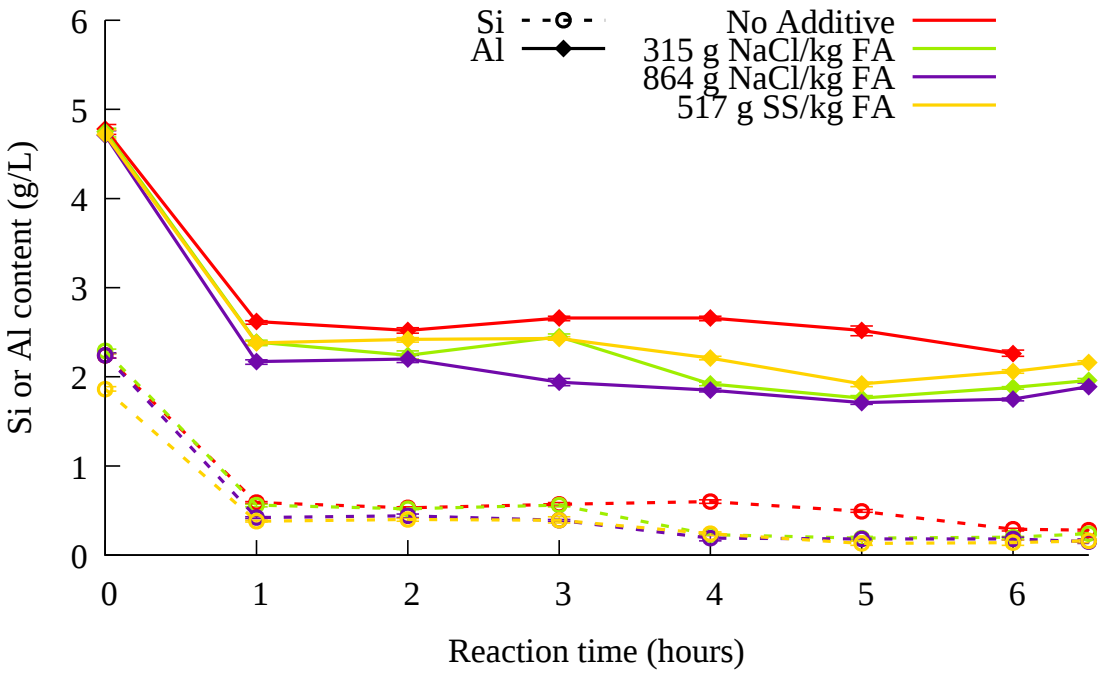

Figure 6.66: AAS results comparing NaCl source

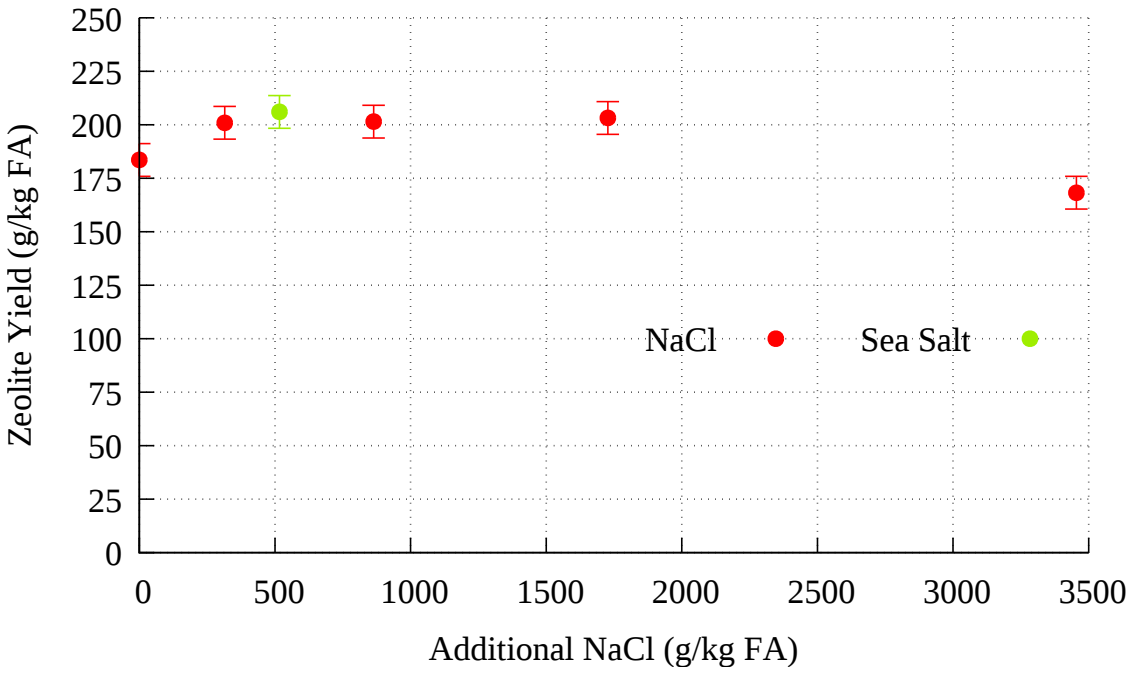

Figure 6.67: Yield results comparing NaCl source

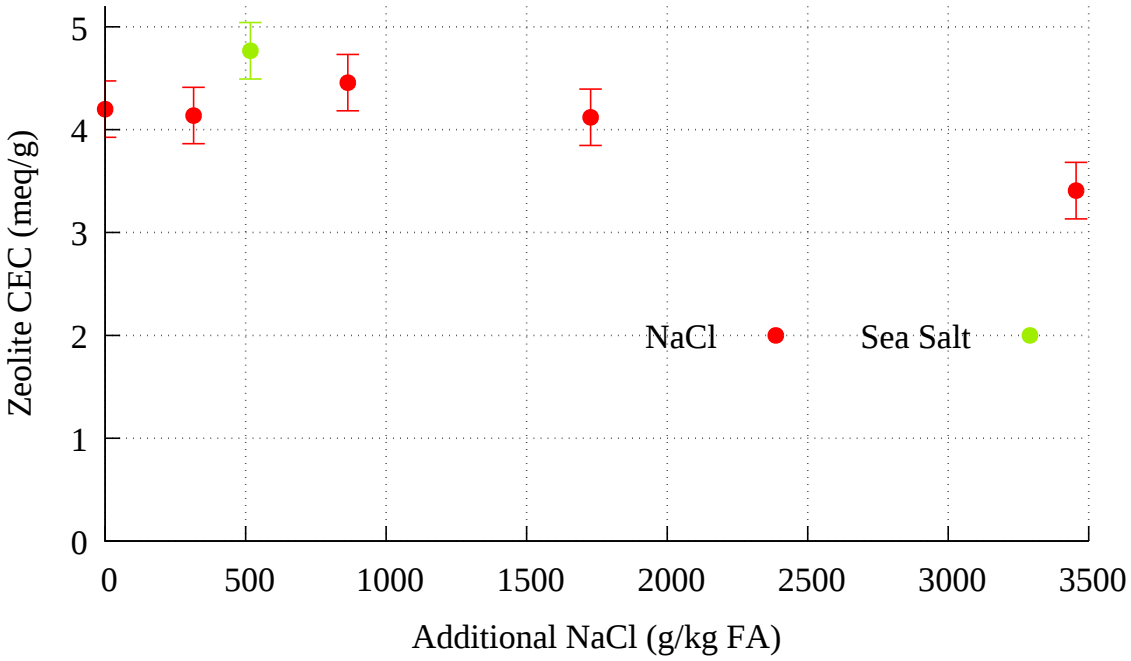

Figure 6.68: CEC results comparing NaCl source

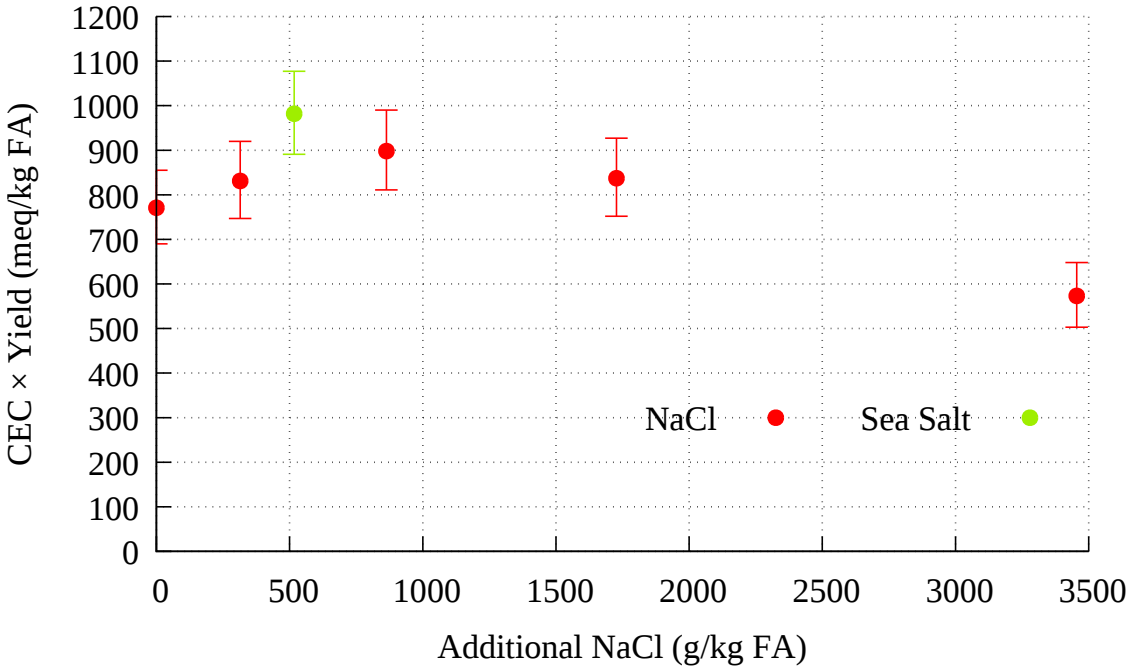

Figure 6.69: CEC × yield results comparing NaCl source

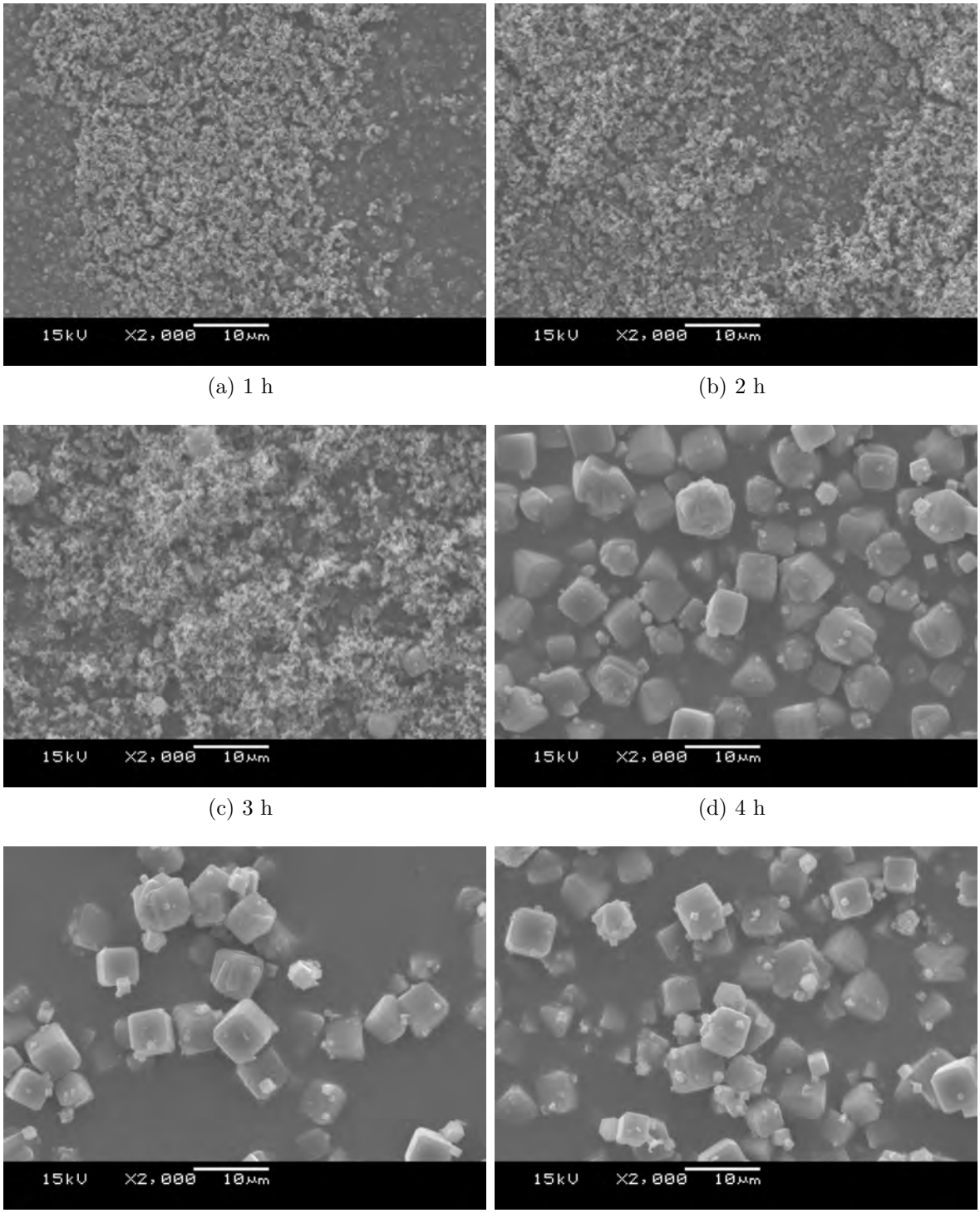

(a) 1 h (b) 2 h

(c) 3 h (d) 4 h

(e) 5 h (f) 6 h

Figure 6.70: SEM images of zeolites from ash leachate crystallised with 517 g of sea salt/kg FA and 222 g SA/kg FA on a stirred hot plate at 90-95°C

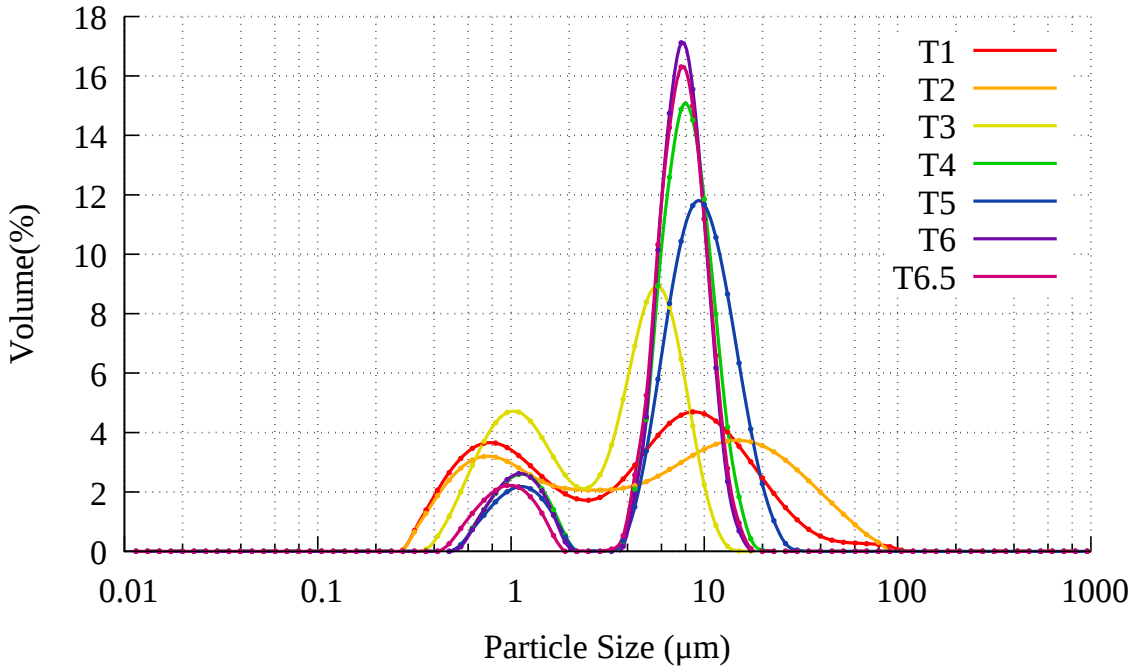

(a) PSD

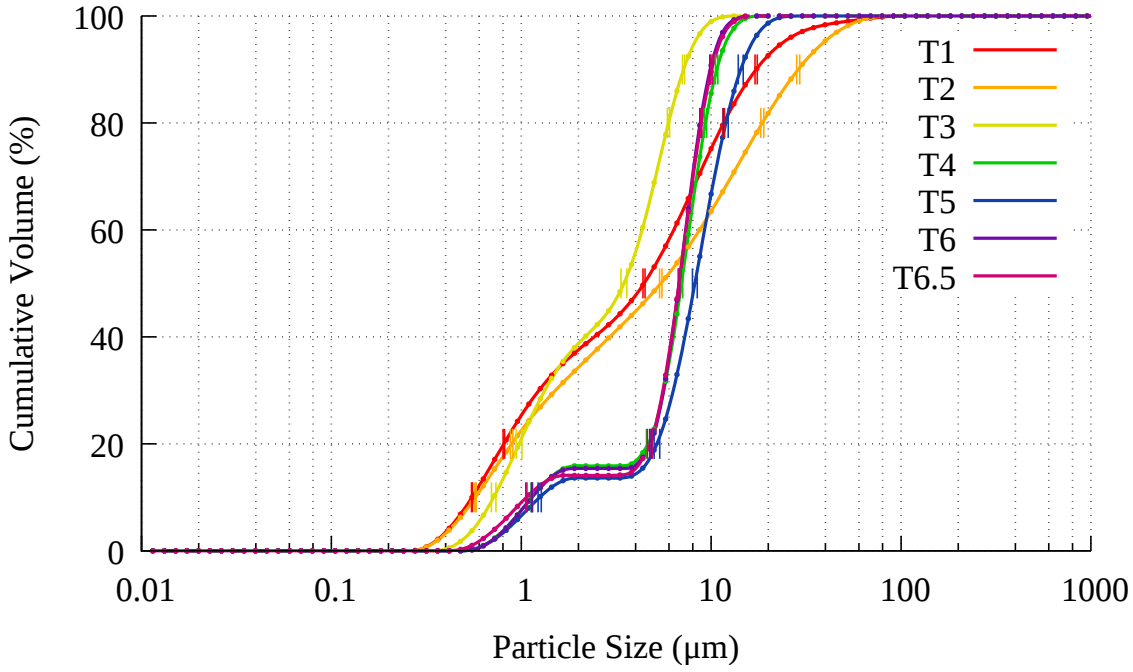

(b) Standard deviation in PSD

Figure 6.71: 90-95°C crystallisation process with 517 g sea salt/kg FA

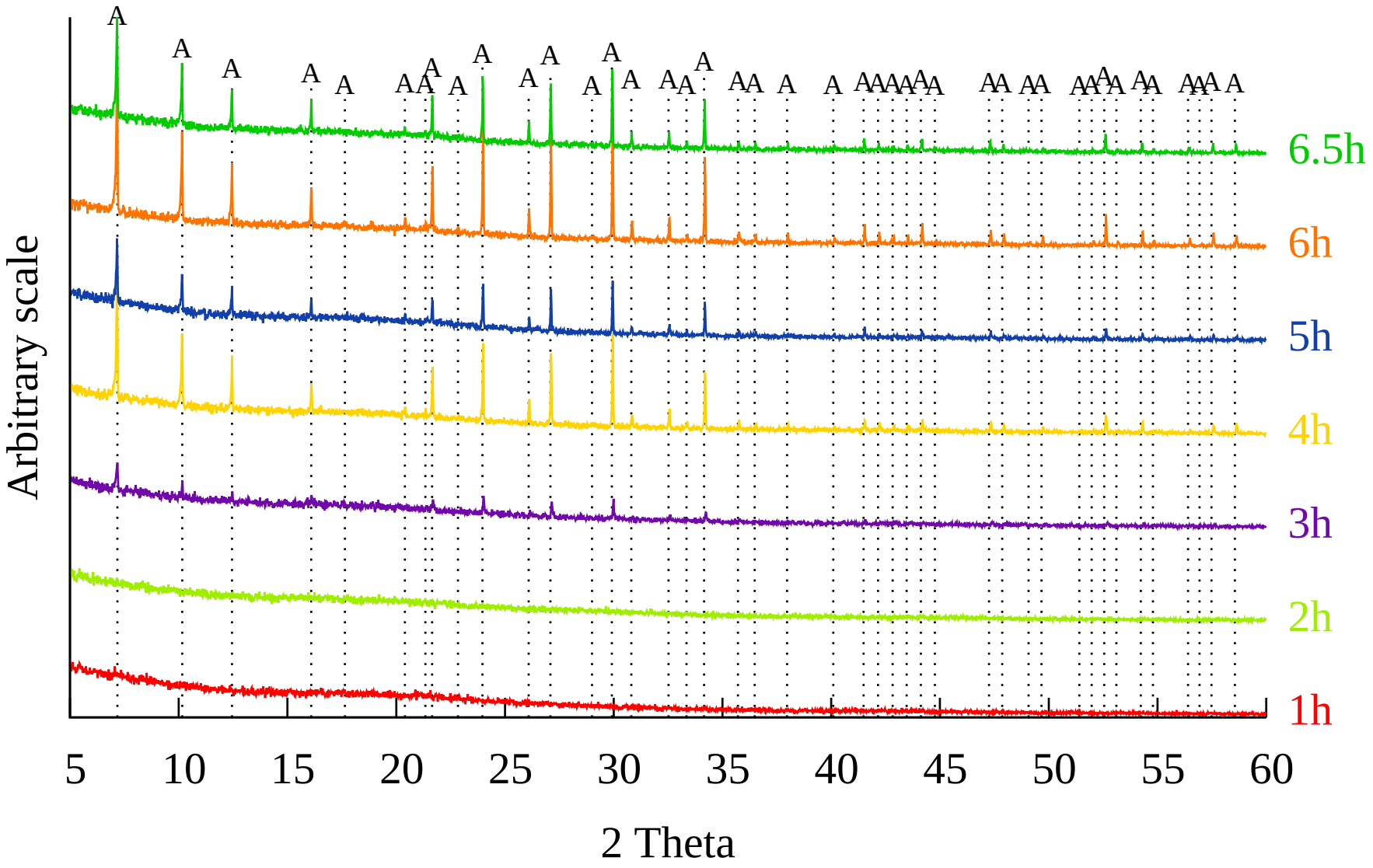

Figure 6.72: XRD patterns of 90-95°C crystallisation with 517 g sea salt/kg FA. A: Zeolite Na-A. $\lambda = 1.5406$ Å

6.7 The Effect of Varied Dosages of Sodium Aluminate with a Constant Dosage of Sea Salt

Experiments were conducted to investigate the effect of varied dosage of sodium aluminate, given a constant quantity of sea salt. The experiments in this section follow the method set out in section 6.1, but with 517 g of sea salt/kg FA added in place of the NaOH. Three dosages of sodium aluminate were investigated, 133, 177 and 222 g/kg FA.

The results of the 222 g SA/kg FA are discussed in section 6.6, and compared to experiments where NaCl was added rather than sea salt.

The AAS results for the experiments are shown in Figure 6.73. As expected, with increasing sodium aluminate content, the consumption of Si increases. The decreases in Si and Al in solution between 4 and 5, and 3 and 5 hours are more pronounced than in the experiments without sea salt in Figures 5.32a and 5.32b. The decrease in Si and Al in the AAS results coincides with the disappearance of the amorphous material between Figures 6.77d and 6.77e and the increased abundance of cubes. In Figures 6.78d and 6.78d the decrease in amorphous material is less apparent, but still visible on the surfaces of the cubes. XRD results in Figures 6.81 and 6.82 show zeolite A detected from 4 hours, in line with AAS and SEM results.

The PSD in Figure 6.79a shows fine particles for the first two hours. Figure 6.79b shows that they both have a d_{50} of 0.4 μm. The PSD for 5 and 6 hours is almost identical, with a larger d_{50} of 6 μm. With a larger dose of sodium aluminate, this behaviour is repeated, with Figure 6.80 showing a finer PSD with a d_{50} of 0.4 μm for the first two hours, with hours 5-6 being very similar, and having a d_{50} of 6 μm.

Yield results in Figure 6.74 show an improvement on the temperature-change results, however the yield is lower than that of experiments with higher quantities of NaCl. Yield appears to increase linearly with increased sodium aluminate dosage. The CEC results are presented in Figure 6.75, and compared with previous CEC results discussed so far. These results show an improvement when compared to all other conditions. It is noted that the

CEC data point for the 177 g SA/kg FA has been taken from the 6 hour experiment in section 6.8. This was done because the conditions were the same in both experiment sets (other than a lack of sampling in the experiment in section 6.8), and the original data point was unexpectedly low and considered anomalous. The CEC yield shown in Figure 6.76 compares the CEC yield to previous results. The linear increase in CEC and yield with increasing SA are clear here, giving the highest CEC yield measured thus far, at 222 g SA/kg FA.

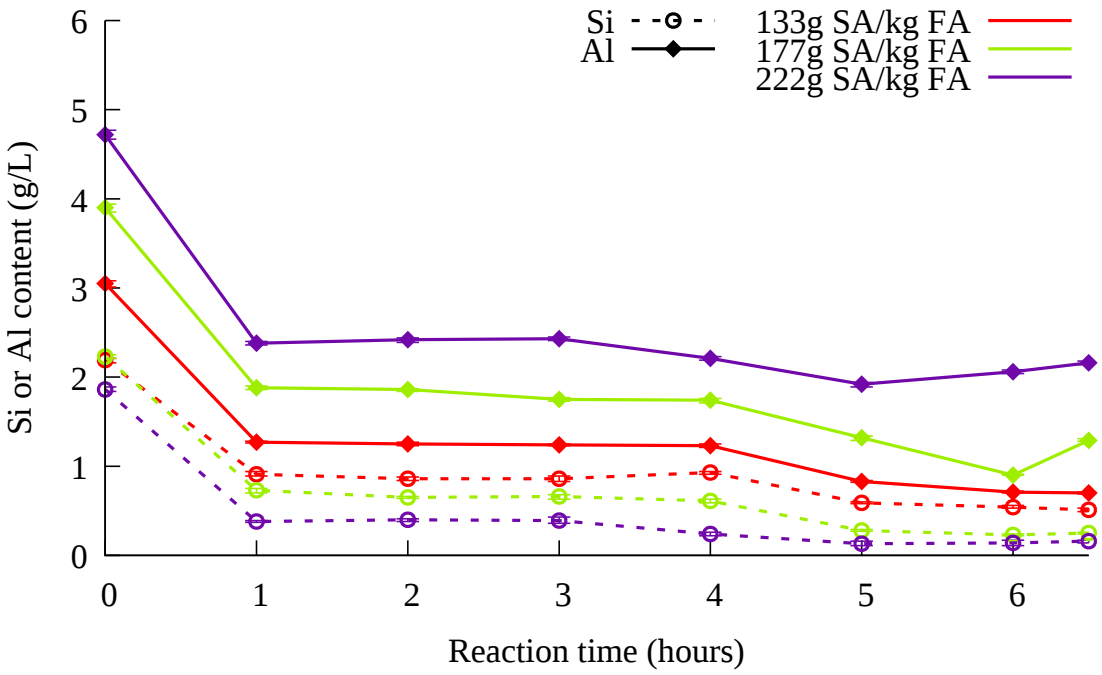

Figure 6.73: AAS results comparing SA dosage with constant sea salt dosage

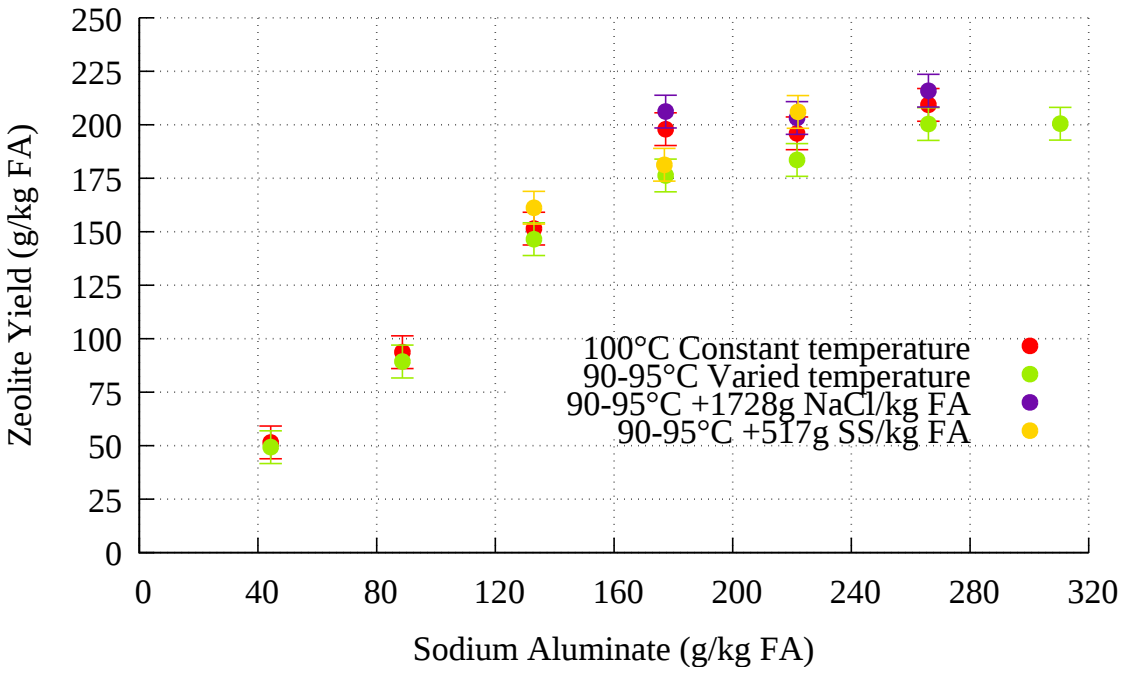

Figure 6.74: Yield results comparing SA dosage with constant sea salt dosage

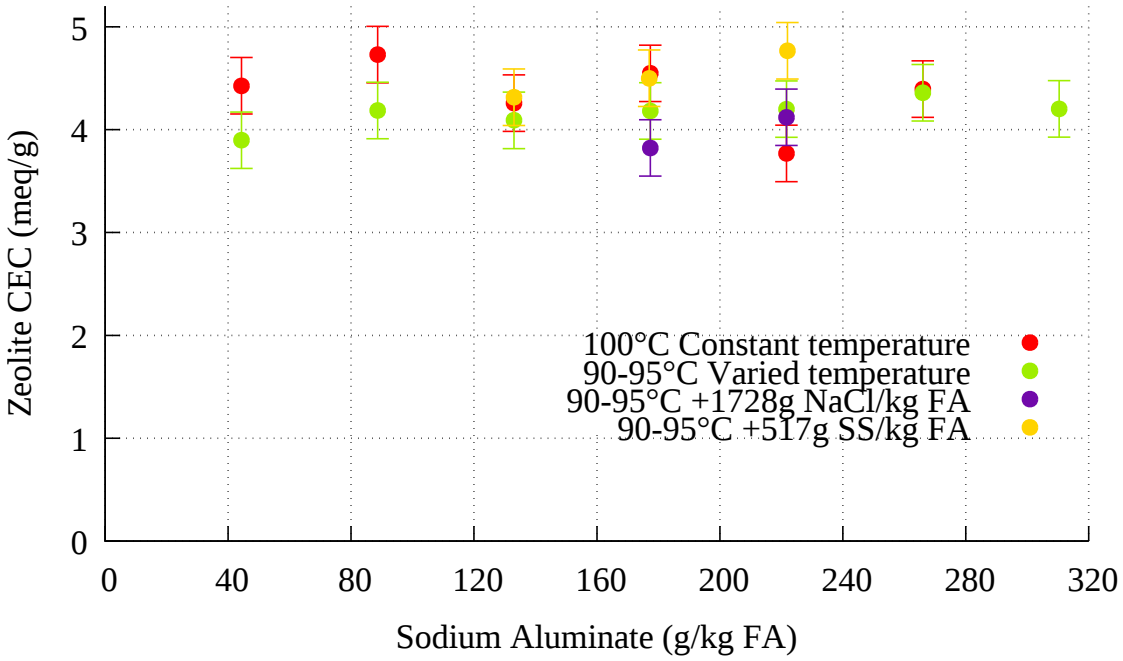

Figure 6.75: CEC results comparing SA dosage with constant sea salt dosage

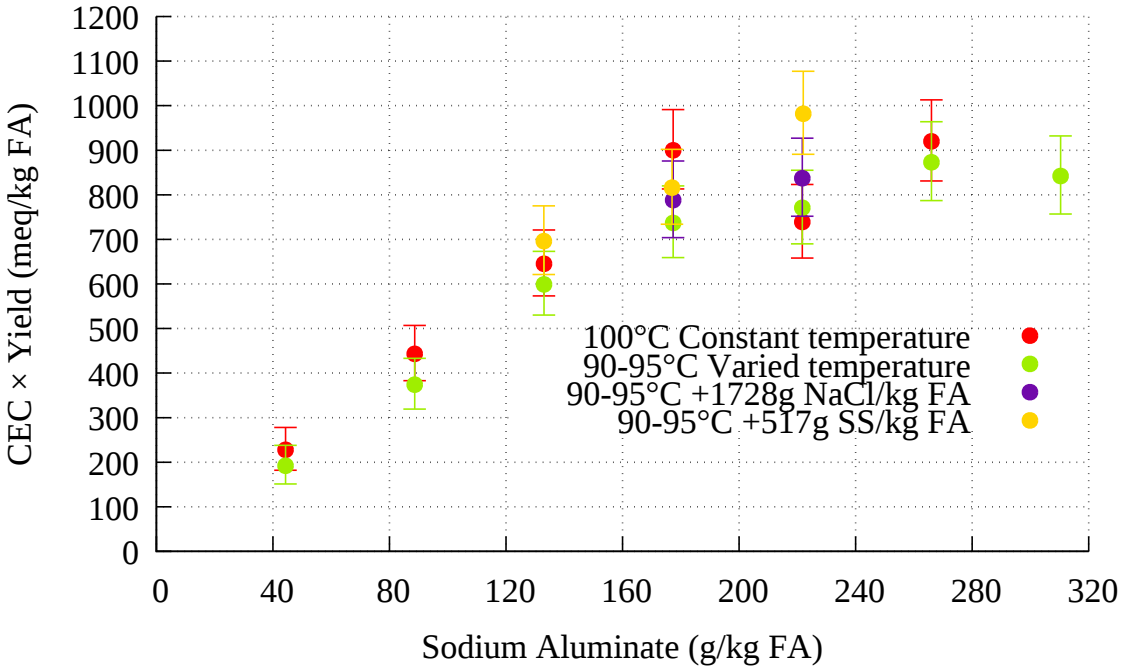

Figure 6.76: CEC × yield results comparing SA dosage with constant sea salt dosage

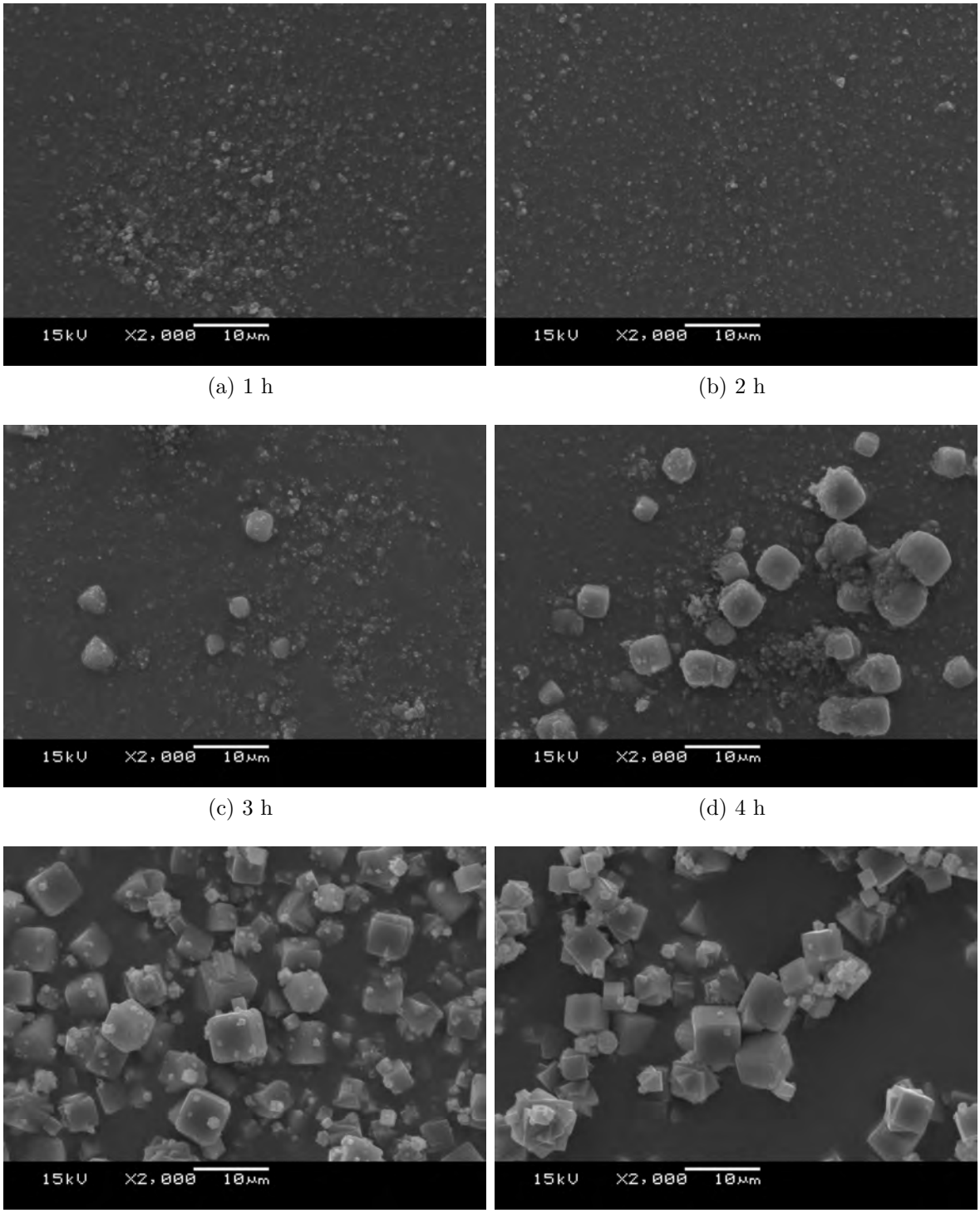

(a) 1 h (b) 2 h

(c) 3 h (d) 4 h

(e) 5 h (f) 6 h

Figure 6.77: SEM images of zeolites from ash leachate crystallised with 517 g of sea salt/kg FA and 133 g SA/kg FA on a stirred hot plate at 90-95°C

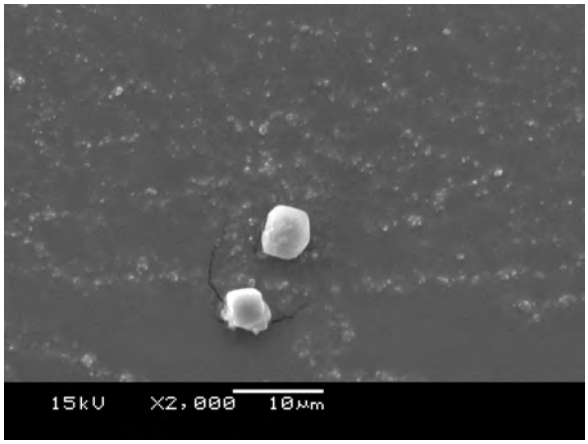

(a) 1 h

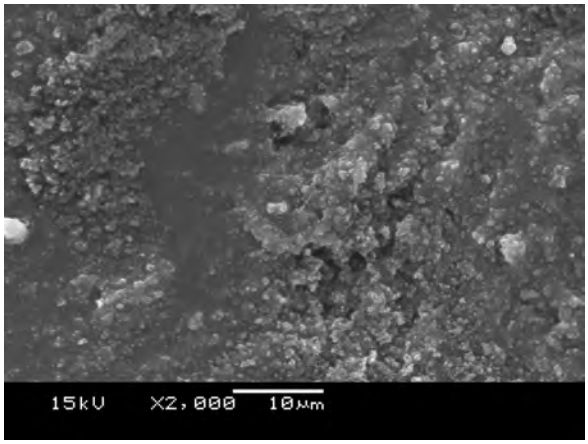

(b) 2 h

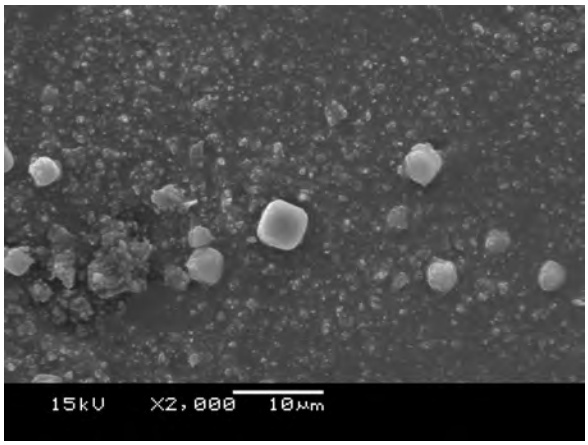

(c) 3 h

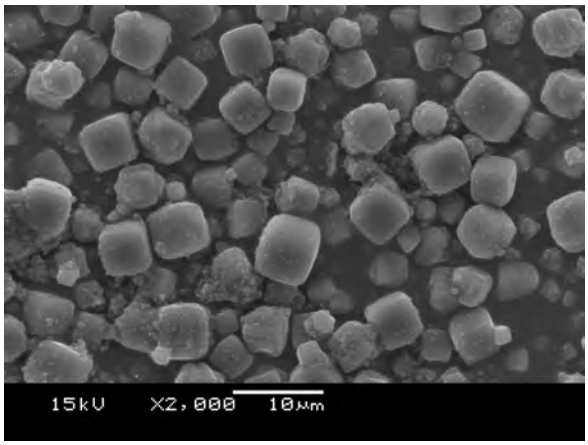

(d) 4 h

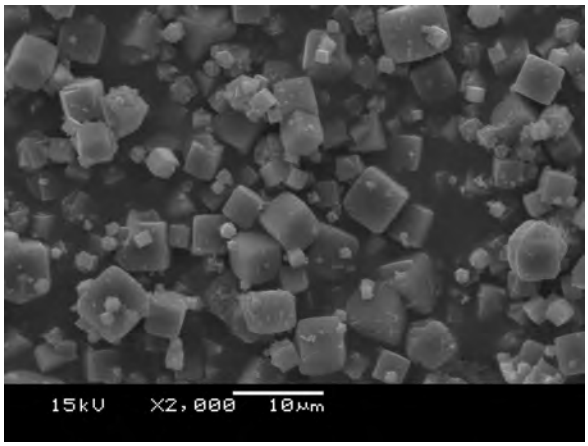

(e) 5 h

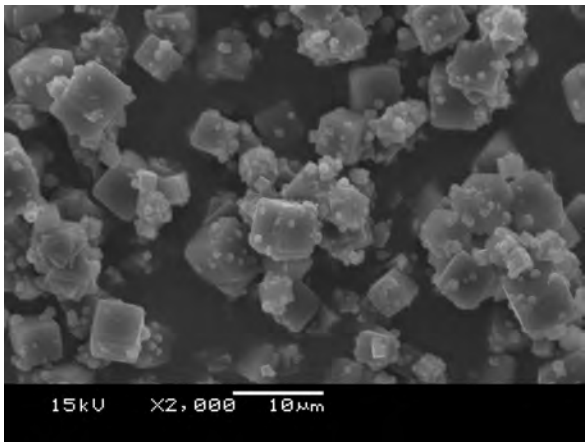

(f) 6 h

Figure 6.78: SEM images of zeolites from ash leachate crystallised with 517 g of sea salt/kg FA and 177 g SA/kg FA on a stirred hot plate at 90-95°C

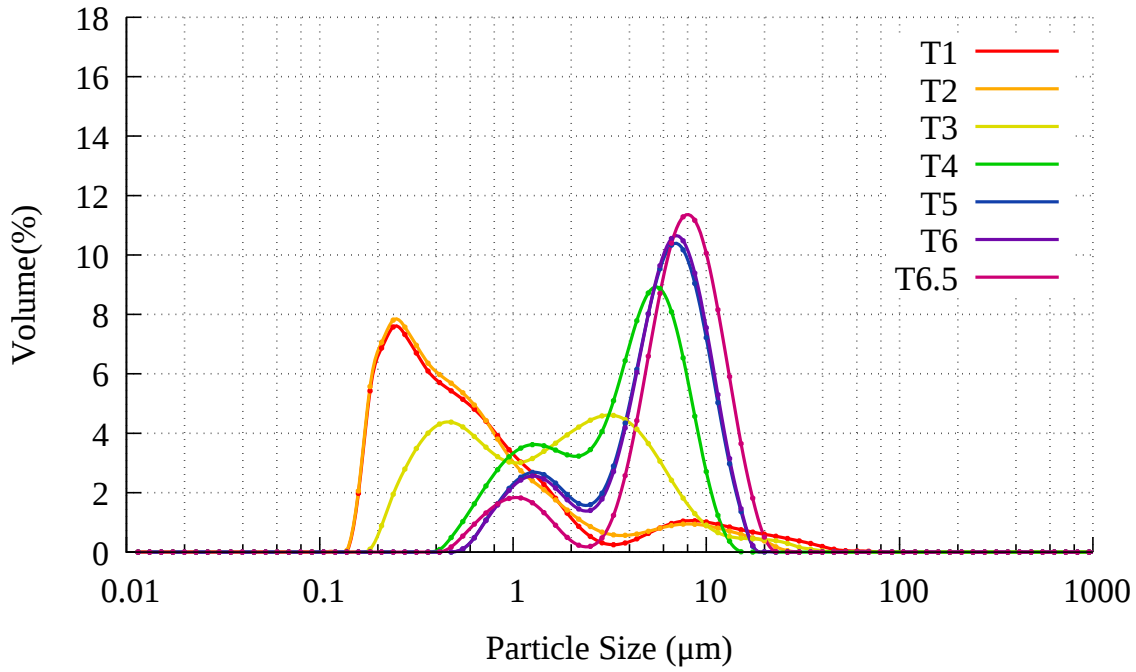

(a) PSD

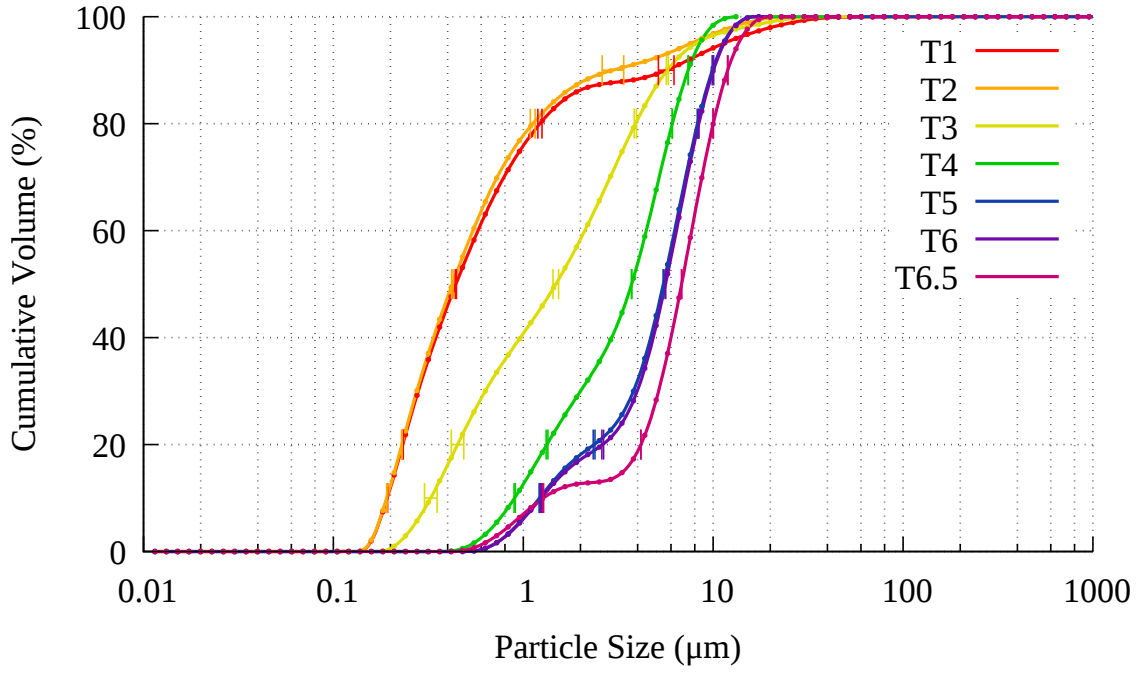

(b) Standard deviation in PSD

Figure 6.79: 90-95°C crystallisation process with 517 g sea salt/kg FA and 133 g SA/kg FA

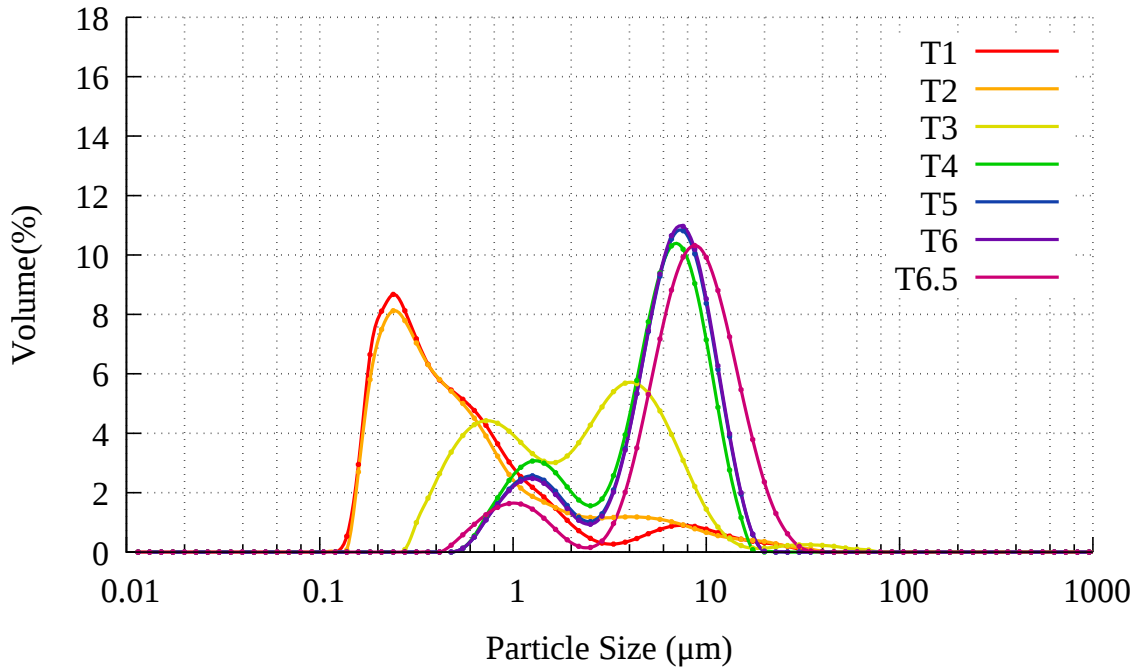

(a) PSD

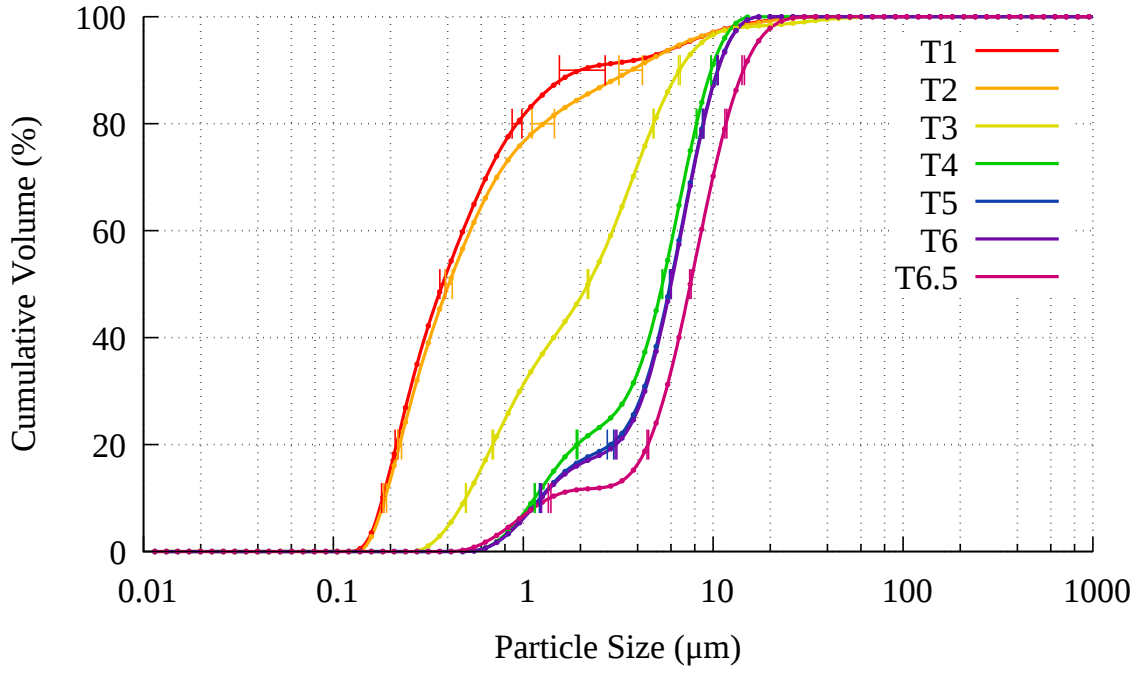

(b) Standard deviation in PSD

Figure 6.80: 90-95°C crystallisation process with 517 g sea salt/kg FA and 177 g SA/kg FA

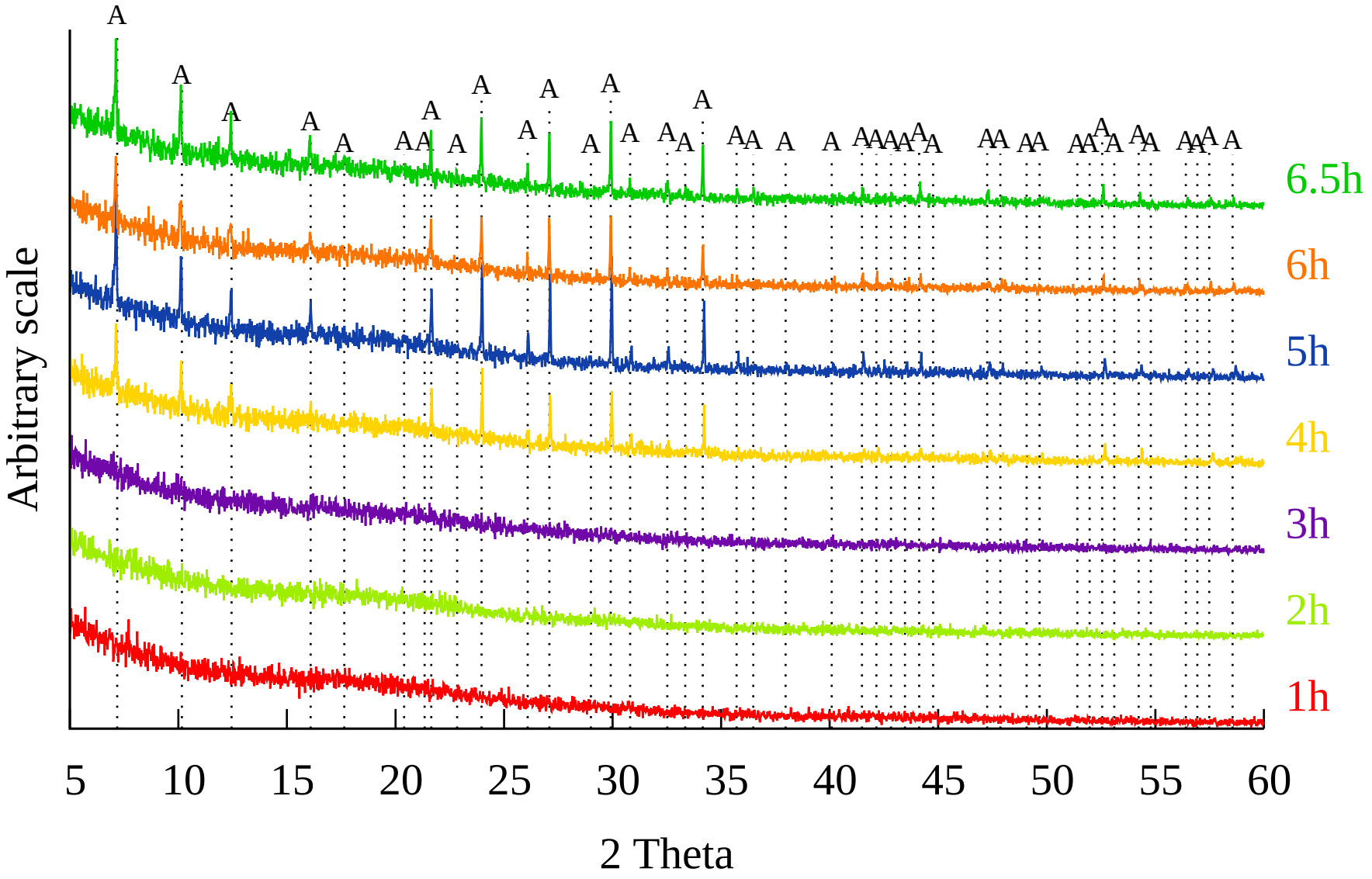

Figure 6.81: XRD patterns of 90-95°C crystallisation with 517 g sea salt/kg FA and 133 g SA/kg FA. A: Zeolite Na-A. $\lambda = 1.5406$ Å

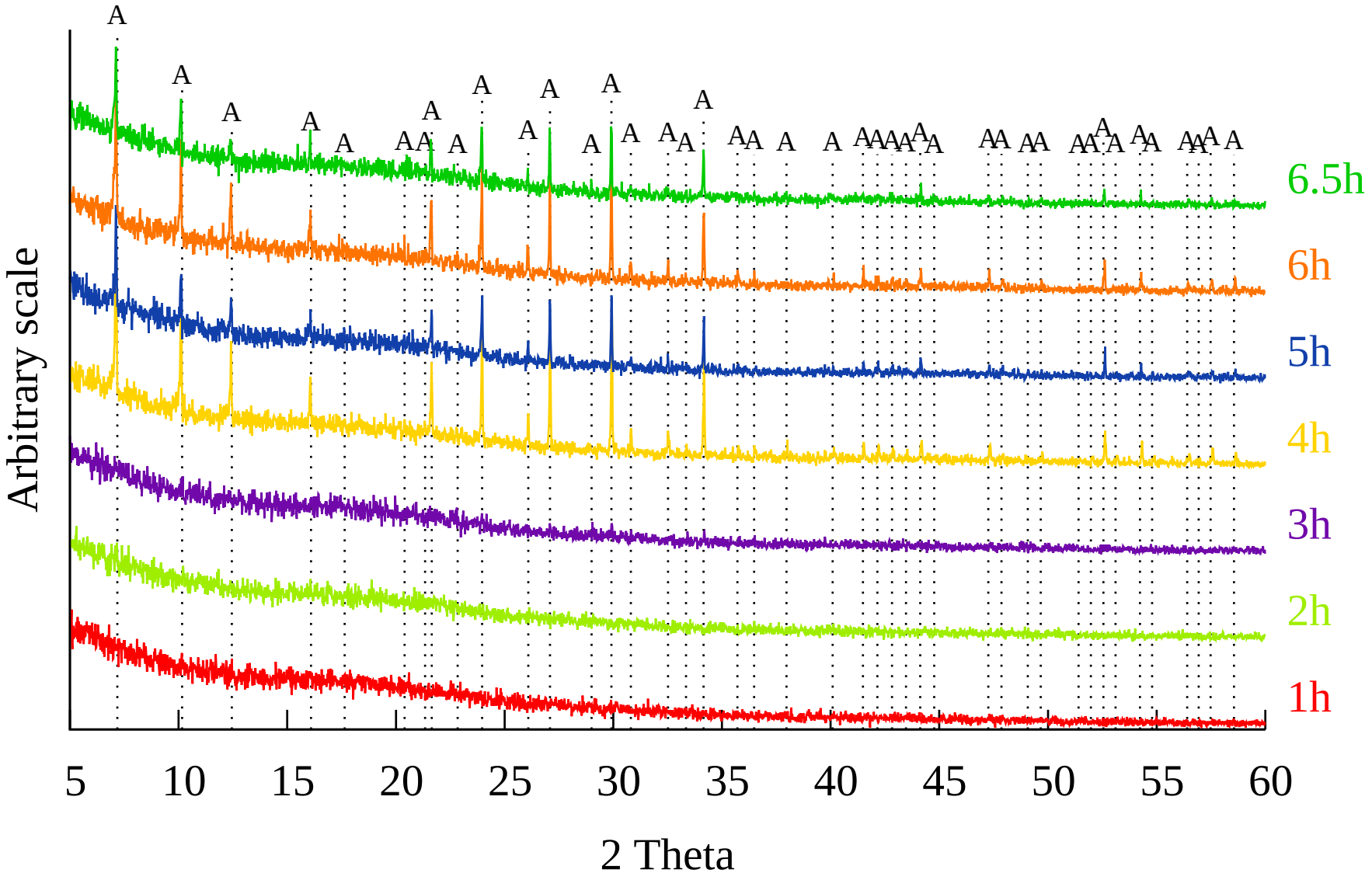

Figure 6.82: XRD patterns of 90-95°C crystallisation with 517 g sea salt/kg FA and 177 g SA/kg FA. A: Zeolite Na-A. $\lambda = 1.5406$ Å

6.8 Repetition

Repetition is necessary in order to assess accuracy, however repetition of each experiment would have been time consuming and costly to such a degree as to have limited the scope of this work. In order to gain an estimate of accuracy, one experiment was repeated and the variation found in these results applied to other experiments. Four experiments were carried out with lengths of 3 to 6 hours, and 5 experiments were conducted for 5 hours (including the 5 hour experiment from the 3-6 hour range) totalling 8 experiments. Samples were not taken throughout, only the final product was measured.

6.8.1 Method

80 g of NaOH were mixed with 67.66 g of Delta ash, and fused in the microwave using the fusion vessel depicted in Figure 4.3. The sample was microwaved for 5 minutes on full power, then mixed, further fused for 5 minutes and then mixed again. The sample was then dissolved in 1 litre of ambient temperature distilled water for 10 minutes, stirred by a PTFE coated stirring rod, powered by a mixer operating at 2000 rpm. The ash was then filtered from the leachate using a sintered glass Büchner funnel, and 900 ml of the leachate was added to a conical flask on the stirred hot plate depicted in Figure 5.1. 35 g of sea salt was then added to the leachate, the 60 mm magnetic stirring bead added and the apparatus set to 90°C. Upon reaching the set temperature, 100 ml of distilled water with 12 g of sodium aluminate dissolved therein was added to the conical flask and the timer started. At 2 hours, the temperature was raised to 95°C. At the end of the experiment, the sample was cooled for 30 minutes, then filtered in a sintered glass Büchner funnel, the leachate retained for analysis. The zeolite was then washed with distilled water and dried overnight in a drying oven.

6.8.2 Results

Figure 6.83a shows the AAS results for the 5 hour experiment repeated in quintuplicate. The standard deviation was derived from this data, and applied to the data points in Figure 6.83b. The same approach was taken for the yield in Figure 6.84, the CEC in Figure 6.85, and the CEC multiplied by yield in Figure 6.86. The final AAS values for the repeated 5 hour experiment seem quite similar, with a relative standard deviation of 23 % for Si and 3 % for Al. The comparatively high RSD for Si could be due to the low Si content. The 5 hour samples measured were found to contain between 0.32 and 0.19 ppm Si, with a mean of 0.25 ppm and a standard deviation of 0.06 ppm. The mean result for the Al values was 1.44 ppm, with a standard deviation of 0.06 ppm.

The yield experiments in Figure 6.84a show a range of 226-245 g of zeolite /kg FA, with a mean of 233 g/kg FA and a standard deviation of 7.7 g (RSD of 3.3 %). This standard deviation was applied to the data in Figure 6.84b, as well as other yield data to produce the error bars shown in all yield graphs. When comparing the 6 hour experiment to the experiment with the same conditions that had samples taken hourly, the regularly sampled experiment was found to have a yield which was 78 % of the experiment from which no samples were taken. The total volume of samples taken should amount to 17.5 % of the total volume of the crystallisation solution ignoring loss through evaporation. Removal of some of the zeolite nuclei from early stages of the crystallisation process is expected to have a greater influence on the final yield than simply removing some of the solution, thus this yield data is treated as quantitative, whilst all other yield data is provided as a qualitative measure of how yield is influenced by experimental conditions. These results are reasonable when compared to literature. Experiments by Yaping et al. [90] had a yield of zeolite A of 314-368 g zeolite/kg FA after 5 hours of crystallisation, although this was for a system seeded with zeolite A crystals following a fusion process at 850°C with sodium carbonate.

The CEC results shown in Figure 6.85 were treated in the same manner as the yield results. The CEC results of the repeated 5 hour experiments were averaged and the

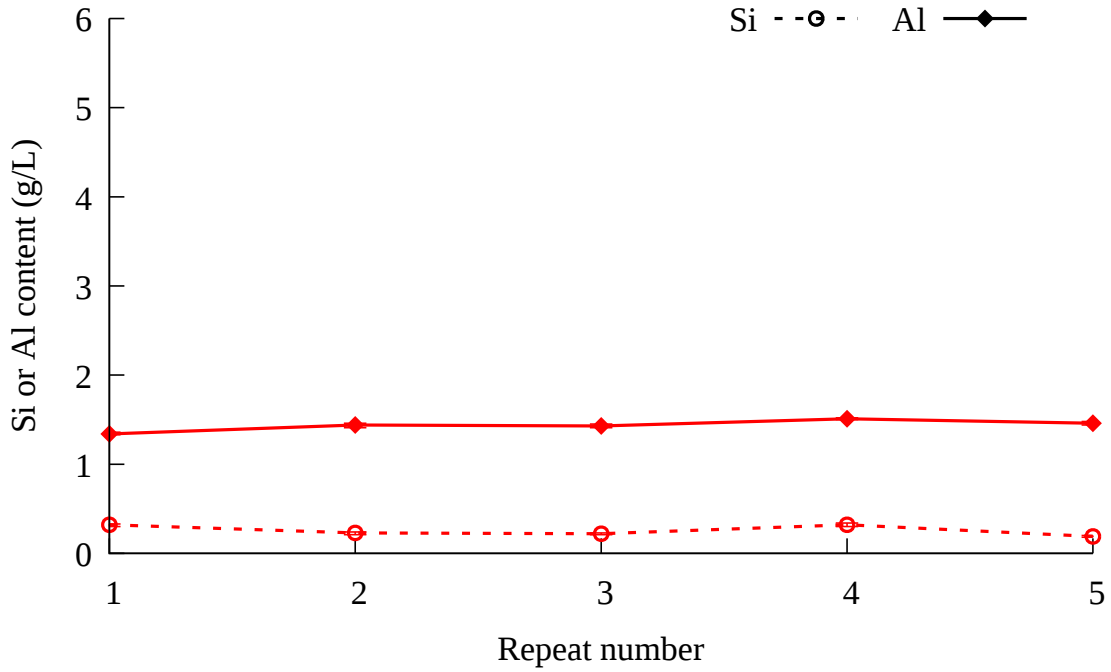

(a) 5 hour repeats

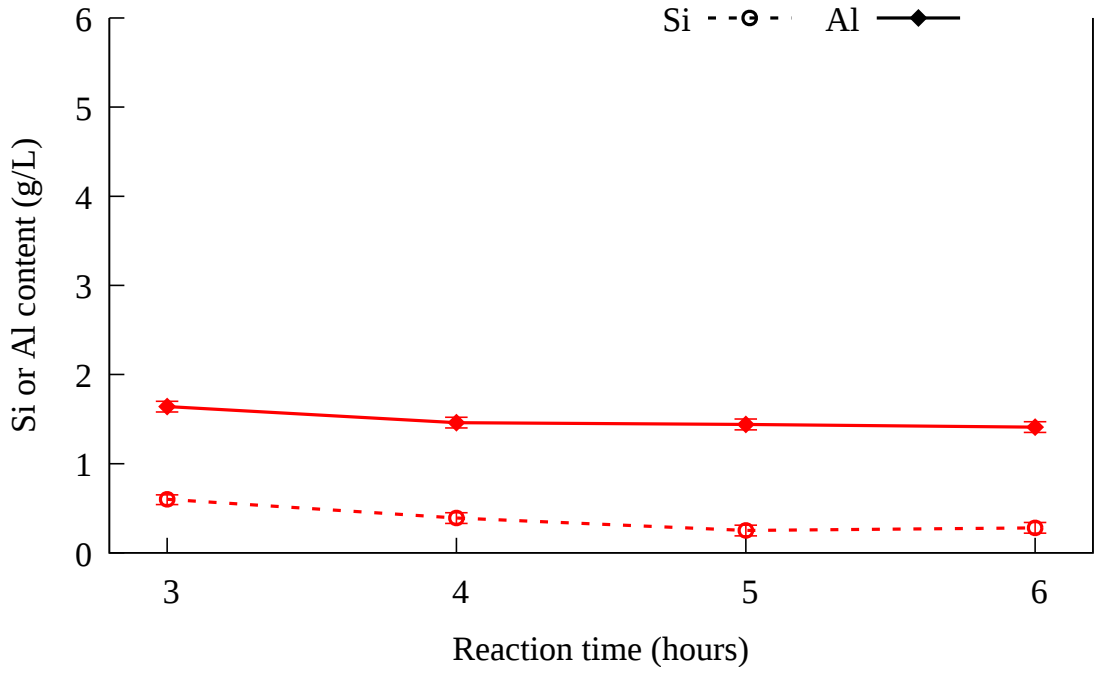

(b) 3-6 hour experiments

Figure 6.83: Repeated 5 hour AAS results with error applied to 3-6 hour experiments

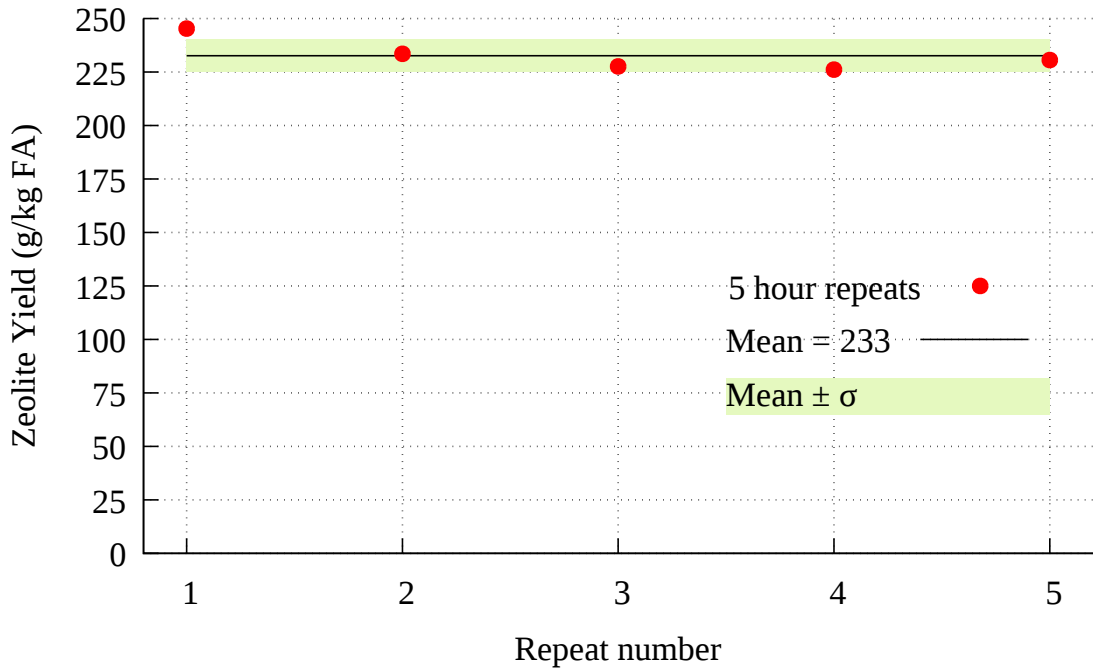

(a) 5 hour repeats, with mean value shown, and standard deviation highlighted in green

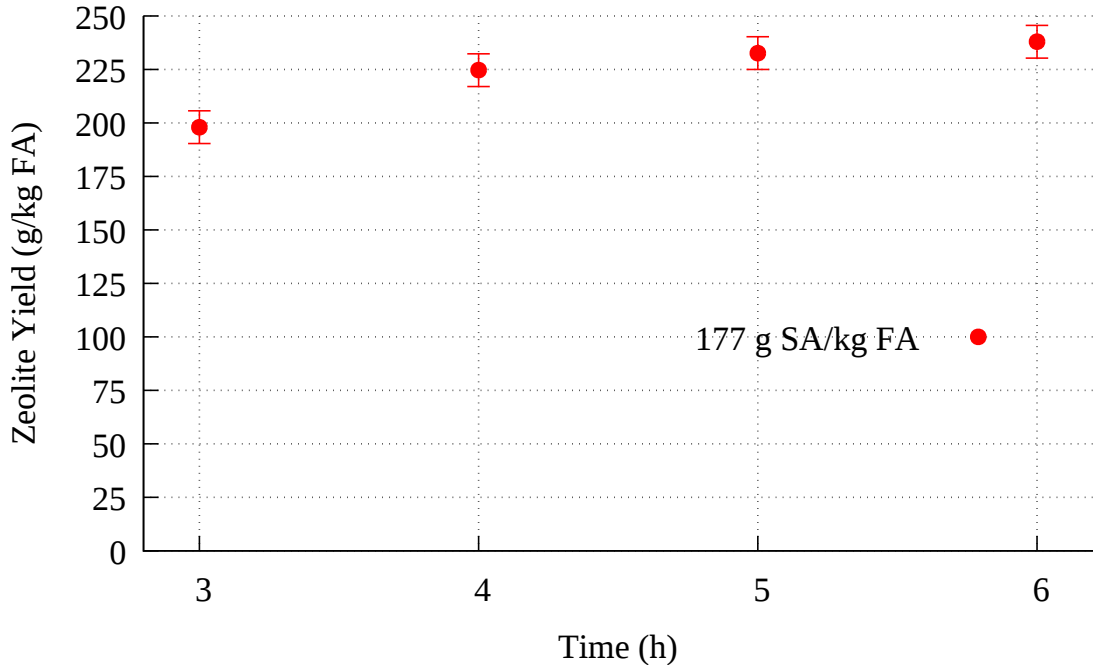

(b) 3-6 hour experiments

Figure 6.84: Repeated 5 hour yield results with error applied to 3-6 hour experiments

standard deviation calculated. The mean CEC was found to be 4.6 meq/g, with a standard deviation of 0.27 (RSD 5.9 %). This standard deviation was applied to the 3-6 hour experiments and is shown in Figure 6.85b. These results are taken as a quantitative assessment of the CEC. When compared to CEC results from literature, these values appear acceptable, and sane, because they are less than the 5 meq/g limit stipulated by literature [3]. Similar experiments by Yaping et al. [90] showed zeolite A to have a CEC of 3.8-4.5 meq/g, whilst Izidoro et al. [54] showed zeolite A to have a CEC of 3.9 from a direct conversion of fused ash method. CEC experiments on zeolites X or P have been shown to have a CEC of 4-4.2 meq/g [44] or 3.1-4.6 meq/g [90].

The CEC yield is shown in Figure 6.86. The mean yield of CEC from the repeated 5 hour experiments was 1074.9 meq/kg FA, with a standard deviation of 54.8 meq/kg FA (RSD 5.1 %). This standard deviation was applied to the 3-6 hour experiments and is shown in Figure 6.86b.

XRD patterns in Figure 6.87 show zeolite A detected at all time points, with the weakest at 3 and 4 hours, with 5 and 6 hour experiments showing little variation between themselves.

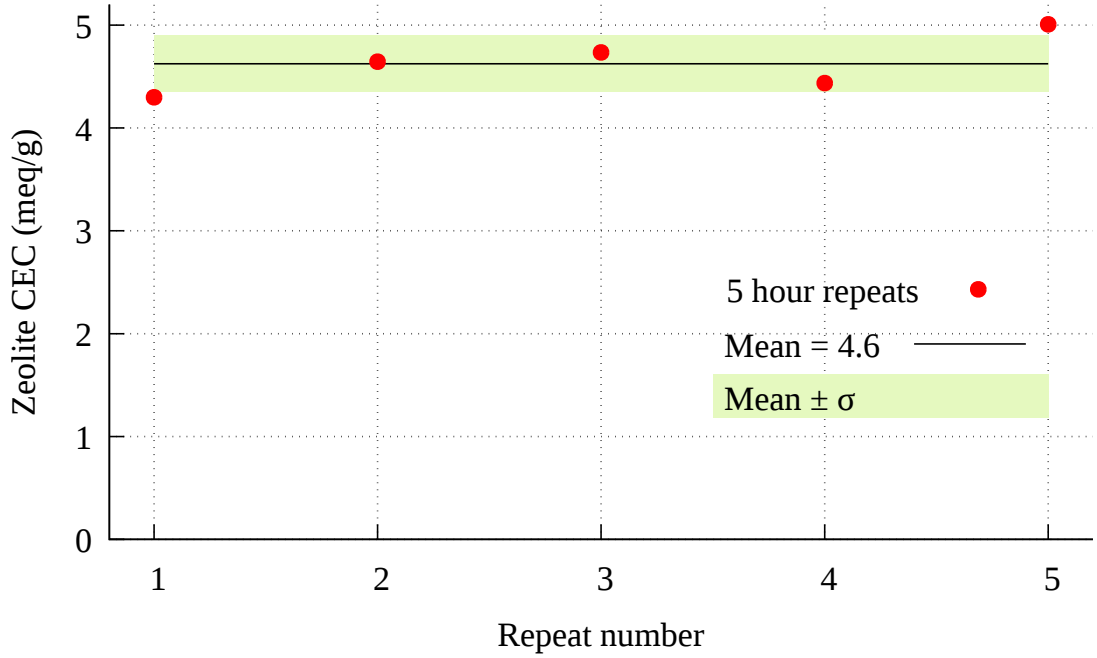

(a) 5 hour repeats, with mean value shown, and standard deviation highlighted in green

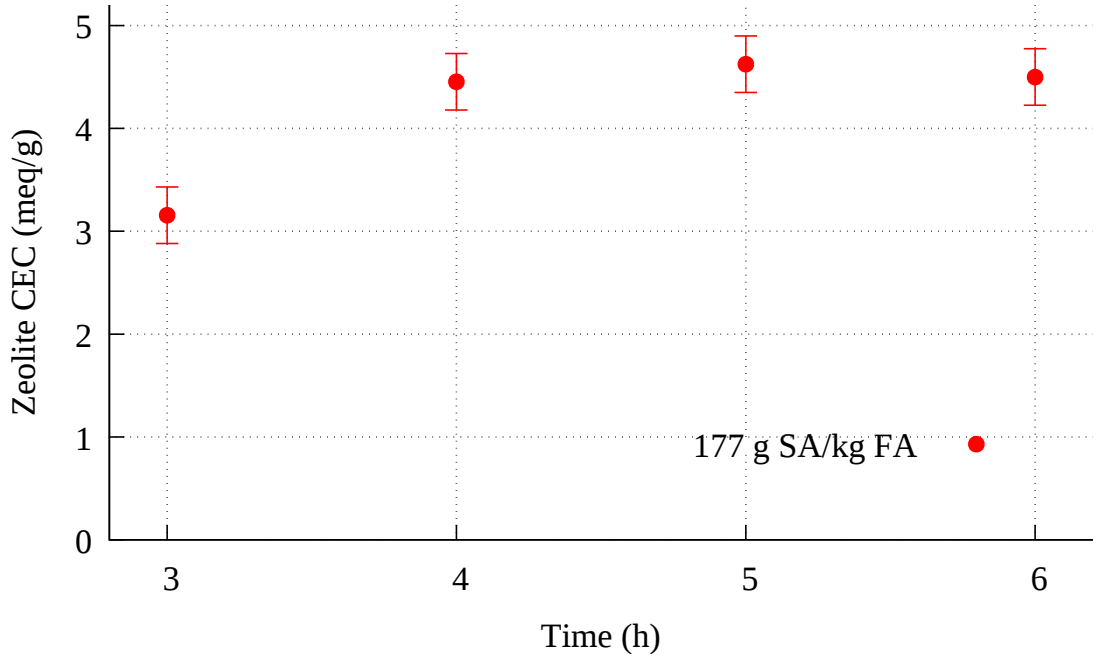

(b) 3-6 hour experiments

Figure 6.85: Repeated 5 hour CEC results with error applied to 3-6 hour experiments

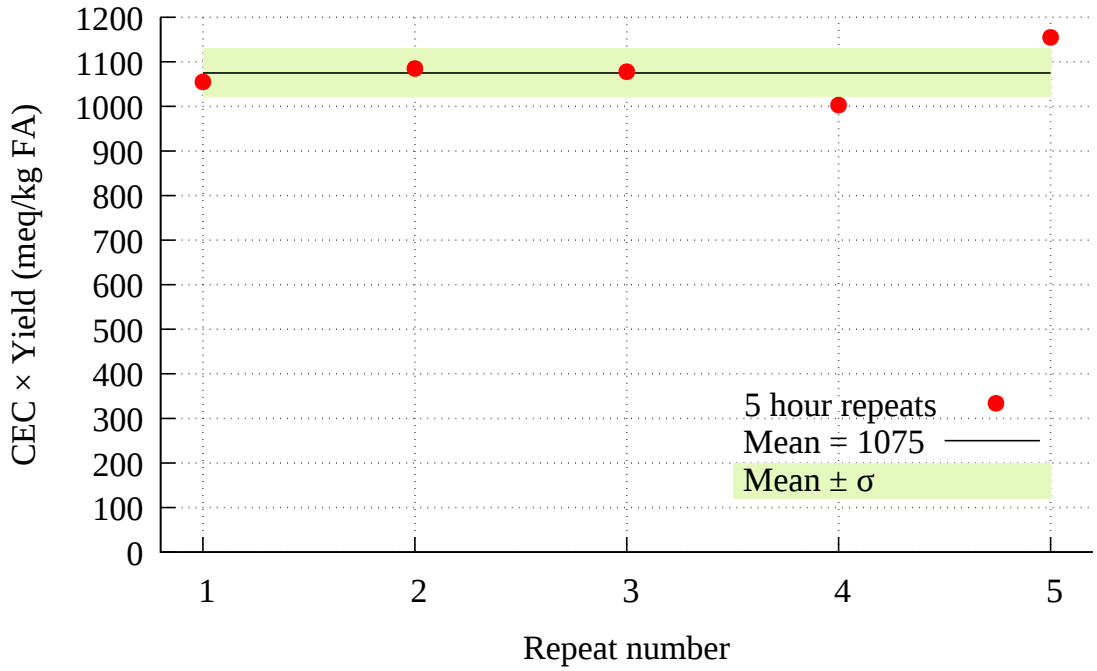

(a) 5 hour repeats, with mean value shown, and standard deviation highlighted in green

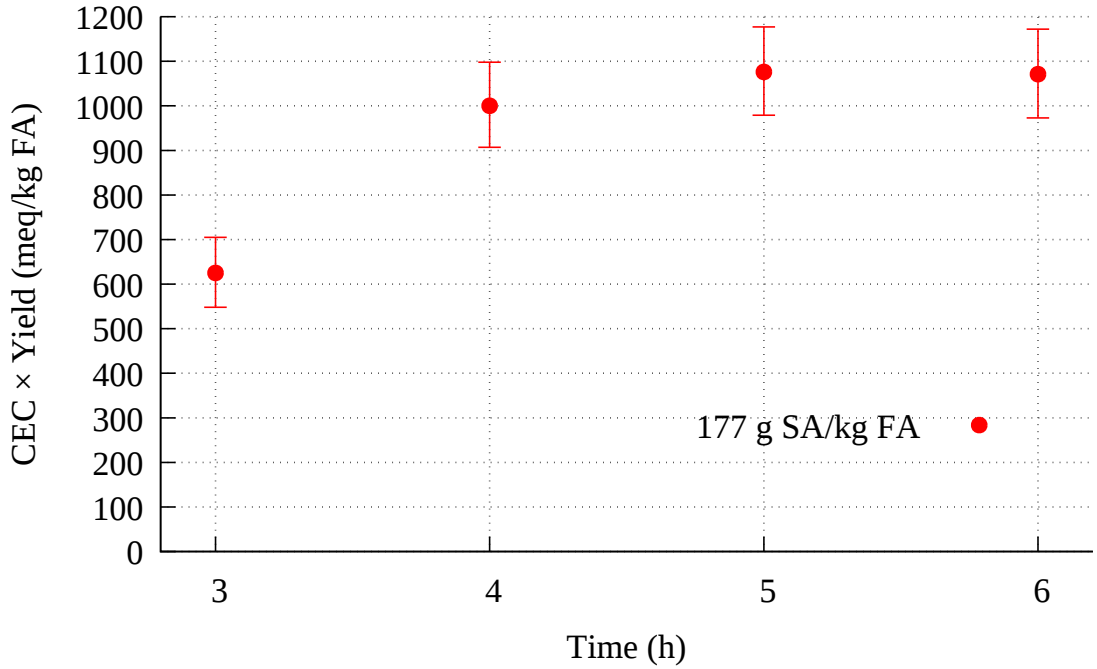

(b) 3-6 hour experiments

Figure 6.86: Repeated 5 hour CEC × yield results with error applied to 3-6 hour experiments

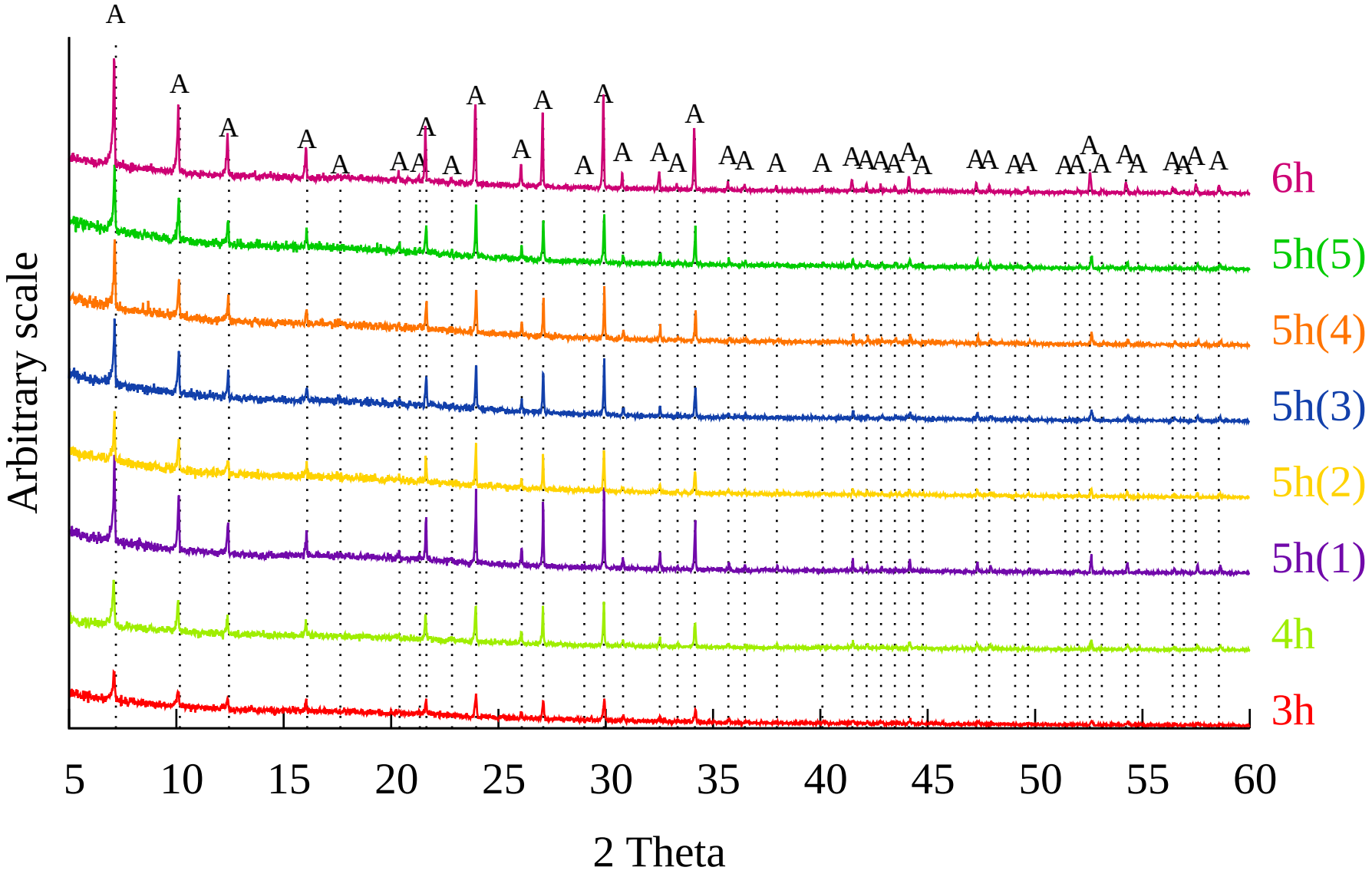

Figure 6.87: XRD patterns of repeated experiments at 90-95°C. A: Zeolite Na-A. $\lambda = 1.5406$ Å

SEM images are shown in Figure 6.88. Figure 6.88a shows the SEM image from the 3 hour experiment, which contains amorphous material as well as some zeolite cubes. In the 4 hour SEM image Figure 6.88b, the amorphous material is no longer present, and smooth surfaced cubes, some of which intersect each other are visible. There is very little change between the 4, 5, and 6 hour experiments. These SEM images are similar to the SEM images produced by Musyoka et al. [35], which show amorphous material early in the experiment, which is replaced with crystalline cubes of zeolite A.

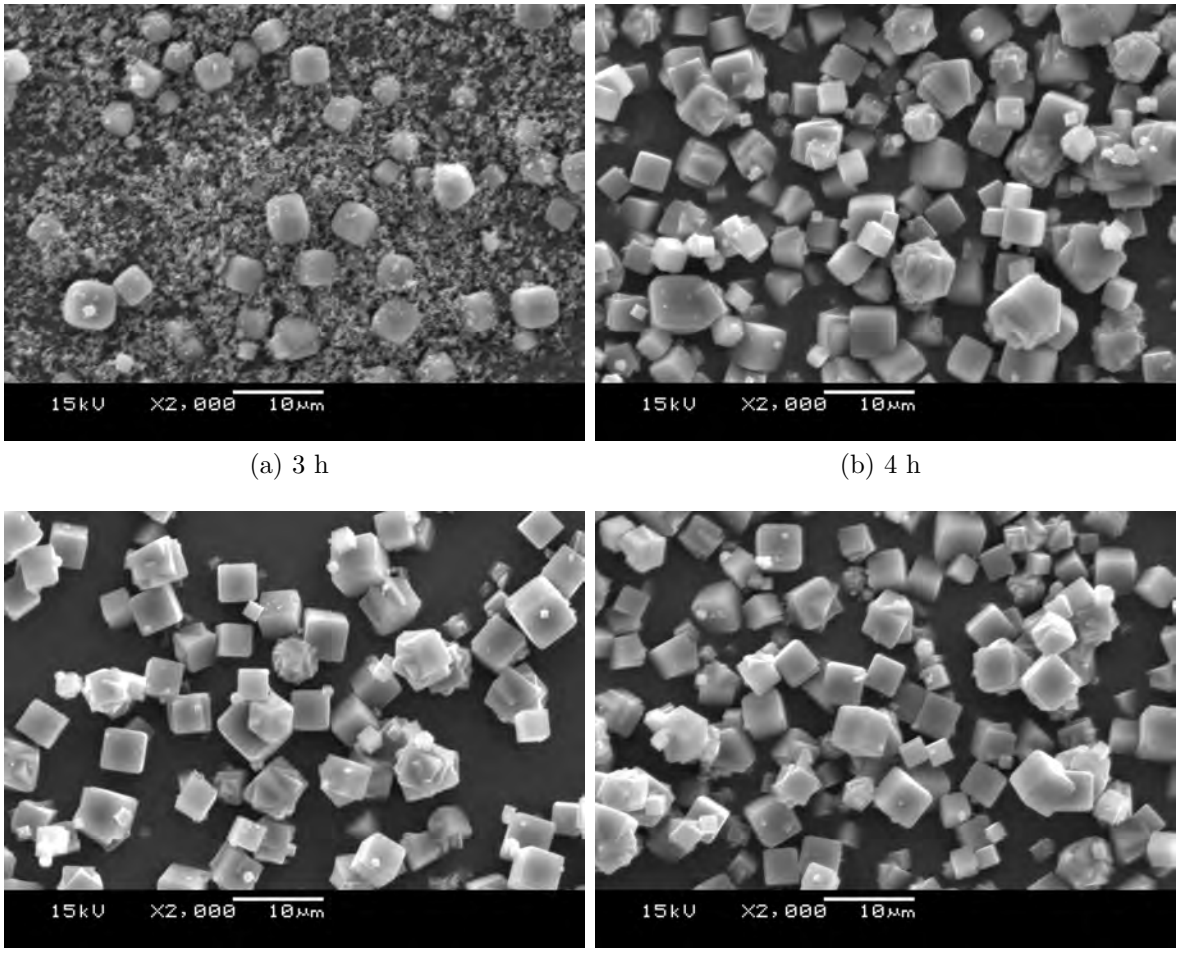

(a) 3 h (b) 4 h

(c) 5 h (d) 6 h

Figure 6.88: SEM images of zeolites from repeated experiments with ash leachate crystallised with 177 g of sodium aluminate/kg FA & 517 g sea salt/kg FA on a stirred hot plate at 90-95°C

Chapter 7

Crystallisation of Zeolites: Effect of Ash Source

7.1 The Effect of Different Ash Sources on the Crystallisation Process

Coal fly ash is a heterogeneous material. Due to this it is necessary to investigate the effects that changing the source ash will have on results. The main ash source used in experiments thus far has been the Delta processed ash product from RockTron. The finer RockTron product Alpha was also tested, along with two unprocessed ashes, an untreated ash from a storage Lagoon, and an untreated ash referred to as FB7.

The experimental method used is outlined in section 6.1. For the crystallisation, 517 g of sea salt and 222 g SA/kg FA were added to the crystallisation conditions.

AAS results are shown in Figure 7.1. The starting Si content of the Lagoon ash is noted to be higher than the Lagoon and FB7, resulting in a correspondingly lower final Al content. This increase in starting Si is better shown in Figure 4.21 on page 108, which displays the proportion of Si and Al extracted from each ash during the extraction process.

The SEM images for the crystallisation products from the Lagoon ash experiments are shown in Figure 7.5. The SEM images show a disappearance of amorphous material

between hours 3 and 4, with chamfered edged cubes apparent from 5 hours. This corresponds with the decrease in Al content between 3 and 4 hours from Figure 7.1. For the FB7 ash, the decrease in amorphous material between 4 and 5 hours shown in Figures 7.6d and 7.6e also corresponds with the AAS results of a decrease in Al content between these two measurements. The 6 hour products also show chamfered edge cubes. The Alpha product experiment SEM images show similar results to the FB7 experiments, but whilst the amorphous material also disappears between the 4 and 5 hour images 7.7d and 7.7e, cubes are in greater abundance in the 4 hour image for the Alpha experiment than the FB7 experiment.

The Lagoon PSD results in Figure 7.8 show the finer PSD for the first two hours, with a d_{50} of 0.5-0.6μm, and a very similar PSD for 4-6 hours with a d_{50} of 6 μm. The FB7 PSD results in Figure 7.9 show similar results, with a 0.4-0.5 μm d_{50} for 1-2 hours, and a 6 μm d_{50} for 5 and 6 hours. For the Alpha ash, the PSD results for the first two hours are distorted by measurements in the 10-20 μm range with high error in Figure 7.10b, which is most likely due to air entrained during measurement. The 4-6.5 hour measurements are all consistent with a d_{50} of 6-7 μm. The PSD of the zeolites at 6 hours is shown in Figure 7.11, and for 6.5 hours in Figure 7.12. The PSD's are broadly similar, however the Delta experiment zeolite has a narrower PSD than the other ashes, and few particles in the 2-4 μm range indicating distinct separation between nucleation and crystal growth phases.

The XRD results for the Lagoon experiment are shown in Figure 7.13, and correspond with the SEM images, showing zeolite A detected from 4 hours, but a weak pattern is also present at 3 hours, which is attributed to the scant cubes visible in Figure 7.5c. For the FB7 experiment, the XRD patten is shown in Figure 7.14. Zeolite A is similarly visible from 5 hours, with a weaker pattern visible at 4 hours. Figure 7.15 compares the final products from all XRD results. This shows zeolite A present in all samples.

The yield experiments shown in Figure 7.2 show that whilst the Delta experiment has the highest yield, the Lagoon sample is second with FB7 and Alpha ash being similarly lower. This increased yield from the Lagoon sample is anticipated from the AAS results

in Figure 7.1, which shows an increased starting quantity of Si. The variation in the starting yields of Si is discussed in section 4.5.2. The CEC shown in Figure 7.3 is similar for all experiments, with Alpha and FB7 being slightly lower than Lagoon and the Delta experiments. The decrease in yield has a significant effect on the CEC × yield results in Figure 7.4 which, is mostly attributed to the higher Si yield during extraction.

The combined results presented in this section indicate that the method used can produce zeolite A from a few different ash sources, however the processing of fly ash to the Delta product by RockTron increases the cation exchange capacity yield of the final product. This is in agreement with literature where magnetic separation of ash has been shown to improve CEC, although literature notes a larger improvement in CEC has been observed in hydrothermal extraction processes than the fusion extraction process used in these experiments [6, 28].

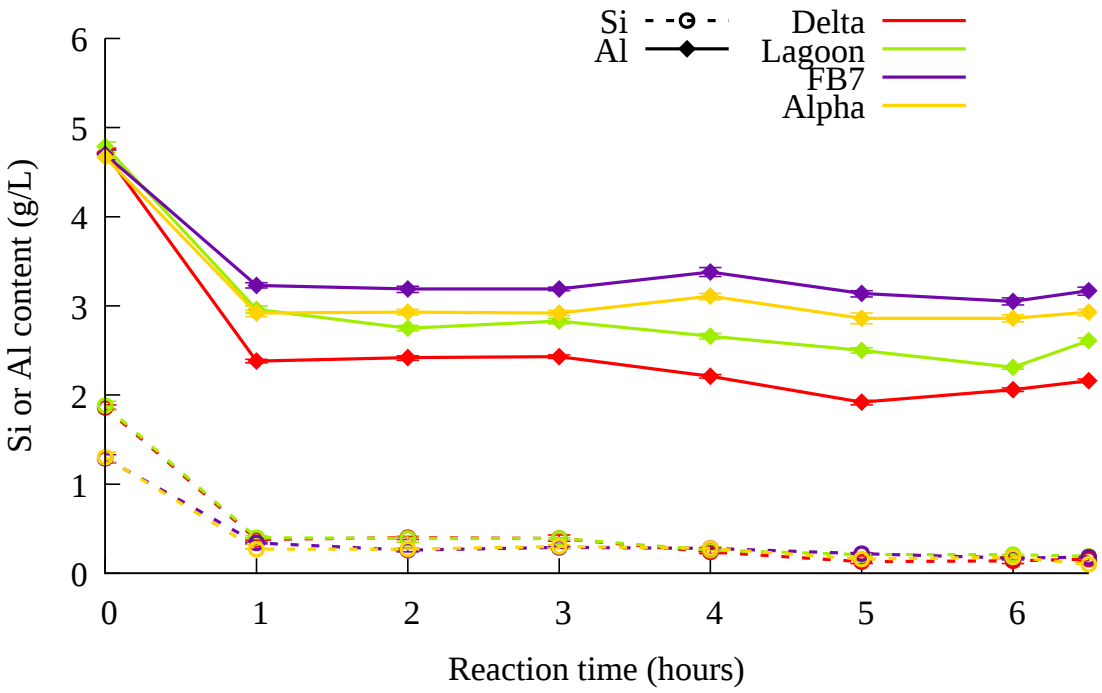

Figure 7.1: AAS results comparing ash source

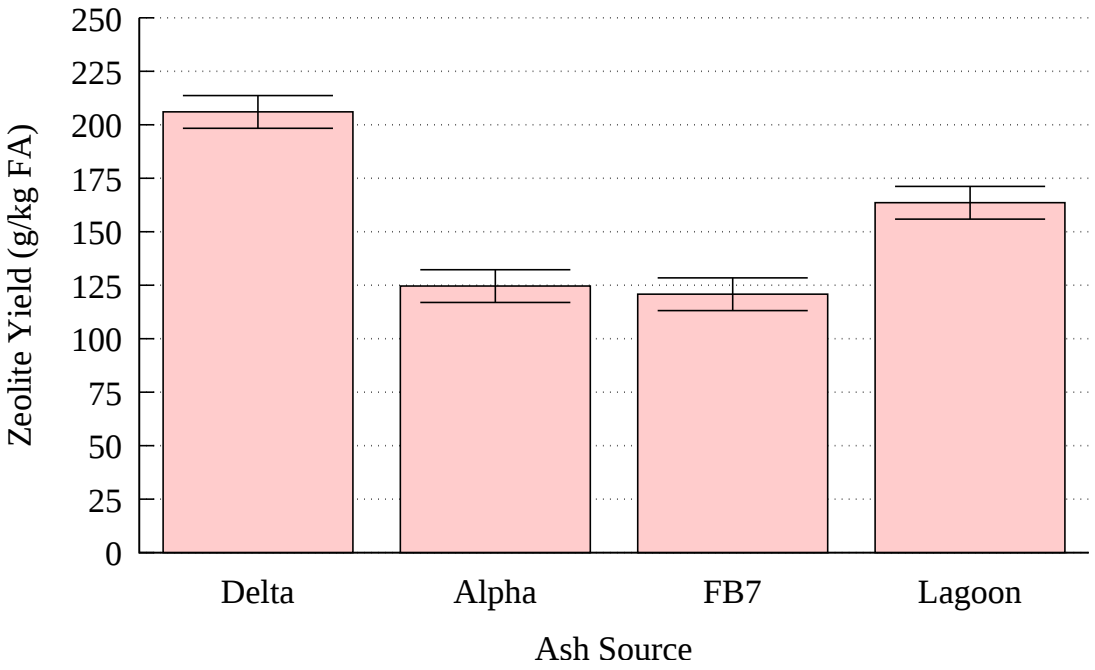

Figure 7.2: Yield results comparing ash source

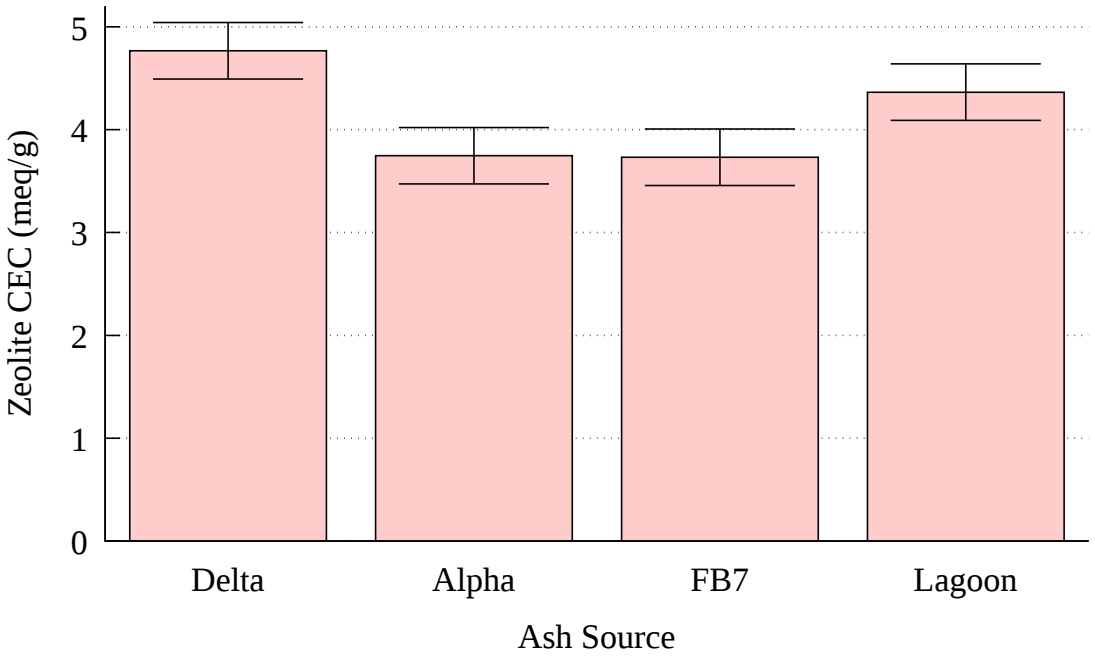

Figure 7.3: CEC results comparing ash source

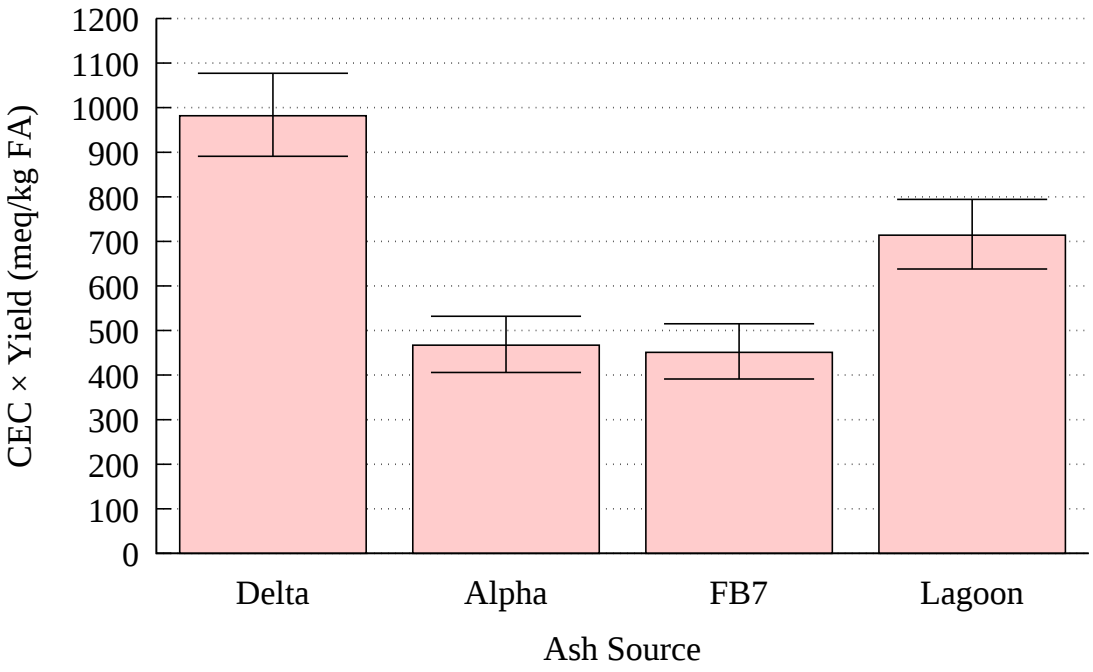

Figure 7.4: CEC × yield results comparing ash source

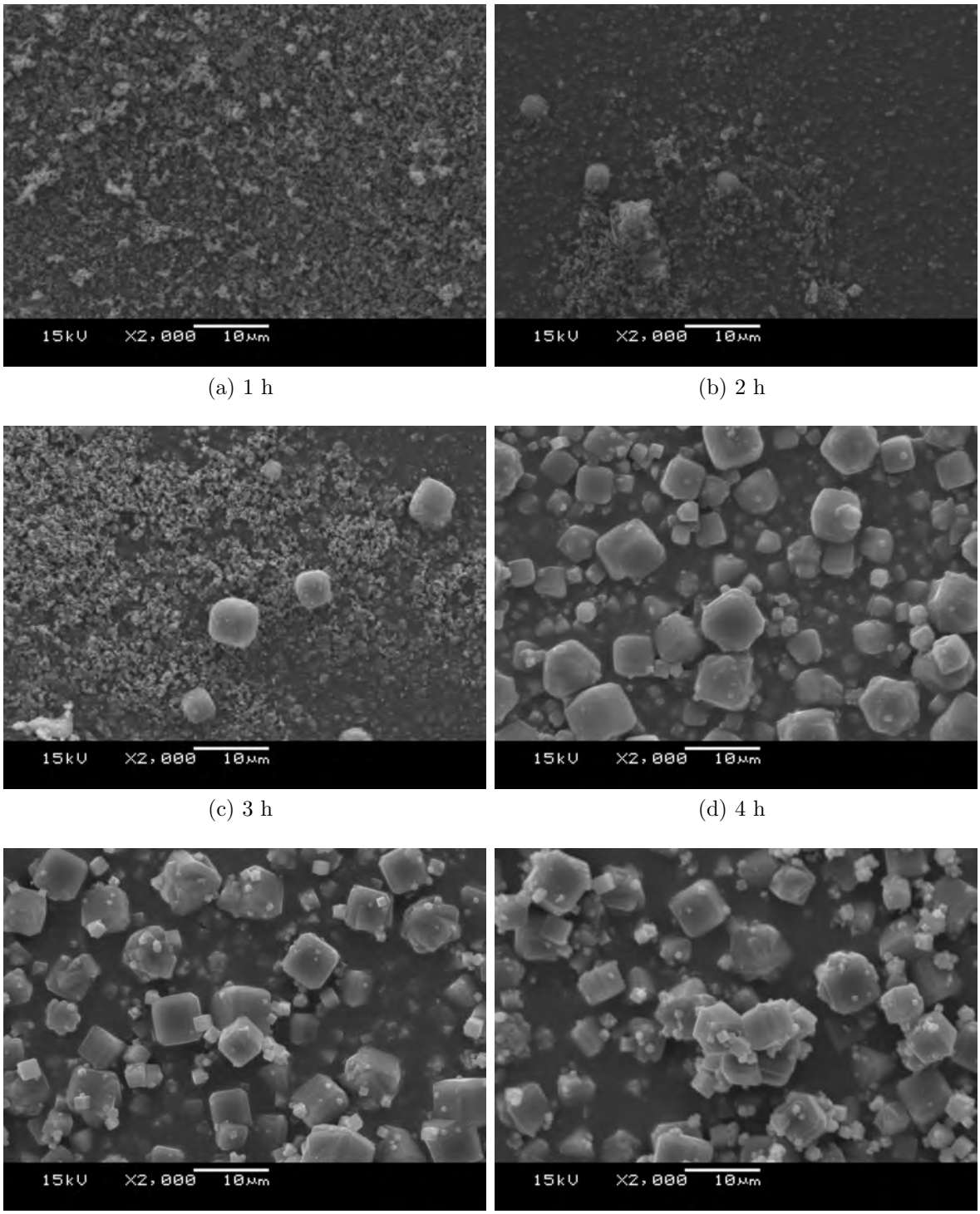

(a) 1 h (b) 2 h

(c) 3 h (d) 4 h

(e) 5 h (f) 6 h

Figure 7.5: SEM images of zeolites from Lagoon ash leachate

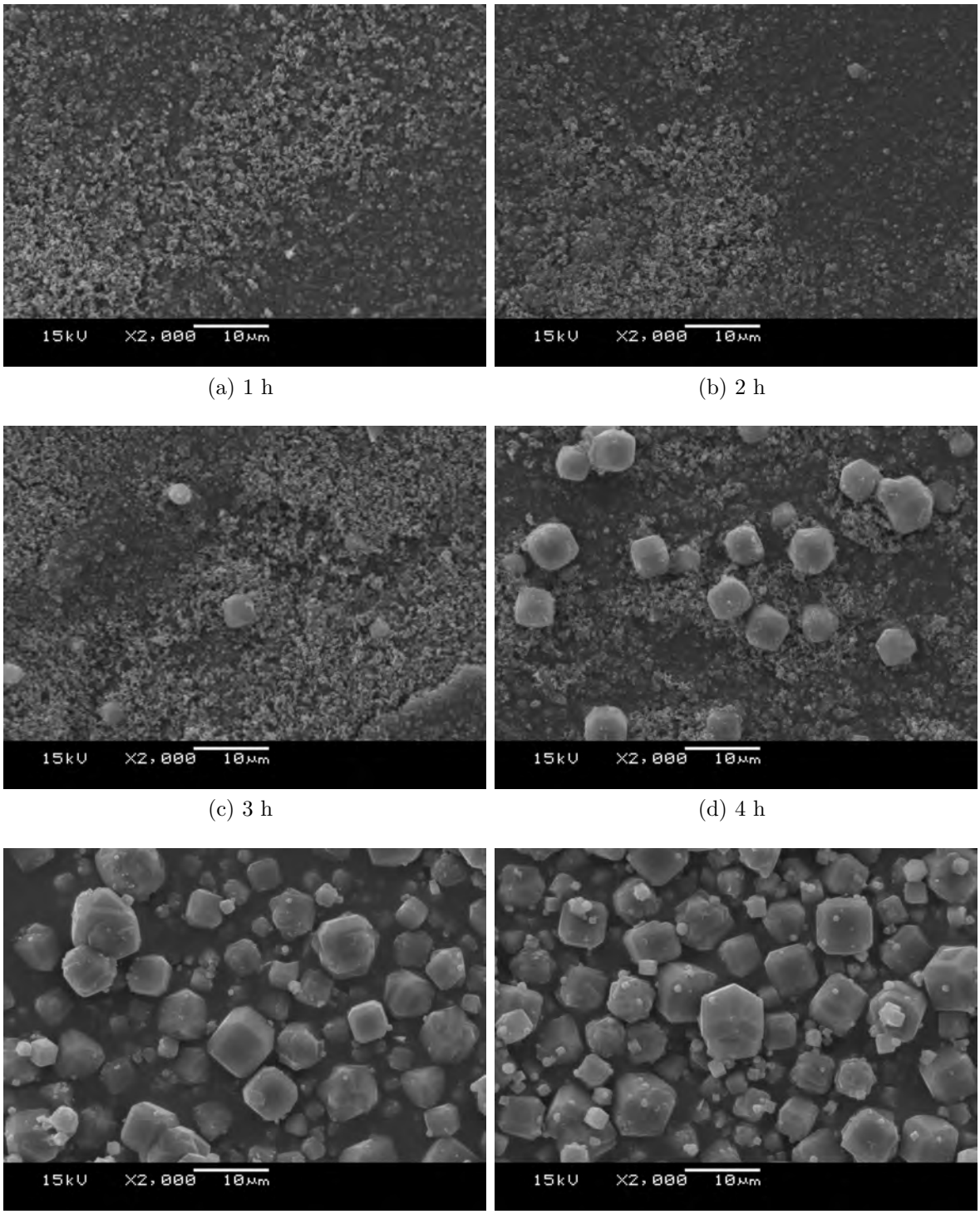

(a) 1 h (b) 2 h

(c) 3 h (d) 4 h

(e) 5 h (f) 6 h

Figure 7.6: SEM images of zeolites from FB7 ash leachate

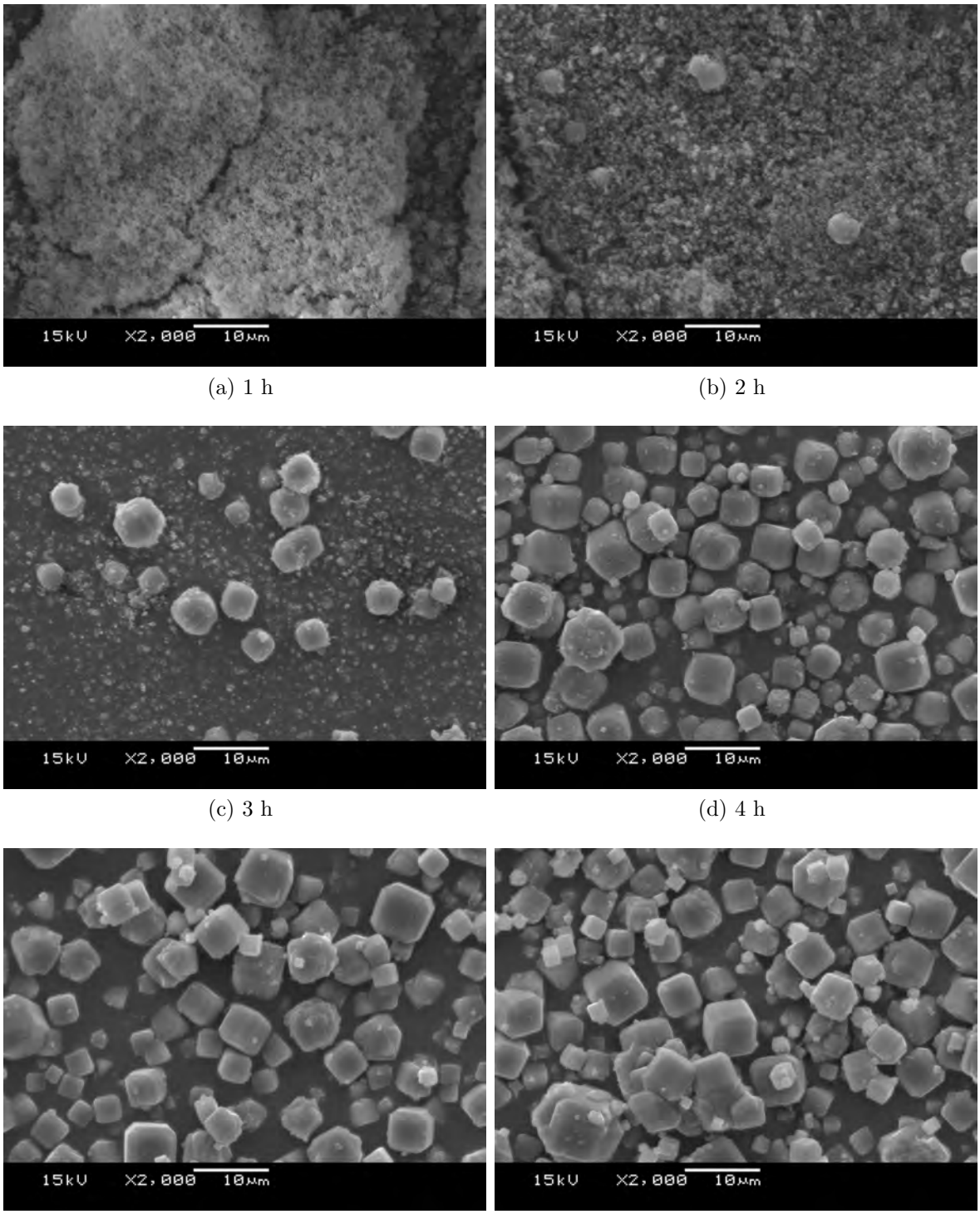

(a) 1 h (b) 2 h

(c) 3 h (d) 4 h

(e) 5 h (f) 6 h

Figure 7.7: SEM images of zeolites from Alpha ash leachate

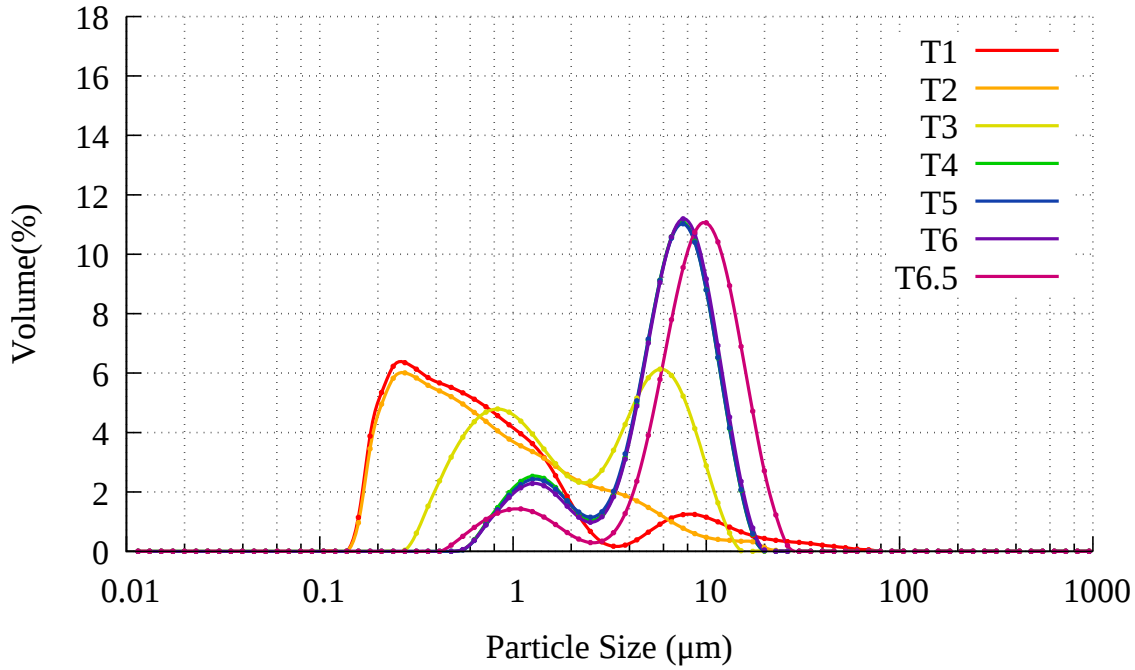

(a) PSD

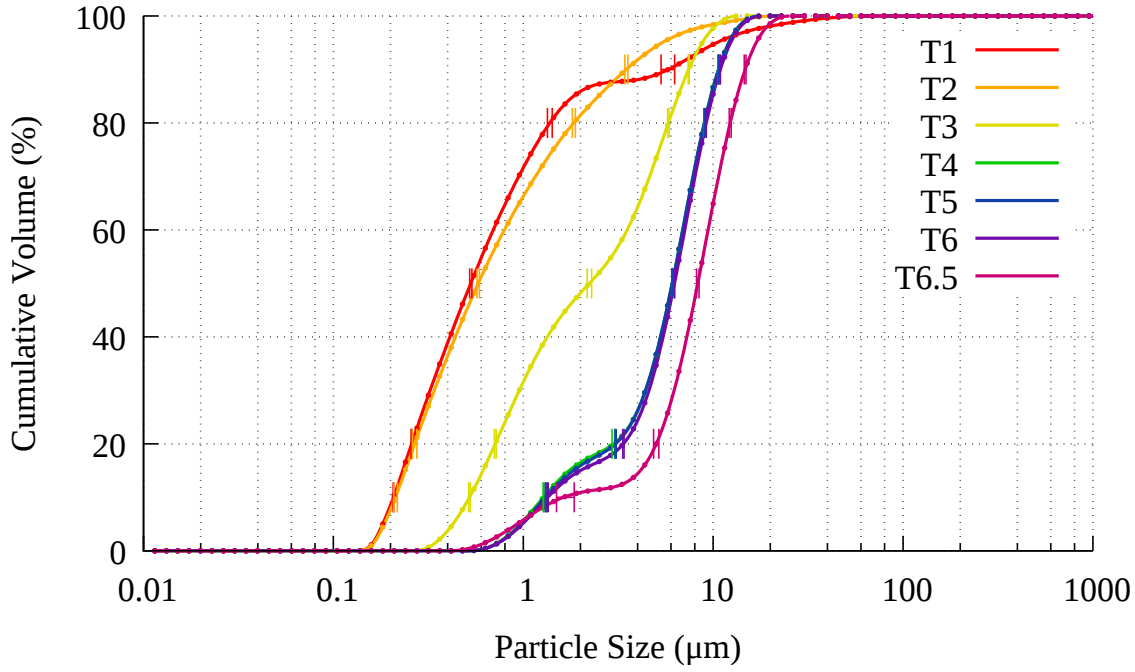

(b) Standard deviation in PSD

Figure 7.8: 90-95°C crystallisation process from Lagoon ash leachate

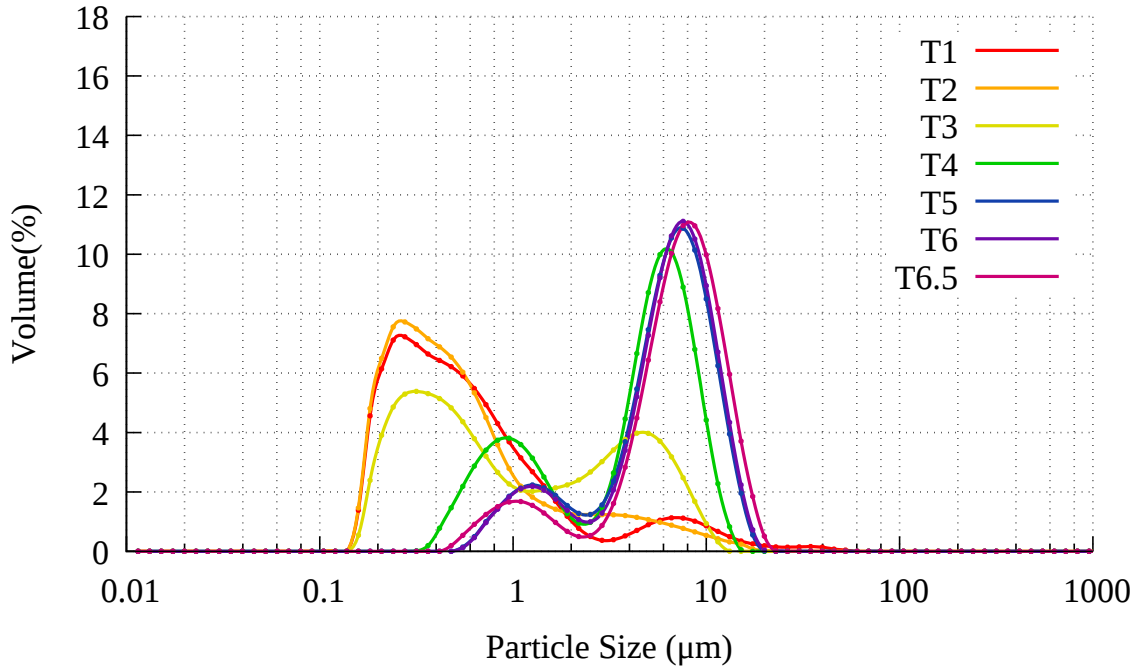

(a) PSD

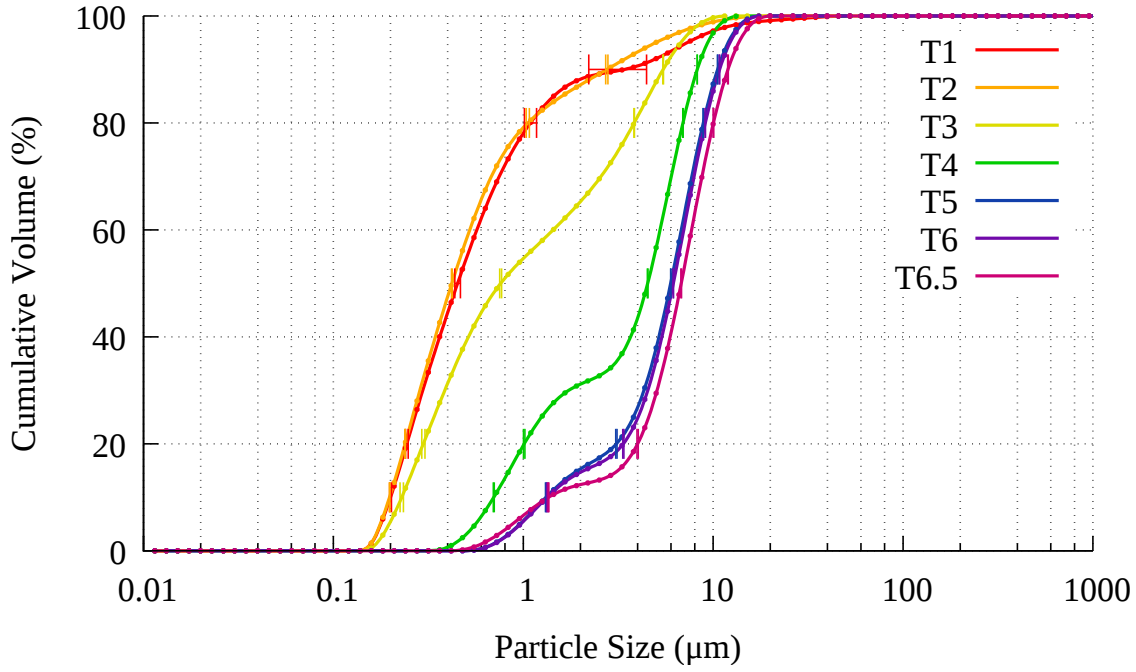

(b) Standard deviation in PSD

Figure 7.9: 90-95°C crystallisation process from FB7 ash leachate

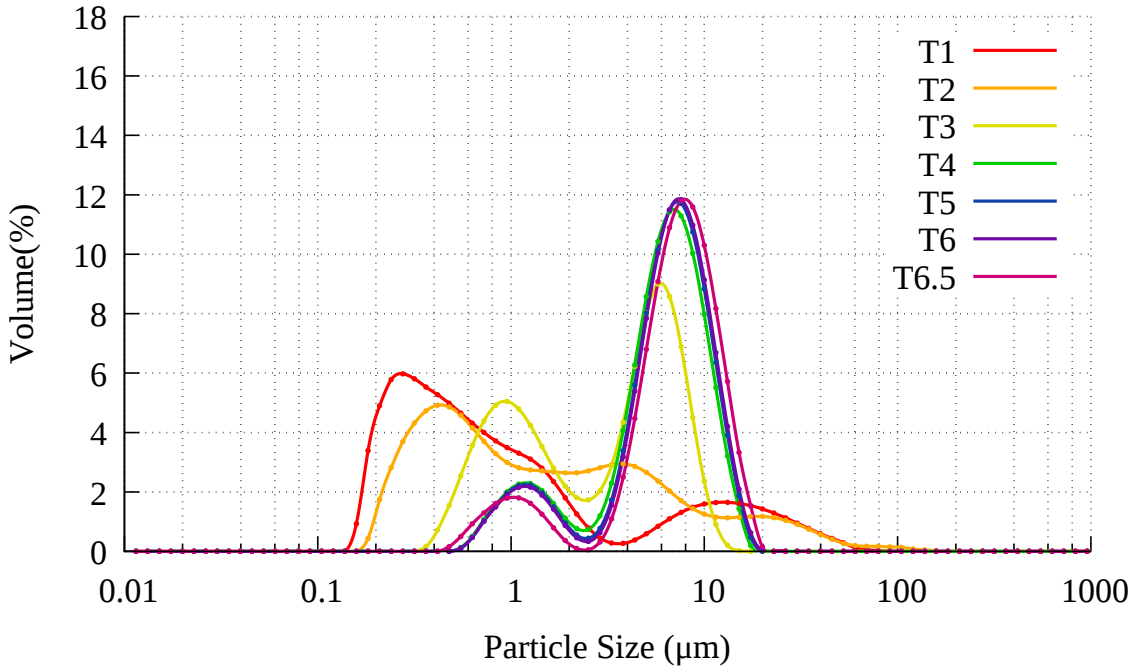

(a) PSD

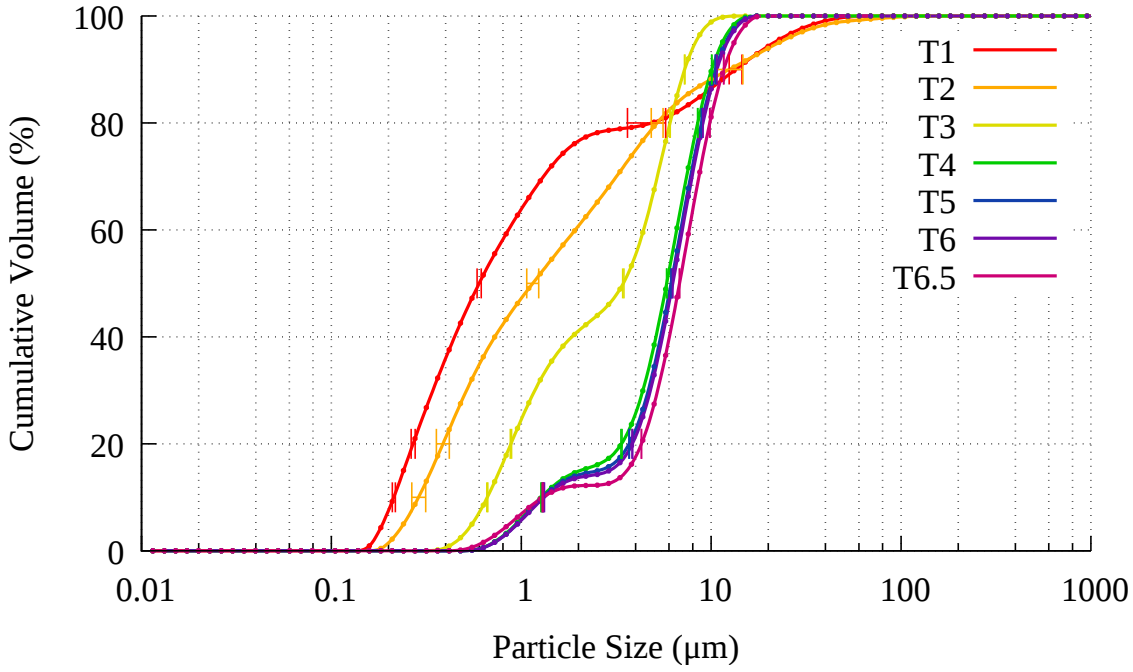

(b) Standard deviation in PSD

Figure 7.10: 90-95°C crystallisation process from Alpha ash leachate

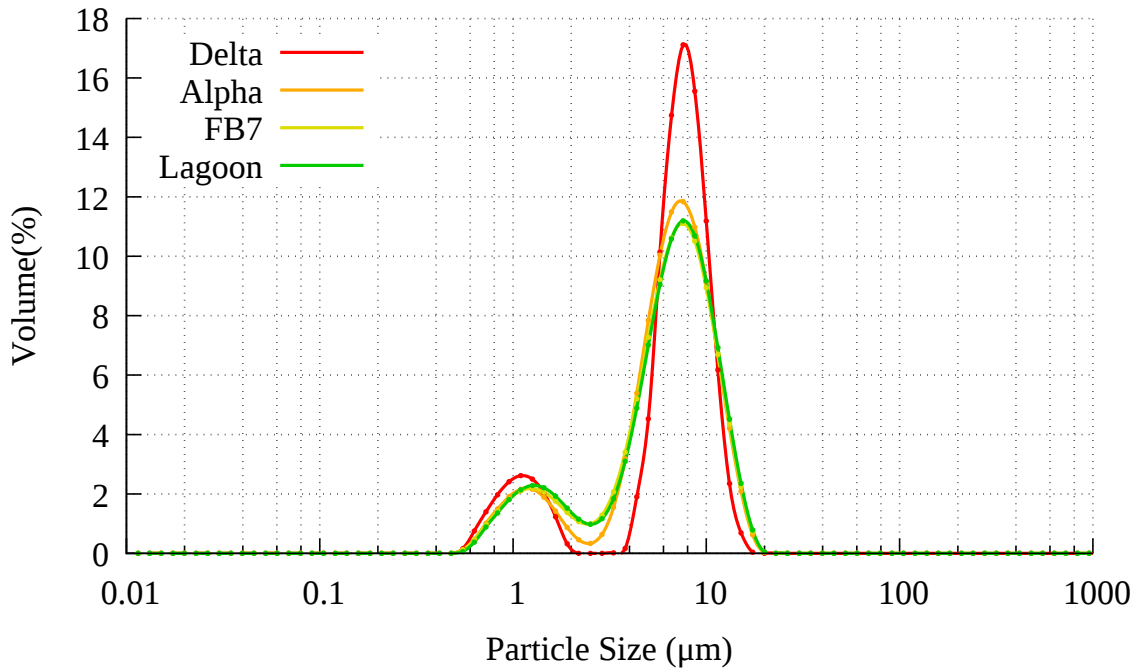

(a) PSD

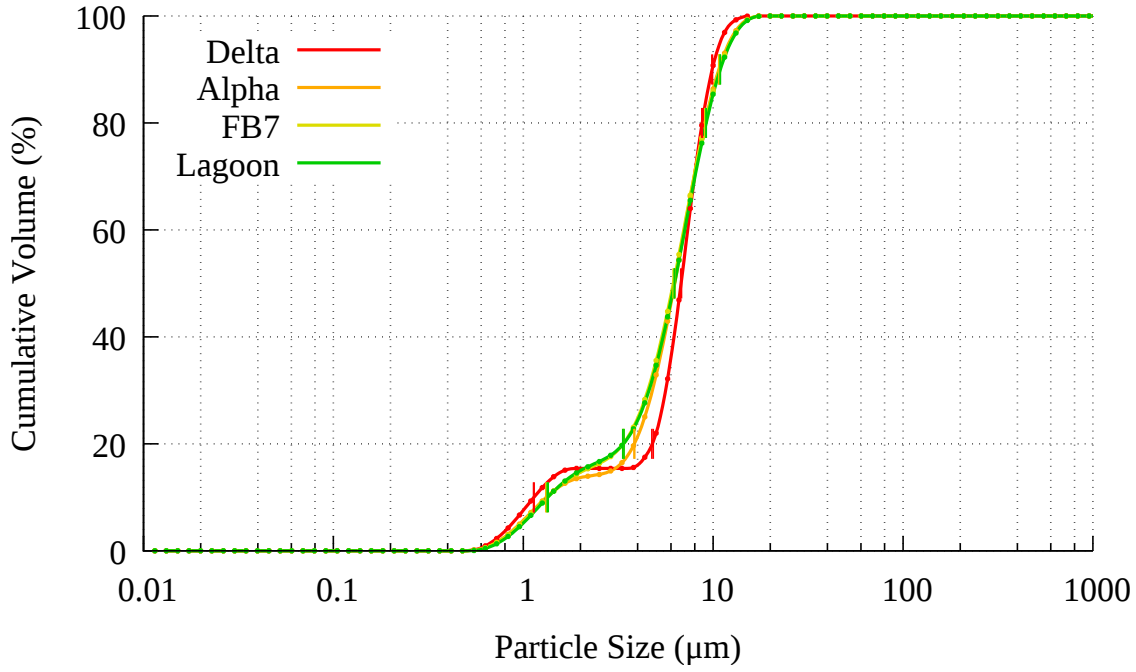

(b) Standard deviation in PSD

Figure 7.11: 90-95°C crystallisation of 4 ashes at 6 hours

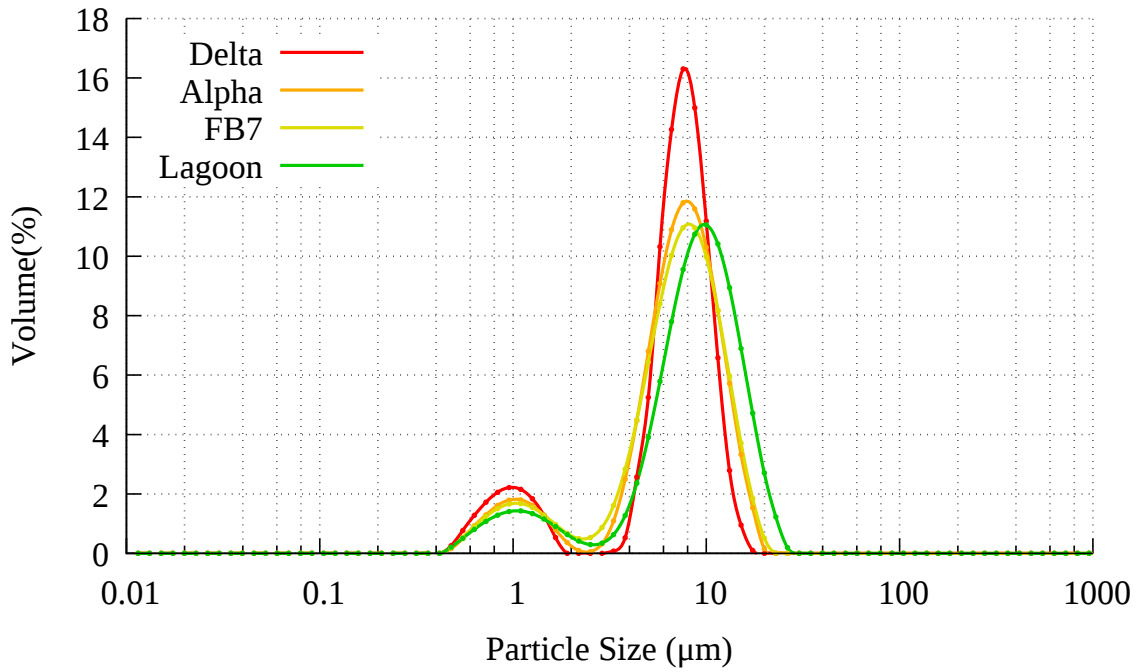

(a) PSD

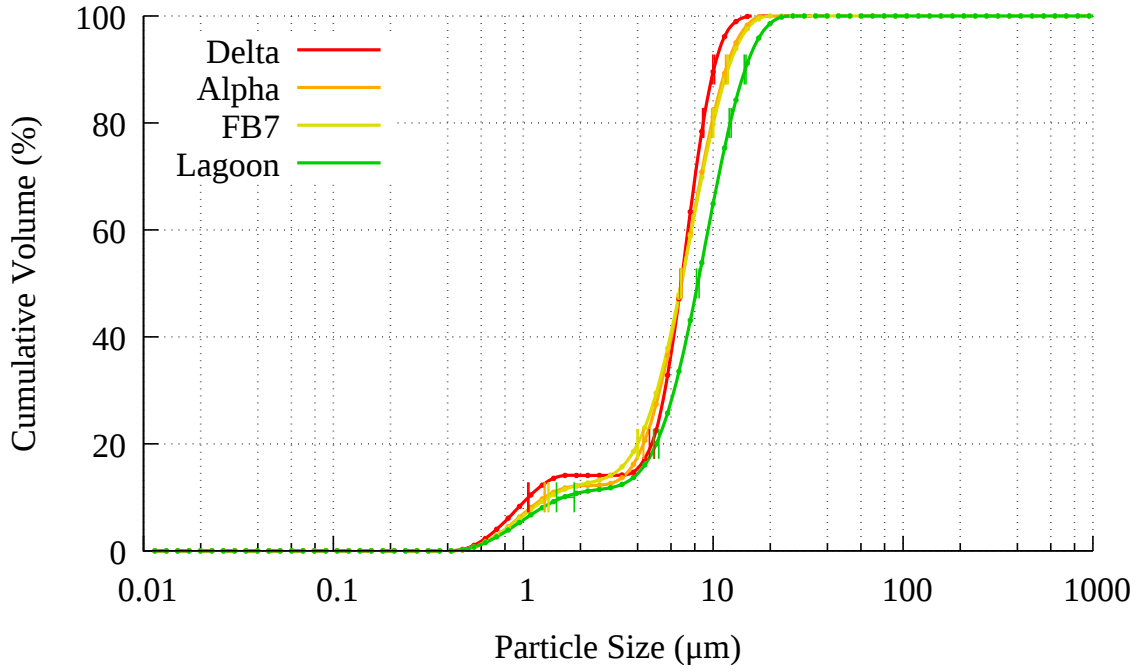

(b) Standard deviation in PSD

Figure 7.12: 90-95°C crystallisation of 4 ashes at 6.5 hours

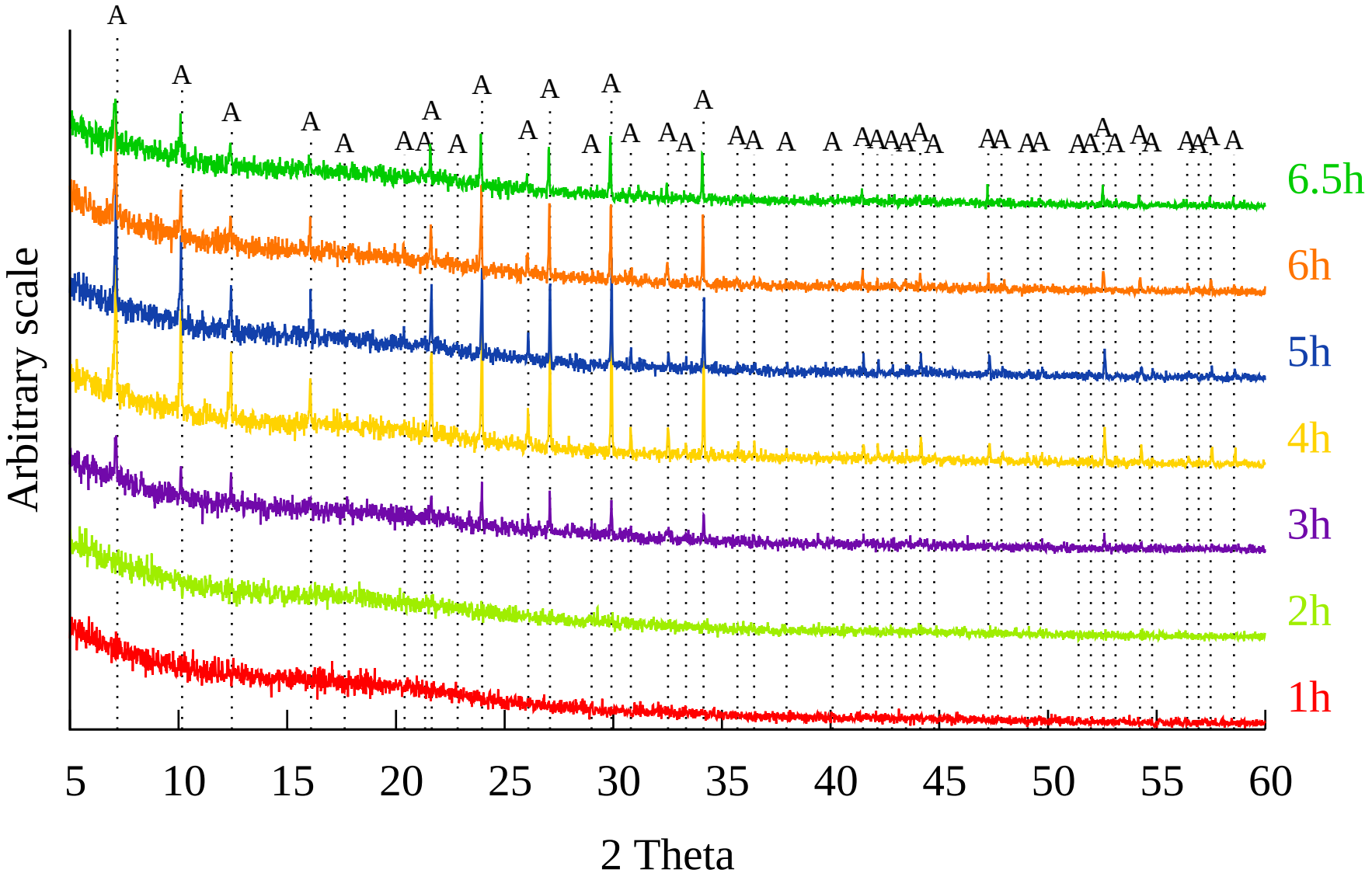

Figure 7.13: XRD patterns of zeolite from Lagoon ash leachate. A: Zeolite Na-A. $\lambda = 1.5406$ Å

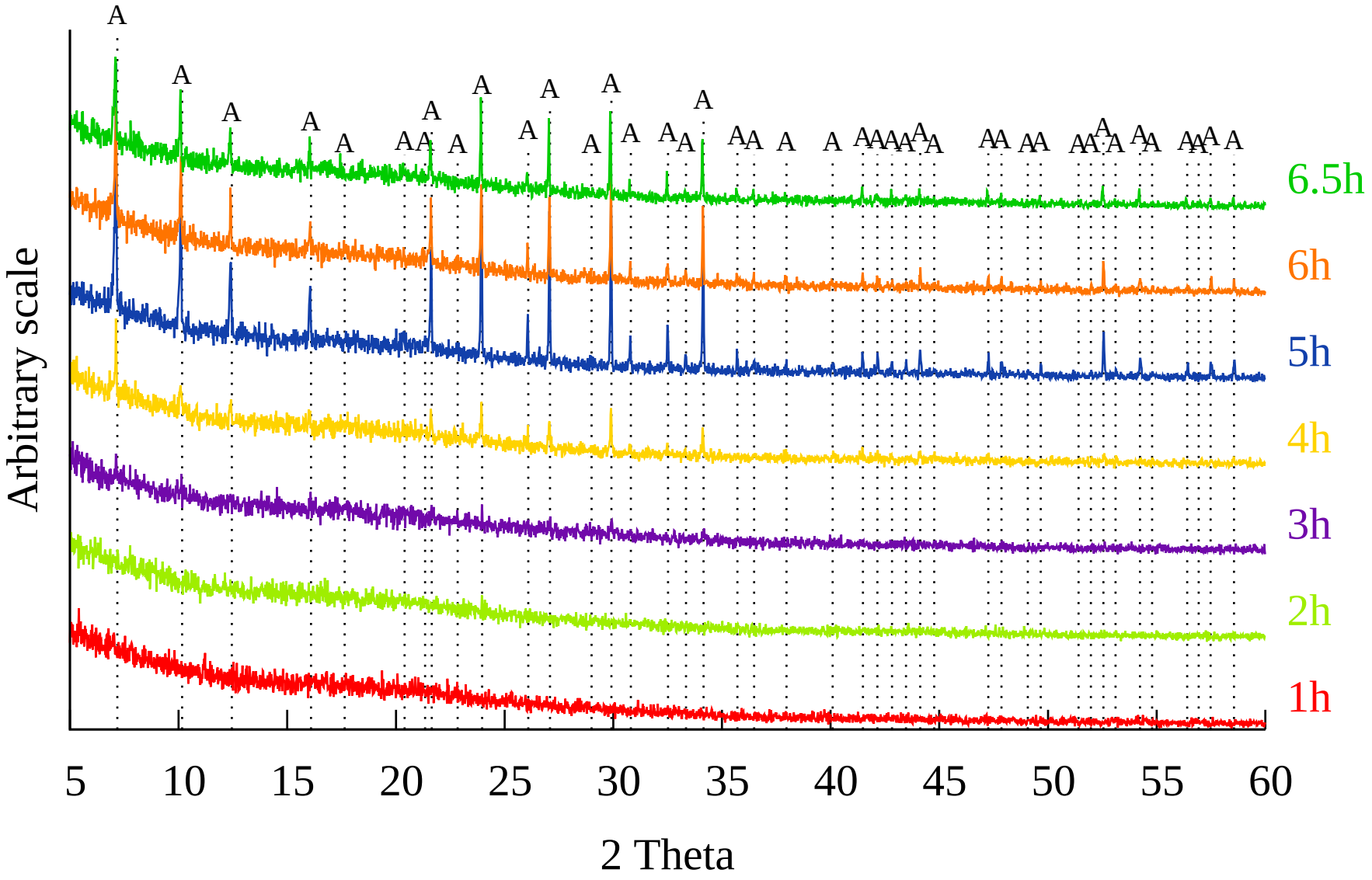

Figure 7.14: XRD patterns of zeolite from FB7 ash leachate. A: Zeolite Na-A. $\lambda = 1.5406$ Å

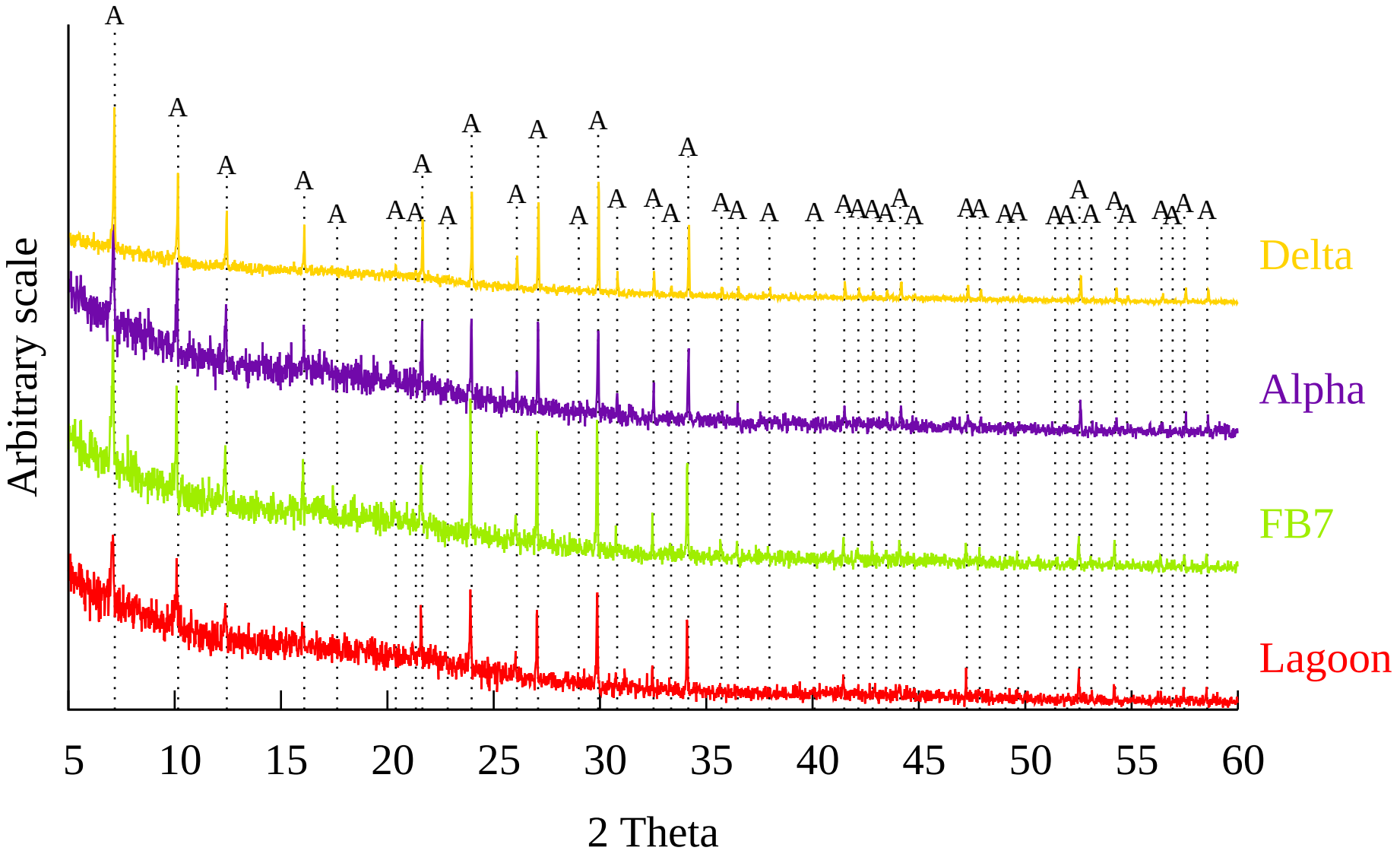

Figure 7.15: XRD patterns of final products from different ash leachates. A: Zeolite Na-A. $\lambda = 1.5406$ Å

7.2 Seeding with Cenospheres

Zeolites are used to exchange cations in aqueous media. Once the zeolites are saturated, the end user is likely to want to separate the zeolite from the aqueous media. In order to make separation easier, it was decided to attempt to create floating zeolites. This was to be achieved through precipitation of zeolites on buoyant media, such as cenospheres. In previous works, the cenospheres were found to be insufficiently buoyant, as when coated with zeolite a proportion sank under the weight of the coating. In order to rectify this, lower density cenospheres were separated from a batch of cenospheres by density separation with ethanol. The cenospheres produced were then added to the crystallisation process. The cenospheres produced are shown in Figure 7.16.

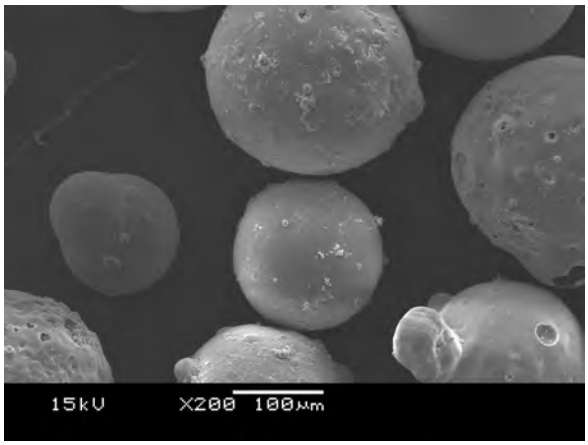

(a) Untreated Cenospheres x200

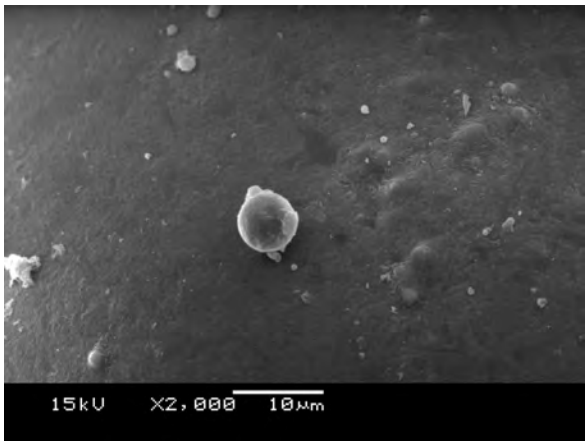

(b) Untreated Cenospheres x2000

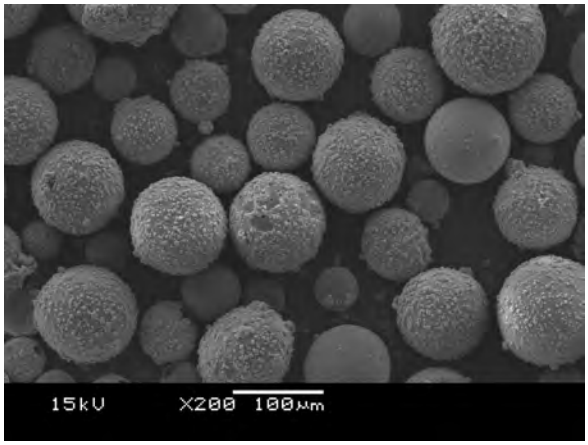

(c) 1475 g Cenospheres/kg FA Float

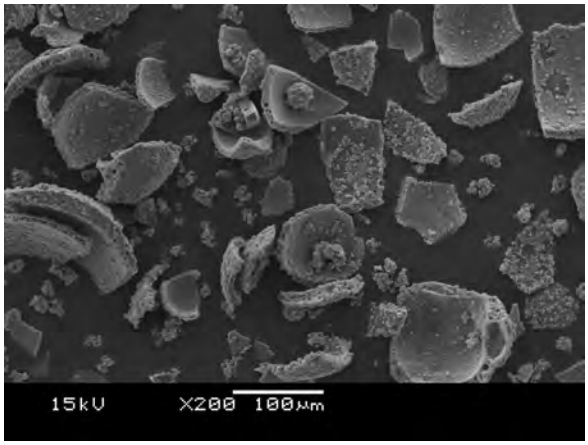

(d) 1475 g Cenospheres/kg FA Sink

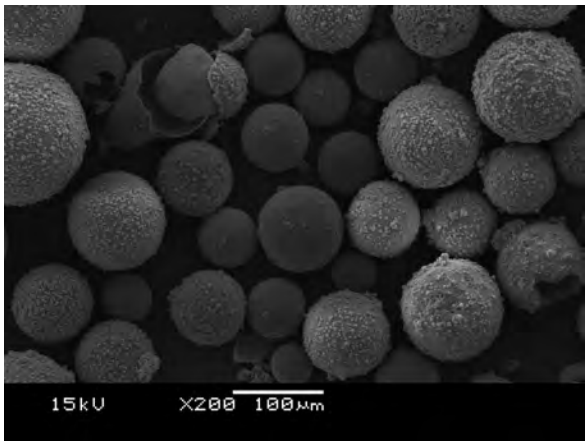

(e) 590 g Cenospheres/kg FA Float

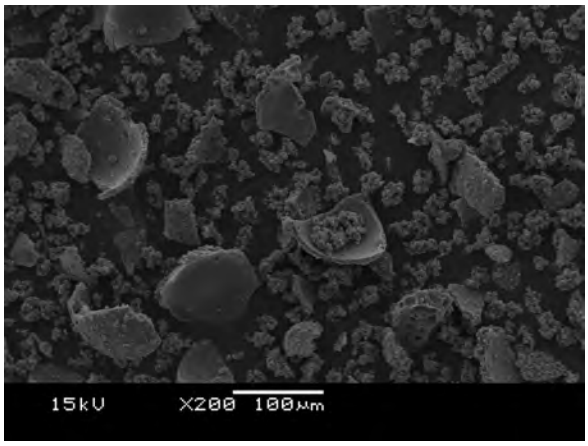

(f) 590 g Cenospheres/kg FA Sink

Figure 7.16: SEM images of untreated and zeolite coated cenospheres

A problem was noted with the process, in that only 2-6 % of the final product floated on water. During the crystallisation process it was noted that the magnetic stirrer bead was making more noise than in previous experiments, and it was believed that the cenospheres were subject to abrasion between the 60 mm magnetic stirrer bead and the conical flask during crystallisation. The stirring beads were also noted to have attracted a coating of magnetic material at each end. Figures 7.16d and 7.16f show broken cenospheres and clumps of zeolite, and the idea that cenospheres were being broken during crystallisation was considered viable.

7.2.1 Avoiding Grinding in Crystallisation

The experimental equipment was reconsidered, and the 60 mm magnetic stirrer bead was replaced with an overhead stirrer that did not touch the sides of the conical flask. The quantities of all reagents used in non-cenosphere experiments were reduced by 20 % in order to fit within a 1 litre conical flask whilst accommodating the volume of cenospheres added. The experiment comprised two experimental conditions: 1111 g cenospheres/kg FA with 222 g SA/kg FA, and 370 g cenospheres with 111 g SA/kg FA. Both conditions had 517 g sea salt/kg FA added to the crystallisation solution. With reference to Figure 2.12 on page 46, 720 ml of leachate (N) was placed in a 1 litre conical flask with 28 g of sea salt (Q), the stated quantity of cenospheres (R) and the hot plate set to 90°C (U). Upon reaching the set temperature, 80 ml of distilled water (P) with 12 g of sodium aluminate (O) was added and the timer started. At 2 hours the temperature was raised to 95°C. Samples were taken every hour, filtered, washed, dried and separated by density with water.

These crystallisation conditions provided much more buoyant materials, with 63 % and 43 % of the final products for each cenosphere loading condition floating on water. As expected, the conditions with a higher proportion of cenospheres produced a product with a higher proportion of buoyant particles. The results for the buoyant products at each hour are shown in Figures 7.17 and 7.18, and the both buoyant and sinking final

products are shown in Figures 7.19 and 7.20.

The proportion of zeolite to cenospheres in the floating zeolite (x) is calculated from the CEC of: the untreated cenospheres (C), the zeolite (Z), and floating zeolite product (F). The CEC of the floating zeolite is described by equation 7.1.

$$\begin{aligned} F &= C \cdot x + Z \cdot (1 - x) \\ x &= \frac{F - Z}{C - Z} \end{aligned} \tag{7.1}$$

For both conditions, zeolite cubes are apparent growing from the surface of the cenospheres from 3 hours, as seen in Figures 7.17c and 7.18c and increasing in abundance and crystallinity as time progresses. These results are as expected, following similar results in experiments without added cenospheres, indicating that the addition of cenospheres does not inhibit the formation of zeolites. The experiment with a lower cenosphere and sodium aluminate content produced a final product of which 43 % floated. Applying equation 7.1, this was found to consist of 7 % zeolite and 93 % cenospheres. The SEM images are shown in Figure 7.20. The experiment depicted by Figure 7.19 with more cenospheres and sodium aluminate formed a final product of which 63 % floated on water. It was calculated to consist of 14 % zeolite and 86 % cenospheres. These calculations are supported by the SEM images. Comparing the images in Figure 7.20 to the images in Figure 7.19 it is clear that the floating product of Figure 7.19 has more zeolite on the surface of the cenospheres.

Due to the low zeolite concentrations in the floating product and the rapid analysis, XRD analysis did not detect any crystalline material in the floating products. The sinking material shows zeolite A detected from 4 hours. XRD spectra of floating and sinking products for high cenosphere content are shown in Figures B.5 and B.6 in the Appendix, pages 376 and 377. For low cenosphere content floating and sinking products see Figures B.7 and B.8, pages 378 and 379.

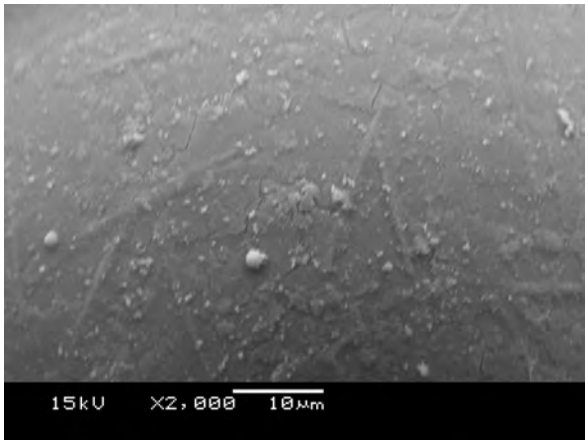

(a) 1 h

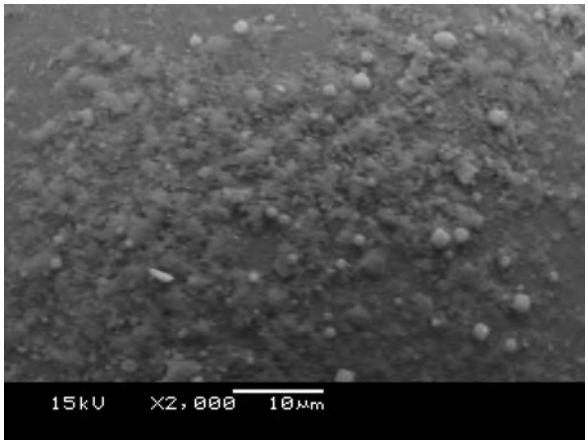

(b) 2 h

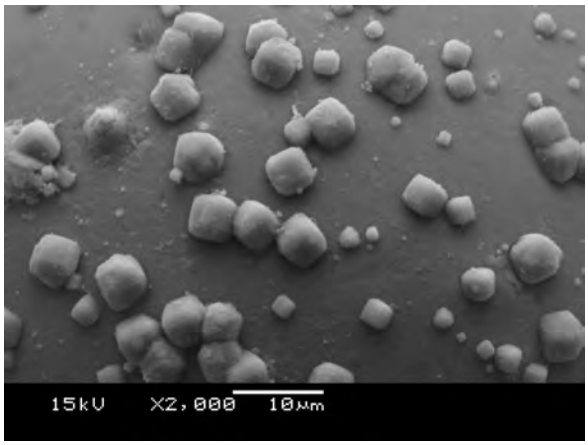

(c) 3 h

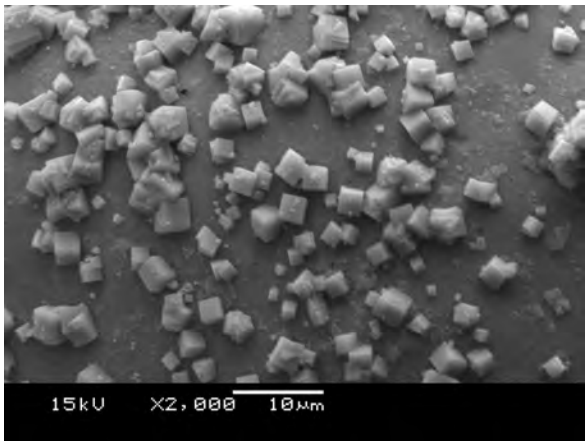

(d) 4 h

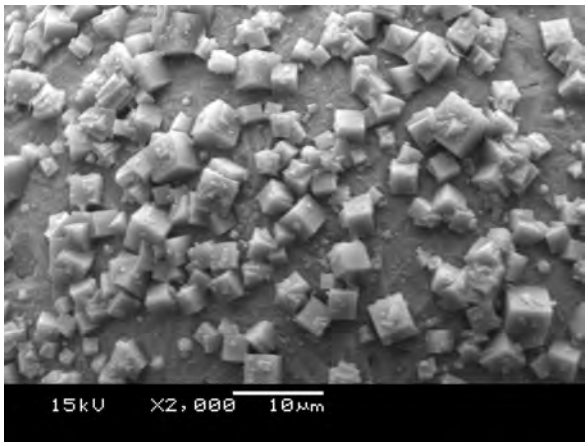

(e) 5 h

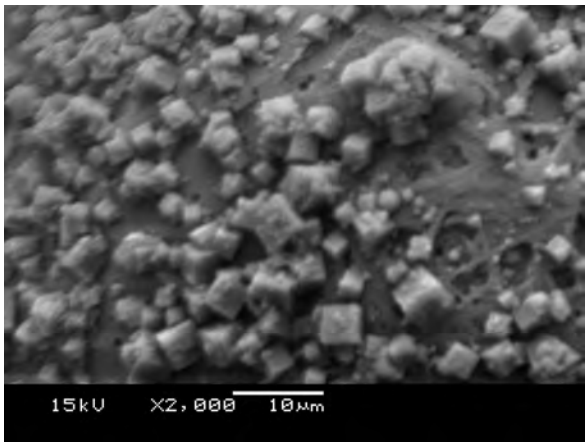

(f) 6 h

Figure 7.17: SEM images of products samples seeded with a high dosage of cenospheres, 1-6 hours

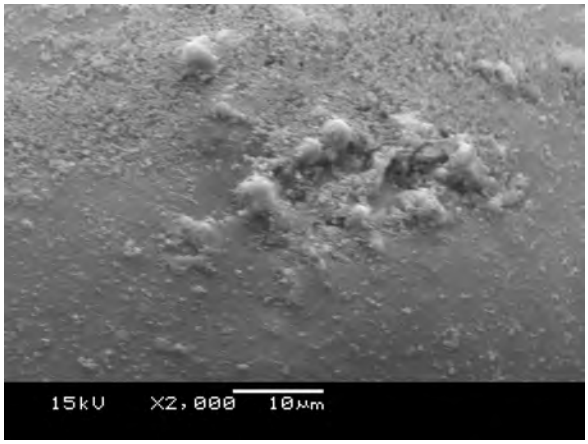

(a) 1 h

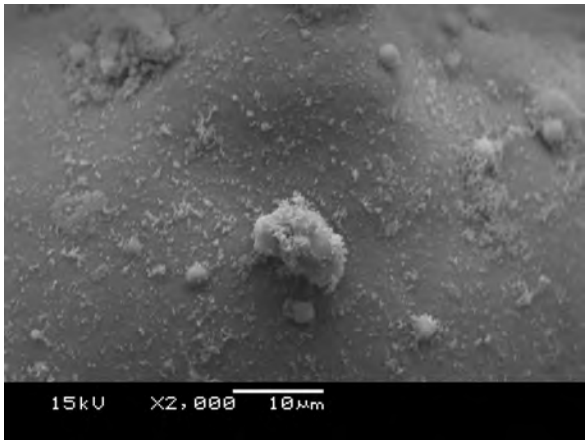

(b) 2 h

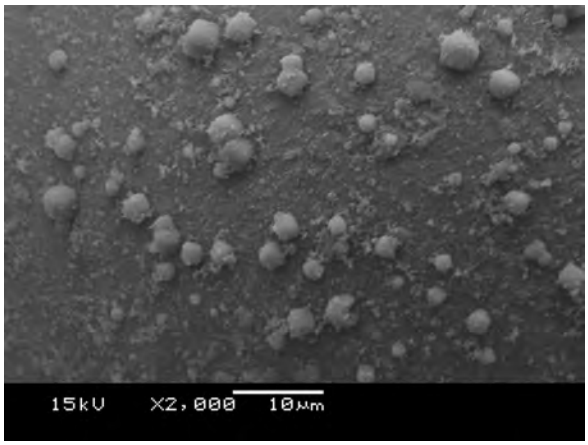

(c) 3 h

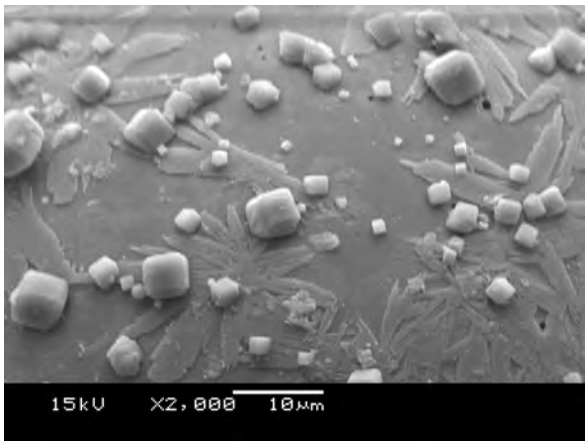

(d) 4 h

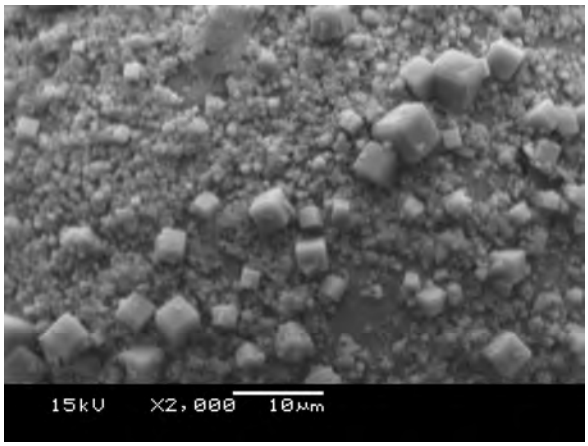

(e) 5 h

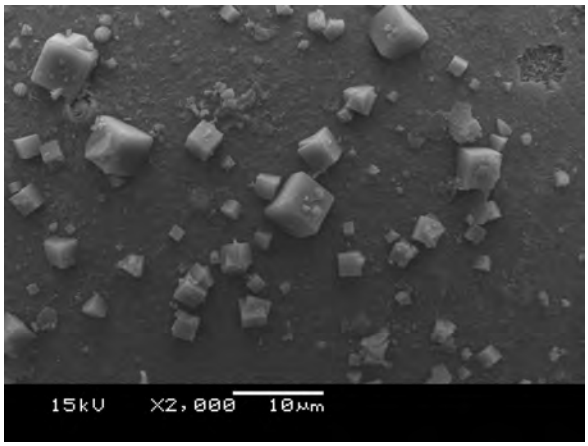

(f) 6 h

Figure 7.18: SEM images of products samples seeded with a low dosage of cenospheres, 1-6 hours

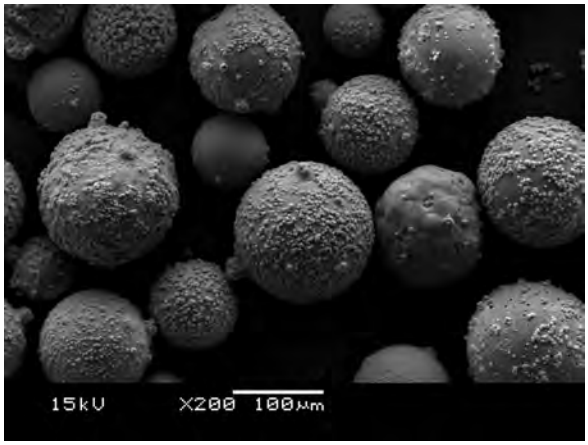

(a) Float x200

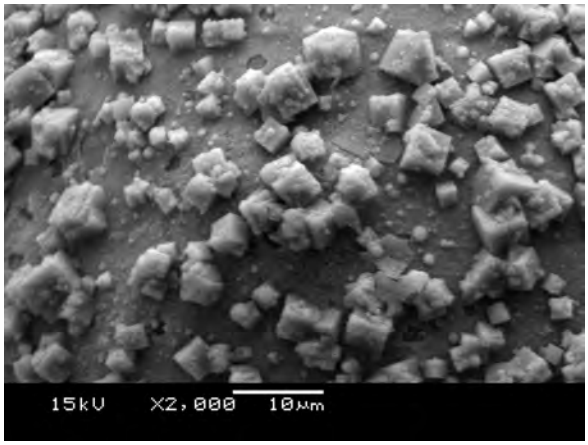

(b) Float x2000

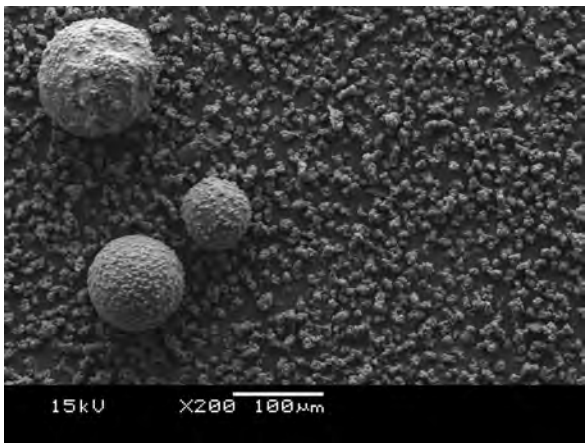

(c) Sink: x200

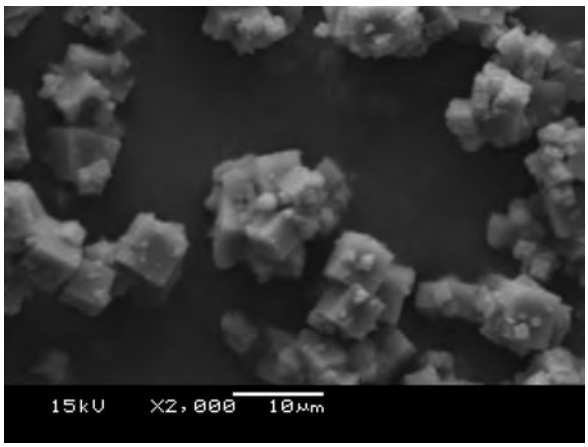

(d) Sink: x2000

Figure 7.19: SEM images of products samples seeded with a high dosage of cenospheres, separated by buoyancy

7.2.2 Increasing Zeolite Buoyancy

Figures 7.19c 7.20c show that much of the material which is not buoyant consists of zeolite which is not attached to a cenosphere. When cenospheres are not added, the crystallisation solution is noted to turn from a transparent yellow to an opaque off-white when the sodium aluminate is added at the start of the experiment. More specifically, the solution turns opaque after the majority of the solution has been poured in, and turns opaque sooner with higher dosages of sodium aluminate. It was also noted that at the end of experiments the zeolite formed sinks to the bottom of the crystallisation vessel during the cooling period to show a transparent yellow solution again. It was considered

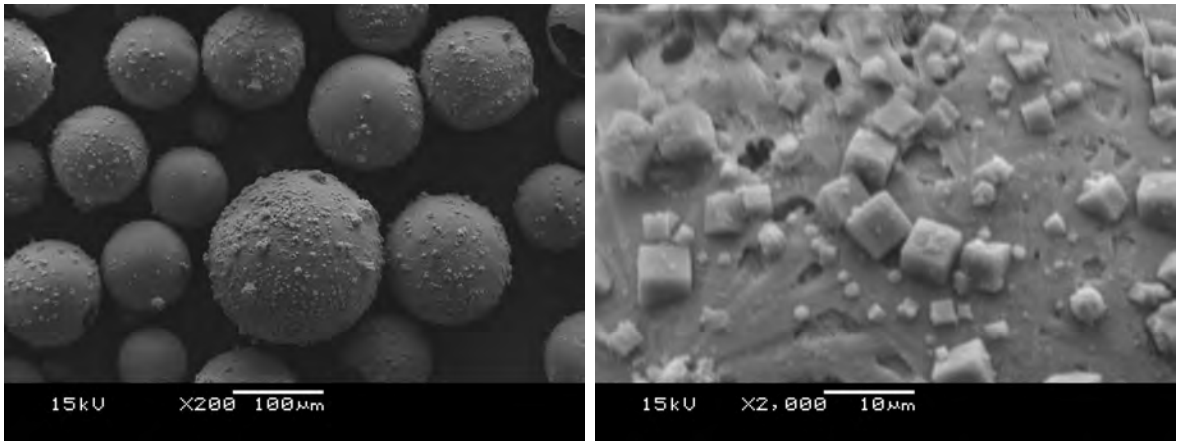

(a) Float x200 (b) Float x2000

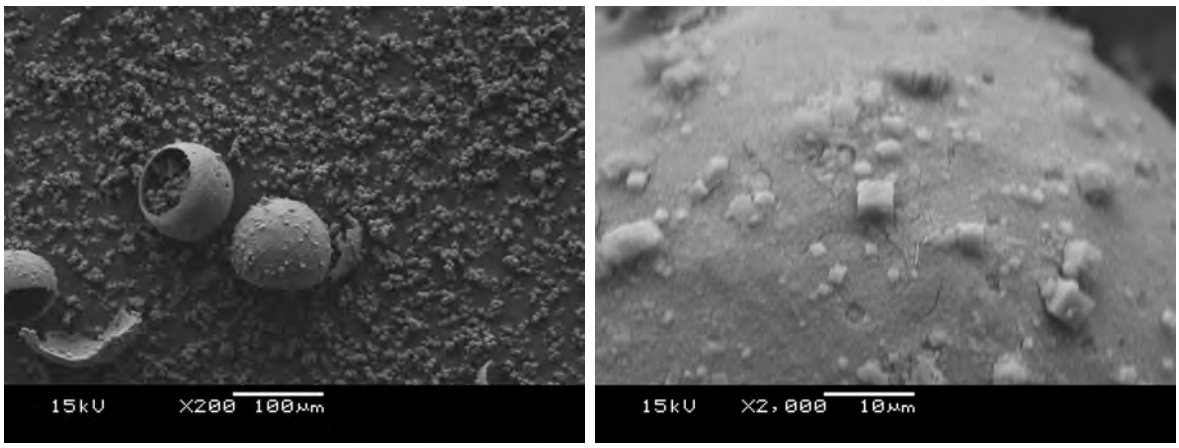

(c) Sink: x200 (d) Sink: x2000

Figure 7.20: SEM images of products samples seeded with a low dosage of cenospheres, separated by buoyancy

likely that this rapid addition of the entire dosage of sodium aluminate may cause zeolite seeds to form, from which zeolite crystals grow. It was considered that if the quantity of sodium aluminate in solution could be kept low enough to avoid turning the crystallisation solution opaque, the seeding process could be reduced and more zeolites may form on the cenospheres, with fewer zeolite nuclei forming.

The higher dosage cenosphere and sodium aluminate experiment depicted in Figure 7.19 was therefore repeated. The 80 ml sodium aluminate solution was added in 10 ml aliquots every 10 minutes from 0-50 minutes, with one 20 ml aliquot at 1 hour. In an attempt to further hinder nucleation and encourage crystallisation, the crystallisation experiment was conducted at a constant 95°C, rather than the previous 90-95°C step

change in temperature. The SEM images for this experiment are shown in Figures 7.21 and 7.22. With the new conditions, scant, rounded zeolite cubes are observed on the surface of the zeolite from 2 hours in Figure 7.21b, rather than 3 hours in Figure 7.21c. As with other experiments, these cubes then grow in size and crystallinity as the experiment progresses.

From the final product, 68 % floated, and of that 68 %, the CEC calculations indicate a composition of 23 % zeolite and 77 % cenospheres. Both the buoyancy and zeolite loading of the floating product are improved under the higher temperature and slower sodium aluminate addition conditions. SEM images appear to show a decreased quantity of zeolite, which is not associated with a cenosphere when comparing Figures 7.19c 7.22c, however the slight increase in zeolite coating of the floating products is difficult to discern solely based on Figures 7.19b and 7.22b.

The AAS results are shown in Figure 7.23. Despite the same dosage of sodium aluminate, the Al consumption for the experiment with slower addition of sodium aluminate is significantly higher in the first hour. It is also noted that the Al content for both conditions does not plateau, but continues to decrease as the experiment progresses, whilst the Si content appears to increase slightly from 4 hours. The continued decrease in Al can be attributed to continued crystallisation of zeolite with Si being drawn from the cenospheres. In previous experiments, Al would plateau due to there being no more Si available to form zeolites with. With the cenospheres present, Si can be leached from the cenospheres into solution due to the alkaline conditions, providing Si in solution which can be used to further consume the available Al. The increased consumption of Al in the first hour can be attributed to the higher temperature and the slow addition of sodium aluminate, both being more conducive to crystallisation than nucleation, allowing for a more rapid consumption of Al as it is incorporated into zeolite structure rather than forming a precursor gel.

The CEC of a control experiment with no added cenospheres is compared with the CEC of the floating products from the 90-95°C cenosphere experiment and the 95°C cenosphere

experiment in Figure 7.24. Also included are CEC results for untreated cenospheres, and the source ash from which the leachates are derived. It is noted that the CEC of the slow addition of SA cenosphere experiment is higher than the cenosphere experiment with all the sodium aluminate added in one dosage, and that the CEC of untreated cenospheres is negligible in comparison to either. All of these results are lower than the control experiment, which consists of exclusively zeolite, however some CEC must be lost in order to achieve a buoyant product.

Figure 7.25 shows the XRD pattern of the final floating product from the cenosphere experiment in comparison to the untreated cenospheres. The untreated cenospheres contain mullite (M), quartz (Q) and calcite (C), whilst the floating product contains these as well as zeolite A (A). These two XRD patterns come from a reflection diffractometer and were analysed for 1 hour rather than the customary 10 minutes in the transmission diffractometer, and thus the zeolite phases, as well as mullite and quartz are detected. Due to the buoyant nature of the products, it was not possible to produce a reliable PSD, as the equipment used relies upon the product being dispersed in water.

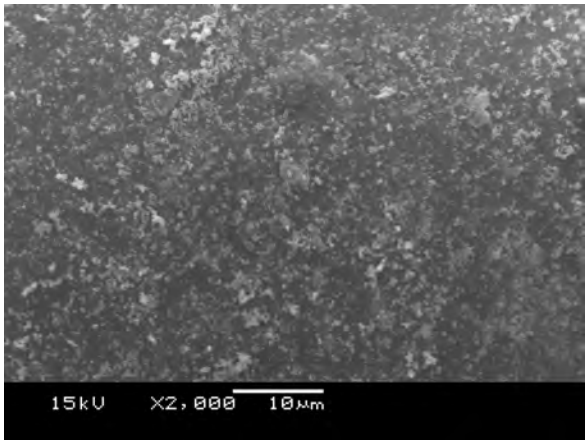

(a) 1 h

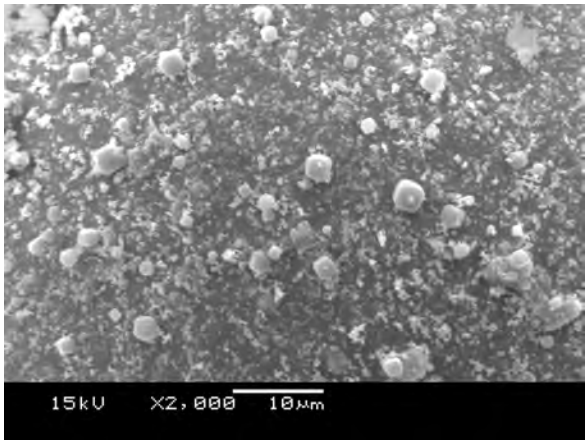

(b) 2 h

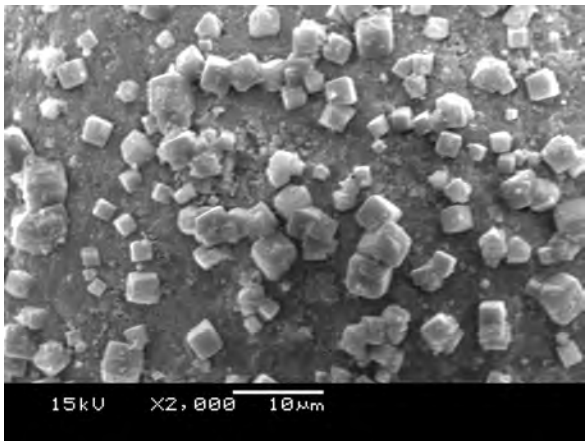

(c) 3 h

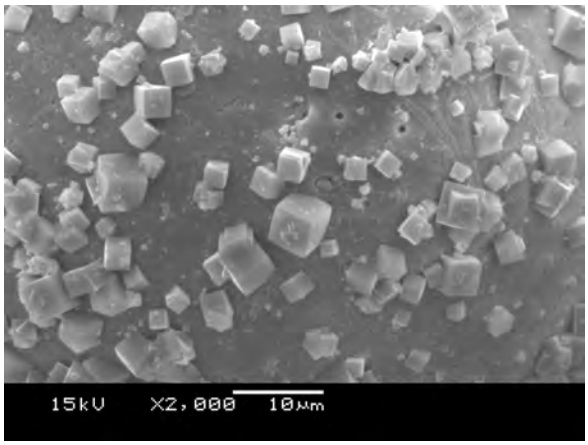

(d) 4 h

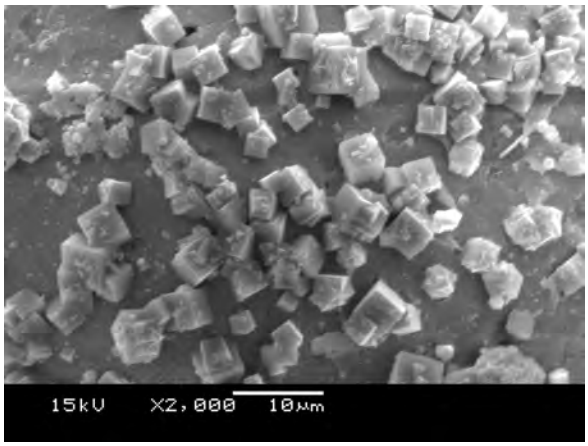

(e) 5 h

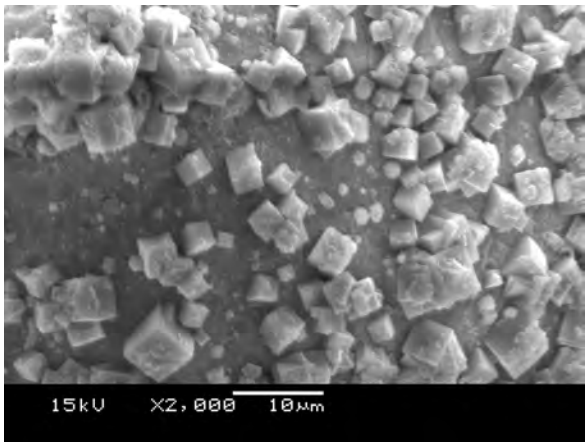

(f) 6 h

Figure 7.21: SEM images of products samples seeded with a high dosage of cenospheres, slow SA addition, 1-6 hours

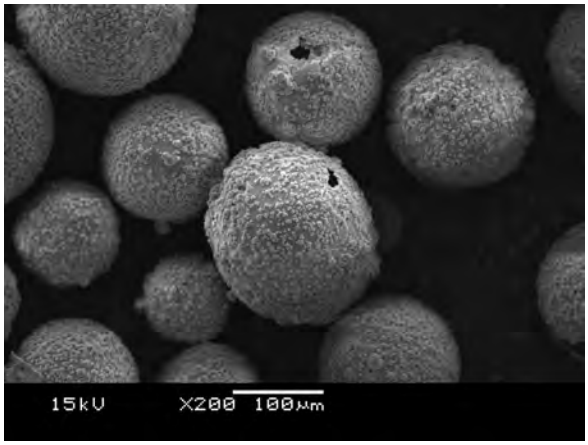

(a) Float x200

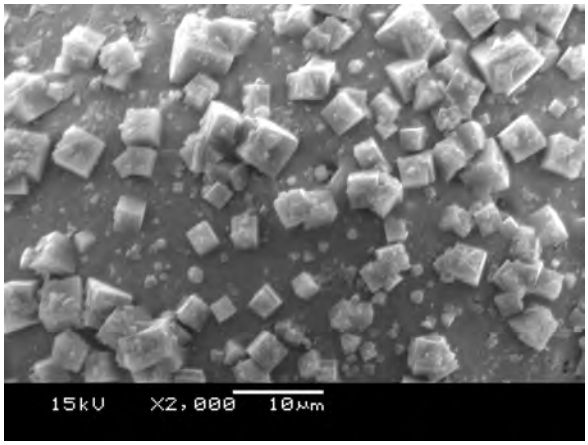

(b) Float x2000

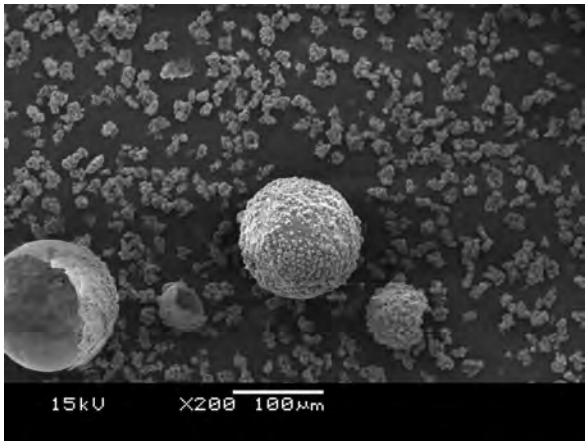

(c) Sink: x200

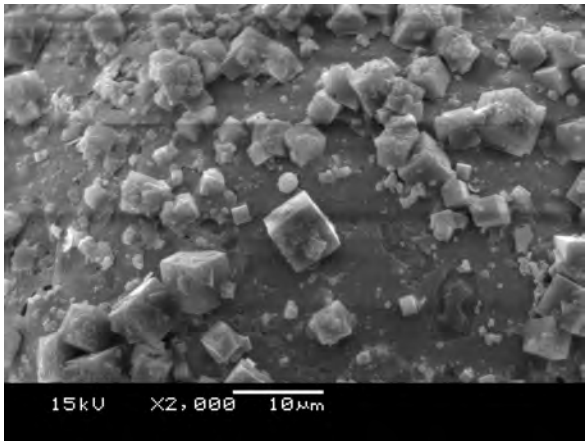

(d) Sink: x2000

Figure 7.22: SEM images of final products. Samples were seeded with a high dosage of cenospheres, crystallised at 95°C, with sodium aluminate added over 1 hour, and separated by buoyancy

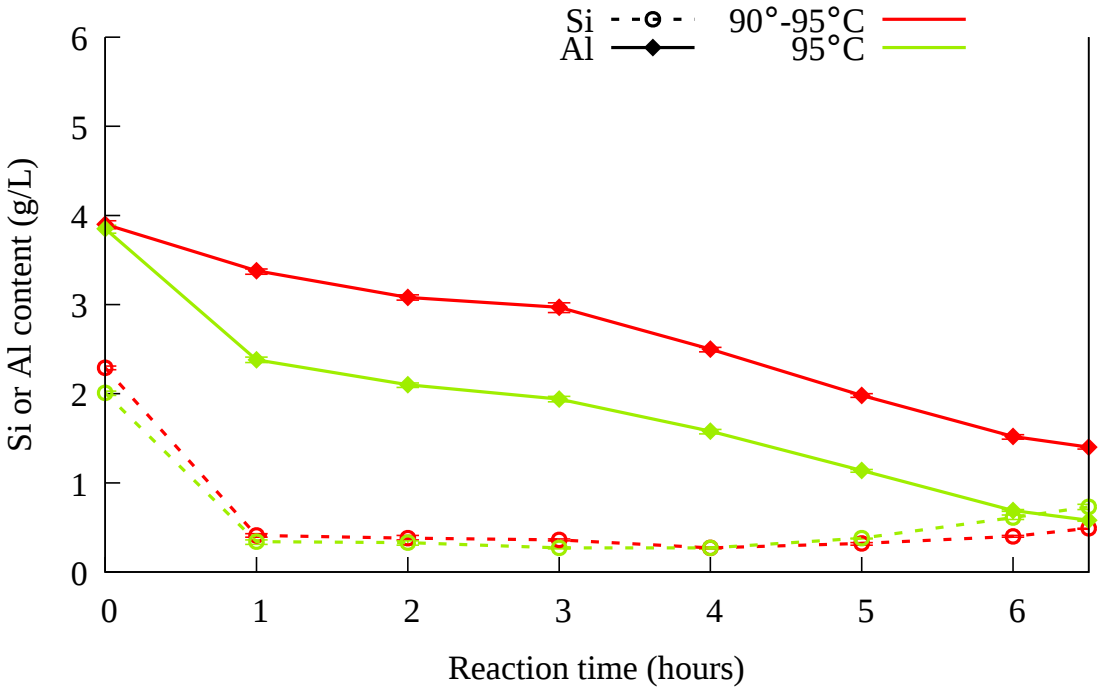

Figure 7.23: AAS results for crystallisation process with high cenosphere content. 95°C crystallisation process compared to 90-95°C process

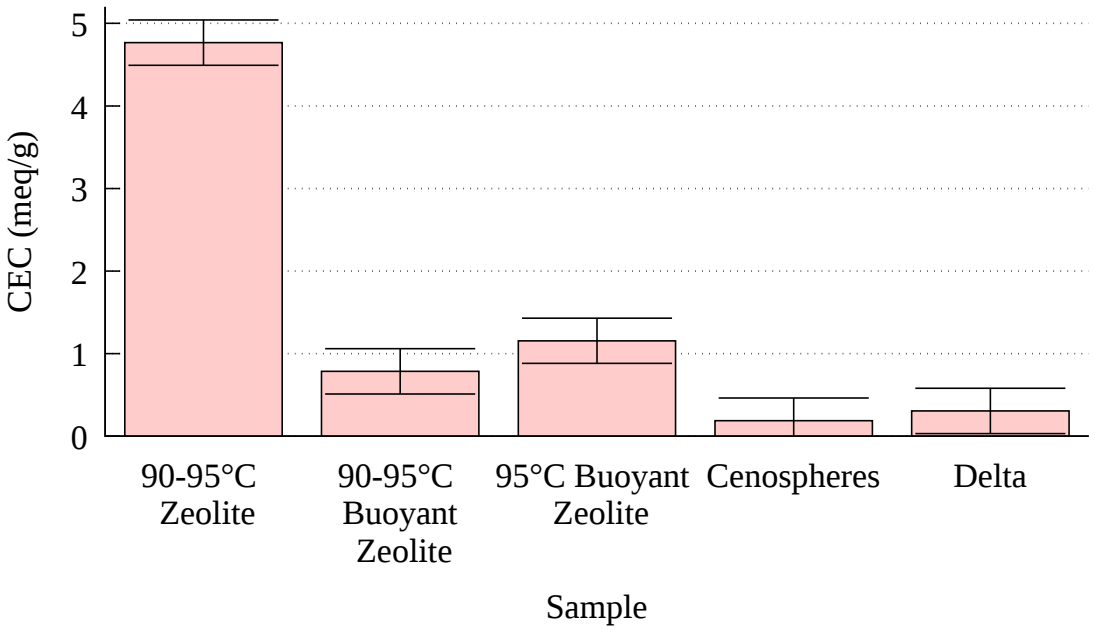

Figure 7.24: CEC results for cenosphere experiments

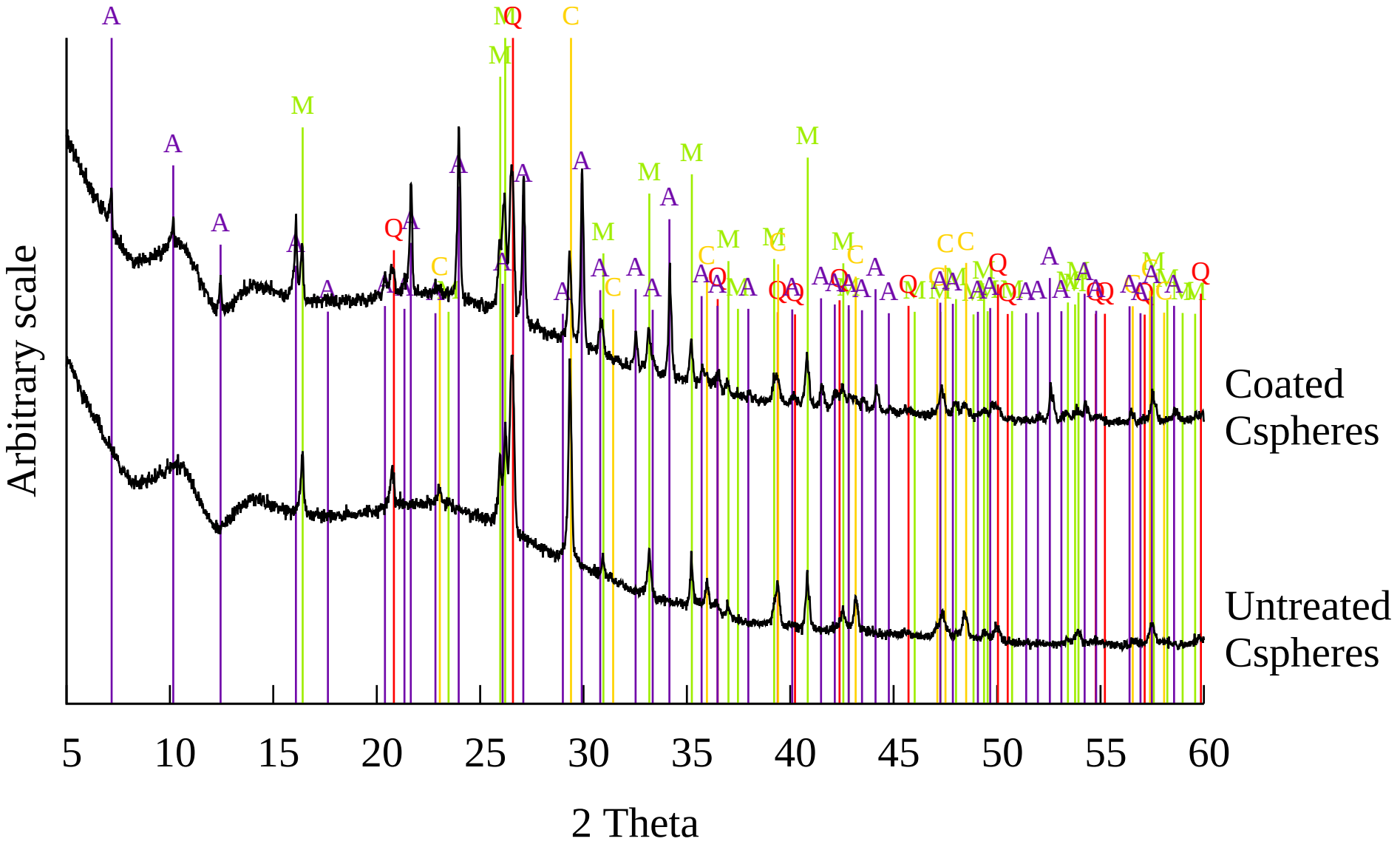

Figure 7.25: XRD patterns of cenospheres and coated cenospheres. A: Zeolite Na-A; Q: Quartz; M: Mullite; C: Calcite. $\lambda = 1.5406$ Å

7.3 Crystallisation of Zeolites from Rice Husk Ash

7.3.1 Method

Figure 4.35 shows the results of three RHA extraction experiments. The final values of the leachate were found to be 7.27 and 3.77 g/L of Si for ratios 3.2 and 6.4 respectively. 620 ml of the 3.77 g/L sample was added to a conical flask (as shown in Figure 5.1), along with 35 g of sea salt, 180 ml of distilled water and a magnetic stirrer bead. This solution was heated on the depicted hot plate to 90°C, then a 200 ml solution of distilled water and 12 g of sodium aluminate was added to the conical flask and a timer started. After dilution, and ignoring any precipitation, the 3.77 g Si/L solution would have had a concentration of 2.34 g Si/L, which is similar to the 2.38 g Si/L concentration which is the mean value of the starting Si concentration of most experiments in this chapter. Similarly the addition of 12 g of sodium aluminate is equivalent to the sodium aluminate additions described as 177 g SA/kg FA in sections such as 5.4.2.4, 6.4.1.1 and 6.5.1.2. Samples were taken in keeping with previous methods, and the temperature was raised to 95°C at 2 hours. Similarly, 600 ml of the 7.27 g Si/L sample were crystallised with 24 g of sodium aluminate. The sodium aluminate content was doubled as the Si content of the starting solution was approximately double.

7.3.2 Results

AAS analysis of the leachates is shown in Figure 7.26a. As with crystallisation from Delta ash, there is a decrease in the Si and Al content, in this case between 4 and 5 hours. For context, these RHA results are compared to two of the 3 result sets in Figure 6.73, and are shown in Figure 7.26b. These comparison experiments follow the same crystallisation method and vary only in the origin of the leachate and sodium aluminate content. The Si results shown in green (the crystallisation from the extraction with lower solids loading NaOH/RHA = 6.4; to which 12 g of sodium aluminate were added) shows a Si content comparable to the Si content of the processed fly ash experiments. The Al content of the

RHA experiment plotted in green does not match up with the processed fly ash experiment of the same sodium aluminate dosage (in blue) due to the Al content extracted from the processed fly ash already in solution, thus the experiment with the next lowest Al content (purple) is also provided for context.

It is noted that the drops in Si and Al in Figure 7.26 observed between 4 and 5 hours also occur in the comparison experiments at the same time. It is also noted that the Si consumption for both experiments are similar to each other and the control experiments, indicating a high consumption of Si by the end of the experiment. The Al values for the RHA experiments are also very low, but are also noted to be lower than the control experiments they are compared to.

The drop in Si and Al in the AAS in Figure 7.26 coincides with the consumption of the amorphous material in the SEM images of Figures 7.28 and 7.29. SEM images show clean cubes by 5 hours, with no observable superfluous material. PSD analysis in Figure 7.27 indicates that some material ~1 μm in size still persists, but the majority of the material is ~4-10 μm in size. Both RHA experiments give similar PSD's.

XRD patterns shown in Figure 7.33 and Figure 7.34 show zeolite A detected from 4 hours, supporting the SEM images which show cubes from 4 hours. The x-ray source for the diffractometer was replaced between the analysis of the 1-6 hour samples in Figure 7.33 and the analysis of the 6.5 hour sample in Figure 7.33 and all samples in Figure 7.34.

Due to the high solubility of RHA in comparison to the processed fly ash, the yield of zeolite is much higher, as shown in Figure 7.30. Whilst the NaOH/RHA = 6.4 experiment has a slightly lower final yield than the other RHA crystallisation experiment, this can be attributed to a slightly decreased starting Si concentration. The performance of the RHA derived zeolites is comparable, and slighty superior to the fly ash zeolite produced under similar conditions, as shown in Figure 7.31. These results combined show a far higher CEC yield for zeolites produced from RHA compared to processed fly ash, as shown in Figure 7.32.

Literature has shown synthesis of zeolite A from RHA to be possible, however sources

of RHA used in literature often contain crystalline material such as quartz and cristobalite, a lower silica content, or insufficient characterisation information [118, 127].

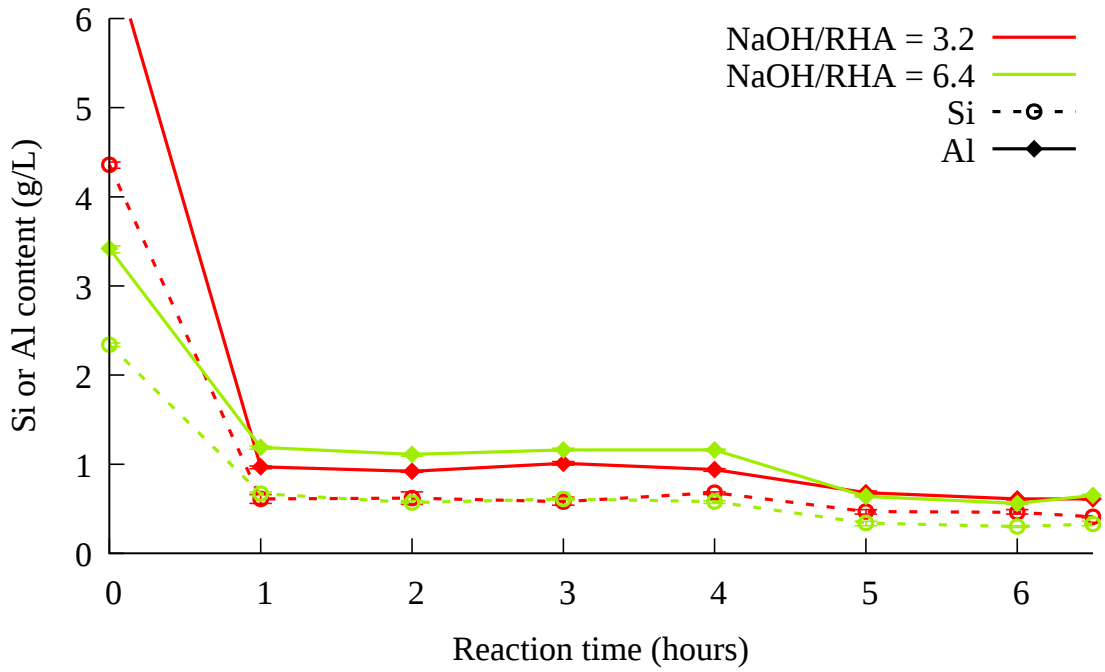

(a) AAS of RHA crystallisation

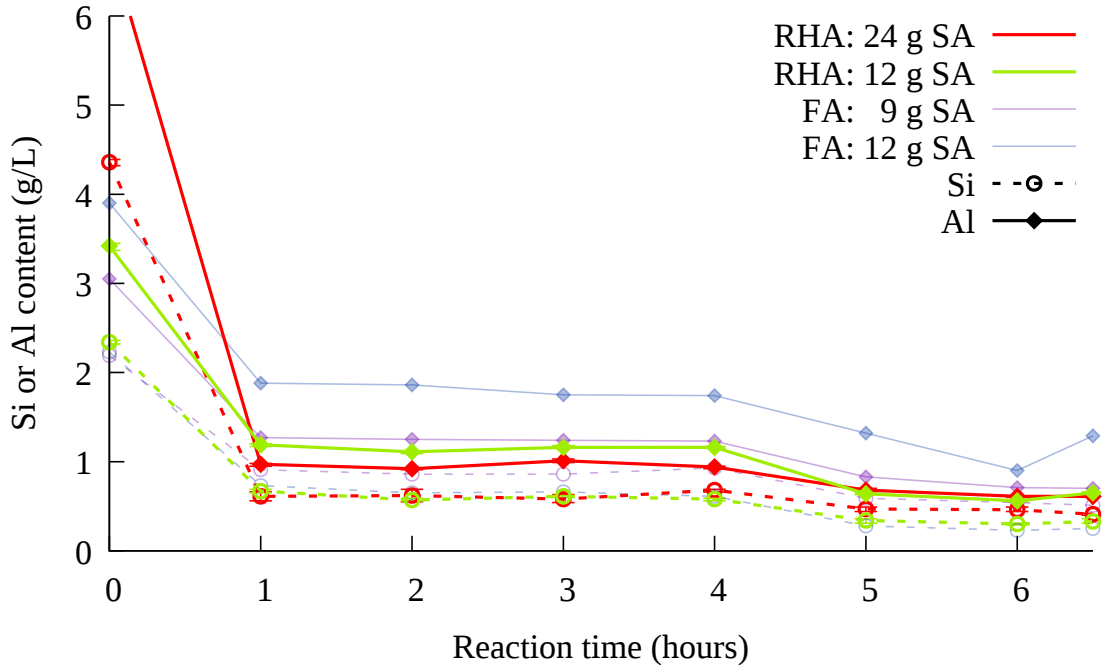

(b) AAS of RHA crystallisation compared to previous experiments

Figure 7.26: 90-95°C crystallisation process with leachate derived from rice husk ash

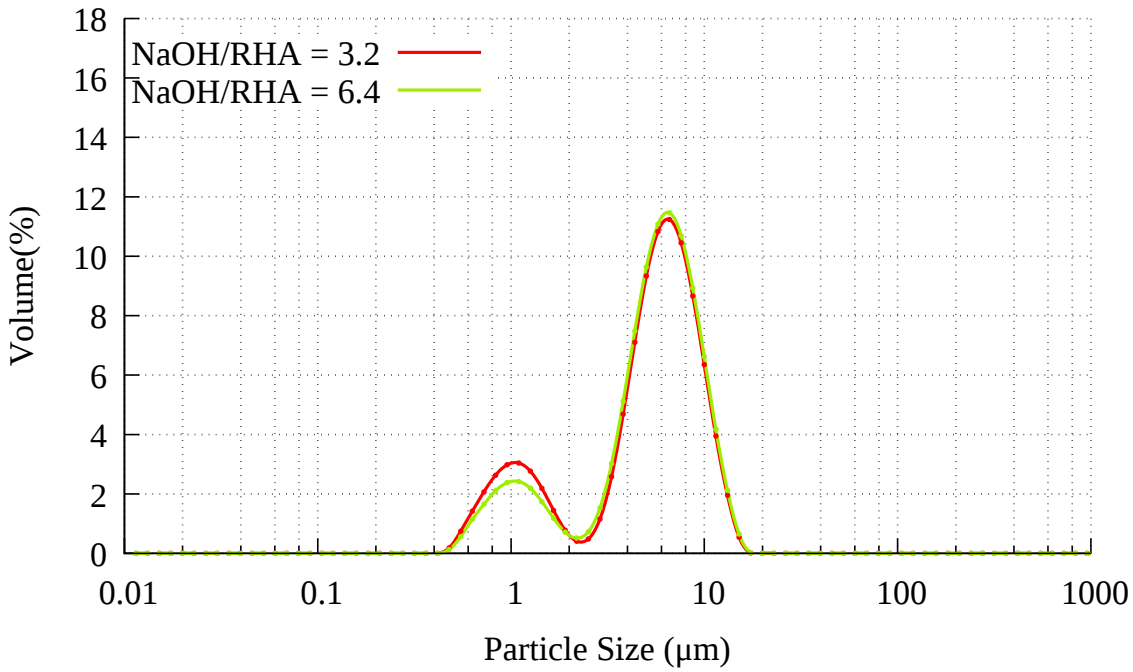

(a) PSD

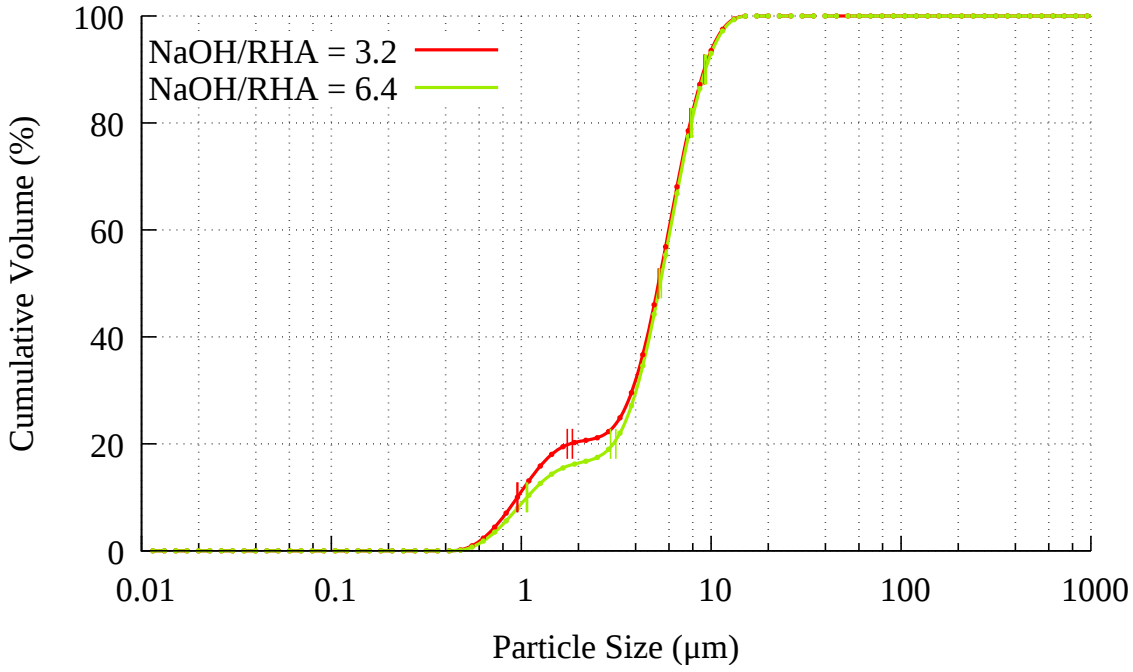

(b) Standard deviation in PSD

Figure 7.27: 90-95°C crystallisation process from rice husk ash leachate

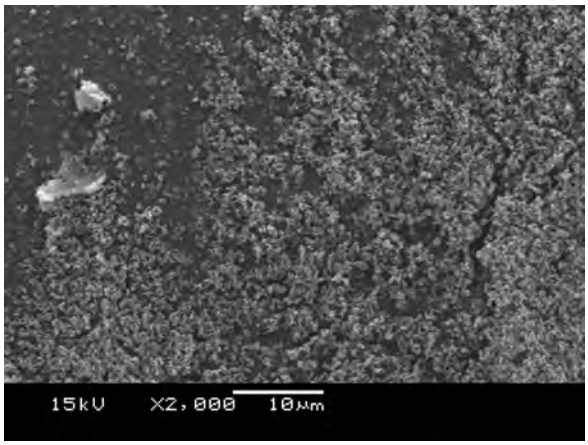

(a) 1 h

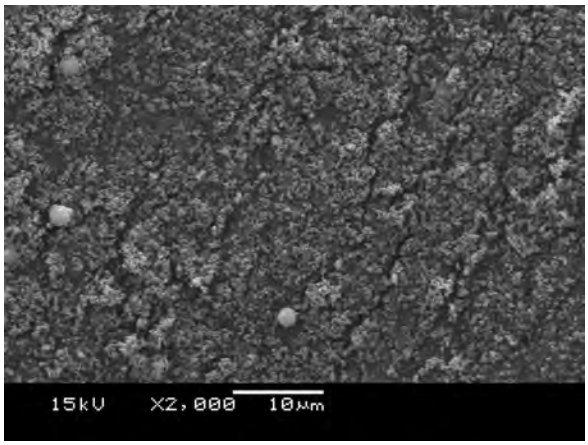

(b) 2 h

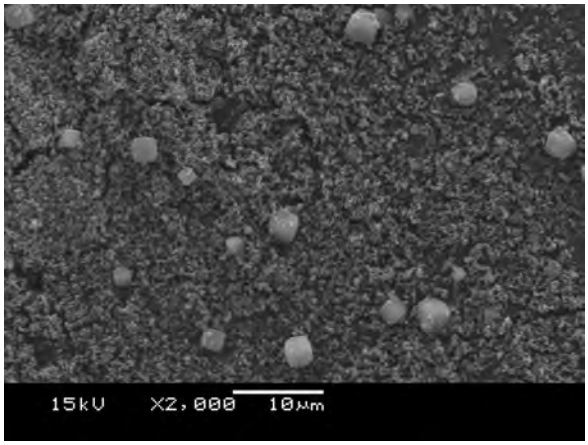

(c) 3 h

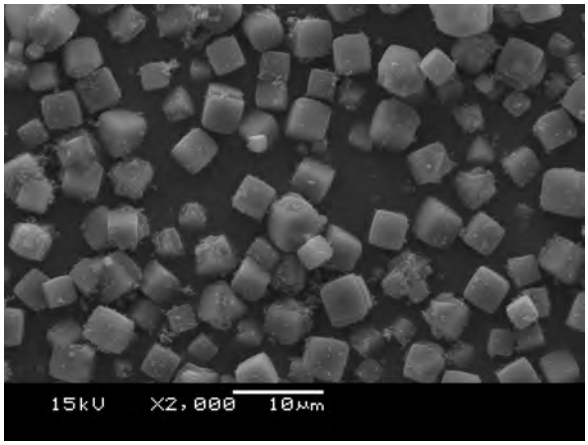

(d) 4 h

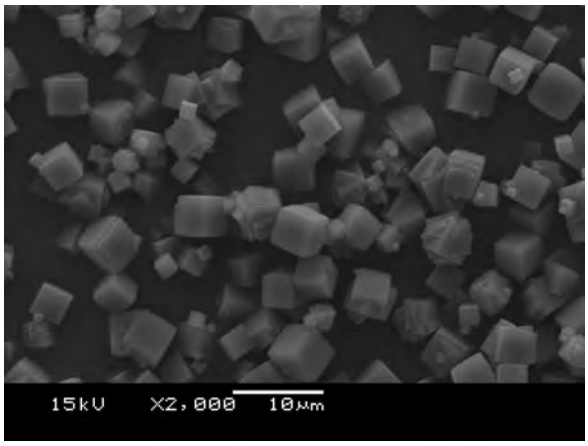

(e) 5 h

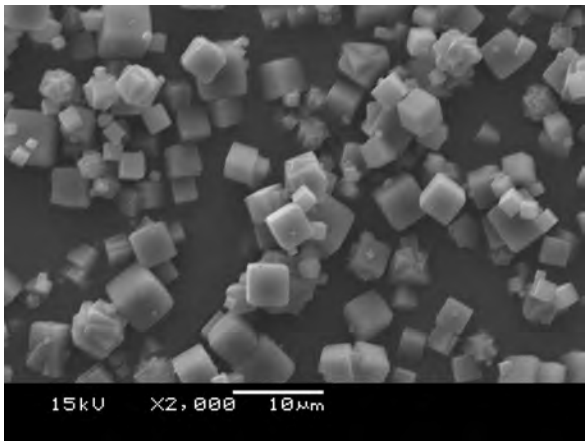

(f) 6 h

Figure 7.28: SEM images of zeolites from RHA extracted at NaOH/RHA = 3.2

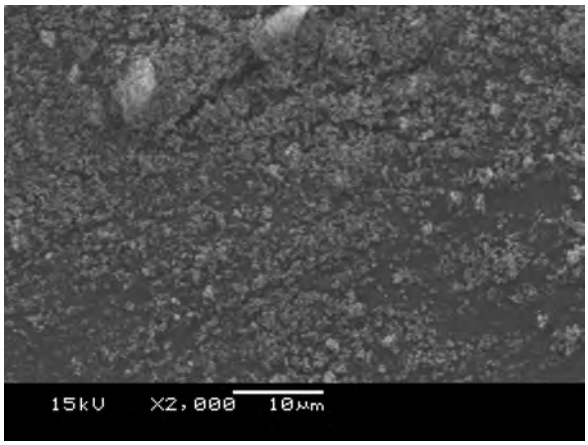

(a) 1 h

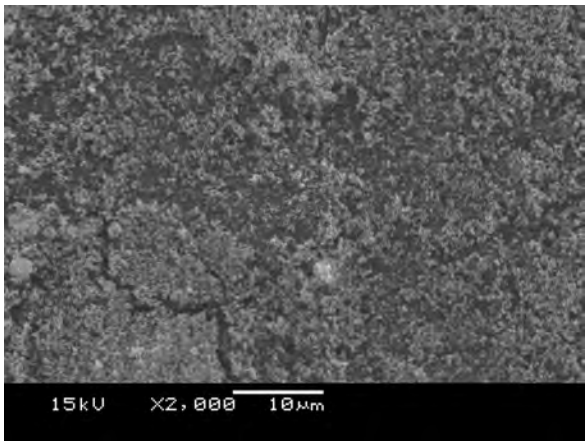

(b) 2 h

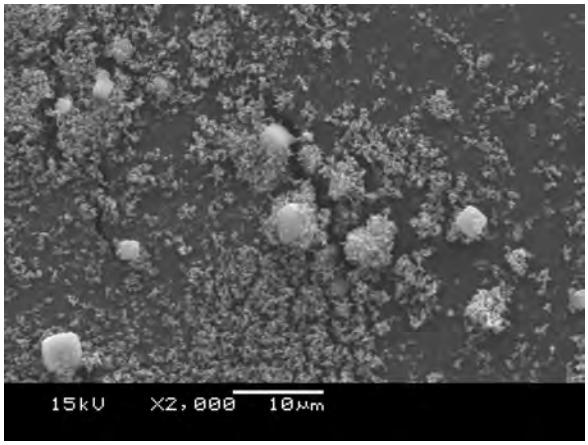

(c) 3 h

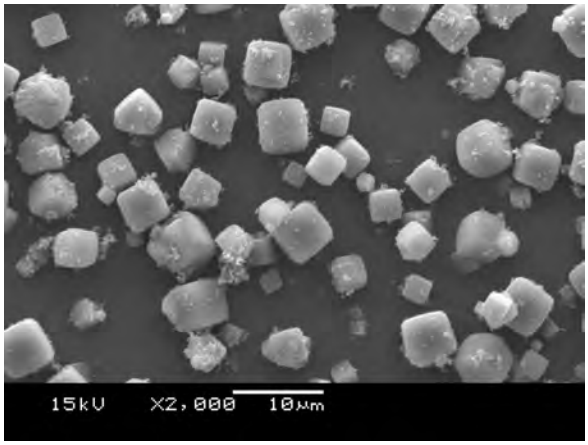

(d) 4 h

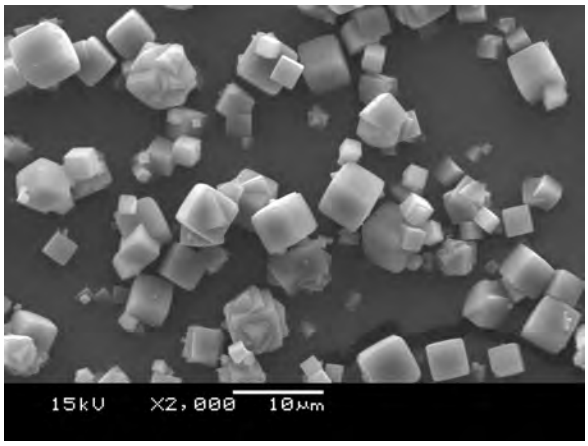

(e) 5 h

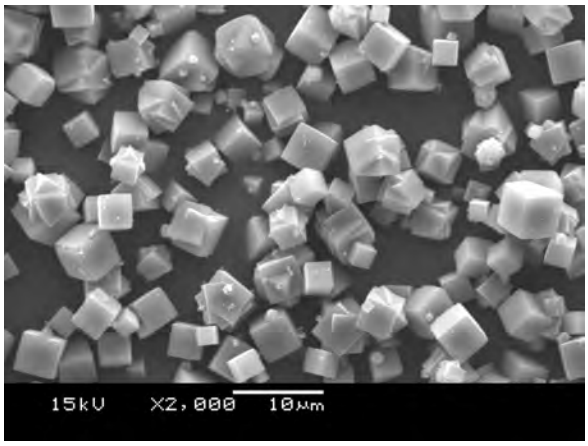

(f) 6 h

Figure 7.29: SEM images of zeolites from RHA extracted at NaOH/RHA = 6.4

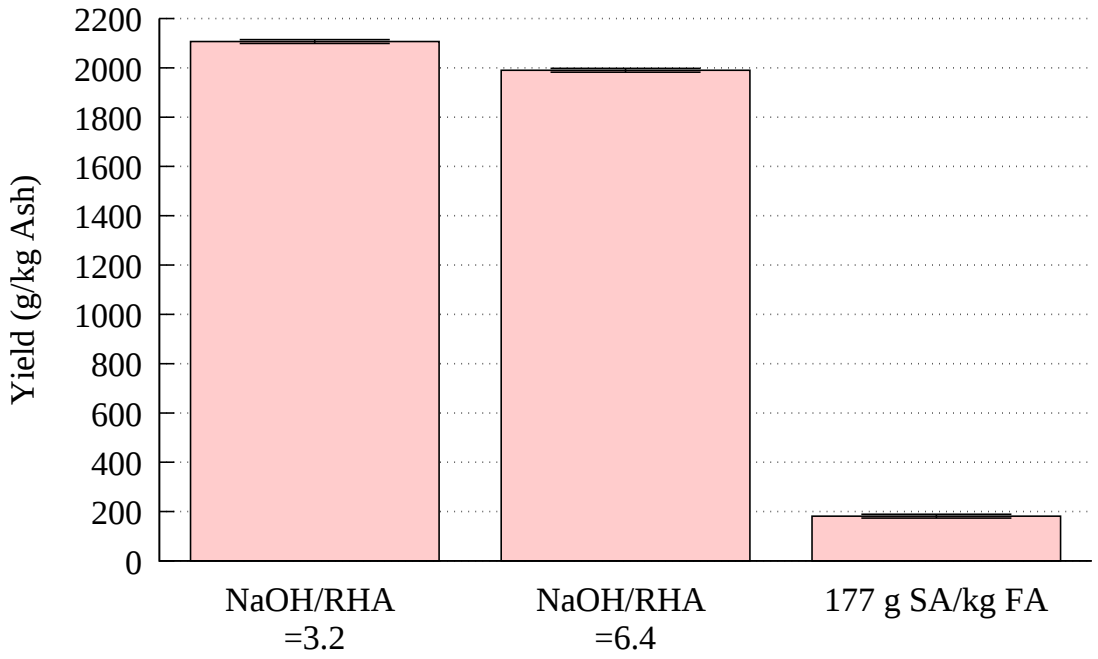

Figure 7.30: Yield comparison for zeolites crystallised from RHA leachates in Figure 4.35, with yield from a Delta extraction for context

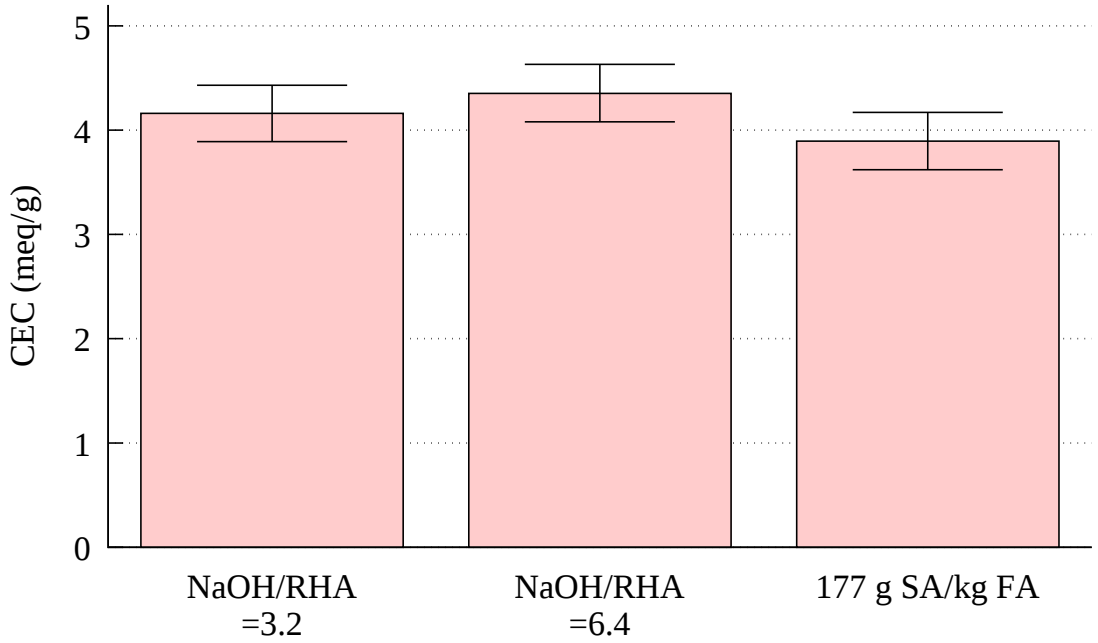

Figure 7.31: CEC comparison for zeolites crystallised from RHA leachates in Figure 4.35, with CEC from a Delta extraction for context

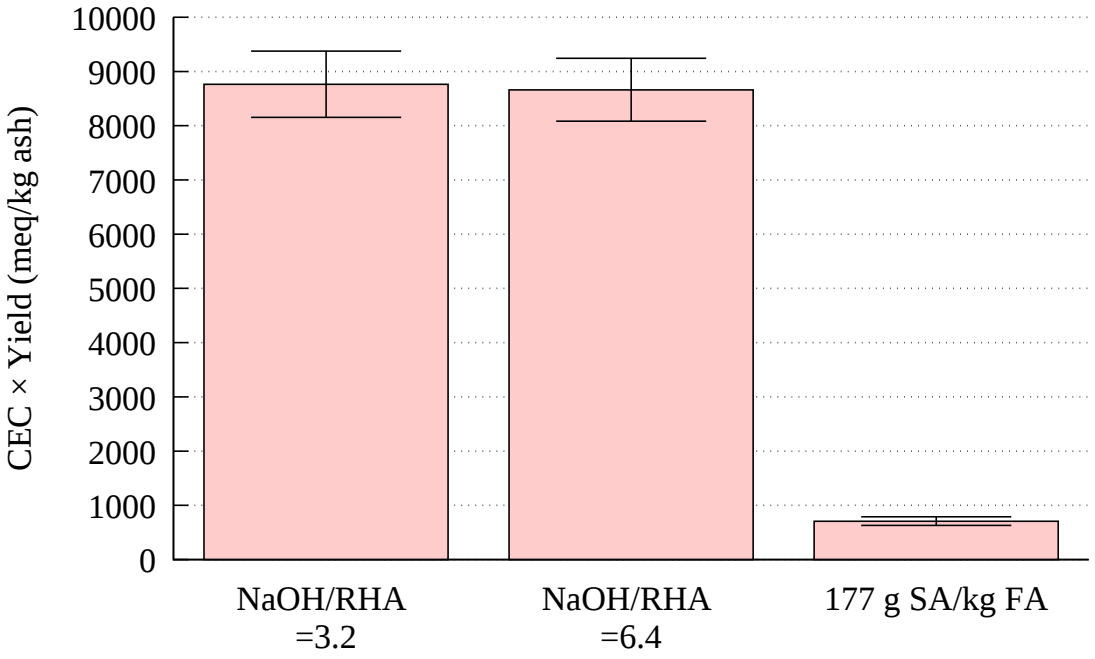

Figure 7.32: CEC Yield comparison for zeolites crystallised from RHA leachates in Figure 4.35, with CEC yield from a Delta extraction for context

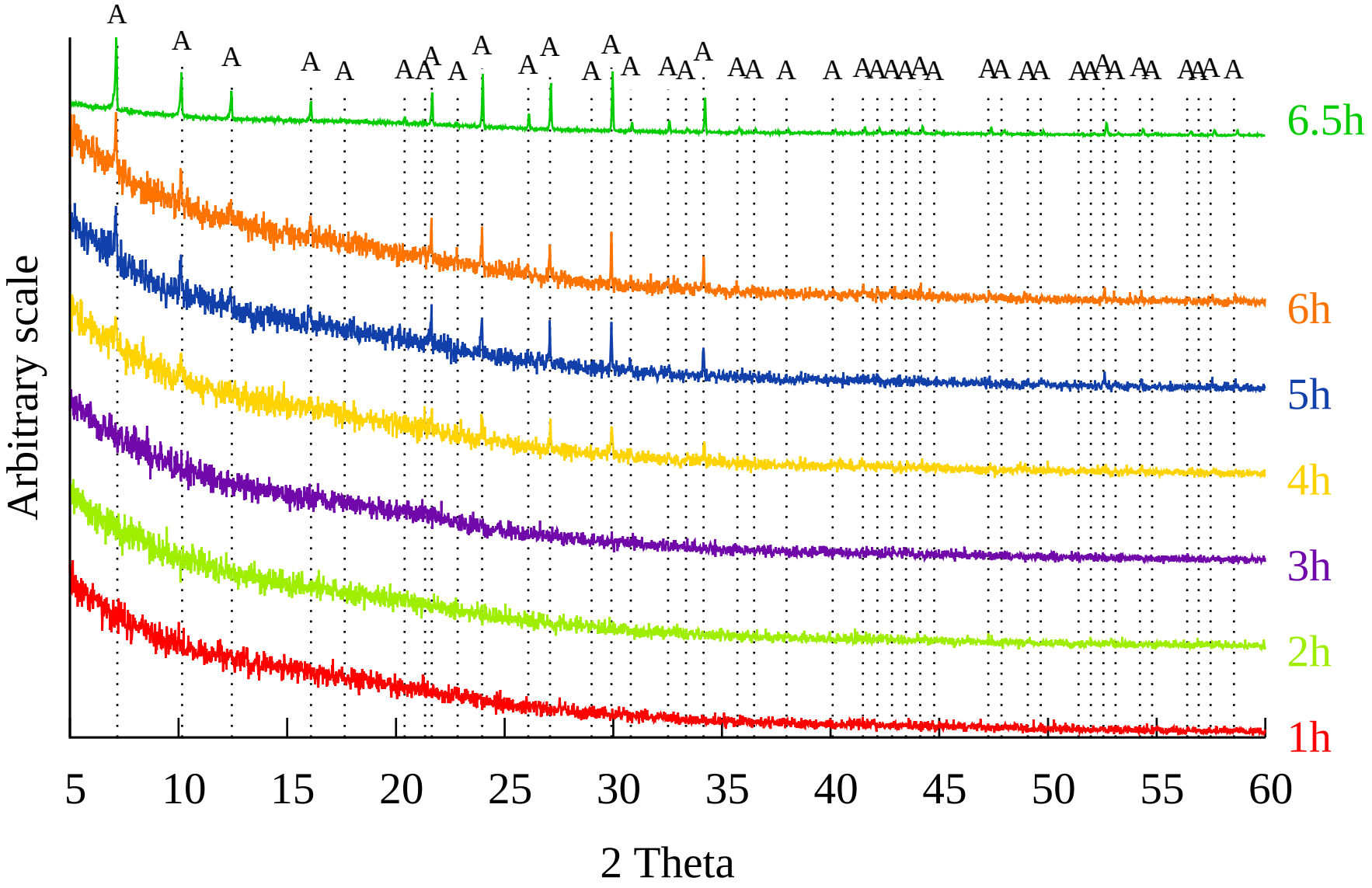

Figure 7.33: XRD patterns of 90-95°C crystallisation from RHA crystallised from leachate extracted at NaOH/RHA = 3.2 shown in Figure 4.35. A different x-ray source was used for the 6.5 hour sample analysis. A: Zeolite Na-A. $\lambda = 1.5406$ Å

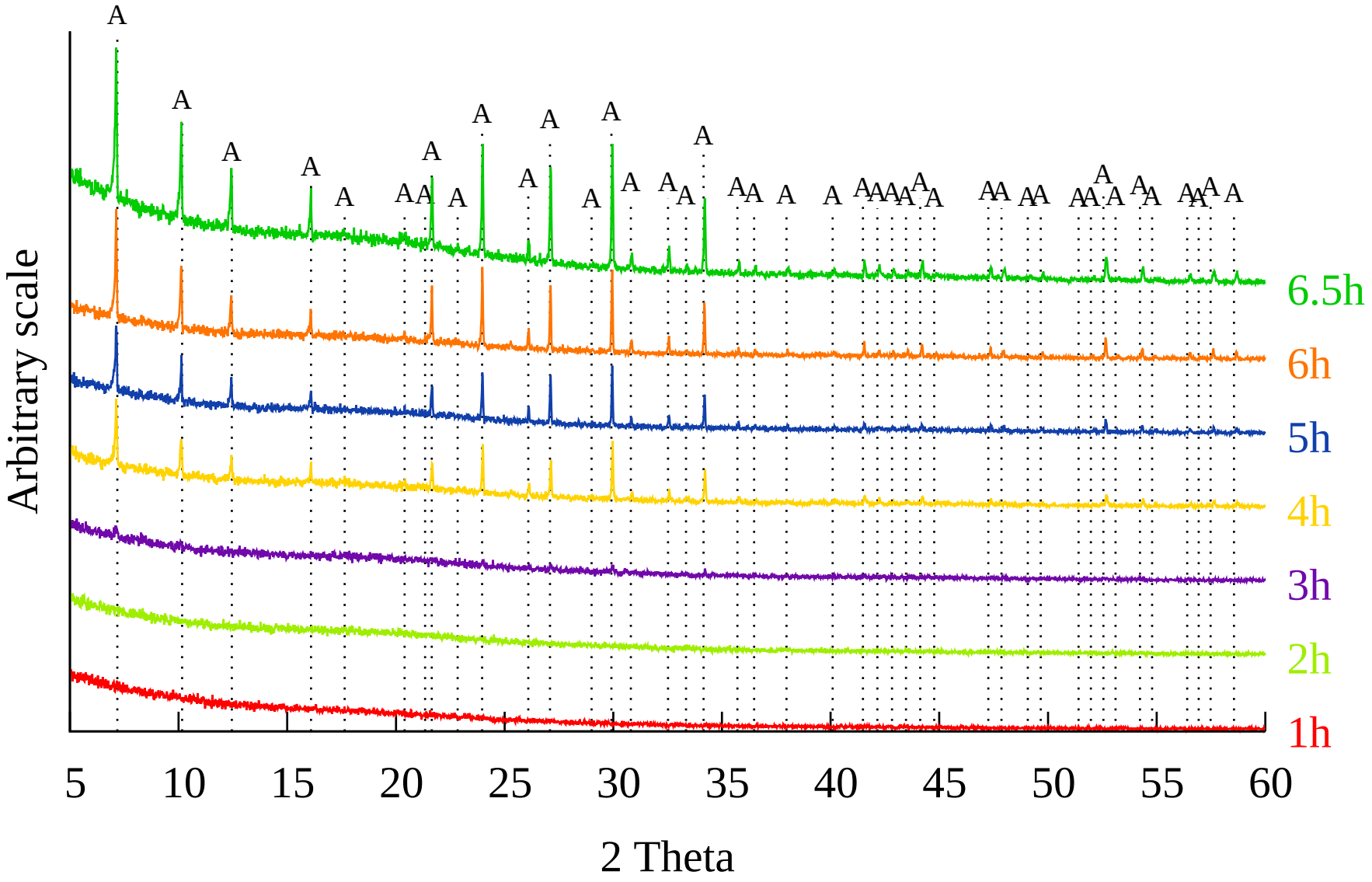

Figure 7.34: XRD patterns of 90-95°C crystallisation from RHA crystallised from leachate extracted at NaOH/RHA = 6.4 shown in Figure 4.35. A: Zeolite Na-A. $\lambda = 1.5406$ Å

7.4 Summmary of Crystallisation Experiments

Early experiments conducted under reflux conditions (~105°C) were noted to produce sodalite as well as zeolite A (figures 5.7-5.11). Reducing the temperature of the crystallisation step by 5°C resulted in synthesis of zeolite A with no sodalite detected in XRD analysis, however SEM analysis showed the presence of material which was not cube-shaped (figures 5.15f-5.20f), indicating an impure product. Yield analysis of these experiments showed that lower concentrations of sodium aluminate reduced the yield, and CEC analysis indicated that sodium aluminate content had little or no influence on the CEC of the final product. Conducting experiments at 90-95°C did not appear to significantly decrease yield, as with the 100°C experiments the yield started to plateau from 177 g SA/kg FA (figure 5.29). The CEC was approximately constant for all dosages of sodium aluminate bar the highest and lowest 5.30. The highest CEC yield was noted at 266 g SA/kg FA. The PSD of the final products was broadly similar at all but the lowest dosages of sodium aluminate, with the majority of particles being 4-20 μm in size.

In order to investigate the influences of the various components of sodium aluminate, experiments were conducted with additional NaOH, and were not found to have improved significantly when compared to the control experiment, however the PSD analysis indicates that the nucleation did not occur during the crystal growth phase of the experiment, due to the lack of particles in the 2-4 μm size. Agglomeration of the zeolite product was also noted during the cooling and filtration step. Addition of NaCl rather than NaOH noticeably decreases the final concentration of Si and Al in the crystallisation solution (figure 6.15) and increases the CEC and yield. A stark contrast is noted in the PSD for the nucleation period (0-2 hours) and the crystal growth period (3-6.5 hours, Figure 6.22a), and the PSD becomes broader and finer for the final product in comparison to NaOH addition. This indicates that NaCl aids the nucleation process. By varying the NaCl dosage, it was found that very high concentrations of NaCl produce a seed-rich solution within the first 2 hours, reducing the crystallinity and particle size of the final product 6.39a. Lower dosages of NaCl improved crystallinity based on XRD and SEM

data (figures 6.29 and 6.30). From these experiments it was clear that lower dosages of NaCl were favourable for CEC, yield and crystallinity.

Variation of SA content with a constant dosage of NaCl followed previous trends, with yield and CEC increasing with higher dosages of SA. The yield and CEC were also improved when compared to experiments without added NaCl. Crystallisation at a constant temperature of 95°C rather than 90°C for 2 hours, then 95°C for a further 4 hours was not found to improve the zeolite product or crystallisation process by any metric, and the similarity of the results to their 90-95°C counterparts indicated good repeatability. Use of sea salt at at the concentration of seawater was found to improve yield and CEC when compared to experiments with added NaCl. Sea salt was also found to encourage crystal growth and inhibit nucleation during the crystal growth phase (2-6 hours) of the crystallisation process due to the lack of particles of 2-4 μm size in Figure 6.71. Variation of SA with constant sea salt was found to follow previous trends, with an increase in yield as SA increases. CEC was also comparable. The highest yield of CEC from Delta ash was produced using sea salt and 222 g SA/kg FA.

Utilisation of different ashes in place of the Delta product was found to produce zeolite A, albeit at lower yields and slightly lower CEC. The lower yields can be attributed to the decrease in the Si content of the starting solution. This would indicate that the process can be used for different ashes, however processing ashes prior to use would produce favourable results. Repetition of experiments found good repeatability for yield and CEC. The highest yield of CEC was found to be at 5 and 6 hours. SEM images of the products show chamfered edge cubes of zeolite A with minimal observable impurities.

Addition of cenospheres to the crystallisation process resulted in the synthesis of zeolites which had crystallised on the surface of buoyant cenospheres. From CEC tests, the best floating zeolite product was found to consist of 23 % zeolite.

RHA was used as a feedstock for the crystallisation process. RHA is much more soluble than CFA, and produces a solution much richer in Si. Due to the higher Si content, more sodium aluminate can be added and almost entirely consumed, rather than leaving a

solution rich in wasted sodium aluminate after the zeolite has been filtered out. Due to the higher solubility of the RHA, the yield is significantly higher, whilst the CEC of the zeolite derived from the RHA is comparable to zeolite derived from CFA under similar conditions.

Commercially available zeolite A is described as having a d_{50} of 4 μm, a mean size of 4 μm or consisting of 90 % less than 4 μm or 10 μm depending on the source [144–148]. Such particle sizes were achieved in conditions with a high NaCl content, however such experiments took a significantly longer period to filter, often resulting in some loss during filtration. If target markets require a particle size of 4 μm, in order to speed up the synthesis on an industrial scale, it suggested that crystallisation conditions should aim for a particle size of 10-20 μm and then grind the product afterwards to allow for a faster filtration process and in order to reduce the quantity of zeolite product lost during filtration.

Chapter 8

Conclusions

8.1 Extraction

Experiments were conducted to optimise the conditions under which a Si rich leachate could be derived from CFA. Hydrothermal extraction, fusion assisted extraction, and microwave-fusion assisted extraction were the main conditions investigated. Commercial synthesis of zeolite A is conducted at atmospheric pressure, thus high pressure processes were not investigated [68].

8.1.1 Hydroxide Content and Source

Hydrothermal extraction experiments with 2-4 M NaOH under reflux conditions found that the extraction of Si from ash increased in proportion with the concentration of NaOH. Si and Al extraction increased rapidly for the first 30-40 minutes, before the Al content of the solution started to decrease, and the Si content continued to increase but at a significantly slower rate. After the initial peak in Al content, the concentration of Al in the solution decreases, which is consistent with the formation of a zeolite coating on the surface of the ash particles, limiting further dissolution of the ash, and consuming Al from solution. Such observations and conclusions are supported by literature [72, 74, 84]. Whilst higher NaOH concentrations increase the proportion of Si extracted, crystallisa-

tion conditions with highly alkaline solutions have been shown to synthesise sodalite, thus subsequent extraction experiments mostly focused on 2 M NaOH, a concentration commonly used in literature [25, 32, 49, 58, 73, 74]. Experiments where a proportion of the NaOH content was replaced with Na_2CO_3 supported literature which stated that Na_2CO_3 is less effective than NaOH at extracting Si from ash, and as the proportion of NaOH replaced increased, the extraction efficiency decreased [68, 74, 75].

8.1.2 Comparison of Hydrothermal Extraction and Fusion Assisted Extraction

The fusion method commonly described by literature grinds ash and NaOH prior to fusion [38, 39, 54, 85]. This method was compared to a fusion step without grinding the ash and NaOH. The fusion products were dissolved under reflux conditions. In the hydrothermal extraction experiment, ash was added to a boiling solution of NaOH. Adding the fusion product to boiling water would have been unsafe, thus the fusion product was added to water at room temperature, and heated to its boiling point at which the experiment's timer was started. No measurements were taken before the experiment reached its boiling point. The "0 minute" samples for both fusion experiments are therefore higher in Si than the hydrothermal experiment with no Si. The ground fusion experiment exhibited lower levels of Si and Al in solution than the other conditions at all time points other than the "0 minute" point. This decreased content is attributed to the dissolved Si and Al crystallising out of solution during the extraction process due to the high temperatures being conducive to crystallisation of zeolites. The Si extraction for the hydrothermal process at 40-60 minutes was comparable to that of the fusion process without grinding at 40 minutes.

Dissolution of the fusion products in distilled water at ambient temperature was investigated. The results showed that the Si and Al content of the solution did not decrease after reaching a maximum. The quantity of ash in ambient temperature 4 M experiment was half the ash content of the other experiments. Thus, the NaOH:ash ratios were 3.2:1

and 0.8:1 for the 4 M and 2 M ambient temperature dissolution experiments. The 3.2:1 experiment had the higher relative extraction of Si, but the absolute yield of Si in solution was similar to the hydrothermal extraction at 60 minutes.

8.1.3 Microwave Fusion Experiments

An experiment was conducted comparing the conventional fusion process with a microwave fusion process and a hydrothermal extraction process. The results indicate that the microwave fusion process performs similarly to the conventional fusion process at NaOH:ash ratios of 1.6:1. The hydrothermal extraction process shows a decrease in the Al content over time, as mentioned earlier. This decrease is attributed to crystallisation of zeolite in the hot hydrothermal conditions. The ambient temperature dissolution of the fusion products displays no great change in the Si or Al content between 10 minutes and 6 hours. SEM images show similar results for the insoluble residue after cold dissolution when comparing microwave fused ash with conventionally fused ash.

8.1.4 Solids Loading in Hydrothermal Experiments

An investigation into the effect that ash content has on Si extraction in hydrothermal experiments indicated that extraction efficiency was higher when less ash was used. The concentration of ash in both experiments was similar at 60 minutes, and the disparity tended to decrease as the experiment progressed and the concentration of Si in solution increased. SEM images show initially smooth ash particles gradually accumulate a crystalline coating over 6 hours. The conclusions drawn from this data were that lower solids loadings may be be preferable for extraction experiments that are shorter in duration in order to increase efficiency.

8.1.5 Solids Loading and Mixing in Fusion Experiments

Investigations into the effect of solids loading on extraction of Si and Al from ash indicated that a higher ratio of NaOH:ash resulted in a higher extraction efficiency. Two sets experiments were conducted, where one set was stirred during the fusion process. The results were very similar, indicating good repeatability, and that stirring does not greatly influence the extraction efficiency. SEM images of samples at varied NaOH:ash ratios appear very similar.

8.1.6 Solids Loading in Microwave Fusion Experiments

As with the conventional fusion experiments, the extraction efficiency increased as the NaOH:ash ratio increased, however the highest concentration of Si in solution was achieved with a ratio of 1.2. The concentration of Al continued to increase despite a decreasing ash content up to a NaOH:ash ratio of 6. As the cost of the ash is low, and the desired outcome of extraction process is a solution rich in Si, subsequent experiments focus on the 1.2:1 NaOH:ash ratio solids loading.

8.1.7 Re-Fusing Used Ash

As the proportion of Si extracted in the fusion process was not particularly high, re-utilising ash in the extraction process was explored in order to increase the extraction efficiency. Ash that had previously undergone fusion and dissolution was filtered from the dissolution solution and dried without washing. The ash was then mixed with NaOH at the same ratio to which it had been previously been mixed for the first fusion process, and fused again. For the NaOH:ash ratio of 1.2:1, the yield of Si in solution was lower, whilst the 3:1 ratio ash rendered a similar concentration of Si in solution.

8.1.8 Effect of Prolonged Dissolution on the Extraction of Si and Al from Microwave Fused Ash

In order to ascertain the minimum necessary duration of the dissolution process that follows the fusion step, a prolonged dissolution experiment was conducted. The experiment was conducted at two ratios of NaOH:ash; 1.6:1 and 3.2:1. Both ratios showed a similar extraction of Si for the first 40 minutes, and the experiment with a lower ash content showed a slightly higher efficiency of extraction from 50 minutes - 6 hours, whilst the experiment with a higher ash content maintained a steady Si extraction from 10 minutes to 3.5 hours before deviating slightly. This experiment indicates that there is little change in the Si content between 10 minutes and several hours, thus the dissolution process could be conducted quite quickly.

8.1.9 Effect of Varying the Duration of the Microwave Fusion Step

The influence of the duration of the microwave fusion process on the dissolution of Si and Al from ash was investigated. The NaOH and ash were fused at a ratio of 1.6:1 for 10-40 minutes. The results indicate very similar extraction efficiencies for Si and Al at all fusion durations, and the yield of Si in solution appears to be stable for all samples taken during dissolution between 10 minutes and 3.5 hours, after which there is a slight variation. The extraction efficiency of Al appears to decrease as the duration of the fusion step increases. SEM images of fused ash at different ratios appear quite similar.

A further investigation into microwave fusion duration was conducted with a 10 minute dissolution step. These experiments were conducted with a fusion period of 5-20 minutes. The quantity of solids fused was also reduced by a factor of 5. The results from these experiments had a similar yield to the experiments with five times as much material, indicating scope for optimisation, with potential to save energy by fusing larger batches.

8.1.10 Source Ash

Comparing the performance of the Delta ash with other CFA samples shows that Delta is the ash with the highest yield of Si for these conditions. Unprocessed ashes have lower Si extractions, with the Alpha ash having the lowest yield of Si in solution. This is attributed to the effect of particle size on the rate of heating [139, 140]. Delta is a coarser ash product with a particle size range > 45 μm, whilst Alpha is finer and has a particle size < 45 μm. The difference in effect of heating is supported by experimental observations, as a greater proportion of the Delta fusion product glowed incandescently after 10 minutes than the Alpha fusion product.

8.1.11 Acid Washing Leached Ash

The zeolite coating that forms on the surface of ash particles hinders further dissolution of Si and Al from ash. Ash that had been previously leached was washed with HCl in order to disrupt the zeolite layer, and then leached again with NaOH. Whilst this did result in further dissolution of the ash, the yield of Si and Al in the second NaOH leaching was low.

8.1.12 Analysis of the Fusion Product

XRD analysis of the fusion product indicates the presence of water soluble sodium silicate, which is no longer present after a 10 minute dissolution step. This is in line with literature, which indicates that the fusion process results in the formation of water soluble sodium silicate [39, 40, 44, 57]. Literature describes the fusion product as being green in colour [85, 86, 90]. This is also observed in the microwave fusion product and is attributed to the iron (II) hydroxide that is eventually replaced with iron (III).

8.1.13 Repeated Acid Washing

In order to break down the zeolite coating on ash particles that prevents further dissolution of Si and Al, the ash was washed with HCl. This was done at hot and ambient temperatures. SEM images indicate that even a short exposure to ambient temperature HCl is sufficient to remove the zeolite coating. Further, more rapid experiments where ash was washed with aliquots of HCl indicated that the zeolite coating was rapidly removed. Acid washing of ash was not pursued further, as the production of a Si, Al and Fe rich acidic solution with no application was not considered advantageous.

8.1.14 Long Term Extraction Average

Analysis of the Si and Al content of leachate from 44 extraction experiments shows a relative standard deviation of 6 % and 10 %. These variations are attributed to the ash being a heterogeneous material, an imperfect mixing process, and uneven heating.

8.1.15 RHA as a Source of Si

Hydrothermal dissolution of Si from RHA gave a much higher extraction efficiency than Delta ash. This is attributed to the RHA being more amorphous, and the lack of any Al present in the solution forming an insoluble zeolite surface layer to inhibit dissolution. RHA combusted at lower temperatures leached faster than samples with crystalline material, but all RHA samples were similar from 2-6 hours.

Experiments conducted investigating solids loading, NaOH:RHA ratio and extraction method indicate these have little effect on the yield of Si within the first 60 minutes. This suggests potential scope for optimisation of the process where savings could be made by reducing the reagents, energy costs and duration of Si extraction processes from RHA.

8.2 Crystallisation of Zeolites

Experiments were conducted investigating the effect of various parameters on the crystallisation process. XRD, SEM, AAS and PSD analysis were used to assess the influence of alkalinity, NaCl content, temperature, and additional reagents on the crystallisation of zeolites.

8.2.1 Crystallisation of Zeolites from Na_2CO_3 Leached Ash

The crystallisation under reflux conditions of zeolite from Na_2CO_3 leached ash produced sodalite and zeolite A. SEM images show cubes of zeolite A with extraneous spherules. The synthesis of sodalite is attributed to the high temperature and longer experiment times, both factors that encourage the formation of sodalite [32, 42, 62–64].

8.2.2 Crystallisation at 100°C Using a Hot Plate

Reducing the temperature of the crystallisation process from reflux temperatures (105°C) to 100°C resulted in the synthesis of zeolite A, with no apparent sodalite impurities. SEM images show fewer extraneous spherules. AAS analysis of the crystallisation solution shows that as more Al is added, Si in solution decreases. AAS also shows concurrent decreases in Si and Al in solution as amorphous material disappears from SEM images, and XRD patterns show the presence of crystalline material. These observations are similar to those by Belviso et al. [40], who also observed a decrease in Si and Al in solution as crystalline materials developed, and are in line with the mechanism described by Cundy and Cox [60]. Crystalline material grows through addition of Si and Al from solution. The solution is in equilibrium with amorphous and less ordered material. As the Si and Al in solution are consumed through crystal growth, the amorphous material is dissolved to replenish the Si and Al in solution, thus SEM images show a decrease in amorphous material, AAS results show a decrease in Si and Al in solution, and XRD results show a growth in crystalline material. As the amount of Al added increases: the yield increases

and plateaus; and the aforementioned observable crystallisation process occurs sooner. These observations are also supported by literature [35, 71]. This behaviour and the aforementioned trends are also observed in subsequent experiments.

8.2.3 Step Change in Temperature During Crystallisation

Literature indicates that heating the crystallisation solution to 90°C to encourage nucleation before raising the temperature to 95°C to encourage crystal growth results in a more rapid crystallisation process [32]. Comparing this step change with the previous 100°C process showed similar or slightly reduced yields for most dosages of sodium aluminate, and a slightly more consistent CEC. AAS and XRD results followed the trends observed in section 8.2.2. SEM results showed cubes with chamfered edges, which appear cleaner than cubes in the 100°C experiment. Some crystals appear to show intertwined cubes. Such particles can be attributed to agglomeration of zeolite nuclei which grow together, as described by [60] .

8.2.4 The Effect of Additional NaOH on Crystallisation

The addition of sodium aluminate increases the alkalinity of the crystallisation solution. Experiments were carried out to investigate the effect of additional NaOH on the crystallisation process. Zeolite A was produced more rapidly with the additional NaOH, whilst the yield was only slightly reduced and the CEC slightly raised with an additional 0.5 moles of NaOH and reduced with 1 additional mole of NaOH. SEM images show agglomerated cubes with additional, finer material on the surface. The additional NaOH was not so high as to produce sodalite, which is supported by authors who have synthesised zeolites at concentrations of 3 M NaOH [25, 35, 68].

8.2.5 Alternative Sources of Sodium

Cations have been noted to influence the crystallisation process [30, 60]. Sodium hydroxide and sodium aluminate both add sodium to the crystallisation solution, thus an experiment was carried out with the intent of comparing additional sodium from NaCl without altering the alkalinity of the crystallisation solution. Results showed that addition of NaCl increased: consumption of Si and Al in solution, yield, and CEC. The particle size of the product was decreased, which was attributed to a seed-rich solution based on the PSD of the product early in the experiment. SEM images indicated the presence of finer particles alongside the chamfered edged cubes.

8.2.6 Effect of NaCl Dosage on the Crystallisation Process

In order to better investigate the influence of additional NaCl, experiments were carried out where various quantities of NaCl were added to the crystallisation process. As NaCl content increases, the Si content drops sooner, which coincides with the crystallisation observations described in section 8.2.2. Low dosages of NaCl show: chamfered edged cubes with minimal fine particles; an increased yield; an increased CEC; and clearer XRD patterns. With increasing dosages of NaCl: the finer particles become more prevalent in SEM images; cubes are less well defined; XRD analysis detects less crystalline material; the yield and CEC decrease; and the particle size decreases.

8.2.7 Increasing Sodium Aluminate with a Constant Dosage of NaCl

The addition of NaCl has been shown to improve results. Variation of the sodium aluminate content in a solution with added NaCl was therefore explored. These results followed the trends discussed in section 8.2.2, but with the improved yield attributed to the NaCl. The reduced CEC was attributed to the concentration of NaCl being too high.

8.2.8 Crystallisation at a Constant Temperature of 95°C

Experiments conducted at a constant 95°C, appeared very similar in every regard to experiments with a 90-95°C temperature change.

8.2.9 Alternative NaCl Sources

Utilising seawater rather than distilled water in the crystallisation process can reduce costs [38, 39]. Replacing the NaCl with sea salt at concentrations appropriate for sea water indicated a similar performance to that of NaCl, with a higher yield, and higher CEC than the control experiment with no added NaCl. Variation of the sodium aluminate content under such conditions followed the behaviour described in section 8.2.2. The CEC and yield both improved linearly with increased dosages of sodium aluminate.

8.2.10 Repetition

In order to accurately assess the yield, experiments were conducted with no samples taken prior to the end of the experiment. These conditions were identical to the median conditions of the previous experiment set. These experiments showed very similar yields and CECs at 5 and 6 hours, however the yield was slightly higher at 6 hours, and the CEC slightly higher at 5 hours, with the CEC yield being slightly higher for the 5 hour experiment. The mean yield was 233 g of zeolite A/kg FA with a RSD of 3.3 %. The mean CEC was found to be 4.6 meq/g with a RSD of 5.9 %. Extrapolating these results for a higher dosage of SA based on data from the previous experiment set would give a yield of 264 g/kg FA and a CEC of 4.8 meq/g. SEM images show chamfered edged cubes with no apparent contaminant. No yield results for the same conditions could be found in literature. The closest comparison had a slightly higher yield by a different method [90]. CEC results are sane, but slightly higher than some reports of achieved CECs in literature [3, 26, 44, 54, 90].

8.2.11 Different Source Ashes

Comparing the performance of Delta ash with Alpha, Lagoon and FB7 ashes shows that whilst the process also works for other ashes, the lower Si content from the extraction process results in a lower yield. The CEC capacity is also reduced, such a reduction attributed to the Si/Al ratio. SEM images show chamfered edged cubes with minimal extraneous material. The PSD is narrowest for the Delta ash, but is similar for the other ashes, whilst being slightly broader.

8.2.12 Floating Zeolites

Cenospheres were separated by density with ethanol in order to acquire the most buoyant cenospheres. These were added to a crystallisation process with the goal of crystallising zeolite A on the surface of the cenospheres. In experiments where the mixing mechanism did not cause attrition, cenospheres were produced with a final product of which 63 % floated on water. From CEC tests, this floating material comprised 86 % cenosphere and 14 % zeolite. This result was improved to 68 % buoyant material comprising 77 % cenospheres and 23 % zeolite by slowing the addition of the sodium aluminate. XRD of the most buoyant material showed zeolite A, mullite, quartz and calcite.

8.2.13 Zeolites from Rice Husk Ash

Synthesis of zeolites from RHA was compared to zeolites from Delta ash. AAS results still show the concurrent drop in Si and Al observed in Delta ash described in section 8.2.2. Due to the high starting concentration of Si, the amount of SA added was increased proportionally, and the yield was significantly higher than the yield derived from RHA. SEM images show clean cubes of zeolite A, XRD shows no other phases present, and the CEC is similar to that of zeolites derived from Delta ash samples. This indicates that RHA can easily be used in the synthesis of zeolites due to the high solubility of Si.

8.3 Comparison of Performance

8.3.1 Zeolite Performance

Table 8.1: Comparison of cation exchange capacities of various zeolites and sources. CEC expressed as meq/g.

Sample	CEC
Zeolite A from Delta ash	4.8
Zeolite A from RHA	4.4
Zeolite A from CFA [54]	3.9
Zeolite A from CFA [26]	4.3
Zeolite A from RHA [127]	4.7
Clinoptilolite [149, 150]	2.2

Table 8.1 compares the CEC of the zeolites synthesised in this project with zeolites produced by studies described by literature, and a natural zeolite, Clinoptilolite. The results show a high CEC for the zeolites made during this study, with the zeolites from Delta ash outperforming zeolites derived from CFA described by literature. Zeolites produced from RHA in an unoptimised process during this study performed at a level slightly lower than optimised processes in literature.

8.3.2 Fusion Process Performance

The power consumed by the furnace for the fusion process was measured. Comparing the power requirements of the microwave fusion process to the conventional fusion process is pertinent as such parameters will help determine if the microwave fusion process is cost effective, and thus if application of the of the microwave fusion process in scaled up processes is feasible. The power drawn by the furnace over the 2 hour process was 1.062 kWh. The microwave was rated as having a 1200 W input, and a 700 W output. As the microwave was operated on full power for 10 minutes, the calculated power consumption was 0.2 kWh. This indicates that the microwave fusion process offers an energy saving of approximately 80 %. The microwave fusion process also offers a time saving of 92 %. The option of saving both time and energy costs indicate that implementation is feasible.

Chapter 9

Further Work

The scope for further work is ample. A brief outline of potential avenues of research are detailed below.

9.1 Microwave Processes

All microwave experiments were conducted at a frequency of 2.45 GHz. Whilst this is suitable for dielectric heating of water, it is possible that use of other frequencies could improve heating rates in CFA. The particle size distribution of the ash and NaOH to be fused could be further investigated in order to find the optimum size range for rapid heating, as literature indicates particle size influences heating rates [140]. The ratio of microwave power to solids being fused could be optimised in order to increase the efficiency of the process. Addition of small amounts of water to the microwave fusion process could improve the rate of heating through superior dielectric heating of the water at the 2.45 GHz frequency range. The crystallisation process could also be improved through microwave assisted crystallisation.

9.2 Leachate Disposal

The alkaline leachate from the crystallisation process presents a disposal cost. The waste solution could be utilised to capture CO_2 from flue gas streams, as described by Amrhein et al. [25]. Another option would be to utilise the leachate in the synthesis of a phosphate fixating product developed by Xie et al. [59]. In this process, the Al-rich solution from the crystallisation solution would be added to the undissolved Delta ash to form zeolitised ash. After zeolitisation is complete, $FeCl_3$ could be added slowly to the solution to make phosphate-immobilising Fe_2O_3 compounds. The resulting leachate would have a neutral pH and be easier to dispose of. The zeolitised Fe-rich product could then have applications as an anti-eutrophication product, which can then be reused as a soil treatment agent to improve soil CEC and slowly release ammonia and phosphates back into soil.

9.3 Optimisation of Synthesis Processes

The methods for the synthesis of added value products was not optimised. The addition of cenospheres to the crystallisation solution provides a source of Si as the cenospheres are dissolved by the alkaline solution. Addition of aluminium at a yet slower rate could also be explored in an attempt to inhibit nucleation of zeolites that are not attached to cenospheres. The process for the synthesis of zeolites from RHA has only been roughly explored. Further optimisation could be pursued in increasing the extraction efficiency of the RHA, and investigating the optimal conditions for zeolitisation.

9.4 Kinetics of RHA Dissolution

The dissolution of RHA in NaOH appears to follow a kinetic model, however does not fit first or second order kinetic models. Further work could be done applying higher order kinetic models to the RHA dissoultion data.

Appendix A

SEM

(a) Parboiled Rice Husk

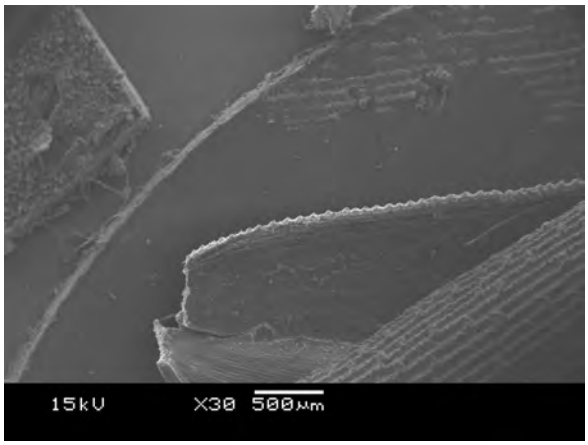

(b) Parboiled Rice Husk

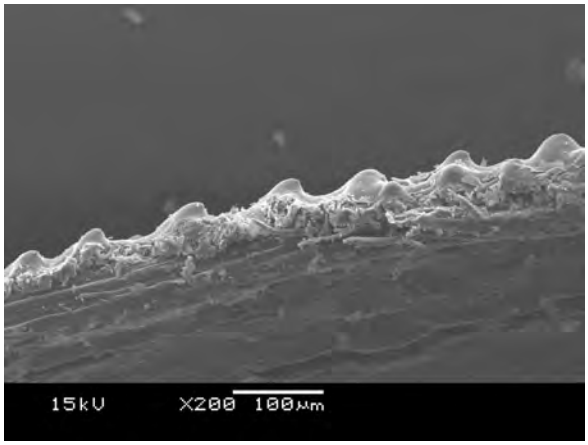

(c) Parboiled Rice Husk

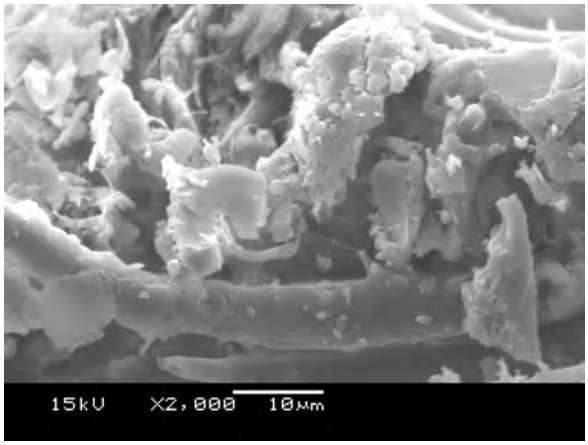

(d) Parboiled Rice Husk

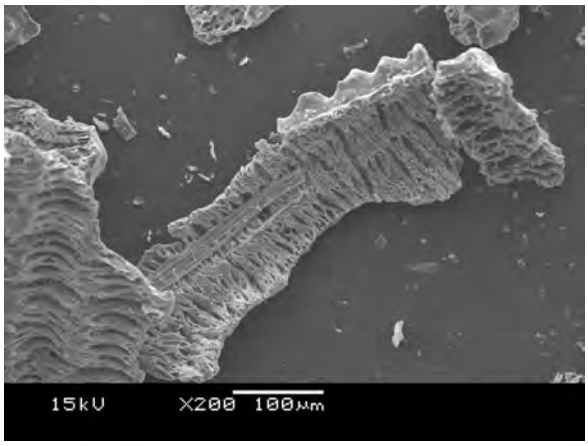

(e) Rice Husk Char

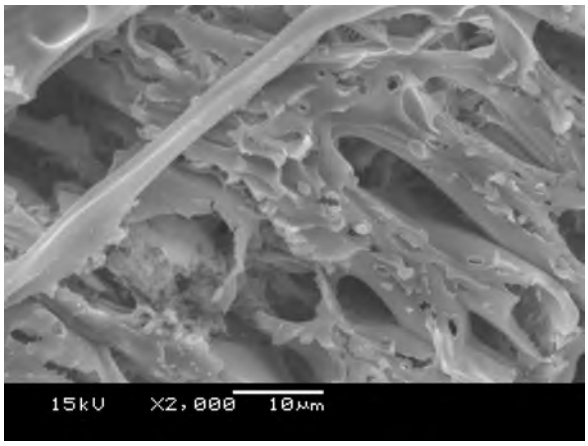

(f) Rice Husk Char

Figure A.1: SEM images of parboiled rice husks and rice husk char

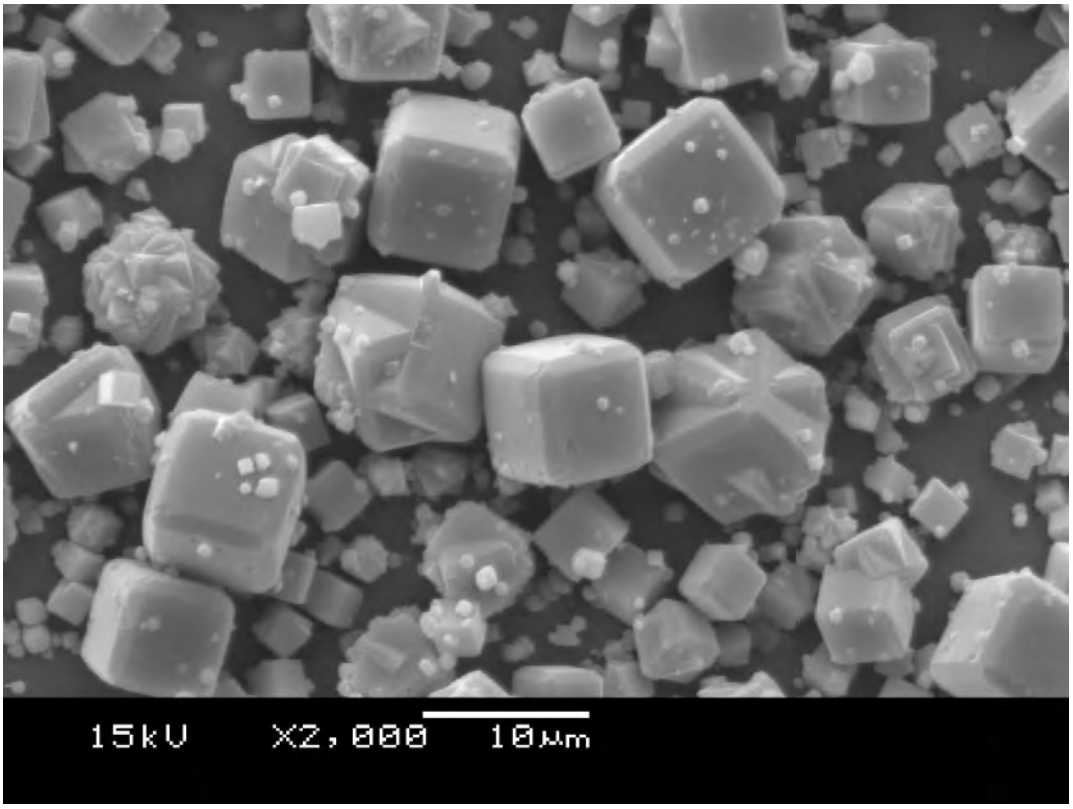

(a) 6 h

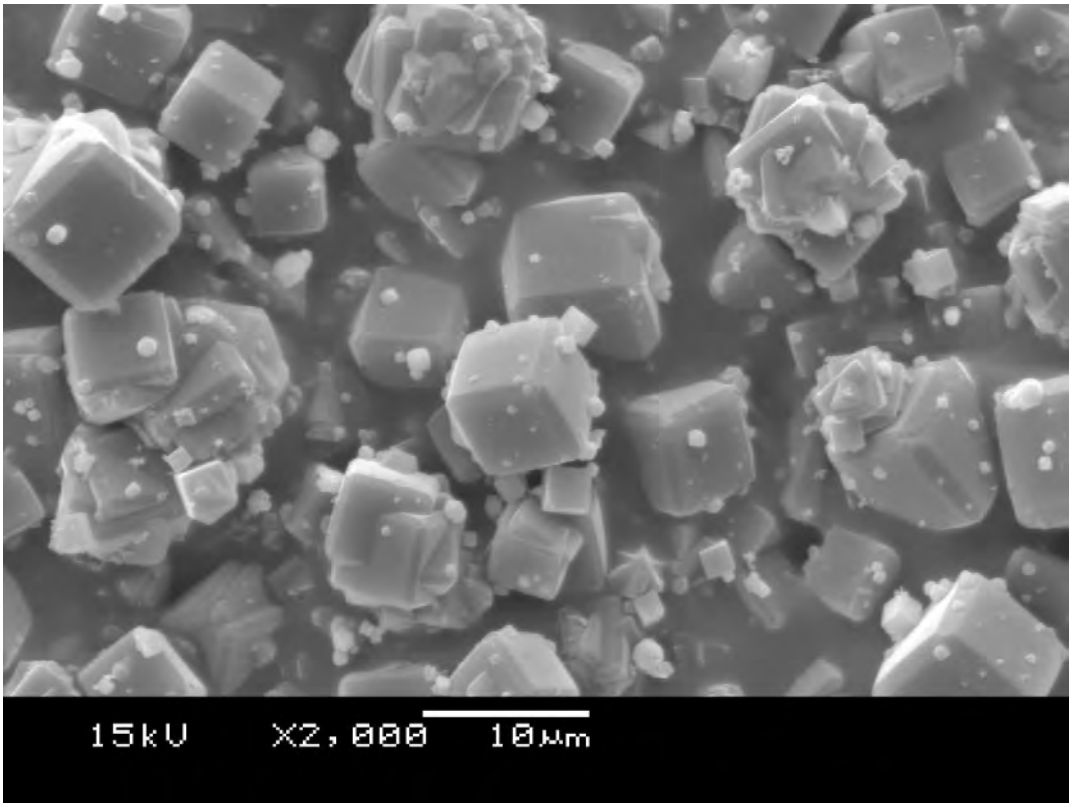

(b) 6.5 h

Figure A.2: SEM images of zeolites from ash leachate crystallised with 222 g of sodium aluminate/kg FA on a stirred hot plate at 90-95° C

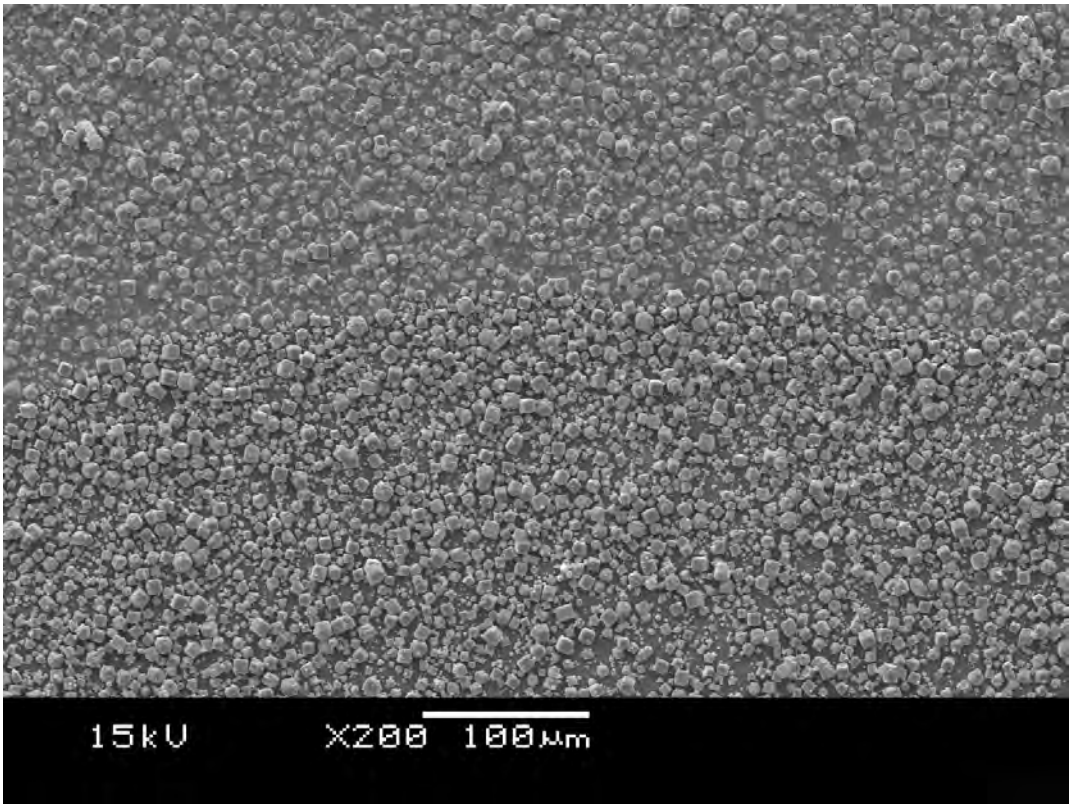

(a) 6 h

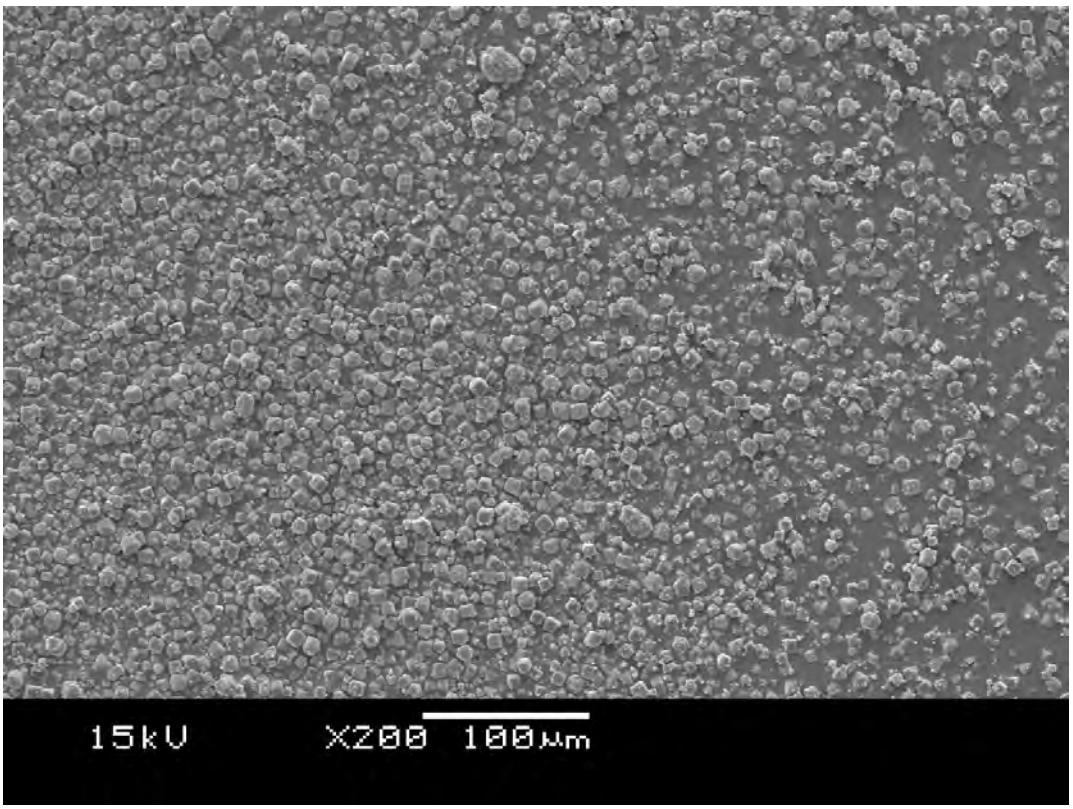

(b) 6.5 h

Figure A.3: SEM images of zeolites from ash leachate crystallised with 222 g of sodium aluminate/kg FA on a stirred hot plate at 90-95° C

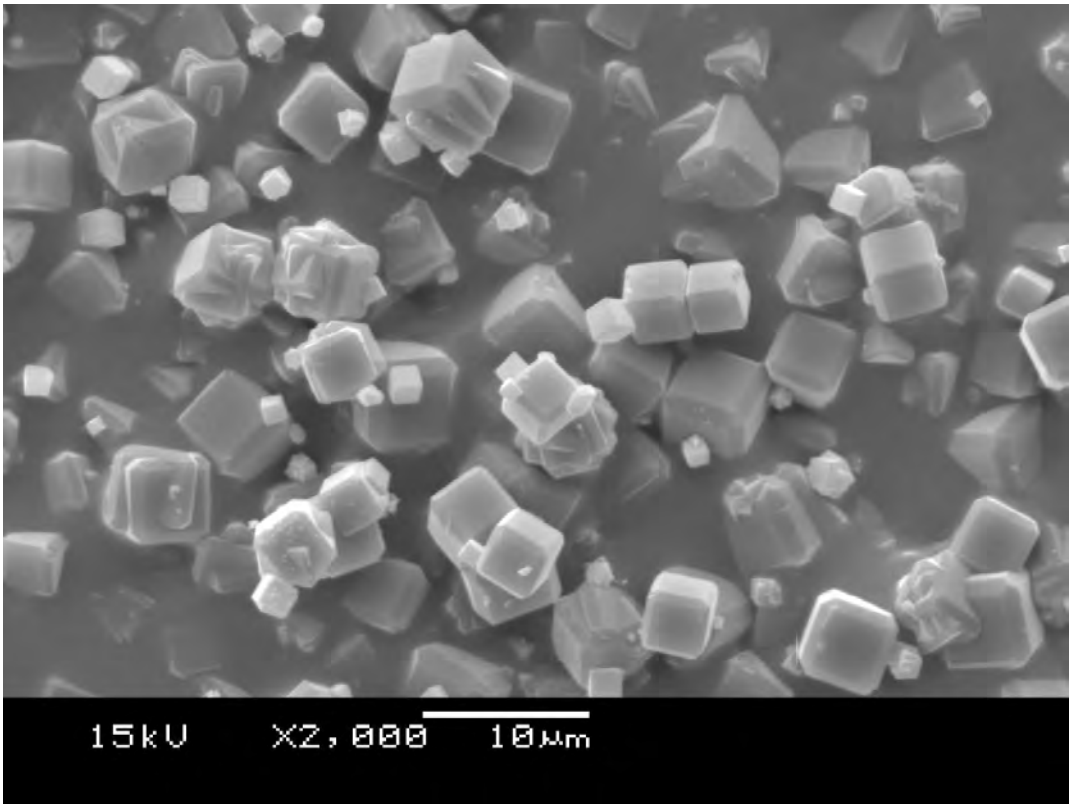

(a) 6 h

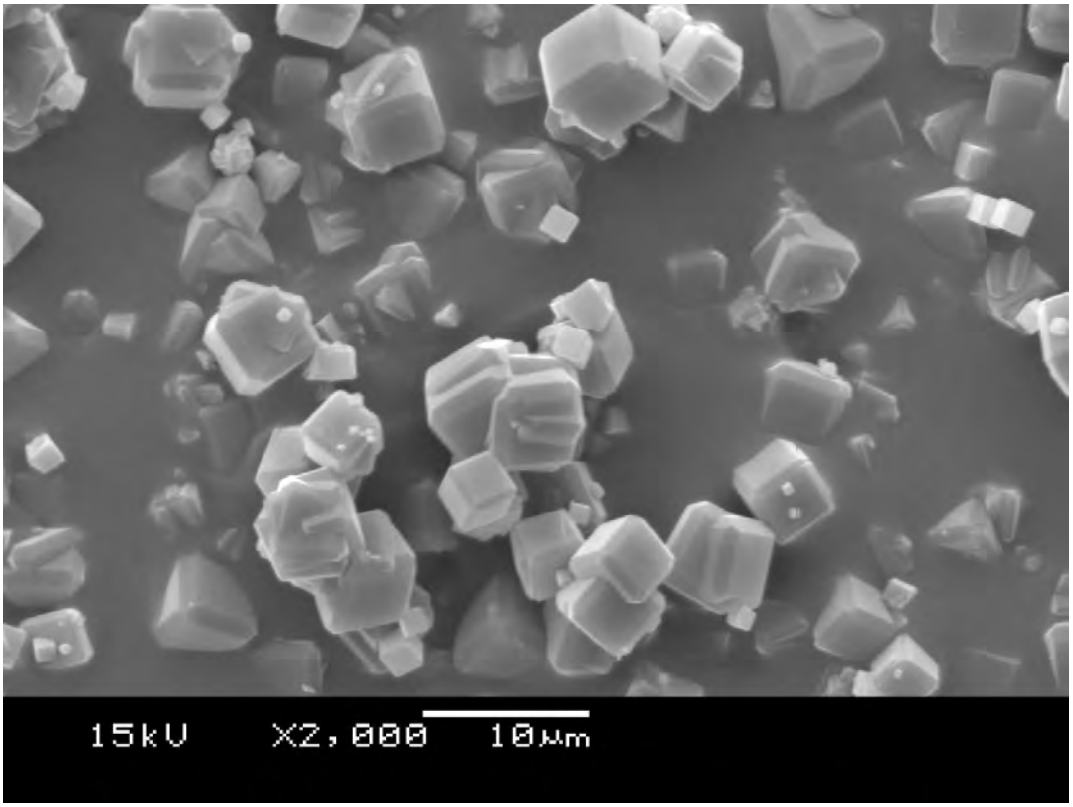

(b) 6.5 h

Figure A.4: SEM images of zeolites from ash leachate crystallised with 266 g of sodium aluminate/kg FA on a stirred hot plate at 90-95° C

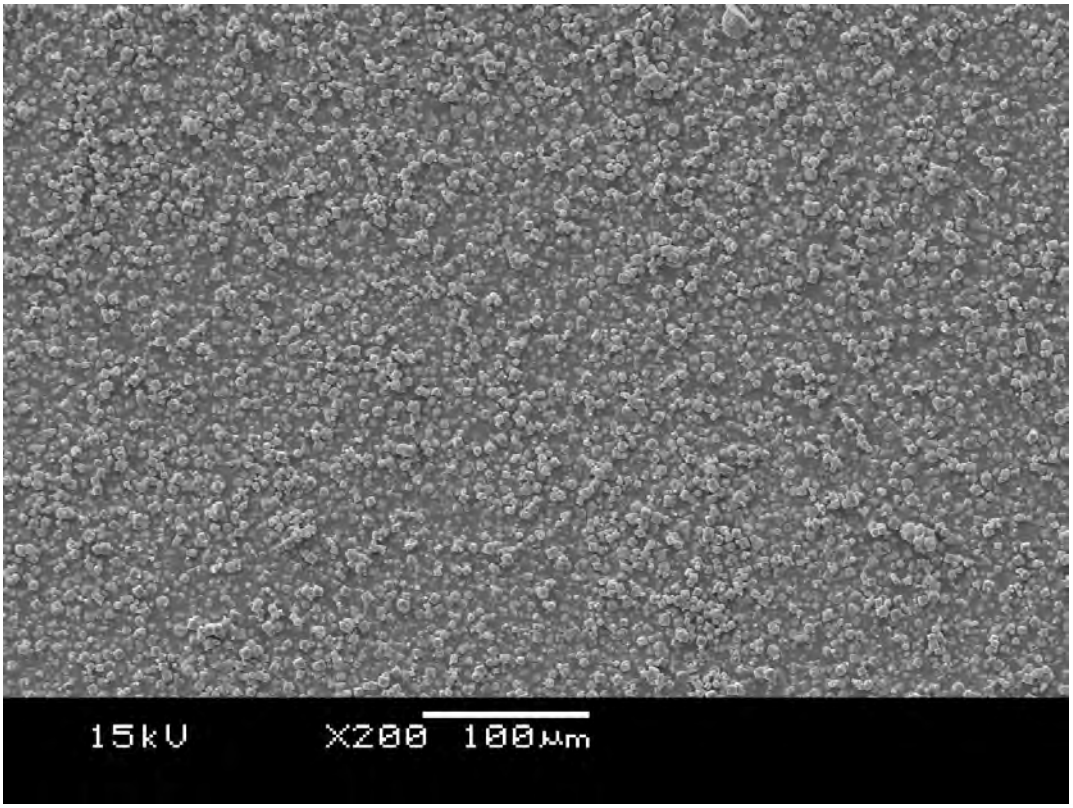

(a) 6 h

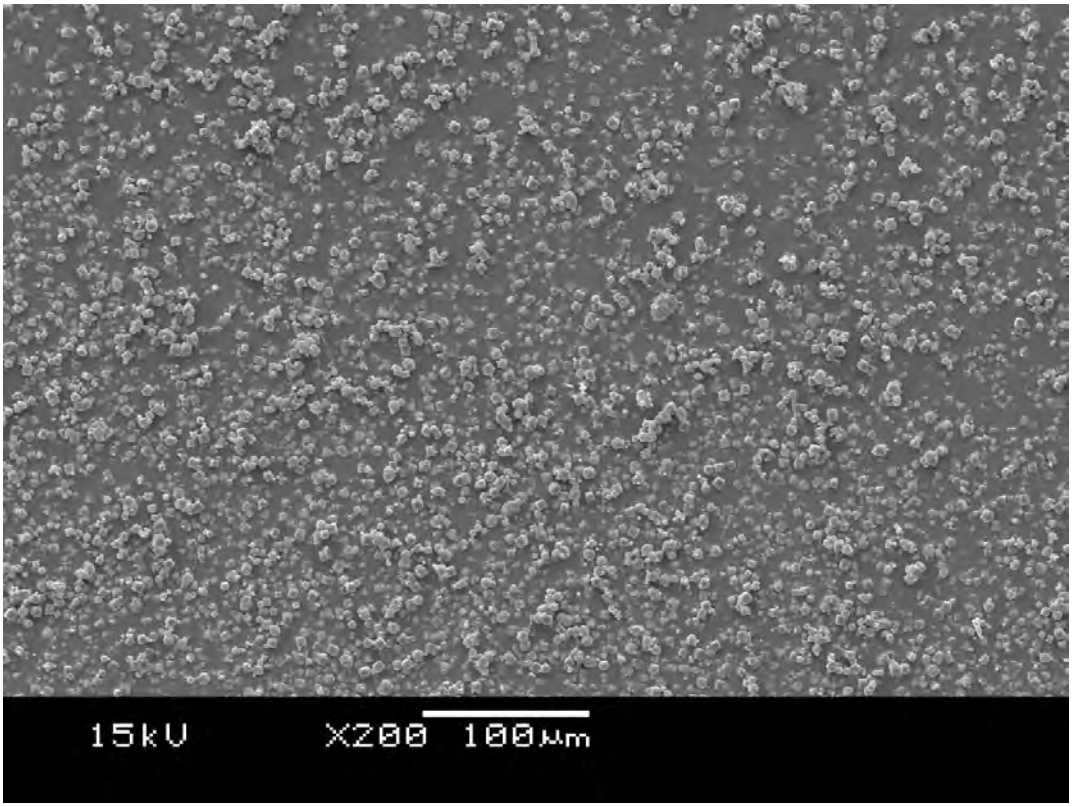

(b) 6.5 h

Figure A.5: SEM images of zeolites from ash leachate crystallised with 266 g of sodium aluminate/kg FA on a stirred hot plate at 90-95° C

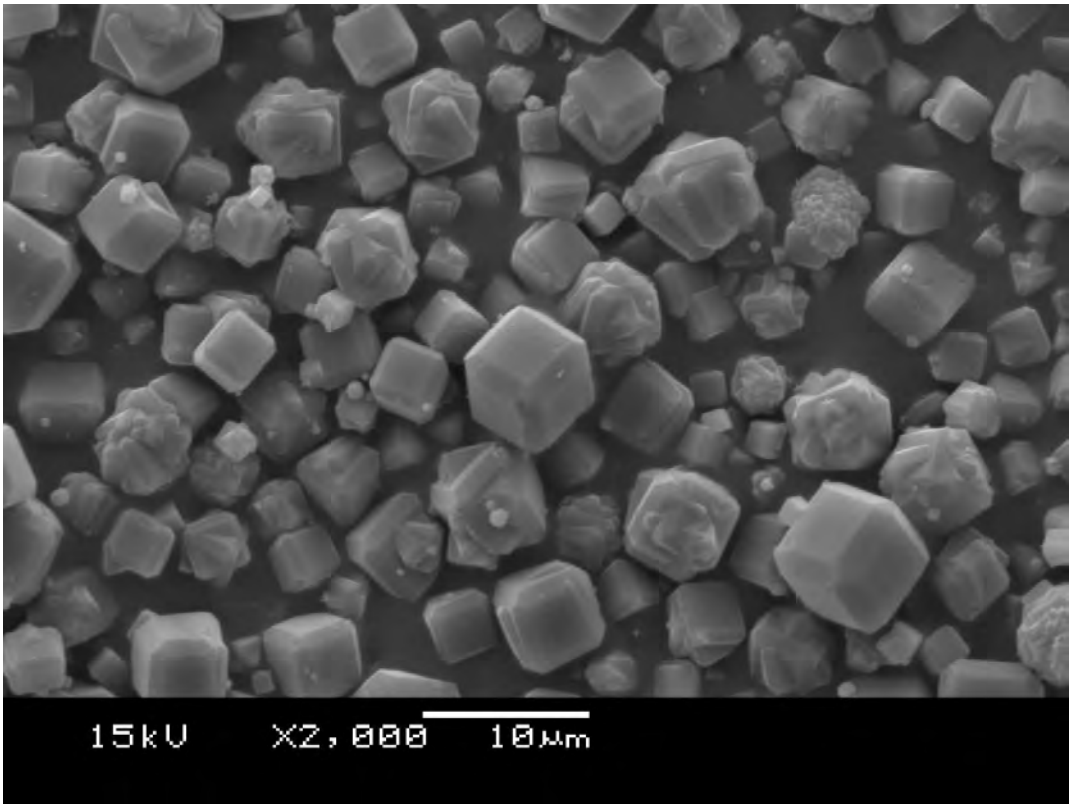

(a) 6 h

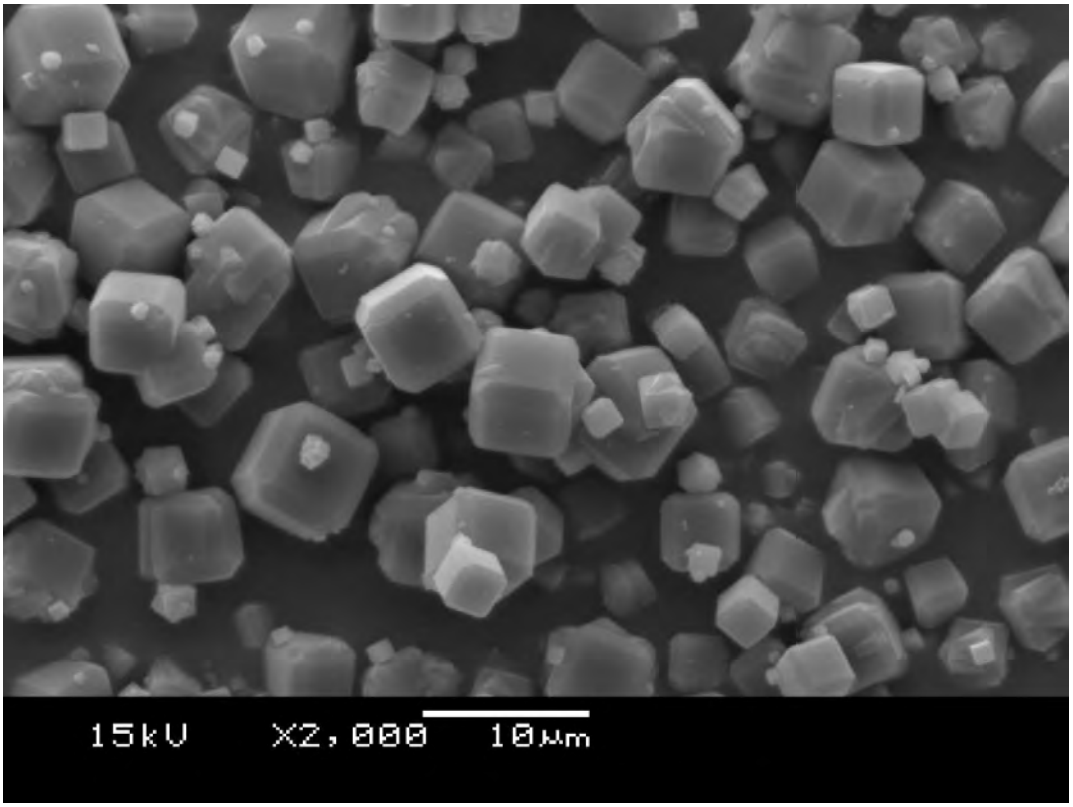

(b) 6.5 h

Figure A.6: SEM images of zeolites from ash leachate crystallised with 310 g of sodium aluminate/kg FA on a stirred hot plate at 90-95° C

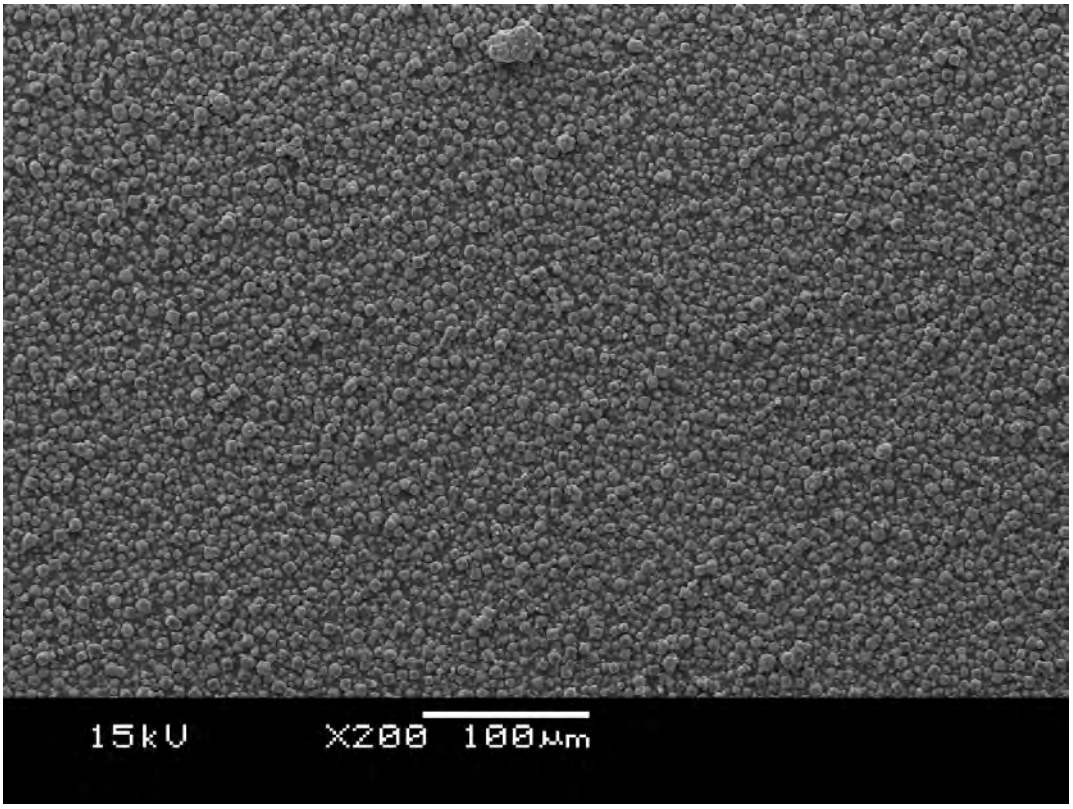

(a) 6 h

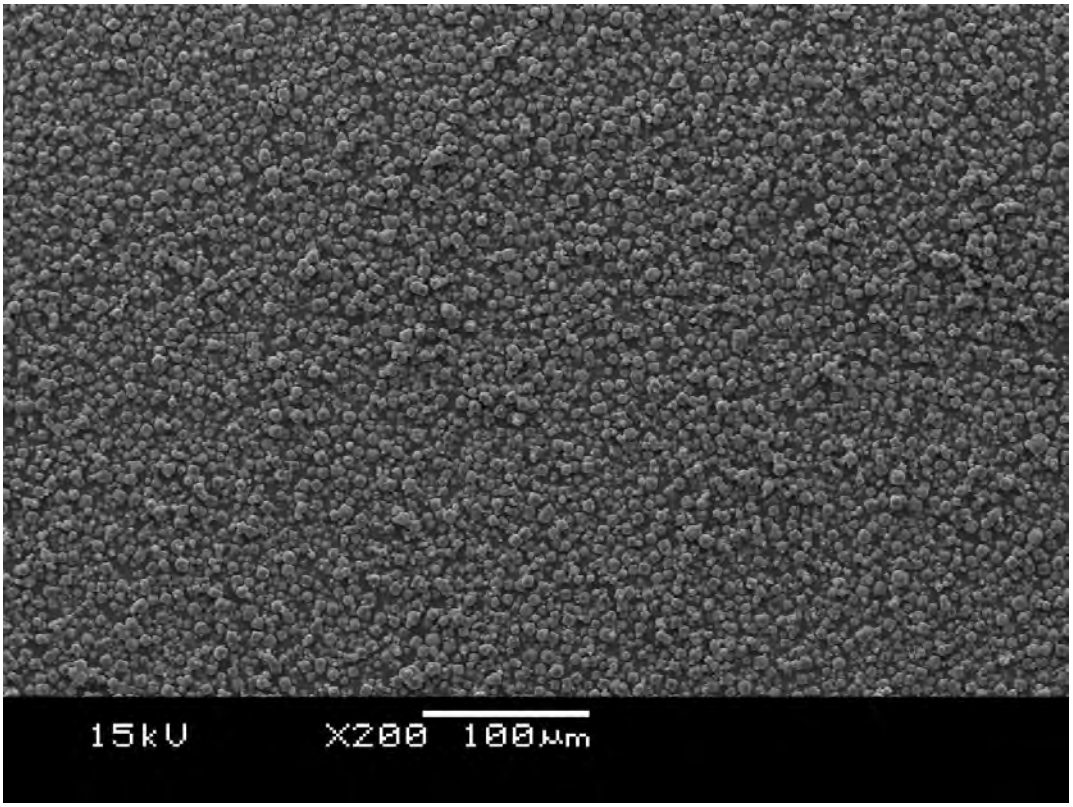

(b) 6.5 h

Figure A.7: SEM images of zeolites from ash leachate crystallised with 310 g of sodium aluminate/kg FA on a stirred hot plate at 90-95° C

Appendix B

XRD

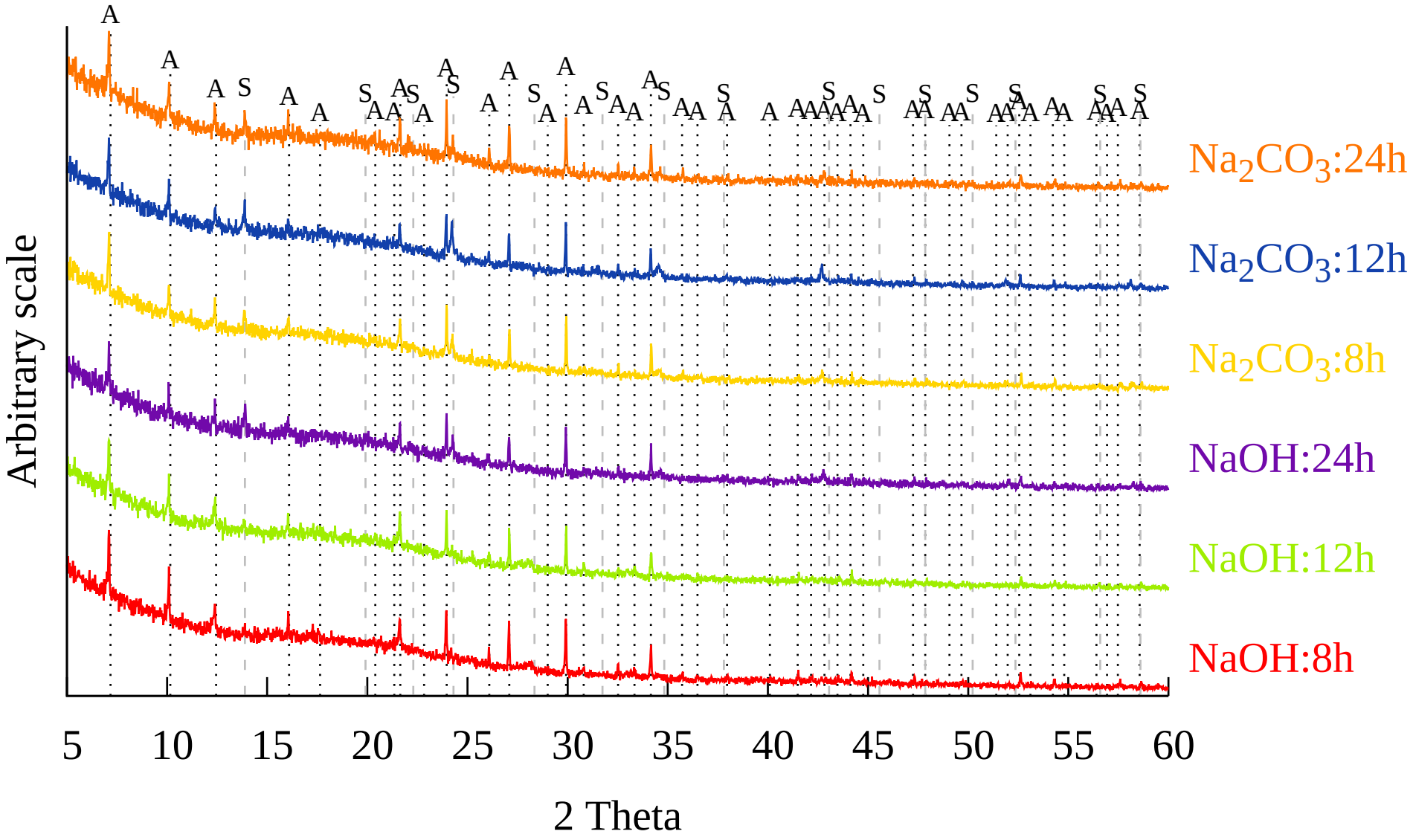

Figure B.1: XRD patterns of NaOH Vs Na_2CO_3 extraction with 160 g sodium aluminate/kg FA added during crystallisation. A: Zeolite Na-A, S: Sodalite. $\lambda = 1.5406$ Å

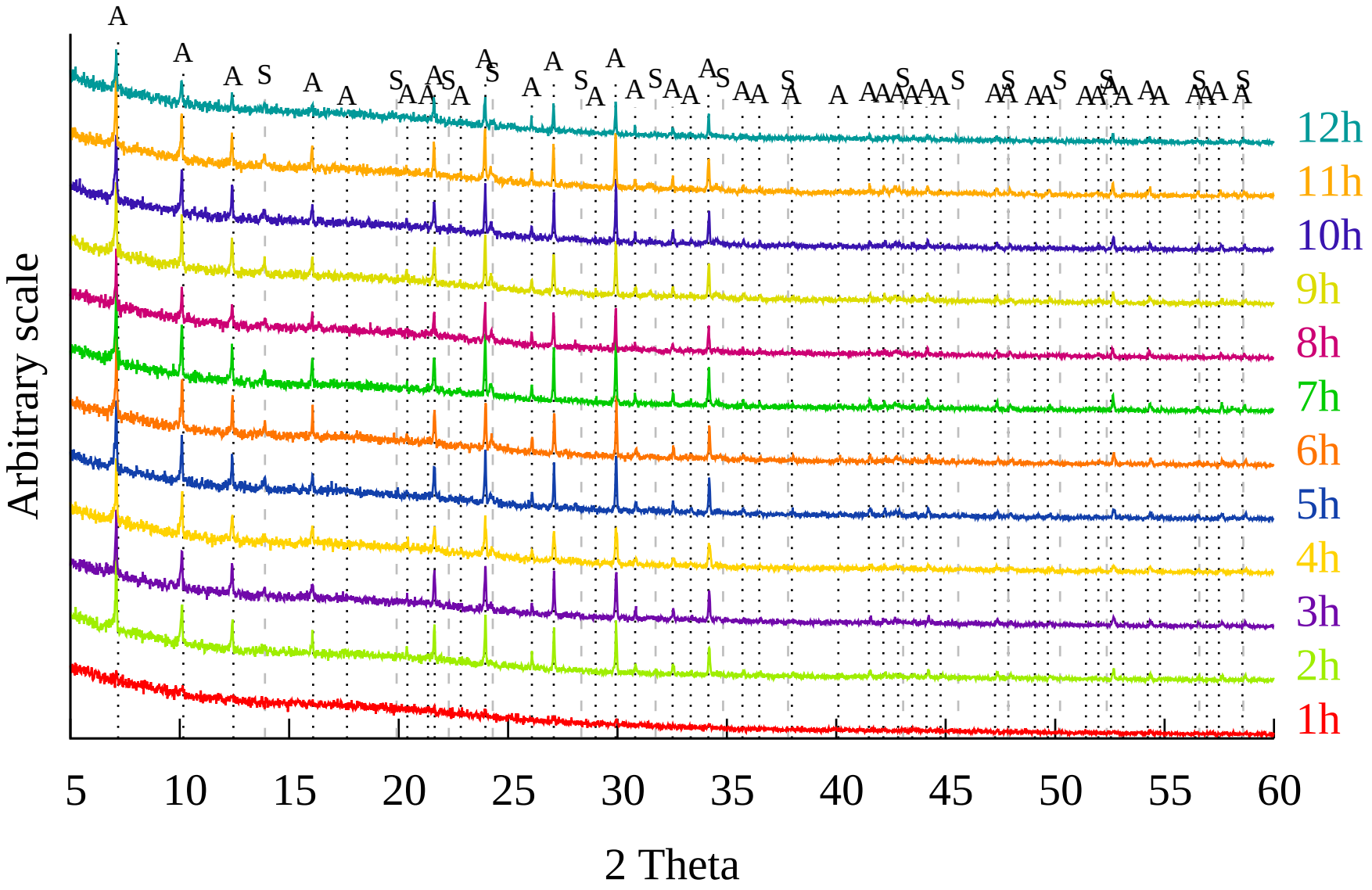

Figure B.2: XRD patterns of NaOH extraction with 200 g sodium aluminate/kg FA added during crystallisation. A: Zeolite Na-A, S: Sodalite. $\lambda = 1.5406$ Å

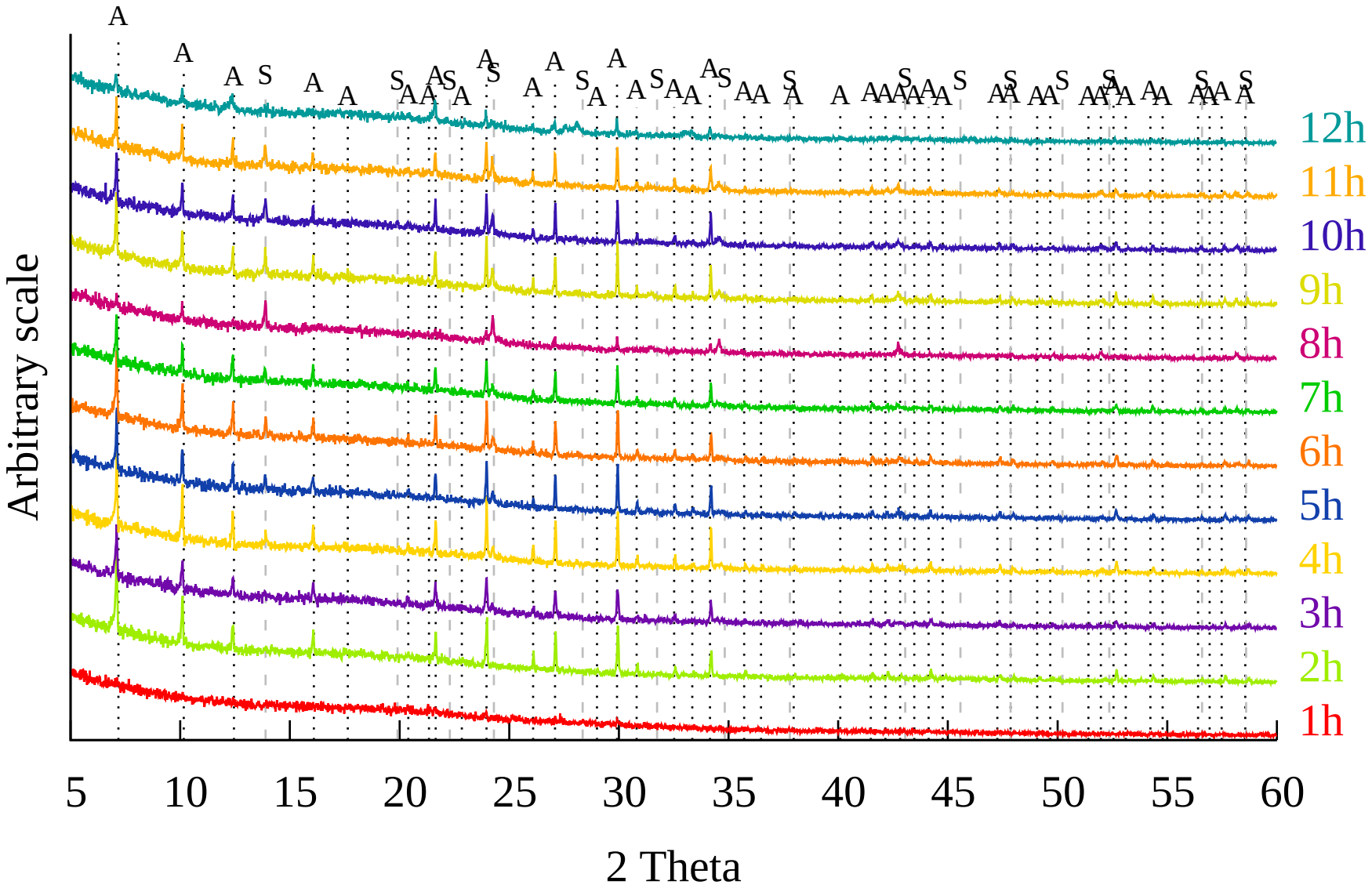

Figure B.3: XRD patterns of Na_2CO_3 extraction with 200 g sodium aluminate/kg FA added during crystallisation. A: Zeolite Na-A, S: Sodalite. $\lambda = 1.5406$ Å

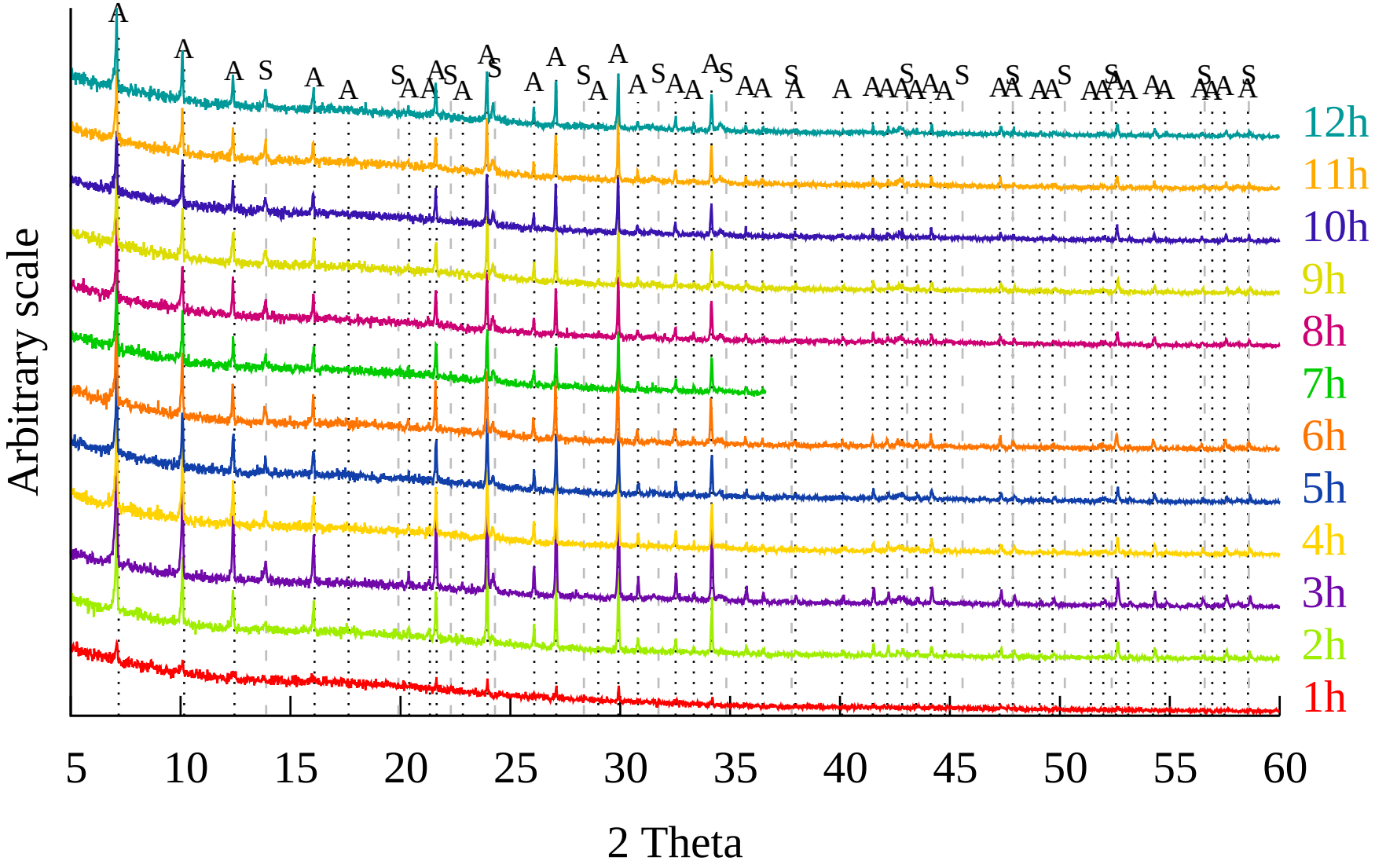

Figure B.4: XRD patterns of NaOH extraction with 240 g sodium aluminate/kg FA added during crystallisation. A: Zeolite Na-A, S: Sodalite. $\lambda = 1.5406$ Å

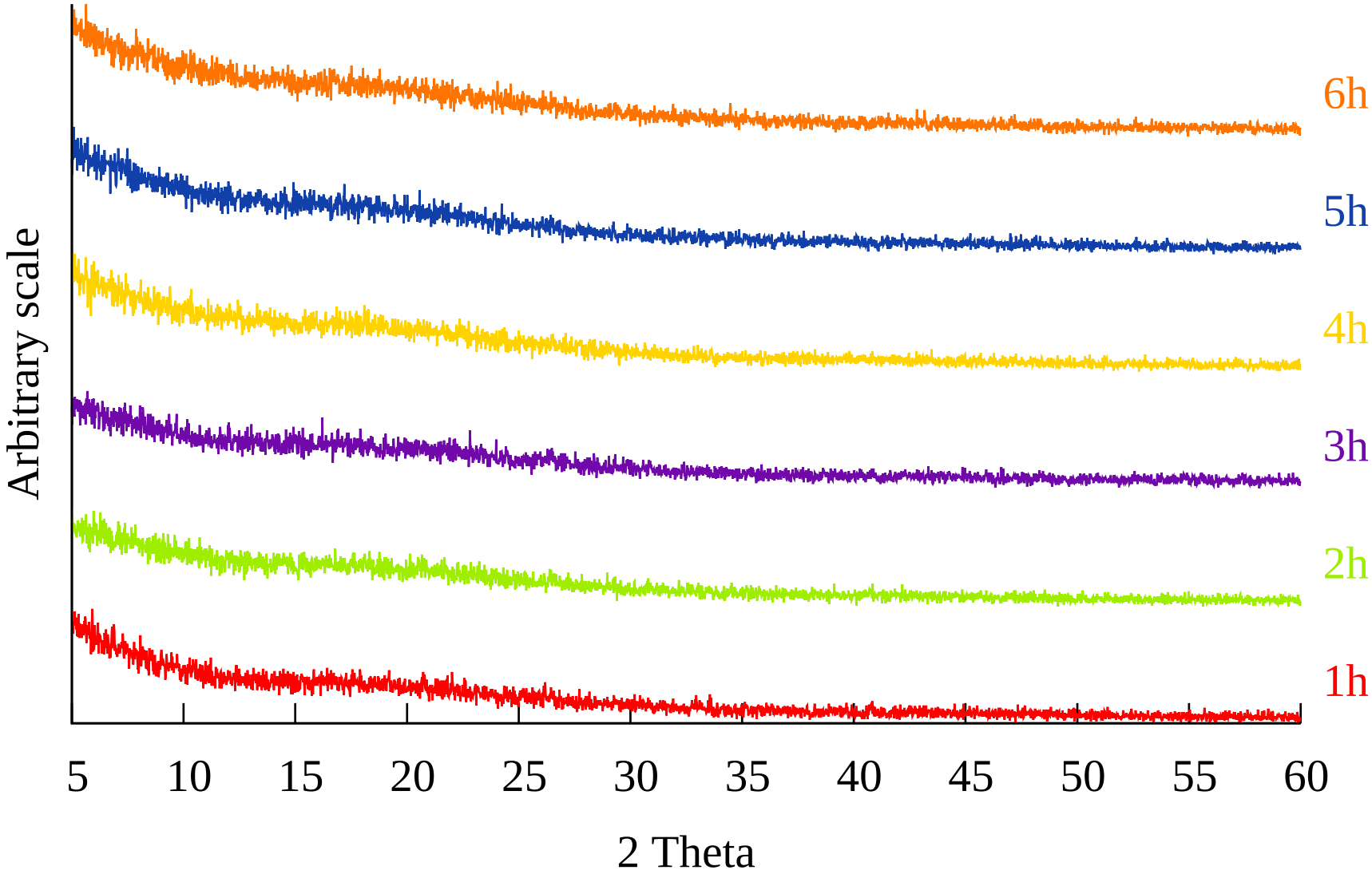

Figure B.5: XRD patterns of floating product: high loading of cenospheres during crystallisation. $\lambda = 1.5406$ Å

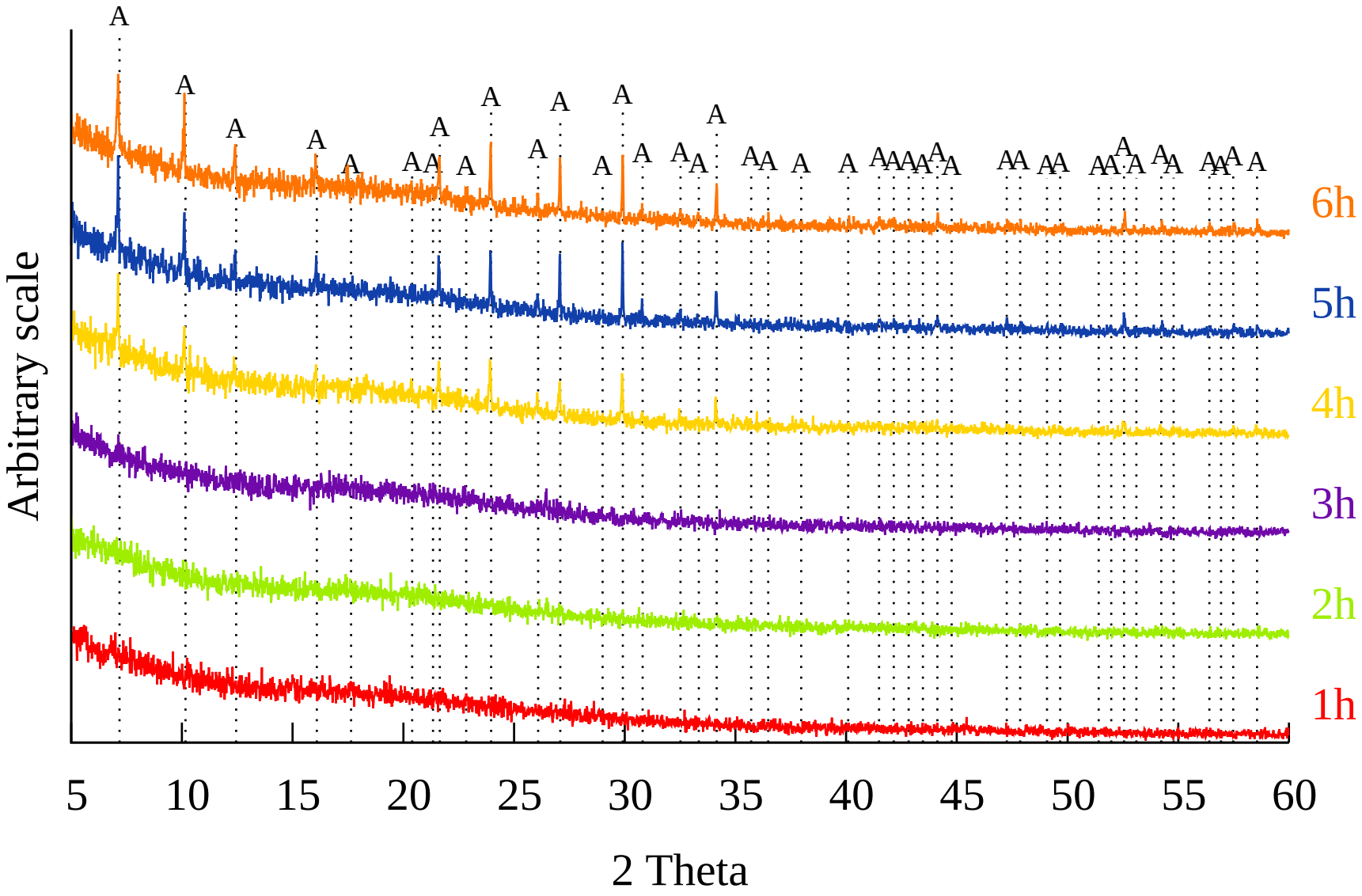

Figure B.6: XRD patterns of sinking product: high loading of cenospheres during crystallisation. A: Zeolite Na-A. $\lambda = 1.5406$ Å

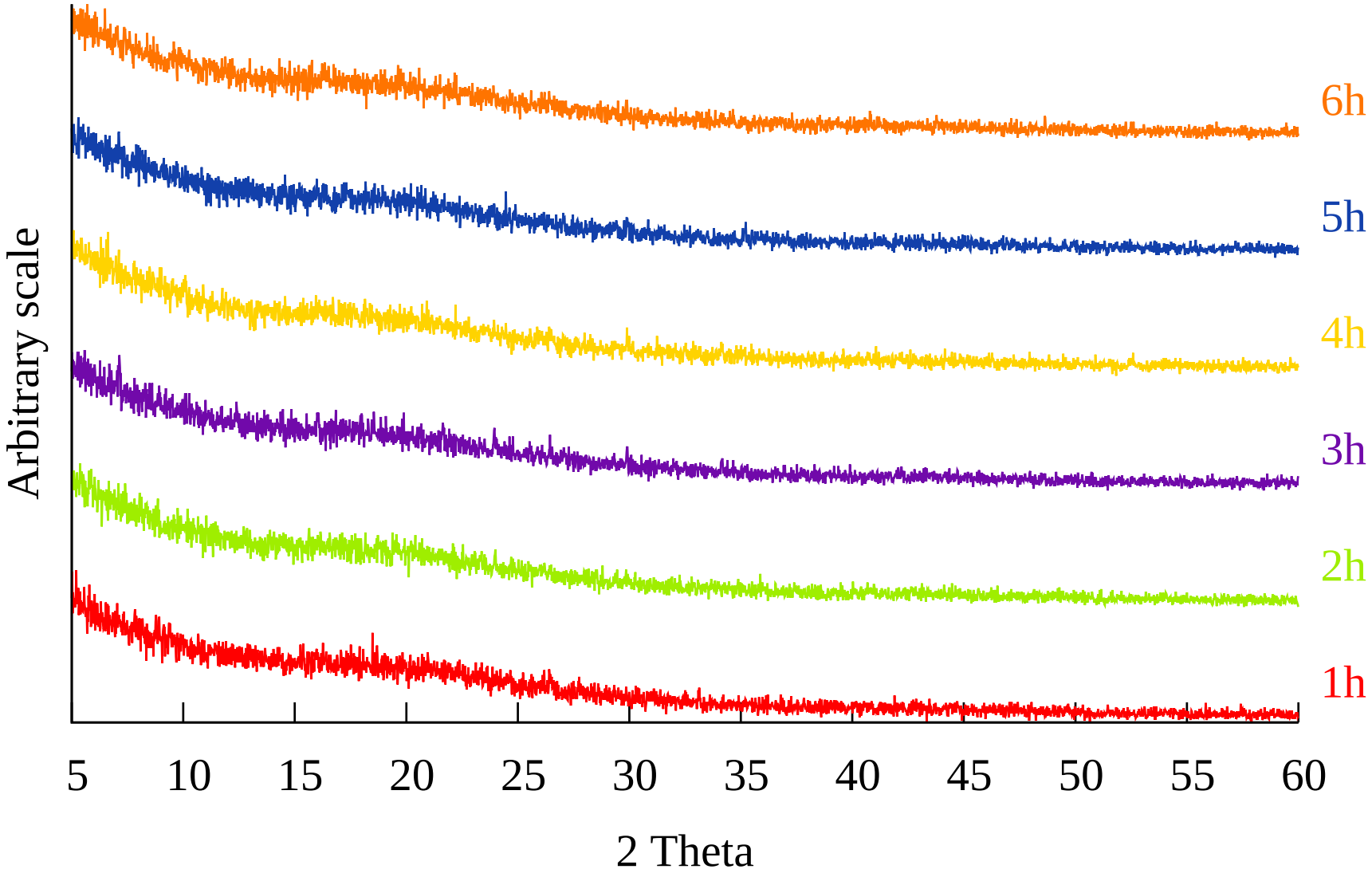

Figure B.7: XRD patterns of floating product: high loading of cenospheres during crystallisation. $\lambda = 1.5406$ Å

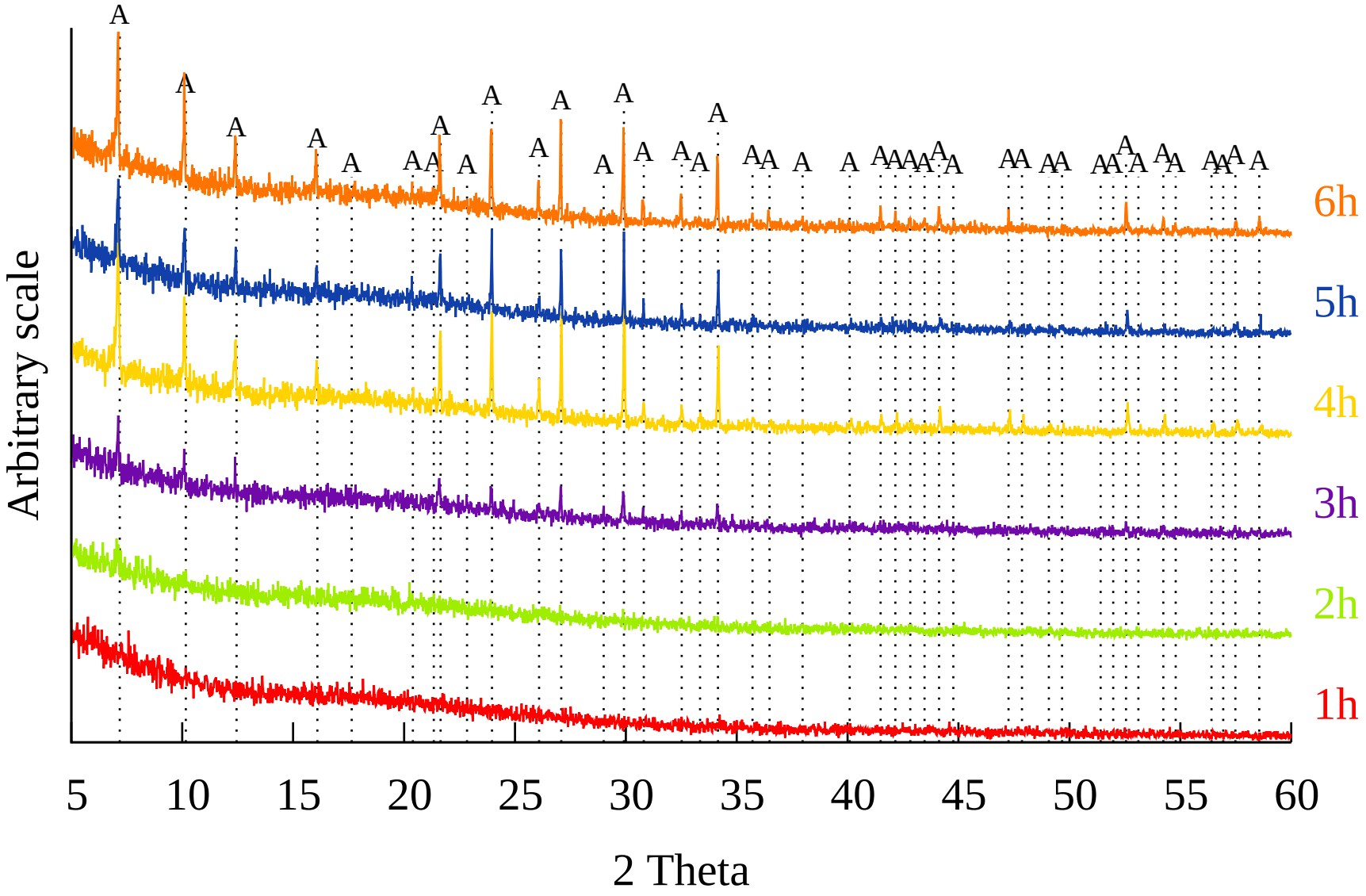

Figure B.8: XRD patterns of sinking product: high loading of cenospheres during crystallisation. A: Zeolite Na-A. $\lambda = 1.5406$ Å

Appendix C

Notes

C.1 XRD Presentation

Due to the large number of phases present in the XRD patterns of Figures 3.10, 4.23 and 4.24, the presentation style is inconsistent with other XRD Figures. Justifications regarding why presentation in one Figure would be impractical are provided below:

- The number of phases present requires each sample to be presented individually for clarity.
- The variation in intensity of different phases requires background to be taken into account for a clearer representation of the peaks.
- The software used did not provide a function to export background-subtracted peak data.
- Powder Diffraction File (PDF) patterns are presented with no background, thus do not properly match the XRD patterns.
- It was not possible to simultaneously account for background and add a Y-offset and present all graphs in the same Figure.
- Other Figures contain one phase, and the error introduced by not removing the background is small relative to the PDF peak height.

C.2 Rietveld Refinement

Rietveld refinement allows for quantitative phase analysis. Rietveld refinement requires all phases in the sample to be correctly identified, and requires good quality data [151, 152]. If an amorphous phase is present in a sample, its proportion must be identified in order to conduct quantitative analysis on the other phases present. This can be achieved by introducing a known quantity of a crystalline reference material and comparing the weight fractions of the added reference material to the identified phases in the sample [151]. CFA has a significant amorphous phase present. Quantification of this amorphous phase, as well as the other phases in the material are necessary for accurate quantitative analysis. Such analysis would require high quality XRD data, data of a higher quality than that which has been produced for this work. Similarly, quantitative analysis of the zeolite products produced would also require higher quality data than that which has been produced for this work. It was therefore decided that Reitveld refinement is not relevant to this work.

Appendix D

Supplementary Material

Sommerville [96] was referenced in this thesis, and is not available online. It is therefore provided here.

RESEARCH PROJECT: RECYCLING COAL FLY ASH IN THE MANUFACTURE OF USEFUL MATERIALS

Robert Sommerville

714332 - rxs632@bham.ac.uk
Module: 04 20546

Abstract

Fly ash is produced from the combustion of pulverised coal, and is a resource with large stockpiles and steady supply. The storage and disposal of fly ash is costly, polluting, unattractive and utilises land which could be used for other purposes. Recycling fly ash presents an environmentally friendly solution to the disposal of fly ash, whilst preserving virgin resources. This paper investigates the chararcterisation of fly ash, and the beneficiation processes implemented by RockTron^{TM}, as well as conversion of fly ash into zeolites for the purposes of metal ion adsorption from acid minewater. Research found that zeolites derived from fly ash were effective at reducing the metal ion content of acid minewater, providing a potential source of diversification and revenue for RockTron^{TM}. Future research and potential variations on the RockTron^{TM}process are also discussed.

1. Introduction

1.1. Origins & Production

Fly ash, scrubbed from flue gasses with electrostatic precipitators forms 60-88% of the residue from the combustion of pulverised coal in thermoelectric power plants. Worldwide production of was estimated in 2009 to be around 500 million tonnes per year [1, 2, 3, 4]. Fly ash (FA) is defined by European standard EN450 as a "fine-grained powder, which is mainly composed of spherical glassy particles, produced during the combustion of pulverised coal" [5].

1.2. Composition

Table 1: Ranges of Composition for fly ashes [4]

Component	Subcomponent	Weight %
Inorganic		90-99 %
Inorganic	Amorphous	34-80 %
Inorganic	Crystalline	17-63 %
Organic		1-9 %
Fluid		<0.5 %

1.2.1. Material Overview

FA is an abrasive refractory powder with a wide PSD made up of mostly spherical particles. FA is polycomponent, heterogeneous and predominantly amorphous but composition varies widely depending on coal rank and plant type [1, 4]. FA surfaces are hydrophilic, and FA is highly porous [3]. Colour varies depending on unburned carbon content. FA is mostly inorganic matter, with some organic matter (predominantly carbon) and a very small fluid component (liquids & gasses) [1, 4]. Primary components are Silica (SiO_2), Alumina (Al_2O_3) and iron oxides (Fe_2O_3) [3, 5]. The most common elements (>1%) are Oxygen, Silicon, Aluminium, Calcium, Iron, Carbon, Potassium, Manganese & Sulphur. The material in fly as can be classified as primary (unaffected by the combustion process), secondary (formed during combustion) and tertiary (formed during transportation and storage) [1, 3, 4, 6]. The smaller size fractions are often enriched in trace elements, such as rare earth elements [7].

1.2.2. Cenospheres

FA includes Cenospheres, unburned carbon, and magnetic components. Cenospheres (formed during the combustion process) are hollow ceramic microspheres frequently larger than the rest of the ash, however con-

tent varies with coal type and combustion process [8, 9]. The smallest hollow spheres are noted to be around 4μm and cenospheres have been defined in literature as having a density of <2.2g cm^{-3} or <1g cm^{-3} [5, 6].

1.2.3. Unburnt Carbon

Unburned carbon makes up 1-25% of the ash, and also contains Oxygen, Nitrogen, Sulphur and Hydrogen. Carbon Concentrates (CC) retrieved from FA have a 21-80% ash yield, a calorific value of 5000-6000 kcal kg^{-1}, a specific surface area of 10-134 m^{2}g^{-1}, and a density of 0.26-0.28 g cm^{-3}. PSD tests show that 100-200 μm fractions contain the majority of the carbon. Carbon is predominantly black in colour, and darkens ash in higher concentrations [1, 10]. The Clean Air Act 1990 in the US limited NO_x emissions to 68g NO_x/million BTU. Cooler burn temperatures result in lower NO_x emissions, but lower combustion efficiency. Many boilers have been retrofitted with low-NO_x burners or otherwise adjusted to lower emissions, resulting in more unburnt carbon in the FA [11].

1.2.4. Magnetic Component

The magnetic components (ferromagnetic, ferrimagnetic, paramagnetic) comprise 0.5-5% of the ash. A concentrate (predominantly Fe enriched aluminosilicate) can be formed with 20-61% Iron by weight. Most of the magnetic content (79%) has a particle size <100μm, and the Loss On Ignition (LOI) for magnetic concentrate is low (1.8%), in comparison to FA (4.9%), suggesting good separation between CC and magnetic components [4, 10].

1.3. Uses

The re-utilisation of FA reduces disposal costs, decreases land usage, and can provide a source of revenue. Increasingly strict regulations make the storage of FA more expensive due to metal leaching. FA currently finds uses in landfill, land reclamation, minefill, cement binder, aggregate, brick manufacture, bitumin filler, road beds & pavement runways, ceramics, adsorbent for organic compounds and gas streams, an ore source for acid leaching, soil pH and clay amendment, chemical fertiliser and as a settling aid and COD reducer.[1, 3, 5, 12]

Currently, the construction industry is the main consumer of FA in agglomerate and bulk applications [1, 5]. It is used as a filler and cement replacement product due to its pozzolanic properties (dependent on calcium content) where silica and CaOH react to form calcium silicate hydrate [1, 3, 11]. Only 10-20% of US FA is reused, mostly in cement or roadbase manufacture [3]. Many regulatory bodies set limits on the carbon content of FA for cementitious applications. Carbon content is frequently measured by LOI. Due to the low-NO_x burners increasing carbon content fewer fly ashes are meeting the US regulation requirement of < 6% LOI to be acceptable for use in cement. This increases costs as ash must be pre-treated or will not be used, further decreasing consumption of FA [11]. Alternative applications include aggregate and structural filler due to appropriate bulk density, permeability, internal angular friction and consolidation properties [1, 2].

1.3.1. RockTron^{TM}

The Beneficiation processes used in this paper follow the separation processes used by RockTron^{TM}to produce their products, as shown in figure 1. The RockTron^{TM}process takes in FA from a power plant or storage, removes cenospheres, CC, and magnetic content before size-classifying the remnants to produce five major products: Cenospheres (CenTron^{TM}), Magnetite (MagTron^{TM}), Coke (volatile-free carbon), Delta Cement Constituent (coarser final product), and Alpha Cement Constituent (finer final product) [13].

After separation and treatment, the main current uses of the CC are in fuel, filler, adsorbents, pigments and catalysts. CC is of use as an adsorbent due to its high relative surface area, porosity, and amorphous nature. CC can be treated to form activated carbon. The magnetic fraction is predominantly used in metallurgy, high density concrete production, and electromagnetic insulators. Cenospheres find a variety of uses due to their low density [8, 9, 10, 12]. The remaining ash is better suited in the production of cement and concrete due to lower carbon content.

1.4. Zeolitisation

A zeolite is defined in *Introduction to Zeolite Science and Practice* as "A crystalline aluminosilicate with a three-dimensional framework structure that forms uniformly sized pores of molecular dimensions" [14]. The structure comprises group I or II element counter-ions with Oxygen-linked $[SiO_4]^{-4}$ and $[AlO_4]^{-5}$ tetrahedra whose inter-tetrahedral voids allow access for cation exchange due to $Si4^+ \Rightarrow Al3^+$ substitutions which produce a net negative charge, as shown in figure 2a [3, 5, 14]. Zeolite can be attained from the hydrothermal alkali treatment of FA (which has a naturally high Si/ Al ratio), to produce zeolites with a low Si content, large

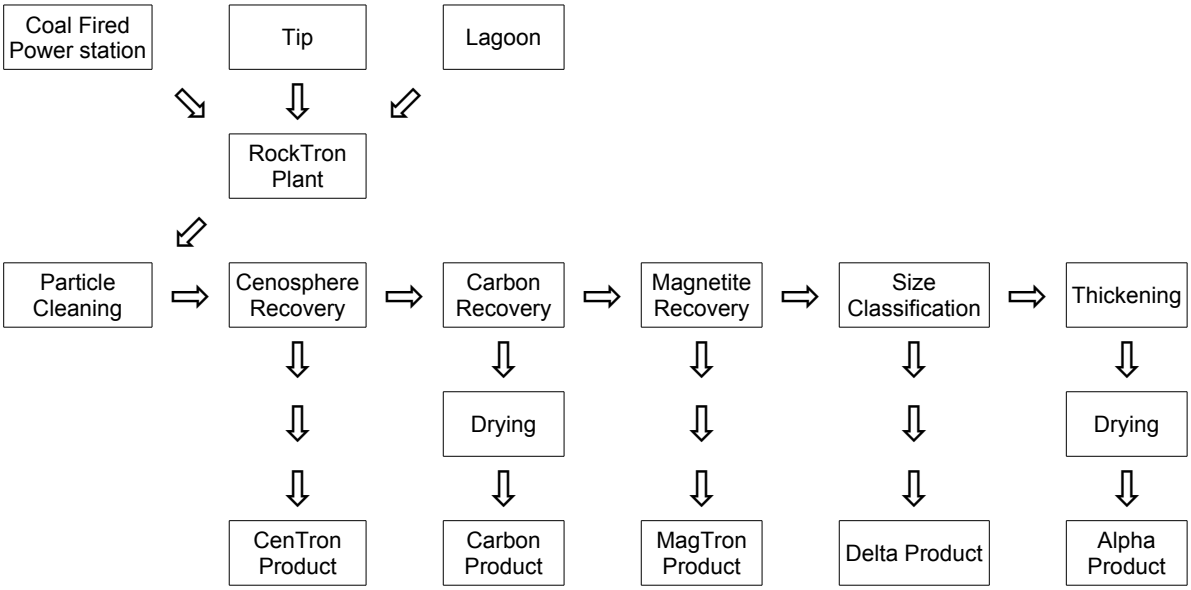

Figure 1: A Summary of The RockTron^{TM}Process [13]

pore volume and high capacity for cation exchange, which makes them highly suited to water decontamination [3, 5, 14, 15, 16, 17]. Zeolite type can be changed by varying alkali concentration, alkali to ash ratio, reaction temperature and duration [5, 16, 17].

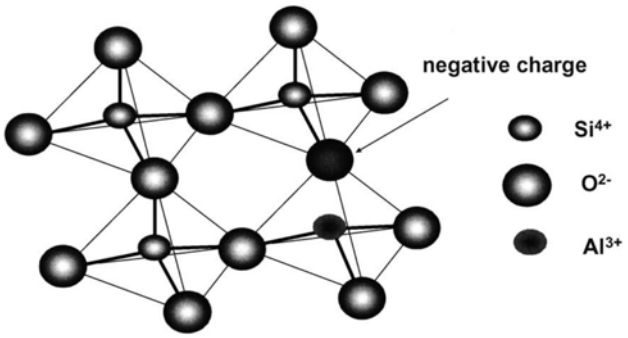

(a)

Figure 2: Theoretical zeolite structure, showing tetrahedral units and negative charged induced by Silicon/ Aluminium substitution [5]

2. Physical Characterisation

2.1. Water & Carbon Content (LOI)

The moisture content of the ash was measured by placing ash in a dehumidifying oven for 1 hour at 100°C until dry. Unless otherwise stated, all weights in this paper were taken using a balance accurate to 4 decimal places. LOI was measured by placing dry ash in a furnace at 900°C for 1 hour and taking weights before and after.

2.2. Size Distribution

Particle size distribution (PSD) tests were conducted in accordance with BS 17961. Dry ash was placed in the top tray of a set of sieves of decreasing mesh size from 2000 μm to 106 μm, and were agitated in a mechanical shaker. Particles larger than 106 μm were agitated for 60 minutes to break up large agglomerates. Particles smaller than 355 μm were sieved for 30 minutes. Weights were recorded for the starting material and the material left in each tray.

2.3. Cenosphere Size Distribution

PSD tests conforming to BS 17961 were conducted on dry cenospheres, placed in the top tray of a set of sieves ranging from 500 μm to 45 μm. The trays were agitated in a mechanical shaker for 30 minutes and the weights were taken for the starting material, and the contents of each tray.

2.4. Scanning Electron Microscopy (SEM)

Images were taken using a Philips XL30 SEM using secondary electron detection at various magnifications.

2.5. ICP-OES

Dried samples of Alpha, Delta, FB7 and Lagoon ash were digested using a lithium carbonate fusion method, and then analysed using Inductivly Coupled Plasma Optical Emission Spectroscopy (ICP-OES).

3. Beneficiation Processes

3.1. Cenosphere Flotation

Cenospheres were removed from dry FA through flotation separation. Dry ash was passed through a 1000 μm sieve to break up agglomerates and remove large particles which may block the separator nozzle. The sieved ash was put into a 2 litre separating funnel (separator) via a funnel, and the funnel was washed through with water to fill the separator. The separator was manually agitated for 30 seconds, returned to a vertical position and allowed to settle for 15 minutes. The separator was drained onto filter paper of a known weight. In the case of blockage, a water bottle with nozzle was used to spray a jet of water upwards into the separator to dislodge the blockage. The filter cake and paper were washed into an enamelled metal tray, the particles removed during the sieving process were added and the tray was placed into a dryer until dry. The remainder of the water in the separator was drained into another tray and placed in the dryer until dry. The dry weights were measured.

3.2. Froth Flotation

Froth floatation was carried out on dry ash without cenospheres using the apparatus shown in figure 3a. 130g of ash was placed in the vessel (4), followed by 2.6 litres of water. The mixer was run for 5 minutes at 1500 rpm with the air valve (2) closed. A measured amount of diesel oil and 0.2 ml of teefroth frothing agents were added, and mixing continued for another 2 minutes. The air valve was opened and froth was scraped off in 3 batches: < 1 minute, 1-3 minutes, and 3-8 minutes. The Froth batches were filtered, dried, weighed, and LOI tests were conducted.

3.3. Magnetic Separation

Dry ash which has undergone cenosphere removal and froth flotation is subjected to several different methods of magnetic separation.

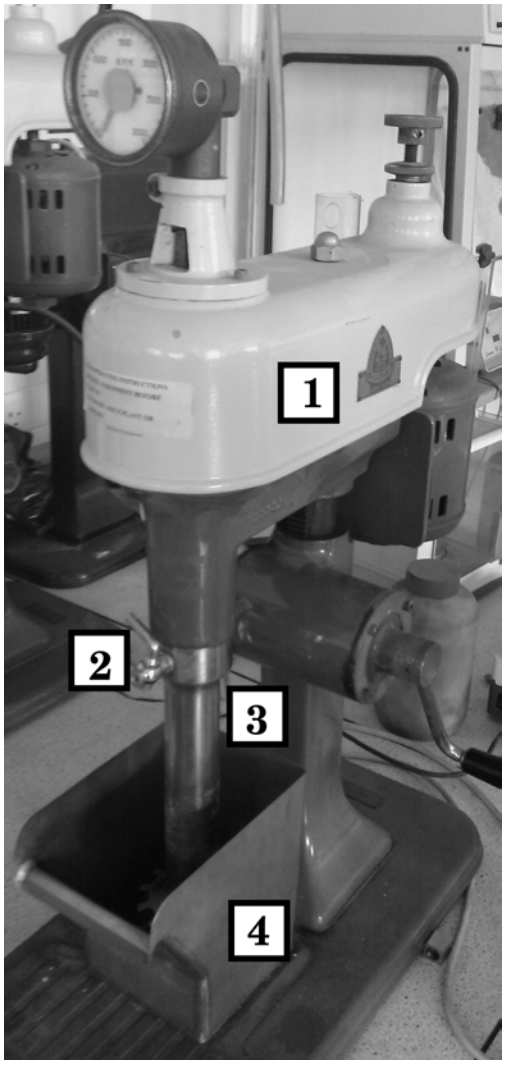

(a)

Figure 3: Froth flotation apparatus. 1: Apparatus body. 2: Air inlet. 3: Downpipe leading to froth head. 4: Vessel, with froth head inside.

3.3.1. Boxmag Rapid High Intensity Wet Magnetic Separation

Magnetic separation was carried out using a Boxmag Rapid type BHW high intensity wet magnetic separator (shown in figure 4a)on dry ash. A wedge wire matrix (6) was used, and in later experiments a coarse expanded metal matrix was used (7 & 8). The matrix was washed and inserted into the assembley (5), and a non-magnetic container (3) was placed underneath to catch the ash. The separator was turned on (1) and adjusted to a current of 0.25A (0.1 Tesla). A solution of a known weight of dry ash was passed through the separator's matrix, followed by excess water to dislodge entrained particles. The run-off was set aside for later use, and the container replaced. The magnetic matrix was dismantled and washed into the container, placed in the dryer, and the matrix reassembled. The process was repeated with the previous run-off at 3.25A (0.7 Tesla). The run-off was filtered through filter paper of a known weight and dried.

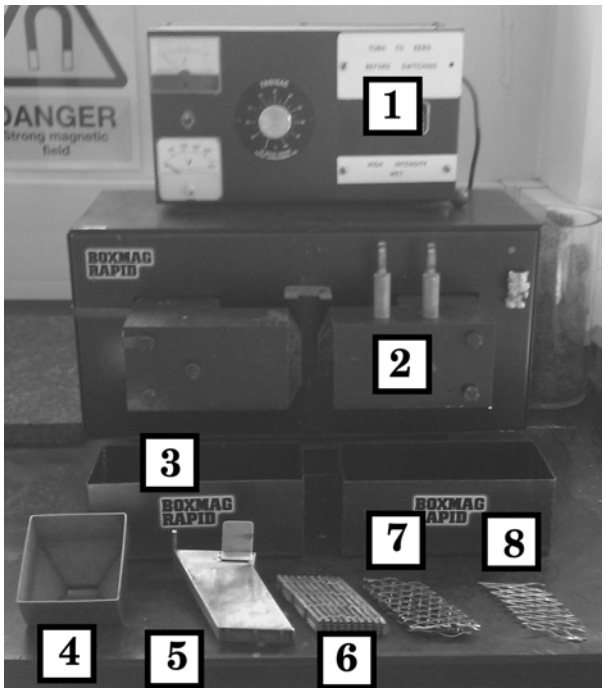

(a)

Figure 4: Boxmag Rapid BHW High Intensity Wet Magnetic Separator. 1: Control unit. 2: Magnetic apparatus. 3: Non-magnetic receptacles. 4: Funnel. 5: Matrix assembley. 6: Wedge Wire Matrix. 7: Stack of course expanded metal matrices. 8: Individual expanded metal matrix.

3.3.2. Barium Ferrite Magnetic Separation

Dry ash was spread onto a clean sheet of A3 paper. A barium ferrite magnet in a plastic beaker was passed through the ash repeatedly, depositing collected matter in a new pile. Once the yield of magnetic ash collected from the first pile dropped significantly, this process was repeated on the second pile, making a third. This process was repeated to produce at least 5 piles. The 5th pile was then transferred using the magnet to a plastic beaker for weighing.

3.3.3. Boxmatic Rapid Magnachute Separation

A known mass of dry ash was placed at the top of a Boxmatic Magnachute separator. A tray was placed at the bottom to receive the non-magnetic ash, and the slope was raised to increase the gradient of the slope till the ash moved down the slope. The slope was then tapped, raised away from the magnet below and disturbed to separate the non-magnetic ash from the magnetic parts until no further separation occurs. Magnetic components were put aside and the process was repeated on the non-magnetic ash.

4. Zeolite Synthesis & Testing

4.1. One Step Synthesis

Following one-step zeolite synthesis instructions from literature [18], a 1 litre quick fit glass leaching vessel with condenser was heated in a water bath with water at 95°C. A known mass of ash was added to the vessel, and washed in with 160 ml of 2M NaOH (which is reported to have a higher conversion efficiency than KOH [5]). This was heated for 5 hours, then left to cool. The leaching vessel was dismantled and the contents washed onto filter paper of known weight and left to drain before being put in a dryer until dry. Weights were taken using a balance accurate to 1 decimal place.

4.2. Metal ion Adsorption Tests

100 ml of Whealjane acid mine drainage with a high metal content was measured into each of 4 plastic beakers, the pH was measured, a known weight of ash was added and the pH was taken again. Lids were attached to the beakers and they were put into a rotating mixing device. Measurements and samples were taken at 15, 30, 60, 120 and 180 minutes. The pH in the beaker was measured, and a 3-5ml sample was taken with a syringe and filtered using a 0.22 μm filter membrane into a beaker for later testing with atomic adsorption spectophotometry. The AAS was first calibrated with water containing known PPM's of metal ions, the PPM's were

plotted against readings, and the values taken from the mine drainage were derived graphically.

5. Results & Discussion

5.1. Physical Characterisation

5.1.1. Water & Carbon Content (LOI)

No literature was found with criticisms on the accuracy of this method of testing, thus it is assumed that these results for water content are reasonably reliable and accurate for these samples. Critical values in the drying process include dryer temperature, quantity of ash being dried and drying duration. Higher temperatures may have resulted in thermal decomposition of minerals or carbon. Longer drying time was deemed unnecessary due to the small volume of the ash sample being dried. Were the volume larger, a longer time period would have been necessary. The water content of the ash as shown in table 2 is higher than the "fluid" content mentioned in literature [4], however, the literature values ostensibly apply to dry powdered FA. The raw ash samples supplied for use in this paper are noticeably moist and highly agglomerated, explaining the higher moisture values.

Table 2: Moisture content and loss on ignition in weight percent

Test	FB7	Lagoon
Moisture	5.09%	2.75%
LOI	11.99%	11.06%

High temperature ashing tests, which are conducted at 700-1000°C are known to be inaccurate due to the dehydration, decomposition, decarbonisation or dehydroxylation of gypsum, anhydrites, calcite, dolomite and portlandite, which occurs at high temperatures, giving unreliable measurements for the organic content of FA. Alternative tests such as low temperature ashing require expensive equipment, are lengthy, and can only be conducted on very small (potentially unrepresentative) samples of ash, thus the conventional LOI test values were used, accounting for inaccuracies [4]. As with the moisture test, the most influential parameters are quantity of ash tested, temperature and duration. Due to the small amount of ash tested, one hour was deemed sufficient to ensure all carbon decomposition. Table 3 shows values for the moisture, LOI, and carbon content according to LECO elemental analysers for a range of coals, tested in literature [2]. The table shows that the Carbon values (taken to be accurate) are not the same as the values for LOI which are always lower, showing that LOI is not entirely reliable for measuring ash carbon content. LOI and moisture results attained through these experiments do not fall within the maximum values in table 3, however as there are many other ranges given in literature (2-12%, >20%, 1-25%), few of which completely agree with each other, but most of which agree with experimental results, the results are considered acceptable even if the values were overestimated due to decomposition of non-organic components [1, 4]. The high LOI values mean that the ashes cannot be used in cement without carbon removal due to regulations [11].

Table 3: Carbon content, Moisture and LOI in wt% for various coals, as analysed in literature [2]

Coal Name	Carbon	Moisture	LOI
Narcea	1.4	0.03	1.9
Barrios	3.4	0.01	3.8
Escucha	4.6	0.03	4.7
Meirama	0.7	2.4	5.2
Teruel	0.6	0.1	2
Espiel	2.4	0.1	3.7
Compostilla	3.2	0.1	4.3
La Robla	1.1	0.1	1.9
As Pontes	1.4	0.3	3.8
S. de Ribera	1.2	0.2	3
Puertollano	0.7	0.1	1.1
Alkaline	1.9	0.2	3
Nijmegen	6.2	0.2	7.5
Neutral	4	0.3	4.8
CCB	3.4	0.3	3.7
Acid	2.7	0.1	3.3
Amer-8	7	0.1	8.1
Amer-9	2.3	0.1	2.8
Hemweg-8	2.3	0.2	2.7
Lignite	1	0.1	3
Fusina	7.6	0.1	7.9
Monfalcone	1.6	0.1	1.9
Sardegna	6.5	0.2	7.6

5.1.2. Size Distributions

Sieve analysis was selected over other methods due to equipment availabilty, simplicity and cost-effectiveness. In order to ensure the PSD test was finished (thus reliable), each tray was tapped to make sure no more material was passing through the sieve before results were

measured. The most influential parameters in this test are vibration strength and duration, which would influence how long the test would run, but otherwise not influence the final result. Although a small amount of material is lost to experimental error (similar tests indicate 2-3% of matter is lost), this is not expected to significantly influence the results. From the first PSD test conducted on the FA (Figure 5a), most of the material (69% for FB7, 64% for Lagoon) is smaller than 106 μm. Thus a second PSD test (Figure 5b) was carried out where the finest mesh size was 45μm. It was still found that the majority of the material (70% for FB7, 56% for Lagoon) was smaller than the smallest mesh size. The results for the PSD on cenospheres is shown in figure 5d. It shows that the smallest particles only make up a small proportion of the cenospheres, and 78% of the cenospheres are between 90μm and 250μm. This is in contrast with untreated ash, where the majority of the matter is smaller than 45μm. PSD experiments in literature confirm the fine grain size shown in figure 5b and show similar ceosphere size distributions [2, 6]. This data shows that the bulk of the mass of the FA consists of very fine particles, which can be easily separated through sieving. The larger size of the cenospheres is to be expected due to the nature in which they are separated. Smaller cenospheres would have a higher relative density due to the thickness of their walls in comparison to their volume, thus would have a lower buoyancy in comparison to the larger cenospheres, assuming similar relative wall thicknesses throughout all cenospheres. If the settling time in the cenosphere recovery process is not high enough this would be exaggerated, with only the most buoyant thus largest cenospheres being recovered.

LOI ignition tests carried out on the individual particle size fractions from figure 5b are assumed to be of a similar reliability to the LOI conducted in section 5.1.1, with the same critical parameters and levels of accuracy. The results concur with findings in literature indicating that the majority of carbon concentrates can be found in the larger grain sizes. The results show that LOI increases with particle size, and a higher LOI occurs for FB7 than for Lagoon ash. This leads to the assumption that most of the carbon in the FA can be found in the larger particle sizes, and that removal of smaller size fractions could increase carbon recovery efficiency.

5.1.3. Scanning Electron Microscopy

Of the various imaging techniques, SEM was selected due to equipment availability, image resolution and size, magnification level and cost. From the SEM images, we can identify the various components of the FA. Figure 6a shows untreated FB7 FA, with various isolated components in the following figures. We can see a smooth glassy cenosphere in figure 6b, highly porous, carbon-rich material in figure 6c, and a ferrosphere with skeletal magnetite crystallisation in figure 6d, which is very similar to SEM images in literature [10]. Images of the finalised alpha and delta products are similar to the untreated ash, which is to be expected, as cenospheres, carbon and magnatite only make up a small proportion of the ash. The difference in size is clear in the SEM images. Alpha (Figure 6e) is shown to be a fine powder made up of spherical particles, somewhat uniform in size, whilst Delta (figure 6f) is made up of coarser, often non-spherical particles. The removal of non-pozzolanic material (CC and magnetic) and alpha's fine particle size increases reactivity (makes the ash more pozzolanic), thus cement can be made using larger proportions of alpha [19]. The larger particle size and reduced non-pozzolanic content of Delta makes it ideally suited as aggregate for use in concrete.

5.1.4. ICP-OES

The ICP-OES results do contain an element of experimental error, in that the percentages only add up to 80%. For this reason, the results should only be taken as an example of which elements are present, and their order of magnitude, rather than a definitive elemental analysis, however it should also be noted that the results for iron are similar to the results for magnetic content in table 7. The results are similar to results in literature [1], showing the ash to be predominantly Alumina and silica, with 10-15% iron compounds. The rest of the ash is made up of minor components (1-10%) in the form of alkali metal oxides Potassium, Sodium, Calcium and Magnesium and trace elements (< 1%).

5.2. Beneficiation Processes

5.2.1. Cenosphere Flotation

Despite some literature definitions giving cenospheres a relative density of <2.2g cm^{-3} [6], water is used as the separation medium for reasons of cost and simplicity as other sources describe cenospheres as having a relative density less than 1 kg dm^{-3} [5]. Using water as the separation medium ensures a higher purity of cenospheres, as using a fluid with a higher relative density may also remove some non-cenospheric, low-density material [6]. The most influential parameters in

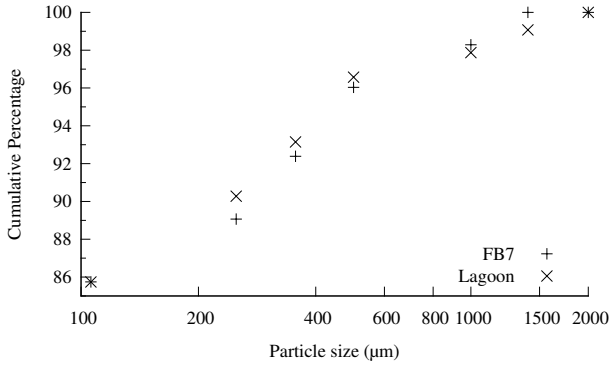

(a) Particle Size Distribution 2000-106μm

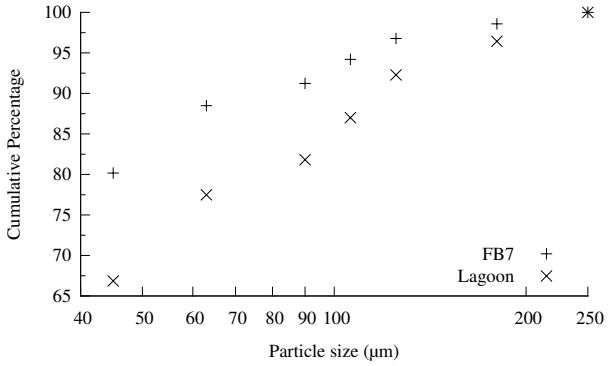

(b) Particle Size Distribution 250-45μm

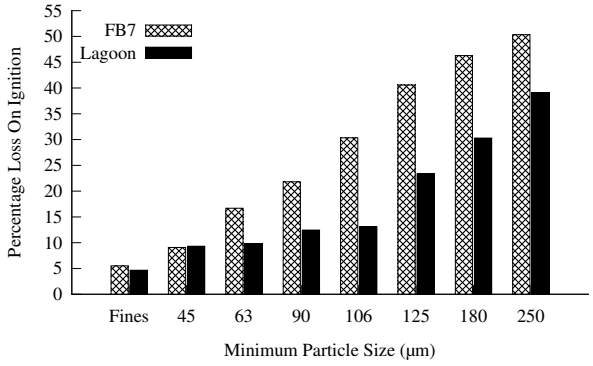

(c) Loss on Ignition per Size 250-45μm

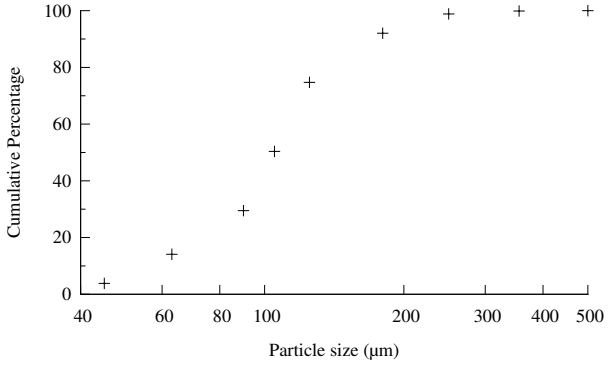

(d) Cenosphere Particle Size Distribution

Figure 5: Particle Size Distributions

cenosphere recovery are settlling time, and solids loading. Through the repeated experiments, solids loading does not appear to have influenced the results, and settling time was longer than was required to render the water unclouded. The cenosphere flotation process resulted in the average loss of around 2.5% of the material, which is attributed to experimental error. It is assumed that this material loss is distributed proportionally between cenosphere and non-cenosphere fractions. The results show a low cenosphere content by mass of around 0.5%, which can be anticipated due to the low density of the cenospheres. Sources in literature mention cenosphere contents which vary between 3.6 wt% and 96.9% [6]. Although these results do not fall strictly within the above boundaries, due to the massive variation in the results in literature, it is assumed that the results are still acceptable.

5.2.2. Carbon Recovery

Froth flotation was selected for the carbon recovery process as it is widely used in industry and considered one of the most effective methods [20]. Parameters influencing the carbon recovery process include solids loading, duration, number of repetitions and concentration of frother and collector. All variables but concentration of collector (diesel oil) were kept constant following experiments already conducted in literature [20]. In order to ascertain the optimal concentration of Diesel oil, the amount of teefroth added was kept constant at 0.2ml per batch, and 3 tests were run for each sample, with 0.1ml, 0.2ml and 0.3ml of Diesel oil added. The effectiveness of the froth flotation is measured by LOI tests, the accuracy of which are discussed in section 5.1.1. Although they may not accurately depict the absolute amount of carbon recovered, they can be used to indicate carbon content relative to each sample. The froth flotation results show that the froth collected has a higher loss on igntion than the bottoms remaining after the froth

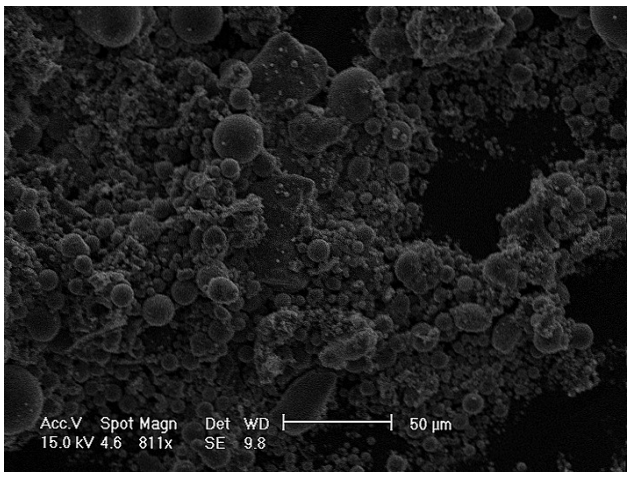

(a) Untreated FB7

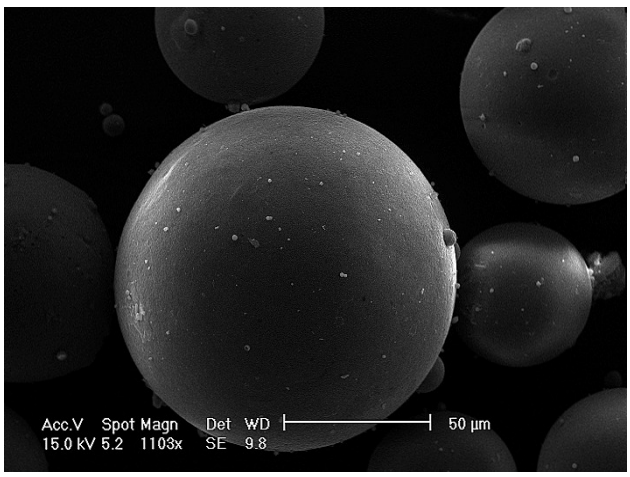

(b) Cenospheres

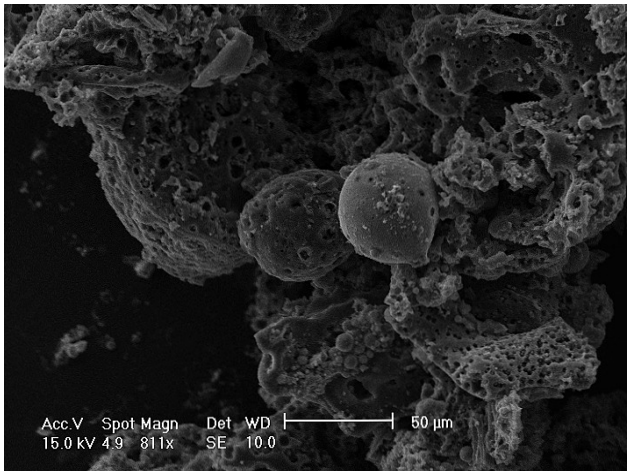

(c) Carbon-Rich Material

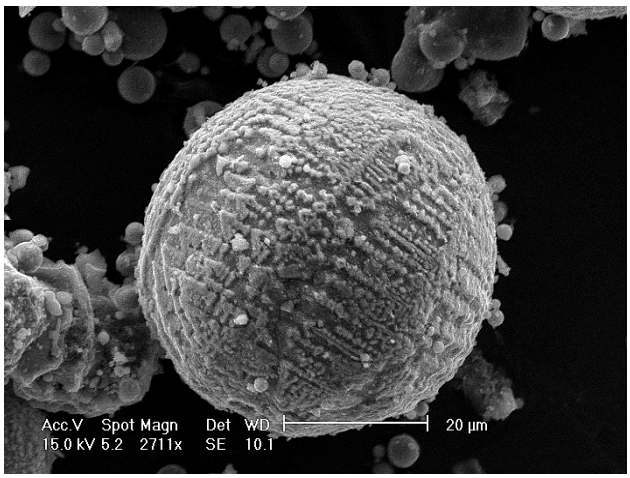

(d) Magnetic Concentrate

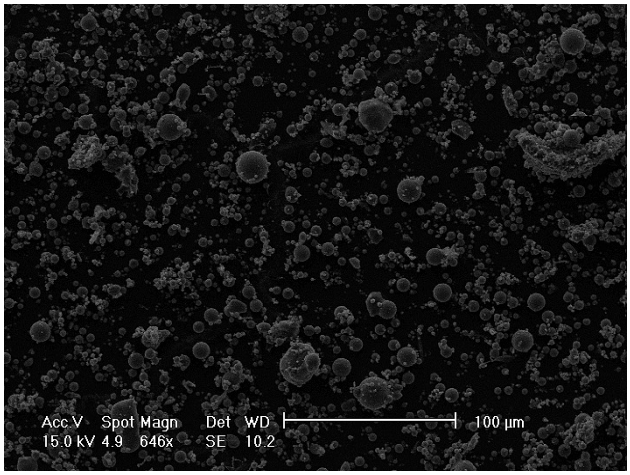

(e) “Alpha” Product

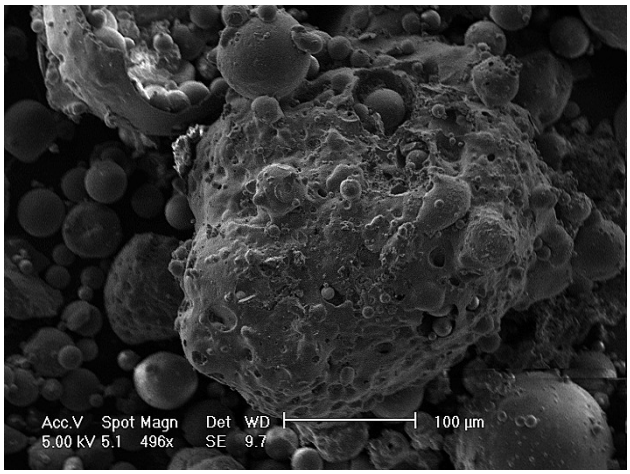

(f) “Delta” Product

Figure 6: SEM images of FA: Major Products

Table 4: Ash Content of 4 ash samples, measured by Inductively Coupled Plasma - Optical Emission Spectroscopy. Results in wt %

Oxide	Alpha FF	Delta	FB7	Lagoon
Al_2O_3	23.60 %	23.34 %	23.23 %	19.46 %
BaO	0.09 %	0.08 %	0.08 %	0.09 %
CaO	2.68 %	2.61 %	2.99 %	2.06 %
Cr_2O_3	0.02 %	0.01 %	0.02 %	0.01 %
CuO	0.02 %	0.01 %	0.01 %	0.01 %
Fe_2O_3	5.07 %	5.09 %	6.04 %	7.36 %
K_2O	3.94 %	3.04 %	2.90 %	2.68 %
MgO	1.35 %	1.37 %	1.72 %	1.26 %
MnO	0.05 %	0.07 %	0.11 %	0.06 %
Na_2O	2.44 %	2.03 %	2.29 %	2.06 %
P_2O_5	0.32 %	0.17 %	0.36 %	0.23 %
SO_2	0.10 %	0.04 %	0.08 %	0.05 %
SiO_2	41.60 %	43.68 %	38.97 %	44.03 %
SrO	0.05 %	0.03 %	0.06 %	0.04 %
TiO_2	0.38 %	0.31 %	0.36 %	0.30 %
V_2O_5	0.02 %	0.01 %	0.02 %	0.02 %
ZnO	0.20 %	0.13 %	0.23 %	0.22 %

Table 5: Mass lost through experimental error, and average cenosphere content by mass

Average Mass Lost:	2.52%
FB7 Cenosphere Content:	0.48%
Lag Cenosphere Content	0.57%

flotation has taken place. This indicates that the froth collected is carbon enriched, as indicated by the darker colour in comparison to the untreated FA. As shown in figure 7a, for the FB7 ash, the highest LOI occurs with the ash collected in the first minute, with decreasing LOI results for each sample following. For the Lagoon FA, the inverse is true; the first collection renders the lowest LOI, and the successive collections increase in LOI. Figure 7b shows the total LOI from the dried froth of each batch as a function of the amount of diesel oil added, and that 0.2ml of diesel oil produces the highest LOI for the froth collected. It should be noted that the ash only underwent one froth flotation procedure, whereas in an industrial context the ash would undergo multiple froth flotations to achieve a higher concentration of carbon in the concentrate, and minimise carbon in the bulk of the product, which explains the relatively low purity of the carbon concentrate.

5.2.3. Magnetic Separation

The Boxmatic Rapid BHW was selected due to its availability, ease of operation and variable magnetic strength. The Boxmatic best mimics the wet magnetic separator used in the RockTron^{TM}process from the apparatus available. Critical parameters in this experiment are magnetic field strength, mesh density and quantity of water used to wash through ash. Magnetic field was limited to two known values. Higher field strength would remove more magnetic matter, but also entrain more non-magnetic matter. Mesh density was varied after poor results with the highest density matrix. The higher the matrix density the more non-magnetic material that will be entrained. Sufficient water was washed through to ensure all loose matter was dislodged. The losses due to experimental error are accounted for in table 6, and are deemed to be acceptable. This method provided rather high results for magnetic content, as shown in table 6. The control test which was run on a lower density matrix showed erroneously high results. The lower density matrix should theoretically retain less matter, thus any error in this test would be even higher in the wedge wire matrix. These results are significantly higher than literature on the subject [4, 10], even taking into account experimental loss. Due to the gross disagreement with literature and discrepancy in the control run the results are considered unreliable. The high values are attributed to poor flow through the matrix resulting in nonmagnetic material being entrained in the matrix, producing erroneously high values.

Table 6: Boxmag Rapid BHW - Mass lost through experimental error and average magnetic content at high and low-power by mass

Wedge Wire Matrix	
Average loss	3.55%
FB7 Highly Magnetic Fraction	22.47%
FB7 Medium Magnetic Fraction	28.14%
FB7 Total Magnetic	50.61%
Lag Highly Magnetic Fraction	33.20%
Lag Medium Magnetic Fraction	18.92%
Lag Total Magnetic	52.12%
Expanded Metal Matrix	
Average Loss	6.95%
Actual Magnetic Content	5.83%
Measured Magnetic Content	13.69%

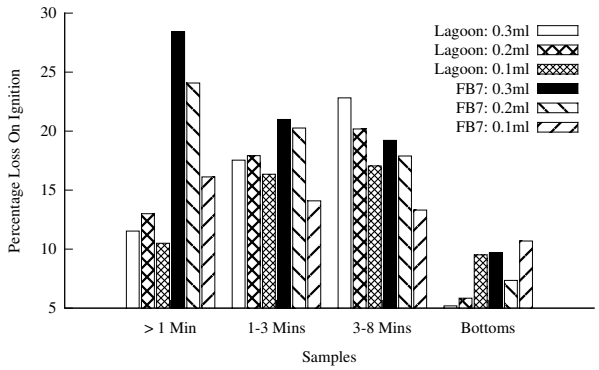

(a) LOI per sample, varying frothing agent

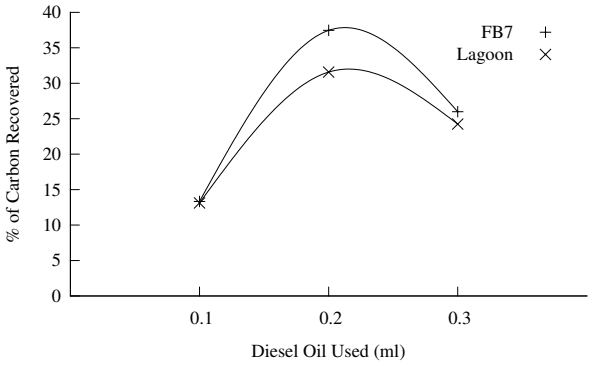

(b) Effect of Frothing agent concentration on Carbon Recovery

Figure 7: Results from the froth flotation of carbon

The Barium Ferrite Magnetic separation method was selected for its simplicity and cost. The method used was repetitive and consistent but still allowed for some variation between each repetition through human error. However this was not reflected in the results, which were all quite consistent. Influencing variables include strength of magnetic field and number of repetitions. The strength of the magnet was selected based on the approximate strength of the magnetic separator at RockTron^{TM}. This method produced lower results for losses through experimental error and the results were closer to literature values, as shown in table 7. Results could have been made more reliable through repetition, which was not achievable at the time. The control sample tests which consisted of a known amount of magnetite and Delta produced a result which was within 0.6% of the expected result for the quantities used. This shows that the barium ferrite magnet separation method is accurate enough to be used in this separation procedure. The results show that the ash which had not been treated with cenosphere removal and froth flotation had a higher magnetic content than the treated ash, indicating that the lagoon ash for example loses 3% of its magnetic content through froth flotation and cenosphere removal, however this value may be anomalous, due to lack of repeated experiments.

The Boxmag magnachute separation process was quicker and easier to precisely repeat than than the barium ferrite separation method. As the separation process yielded magnetic material each time it was repeated (as was the case for the barium ferrite magnet separation), the magnetic content of the Delta ash was questioned. For this reason, the magnetic separation on purely delta ash was conducted. The results from the control samples, as shown in table 8 were closer to the expected results than the barium ferrite control separation results, thus the accuracy of this method is taken to be acceptable. This process produced a loss result similar to the previous Boxmag procedure, and was tested only on control samples and Delta. According to the RockTron^{TM}process, Magnetic content has been removed from the delta product. This should result in less magnetic content being removed from the delta product, which did not appear to be the case. From this information one could infer that the dry magnetic separation techniques remove a proportion of the magnetic content. To fully characterise the magnetic content, a longer, more thorough magnetic separation process would have to be carried out. In the industrial context, complete separation would not necessarily be required, especially as each repetition of the process is likely to produce a smaller and smaller ash yield.

Table 7: Barium Ferrite Separation - Loss through experimental error, Magnetic content for Raw and Processed ash, and control sample error

Average Loss	0.98%
FB7 Magnetic Content	3.73%
Lag Magnetic Content	4.13%
FB7 Raw Magnetic Content	3.97%
Lag Raw Magnetic Content	7.02%
Average Difference (Control Sample)	0.57%

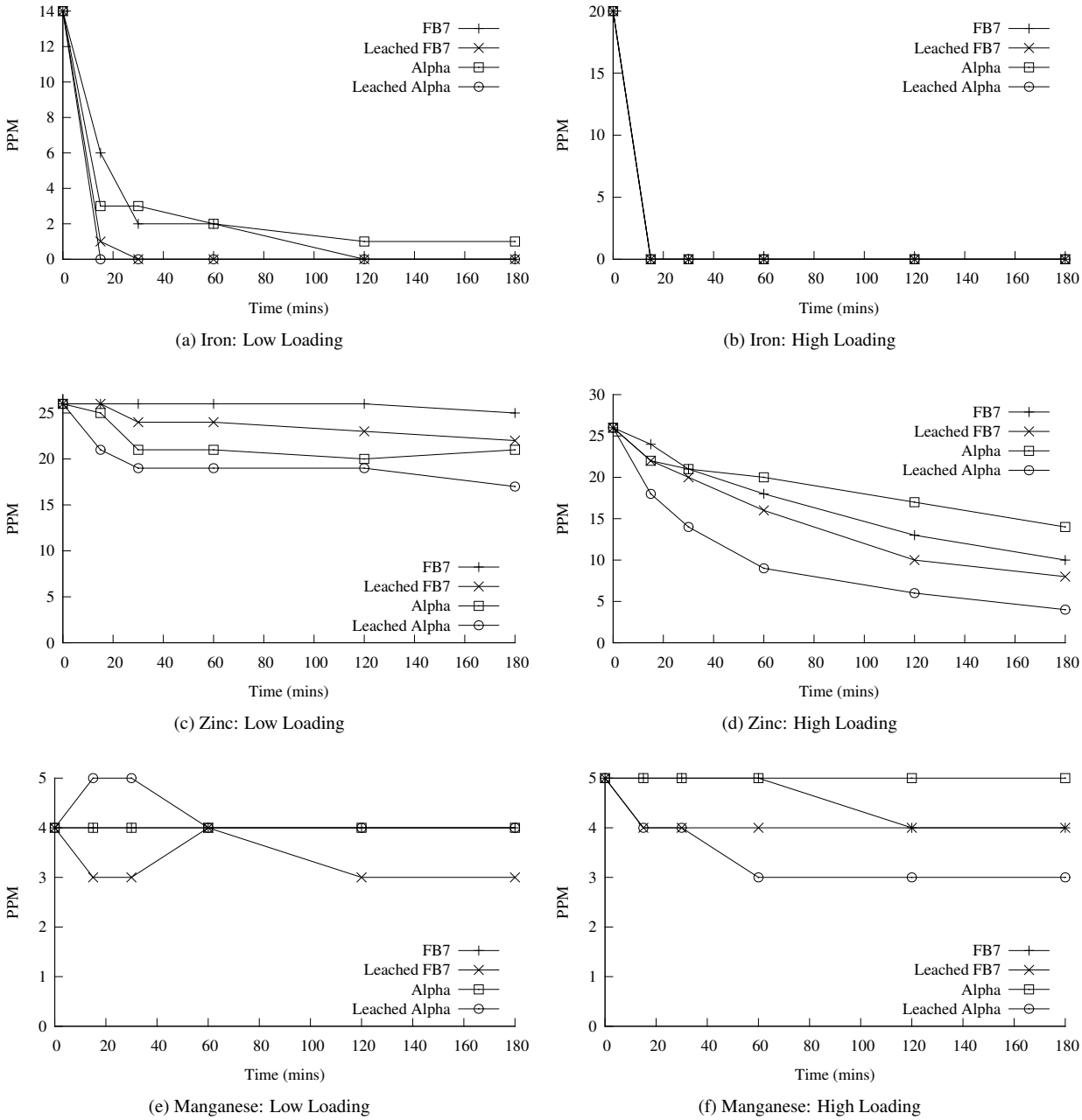

(a) Iron: Low Loading

(b) Iron: High Loading

(c) Zinc: Low Loading

(d) Zinc: High Loading

(e) Manganese: Low Loading

(f) Manganese: High Loading

Figure 8: Concentrations of metal ions in minewater as a function of time with low (0.2g/ 100ml) and high (1g/100ml) ash loading

Table 8: Boxmag Rapid Magnachute - Loss through experimental error, error in control sample, and magnetic content of Delta

Average Loss	3.82%
Average Difference (Control Sample)	0.39%
Magnetic Content of Delta	3.26%

5.3. Zeolite Testing

5.3.1. Adsorption of Metal Ions by Zeolitised Ash

The metal ion adsorption method was chosen as it is a smaller scale example of the intended application of the FA, thus is ideally suited for these purposes. Critical process parameters are experiment length, temperature, agitation and pH. In application the zeolites would be left for a long period, but would not be agitated. In order to complete this experiment at a laboratory time scale, the zeolite-minewater was agitated to aid diffusion and adsorption and reduce the time scale necessary. Experiments were conducted at room temperature. Increasing or decreasing temperature would not have accurately reflected the intended application. Discussion on pH follows separately. The AAS calibration curve values for low PPM's, especially manganese are very closely grouped, so a small variation in the AAS readings results (which is commonplace) in a change of one PPM, equivalent to a 20% change in manganese content. This would be less significant for metals such as iron and zinc, where the minewater concentrations start off at 20 and 26 respectively, thus a 1PPM variation produces only a 4-5% variation. The results shown in figure 8 show that the FA can be used as an aborption medium for the treatment of minewater contaminated with a high metal content. The results show that Alpha adsorbs more metal ions over the given time period than untreated FB7 ash, and that the leached alpha and FB7 are better than their untreated counterparts. The treatment is highly effective at removing Iron, as shown in figure 8b, effective at removing Zinc, shown by figure 8d, and can remove some Manganese, shown in figure 8f. For the second set of adsorption experiments (with zeolitised Alpha and Delta) figure 9 shows that the alpha-product ash, which has the higher surface area is the more effective metal adsober after treatment with NaOH. This is shown to be the case for all metals. Although the ash was treated in the two-step leaching method, data for the high purity zeolite formed from precipitation of the filtrate is unavailable.

Figure 8 shows that an increased ash loading results in

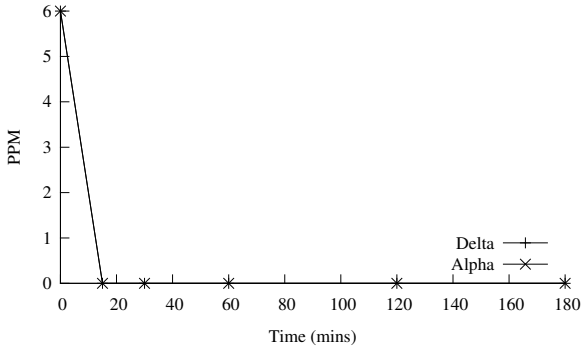

(a) Iron

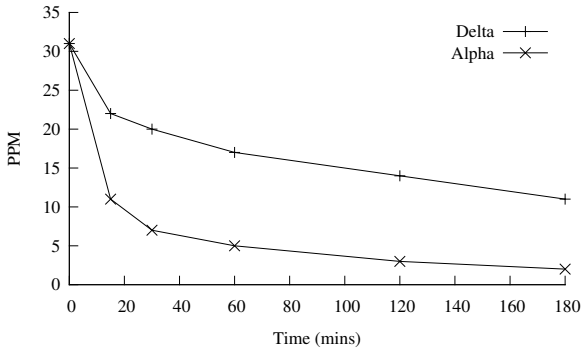

(b) Zinc

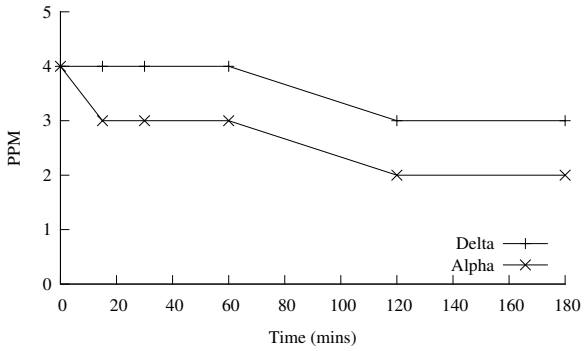

(c) Manganese

Figure 9: Concentrations of metal ions in minewater as a function of time using 2-stage zeolitised ash (1g/ 100ml)

increased metal adsorption, demonstrating scalability. The fluctuations for Manganese adsorption at low loading (figure 8e) can be attributed to variation in the AAS readings or to leaching of Manganese from the FA into the minewater, temporarily increasing the concentration of Manganese in the minewater.

Influence of pH: Addition of zeolite raises pH. It is important to ascertain whether the decrease in metal content is due to solid precipitation of metals, or due to cation exchange in zeolites [5, 16]. Alkali water treatment is utilised to precipitate metals in some circumstances, but must be done carefully so as not to damage the environment. Overdosing results in detrimental environmental effects, whereas a zeolite overdose has no discernible environmental effects, thus can be used on water which has been partially treated with NaOH. Zeolite is also ideal for treatment which leaves no solid residue through suspension in permeable membranes [16].

The pH of the various minewater samples are available in tables 9 & 10 which show that the highest pH reached is around 6.8, from the starting value (for untreated minewater) of around 3.2. It should be noted that the pH values for low solids loading in table 9 are high due to incorrectly calibrated pH meters, however, due to the lower ash loading it is safe to assume that the pH is lower than in the high solids loading and in table 10. The highest concentrations of metals in the minewater were 20 ppm (Iron), 31 ppm (Zinc) and 5 ppm (Manganese). Data on precipitation pH's of acid mine drainage indicates that the pH would need to be higher than 6.8 in order to induce metal ion precipitation [21, 22]. It can thus be assumed that the reduction in concentration of metal ions in the Whealjane acid minewater is due to the ion exchange activity of the synthesised zeolite.

5.3.2. Scanning Electron Microscopy

The images in figures 10 and 11 are SEM images of FB7 and Alpha product FA after leaching with NaOH to deposit zeolites on the surfaces of the ash particles. Figures 10a and 11a show the untreated FB7 and Alpha-product ashes, and figures 10b and 11b show their zeolitised counterparts. Although image quality is poor, figures 10b and 11b do demonstrate rougher surfaces than their counterparts 10a and 11a. This can be attributed to zeolite deposits on the ash surface, characterised by the metal ion adsorption tests in figure 8.

Table 9: pH values over time for Metal Ion adsorption tests

Low Loading				
TIME	FB7	FB7-Z	α	α-Z
0	5.47	5.47	5.47	5.47
15	5.77	6.24	5.83	6.45
30	5.83	6.41	5.85	6.57
60	5.91	6.52	5.87	6.55
120	6.00	6.55	5.89	6.66
180	6.08	6.53	5.89	6.66
High Loading				
TIME	FB7	FB7-Z	α	α-Z
0	3.23	3.23	3.23	3.23
15	5.25	4.55	5.44	5.46
30	5.32	5.02	5.34	5.58
60	6.24	6.64	6.60	6.53
120	6.51	6.45	6.40	6.45
180	6.51	6.51	6.56	6.70

Table 10: pH values over time for Metal Ion adsorption tests: Alpha and Delta

TIME	Delta	α
0	3.20	3.20
15	5.07	6.31
30	5.78	6.55
60	6.00	6.64
120	6.25	6.76
180	6.35	6.83

6. Recommendations

As suggested by literature [3], a life cycle analysis on FA products would be expedient, in order to analyse the economic and environmental impacts of FA reutilisation.

Further research can be carried out in several areas. The observation that LOI for the magnetic concentrate is quite low [4], suggests that there is good separation between CC and magnetite. The efficiency of the carbon reclamation process could be improved were magnetic separation to be conducted before carbon recovery.

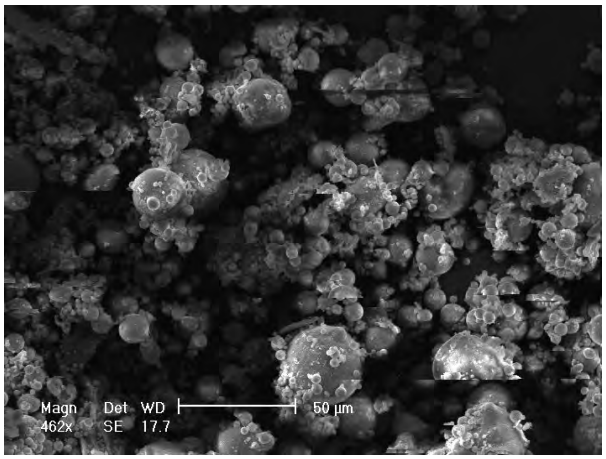

(a) Non Zeolitised FB7

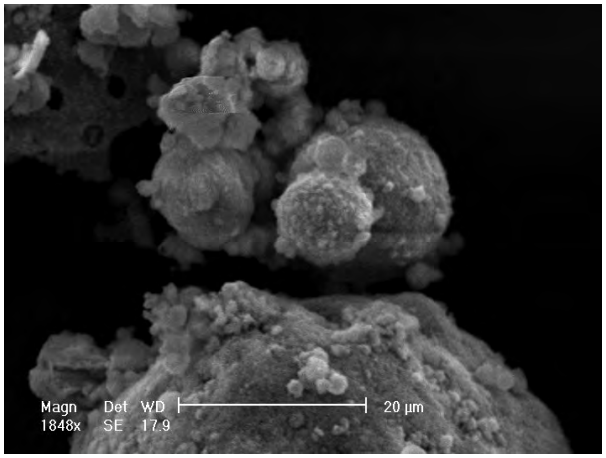

(b) Zeolitised FB7

Figure 10: SEM images of fly ash: zeolitised and non-zeolitised FB7

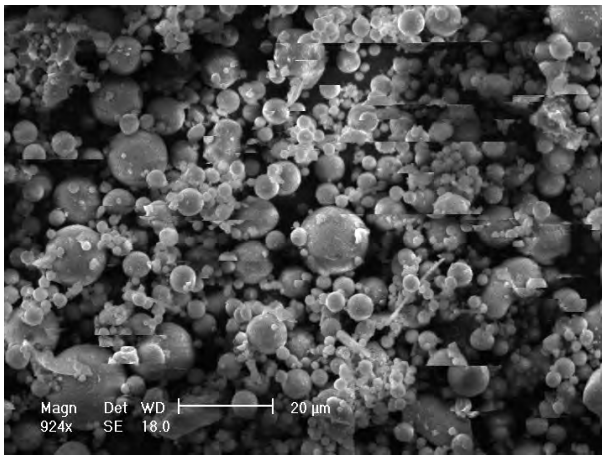

(a) Non Zeolitised Alpha

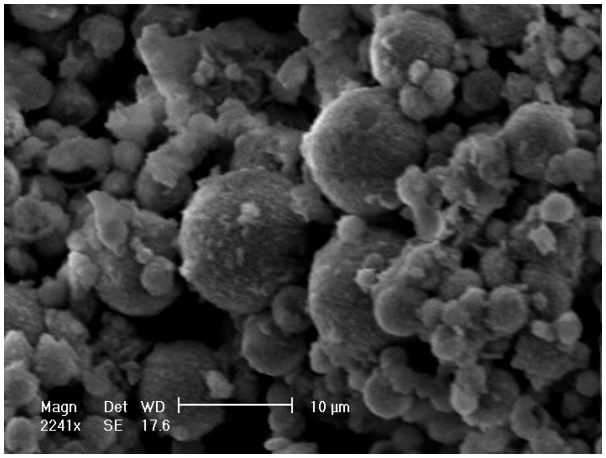

(b) Zeolitised Alpha

Figure 11: SEM images of fly ash: zeolitised and non-zeolitised Alpha

Speed and efficiency of carbon recovery could be increased using sieving to remove smaller sized particles which are low in carbon, performing froth flotation only on the larger particles, where the majority of the carbon is found. Experiments conducted in literature claim to recover 85% of the carbon for fractions larger than 100μm [10, 11]. Figures 5b & 5c show that 55-70% of the FA is smaller than 45μm, with a LOI of 5%.

Density classification could be achieved using fluids of varying densities, such as halogenated organic compounds (a mix of CCl_4, CH_2Br_2 and CH_2I_2) or lithium heteropolytungstate (LST) salts. Densities for separating the fly should mostly fall between 2 and 3 g cm^{-3}, as demonstrated by literature [4, 6, 11]. LST salts have the advantage of being nonreactive, noncorrosive and non-toxic [11]. Carbon enrichment processes could then be applied to density-classified ash, to provide higher purity CC and ash with lower Carbon content.

Two step zeolite synthesis could be implemented with minimal effect on the yield of zeolitised ash. Two step zeolite synthesis involves retaining the filtrate following the leaching process and treating it with aluminium solution to precipitate high purity zeolite. Unoptimised yields in literature currently stand at 5-8.5% as a weight percentage of ash input [18]. Synthetic zeolite has been found to have ten times the adsorption capacity of natural zeolite [15], and could thus be sold for at a higher price, increasing revenue. The remaining ash is still suitable for use as zeolitised ash in the conventional one-step method [17].

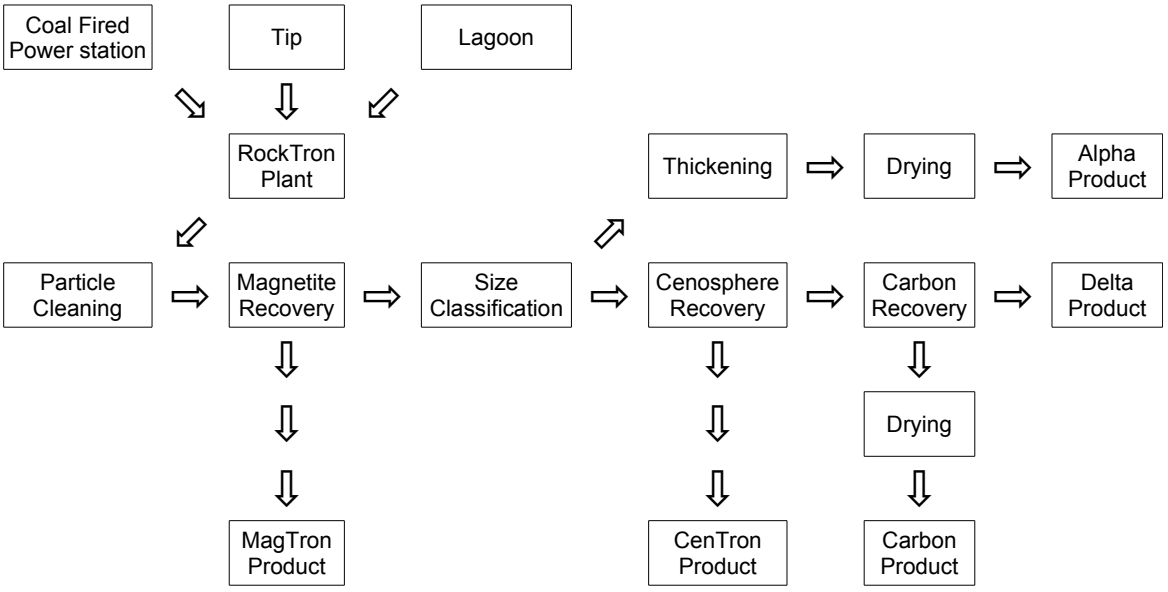

Figure 12: A Summary of the proposed Process

7. Conclusion

In conclusion the RockTron^{TM}beneficiation process is effective in turning a readily available and bountiful waste product into several value-added products, including cenospheres, magnetite, carbon concentrates, fly ash with a sufficiently low carbon content and high enough pozzolanic properties to be used in the manufacture of cement, and a metal ion adsorbing zeolite. Improvements in efficiency could be made through a re-ordering and alteration of the process as shown in figure 12. Magnetic separation is brought to the front of the process due to the good separation between carbon and magnetic content. The non-magnetic material is classified to 45μm. The smaller fraction with 4.5-5.5% LOI, low magnetic and cenospheric content is then suitable for use as alpha product. The remaining stream which should contain > 99% of the cenospheres (see figure 5d) and the majority of the carbon (see figure 5c), can undergo cenosphere and carbon removal in the same way as before. As only 30-45% of the ash need undergo cenosphere and carbon removal and assuming these are the most costly pieces of equipment, production could be increased 222-333% with an investment in a larger magnetic separation capacity.

The one-step zeolitisation process has been shown to produce a product highly effective at removing Iron and Zinc and quite effective at removing Manganese from mine water. RockTron^{TM}may also stand to gain if using the two-step zeolitisation process to produce high-purity zeolites. The zeolitisation of fly ash is feasible, and has practical applications in the treatment of acid mine water, which is a problem increasingly coming to the attention of environmental agencies. RockTron^{TM}stand to increase their revenue and diversify their consumer base.

8. Acknowledgments

Many thanks for the invaluable guidance and support provided by Dr N. Rowson and R. Blissett, and to D. Baratta for the lab work.

9. References

[1] M. Ahmaruzzaman, A review on the utilization of fly ash, Progress in Energy and Combustion Science 36 (2010) 327–363.

[2] N. Moreno, X. Querol, J. Andres, K. Stanton, M. Towler, H. Nugteren, M. Janssenjurkovicova, R. Jones, Physico - chemical characteristics of european pulverized coal combustion fly ashes, Fuel 84 (2005) 1351–1363.

[3] R. Iyer, J. Scott, Power station fly ash — a review of value-added utilization outside of the construction industry, Resources, Conservation and Recycling 31 (2001) 217–228.

[4] S. V. Vassilev, C. G. Vassileva, Methods for characterization of composition of fly ashes from Coal-Fired power stations: a critical overview, Energy & Fuels 19 (2005) 1084–1098.
[5] X. Querol, Synthesis of zeolites from coal fly ash: an overview, International Journal of Coal Geology 50 (2002) 413–423.
[6] S. Ghosal, Particle size-density relation and cenosphere content of coal fly ash, Fuel 74 (1995) 522–529.
[7] J. A. Campbell, J. C. Laul, K. K. Nielson, R. D. Smith, Separation and chemical characterization of finely-sized fly-ash particles, Analytical Chemistry 50 (1978) 1032–1040.
[8] S. P. McBride, A. Shukla, A. Bose, Processing and characterization of a lightweight concrete using cenospheres, Journal of Materials Science 37 (2002) 4217–4225. 10.1023/A:1020056407402.
[9] S. Shukla, Electroless copper coating of cenospheres using silver nitrate activator, Materials Letters 57 (2002) 151–156.
[10] S. Vassilev, Phase -mineral and chemical composition of coal fly ashes as a basis for their multicomponent utilization. 3. characterization of magnetic and char concentrates, Fuel 83 (2004) 1563–1583.
[11] M. M. Maroto-Valer, D. N. Taulbee, J. C. Hower, Novel separation of the differing forms of unburned carbon present in fly ash using density gradient centrifugation, Energy & Fuels 13 (1999) 947–953.
[12] G. Ferraiolo, M. Zilli, A. Converti, Fly ash disposal and utilization, Journal of Chemical Technology & Biotechnology 47 (2007) 281–305.
[13] R. Ltd, Fly ash beneficiation process & benefits - rktron.com, http://rktron.com/us-rocktron-fly-ash-beneficiation-process-benefits, 2011.
[14] T. Maesen, B. Marcus, The zeolite scene–An overview, in: H. V. Bekkum, J. Jansen, E. Flanigen (Eds.), Introduction to Zeolite Science and Practice, volume 137 of *Studies in Surface Science and Catalysis*, Elsevier, 2001, pp. 1 – 9.
[15] K. Hui, C. Chao, S. Kot, Removal of mixed heavy metal ions in wastewater by zeolite 4A and residual products from recycled coal fly ash, Journal of Hazardous Materials 127 (2005) 89–101.
[16] N. Moreno, X. Querol, C. Ayora, C. F. Pereira, M. Janssen-Jurkovicová, Utilization of zeolites synthesized from coal fly ash for the purification of acid mine waters, Environmental Science & Technology 35 (2001) 3526–3534.
[17] X. Querol, J. C. U. na, F. Plana, A. Alastuey, A. Lopez-Soler, A. Medinaceli, A. Valero, M. J. Domingo, E. Garcia-Rojo, Synthesis of na zeolites from fly ash in a pilot plant scale. examples of potential environmental applications, Fuel 80 (2001) 857–865.
[18] G. Hollman, A two step process for the synthesis of zeolites from coal fly ash, Fuel 78 (1999) 1225–1230.
[19] R. Ltd, Product ranges - rktron.com, http://www.rktron.com/media/pdfs/JD-RT-4230-AlphaSalesPresenter-27-04-10.pdf, 2011.
[20] M. Uçurum, Influences of jameson flotation operation variables on the kinetics and recovery of unburned carbon, Powder Technology 191 (2009) 240–246.
[21] R. Apak, Correlation between the limiting pH of metal ion solubility and total metal concentration, Journal of Colloid and Interface Science 211 (1999) 185–192.
[22] D. Feng, Treatment of acid mine water by use of heavy metal precipitation and ion exchange, Minerals Engineering 13 (2000) 623–642.

References

[1] Robert Blissett. *Coal fly ash and the circular economy.* EngD thesis, University of Birmingham, 2015.

[2] M Ahmaruzzaman. A review on the utilization of fly ash. *Progress in Energy and Combustion Science*, 36(3):327–363, 2010.

[3] Xavier Querol, N Moreno, JC t Umaña, A Alastuey, E Hernández, A Lopez-Soler, and F Plana. Synthesis of zeolites from coal fly ash: an overview. *International Journal of Coal Geology*, 50(1):413–423, 2002.

[4] Stanislav V Vassilev and Christina G Vassileva. Methods for characterization of composition of fly ashes from coal-fired power stations: a critical overview. *Energy & Fuels*, 19(3):1084–1098, 2005.

[5] Paola Catalfamo, Sebastiana Di Pasquale, Francesco Corigliano, and Letterio Mavilia. Influence of the calcium content on the coal fly ash features in some innovative applications. *Resources, Conservation and Recycling*, 20(2):119–125, 1997.

[6] A Molina and C Poole. A comparative study using two methods to produce zeolites from fly ash. *Minerals Engineering*, 17(2):167–173, 2004.

[7] Pieter W Du Plessis, Tunde V Ojumu, Ojo O Fatoba, Richard O Akinyeye, and Leslie F Petrik. Distributional fate of elements during the synthesis of zeolites from south african coal fly ash. *Materials*, 7(4):3305–3318, 2014.

[8] Hidekazu Tanaka, Hajime Eguchi, Satoshi Fujimoto, and Ryozi Hino. Two-step process for synthesis of a single phase Na-A zeolite from coal fly ash by dialysis. *Fuel*, 85(10):1329–1334, 2006.

[9] Giuseppe Ferraiolo, Mario Zilli, and Attilio Converti. Fly ash disposal and utilization. *Journal of Chemical Technology and Biotechnology*, 47(4):281–305, 1990.

[10] Richard A Kruger. Fly ash beneficiation in south africa: creating new opportunities in the market-place. *Fuel*, 76(8):777–779, 1997.

[11] Orava Hanne, Nordman Timo, and Kuopanportti Hannu. Increase the utilisation of fly ash with electrostatic precipitation. *Minerals Engineering*, 19(15):1596–1602, 2006.

[12] IEA. Key world energy statistics. Technical report, International Energy Agency, 2015. URL http://www.iea.org/publications/freepublications/publication/KeyWorld_Statistics_2015.pdf.

[13] RS Blissett and NA Rowson. A review of the multi-component utilisation of coal fly ash. *Fuel*, 97:1–23, 2012.

[14] RS Iyer and JA Scott. Power station fly ash—a review of value-added utilization outside of the construction industry. *Resources, Conservation and Recycling*, 31(3): 217–228, 2001.

[15] M Mercedes Maroto-Valer, Darrell N Taulbee, and James C Hower. Novel separation of the differing forms of unburned carbon present in fly ash using density gradient centrifugation. *Energy & Fuels*, 13(4):947–953, 1999.

[16] RJ Haynes. Reclamation and revegetation of fly ash disposal sites–challenges and research needs. *Journal of Environmental Management*, 90(1):43–53, 2009.

[17] Vimal Chandra Pandey, Jay Shankar Singh, Rana P Singh, Nandita Singh, and M Yunus. Arsenic hazards in coal fly ash and its fate in Indian scenario. *Resources, Conservation and Recycling*, 55(9):819–835, 2011.

[18] MG Dosskey and DC Adriano. Trace element toxicity in VA mycorrhizal cucumber grown on weathered coal fly ash. *Soil Biology and Biochemistry*, 25(11):1547–1552, 1993.

[19] Raymond E Davis. A review of pozzolanic materials and their use in concretes. In *Symposium on Use of Pozzolanic Materials in Mortars and Concretes*. ASTM International, 1950.

[20] A Moutsatsou, E Stamatakis, K Hatzitzotzia, and V Protonotarios. The utilization of Ca-rich and Ca-Si-rich fly ashes in zeolites production. *Fuel*, 85(5):657–663, 2006.

[21] Vinay Kumar Jha, Motohide Matsuda, and Michihiro Miyake. Resource recovery from coal fly ash waste: an overview study. *Journal of the Ceramic Society of Japan*, 116(1350):167–175, 2008.

[22] D Feng, C Aldrich, and H Tan. Treatment of acid mine water by use of heavy metal precipitation and ion exchange. *Minerals Engineering*, 13(6):623–642, 2000.

[23] Oriol Font, Xavier Querol, Roberto Juan, Raquel Casado, Carmen R Ruiz, Ángel López-Soler, Pilar Coca, and Francisco García Peña. Recovery of gallium and vanadium from gasification fly ash. *Journal of Hazardous Materials*, 139(3):413–423, 2007.

[24] Fatima Arroyo and Constantino Fernandez-Pereira. Hydrometallurgical recovery of germanium from coal gasification fly ash. solvent extraction method. *Industrial & Engineering Chemistry Research*, 47(9):3186–3191, 2008.

[25] Christopher Amrhein, Gholam H Haghnia, Tai Soon Kim, Paul A Mosher, Ryan C Gagajena, Tedros Amanios, and Laura De La Torre. Synthesis and properties of zeolites from coal fly ash. *Environmental Science & Technology*, 30(3):735–742, 1996.

[26] GG Hollman, G Steenbruggen, and M Janssen-Jurkovičová. A two-step process for the synthesis of zeolites from coal fly ash. *Fuel*, 78(10):1225–1230, 1999.

[27] Natalia Moreno, Xavier Querol, Carles Ayora, Constantino Fernández Pereira, and Maria Janssen-Jurkovicová. Utilization of zeolites synthesized from coal fly ash for the purification of acid mine waters. *Environmental Science & Technology*, 35(17): 3526–3534, 2001.

[28] R Sommerville, R Blissett, N Rowson, and S Blackburn. Producing a synthetic zeolite from improved fly ash residue. *International Journal of Mineral Processing*, 124:20–25, 2013.

[29] L. Puppe J. Weitkamp, editor. *Catalysis and Zeolites: Fundamentals and Applications*. Springer, Berlin, 1999. doi: 10.1007/978-3-662-03764-5.

[30] Richard M Barrer. Zeolites and their synthesis. *Zeolites*, 1(3):130–140, 1981.

[31] Theo Maesen and Bonnie Marcus. The zeolite scene—an overview. *Studies in surface science and catalysis*, 137:1–9, 2001.

[32] KS Hui and Christopher Yu Hang Chao. Effects of step-change of synthesis temperature on synthesis of zeolite 4A from coal fly ash. *Microporous and Mesoporous Materials*, 88(1):145–151, 2006.

[33] Lidia Bandura, Małgorzata Franus, Grzegorz Józefaciuk, and Wojciech Franus. Synthetic zeolites from fly ash as effective mineral sorbents for land-based petroleum spills cleanup. *Fuel*, 147:100–107, 2015.

[34] K Byrappa and Masahiro Yoshimura. *Handbook of Hydrothermal Technology A technology for Crystal Growth and Materials Processing*. William Andrew Inc, 2001.

[35] Nicholas M Musyoka, Leslie F Petrik, Eric Hums, Hasan Baser, and Wilhelm Schwieger. In situ ultrasonic monitoring of zeolite A crystallization from coal fly ash. *Catalysis Today*, 190(1):38–46, 2012.

[36] Ch Baerlocher, Lynne B McCusker, and David H Olson. *Atlas of zeolite framework types*. Elsevier, 2007.

[37] Harry Robson. *Verified synthesis of zeolitic materials*. Gulf Professional Publishing, 2001.

[38] Claudia Belviso, Francesco Cavalcante, and Saverio Fiore. Synthesis of zeolite from italian coal fly ash: differences in crystallization temperature using seawater instead of distilled water. *Waste management*, 30(5):839–847, 2010.

[39] Claudia Belviso, Francesco Cavalcante, F Javier Huertas, Antonio Lettino, Pietro Ragone, and Saverio Fiore. The crystallisation of zeolite (X-and A-type) from fly ash at 25°C in artificial sea water. *Microporous and Mesoporous Materials*, 162: 115–121, 2012.

[40] Claudia Belviso, Lorena C Giannossa, F Javier Huertas, Antonio Lettino, Annarosa Mangone, and Saverio Fiore. Synthesis of zeolites at low temperatures in fly ash-kaolinite mixtures. *Microporous and Mesoporous Materials*, 212:35–47, 2015.

[41] Nicholas Mulei Musyoka, Leslie Petrik, and Eric Hums. Synthesis of zeolite A, X and P from a South African coal fly ash. In *Advanced Materials Research*, volume 512, pages 1757–1762. Trans Tech Publ, 2012.

[42] Annie Shoumkova and Valeria Stoyanova. Zeolites formation by hydrothermal alkali activation of coal fly ash from thermal power station Maritsa 3, Bulgaria. *Fuel*, 103: 533–541, 2013.

[43] Hidekazu Tanaka, Yasuhiko Sakai, and Ryozi Hino. Formation of Na-A and-X zeolites from waste solutions in conversion of coal fly ash to zeolites. *Materials Research Bulletin*, 37(11):1873–1884, 2002.

[44] V Berkgaut and A Singer. High capacity cation exchanger by hydrothermal zeolitization of coal fly ash. *Applied Clay Science*, 10(5):369–378, 1996.

[45] KS Hui, Christopher Yu Hang Chao, and SC Kot. Removal of mixed heavy metal ions in wastewater by zeolite 4A and residual products from recycled coal fly ash. *Journal of Hazardous Materials*, 127(1):89–101, 2005.

[46] X Querol, JC Umana, F Plana, A Alastuey, A Lopez-Soler, A Medinaceli, A Valero, MJ Domingo, and E Garcia-Rojo. Synthesis of zeolites from fly ash at pilot plant scale. examples of potential applications. *Fuel*, 80(6):857–865, 2001.

[47] Savvaki Savva. *New materials for strontium removal from nuclear waste streams.* PhD thesis, University of Birmingham, 2016.

[48] G Blanchard, M Maunaye, and G Martin. Removal of heavy metals from waters by means of natural zeolites. *Water research*, 18(12):1501–1507, 1984.

[49] KS Hui and Christopher Yu Hang Chao. Pure, single phase, high crystalline, chamfered-edge zeolite 4A synthesized from coal fly ash for use as a builder in detergents. *Journal of Hazardous Materials*, 137(1):401–409, 2006.

[50] European Comission. Commission staff working document accompanying document to the proposal for a regulation (eu) no .../... of the european parliament and of the council amending regulation (ec) no 648/2004 as regards the use of phosphates and other phosphorous compounds in household laundry detergents impact assessment /* sec/2010/1277 final - cod 2010/0298 */. Technical report, European Comission, 2010. URL http://eur-lex.europa.eu/legal-content/EN/TXT/PDF/?uri=CELEX:52010SC1278&from=EN.

[51] Henkel KGaA. Human & environmental risk assessment on ingredients of european household cleaning products zeolite a. Technical report, HERA, January 2004. URL www.zeolites.eu/downloads/HERA_Zeolite_v3.pdf.

[52] Zeodet. Zeolites for detergents. Online, 2000. URL http://www.zeolites.eu/downloads/Zeolites.pdf.

[53] Hsiao-Lan Chang and Wei-Heng Shih. Synthesis of zeolites A and X from fly ashes and their ion-exchange behavior with cobalt ions. *Industrial & Engineering Chemistry Research*, 39(11):4185–4191, 2000.

[54] Juliana de C Izidoro, Denise A Fungaro, Jennifer E Abbott, and Shaobin Wang. Synthesis of zeolites X and A from fly ashes for cadmium and zinc removal from aqueous solutions in single and binary ion systems. *Fuel*, 103:827–834, 2013.

[55] RM Barrer and BM Munday. Cation exchange reactions of zeolite Na-P. *Journal of the Chemical Society A: Inorganic, Physical, Theoretical*, pages 2909–2914, 1971.

[56] AM Taylor and Rustum Roy. Zeolite studies 4-Na-P zeolites+ ion-exchanged derivatives of tetragonal Na-P. *American Mineralogist*, 49(5-6):656, 1964.

[57] Hsiao-Lan Chang and Wei-Heng Shih. A general method for the conversion of fly ash into zeolites as ion exchangers for cesium. *Industrial & Engineering Chemistry Research*, 37(1):71–78, 1998.

[58] Deyi Wu, Yanming Sui, Xuechu Chen, Shengbing He, Xinze Wang, and Hainan Kong. Changes of mineralogical–chemical composition, cation exchange capacity, and phosphate immobilization capacity during the hydrothermal conversion process of coal fly ash into zeolite. *Fuel*, 87(10):2194–2200, 2008.

[59] Jie Xie, Zhe Wang, Deyi Wu, and Hainan Kong. Synthesis and properties of zeolite/hydrated iron oxide composite from coal fly ash as efficient adsorbent to simultaneously retain cationic and anionic pollutants from water. *Fuel*, 116:71–76, 2014.

[60] Colin S Cundy and Paul A Cox. The hydrothermal synthesis of zeolites: Precursors, intermediates and reaction mechanism. *Microporous and Mesoporous Materials*, 82 (1):1–78, 2005.

[61] Barrie M Lowe. An equilibrium model for the crystallization of high silica zeolites. *Zeolites*, 3(4):300–305, 1983.

[62] Dimitar Georgiev, Bogdan Bogdanov, Krasimira Angelova, Irena Markovska, and Yancho Hristov. Synthetic zeolites–structure, classification, current trends in zeolite synthesis. review. In *International Science Conference*, pages 4–5, 2009.

[63] B Subotic and L Sekovanic. Transformation of zeolite a into hydroxysodalite. ii: Growth kinetics of hydroxysodalite microcrystals. *Journal of Crystal Growth*, 75 (3):561–572, 1986.

[64] B Subotić, D Škrtić, I Šmit, and L Sekovanić. Transformation of zeolite a into hydroxysodalite: I. an approach to the mechanism of transformation and its experimental evaluation. *Journal of Crystal Growth*, 50(2):498–508, 1980.

[65] Boris Subotić, Ivan Šmit, Olga Madžija, and Lavoslav Sekovanić. Kinetic study of the transformation of zeolite A into zeolite P. *Zeolites*, 2(2):135–142, 1982.

[66] Kunihiro Fukui, Keiji Kanayama, Tetsuya Yamamoto, and Hideto Yoshida. Effects of microwave irradiation on the crystalline phase of zeolite synthesized from fly ash by hydrothermal treatment. *Advanced Powder Technology*, 18(4):381–393, 2007.

[67] Miki Inada, Hidenobu Tsujimoto, Yukari Eguchi, Naoya Enomoto, and Junichi Hojo. Microwave-assisted zeolite synthesis from coal fly ash in hydrothermal process. *Fuel*, 84(12):1482–1486, 2005.

[68] Jae Kwan Kim and Hyun Dong Lee. Effects of step change of heating source on synthesis of zeolite 4A from coal fly ash. *Journal of Industrial and Engineering Chemistry*, 15(5):736–742, 2009.

[69] Xavier Querol, Andrés Alastuey, Angel López-Soler, Felicià Plana, Jose M Andrés, Roberto Juan, Pedro Ferrer, and Carmen R Ruiz. A fast method for recycling fly ash: microwave-assisted zeolite synthesis. *Environmental Science & Technology*, 31 (9):2527–2533, 1997.

[70] Tomasz T Wałek, Fumio Saito, and Qiwu Zhang. The effect of low solid/liquid ratio on hydrothermal synthesis of zeolites from fly ash. *Fuel*, 87(15):3194–3199, 2008.

[71] Z Miladinović, J Zakrzewska, and V Dondur. Kinetic analysis of experimental intensity curves obtained during zeolite a synthesis using in situ 27Al NMR spectroscopy. *Russian Journal of Physical Chemistry A*, 83(9):1478–1484, 2009.

[72] Nicholas M Musyoka, Leslie F Petrik, Wilson M Gitari, Gillian Balfour, and Eric Hums. Optimization of hydrothermal synthesis of pure phase zeolite Na-P1 from south african coal fly ashes. *Journal of Environmental Science and Health, Part A*, 47(3):337–350, 2012.

[73] Deyi Wu, Bohua Zhang, Li Yan, Hainan Kong, and Xinze Wang. Effect of some additives on synthesis of zeolite from coal fly ash. *International Journal of Mineral Processing*, 80(2):266–272, 2006.

[74] Miki Inada, Yukari Eguchi, Naoya Enomoto, and Junichi Hojo. Synthesis of zeolite from coal fly ashes with different silica–alumina composition. *Fuel*, 84(2):299–304, 2005.

[75] Norihiro Murayama, Hideki Yamamoto, and Junji Shibata. Mechanism of zeolite synthesis from coal fly ash by alkali hydrothermal reaction. *International Journal of Mineral Processing*, 64(1):1–17, 2002.

[76] Ryo Moriyama, Shohei Takeda, Masaki Onozaki, Yukuo Katayama, Kouji Shiota, Tomoya Fukuda, Hiroaki Sugihara, and Yuichi Tani. Large-scale synthesis of artificial zeolite from coal fly ash with a small charge of alkaline solution. *Fuel*, 84(12): 1455–1461, 2005.

[77] Nicholas M Musyoka, Leslie F Petrik, Gillian Balfour, Wilson M Gitari, and Eric Hums. Synthesis of hydroxy sodalite from coal fly ash using waste industrial brine solution. *Journal of Environmental Science and Health, Part A*, 46(14):1699–1707, 2011.

[78] Man Park, Choong Lyeal Choi, Woo Taik Lim, Myung Chul Kim, Jyung Choi, and Nam Ho Heo. Molten-salt method for the synthesis of zeolitic materials: II. characterization of zeolitic materials i. *Microporous and Mesoporous Materials*, 37 (1):81–89, 2000.

[79] NM Musyoka, LF Petrik, G Balfour, P Ndungu, WM Gitari, and E Hums. Synthesis of zeolites from coal fly ash: Application of a statistical experimental design. *Research on Chemical Intermediates*, 38(2):471–486, 2012.

[80] IZA. Analcime, iza comission on natural zeolites. Online 2016-09-14, . URL http://www.iza-online.org/natural/Datasheets/Analcime/analcime.htm.

[81] IZA. Chabazite series, iza commission on natural zeolites. Online 2016-09-14, . URL http://www.iza-online.org/natural/Datasheets/Chabazite/chabazite.htm.

[82] P. W. DuPlessis, Tunde V Ojumu, and Leslie F Petrik. Waste minimization protocols for the process of synthesizing zeolites from south african coal fly ash. *Materials*, 6(5):1688–1703, 2013.

[83] Ubolluk Rattanasak and Prinya Chindaprasirt. Influence of NaOH solution on the synthesis of fly ash geopolymer. *Minerals Engineering*, 22(12):1073–1078, 2009.

[84] Chun-Feng Wang, Jian-Sheng Li, Lian-Jun Wang, and Xiu-Yun Sun. Influence of NaOH concentrations on synthesis of pure-form zeolite A from fly ash using two-stage method. *Journal of Hazardous Materials*, 155(1):58–64, 2008.

[85] Nicholas M Musyoka, Leslie F Petrik, Eric Hums, Hasan Baser, and Wilhelm Schwieger. In situ ultrasonic diagnostic of zeolite X crystallization with novel (hierarchical) morphology from coal fly ash. *Ultrasonics*, 54(2):537–543, 2014.

[86] Y Soong, ML Gray, TA Link, KJ Champagne, and MR Schoffstall. Separation and utilization of value-added products from combustion fly ash. In *Abstracts of papers of the American Chemical Society*, volume 220, pages U390–U390. Amer Chemical Soc 1155 16th st, NW, Washington, DC 20036 USA, 2000.

[87] Clive L. Roberts Carlos A. Ríos R., Craig D. Williams. A comparative study of two methods for the synthesis of fly ash-based sodium and potassium type zeolites. *Fuel*, 88(8):1403–1416, 2009.

[88] Dana R Kester, Iver W Duedall, Donald N Connors, and Ricardo M Pytkowicz. Preparation of artificial seawater. *Limnology and Oceanography*, 12(1):176–179, 1967.

[89] IZA. Phillipsite, iza commission on natural zeolites. Online 2016-09-14, . URL http://www.iza-online.org/natural/Datasheets/Phillipsite/phillipsite.htm.

[90] Ye Yaping, Zeng Xiaoqiang, Qian Weilan, and Wang Mingwen. Synthesis of pure zeolites from supersaturated silicon and aluminum alkali extracts from fused coal fly ash. *Fuel*, 87(10):1880–1886, 2008.

[91] Jong-Wan Kim and Hae-Geon Lee. Thermal and carbothermic decomposition of Na_2CO_3 and Li_2CO_3. *Metallurgical and Materials Transactions B*, 32(1):17–24, 2001.

[92] Man Park, Choong Lyeal Choi, Woo Taik Lim, Myung Chul Kim, Jyung Choi, and Nam Ho Heo. Molten-salt method for the synthesis of zeolitic materials: II. characterization of zeolitic materials ii. *Microporous and Mesoporous Materials*, 37 (1):91–98, 2000.

[93] RS Blissett and NA Rowson. An empirical model for the prediction of the viscosity of slurries of coal fly ash with varying concentration and shear rate at room temperature. *Fuel*, 111:555–563, 2013.

[94] JA Campbell, JC Laul, KK Nielson, and RD Smith. Separation and chemical characterization of finely-sized fly-ash particles. *Analytical Chemistry*, 50(8):1032–1040, 1978.

[95] RockTron. Fly ash beneficiation process & benefits - rktron.com. Online, 2011. URL http://rktron.com/us-rocktron-fly-ash-beneficiation-process-benefits.

[96] R P Z Sommerville. Recycling coal fly ash in the manufacture of useful materials. MEng thesis, University of Birmingham, 2011.

[97] Sarbajit Ghosal and Sidney A Self. Particle size-density relation and cenosphere content of coal fly ash. *Fuel*, 74(4):522–529, 1995.

[98] Prabir K Kolay and Sudha Bhusal. Recovery of hollow spherical particles with two different densities from coal fly ash and their characterization. *Fuel*, 117:118–124, 2014.

[99] Shawn Patrick McBride, A Shukla, and A Bose. Processing and characterization of a lightweight concrete using cenospheres. *Journal of Materials Science*, 37(19): 4217–4225, 2002.

[100] S Shukla, S Seal, Z Rahaman, and K Scammon. Electroless copper coating of cenospheres using silver nitrate activator. *Materials Letters*, 57(1):151–156, 2002.

[101] Zeng Aixiang, Xiong Weihao, Wang Caifang, and Zhou Qionghua. Structure and properties of $BaFe_{12}O_{19}$ coated fly ash cenospheres by sol-gel process. *Journal of Wuhan University of Technology-Mater. Sci. Ed.*, 21(3):129–131, 2006.

[102] Roberto Peter Zygmunt Sommerville. Utilisation of coal fly ash in the manufacture of useful materials. MRes thesis, University of Birmingham, 2013.

[103] Pengwei Huo, Yongsheng Yan, Songtian Li, Huaming Li, Weihong Huang, Songtao Chen, and Xiaojie Zhang. H_2O_2 modified surface of TiO_2/fly-ash cenospheres and enhanced photocatalytic activity on methylene blue. *Desalination*, 263(1):258–263, 2010.

[104] M Koopman, KK Chawla, W Ricci, K Carlisle, GM Gladsyz, M Lalor, ML Jones, K Kerr, MP George, G Gouadec, et al. Titania-coated glass microballoons and cenospheres for environmental applications. *Journal of Materials Science*, 44(6): 1435–1441, 2009.

[105] Praveen K Surolia, Rajesh J Tayade, and Raksh V Jasra. TiO_2-coated cenospheres as catalysts for photocatalytic degradation of methylene blue, p-nitroaniline, n-decane, and n-tridecane under solar irradiation. *Industrial & Engineering Chemistry Research*, 49(19):8908–8919, 2010.

[106] Bing Wang, Qin Li, Wei Wang, Ying Li, and Jianping Zhai. Preparation and characterization of Fe^{3+}-doped TiO_2 on fly ash cenospheres for photocatalytic application. *Applied Surface Science*, 257(8):3473–3479, 2011.

[107] *Directive 2001/80/EC of the European Parliament and of the Council of 23 October 2001 on the limitation of emissions of certain pollutants into the air from large combustion plants*, 2001. EU Comission. URL http://eur-lex.europa.eu/legal-content/EN/TXT/PDF/?uri=CELEX:32001L0080&from=EN.

[108] *Directive 2010/75/EU of the European Parliament and of the Council of 24 November 2010 on industrial emissions (integrated pollution prevention and control)*, 2010. European Parliament, Council of the European Union. URL http://data.europa.eu/eli/dir/2010/75/oj.

[109] Stanislav V Vassilev, Rosa Menendez, Mercedes Diaz-Somoano, and M Rosa Martinez-Tarazona. Phase-mineral and chemical composition of coal fly ashes as a basis for their multicomponent utilization. 2. Characterization of ceramic cenosphere and salt concentrates. *Fuel*, 83(4):585–603, 2004.

[110] M Uçurum. Influences of jameson flotation operation variables on the kinetics and recovery of unburned carbon. *Powder Technology*, 191(3):240–246, 2009.

[111] RK Dwari and K Hanumantha Rao. Fine coal preparation using novel tribo-electrostatic separator. *Minerals Engineering*, 22(2):119–127, 2009.

[112] VV Zyryanov, SA Petrov, and AA Matvienko. Characterization of spinel and magnetospheres of coal fly ashes collected in power plants in the former ussr. *Fuel*, 90 (2):486–492, 2011.

[113] David M Bibby. Composition and variation of pulverized fuel ash obtained from the combustion of sub-bituminous coals, New Zealand. *Fuel*, 56(4):427–431, 1977.

[114] Jianping Yang, Yongchun Zhao, Vladimir Zyryanov, Junying Zhang, and Chuguang Zheng. Physical–chemical characteristics and elements enrichment of magnetospheres from coal fly ashes. *Fuel*, 135:15–26, 2014.

[115] RockTron. Product ranges. Online 2011-05-06. URL http://www.rktron.com/media/pdfs/JD-RT-4230-AlphaSalesPresenter-27-04-10.pdf.

[116] Ramchandra Pode. Potential applications of rice husk ash waste from rice husk biomass power plant. *Renewable and Sustainable Energy Reviews*, 53:1468–1485, 2016.

[117] DS Chaudhary and MC Jollands. Characterization of rice hull ash. *Journal of Applied Polymer Science*, 93(1):1–8, 2004.

[118] Seyed Naser Azizi and Maryam Yousefpour. Synthesis of zeolites naA and analcime using rice husk ash as silica source without using organic template. *Journal of Materials Science*, 45(20):5692–5697, 2010.

[119] Alireza Naji Givi, Suraya Abdul Rashid, Farah Nora A Aziz, and Mohamad Amran Mohd Salleh. Contribution of rice husk ash to the properties of mortar and concrete: a review. *Journal of American Science*, 6(3):157–165, 2010.

[120] Wanvimon Arayapranee, Nuchanat Na-Ranong, and Garry L Rempel. Application of rice husk ash as fillers in the natural rubber industry. *Journal of Applied Polymer Science*, 98(1):34–41, 2005.

[121] MY Ahmad Fuad, Z Ismail, ZA Mohd Ishak, and AK Mohd Omar. Application of rice husk ash as fillers in polypropylene: effect of titanate, zirconate and silane coupling agents. *European Polymer Journal*, 31(9):885–893, 1995.

[122] S Chandrasekhar, KG Satyanarayana, PN Pramada, P Raghavan, and TN Gupta. Review processing, properties and applications of reactive silica from rice husk—an overview. *Journal of Materials Science*, 38(15):3159–3168, 2003.

[123] Teong Guan Chuah, A Jumasiah, I Azni, Saed Katayon, and SY Thomas Choong. Rice husk as a potentially low-cost biosorbent for heavy metal and dye removal: an overview. *Desalination*, 175(3):305–316, 2005.

[124] EA Basha, R Hashim, HB Mahmud, and AS Muntohar. Stabilization of residual soil with rice husk ash and cement. *Construction and Building Materials*, 19(6): 448–453, 2005.

[125] AA Boateng and DA Skeete. Incineration of rice hull for use as a cementitious material: the Guyana experience. *Cement and Concrete Research*, 20(5):795–802, 1990.

[126] Margandan Bhagiyalakshmi, Lee Ji Yun, Ramani Anuradha, and Hyun Tae Jang. Utilization of rice husk ash as silica source for the synthesis of mesoporous silicas and their application to CO_2 adsorption through TREN/TEPA grafting. *Journal of Hazardous Materials*, 175(1):928–938, 2010.

[127] Chawikarn Santasnachok, Winarto Kurniawan, Chris Salim, and Hirofumi Hinode. The utility of rice husk ash from biomass power plant: Synthesis of Na-A and Na-X zeolites using the two step method hydrothermal. *Journal of Advanced Agricultural Technologies Vol*, 1(2), 2014.

[128] M Rozainee, SP Ngo, AA Salema, KG Tan, M Ariffin, and ZN Zainura. Effect of fluidising velocity on the combustion of rice husk in a bench-scale fluidised bed combustor for the production of amorphous rice husk ash. *Bioresource Technology*, 99(4):703–713, 2008.

[129] Daniel C. Harris, editor. *Quantitative Chemical Analysis*. W. H. Freeman and Company, 2003.

[130] Keiichiro Fuwa and BL Valle. The physical basis of analytical atomic absorption spectrometry. the pertinence of the beer-lambert law. *Analytical Chemistry*, 35(8): 942–946, 1963.

[131] Barry A. Wills and James A. Finch. *Wills' Mineral Processing Technology*. Butterworth-Heinemann, Boston, eighth edition edition, 2016. ISBN 978-0-08-097053-0. doi: http://dx.doi.org/10.1016/B978-0-08-097053-0.00005-4. URL http://www.sciencedirect.com/science/article/pii/B9780080970530000054.

[132] Ray F Egerton. *Physical Principles of Electron Microscopy An Introduction to TEM, SEM, and AEM*. Springer Science+Business Media, Inc, Boston, MA, 2005. ISBN 9780387260167 0387260161.

[133] P. W Hawkes and John C. H Spence. *Science of microscopy*. Springer, New York, 2007. ISBN 9780387252964 0387252967 9780387497624 0387497625.

[134] S Amelinckx, D Van Dyck, J Van Landuyt, and G Van Tendeloo. *Handbook of microscopy*. VCH, Weinheim [u.a., 1997. ISBN 3527294732 9783527294732.

[135] Vangipuram Seshachar Ramachandran and James J Beaudoin. *Handbook of analytical techniques in concrete science and technology: principles, techniques and applications*. Elsevier, 2000.

[136] H Saisho and H Hashimoto. X-ray fluorescence analysis. In *Applications of Synchrotron Radiation to Materials Analysis*, chapter 2, pages 79–169. Elsevier Science, B.V., 1996.

[137] Philip J Potts and Peter C Webb. Wavelength dispersive x-ray fluorescence. In *Encyclopedia of Analytical Science*, volume 44, pages 419–429. Elsevier, 2005. doi: 10.1016/B0-12-369397-7/00674-9.

[138] DD Williams, JA Grand, and RR Miller. The reactions of molten sodium hydroxide with various metals. *Journal of the American Chemical Society*, 78(20):5150–5155, 1956.

[139] Philip W Schutz and EK McMahon. Dielectric heating of granular materials. *Industrial & Engineering Chemistry*, 38(2):179–184, 1946.

[140] Patrick Charles Harrison. *A Fundamental Study Of The Heating Efffect Of 2.45 GHz Microwave Radiation On Minerals*. PhD thesis, University of Birmingham, 1997.

[141] Robert V Jelinek, Henry B Linford, EK McMahon, and Philip W Schutz. Dielectric heating of granular materials. *Industrial & Engineering Chemistry*, 41(4):852–856, 1949.

[142] Youjun Deng, Markus Flury, James B Harsh, Andrew R Felmy, and Odeta Qafoku. Cancrinite and sodalite formation in the presence of cesium, potassium, magnesium, calcium and strontium in hanford tank waste simulants. *Applied Geochemistry*, 21 (12):2049–2063, 2006.

[143] Andrew R Hind, Suresh K Bhargava, and Stephen C Grocott. The surface chemistry of bayer process solids: a review. *Colloids and Surfaces A: Physicochemical and Engineering Aspects*, 146(1):359–374, 1999.

[144] Alibaba.com. Zeolite 4a/sudium alumino silicate. Online 2016-09-09, . URL https://www.alibaba.com/product-detail/Zeolite-4A-Sudium-Alumino-Silicate_60324416068.html.

[145] Alibaba.com. 4a zeolite factory used in detergent industry. Online 2016-09-09, . URL https://www.alibaba.com/product-detail/4A-Zeolite-factory-used-in-detergent_60495788907.html.

[146] Alibaba.com. Zeolite 4a for detergent, plastic, paper chemicals. Online 2016-09-09, . URL https://www.alibaba.com/product-detail/Zeolite-4A-for-detergent-plastic-paper_142002527.html.

[147] Alibaba.com. detergent oxygen generator and water adsorber zeolite 4a. Online 2016-09-09, . URL https://www.alibaba.com/product-detail/detergent-oxygen-generator-and-water-adsorber_1918350720.html.

[148] Alibaba.com. detergent powder raw materials 4a zeolite/zeolite powder. Online 2016-09-09, . URL https://www.alibaba.com/product-detail/detergent-powder-raw-materials-4A-zeolite_60366694854.html.

[149] Douglas W Ming and Joe B Dixon. Quantitative determination of clinoptilolite in soils by a cation-exchange capacity method. *Clays and Clay Minerals*, 35(6): 463–468, 1987.

[150] A Langella, M Pansini, P Cappelletti, B De Gennaro, M de'Gennaro, and C Colella. NH^{4+}, Cu^{2+}, Zn^{2+}, Cd^{2+} and Pb^{2+} exchange for Na^{+} in a sedimentary clinoptilolite, North Sardinia, Italy. *Microporous and Mesoporous Materials*, 37(3):337–343, 2000.

[151] Ruben Snellings, Lieven Machiels, Gilles Mertens, and Jan Elsen. Rietveld refinement strategy for quantitative phase analysis of partially amorphous zeolitized tuffaceous rocks. *Geologica Belgica*, 13(3):183–96, 2010.

[152] LB McCusker, RB Von Dreele, DE Cox, D Louer, and P Scardi. Rietveld refinement guidelines. *Journal of Applied Crystallography*, 32(1):36–50, 1999.

Publications